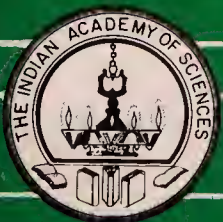


PHOTONS GALAXIES & STARS



R HANBURY BROWN

Photons, Galaxies and Stars

Selected Papers
of
R. Hanbury Brown
Raman Professor, 1974



INDIAN ACADEMY OF SCIENCES
BANGALORE 560 080

1985

© INDIAN ACADEMY OF SCIENCES, BANGALORE

The copyright of individual papers rests with the original publishers *viz.*, Royal Astronomical Society, London; Macmillan Journals Limited, London; Royal Society, London; Taylor and Francis Limited, London; The Astrophysical Journal, University of Chicago Press, Illinois; Royal Greenwich Observatory, Sussex; Australian Academy of Sciences, Canberra; Indian Institute of Science, Bangalore; Free University, Amsterdam; University of Sydney, Australia.

FOREWORD

The Raman Chair was established by the Indian Academy of Sciences in 1972 with an endowment from the Government of India to honour the memory of the Academy's founder Prof. C. V. Raman.

Professor Robert Hanbury Brown (then with the Chatterton Astronomy Department, School of Physics, University of Sydney, Australia) was invited by the Academy to be the first occupant of this prestigious Chair. Prof. and Mrs Hanbury Brown visited India in the summer of 1974 and were in residence at the Raman Research Institute, Bangalore.

During his stay in India, Prof. Hanbury Brown attended and delivered lectures at the National Symposium on Statistical Physics held at Bangalore, to celebrate 50 years of Bose Statistics. Since his pioneering work brings out the fundamental role of Bose statistics in optics, his presence was a major contribution to the success of the symposium.

He visited several universities and scientific institutions and establishments at Kodaikanal, Ootacamund, Bombay, Ahmedabad, Jaipur, Delhi, Nainital, Hyderabad and Madras and delivered a total of 15 lectures during this period. His visit to India greatly stimulated interest amongst astronomers, young and old.

In order to commemorate his visit, the Academy considered it appropriate to bring out a volume of his selected papers in astronomy and astrophysics which surprisingly did not exist. Such a volume would obviously be of great value to all workers in this field, both in India and abroad. Prof. Hanbury Brown most kindly permitted the publication of this volume and also made valuable suggestions as to the papers that could go into the volume. Also included at the end of the volume are a few of his very interesting lectures on general topics.

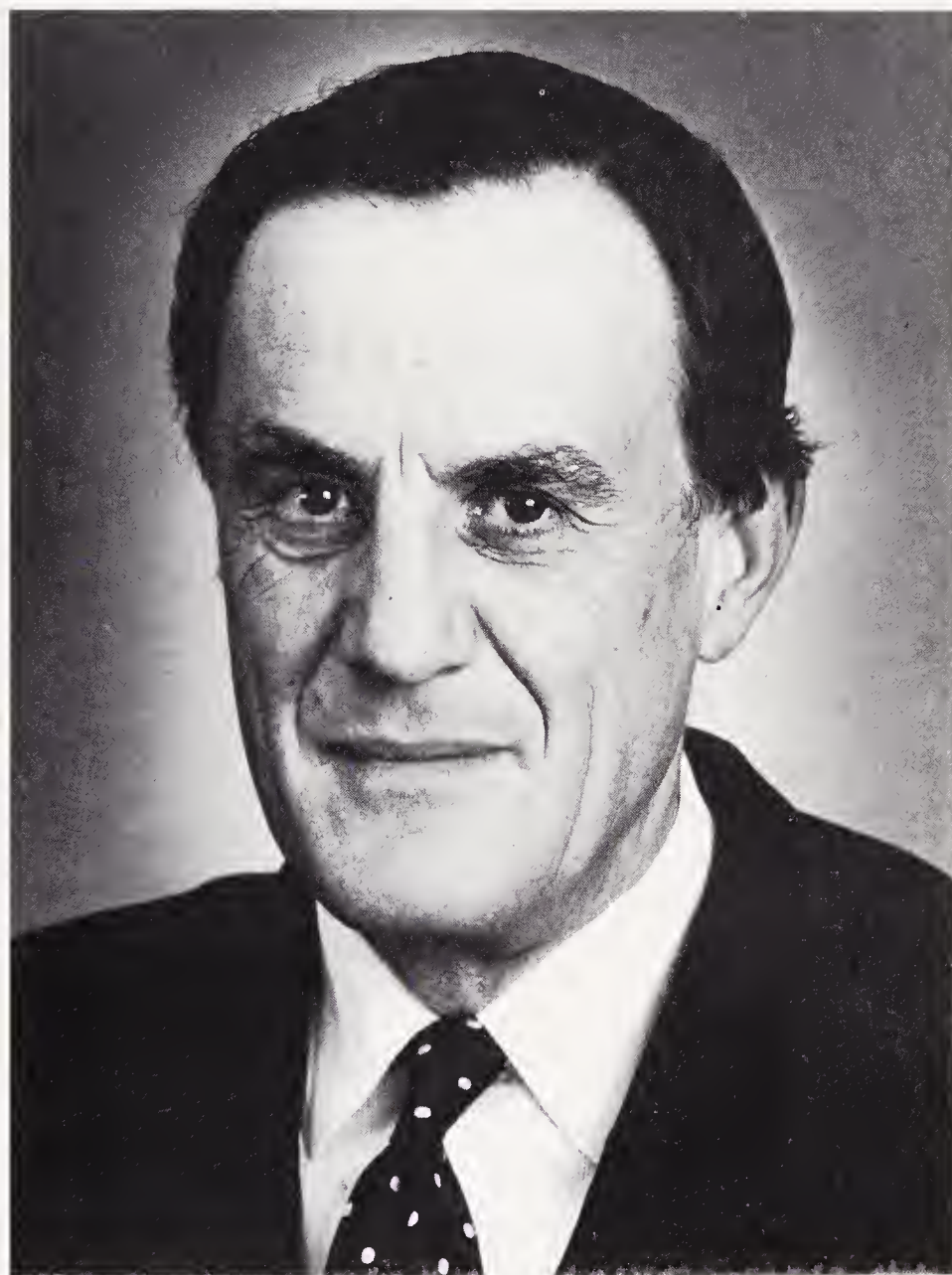
We thank the publishers of these papers and articles—Royal Astronomical Society, London; Macmillan Journals Limited, London; Royal Society, London; Taylor and Francis Limited, London; The Astrophysical Journal, University of Chicago Press, Illinois; Royal Greenwich Observatory, Sussex; Australian Academy of Sciences, Canberra; Indian Institute of Science, Bangalore; Free University, Amsterdam; University of Sydney, Australia—for permitting us to reproduce them.

S. RAMASESHAN
President
Indian Academy of Sciences
Bangalore



Digitized by the Internet Archive
in 2018 with funding from
Public.Resource.Org

<https://archive.org/details/photonsgalaxiess00unse>



Prof. R. Hanbury Brown

BIOGRAPHICAL SKETCH

Prof. R. Hanbury Brown was born at Aruvankadu, Nilgiri Hills, India on August 31, 1916, and had his schooling in England. After a post graduate degree in electronics from the City and Guilds College of London University, he joined the Air Ministry in 1936 to work on radar, making important contributions to the development of airborne instruments during the war years. In 1949, he commenced work on the radio emission from our galaxy and other galaxies at Jodrell Bank devising and developing long baseline interferometric techniques to achieve high angular resolution. In the preface to his book 'The Intensity Interferometer', he writes of 'being fortunate to take part in two other scientific adventures—the early work on radar and the beginnings of radio astronomy'. The third adventure, which he himself initiated, is of course intensity interferometry itself. This originated in the fifties as an elegant and experimentally convenient alternative to conventional amplitude interferometry. The principle is that intensity fluctuations as measured by radio telescopes at two separate points will have a correlation, depending on the baseline and the angular size of the source. While this is not difficult to visualise for radio waves, the extension to visible light proposed by Hanbury Brown and Twiss met with widespread misunderstanding and disbelief in the physics community. With hindsight, this can be attributed to a misuse of the photon picture of light. There was also some uncertainty about how faithfully photocurrents in the detectors could follow fluctuations in the light. The first laboratory test of the idea by Hanbury Brown and Twiss in 1956 was soon followed by the first astronomical application, *viz* the measurement of the angular diameter of Sirius.

This work undoubtedly stimulated a rethinking of the theoretical description of light. The dual nature of light has been a preoccupation of physicists from the turn of the century. That a new manifestation was discovered more than fifty years later is both a warning against regarding a subject as closed and a tribute to the insight of the discoverers. A basic paper by Purcell showed that the correlated appearance of photons in two separate detectors followed from their Bose statistics. A substantial part of the experimental technique and formalism of modern quantum optics can trace its origin to the Hanbury Brown-Twiss experiment.

With a view to measuring stellar angular diameters, an intensity interferometer was constructed at Narrabri, Australia, and Prof. Hanbury Brown moved to the University of Sydney as Professor of Physics and Astronomy in 1964. This unique instrument, going to baselines as large as 180 metres has measured accurate angular diameters for 32 main sequence stars and led to a wholly observational scale of effective temperatures against which astrophysical theory can be checked. In addition, several interesting results on binary, rotating, and emission-line stars have emerged. In his more recent writings, Prof. Hanbury Brown has emphasized the exciting contributions that an instrument with higher sensitivity, accuracy and resolving power can make to astronomy. As an example, the study of pulsating stars would greatly strengthen one important rung of the shaky cosmological distance ladder. With characteristic openness, he has been exploring the possibility of a return to the Michelson interferometer, armed with modern electronic and optical techniques.

The many honours which Prof. Hanbury Brown has received include the Fellowship and the Hughes medal of the Royal Society, the Fellowship and the Eddington

medal of the Royal Astronomical Society and the Honorary Fellowship of the Indian Academy of Sciences. In view of his contributions to our understanding of light, techniques for studying it, and particularly to the problem of measuring the angular sizes of stars, it is indeed appropriate that the Franklin Institute has awarded him its Albert Michelson medal. This collection of his papers, brought out by the Indian Academy of Sciences, should enable a wider circle of readers to appreciate his work which cuts across conventional distinctions like engineer/physicist/astronomer or even experimenter/theorist and leaves us with a picture of a remarkably integrated scientist.

R. Nityananda
Raman Research Institute
Bangalore

LIST OF PAPERS REPRODUCED

	<i>Page</i>
I <i>The Emission from Radio Sources</i>	
1. Radio emission from the Andromeda Nebula. R. H. Brown and C. Hazard. 1951. <i>Mon. Not. R. astr. Soc.</i> 111 , 357-367	1
2. The radio emission from normal galaxies. I. Observations of M31 and M33 at 158 Mc/s and 237 Mc/s. R. H. Brown and C. Hazard. 1959. <i>Mon. Not. R. astr. Soc.</i> 119 , 297-308	15
3. The radio emission from normal galaxies. II. A study of 20 spirals at 158 Mc/s. R.H. Brown and C. Hazard. 1961. <i>Mon. Not. R. astr. Soc.</i> 122 , 479-490	27
4. The radio emission from normal galaxies. III. Observations of irregular and early-type galaxies at 158 Mc/s and a general discussion of the results. R.H. Brown and C. Hazard. 1961. <i>Mon. Not. R. astr. Soc.</i> 123 , 279-283	39
5. A radio survey of the Great Loop in Cygnus. D. Walsh and R. H. Brown. 1955. <i>Nature (London)</i> . 175 , 808-810	45
6. The remnants of supernovae as radio sources in the galaxy. R.H. Brown. 1954. <i>Observatory</i> . 74 , 185-194	49
II <i>The Angular Diameters of Radio Sources</i>	
7. Apparent angular sizes of discrete radio sources. R.H. Brown, R.C. Jennison and M.K. Das Gupta. 1952. <i>Nature (London)</i> . 170 , 1061-1066	59
8. Galactic radio sources of large angular diameter. R.H. Brown, H.P. Palmer and A.R. Thompson. 1954. <i>Nature (London)</i> . 173 , 945-949	65
9. An analysis of the angular sizes of radio sources. L.R. Allen, R.H. Brown and H.P. Palmer. 1962. <i>Mon. Not. R. astr. Soc.</i> 125 , 57-74	71
III <i>Techniques of Measuring Angular Size</i>	
10. A new type of interferometer for use in radio astronomy. R.H. Brown and R.Q. Twiss. 1954. <i>Philos. Mag.</i> 45 , 663-682	89
11. A rotating-lobe interferometer and its application to radio astronomy. R.H. Brown, H.P. Palmer and A.R. Thompson. 1955. <i>Philos. Mag.</i> 46 , 857-866	109
IV <i>Photon Optics</i>	
12. Correlation between photons in two coherent beams of light. R.H. Brown and R.Q. Twiss. 1956. <i>Nature (London)</i> . 177 , 27-29	119
13. Correlation between photons, in coherent beams of light, detected by a coincidence counting technique. R.Q. Twiss, A.G. Little and R.H. Brown. 1957. <i>Nature (London)</i> . 180 , 324-326	125

V *Optical Astronomy*

14. A test of a new type of stellar interferometer on Sirius. R.H. Brown and R.Q. Twiss. 1956. *Nature (London)*. **178**, 1046-1948 131
15. Interferometry of the intensity fluctuations in light. I. Basic theory: the correlation between photons in coherent beams of radiation. R.H. Brown and R.Q. Twiss. 1957. *Proc. R. Soc. (London)*. **A242**, 300-324 139
16. Interferometry of the intensity fluctuations in light. II. An experimental test of the theory for partially coherent light. R.H. Brown and R.Q. Twiss. 1957. *Proc. R. Soc. (London)*. **A243**, 291-319 164
17. Interferometry of the intensity fluctuations in light. III. Applications to astronomy. R.H. Brown and R.Q. Twiss. 1958. *Proc. R. Soc. (London)*. **A248**, 199-221 193
18. Interferometry of the intensity fluctuations in light. IV. A test of an intensity interferometer on Sirius A. R.H. Brown and R.Q. Twiss. 1958. *Proc. R. Soc. (London)*. **A248**, 222-237 216
19. The stellar interferometer at Narrabri Observatory. I. A description of the instrument and the observational procedure. R.H. Brown, J. Davis and L.R. Allen. 1967. *Mon. Not. R. astr. Soc.* **137**, 375-392 233
20. The stellar interferometer at Narrabri Observatory. II. The angular diameters of 15 stars. R.H. Brown, J. Davis, L.R. Allen and J.M. Rome. 1967. *Mon. Not. R. astr. Soc.* **137**, 393-417 251
21. The angular diameters of 32 stars. R.H. Brown, J. Davis and L.R. Allen. 1974. *Mon. Not. R. astr. Soc.* **167**, 121-136 277
22. Empirical effective temperatures and bolometric corrections for early type stars. A.D. Code, J. Davis, R.C. Bless and R.H. Brown. 1976. *Astrophys. J.* **203**, 417-434 293
23. A study of γ^2 Velorum with a stellar intensity interferometer. R.H. Brown, J. Davis, D. Herbison-Evans and L.R. Allen. 1970. *Mon. Not. R. astr. Soc.* **148**, 103-117 311
24. A study of α Virginis with an intensity interferometer. D. Herbison-Evans, R.H. Brown, J. Davis and L.R. Allen. 1971. *Mon. Not. R. astr. Soc.* **151**, 161-176 327
25. An attempt to detect a corona around β Orionis with an intensity interferometer using linearly polarized light. R.H. Brown, J. Davis and L.R. Allen. 1974. *Mon. Not. R. astr. Soc.* **168**, 93-100 343

VI *Gamma Ray Astronomy*

26. Evidence for the detection of gamma rays from Centaurus A at $E_\gamma \geq 3 \times 10^{11}$ eV. J.E. Grindlay, H.F. Helmken, R.H. Brown, J. Davis and L.R. Allen. 1975. *Astrophys. J.* **197**, L9-L12 351
27. Results of a southern hemisphere search for gamma-ray sources at $E_\gamma \geq 3 \times 10^{11}$ eV. J.E. Grindlay, H.F. Helmken, R.H. Brown, J. Davis and L.R. Allen. 1975. *Astrophys. J.* **201**, 82-89 355

	<i>Page</i>
28. The detection of very high energy gamma rays by Čerenkov light. R.H. Brown. 1974. Lecture, Raman Research Institute, Bangalore.	363
VII <i>Lectures</i>	
29. Measuring the size of the stars. R.H. Brown. 1982. The Matthew Flinders Lecture, Australian Academy of Science, Occasional Paper Series No. 3	369
30. Bosons and stars. R.H. Brown, 1975. <i>In Statistical physics</i> (eds.) N. Mukunda, A.K. Rajagopal and K.P. Sinha. Lecture given at Symposium to celebrate fifty years of Bose Statistics, Indian Institute of Science, Bangalore, July 1974	391
31. Concern about the control of science. R.H. Brown. 1982. Proc. Academic Congress, <i>Concern about science</i> , Centennial Free University, Amsterdam, 1980. pp. 75-84	403
32. Science and faith. R.H. Brown. 1979. <i>Curr. Affairs Bull.</i> 56 , 14-21	415

RADIO EMISSION FROM THE ANDROMEDA NEBULA

R. Hanbury Brown and C. Hazard

(Communicated by A. C. B. Lovell)

(Received 1951 March 29)

Summary

A detailed account is given of the measurement of the radio-frequency radiation from the Great Nebula in Andromeda (M31) using a wave-length of 1.89 m. It is shown that the measured intensity is in good agreement with that to be expected on the assumption that the generation of the radiation is similar to that in the Galaxy. From these results it is estimated that the total extra-galactic radio emission amounts to about 1 per cent of the whole radio flux observed on the Earth.

1. *Introduction.*—The experiments of Jansky (1) in 1931 showed that radio-frequency radiation is reaching the Earth from the general direction of the Milky Way. Subsequent measurements by Hey, Parsons and Phillips (2), by Reber (3) and by Bolton and Westfold (4) have shown that the intensity contours of this radiation correspond well with the structure of the Galaxy derived from visual observations. Although the source of the radiation remains unknown, it is generally accepted that the major part of the radiation must be generated by some mechanism which is widespread in the Galaxy.

Attempts have been made in the past to discover whether or not the extra-galactic nebulae generate similar radio emissions. For example, Reber (3) used a paraboloid of 30 feet aperture on a wave-length of 1.87 metres, but failed to find any conclusive evidence of radiation from the nebula M31. During the last few years, however, a much larger paraboloid of aperture 218 feet has been available at the Jodrell Bank Experimental Station. Calculations of the intensity to be expected from M31 based on the assumption that it radiates in a similar way to the Galaxy suggested that with this paraboloid, used in conjunction with the best available receiver, it might be possible to detect the radiation if it existed.

This paper describes the results of an experiment designed to test if such radio-frequency radiation is being emitted by the Great Nebula in Andromeda (M31). A short account of the results has been published previously (5).

2. *Description of apparatus.*—Fig. 1 shows a block diagram of the apparatus. The aerial is a paraboloid of diameter 218 feet and focal length 126 feet. The reflecting surface is formed by long wires which are spaced 8 inches apart and which run parallel to one fixed plane of polarization.

Electromagnetic waves of wave-length large compared with 8 inches and whose polarization is parallel to the wires are reflected by this surface and are focused on to the primary feed which consists of two dipoles and their reflectors mounted on a central mast 126 feet high. This mast is pivoted at its base in such a way that it may be tilted in the north-south plane to 15 degrees on either side of the vertical. The latitude of the system is N. 53° 14' and it is therefore possible to

direct the beam to declinations between N. 38° and N. 68° . The direction of the beam is estimated by measuring the angle through which the primary feed is displaced from the vertical and applying to this angle a correction established from experiments (6) carried out with small paraboloids.

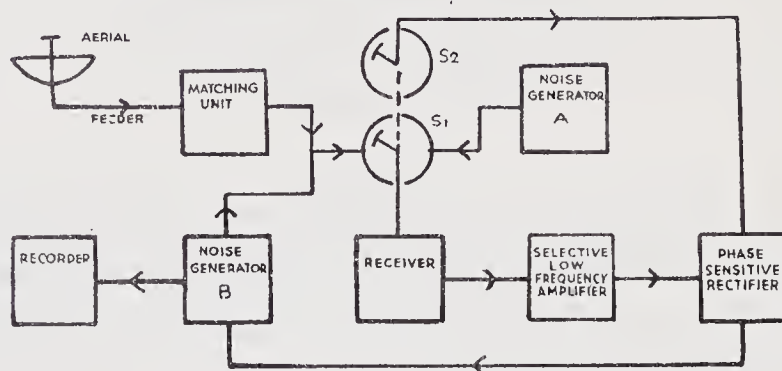


FIG. 1.—Block diagram of apparatus.

The gain and beam-width of the aerial have been calculated for various wave-lengths, taking into account the polar diagram of the primary feed, the actual shape of the reflecting surface and the reflection coefficient of the system of wires. They have also been measured at 4.2 metres using an aircraft as a transmitting source. The beam-width at 1.89 metres has been measured by observations of the radio source in Cygnus. The values obtained are shown in Table I.

TABLE I
Characteristics of Aerial System

	72 Mc./s.		158.5 Mc./s.	
	Theoretical	Measured	Theoretical	Measured
Gain (over half-wave dipole)	690	700	2130	∞
Beam-width to half power	$4^\circ 30'$	$4^\circ 20'$	$2^\circ 00'$	$1^\circ 58'$

Fig. 2 shows the shape of the beam measured in both planes by observations of the source in Cygnus, that is with the beam tilted about 14 degrees from the vertical. The broken line in Fig. 2(a) shows the theoretical beam shape when the beam is directed to the zenith.

The aerial system is connected to the receiver through 294 feet of coaxial feeder which has a loss of 2.7 decibels at 1.89 metres.

The receiving equipment is based on that described by Ryle and Vonberg (7). Their arrangement has been modified to allow the measurement of aerial temperatures below room temperature. A rotating switch S_1 (Fig. 1) revolves at about 1200 r.p.m. and switches the receiver alternately to a noise generator A and to the aerial in parallel with a noise generator B. Both noise generators are tungsten filament diodes type CV 172. Any difference between the power received in the two positions of the switch appears as a low-frequency modulation of the receiver output. This low-frequency component is amplified by a selective low-frequency amplifier and is applied to a phase-sensitive rectifier operated from a switch S_2 which is synchronous with the aerial switch. The output of the phase sensitive rectifier controls the power delivered from the noise generator B which is in parallel with the aerial. The system automatically maintains a balance such that the power from the aerial plus that from the generator B balances the

power from the generator A. The power from the generator A is kept constant and the variations in the power from the aerial are recorded as variations in power output from the generator B. These variations are recorded continuously by a standard recording milliammeter on a moving chart.

In the region of sky around M₃₁ the effective aerial temperature remained below room temperature and, except when calibrating, the output from the generator A was simply that of a resistance at room temperature. The load impedance of the generator A is accurately pre-set and an adjustable matching unit is used to equalize the impedances of the two branches at the switch S₁. As a further precaution the output of the generator B is calibrated by means of the generator A.

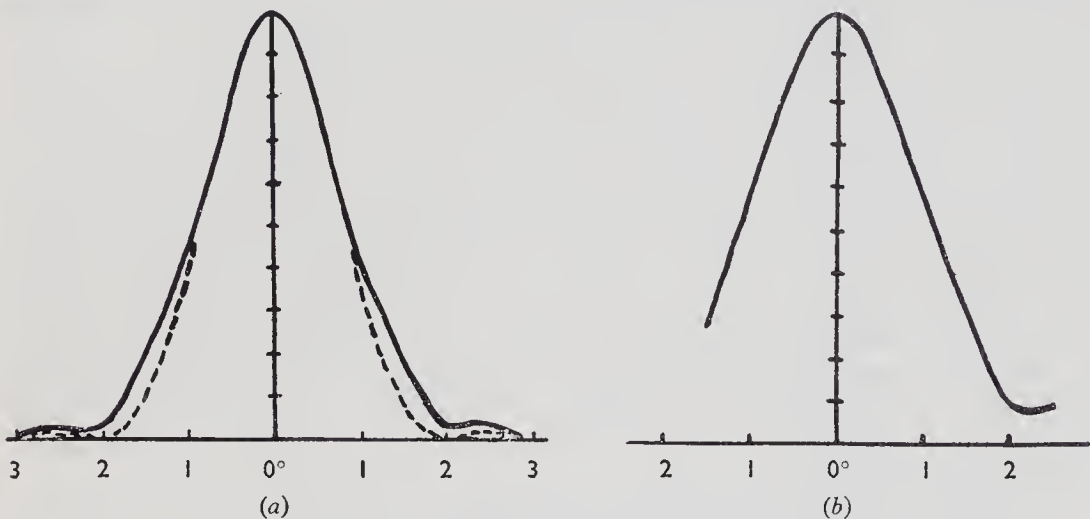


FIG. 2.—Polar diagrams of 218-ft. aperture paraboloid. ($\lambda=1.89$ metres.)

- (a) Beam shape in right ascension.
- (b) Beam shape in declination.
- Ordinates: Intensity in arbitrary units.
- Abscissae: Degrees.

The receiver has a midband frequency of 158.5 Mc./s. determined by a crystal-controlled local oscillator. The pre-detector band-width is 1.5 Mc./s., and the radio-frequency amplifier is a “cascode” (8) with a noise factor of 3.5. The time constant of response of the whole system is about 10 seconds which is small compared with the 10 minutes taken by a point source at declination N. 40° to transit the aerial beam.

The minimum power incident on the aerial, which can be detected by such an equipment, can be estimated theoretically, assuming that the limit is set by the random fluctuations inherent in the equipment, and not by external interference.

Assuming that

- N = noise factor of the receiver,
- B = band-width of receiver in cycles per second,
- t = time constant of response of the equipment,
- T = total effective temperature at input to receiver,
- ΔT = r.m.s. fluctuations of output meter,

it can be shown (9) that

$$\Delta T \sim NT \sqrt{\left(\frac{2\pi}{Bt}\right)}. \tag{1}$$

Substituting the parameters of the equipment described above, $\Delta T \sim 0.7$ deg. C. Practical experience shows that under the conditions of this experiment the minimum deflection which can be detected on a single trace is about twice the r.m.s. fluctuation of the output indicator. Using the theoretical value of ΔT derived above, the minimum change of aerial temperature which can be detected should be about 1.4 deg. C.

Allowing for the loss in the feeder cable and for the decrease in gain of the aerial system when the beam is tilted 14 degrees from the zenith, this value of ΔT corresponds (at 1.89 metres wave-length) to an incident randomly polarized flux of 10^{-25} watts/square metre/c.p.s. Practical experience shows that the minimum detectable flux depends upon the time of day and on the weather. During the day, and in fine weather, the noise level of the equipment is controlled by reception of the "quiet" Sun in minor lobes of the aerial, and by man-made static. Charged rain, electrical disturbances in the atmosphere and radiation from the "disturbed" Sun overload the equipment. During the night the noise level falls off gradually until about midnight and increases again at sunrise. Between midnight and sunrise the minimum detectable flux appears to be controlled sometimes by the theoretical limits discussed in equation (1) and sometimes by unidentified signals which appear to vary with the weather and which probably have a terrestrial origin. On favourable nights it is about 10^{-25} watts/square metre/c.p.s., which is the limit estimated theoretically. By averaging the results of several independent observations it is possible to extend this limit by an amount which has not yet been established by a quantitative experiment. In the present work the limit has been successfully reduced to 5×10^{-26} watts/square metre/c.p.s. by averaging four records.

3. *Method of observation.*—The experiment was carried out by fixing the beam at a number of different elevations corresponding to the region around M31, so that for each diurnal rotation of the Earth the beam swept out a strip of sky 2 degrees wide in declination and 24 hours in right ascension. For each elevation of the beam the intensity of the radio flux received was recorded continuously for about 100 to 200 hours. Altogether, recordings were made for several elevations of the beam, corresponding to declinations between N. $38^{\circ} 47'$ and N. $43^{\circ} 00'$. The variation with right ascension of the flux received at each declination was found by averaging the results obtained on several successive sweeps.

4. *Results.*—The total number of records obtained by the method described above was 90, of which 20 were spoiled by the effects of heavy rain which persisted throughout 1950 August and September. Of the remaining records 50 showed the existence of a localized source of radio-frequency radiation at $00^{\text{h}} 40^{\text{m}}$ R.A. Plate 4 shows one of these records taken with the beam at declination N. $40^{\circ} 11'$. The remaining 20 were either taken when the beam was directed to declinations N. 38° and N. 43° , or interpretation of the records was made difficult by interference in the period $23^{\text{h}} 30^{\text{m}}$ R.A. to $01^{\text{h}} 40^{\text{m}}$ R.A. The curves shown in Fig. 3 were constructed from 30 records which were undisturbed by interference. In order to show clearly the change in intensity with right ascension along each sweep the records have been displaced by an arbitrary amount, corresponding to different declinations, so that the ordinate represents only the relative intensities for the points in each sweep. The sweeps between declinations N. $39^{\circ} 48'$ and N. $41^{\circ} 58'$ indicate a localized source of radiation about $00^{\text{h}} 40^{\text{m}}$ R.A., superimposed on a slow change of intensity which reaches a minimum between

00^h 20^m and 00^h 30^m R.A. This slow change corresponds to a gradient of the galactic background radiation, which reaches a minimum when the beam is near its maximum southern galactic latitude.

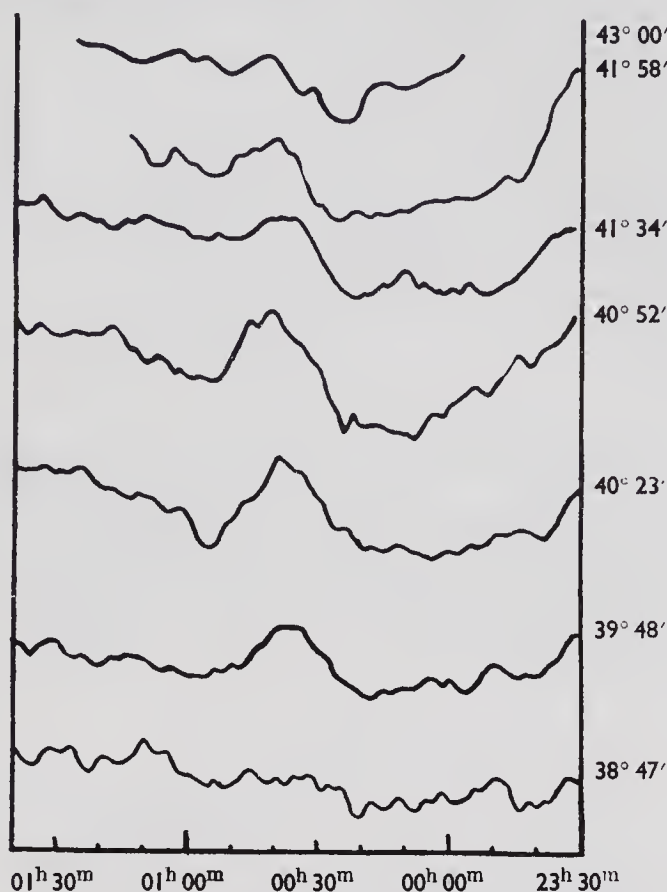


FIG. 3.—Intensity recorded during transit of the source in Andromeda with the aerial beam directed to different declinations.

Ordinates : Relative intensity in arbitrary units.

Abscissae : Hours and minutes of right ascension.

These curves cannot be converted into true contours of the intensity from this region because the change of aerial impedance with beam tilt did not permit the difference in absolute intensity between observations at different declinations to be measured reliably. Therefore the background intensity was extrapolated to 00^h 40^m R.A. for each curve and the intensity of the background radiation at this point was taken as the zero for each curve when plotting the contours shown in Fig. 4. The contour system (Fig. 4) therefore represents the intensity relative to the background intensity at 00^h 40^m R.A., the gradient in declination of the galactic radiation having been removed. The gradient in right ascension has not been removed and so causes a distortion of the contours.

Analysis of the results yields the data shown in Table II. The source has a finite apparent width in right ascension and declination, as can be seen by comparing the apparent widths with the corresponding widths of the intense source in Cygnus, which is at approximately the same declination as the observed source, and whose apparent width is known to be less than 1.5 of arc (10). This comparison eliminates any uncertainty due to possible distortion of the beam. The appropriate curves are shown at (a) and (c) in Fig. 5. Record (b) in Fig. 5

shows the intensity received from another weak source at approximately the same declination as the observed source.

The intensity given in Table II is an integrated value over the source and is twice the intensity observed on one polarization, as it is assumed that the radiation

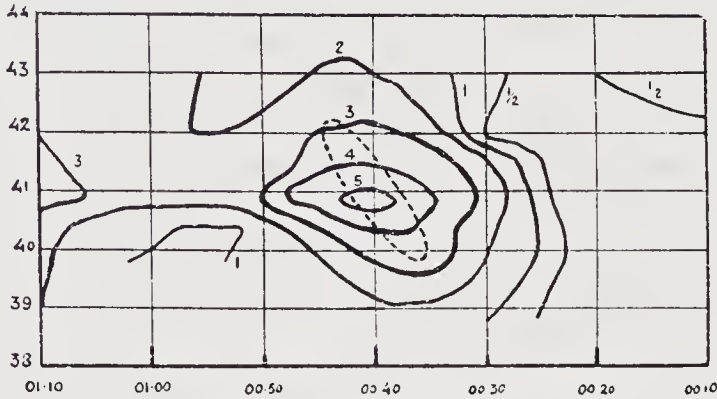


FIG. 4.—Contours of radio-frequency flux observed near the source in Andromeda with a 2-degree beam. (1 unit = 10^{-26} watts/square metre/c.p.s. $\lambda = 1.89$ metres.)

The contours do not represent the absolute intensity of the radio flux at each point. As explained in the text the gradient of background flux in declination has been removed and the contours show the intensity for each point above the background flux at 00^h 40^m R.A. The gradient of background flux in right ascension has not been removed and therefore distorts the contours.

The broken line shows the outline of the nebula derived from a photograph.

Ordinates : Declination (degrees north).

Abscissae : Right ascension (1 division represents 10 minutes).

TABLE II

Data on Source in Andromeda

Right Ascension	00 ^h 40 ^m 15 ^s ± 30 ^s
Declination	40° 50' N. ± 20'
Apparent widths to half-power	3° (dec.) × 3½° (R.A.)
Apparent widths to half-power of the source in Cygnus	2¼° (dec.) × 2° (R.A.)
Intensity (integrated over source)	10^{-24} watts/sq. metre/c.p.s. ± 25 per cent

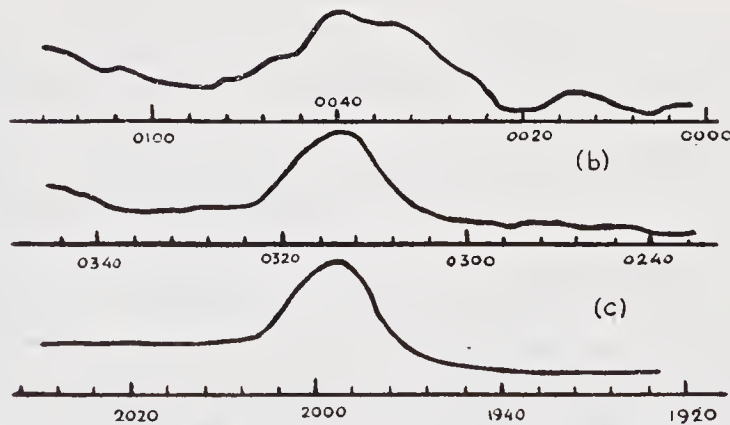


FIG. 5.—Intensity recorded during transit of three sources through the aerial beam. The scale of intensity for each diagram has been adjusted so that the widths in right ascension can be compared easily.

(a) Source in Andromeda.

(b) Weak source in Perseus.

(c) Intense source in Cygnus.

Ordinates : Intensity (arbitrary units).

Abscissae : Hours and minutes of right ascension.

is randomly polarized. The previously published (5) value of 4×10^{-25} watts/square metre c.p.s. was calculated assuming the apparent diameter of the source to be small compared with the beam-width, and radiation from the outer regions of the source was neglected. Further measurements and analysis showed the extension of the source to be so great that this assumption was not justified.

The intensity of the source is so small compared with the background radiation and with the random fluctuations in the receiver that the difficulty in interpreting the records is the main cause of errors in the data in Table II. There is no significant systematic error in right ascension as the position of the beam in this coordinate was checked by reference to the intense source in Cygnus whose right ascension is well established. As the declination of the source in Cygnus is not yet known with satisfactory accuracy (10) it was not possible to check the position of the beam in declination in the same way. This introduces an additional error into the determination of declination, as the relationship between the angle of tilt of the mast and the angle of the beam is not yet known to better than 1 per cent. Therefore there may be a systematic error of the order of $\pm 10'$ in the measurements of declination. The error in measuring the actual tilt of the mast was negligible.

The error in the measurement of intensity is caused partly by the weakness of the source and partly by inaccuracy in the calibration, these two errors being of comparable magnitude.

5. *Discussion of results.*—The coordinates of the observed source lie close to the centre of the Great Nebula in Andromeda M31 (R.A. $00^{\text{h}}40^{\text{m}}$, declination $N. 41^{\circ}00'$, Epoch 1950). The apparent dimensions of the source are consistent with a source of radio-frequency radiation of size comparable with the main body of the nebula M31.* It is possible that these results could be due to a fortuitous grouping of two or more point sources with their effective centre coincident with that of M31. From a consideration of the number of observed point sources of intensity comparable to 10^{-24} watts/square metre/c.p.s. and, assuming a random distribution of sources, it can be shown that the probability of observing two sources simultaneously in the beam is about $\frac{1}{4000}$. It is therefore improbable that the finite width of the source is due to a coincidence of two point sources.

The celestial coordinates and finite size of the source indicate with a high degree of probability that the source may be identified with the nebula M31. It is assumed that the two companion nebulae NGC 205 and NGC 221 (which have apparent photographic magnitudes of 10.8 and 9.5 respectively compared with the apparent photographic magnitude 5 of M31 (11)) are not contributing substantially to the radiation received.

* *Note added in proof.*—The apparent extension of the source can, in principle, be deduced by applying to the observed results a correction for the finite beam-width of the aerial. However, the low intensity of the source in comparison with the gradient of background radiation precludes an accurate analysis of the extension, particularly in right ascension. The values for the extension of the source given in a previous publication (5) were underestimated. A subsequent analysis showed that the observed variation of intensity with declination could be accounted for by a source in which the intensity is a maximum at the centre and decreases to 10 per cent of the central intensity at points separated by $150'$. The apparent extension of the source in right ascension appears to be of the same order, but the gradient of background radiation makes this result unreliable.

Inspection of the contour system given in Fig. 4 shows that, when allowance is made for the distortion in right ascension of the contours by the gradient of background radiation, it is possible to interpret the results as due to an elliptical source orientated in a similar manner to M31.

The authors are obliged to Mr J. H. Piddington of the Radiophysics Laboratory, Sydney, whose criticisms have led to the inclusion of this footnote.

6. *Comparison of the radio emission from M₃₁ and the Galaxy.*—From the results described above it appears evident that radio emissions from M₃₁ are being received on the Earth. In this section we compare the measured intensity of this emission with that to be expected if M₃₁ is similar to the Galaxy. An estimate of the intensity to be expected from M₃₁ has been made in two ways, (a) by consideration of the luminosities and (b) by analysis of the contours of radio flux from the Galaxy.

(a) *Comparison of radio flux and light flux.*—This method makes the assumption that the ratio of the radio flux from M₃₁ to the radio flux from a volume near the Sun equals the ratio of the light flux from M₃₁ to the light flux from the same volume near the Sun.

The aggregate luminosity per cubic parsec near the Sun is known to be 0.045 suns. The radio flux from the same volume can be estimated from the temperatures observed (4) in the directions of the galactic poles, if it is assumed that the radio flux originates in bodies distributed in a manner similar to the visible stars and that absorption is negligible. The temperatures of the galactic poles have been used because in these directions the estimates of stellar distribution are the most reliable.

Consider an aerial with a beam of solid angle ω , effective area A and gain G directed towards a galactic pole and receiving radiation of wave-length λ metres.

Let

ρ_r = the density of sources per cubic metre at a distance r metres from the Sun,

ρ_0 = the density of sources near the Sun,

$4\pi\alpha$ = the total power radiated by an average source (watts/c.p.s.),

I = the intensity of the radio flux at the Earth (watts/square metre/c.p.s.),

P = the power received by the aerial (watts/c.p.s.),

T = the effective temperature of the aerial (deg. K.),

then
$$I = \int_0^R \frac{\alpha}{r^2} \rho_r \frac{\omega}{4\pi} \cdot 4\pi r^2 dr = \alpha\omega \int_0^R \rho_r dr, \quad (2)$$

where R is the distance from the Sun to the boundary of the Galaxy in a direction perpendicular to the galactic plane, the boundary being taken as the distance at which the stellar density falls to 1 per cent of that near the Sun. Therefore

$$P = kT = \frac{\alpha\omega A}{2} \int_0^R \rho_r dr,$$

where k is Boltzmann's constant (the factor $\frac{1}{2}$ is included because the aerial receives radiation in one polarization only), but

$$G = \frac{4\pi A}{\lambda^2} = \frac{4\pi}{\omega}. \quad (3)$$

Hence

$$kT = \frac{\alpha\lambda^2}{2} \int_0^R \rho_r dr. \quad (4)$$

The integral $\int_0^R \rho_r dr$, evaluated by using the star density/distance tables given by Bok (12), equals $1.4 \times 10^{10} \rho_0$.

Taking (4) $T = 600$ deg. K. and $\lambda = 3$ metres,

$$\begin{aligned} \alpha\rho_0 &= 1.3 \times 10^{-40} \text{ watts/steradian/cu. metre/c.p.s.} \\ &= 3.8 \times 10^9 \text{ watts/steradian/cu. parsec/c.p.s.,} \end{aligned}$$

it has been shown that the law connecting the intensity (I) of the background radiation with wave-length (λ) is $I = \text{constant} \times \lambda^a$, where $0.35 < a < 0.65$ (10).

By assuming $I \propto \lambda^{0.5}$,

$$\alpha\rho_0 = 3 \times 10^9 \text{ watts/steradian/cu. parsec/c.p.s.}$$

at a wave-length of 1.89 metres. This is the radio flux per steradian from a cubic parsec near the Sun.

The ratio of the light flux from M31 to that from a cubic parsec near the Sun is 2.2×10^{10} . (The luminosity of M31 is taken as 10^9 suns and that of a cubic parsec near the Sun as 0.045 suns.)

Assuming this same ratio for radio-frequency radiation, then the total radio-frequency radiation from M31 is $2.2\alpha\rho_0 \times 10^{10}$ watts/steradian/c.p.s. The intensity of this radiation at the Earth should therefore be

$$\frac{2.2\alpha\rho_0 \times 10^{10}}{l^2} \text{ watts/square metre/c.p.s.,}$$

where l is the distance of M31 in metres.

If $l = 230,000$ parsecs, then $I_{M31} = 1.2 \times 10^{-24}$ watts/square metre/c.p.s. which is of the same order as the observed value.

(b) *Analysis of contours of radio flux from the Galaxy.*—The contours of radio-frequency radiation over most of the celestial sphere have been measured by Bolton and Westfold (4) at a wave-length of 3 metres. These have been used to construct a rough model of the Galaxy as it would appear from the distance of M31.

If absorption is negligible, then the intensity of the radiation observed from this distance will be approximately independent of the orientation of the Galaxy with respect to the observer. In this analysis the Galaxy was assumed to be viewed along the equatorial plane. The observed contours were projected on to a cross-section of the Galaxy through the galactic centre and perpendicular to the observer. The Galaxy was assumed to be a spheroid with dimensions $30,000 \times 5,000$ parsecs and to have a distribution of mass symmetrical about its minor axis. The projection was made on the assumption that the radiation from any volume of the Galaxy is proportional to the mass in that volume. From these projected contours $\int T(\Omega) d\Omega$ was evaluated over the whole cross-section of the Galaxy, where $T(\Omega)$ is the effective temperature observed over an elementary solid angle $d\Omega$ subtended at an observer at a distance of 230,000 parsecs. The intensity (I_G) observed at this distance will be *

$$I_G = \frac{2k}{\lambda^2} \int T(\Omega) d\Omega.$$

* This expression can be derived as follows:—

Consider a beam of solid angle ω where ω is large compared with the apparent diameter of the source. The effective temperature (T_ϵ) of this beam will be given by

$$T_\epsilon = \frac{\int T(\Omega) d\Omega}{\omega}$$

using the same notation as in the text. The power (P) received by the beam is given by

$$P = kT_\epsilon = \frac{k \int T(\Omega) d\Omega}{\omega} = \frac{I_G}{2} \cdot A,$$

$$I_G = \frac{2k \int T(\Omega) d\Omega}{A\omega}.$$

From equation (3) $A\omega = \lambda^2$,

$$\therefore I_G = \frac{2k}{\lambda^2} \int T(\Omega) d\Omega.$$

Evaluating the integral as described above, the value of I_G is found to be 9×10^{-24} watts/square metre/c.p.s. at a wave-length of 3 m. Then, assuming $I : \lambda^{0.5}$ as before, the intensity on the wave-length of 1.89 m. used in the present work should be 7×10^{-24} watts/square metre/c.p.s. for the Galaxy observed at the distance of M31.

By assuming, as above, that the radio flux is proportional to the mass, then the intensity to be expected from M31 can be estimated by comparing its mass with that of the Galaxy. Estimates of the mass of M31 vary from 3×10^{10} to 10^{11} solar masses compared with an estimate of 10^{11} to 2×10^{11} for the Galaxy. The intensity of the radio-frequency radiation from M31 observed on the Earth would thus be expected to be within the range 1×10^{-24} to 7×10^{-24} watts/square metre/c.p.s. which, in fact, includes the observed value.

The agreement between the theoretical values calculated above and the measured intensity suggests that as far as radio-frequency emission is concerned M31 possesses similar characteristics to the Galaxy.

7. *The total radiation from extra-galactic nebulae.*—The contribution to the radio flux incident on the Earth from extra-galactic nebulae has been calculated for a very simple model of the universe, assuming that the ratio of radio flux to light flux found for M31 is true for all nebulae independent of type.

The intensity of the radio flux from M31 observed on the Earth at a wave-length of 1.89 metres is 10^{-24} watts/square metre/c.p.s. and therefore assuming it to be an isotropic radiator the total radio flux emitted is 5×10^{19} watts/steradian/c.p.s. M31 has an absolute visual magnitude of -17.5 compared with -15.2 for the average nebula. Therefore the radio flux from an average nebula will be about 5×10^{18} watts/steradian/c.p.s.

If σ = the average space density of nebulae (assumed isotropic),
 $4\pi\gamma$ = the total radio flux from an average nebula,
 I_E = the intensity at the Earth of extra-galactic radiation per steradian,
 then if radiation is received from nebulae in a sphere of radius D and the effects of absorption and recession are neglected,

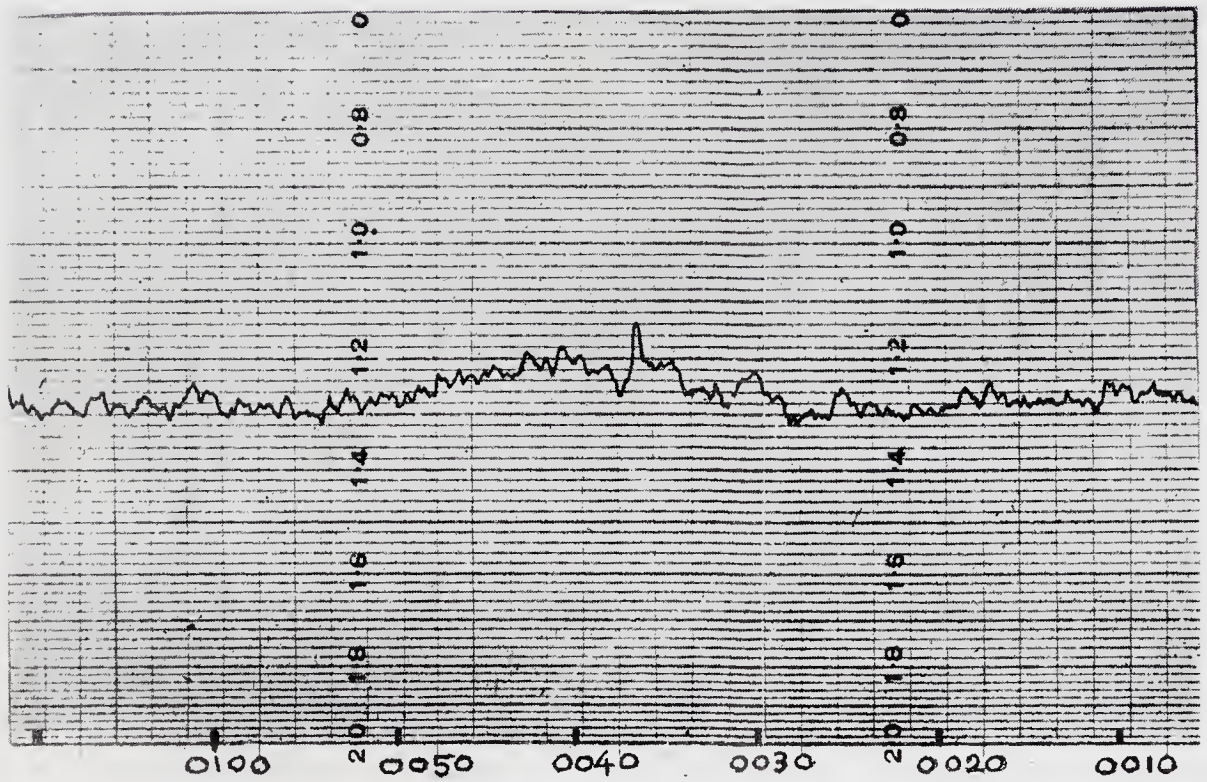
$$I_E = \gamma\sigma D \quad (\text{from equation (2)}).$$

Putting $\gamma = 5 \times 10^{18}$ watts/steradian/c.p.s., $\sigma = 1.9 \times 10^{-19}$ nebulae per cubic light-year, then for a universe of radius 5×10^8 light-years (corresponding to the range of the 100-inch telescope), $I_E = 4.75 \times 10^{-24}$ watts/square metre/steradian/c.p.s. If the radius of the visible universe is taken as 1.8×10^9 light-years, as suggested by the apparent recession of the nebulae,

$$I_E = 1.7 \times 10^{-23} \text{ watts/square metre/steradian/c.p.s.}$$

This latter value of I_E corresponds to an effective aerial temperature at 1.89 metres of about 2 deg. K. The average aerial temperature observed over the whole celestial sphere at this wave-length is about 200 deg. K., and this calculation therefore suggests that the extra-galactic radiation contributes about 1 per cent of the total radio flux incident on the Earth.

8. *Acknowledgments.*—The work has been carried out at the Jodrell Bank Experimental Station of the University of Manchester. The aerial system was designed by Dr J. A. Clegg. The construction of the aerial and apparatus was made possible by financial assistance from the Department of Scientific and Industrial Research. We wish to thank Dr A. C. B. Lovell for his interest in



*Facsimile of a single record of the transit of the source in Andromeda taken on 1950 October 31 with the aerial beam directed to declination $40^{\circ}11'N$.
 Ordinates : Intensity in arbitrary units.
 Abscissae : Hours and minutes of right ascension.*

R. Hanbury Brown and C. Hazard, Radio emission from the Andromeda nebula.

the investigation. One of us (R. H. B.) is indebted to I.C.I. Ltd. for a research fellowship, and the other (C. H.) to the Department of Scientific and Industrial Research for a maintenance grant.

University of Manchester,
Jodrell Bank Experimental Station,
Holmes Chapel, Cheshire:
1951 March 28.

References

- (1) K. G. Jansky, *Proc. I.R.E.*, **20**, 1920, 1932.
- (2) J. S. Hey, J. W. Phillips and S. J. Parsons, *Proc. Roy. Soc. A*, **192**, 425, 1948.
- (3) G. Reber, *Ap. J.*, **100**, 279, 1944.
- (4) J. G. Bolton and K. C. Westfold, *Aust. J. Sci. Res. A*, **3**, 19, 1950.
- (5) R. Hanbury Brown and C. Hazard, *Nature*, **166**, 901, 1950.
- (6) S. Silver and C. S. Pao, *Radiation Laboratory Report*, 479, 1944.
- (7) M. Ryle and D. D. Vonberg, *Proc. Roy. Soc. A*, **193**, 98, 1948.
- (8) H. Wallman, *Proc. I.R.E.*, **36**, 700, 1948.
- (9) R. H. Dicke, *Rev. Sci. Instr.*, **17**, 268, 1946.
- (10) G. J. Stanley and O. B. Slee, *Aust. J. Sci. Res. A*, **3**, 234, 1950.
- (11) H. Shapley and A. Ames, *Harv. Ann.*, **88**, No. 2, 52, 1932.
- (12) B. J. Bok, *Distribution of the Stars in Space*, University of Chicago Press, p. 22, 1937.

THE RADIO EMISSION FROM NORMAL GALAXIES

I. OBSERVATIONS OF M₃₁ AND M₃₃ AT 158 MC/S AND 237 MC/S

R. Hanbury Brown and C. Hazard

(Received 1959 March 9)

Summary

A survey of the radio emission from bright normal galaxies has been carried out at 158 Mc/s. This paper reports the results obtained on M₃₁ and M₃₃. The integrated radio magnitude (m_r) of these two galaxies has been measured and compared with their photographic magnitude (m_p); it is found that the difference ($m_r - m_p$) is almost the same for both.

The distribution of intensity across M₃₁ shows two major components: a *disk* and a *corona*. The corona is responsible for 90 per cent of the total emission, has a true axial ratio of about 0.6, and has a major axis which is about three times greater than that of the visible nebula. The results show that M₃₃ also has a corona; the ellipticity, emissivity and dimensions of the corona relative to the visible object are closely similar to the values found for M₃₁.

A comparison between M₃₁, M₃₃ and the Galaxy suggests that the emissivity of the corona of the Galaxy is significantly higher than that of the other two galaxies.

1. *Introduction.*—In previous papers (1, 2, 3) we reported some observations of galaxies which were carried out at 158 Mc/s with the 218 ft fixed paraboloid at Jodrell Bank. The recent completion of the 250 ft steerable paraboloid (4), with its wider field of view and greater gain, has made it possible to observe a greater number of galaxies and also to improve the previous measurements. A survey has therefore been made at 158 Mc/s of the brightest normal* galaxies in the northern sky in an attempt to establish the relationship between their photographic and radio magnitudes. Subsequently a few galaxies have also been observed at 237 Mc/s; this was only done in those cases where the improved resolving power was considered to be useful in interpreting the results obtained at 158 Mc/s.

The account of this survey has been divided into two parts. The present paper (I) has been restricted to the two brightest spirals M₃₁ and M₃₃; these two objects have been studied in greater detail than the other galaxies and require individual discussion. A second paper (II) contains the results on the remaining galaxies together with a discussion of all the data.

2. *Description of apparatus.*—The observations were made at frequencies of 158 Mc/s and 237 Mc/s, using a receiver based on that described by Ryle and Vonberg (6). The parameters of this receiver are substantially the same as those of the equipment used in our earlier observations of M₃₁ (1).

* In this context a *normal* galaxy, following Baade and Minkowski (5), is taken to be a galaxy which appears to be normal when examined photographically.

The aerial system used was the 250 ft steerable paraboloid (4). The primary feeds at the two frequencies were similar and consisted of a simple dipole and reflector connected to the receiver through 85 ft of low-loss coaxial cable. The shape of the aerial beam was measured in detail by observing the intense radio sources in Cygnus and Cassiopeia; as expected, it was found to be elliptical with the major axis parallel to the dipole. The values obtained for the total width of the beam between half-power points are given in Table I. The same observations were also used to determine the direction of the axis of the beam relative to the axis of the paraboloid. At both frequencies the misalignment between the two axes was about 10' and the appropriate corrections have been applied to all the observations.

TABLE I

The beam-width of the aerial

Frequency (Mc/s)	Beam-width* in E plane	Beam-width* in H plane
158	2°·2	1°·6
237	1°·5	1°·1

* The beam-width is the total width between directions of half-power gain.

3. *Calibration of the intensity scale.*—In a previous paper (2) we defined a scale of radio magnitude, using NGC 5194/5 as a comparison source, which was intended to make the radio and photographic magnitudes of normal spiral galaxies numerically equal. On that scale a source with a flux density of S_{158} w. m. $^{-2}$ (c/s) $^{-1}$ at 158 Mc/s has a radio magnitude m_r defined by the equation

$$m_r = -53.45 - 2.5 \log S_{158}. \quad (1)$$

For the purpose of the present work it is more convenient to use the discrete source 14N5A as a standard of comparison instead of NGC 5194/5. This source has a small angular diameter (7) and is circumpolar at Jodrell Bank; the equipment was calibrated by observing it at least once during each observing period. Preliminary measurements show that it has a flux density of 75×10^{-26} w. m. $^{-2}$ (c/s) $^{-1}$ at 158 Mc/s which, from equation (1), corresponds to a radio magnitude of +6.86. Whitfield (8) finds that it has a spectral index of -0.6.

It is desirable, when observations of sources at different frequencies are to be compared, that their radio magnitudes should be defined in such a way that they do not vary greatly with frequency; in particular it is convenient that the magnitude of the comparison source should be independent of frequency. For this reason we have assumed arbitrarily that the radio magnitude of 14N5A is independent of frequency and has the value $m_r = +6.86$ derived at 158 Mc/s.

To facilitate comparison of our results with those of southern observers we have compared the intensity of 14N5A with that of 12N1A in Virgo. The 12N1A source is the more intense by 2.77 mag. at 158 Mc/s and hence at this frequency its radio magnitude is +4.09.

4. Observations of M31 (NGC 224)

4.1. *Method of observation.*—The observations were made during the late summer and autumn of 1958. The region surveyed was bounded by declinations

$N 34^\circ$ and $N 47^\circ$ and right ascensions $00^h 10^m$ and $01^h 10^m$. The beam of the 250 ft paraboloid was scanned over the region at one degree per minute along lines of constant declination, the scans being separated by 0.5° in the central parts of the survey and 0.75° in the outer parts. These scans were then linked together by scanning along lines of constant right ascension at $00^h 10^m$, $00^h 40^m$ and $01^h 10^m$. Finally, to make certain of the extent of the nebula, the beam was scanned along the major and minor axes. Each scan was repeated several times to minimize the effects of interference and receiver drift; all the measurements were made at both 158 Mc/s and 237 Mc/s. Some sample scans are shown in Fig. 1.

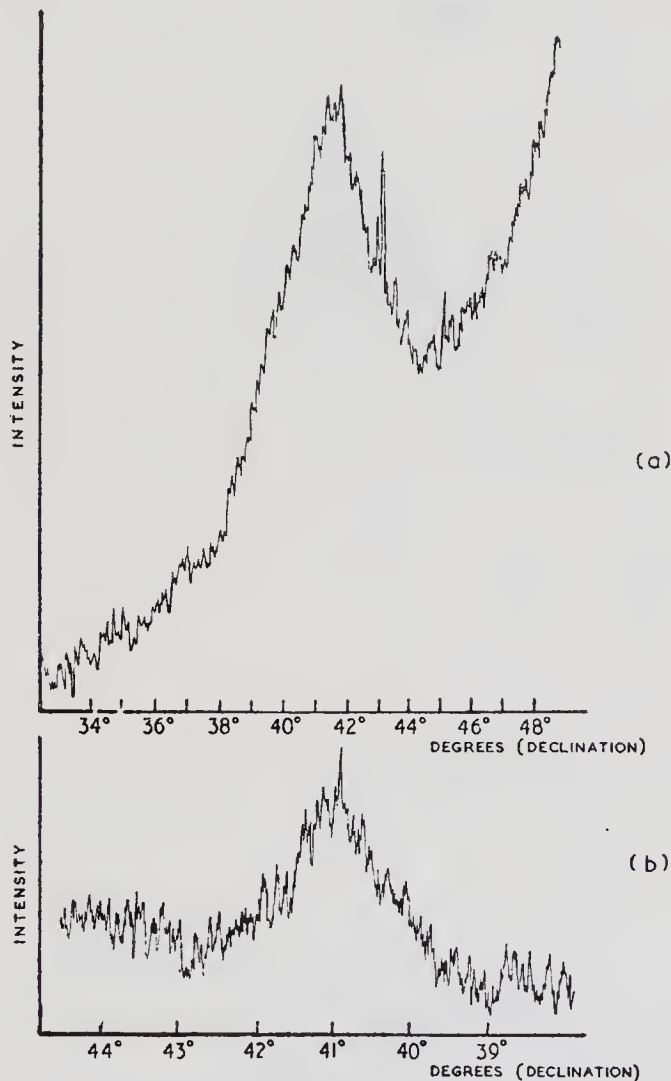


FIG. 1.—Sample scans across M_{31} . (a) A scan along the major axis at 158 Mc/s.
 (b) A scan along the minor axis at 237 Mc/s.
 Ordinates : intensity in arbitrary units.
 Abscissae : declination in degrees.

4.2. *The radio isophotes of M_{31} .*—The records have been converted into contours which show the distribution of brightness over the region; the results are shown in Figs. 2, 3 and 4. The contours represent lines of equal observed brightness and they have been plotted above an arbitrary zero.

The outline of the visible nebula is indicated in Fig. 4 by the broken line which, following de Vaucouleurs (9), encloses 95 per cent of the total luminosity. It can be seen clearly that the radio emission is much more widely distributed than the light, although the shape of the contours is obviously distorted by localized sources and irregularities in the general background radiation.

The localized sources are more prominent on the 237 Mc/s contours, as would be expected with the narrower beam. The source at $00^{\text{h}} 33^{\text{m}}$, $N 39^{\circ}$ is particularly prominent, and is probably the source originally identified with

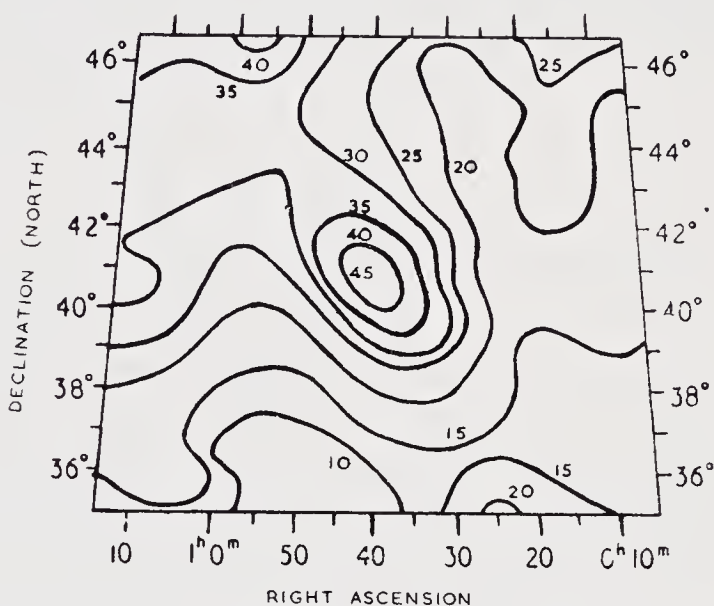


FIG. 2.—Isophotes of M31 observed at 158 Mc/s. The contours are marked in arbitrary units of brightness temperature. Epoch 1950.

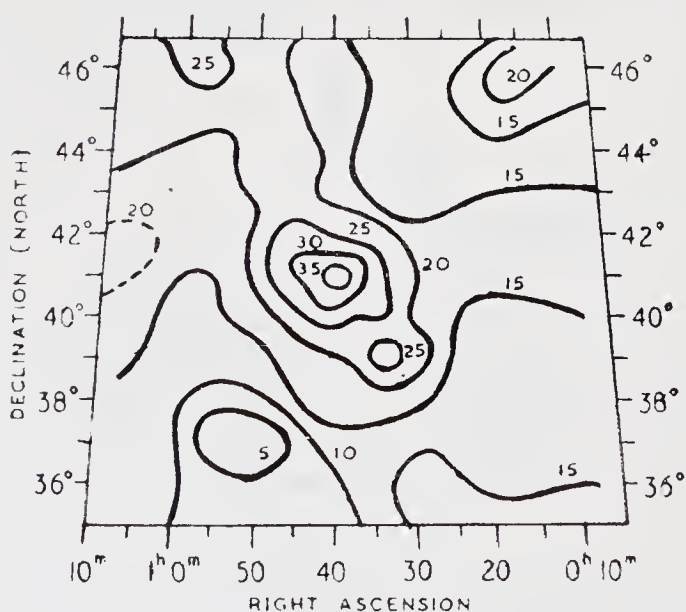


FIG. 3.—Isophotes of M31 observed at 237 Mc/s. The contours are marked in arbitrary units of brightness temperature. Epoch 1950.

M31 by Ryle, Smith and Elsmore (10). It is now known to have an angular diameter which is considerably less than that of the visible nebulae and this fact, together with the discrepancy between the positions of the two objects, makes it unlikely that they are physically associated.

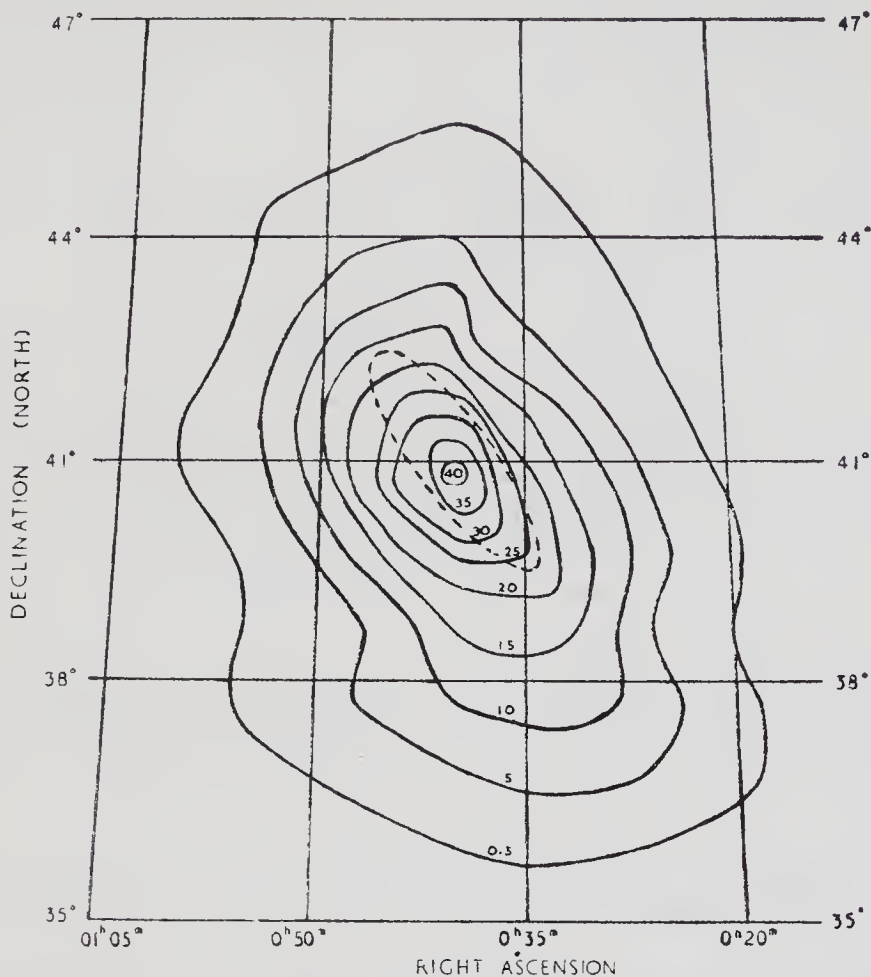


FIG. 4.—Isophotes of M31 at 158 Mc/s with the background radiation removed. The contours are marked in arbitrary units of brightness temperature. The broken line shows the outline of the visible nebula. Epoch 1950.

The small irregularity which appears on the 237 Mc/s contours at about one degree from the centre of the nebula may be a discrete source with a radio magnitude of about +9.6; at the distance of M31 this corresponds to a source with a total radio emission about 2.5 mag. greater than that of Cassiopeia A. The possibility cannot be excluded that it is a discrete source in M31.

In an attempt to show the radiation from the nebula more clearly the background brightness has been removed from the contours observed at 158 Mc/s. The background was extrapolated smoothly over the region of the nebula and contours of brightness measured above this somewhat arbitrary baseline are shown in Fig. 4. At 158 Mc/s the outlines of the nebula are clearly defined on the original records and the distorting effects of discrete sources appear to be comparatively small; it is therefore likely that the derived contours in Fig. 4 give a reasonably accurate picture of the radio emission associated with the nebula when smoothed with a 2° beam

An attempt was also made to remove the background radiation from the contours observed at 237 Mc/s. The derived contours proved to be similar to those obtained at 158 Mc/s but are not so reliable on account of their lower signal-to-noise ratio.

4.3. *The integrated radio magnitude of M₃₁.*—The contours at both frequencies have been analysed to find the integrated radio magnitude of M₃₁. At 158 Mc/s the radio magnitude was found to be $m_r = +5.7$, which includes all the radiation within the 1 per cent contour. This value also includes the localized source at $00^h 33^m, N 39^\circ$; this source has a radio magnitude of $+9.0$ at 237 Mc/s and, if it has a spectrum similar to 14N5A, it must contribute about 5.5 per cent of the integrated emission from M₃₁ at 158 Mc/s. Subtracting the contribution from this source the integrated magnitude of M₃₁ at 158 Mc/s is $m_r = +5.8$.

At 237 Mc/s it was possible to measure the radiation with reasonable certainty only out to the 5 per cent contour. The integrated magnitude out to this level is $+6.1$. Extrapolation to the 1 per cent contour shows that the additional radiation is negligible for the present purpose, and the integrated magnitude of M₃₁ at 237 Mc/s may therefore be taken as $+6.1$. A comparison of this result with the value of $+5.8$ at 158 Mc/s suggests that the spectrum of M₃₁ may perhaps be steeper than that of 14N5A. The measurements of Seeger, Westerhout and Conway (11) show that at 400 Mc/s the integrated magnitude of M₃₁ is 0.6 mag. brighter than 14N5A and therefore support this suggestion. Assuming the spectral index of 14N5A to be -0.6 (8), the spectral index of the integrated emission from M₃₁ averaged over the range 158 to 400 Mc/s is -1.1 .

It follows from the values given above that the total power emitted by M₃₁ at 158 Mc/s is $7.8 \times 10^{20} \text{ w. (c/s)}^{-1} \text{ ster}^{-1}$. It has been assumed in calculating this power that the distance is 630 kpc and that the flux density of the comparison source 14N5A is $75 \times 10^{-26} \text{ w.m.}^{-2} \text{ (c/s)}^{-1}$ at 158 Mc/s.

4.4. *The general distribution of emission from M₃₁.*—An inspection of the individual scans over the centre of M₃₁, especially those at 237 Mc/s, suggests immediately that there are two superimposed distributions with very different widths. The first distribution appears to be two or three times as broad as the visible nebula, while the second distribution is much narrower than the first and by comparison is highly concentrated towards the centre of the nebula. A sample scan along the minor axis at 237 Mc/s is shown in Fig. 1.

We propose to treat these two distributions as distinct, and to discuss them separately. On the basis of the present results alone such a division is necessarily rather arbitrary; however, it is supported by a study of the Galaxy. Surveys of the non-thermal radiation from the Galaxy have shown that there are at least two principal components of the emission: (i) an extended *corona* which is almost spherical and is responsible for the majority of the emission (12); and (ii) a second component which is concentrated towards the galactic plane and which appears to be roughly coextensive with the visible parts of the Galaxy. The second component has been called the *disk* by Mills (13). We shall therefore tentatively identify the two distributions which appear to exist in M₃₁ with those found in the Galaxy, and we shall refer to the broad component as the *corona* and to the narrow component as the *disk*.

4.5. *The disk component of M₃₁.*—The disk component has been separated from the corona by extrapolating the broad distribution over the centre of the

nebula as illustrated by the broken line in Fig. 5. The width of the disk component obtained in this way is clearly subject to considerable uncertainty; nevertheless we have concluded that the 237 Mc/s records do not show any significant broadening of the beam, and it follows that the total width between half-power points cannot exceed about 1° .

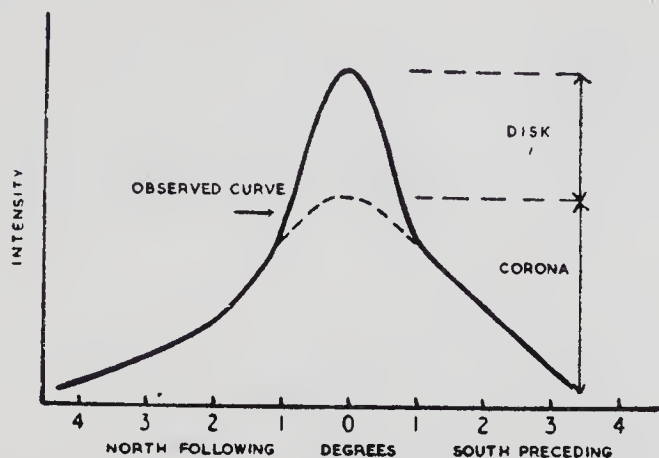


FIG. 5.—Illustrating the method of separating the disk component from the corona. The solid line represents the observed distribution along the major axis of M31 at 237 Mc/s.

Ordinates : intensity.

Abscissae : degrees measured along major axis.

Some further evidence on the width of this narrow distribution has been provided by Palmer and his colleagues (14) who have surveyed M31 at 160 Mc/s using an interferometer with a baseline of 220λ . The records show that there is no source near the optical centre of M31 with an intensity greater than about 0.05 of that of 14N5A. It follows that the maximum width between half-power points of the disk component must be at least 20.

A comparison of the integrated emission from the disk component with that from the corona shows that the disk is responsible for about 10 per cent of the total emission from the nebula.

4.6. The corona of M31

(i) *The apparent distribution of intensity over the corona.*—Since the contribution of the disk component is only 10 per cent of the total radiation, the 158 Mc/s measurements in Fig. 4 are effectively contours of the corona smoothed with a 2° beam. The irregularities in the outline of the corona, which are particularly marked on the outside contour, are probably not significant and may represent minor errors in the separation of the corona from the background.

The general shape of the contours is elliptical and the observed widths of the 1 per cent contour are about 10° (major axis) \times 7° (minor axis). The position angle of the major axis is about 44° and, taking into account the uncertainty in the radio isophotes, this is in reasonable agreement with the value of $37^\circ.7$ given by de Vaucouleurs (9) for the visible nebula.

The observed results were analysed in an attempt to arrive at a closer approximation to the true distribution of the coronal component. The radiation due to the disk was subtracted from the observed distribution, and corrections were made for the smoothing effects of the aerial beam. The analysis

showed that the observations can be reproduced closely if the true isophotes of the corona are elliptical with gaussian brightness distributions along both axes. The total apparent widths of these distributions are $4^{\circ} \cdot 1$ (major axis) $\times 2^{\circ} \cdot 6$ (minor axis) between half-brightness points, and $10^{\circ} \cdot 6$ (major axis) $\times 6^{\circ} \cdot 7$ (minor axis) between 1 per cent contours. The apparent axial ratio of the corona is therefore 0.6, the axial ratio being defined as the ratio of the minor axis to the major axis.

These results have been compared with those obtained by Seeger, Westerhout and Conway (11) who used a 2° beam at 400 Mc/s. The two sets of observations are in reasonable agreement. One obvious discrepancy is that the 400 Mc/s contours show some curious structure at the extreme north and south of the corona. The results presented in the present paper suggest that this structure is not associated with M31, but is due to extraneous features of the background radiation.

(ii) *The distribution of emissivity in the corona.*—We shall discuss the emissivity of the corona of M31 on the assumption that the absorption in the nebula at 158 Mc/s can be neglected, since calculations for our own Galaxy (15) indicate that such an assumption is justified. We shall also assume that the corona is an oblate spheroid whose principal axes coincide with those of the visible nebula. On these assumptions it can be shown (16) that p , the true axial ratio of the ellipsoid, is given by

$$p^2 = \frac{(b/a)^2 - \sin^2 i}{1 - \sin^2 i} \quad (2)$$

where i is the inclination of the nebula to the line of sight and b/a is the apparent axial ratio of the corona. Taking $i = 14^{\circ} \cdot 5$ and $b/a = 0.6$ the true axial ratio of the corona is 0.57.

It was stated in the previous section that the apparent variation of brightness along the principal axes of the corona may be represented by gaussian distributions. It is simple to show that these distributions are exhibited by a model of the corona in which the surfaces of equal emissivity are concentric ellipsoids of fixed axial ratio and in which the emissivity follows a gaussian decrease with distance from the centre. In this model the emissivity $\epsilon(a, z)$ at a point with coordinates a, z with respect to the centre of the corona is given by

$$\epsilon(a, z) = \epsilon_0 \exp \left(-\frac{a^2}{2\sigma_1^2} - \frac{z^2}{2\sigma_2^2} \right) \quad (3)$$

where ϵ_0 is the emissivity at the centre, a is measured in the plane of the nebula and z is measured perpendicular to the plane.

Assuming the distance of M31 to be 630 kpc and taking the widths of the apparent distributions given in the previous section, it can be shown that $\sigma_1 = 19.3$ and $\sigma_2 = 11.0$, where a and z are measured in kiloparsecs. It follows that the total widths of the corona between half-emissivity points are 45 kpc (major axis) $\times 26$ kpc (minor axis), and that the total widths between the 1 per cent contours are 117 kpc (major axis) $\times 67$ kpc (minor axis).

The emissivity of the corona was found by integrating the radiation from the model and equating the result to the observed total power from the nebula. The emissivity at the centre of the corona was found to be 0.12×10^8 w. (c/s) $^{-1}$ ster $^{-1}$ pc $^{-3}$ at 158 Mc/s. This result is in reasonable agreement with the value given by Baldwin (17) of $0.24-0.35 \times 10^8$ w. (c/s) $^{-1}$ ster $^{-1}$ pc $^{-3}$ at

81.5 Mc/s for the mean emissivity of the corona of M31. He assumed in deriving this value that the corona is spherical with a diameter of 36 kpc.

It is interesting to note that, taking the dimensions of the *disk* component suggested in Section 4.5, the emissivity in the disk must be significantly greater than that in the corona.

5. Observations of M33 (NGC 598)

5.1. *The region around M33.*—A detailed survey of M33 was carried out at 158 Mc/s, the region covered being bounded by declinations N26° and N36° and right ascensions 01^h15^m and 01^h55^m. The results of the surveys are plotted as isophotes in Fig. 6. The outline of the visible nebula has been superimposed as a broken line.

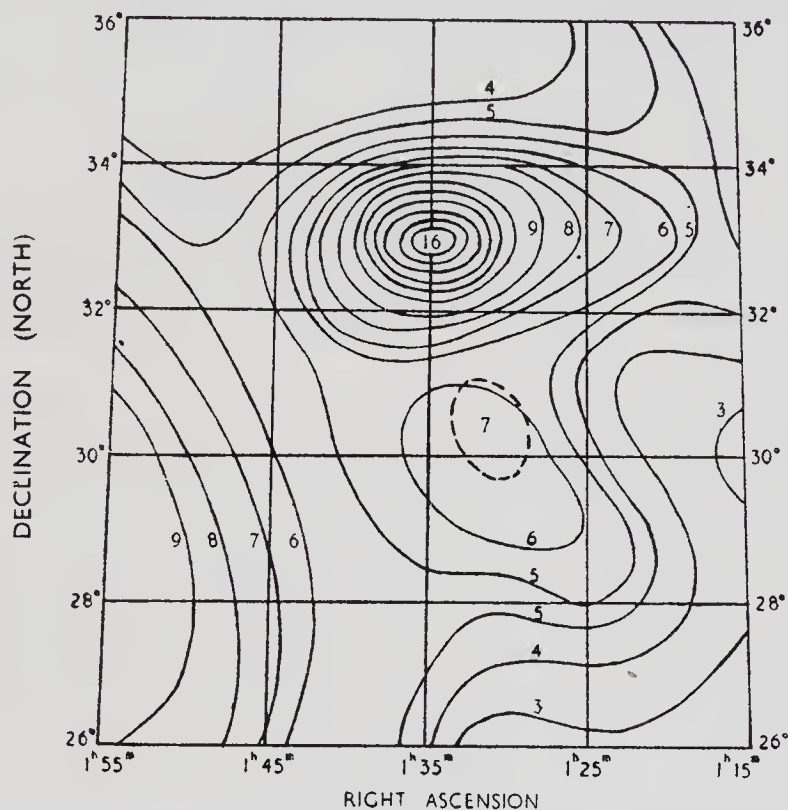


FIG. 6.—Isophotes of M33 observed at 158 Mc/s. The contours are marked in arbitrary units of brightness temperature. Epoch 1950.

The most prominent feature of the map is the source at approximately N 33°, 01^h35^m, which has an intensity of about $60 \times 10^{-26} \text{ w.m.}^{-2} (\text{c/s})^{-1}$ at 158 Mc/s. Some observations made on this source at 237 Mc/s show that it has an angular diameter which is considerably less than 1°. Its position is so close to M33 that it complicates the observations of the radiation from the nebula, and in an early interferometer survey made by Ryle, Smith and Elsmore (10) it was itself identified with the nebula.

The isophotes also show an extended region of low intensity whose centre appears to lie somewhat to the south of the nebula. However, the contour system is distorted by severe gradients in the background radiation and an inspection of the individual records shows that in fact this extended region consists of two sources. One of these sources, which has a small angular diameter

and an intensity of 13×10^{-26} w.m. $^{-2}$ (c/s) $^{-1}$, lies at about $01^{\text{h}} 25^{\text{m}}$, N 29° . The other source, which has a large angular diameter, is centred at $01^{\text{h}} 32^{\text{m}}$, N $30^{\circ} 15'$. These latter coordinates agree closely with the optical centre of M33 and we therefore propose to identify this extended source with the nebula.

After correcting for the effects of the confusing sources, it was found that at 158 Mc/s the apparent widths of the extended source associated with the nebula were $2^{\circ} 45'$ in right ascension and $2^{\circ} 8'$ in declination between points of half-intensity. When allowance is made for the smoothing produced by the aerial beam these figures give the corresponding widths of the radio nebula as $1^{\circ} 5'$ (R.A.) \times $2^{\circ} 1'$ (Dec.). These figures have been checked by making some scans through the centre of the visible nebula at 237 Mc/s. At this higher frequency the confusion effects were considerably reduced and it was therefore possible to measure the widths of the source with more certainty. It was found that the apparent widths were $1^{\circ} 9'$ (R.A.) \times $2^{\circ} 5'$ (Dec.) which correspond to true widths of $1^{\circ} 4'$ \times $2^{\circ} 1'$. These figures are in excellent agreement with those at 158 Mc/s and will be taken as the true size of the nebula.

The measurements imply that the source is elliptical with an apparent axial ratio of about 0.66; although the ellipticity is small, direct comparison of individual records shows that it is real. The observations are not sufficiently accurate to give the orientation of the radio source, but show that the position angle must lie between 0° and 40° . This range includes the position angle of the visible nebula, which is 20° .

The integrated magnitude of M33 was estimated from the observed peak intensity and width of the radio source. It was found to be +7.8 at 158 Mc/s and +7.7 at 237 Mc/s. Assuming the distance to be 630 kpc the total emission from the nebula at 158 Mc/s is therefore 1.3×10^{20} w. (c/s) $^{-1}$ ster $^{-1}$.

5.2. *The corona of M33.*—The radio source associated with M33 is more extensive than the visible nebula and, by analogy with the Galaxy and M31, this suggests that in M33 the majority of the radio emission is also generated in an extensive corona which envelops the visible nebula. If it is assumed that the corona is an oblate spheroid orientated in the same manner as the visible nebula, then it follows from equation (2) that its true axial ratio is 0.45. Taking the distance of M33 as 630 kpc the total widths of the corona between half-emissivity points are 23 kpc (major axis) \times 11 kpc (minor axis).

The emissivity of the corona was estimated by assuming that, as in the case of M31, the emissivity follows a gaussian decrease with distance from the centre. The value of the emissivity at the centre of the corona was found to be 0.15×10^8 w. (c/s) $^{-1}$ ster $^{-1}$ pc $^{-3}$ at 158 Mc/s.

6. Comparison of M31 and M33

6.1. *Comparison of the radio and photographic magnitudes.*—The photographic and radio magnitudes (at 158 Mc/s) for the two nebulae are given in Table II.

TABLE II

Comparison of the radio and photographic magnitudes of M31 and M33

Object	Type	Photographic magnitude (18)	Radio magnitude	$m_r - m_p$
M31 (NGC 224)	Sb	+4.3	+5.8	+1.5
M33 (NGC 598)	Sc	+6.2	+7.8	+1.6

It can be seen from Table II that, if it is assumed that the distances of the two nebulae are the same, then the total radio emission from M31 is greater by two magnitudes than the total radio emission from M33. However, the ratio of the total radio emission to the total light emission ($m_r - m_p$) shows no significant difference although the two nebulae differ in type. This subject will be discussed more fully in Part II of this paper.

The measurements of M33 are not sufficiently accurate and cover too small a frequency range to decide if there is a significant difference between the spectral indices of the two nebulae.

6.2. *Comparison of the corona of M31 with the corona of M33.*—The results presented here show that in the case of both M31 and M33 the majority of the radio emission arises in an extensive corona which envelops the visible nebula. The relevant data on the two coronae are given in Table III. The widths quoted are the total widths between the 1 per cent contours.

TABLE III

The coronae of M31 and M33

Nebula	Size of corona	Axial ratio of corona	Emissivity at centre, w. (c/s) ⁻¹ ster ⁻¹ pc ⁻³ at 158 Mc/s
M31 (NGC 224)	10°·6 × 6°·1	0·57	0·12 × 10 ⁸
M33 (NGC 598)	5°·4 × 2°·4	0·45	0·15 × 10 ⁸

The maximum extension of the corona of M31 is about twice the maximum extension of M33. However, within the limits of experimental error, the axial ratios and the emissivities are equal.

The visual sizes of both M31 and M33 have been measured by Holmberg (18), who obtained a value for M31 of 197' along the major axis, and 83' for M33. These values may be compared in each case with the size of the major axis of the corona; the maximum extent of the corona of M31 is greater than the maximum extent of the visible nebula by a factor of 3·2 while the corresponding factor for M33 is 3·9. To compare the axial ratio of the corona with the axial ratio of the visible nebula it is first necessary to take into account the effects of inclination. Examination of several edge-on spirals (19) indicates that, neglecting the central bulge, the minor and major axes of Sb and Sc type spirals are in the ratio of about 1 : 12 and therefore they have an axial ratio of about 0·08 : 1. This is much smaller than the axial ratio of the corona of M31 and M33 given in Table III. However, although the distributions of the radio emission perpendicular to the planes of M31 and M33 are much broader than the distributions of light the ratio of the widths appears to be much the same for each nebula. It may, therefore, be concluded that the sizes of the coronae of M31 and M33 are approximately proportional to the sizes of the visible nebulae, the maximum extent of the coronae being about three times greater than the maximum extent of the visible nebulae.

7. *Comparison with the Galaxy.*—It has been shown by Mills (13) that about 90 per cent of the total radiation from the Galaxy arises in the corona and about 10 per cent in the disk component; this result is in agreement with the relative

proportions of the two components in M31. He also concluded that the corona of the Galaxy is spheroidal with a ratio of minor to major axis of 0.69 and that the central emissivity is $4.3 \times 10^8 \text{ w. (c/s)}^{-1} \text{ ster}^{-1} \text{ pc}^{-3}$ at a frequency of 85 Mc/s. In an earlier study of the corona of the Galaxy at 81.5 Mc/s, Baldwin (12) showed that the axial ratio was greater than 0.5, and he estimated the mean emissivity as $1.8 \times 10^8 \text{ w. (c/s)}^{-1} \text{ ster}^{-1} \text{ pc}^{-3}$ in good agreement with the results of Mills.

The axial ratio of the corona of the Galaxy therefore appears to be similar to the axial ratio of the corona of M31. The central emissivity of $4.3 \times 10^8 \text{ w. (c/s)}^{-1} \text{ ster}^{-1} \text{ pc}^{-3}$ at 85 Mc/s, which corresponds to an emissivity of about $2.3 \times 10^8 \text{ w. (c/s)}^{-1} \text{ ster}^{-1} \text{ pc}^{-3}$ at 158 Mc/s, is greater by a factor of about 16 than the corresponding emissivities of M31 and M33. As the total radio emission from the Galaxy appears to be comparable to the total emission from M31, it follows that the corona of the Galaxy is probably smaller than that of M31 by a factor of about 2.5 and that it is more nearly equal in size to the corona of M33. These conclusions are in reasonable agreement with the results of Baldwin (17); he found the emissivity of the corona of the Galaxy to be greater by a factor of 6 than that of M31, and his figures also show that the corona of the Galaxy is significantly smaller than that of M31.

8. *Acknowledgments.*—We thank Professor A. C. B. Lovell for making available the facilities for this investigation, and Dr H. P. Palmer for the use of his unpublished results on the Andromeda Nebula.

Jodrell Bank Experimental Station,
Macclesfield,
Cheshire :
 1959 *February.*

References

- (1) R. Hanbury Brown and C. Hazard, *M.N.*, **111**, 357, 1951.
- (2) R. Hanbury Brown and C. Hazard, *Phil. Mag.*, **43**, 137, 1952.
- (3) R. Hanbury Brown and C. Hazard, *Nature*, **172**, 853, 1953.
- (4) A. C. B. Lovell, *Nature*, **180**, 60, 1957.
- (5) W. Baade and R. Minkowski, *Ap. J.*, **119**, 215, 1954.
- (6) M. Ryle and D. D. Vonberg, *Proc. Roy. Soc. A*, **193**, 98, 1948.
- (7) D. Morris, H. P. Palmer and A. R. Thompson, *Observatory*, **77**, 103, 1957.
- (8) G. R. Whitfield, *M.N.*, **117**, 680, 1957.
- (9) G. de Vaucouleurs, *Ap. J.*, **128**, 465, 1958.
- (10) M. Ryle, F. G. Smith and B. Elsmore, *M.N.*, **110**, 503, 1950.
- (11) C. L. Seeger, G. Westerhout and R. G. Conway, *Ap. J.*, **126**, 585, 1957.
- (12) J. E. Baldwin, *M.N.*, **115**, 690, 1955.
- (13) B. Y. Mills, at the Paris Symposium on Radio Astronomy, 1958.
- (14) H. P. Palmer, private communication.
- (15) R. Hanbury Brown and C. Hazard, *Phil. Mag.*, **44**, 939, 1953.
- (16) E. Hubble, *Ap. J.*, **64**, 321, 1926.
- (17) J. E. Baldwin, Symposium No. 5 of the I.A.U., ed. N. Roman, p. 44, Cambridge, 1958.
- (18) E. Holmberg, *Medd. Lund. Obs. Ser. 2*, No. 136, 1957.
- (19) A. B. Wyse and N. U. Mayall, *Ap. J.*, **95**, 24, 1942.

THE RADIO EMISSION FROM NORMAL GALAXIES

II. A STUDY OF 20 SPIRALS AT 158 MC/S

R. Hanbury Brown and C. Hazard

(Received 1961 March 3)

Summary

A survey has been made of the radio emission at 158 Mc/s from twenty bright spiral galaxies. A radio index R has been defined by the equation $R = m_r - m_{pg}$, where m_r and m_{pg} are the radio and photographic magnitude respectively. The results indicate that R is a function of the inclination and galactic latitude of a galaxy and it is suggested that this effect is due to the absorption of light. The mean value of R for spirals of type Sb and Sc is $+1.3$ with an r.m.s. dispersion ± 0.7 . No significant difference was found between the mean values of R for the two types of galaxy.

1. *Introduction*

A survey of the radio emission from some bright normal* galaxies has been made at 158 Mc/s using the 250 ft steerable paraboloid at Jodrell Bank. The object of this survey was to establish the integrated radio magnitudes of these galaxies, and in particular to investigate how the ratio of the total light to the total radio flux varies among galaxies of the same type and also how it depends upon type. In Part I (1) we described the apparatus used in this survey and reported the results obtained on M31 and M33; the present paper (Part II) contains the results on twenty spiral galaxies of types Sb and Sc. The observations of other types of galaxy will be published in a further paper (Part III) together with a discussion of all the data.

2. *Method of observation*

A description of the apparatus was given in Part I together with the method of observation of M31 and M33. For the remainder of the galaxies the observations were carried out as follows. First, a preliminary survey was made in an effort to detect radio emission from a particular galaxy. In this survey two sets of scans were made through the expected position, one set of scans being made at constant right ascension and the other at constant declination; each scan was repeated several times as a check on its reliability. In some regions these scans sufficed to give the position and intensity of the radio source associated with the galaxy, and an example of such a region is illustrated in Fig. 1 which shows two scans made over NGC 253. In other more confused regions it was found necessary to survey a considerable area around the expected position as an aid to the interpretation of the observations.

* In this context a normal galaxy, following Baade and Minkowski (2), is taken to be a galaxy which appears to be normal when examined photographically.

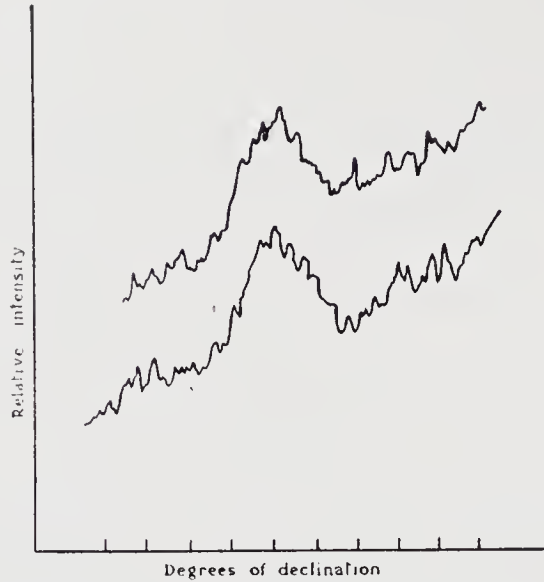


FIG. 1.—Two scans in declination across NGC 253. These scans were both made at a constant right ascension ($00^{\text{h}} 45^{\text{m}}.1$) with a beamwidth of 2° at 158 Mc/s (July, 1958).

Before each set of observations the equipment was calibrated on the source I.A.U. 14N5A and all the magnitudes in the present paper were measured relative to that source. The scale of radio magnitude (m_r) is defined by the equation

$$m_r = -53.45 - 2.5 \log S_{158} \quad (1)$$

where $S_{158} \text{ w. m}^{-2} (\text{c/s})^{-1}$ is the flux density of a source at 158 Mc/s. Following Part I we have taken the magnitude of 14N5A to be +6.86.

3. Results

Observations were made on the twenty galaxies listed in Table I. All these galaxies are brighter than $m_{pg} = 10.6$ on the scale of Holmberg (3) and were in convenient positions to be surveyed during the autumn of 1958 when this work was carried out.

The results are summarized in Table I, which gives the positions and apparent magnitudes of the radio sources; some detailed remarks on the individual galaxies are contained in the notes. In fifteen cases a radio source was found close to the position of the galaxy, and the measurements are sufficiently precise to allow an identification to be made. It is of course possible that some of the suggested identifications represent chance coincidences with discrete sources; but at 158 Mc/s there is about one source per 20 square degrees with an intensity above the limiting sensitivity of the present survey and it is therefore unlikely that more than two of the identifications suggested in Table I represent a chance coincidence. In the remaining five cases the isophotes of the region around the galaxies were too complicated to be interpreted unambiguously and a definite conclusion would require superior resolving power; in four of these cases there was evidence of a radio source close to the position of the galaxy but the position could not be established with satisfactory precision. When no radio source could be identified with a galaxy an upper limit to the radio emission was estimated from the records and this limit is given in Table I.

TABLE I
Radio data at 158 Mc/s

Galaxy	Position of visible nebula (1950)		Position of radio source (1950)		Observed magnitude $m_r(\theta)$	radio limits	Angular size of visible nebula $a \times b$	Estimated angular size of radio source $a' \times b'$	Integration correction† $\Delta m(\theta, a', b')$	Integrated radio magnitude m_r
	R.A. h m	Dec. ° ' "	R.A. h m	Dec. ° ' "						
224(M31)	00 40	+41 00	00 40.3	+40 44 ± 15'	+6.99	7.01 6.96	197' × 92'	246' × 156'	-1.29	+5.70
253*	00 45.1	-25 34	00 44.8	15	8.32	8.42 8.23	35 × 8	46 × 23	0.10	8.22
598(M33)	01 31.1	+30 24	01 31.8	+30 16 30	8.43	8.55 8.34	83 × 53	126 × 84	0.67	7.76
IC 342*	03 41.9	+67 57	03 42	+68 00 15	7.92	8.05 7.80	25 × 20	33 × 28	0.08	7.84
2403	07 32.0	+65 43	—	—	—	> 9.1	29 × 15	38 × 22	0.08	> 9.0
2683	08 49.6	+33 38	—	—	—	> 9.3	12.1 × 3.9	16 × 9	0.01	> 9.3
3031	09 51.5	+69 18	—	—	9.56	10.1 9.06	35 × 14.4	46 × 27	0.11	9.45
4236	12 14.3	+69 45	—	—	—	> 8.7	26 × 8.7	34 × 19	0.06	> 8.6
4244	12 15.0	+38 05	12 16.5	+38 15 30	9.34	9.63 9.05	18 × 2.9	23 × 12	0.03	9.31
4258	12 16.5	+47 35	12 16.8	+47 30 60	9.34	9.80 9.25	24 × 9.6	31 × 18	0.05	9.29
4490	12 28.3	+41 55	12 29	+41 38 20	9.49	9.69 9.32	8.9 × 4.7	12 × 7	0.01	9.48
4565	12 33.9	+26 16	12 34.5	+26 23 15	9.80	10.0 9.49	20 × 3.6	26 × 13	0.04	9.76
4631	12 39.8	+32 49	12 40.5	+32 58 15	9.49	9.80 9.25	19 × 4.4	25 × 13	0.03	9.46
4736	12 48.6	+41 23	12 45	+41 50 30	9.49	9.80 9.34	15 × 13.3	20 × 18	0.03	9.46
4826	12 54.3	+21 47	12 53	+21 43 15	9.34	9.46 9.22	12.3 × 8.3	16 × 12	0.02	9.32
5055	13 13.5	+42 17	—	—	—	> 9.6	16.0 × 10.1	21 × 15	0.03	> 9.6
5194	13 27.8	+47 27	13 28.3	+47 45 20	9.05	9.25 8.88	14.2 × 9.5	18 × 14	0.02	9.03
5236*	13 34.3	-29 37	13 35	-29 47 20	7.86	8.00 7.74	18 × 18	23 × 23	0.04	7.82
5457	14 01.4	+54 35	14 03	+54 00 30	9.51	9.82 9.21	28 × 28	36 × 36	0.11	9.40
6946	20 33.9	+59 58	20 32.8	+60 00 30	9.50	10.0 9.2	14.4 × 12.6	19 × 17	0.03	9.47

† The estimated angular size of the radio source is the total width between points of half-intensity.
 ‡ The integration correction is defined by equation (3) in the text.
 * Not included in Holmberg's list. Data from the revision of the Harvard Survey of Bright Galaxies by de Vaucouleurs (4).

Notes on Table I

NGC 224. See Part I for a detailed discussion.

NGC 253. The radio source is clearly defined. It has also been reported by Mills (9).

NGC 598. See Part I.

IC 342. Although the radio source lies on a steep gradient in both right ascension and declination it is clearly defined.

NGC 2403. This galaxy lies in a difficult region to interpret. On right ascension scans it lies in a sharp minimum of the background radiation and the radio source cannot be observed distinctly. The records indicate the presence of a source in the correct position. The declination scans are confused by nearby sources.

NGC 2683. Region complicated by nearby sources.

NGC 3031. The source lies in a region of enhanced emission extending about fifteen degrees in both declination and right ascension which contains a number of weak sources. Observations are confused by a weak source about half a degree to the north of the galaxy. This confusing source has been shown by Palmer (6) to have a diameter of about 2 minutes of arc. The source in the position of NGC 3031 appears to have a diameter greater than 40 minutes of arc and it seems reasonable to assume that this source may be identified with NGC 3031. Its intensity has been estimated by subtracting the calculated contribution of the small diameter source from the flux density observed, an allowance being made for the different positions of the sources in the beam; the intensities in each case were measured relative to the source I.A.U. 14N5A in order to avoid errors in calibration.

NGC 4236. This region is complicated by nearby sources.

NGC 4244. Declination scans show a clearly defined radio source close to the position of the galaxy which is situated on the edge of a localized region of enhanced intensity. The right ascension scans were of poor quality and it was not possible to measure an accurate right ascension. The identification is therefore rather uncertain.

NGC 4258. The radio source was well resolved on right ascension scans but the declination scans are too confused to permit the determination of an accurate declination.

NGC 4490. The radio source is well resolved in declination but the measurement of its right ascension is complicated by the region of enhanced intensity in which it lies.

NGC 4565. A well defined source on a moderately steep gradient in right ascension.

NGC 4631. A well defined radio source.

NGC 4736. The radio source is well resolved in declination but in right ascension the records are confused and it was therefore not possible to make accurate measurements of this coordinate. A provisional identification.

NGC 4826. Although near a minimum in the background radiation this is a clearly defined radio source.

NGC 5055. This region is complicated by nearby sources and gradients in background radiation. There appears to be a radio source at the correct declination but it is to the west of the visible nebula. However, the interpretation of the records is subject to considerable uncertainty and there is some evidence that the observed source is a double source, the two components having approximately the same declination but differing in right ascension. One of these components may be due to the galaxy.

NGC 5194. Although the observations are complicated by the position being near the centre of a region of enhanced intensity the radio source is well defined.

NGC 5236. This region is confused by a nearby source and a steep gradient, but the radio source in the position of the visible nebula can be clearly observed.

NGC 5457. This region is complicated by the presence of the intense source 14N5A. In the present survey the radio source associated with the galaxy and 14N5A are well resolved.

NGC 6946. This galaxy lies in a pronounced minimum of the background radiation which accounts for the uncertainty in the measured intensity.

4. *The integrated radio magnitude*

The radio magnitude $m_r(\theta)$, tabulated in Table I, was calculated from the observed peak deflection. It is therefore a function of the aerial beamwidth θ and the angular size of the source. The integrated radio magnitude m_r , which is also shown in Table I, is a measure of the total flux received from a source and is independent of beamwidth. It is obtained by integrating the flux over the disk of the source, and therefore corresponds to the magnitude which would be observed with a beamwidth large compared with the angular size of the source.

In the case of M31 and M33 the values of m_r were found by integrating the detailed isophotes of the region around each source as discussed in Part I. For the remaining sources in the table, which have a smaller angular size than the beam, the differences between the observed magnitudes $m_r(\theta)$ and the integrated magnitudes m_r are small, and we have calculated these differences by estimating the angular size of the radio sources as follows.

It was shown in Part I that in both M31 and M33 the majority of the radio emission arises in an extensive corona which envelopes the visible nebula and we have assumed that other galaxies of types Sb and Sc possess similar coronae. This assumption is supported by an examination of some records made with an interferometer at 158 Mc/s (6). These records cover the regions around NGC 3031, 4736 and 5194 and were made with baselines of 60λ and 330λ . They show that the majority of the radio emission from both NGC 4736 and 5194 arises in a source with a diameter of about $25'$, while in NGC 3031 the corresponding diameter exceeds $40'$. These diameters have been estimated on the assumption that the sources are circular disks with a gaussian radial variation of brightness. Although these results are approximate they indicate that for these three galaxies the ratios of optical to radio diameter are similar to those found for M31 and M33 and they support the assumption that all Sb and Sc galaxies have extensive coronae.

In order to estimate the angular sizes of the sources shown in Table I we have therefore assumed that every galaxy has a corona whose ellipticity and size relative to the visible nebula are similar to those found in M31 and M33. Following the results in Part I we have taken this corona to be ellipsoidal with an axial ratio of 0.5 and have assumed that the principal planes of the corona and the visible nebula coincide; the apparent angular size of the major axis of the corona between half intensity points has been taken as 1.3 times the maximum extent of the visible nebula as measured by Holmberg (3). On these assumptions the angular size of the radio source associated with any particular galaxy can be estimated from the angular size of the visible nebula. The major axis is simply proportional to the maximum extent of the nebula as stated in the previous paragraph, while the minor axis can be calculated from the inclination. The inclination may be calculated to a sufficient degree of accuracy on the assumption that the visible nebula is also spheroidal, from the equation

$$\sin^2 i = \frac{(b/a)^2 - p^2}{1 - p^2} \quad (2)$$

where i is the angle of inclination of the principal plane of the visible nebula to the line of sight, p is the axial ratio of the spheroid and b/a is the axial ratio of the nebula image. We have calculated the inclination of all the spirals in Table I assuming $p = 0.2$ (3); in cases where $(b/a) < 0.2$ we have taken the inclination to be zero. These values of inclination have been used to estimate the apparent

angular dimensions $a' \times b'$ of the radio sources, again by means of equation (2), taking $p = 0.5$ which is the value appropriate to the coronae.

The estimated angular dimensions of each radio source have been used to calculate the integration correction $\Delta m(\theta, b', a')$ which was applied to the observed magnitude $m_r(\theta)$ to find the integrated magnitude m_r . It was assumed in this calculation that the distribution of intensity across the elliptical disk of a radio source follows a gaussian variation along both axes, and that the aerial beam is circularly symmetrical with a gaussian profile. On these assumptions it is simple to show that

$$\Delta m(\theta, b', a') = m_r - m_r(\theta) = -2.5 \log [(1 + s^2)(1 + s^2 r^2)]^{1/2} \quad (3)$$

where s is the ratio of the width of the major axis of the radio source to the width of the beam, and r is the apparent axial ratio (b'/a') of the radio source.

The calculated values of $\Delta m(\theta, a', b')$ are given in Table I together with the corresponding integrated magnitudes m_r ; for M31 and M33 the integrated magnitudes are those measured directly from the isophotes (see Part I). The table shows that, with the exception of these two galaxies, the integration corrections are small and in most cases less than the probable errors in measurement. It is therefore unlikely that the values of m_r are significantly in error due to the finite angular size of the radio sources, serious errors could only be introduced if the ratio of the size of the corona to the visible nebula is much greater in some of the galaxies than in M31 and M33.

5. Comparison of the radio and photographic magnitudes

5.1. *Introductory remarks.*—Since we are concerned in the present work to establish the ratio of the *total* light to the *total* radio flux emitted by a galaxy it is convenient to define a measure of this ratio. By analogy with the concept of colour index we propose to define the *radio* index R of a galaxy as the difference between the integrated radio and photographic magnitudes. Thus

$$R = m_r - m_{pg} \quad (4)$$

where m_r and m_{pg} are the radio and photographic magnitudes respectively.

It is clear that the value of R , as observed for any particular galaxy, will depend upon the absorption of light and also of radio waves. In an effort to arrive at values of R which can be usefully compared, we have therefore corrected the observed results for the effects of absorption. We have assumed, following an earlier analysis (7), that for all directions of observation the radio absorption both in our Galaxy and in external galaxies is negligibly small, and we have also assumed that the radio emission from a galaxy is isotropic in direction. On the other hand the absorption of light cannot be neglected and may take place both in our Galaxy and in the galaxy under observation; these two cases will be considered in turn.

5.2. *The effect of the internal absorption of light in a galaxy on the radio index.*—The internal absorption of light in a spiral is mainly due to obscuring clouds concentrated in the plane of the galaxy and will therefore depend on its orientation with respect to the observer. This effect will cause the observed radio index to depend on the orientation of the galaxy, and hence there should be a correlation between the measured values of R and the apparent axial ratio b/a of the photographic image; if the radio absorption is negligible, as assumed above, then spirals seen edge-on should exhibit low values of R . We have analysed our results to test for this effect as follows.

First, we have restricted our analysis to galaxies in Holmberg's catalogue so that measurements of m_{pg} shall be homogeneous. Secondly, in order to avoid confusion with the effects of absorption in the Galaxy, we have further restricted the analysis to those galaxies which are more than 40° from the galactic plane; this excludes M31 and M33 and has the advantage that for all the galaxies included in the analysis the integration corrections are small and are therefore less likely to introduce error into the following discussion.

The ten galaxies which fulfil the necessary criteria are shown in Table II, and in Fig. 2 the radio index for these galaxies is plotted against the apparent axial ratio b/a of the associated visible nebulae. Although the scatter of the results in Fig. 2 is large, they indicate that the radio index decreases with b/a and hence depends upon the inclination of the visible nebula.

TABLE II

The effect of the internal absorption of light on the radio index of a spiral galaxy

Galaxy	Type (after Holmberg)	b/a	$R(i, \beta)$
NGC			
4244	Sc+	0.16	-1.2
4565	Sb+	0.18	-0.5
4631	Sc+	0.23	-0.3
4258	Sb+	0.40	+0.4
3031	Sb-	0.41	+1.6
4490	Sc+	0.53	-0.6
5194	Sc-	0.67	+0.2
4826	Sb-	0.67	+0.1
4736	Sb-	0.90	+0.6
5457	Sc-	1.00	+1.2

b/a is the apparent axial ratio of the visible nebula; $R(i, \beta)$ is the radio index ($m_r - m_{pg}$), where i and β represent the inclination and galactic latitude of the galaxy respectively.

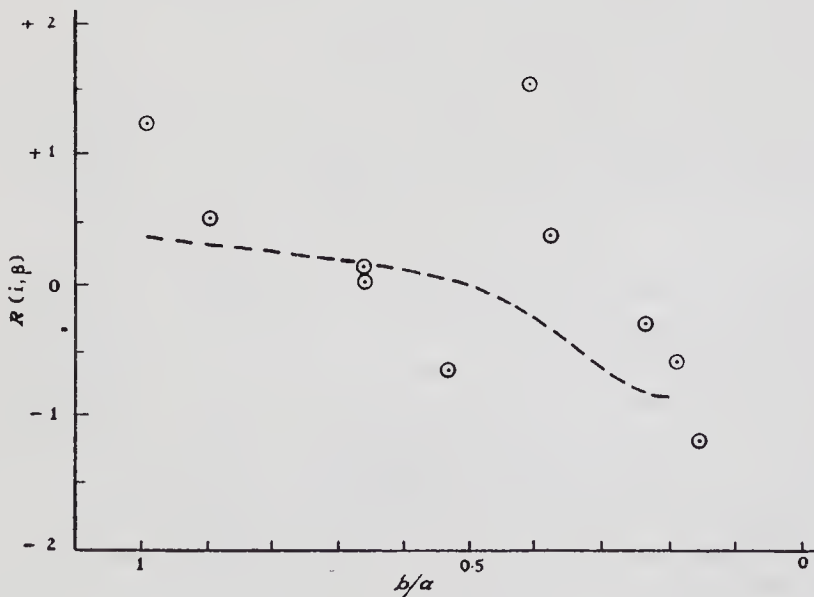


FIG. 2.—The relation between the inclination of a spiral and the radio index.
Ordinate: The radio index $R(i, \beta)$.
Abcissa: The apparent axial ratio b/a of the photographic image of the nebula.

These results may be compared with the measurements of the internal absorption in spirals made by Holmberg (3). He gives a plot of the total photographic absorption as a function of the apparent axial ratio for two groups of spirals, the first group comprises spirals of types Sc+ and Sc- and the second group comprises types Sb+, Sb- and Sa. His results for the two groups have been averaged and the variation of absorption with b/a is shown by the broken line in Fig. 2; the zero of this curve has been arbitrarily chosen to facilitate a comparison between the results. The radio observations are in reasonable agreement with the photographic measurements and this comparison therefore confirms the suggestion that the dependence of the radio index on b/a is due to the internal absorption of light. It is interesting to note that similar radio observations, if conducted on a sufficiently large number of galaxies, might provide a valuable technique for measuring the internal absorption of light.

In view of the agreement between the present observations and those of Holmberg, we have used his values to apply an *inclination correction* $\Delta m(i)$ to the observed values of the radio index in order to correct them all to a standard inclination of 90° . These values of $\Delta m(i)$ are shown in Table III and have been added to the observed radio index $R(i, \beta)$ to give the radio index $R(90, \beta)$ corrected to an inclination of 90° .

However, it should be pointed out that the observations of Holmberg show a considerable variation in the internal absorption between individual galaxies; the broken line in Fig. 2 being an average of measurements of a large number of objects. It is only for values of b/a less than about 0.4 that the mean value of the absorption becomes significantly greater than the dispersion between individual galaxies. The radio measurements show a similar effect, a significant change of radio index with b/a being apparent only for the three almost edge-on spirals. It follows that when dealing with individual galaxies it is only worthwhile to apply an inclination correction when the value is of b/a less than about 0.4. However, for less inclined galaxies the corrected values are of importance when considering the average radio index of a number of galaxies.

5.3. *The effect of the absorption of light in our Galaxy on the radio index.*—The effect of absorption of light in our Galaxy would be to decrease the observed radio indices at low galactic latitudes. Only two of the galaxies observed lie close to the galactic plane where this absorption is likely to be serious, namely IC 342 and NGC 6946. The average radio index of these galaxies, corrected to inclination 90° is -0.2 compared with the average for the remainder of $+0.9$, suggesting that the absorption at latitude 11° is about 1.1 magnitude.

The results therefore suggest that the radio index increases with galactic latitude although the data are obviously too scanty to establish the law of this variation. The correction for galactic absorption found by Hubble (8) gives the average increase of photographic absorption relative to the galactic pole as $0.25 (\operatorname{cosec} \beta - 1)$. Thus the absorption at latitude 11° should be 1.1 magnitude which is in agreement with the value deduced above from the radio data.

5.4. *The average radio index of a spiral galaxy.*—The radio index $R(90, 90)$ for galaxies with $m'_{pg} < 9.1$ is plotted in Fig. 3 against m'_{pg} , the photographic magnitude corrected for the absorption of light, where

$$m'_{pg} = m_{pg} - \Delta m(i) - \Delta m(\beta). \quad (5)$$

TABLE III
The radio index at 158 Mc/s

Galaxy	Type	Photographic magnitude	Axial ratio of visible nebula	Galactic latitude	Integrated radio magnitude	Inclination correction	Galactic latitude correction	Radio index uncorrected	Radio index corrected for inclination	Radio index corrected for inclination and to galactic pole
		m_{pg}	b/a	β	m_r	$\Delta m(i)$	$\Delta m(\beta)$	$R(i, \beta)$	$R(90, \beta)$	$R(90, 90)$
NGC 224 (M31)	Sb-	4.33	0.47	-21	5.70	0.60	0.4	+1.37	+1.97	+2.4
253	Sc	7.6†	0.22	-88	8.22	1.05	0	+0.62	+1.67	+1.7
598 (M33)	Sc+	6.19	0.64	-30	7.76	0.20	0.25	+1.57	+1.77	+2.0
IC 342	Sc	8.2†	0.80	+11	7.84	0.10	1.05	-0.36	-0.26	+0.8
2403	Sc+	8.80	0.52	+30	> 9.0	0.30	0.25	> +0.2	> +0.5	> +0.8
2683	Sb-	10.53	0.32	+40	> 9.3	1.20	0.10	> -1.23	> 0	> +0.1
3031	Sb-	7.85	0.41	+41	9.45	0.70	0.10	+1.60	+2.30	+2.4
4236	Sc+	10.05	0.34	+47	> 8.6	0.70	0.10	> -1.45	> -0.70	> -0.6
4244	Sc+	10.48	0.16	+78	9.31	1.05	0	-1.17	-0.12	-0.1
4258	Sb+	8.9	0.40	+69	9.29	0.80	0	+0.39	+1.19	+1.2
4490	Sc+	10.09	0.53	+73	9.48	0.30	0	-0.61	-0.31	-0.3
4565	Sb+	10.30	0.18	+87	9.76	1.35	0	-0.54	+0.81	+0.8
4631	Sc+	9.71	0.23	+84	9.46	1.0	0	-0.25	+0.75	+0.8
4736	Sb-	8.91	0.90	+76	9.46	0.05	0	+0.55	+0.60	+0.6
4826	Sb-	9.27	0.67	+83	9.32	0.20	0	+0.05	+0.25	+0.3
5055	Sb+	9.26	0.63	+74	> 9.6	0.30	0	> +0.34	> +0.64	> +0.6
5194	Sc-	8.88	0.67	+68	9.03	0.15	0	+0.15	+0.30	+0.3
5236	Sc	7.4†	1.00	+32	7.82	0	0.20	+0.42	+0.42	+0.6
5457	Sc-	8.20	1.00	+59	9.40	0	0.05	+1.20	+1.20	+1.2
6946	Sc-	9.67	0.88	+11	9.47	0.05	1.05	-0.20	-0.15	+0.9

* The corrected photographic magnitude m'_{pg} is the observed photographic magnitude corrected for internal absorption and absorption in the Galaxy, thus: $m'_{pg} = m_{pg} - \Delta m(i) - \Delta m(\beta)$.

† Not included in Holmberg's list. Data from the revision of the *Harvard Survey of Bright Galaxies* by de Vaucouleurs (4).

The distribution of results in Fig. 3 suggests that the two bright galaxies M31 and M33 have unusually high values of R . Since both these galaxies have low photographic magnitudes and comparatively large angular diameters it seems possible that this result may have been produced by some systematic error which is correlated with photographic magnitude. However a re-examination of the original measurements and the associated corrections with this possibility in mind failed to explain these high values of R , and we have therefore reached the conclusion that both these galaxies emit less radio flux in relation to their light than an average spiral.

Fig. 3 also suggests that galaxies with $m_{pg} > +8$ have low values of R . However for these fainter objects the distribution is seriously affected by observational selection introduced by the limited sensitivity of the radio equipment. To illustrate this latter effect the limits of detection have been shown in Fig. 3 as a broken line; any galaxy with an uncorrected radio index lying above this line could not be detected.

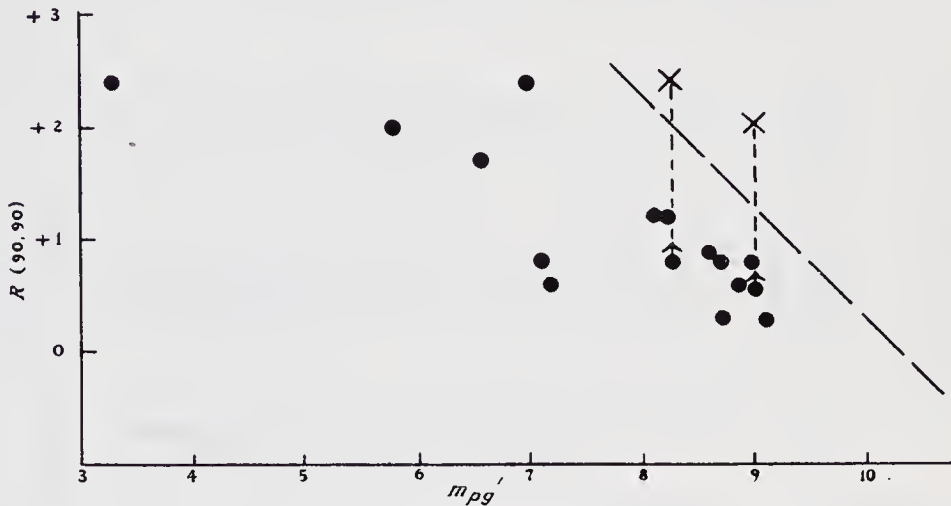


FIG. 3.—The relation between radio index and photographic magnitude for spirals. Ordinate: The radio index $R(90, 90)$ corrected to inclination 90° and to the galactic pole. Abscissa: The photographic magnitude m'_{pg} corrected for the internal absorption of light in the emitting galaxy and also in our Galaxy.

It follows from Fig. 3 that the average radio index for those galaxies which were detected is likely to be significantly lower than the true value for the whole group. In an attempt to overcome this difficulty we have made another survey of two of the galaxies (NGC 2403, 5055) with equipment of higher sensitivity and resolving power. In this survey, which was made at 240 Mc/s, the two galaxies were detected successfully and the resulting values of radio index are shown by the crosses in Fig. 3; it has been assumed in reducing these results to 158 Mc/s that the spectral index of both galaxies is equal to that of the reference source 14N5A. If the two measurements at 240 Mc/s are included, then the results are complete for all the sixteen galaxies with a corrected photographic magnitude ≤ 9.1 , and the following analysis of the average radio index refers only to this group.

The average radio index for all sixteen galaxies is $+1.3$ with an r.m.s. deviation of ± 0.8 . The probable error of measurement in the index for a single galaxy is about ± 0.2 ; this has been estimated from the errors in the radio magnitudes alone and the relatively small errors in the photographic magnitudes have been neglected. It is therefore likely that the observed r.m.s. deviation in the radio index is a true dispersion in the properties of spirals and is not due to errors of measurement.

As a check on the effect of the corrections which we have made for the absorption of light we have also calculated the average radio index for those galaxies in the group which have low inclinations ($b/a \geq 0.4$) and which are far from the galactic plane ($\beta \geq 30^\circ$). The mean value of the index for these galaxies is the same as that for the whole group. Thus we may conclude that at 158 Mc/s the radio index of type Sb and Sc spirals is $+1.3$ with an r.m.s. deviation of ± 0.8 .

If we now separate the spirals of type Sb and Sc the corresponding mean values of radio index are $+1.4$ and $+1.2$, and the associated r.m.s. deviations are ± 0.8 and ± 0.7 respectively. Since the probable error of measurement in each of these mean values is about ± 0.1 , it follows that the present survey shows no significant difference between the radio index of the two types; any difference which may exist must be considerably less than the dispersion in the index between individual galaxies of the same type.

It should be noted that, strictly speaking, this comparison refers only to the ratio of the radio to light flux *received* from the two types of galaxy, and does not take into account any difference in the internal absorption of light when received at an inclination of 90° . However, according to Holmberg (3), this difference is small (< 0.2 magnitude) and therefore the comparison may also be taken as valid for the ratio of radio to light flux *generated* in the two types of galaxy.

In an earlier analysis of the radiation from normal galaxies at 85 Mc/s, Mills (9) found values for Sb and Sc spirals of $+0.3(\pm 0.4)$ and $+1.6(\pm 0.2)$ respectively but concluded that "the difference between Sb and Sc galaxies is hardly significant". The results presented here are in agreement with his general conclusion, but do not show a difference of 1.3 magnitudes between the two types.

6. Conclusions

The results of the present survey indicate that at 158 Mc/s the observed radio index of a spiral galaxy of type Sb and Sc, which is a measure of the ratio of the received radio flux to light flux, is a function of the inclination of the visible nebula to the line of sight and of its galactic latitude; they also suggest that these effects are due to the internal absorption of light in spirals and in the Galaxy respectively. In any comparison of the total radio and light flux emitted by a galaxy, it is therefore necessary to take into account these absorption effects.

When corrected for the absorption of light the mean value of the radio index for spirals of type Sb and Sc is $+1.3$ with a dispersion of ± 0.8 magnitude. No significant difference was found between the two types and any difference which exists is less than the dispersion between individual galaxies of either type. It must be emphasized that these conclusions refer only to a frequency of 158 Mc/s and it is possible that the difference between the radio indices of the two types of galaxy may be a function of frequency.

7. *Acknowledgments*

We thank the Director of the Nuffield Radio Astronomy Laboratories for making available the facilities for this investigation and Dr H. P. Palmer for the use of his unpublished results.

*Nuffield Radio Astronomy Laboratories,
Jodrell Bank,
Macclesfield,
Cheshire:*

1961 March.

References

- (1) R. Hanbury Brown and C. Hazard, *M.N.*, **119**, 297, 1959.
- (2) W. Baade and R. Minkowski, *Ap. J.*, **119**, 215, 1954.
- (3) E. Holmberg, *Medd. Lund. Obs.*, Ser. 2, No. 136, 1957.
- (4) G. de Vaucouleurs, *A revision of the Harvard Survey of Bright Galaxies*, Australian National University Monograph, 1952.
- (5) D. O. Edge, P. A. G. Scheuer and J. R. Shakeshaft, *M.N.*, **118**, 183, 1958.
- (6) H. P. Palmer, private communication.
- (7) R. Hanbury Brown and C. Hazard, *Phil. Mag.*, **44**, 939, 1953.
- (8) E. Hubble, *Ap. J.*, **79**, 8, 1934.
- (9) B. Y. Mills, *Austr. J. Phys.*, **8**, 368, 1955.

THE RADIO EMISSION FROM NORMAL GALAXIES

III. OBSERVATIONS OF IRREGULAR AND EARLY-TYPE GALAXIES AT 158 MC/S AND A GENERAL DISCUSSION OF THE RESULTS

R. Hanbury Brown and C. Hazard

(Received 1961 August 31)*

Summary

A survey of the radio emission at 158 Mc/s has been made from twenty bright spiral, four irregular and four early-type galaxies. This paper reports the measurements of the irregular and early-type galaxies; the results obtained from the spirals were given in the two previous parts. The variation of the radio index R with type of galaxy is discussed; R is defined by the equation $R = m_r - m_{pg}$ where m_r and m_{pg} are the radio and photographic magnitude respectively. It is shown that the value of R for irregular galaxies is significantly greater than that for Sb and Sc spirals, and that this is probably also true of early-type galaxies.

1. *Introduction*

The present paper completes an account of a survey of bright *normal* galaxies which was carried out in 1958 with the 250 ft steerable paraboloid at Jodrell Bank working at 158 Mc/s. A *normal* galaxy, following Baade and Minkowski (1), is taken to be a normal member of the population of galaxies observed photographically. In Paper I (2) we described the apparatus and also the results obtained on M31 and M33; in Paper II (3) we reported measurements on twenty spirals of type Sb and Sc. In the present paper (III) we report some observations of a few irregular and early-type galaxies; we also discuss how the radio emission from a *normal* galaxy depends upon type.

2. *Observations*

An attempt was made to observe the radio emission at 158 Mc/s from four irregular galaxies of magellanic type and four early-type galaxies. A radio source was observed close to the position of IC 1613; the regions of sky near the other galaxies were complicated by the proximity of other sources and irregularities in the general background radiation and it was possible only to set an upper limit to their emission. The results are shown in Table I. We have tabulated m_{pg} , the photographic magnitude according to Holmberg (4) or de Vaucouleurs (5), m_r , the observed integrated radio magnitude at 158 Mc/s, and R the radio index, where $R = m_r - m_{pg}$. We have not corrected the values of R , as discussed in Paper II, for the absorption of light; an estimate of these corrections shows that they are less than 0.5 mag. and for the purposes of the present paper they can be neglected.

* Received in original form 1961 July 10.

TABLE I

Observations at 158 Mc/s of irregular and early-type galaxies

Galaxy NGC	Type	m_{20}	m_r	$R = m_r - m_{20}$
4449	Ir1	9.9	≥ 10.6	$\geq +0.7$
4214	Ir1	10.1	≥ 11.0	$\geq +0.9$
6822	Ir1	9.2	≥ 10.7	$\geq +1.5$
IC 1613	I	8.9*	9.1	+0.2
4594	Sa	9.2	≥ 10.6	$\geq +1.4$
3368	Sa	10.1	≥ 10.4	$\geq +0.3$
4472	E	9.3	≥ 10.2	$\geq +0.9$
1023	SO	10.5	≥ 9.8	≥ -0.7

* The optical data for this galaxy has been taken from de Vaucouleurs (5).

3. The radio index of different types of galaxy

3.1. *The radio index of Sb and Sc spirals.*—It was shown in Paper II that the average radio index of Sb and Sc spirals is +1.4 and +1.2 respectively, the associated r.m.s. deviations about these mean values being ± 0.8 and ± 0.7 . These conclusions were based on measurements of sixteen galaxies selected from a survey of twenty bright spirals.

3.2. *The radio index of early-type galaxies.*—In view of the scarcity of observational data we shall assume that types E, SQ and Sa all have the same average radio index and consider these three types as a single group.

Table II is a list of all the early-type galaxies which have been surveyed individually for radio emission. For the purpose of comparison the measurements at different frequencies have been scaled to 158 Mc/s on the assumption that the spectral index is -0.6 since this was the median value found by Harris and Roberts (10) for all sources in their survey. If also, following Harris and Roberts, we assume that the dispersion about this mean spectral index is such that 50 per cent of the sources have values in the range -0.4 to -0.8 , then we can calculate the associated uncertainty in scaling the values in Table II; the greatest uncertainty, which arises in scaling the 1400 Mc/s results, is about ± 0.5 mag. and is not significant in the present discussion.

The table shows that, out of a total of eighteen galaxies, in only one case (NGC 4526) was a radio source observed; the remainder were below the limit of detection and may therefore have any value of radio index greater than that shown in Table II. The results cannot, therefore, be used to derive a mean radio index, but they can be used to estimate a lower limit if we assume a value for the dispersion about the mean. Thus if we assume that individual early-type galaxies have radio indices which are distributed about the mean with a similar dispersion to that observed for Sb and Sc spirals (± 0.7 mag.), then the probability of occurrence of the distribution of limits given in Table II can be calculated for different values of the mean. This calculation shows that there is roughly a 50 per cent probability that the observed distribution would arise by chance if the mean index is as low as +2.5, and only a 10 per cent probability, if the mean value is +2.0. Thus, given the assumed dispersion, it is probable that the mean radio index of early-type galaxies is greater than +2.0 and is therefore greater than that (+1.3) of Sb and Sc spirals.

TABLE II
Observations of single early-type galaxies

Galaxy	Type	m_{pg}	$m_r(158 \text{ Mc/s})$	$R(158 \text{ Mc/s})$
NGC				
185	E	10.3	> 11.0 (H)	> +0.7
205	E	8.9	> 10.2 (L)	> +1.3
1023	SO	10.5	> 9.8 (BH)	> -0.7
1052	E	11.7	> 11.0 (H)	> -0.7
1291*	SBO	9.4	> 11.1 (M)	> +1.7
3115*	E	10.2	> 11.3 (M)	> +1.1
3368	Sa	10.1	> 10.4 (BH)	> +0.3
3379*	E	10.3	> 10.8 (Le)	> +0.5
3623	Sa	10.2	> 10.8 (Le)	> +0.6
4278	E	11.2	> 11.0 (H)	> -0.2
4382	SO	10.1	> 10.0 (Le)	> -0.1
4472	E	9.3	> 10.2 (BH)	> +0.9
4494*	E	10.8	> 10.1 (Le)	> -0.7
4526*	Sa	10.5	10.0 (Le)	-0.5
4594	Sa	9.2	> 11.2 (M)	> +2.0
4636*	E	10.0	> 10.3 (Le)	> +0.3
4649*	E	9.9	> 10.3 (Le)	> +0.3
5866*	SO	11.1	> 11.0 (H)	> -0.1

H D. S. Heeschen (6) at 1400 Mc/s.

L M. I. Large (7) at 408 Mc/s.

BH Present survey at 158 Mc/s.

M B. Y. Mills (8) at 85 Mc/s.

Le P. R. R. Leslie (9) at 178 Mc/s.

* Optical data according to de Vaucouleurs (5); the data for the other galaxies was taken from Holmberg (4).

3.3. *The radio index of irregular galaxies.*—Table III is a list of the available observations of irregular galaxies. The measurements have been adjusted to 158 Mc/s on the assumption that the spectral index of the sources is -0.6 . All the galaxies in the list contain a substantial proportion of Population I; in the classification of Holmberg they appear as type Ir1, and in the system of de Vaucouleurs they are referred to as Magellanic. One galaxy, IC 1613, appears to have a radio emission which is markedly different from the others. We have therefore surveyed this galaxy also at 240 Mc/s and have confirmed the presence

TABLE III
Observations of single magellanic irregular galaxies.

Galaxy	m_{pg}	$m_r(158 \text{ Mc/s})$	$R(158 \text{ Mc/s})$
LMC	0.6	3.3 (M)	+2.7
SMC	2.5	5.4 (M)	+2.9
NGC 55	7.8	10.8 (M)	+3.0
NGC 4449	9.9	≥ 10.6 (BH)	$\geq +0.7$
NGC 4214	10.1	≥ 11.0 (BH)	$\geq +0.9$
NGC 6822	9.2	≥ 10.7 (BH)	$\geq +1.5$
IC 1613	8.9	9.1 (BH)	+0.2

M B. Y. Mills (8) at 85 Mc/s.

BH The present survey at 158 Mc/s.

of a source close to the optical position; however, the value of radio index measured at 240 Mc/s was +1.3 which differs considerably from the value of +0.2 obtained at 158 Mc/s. This discrepancy suggests that the observations are affected by confusion with other sources and that the association of this radio source with IC 1613 must be regarded as doubtful, although the possibility cannot be excluded that IC 1613 is an excited or *radio* galaxy.

If we exclude the result on IC 1613, then the data in Table III indicate that the average radio index of magellanic galaxies is certainly greater than that of spirals; the measurements on NGC 55 and the Magellanic Clouds suggest that it has a value of about +3.0

3.4. *Summary.*—Fig. 1 summarizes the results of the previous sections. It shows that the ratio of total radio emission to the total light, as measured by the radio index is greatest for Sb and Sc spirals and decreases significantly for irregular galaxies. It also seems likely that it decreases for early-type galaxies, although this conclusion cannot be established by the data. These results confirm the conclusions reached by Mills (11) from earlier surveys.

There appears to be no simple correlation between the radio index of normal galaxies and their mass, linear size or colour index. However, the results in Fig. 1 suggest one particular conclusion. It appears that the ratio of coronal to disk radiation in an irregular galaxy is much less than that found in an Sb or Sc spiral. The absence of a corona around irregular galaxies is suggested by an examination of the radio isophotes of the Magellanic Cloud (8), but their large angular size and proximity to our own Galaxy makes this conclusion somewhat uncertain. However, if we assume that NGC 55 and the other four irregulars in Table I are similar to the Magellanic Clouds, then all the measurements taken together show that irregulars do not have extensive and powerful radio coronae

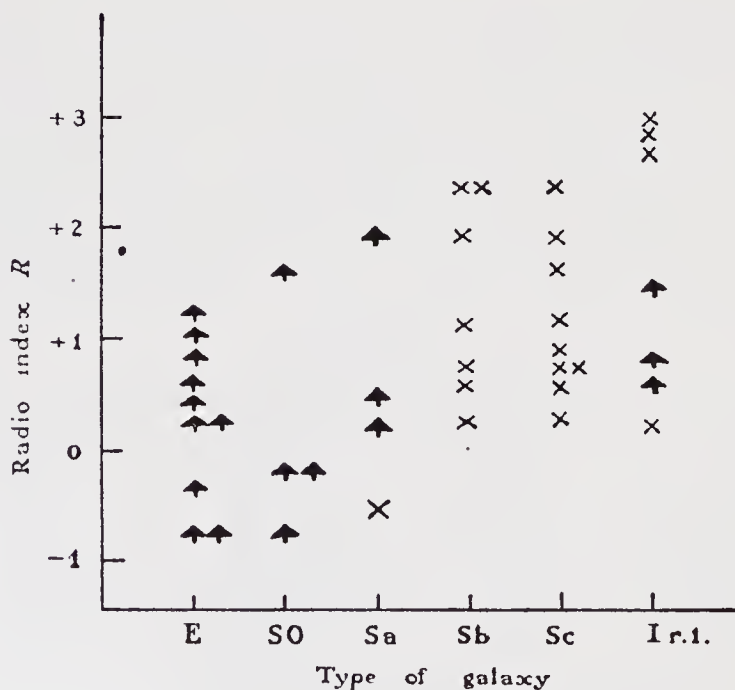


FIG. 1.—The radio index of different types of galaxy.

similar to those found in Sb and Sc spirals, otherwise we would expect their radio indices to be much lower than the radio indices of the Clouds. It follows that any corona which may exist in an irregular must emit less than the main body of the nebula.

The above conclusion is supported by a comparison of the emission from the disk of a spiral and from the body of an irregular. Thus the radio index of an average Sb or Sc spiral, if we exclude about 90 per cent of the emission which is due to the corona, probably lies between +3 and +4 and is therefore comparable with the value of +3 shown in Fig. 1 for irregulars. This suggests that the radio emissivity of the disk of a late-type spiral is comparable with that of the body of an irregular galaxy and that the emission processes are similar in the two cases.

The present limits to the radio index of early-type galaxies do not permit any positive conclusions to be drawn about their radio emission; nevertheless it appears likely that they are relatively weak radio emitters in comparison with Sb and Sc spirals.

4. *Acknowledgments.*—We thank the Director of the Nuffield Radio Astronomy Laboratories for making available the facilities for this investigation.

*Nuffield Radio Astronomy Laboratories,
Jodrell Bank,
Macclesfield, Cheshire:
1961 July.*

*School of Physics,
University of Sydney,
New South Wales,
Australia.*

References

- (1) Baade, W., and Minkowski, R., *Ap. J.*, **119**, 215, 1954.
- (2) Brown, R. Hanbury and Hazard, C., *M.N.*, **119**, 297, 1959.
- (3) Brown, R. Hanbury and Hazard, C., *M.N.*, **122**, 479, 1961.
- (4) Holmberg, E., *Medd. Lund. Obs.*, Ser. 2, No. 136, 1957.
- (5) de Vaucouleurs, G., *A revision of the Harvard Survey of Bright Galaxies*. Australian National University Mimeograph, 1952/53.
- (6) Heeschen, D. S., *P.A.S.P.*, **72**, 368, 1960.
- (7) Large, M. I., Matthewson, D. S., and Haslam, C. G. T., *Nature*, **183**, 1250, 1959.
- (8) Mills, B. Y., *Handbuch der Physik*, Vol. 53, p. 237, Springer-Verlag, Berlin, 1959.
- (9) Leslie, P. R. R., *Observatory*, **80**, 216, 1960.
- (10) Harris, D. E., and Roberts, J. A., *P.A.S.P.*, **72**, 237, 1960.
- (11) Mills, B. Y., *Aust. J. Phys.*, **8**, 368, 1955.
- (12) Mills, B. Y., *Aust. J. Phys.*, **13**, 550, 1960.

A Radio Survey of the Great Loop in Cygnus

DURING the past few years, intense radio sources have been identified with galactic nebulosities in Taurus¹ (the Crab Nebula), Cassiopeia², Puppis³, Gemini⁴ (*I.C.443*) and Auriga⁵. One of these five objects (*I.C.443*) bears a marked resemblance to the Great Loop in Cygnus, and it has been suggested⁴ that the latter may also be a radio source. The Loop comprises the well-known Network nebulae *N.G.C. 6960* and *N.G.C.6992-5*, together with several other patches of nebulosity. A rough sketch of the brighter parts of the system is shown in Fig. 1.

A radio survey of the Loop has been made with the 218-ft. fixed paraboloid at Jodrell Bank, operating at 92.5 Mc./s. At this frequency the paraboloid has a beam-width of about 3° between points of half-power. The results of the survey disclosed the existence of a radio source with the co-ordinates and intensity given in Table 1.

Table 1. DATA ON RADIO SOURCE (EPOCH 1950)

Right ascension	20h. 49m. 30s. ± 1m. 30s.
Declination	N. 29° 50' ± 1°
Intensity	220 ± 100 × 10 ⁻²⁶ watts m. ⁻² (c./s.) ⁻¹ at 92.5 Mc./s.

The zenith angle of the source is about 23° at Jodrell Bank and it lies at the edge of the field of view of the large paraboloid. At these large zenith angles the elevation and shape of the beam are uncertain, and hence there may be considerable errors in the observed values of declination and intensity. However, in the present case it was possible to check the calibration of the aerial by observing a reference source of known position and intensity (private communication from M. Ryle) at approximately the same declination (N. 29° 32.5') as the Loop. As a result of this check, the limits of error shown in Table 1 were established.

An examination of the records suggests that the angular diameter of the source lies in the range 3-6°. Furthermore, this suggestion is strengthened by the fact that the source has not been reported in previous surveys made with interferometers of comparatively high resolving power.

The estimated limits of the position of the centre of the radio source have been plotted in Fig. 1, and it can be seen that it lies close to the Loop. If the nebulosities form part of a roughly spherical object, as photographs of the region indicate, then the

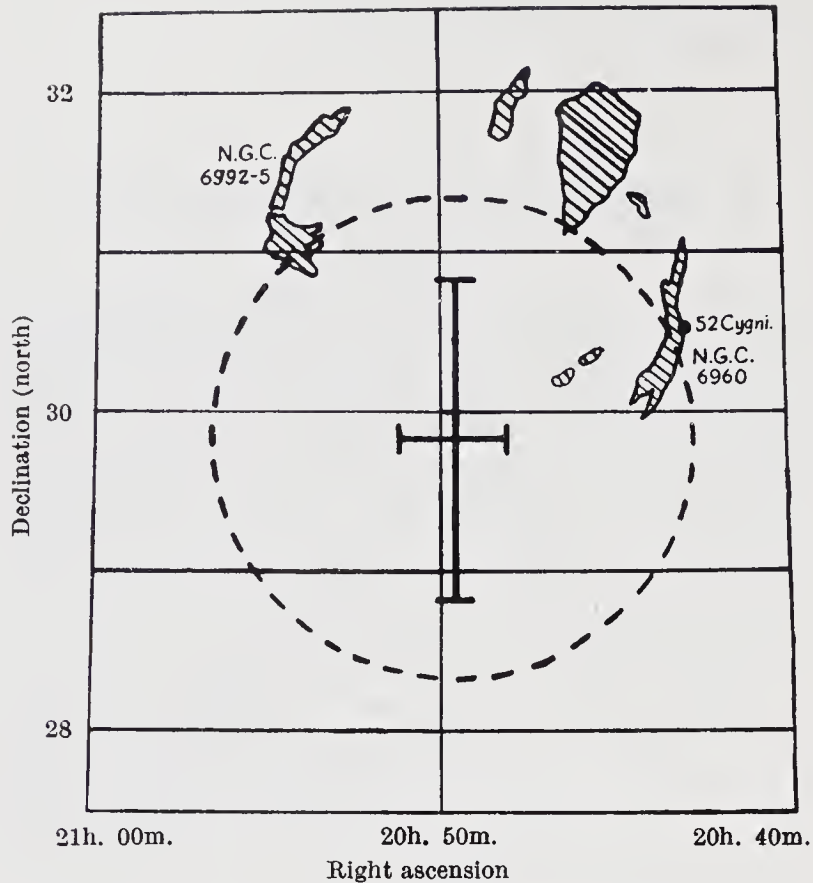


Fig. 1. A sketch of the more prominent nebulosities forming the Great Loop in Cygnus. The position and estimated limits of the centre of the radio source are shown by the cross (full line). The minimum angular diameter of the source is indicated by the circle (broken line)

position of the radio source probably lies within the outline of this object and towards the lower edge. The angular size of the source has been shown by a circle of diameter 3° and, since this is the minimum value given above, it is clear from the sketch that the angular size of the source is at least as great as that of the Loop.

On the basis of the evidence presented above, it is reasonable to conclude, but only tentatively, that the Loop in Cygnus is associated with the radio source. A more positive identification must await improved values for the declination and angular diameter of the source, and these can only be obtained from some other large instrument with a more favourable field of view.

The presence of this source close to the Loop is of considerable interest and indicates that this object may belong to the class of galactic nebulosities which are radio sources. It also supports the suggestion that the Loop is similar to *I.C.443* in Gemini, and it is interesting to note that the intensity of the source given in Table 1 is comparable with that observed⁴ from *I.C.443* (425×10^{-26} watts m.^{-2} (c./s.)¹)

at 3.7 m.). Finally, a radio source in association with the Loop might provide an unrivalled opportunity for studying in detail the correlation between the radio emission and the visible structure of a nebulosity.

We thank Prof. A. C. B. Lovell for his interest in this investigation, and Prof. Z. Kopal for directing our attention to the problem in the course of a lecture given in 1953. One of us (D. W.) is indebted to the Department of Scientific and Industrial Research for a maintenance grant.

D. WALSH
R. HANBURY BROWN

Jodrell Bank Experimental Station,
Lower Withington,
Cheshire.
March 16.

- ¹ Bolton, J. G., Stanley, G. J., and Slee, O. B., *Nature*, 164, 101 (1949).
² Ryle, M., and Smith, F. G., *Nature*, 162, 462 (1948).
³ Baade, W., and Minkowski, R., *Astrophys. J.*, 119, 206 (1954).
⁴ Baldwin, J. E., and Dewhirst, D. W., *Nature*, 173, 164 (1954).
⁵ Hanbury Brown, R., Palmer, H. P., and Thompson, A. R., *Nature*, 173, 945 (1954).

THE REMNANTS OF SUPERNOVAE AS RADIO SOURCES IN THE GALAXY

By R. Hanbury Brown

The origin of the majority of discrete radio sources, or so-called radio stars, remains unexplained and the suggestion has been repeatedly advanced that the sources are associated with some unknown type of object in the Galaxy. Before accepting this suggestion it is important to examine whether the observations can possibly be explained in terms of types of object which have already been identified as radio sources. At the present time the only discrete sources known to be members of the Galaxy are the intense sources of Class I¹ which show a marked concentration into the galactic plane. During the past few years a number of these sources have been identified with peculiar nebulosities^{2, 3, 4, 5, 6} which exhibit filamentary structure and high internal velocities; a list of these objects is shown in Table I. This list, together with the whole of the subsequent discussion, is restricted to sources which have been observed at metre wave-lengths.

The data in Table I show that, in the metre-wave domain, the only recognized type of object in the Galaxy with which a radio source is known to be associated is the remnant of the supernova of A.D. 1054 (the Crab Nebula). This identification suggests that radio sources may be associated with the remnants of other supernovae and it is supported by the discovery of a radio source in the position of the supernova of A.D. 1572⁷. An attempt has therefore been made in the present paper to explore the properties of the radio sources associated with old supernovae and to compare them with the available observational data. Since these data are extremely limited much of the following discussion must necessarily be speculative.

It has been shown⁸ that, at metre-wavelengths, the thermal radiation from the Crab Nebula is negligibly small in comparison with its total emission, and therefore the majority of its radio energy must be generated

by some non-thermal process. It will be assumed in the following discussion that the remnants of all supernovae are radio sources and that, at metre-wavelengths, their radio emission is produced by the non-thermal conversion of the kinetic energy of their expanding shells into radio energy. Furthermore it is assumed that the non-thermal process is excited by the collision of the expanding shell with the interstellar gas,

TABLE I
Galactic objects identified with radio sources

Galactic latitude	Intensity $\text{watts m}^{-2}(\text{c/s})^{-1} \times 10^{-26}$	Apparent angular diameter of radio source	P_R^* $\text{ergs sec}^{-1} \times 10^{32}$	Description of Object
- 4	1900†	$3.5' \times 5.5'$	4.3	Crab Nebula in Taurus, relic of supernova of A.D. 1054.
- 2.0	17000†	$4' \times 5'$	38.2	A peculiar nebulosity in Cassiopeia.
- 2.5	3500†	$\sim 1\frac{1}{2}^\circ$	7.9	A peculiar nebulosity in Puppis.
+ 3.8	100‡	$1^\circ.4$	0.2	A faint nebulosity in Auriga.
+ 4	400†	$50'$	0.9	A peculiar nebulosity (I.C. 443) in Gemini.

* P_R is the total radio power emitted in ergs. sec^{-1} , assuming that the object is at a distance of 1000 ps. and that the energy is radiated over an equivalent bandwidth of 200 Mc/s.

† Intensity at about 100 Mc/s.

‡ Intensity at 160 Mc/s.

and that the rate at which radio energy is produced is proportional to the rate at which the kinetic energy of the shell is exchanged in the collision.

Following Oort⁹ and Öpik,¹⁰ it will be assumed that the expanding shell sweeps up the interstellar gas and that, for a simple model, the equations of motion may be written

$$M/M_0 = V_0/V = 1 + \frac{4}{3}\pi\rho R^3 \quad (1)$$

$$t = \left[1 + \frac{\pi}{3M_0}\rho R^3 \right] \frac{R}{V_0} \quad (2)$$

where M_0 , V_0 are the initial mass and velocity of the shell; M , V , R are the total mass, velocity and radius of the shell after a time t ; ρ is the density of the interstellar gas.

The rate at which kinetic energy is exchanged between the expanding shell and the interstellar gas is

$$2\pi R^2 \rho V^3 \tag{3}$$

and the total radio power (P_R) is therefore given by

$$P_R = 2\pi R^2 \rho V^3 \eta \tag{4}$$

where η is the fraction of the kinetic energy which appears as radio emission.

In the absence of a detailed theory of the non-thermal process the value of the efficiency (η) is unknown. It seems probable that in at least three well-known cases the kinetic energy of a rapidly moving gas is being converted into radio energy by a non-thermal process, namely in the

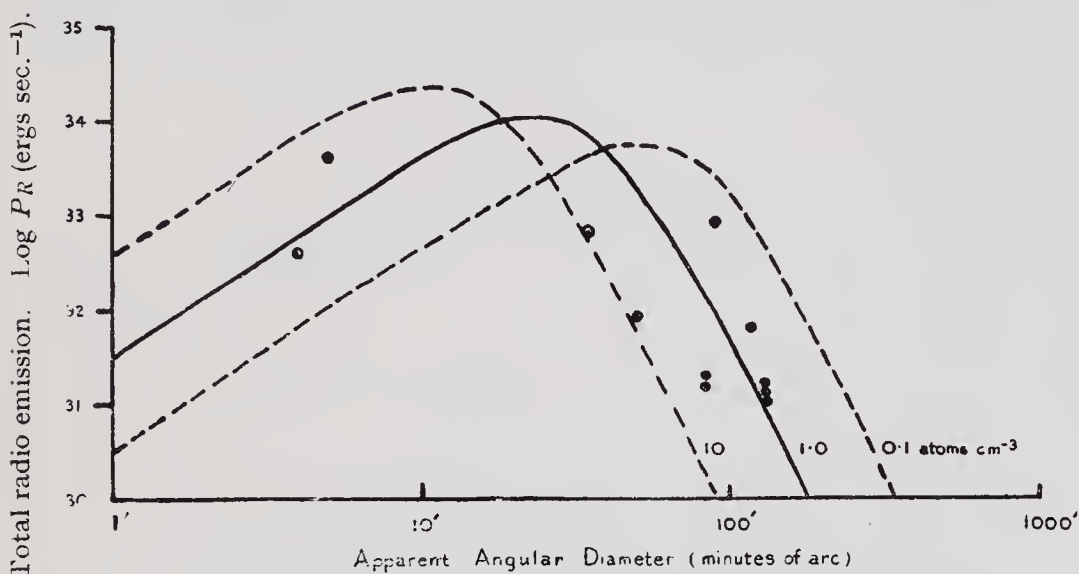


FIG. 1. THE CALCULATED RELATIONSHIP BETWEEN THE APPARENT ANGULAR DIAMETER AND THE TOTAL RADIO EMISSION OF THE SOURCES ASSOCIATED WITH THE REMNANTS OF SUPERNOVAE.

The values in eqn. (4) have been taken as: $M_0 = 15 M_{\odot}$'s, $V_0 = 1000$ kms. sec.⁻¹, $\rho = 0.1, 1.0$ and 10 atoms cm.⁻³, $\eta = 2 \times 10^{-5}$. The distance of the sources has been taken as 1000 pcs. The points represent the observed data as shown in Table II.

Crab Nebula, in the collision of two spiral galaxies in Cygnus² and in the passage of ejected material through the Sun's corona. On the assumption that in each of these cases the radio energy is produced by the collision of gas, the minimum value of η may be estimated very roughly and it can be shown that it must exceed about 10^{-5} . It has been assumed in deriving this value that the radio flux is distributed over an equivalent bandwidth of 200 Mc/s with an average value equal to that observed at 100 Mc/s.

On the assumption that $\eta = 2 \times 10^{-5}$ equations (1), (2) and (4) have been used to calculate the relationship between the angular diameter of the sources and their radio emission and the results are shown in Fig. 1. It has been assumed that the initial mass and velocity of the supernova shell are $15 M_{\odot}$'s, and 1000 kms. sec.⁻¹, and that the density of the inter-

stellar gas is 0.1, 1.0 and 10 atoms cm^{-3} . The apparent angular diameter of the radio sources has been calculated on the assumption that their distance is 1000 pcs.

The variation with time of the radiation from a source has also been calculated on the same assumptions and the results are shown in Fig. 2. An interesting feature of these curves is that the emission increases rapidly after the explosion and reaches a maximum after a time determined by the initial mass and velocity of the shell and by the density of the interstellar gas; after this maximum the emission decreases comparatively slowly. This property of the model is, of course, a consequence of the assumption that the radio energy is produced in an expanding shell and that the efficiency of the process is independent of the velocity and density of the gas.

An obvious weakness of the model is that it assumes that the non-thermal generation of radio energy takes place at velocities of collision which are very low compared with that observed in the Crab Nebula.

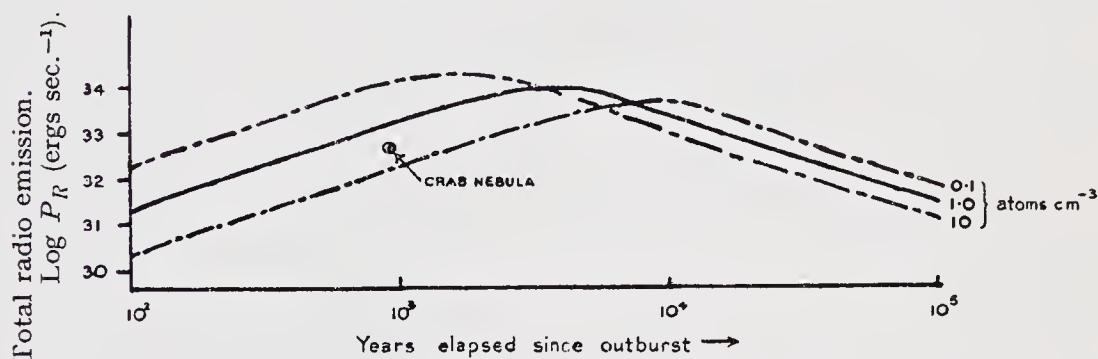


FIG. 2. THE CALCULATED VARIATION WITH TIME OF THE RADIO EMISSION FROM THE REMNANTS OF SUPERNOVAE.

The values assumed in the calculation are the same as those for Fig. 1. The point representing the Crab Nebula is plotted on the assumption that it is at 1000 pcs.

For example after about 10^5 years the velocity will have decreased to about 50 kms. sec^{-1} and it seems unlikely that the efficiency of any non-thermal process will be maintained at such a low velocity. This objection is not necessarily serious since the majority of the radio energy is generated at velocities of several hundred kilometres per second. Thus it can be shown that Figs. 1 and 2, and the discussion presented later, would not be materially altered by assuming that the efficiency of the non-thermal process decreases rapidly to zero at velocities below about 100 kms. sec^{-1} . A further weakness of the model is that the thermal radiation from the shell has been neglected. Although this may be permissible for the Crab Nebula, it is not justified for much older objects. For example, it can be shown that for shells exceeding about 10^5 years in age the thermal component of the radiation is probably significant.

If the model presented above is roughly correct, then it should be possible to observe a population of discrete sources associated with the remnants of supernovae in the Galaxy. The properties of these sources will now be compared with the observed data on the Class I sources. Table II shows a list of sources which have been observed within $\pm 5^\circ$ of

the galactic plane and of which the apparent angular diameter and intensity have been measured. The total power (P_R) radiated by each source is shown and has been calculated from the observed intensity assuming that the energy is distributed uniformly over an equivalent bandwidth of 200 Mc/s. The angular dispersion of these sources about the

TABLE II
Class I radio sources of known diameter

<i>Galactic latitude</i>	<i>Apparent angular diameter</i>	<i>Intensity</i> $\text{watts m}^{-2}(\text{c/s})^{-1}$ $\times 10^{-26}$	$P_R \dagger$ $\text{ergs sec.}^{-1} \times 10^{32}$	<i>Photographic Identification</i>
- 4	3.5' \times 5.5'	1900*	4.3	Crab Nebula
- 2.0	4' \times 5'	17000*	38	Nebulosity in Cassiopeia.
- 2.5	$\sim 1\frac{1}{2}^\circ$	3500*	7.9	Nebulosity in Puppis.
+ 4	50'	400*	0.9	Nebulosity in Gemini.
+ 3.8	1.4°	100*	0.2	Nebulosity in Auriga.
+ 4	35'	3000*	6.7	Unidentified.
+ 2.1	$> 1^\circ.5 < 3^\circ$	80‡	0.18	Unidentified.
- 0.3	$> 1^\circ.5 < 3^\circ$	60‡	0.13	Unidentified.
- 1.5	$> 1^\circ.5 < 3^\circ$	50‡	0.11	Unidentified.
+ 0.8	$\sim 2^\circ$	300‡	0.67	Cygnus X. Identified with traces of filamentary nebulosity.
+ 4.1	1.5°	200‡	0.45	Unidentified.

* Intensity at 100 Mc/s.

† P_R is the total radio power emitted in $\text{ergs sec.}^{-1} \times 10^{32}$, assuming that the object is at a distance of 1000 pcs. and that the energy is radiated over a band of 200 Mc/s.

‡ Intensity at 160 Mc/s.

galactic plane indicates that they are at great distances from the Sun and, as suggested in a previous discussion,¹¹ their mean distance has been taken as 1000 pcs.

The calculated relationship between the power radiated by a source and its apparent angular diameter has already been given in Fig. 1 and the data in Table II have been plotted on the same diagram for comparison. It can be seen that, making the crude assumption that all the sources are at the same distance, the intensities and angular diameters of the observed

sources are in reasonable agreement with the relationship given by the model.

The relative numbers of sources with different intensities have also been calculated and compared with the observed data. Although such a comparison shows that the data in Table II are consistent with the model, this agreement cannot be regarded as significant since the number of observed sources is too small. Nevertheless it can be shown that the mean power of the sources in Table II ($\sim 5 \times 10^{32}$ ergs. sec.⁻¹) agrees closely with the corresponding value given by the model.

The space-density of the observed sources has also been compared with that given by the model. Thus Fig. 2 shows that the lifetime of a source is about 10^5 years and, if supernovae appear with a frequency of 1 per 200 years, the total number of sources of comparable power to those listed in Table II ($P_R > 10^{31}$ ergs. sec.⁻¹) would be about 500. If these sources are observed within 1 or 2 kpcs of the Sun, that is to say in about 1—2 per cent of the volume of the Galaxy, then the corresponding number of intense sources observed close to the galactic plane should be about 5 or 10. Although this estimate is in rough agreement with the number of sources in Table II, such close agreement may be largely accidental. Firstly it is probable that more intense sources will be discovered when complete surveys of the galactic plane have been made; secondly, if supernovae show a pronounced concentration towards the galactic centre, then the space-density of the radio sources associated with their remnants near the Sun will be less than the value calculated above. Thus it appears more likely that the space-density of the sources observed in the Galaxy is higher, say by five or ten times, than that estimated on the assumption that one supernova appears every 200 years. However, it is pointed out later that the frequency of supernovae is itself uncertain and may be significantly higher than the value which has been assumed.

An important objection to the suggestion that many of the Class I sources are the remnants of supernovae is that, in the visual spectrum, the Crab Nebula does not resemble the other four objects which have been identified as radio sources. In the case of three of these sources, Nos. 3, 4 and 5 in Table I, the observed angular diameter of the associated nebulosity is much greater than that of the Crab Nebula, while the surface brightness and velocity of expansion are much lower. These differences suggest that these three objects are much older than the Crab Nebula and the possibility that they are the remnants of supernovae is not excluded.

In the case of source No. 2 in Cassiopeia, the associated nebulosity has about the same angular size as the Crab Nebula but differs from it in appearance. The surface brightness, spectrum and structure of the two objects are dissimilar, also the velocity dispersion of the filaments in the Cassiopeia object is believed to be much greater than the velocity of expansion, while in the Crab Nebula the reverse is true. The significance of the differences between these nebulosities is far from clear since the origin of their light has not yet been established; furthermore the failure to photograph any trace of the supernovae of A.D. 1572 suggests that the appearance of the remnants of supernovae of comparable age may be greatly dissimilar. It must be also noted that the low velocity of expansion and the intense radio emission from the object in Cassiopeia can be ex-

plained in terms of the simple model, if it is assumed that the density of the interstellar gas surrounding the nebulosity is of the order of 100 atoms cm^{-3} . Since regions of such high density must be rare, this explanation is open to considerable doubt.

Another difference between the Crab Nebula and the nebulosity in Cassiopeia is that their associated radio sources have different spectra. Thus measurements in the metre-wave region show that the flux from the source in Cassiopeia decreases with increasing frequency at a rate higher than that observed from the Crab Nebula. However it has been shown¹² that the Crab Nebula may have an appreciable "optical depth" at metre-waves and that this will tend to flatten its spectrum. It is therefore possible that the difference between the radio spectra of the two sources is a function of the difference in density of their associated nebulosities.

Thus, although there are a number of significant differences between the Crab Nebula and the object in Cassiopeia, the present evidence does not exclude the possibility that both these objects are the relics of supernovae. The high velocities, the small angular diameter and the roughly circular outline of the nebulosity in Cassiopeia suggests strongly that it originated by a central explosion, and that this explosion was recent; furthermore the power emitted by the associated radio source is so great that it is difficult to suggest any alternative source of energy to the explosion of a supernova. This conclusion receives support from the historical records¹⁸ of the appearance of a bright star in A.D. 369 in the approximate position of the nebulosity.

It has been shown above that, on the basis of a simple model, the remnants of supernovae may be expected to form a population of radio sources with characteristics similar to those which have been observed close to the galactic plane. Photographic observations of some of these sources show that they are associated with extended nebulosities and do not exclude the possibility that they are the relics of supernovae. At the present time the surveys of the Class I sources are far from complete and the properties of these sources are therefore uncertain; however, the present analysis suggests that at least a significant number of these sources are associated with the remnants of supernovae.*

It was suggested above that the majority of the radio energy emitted by the remnants of a supernova is generated by some non-thermal process which takes place when the expanding shell collides with the interstellar gas. If it is assumed that a similar non-thermal process occurs in the shell of a nova, then the equations derived previously can be used to calculate the radio energy emitted by some of the principal novae.

A list of four principal novae is given in Table 3. These novae have been selected because at maximum light they were among the brightest known and also because they have high velocity shells. The total radio emission (P_R) from their shells has been calculated for epoch 1950 by means of equation (4), on the assumption that their velocity of expansion has remained constant over the period considered. The efficiency (η) of the non-thermal process has been taken as 2×10^{-5} and the density of the interstellar gas as 0.1 and 1 atoms cm^{-3} . These values of P_R have been used, together with the distances shown, to calculate the flux

* In a recent paper Shklovsky¹⁴ has proposed that a number of the intense sources found by Mills may be identified with old supernovae.

densities (I_R) at 100 Mc/s to be expected at the Earth's surface, and the results are also shown. It has been assumed that the total radio energy is distributed over an equivalent bandwidth of 200 Mc/s with an average flux density equal to I_R .

The minimum value of flux density which has been detected reliably in general surveys of the sky is of the order of 50×10^{-26} watts $m^{-2}(c/s)^{-1}$. Thus the calculated intensities suggest that there should be a detectable radio source in the position of N. Aquila (1918)†, and that in the position of N. Persei (1901) there should be a fainter source near the limits of detection. In the case of the N. Lacerta (1936) and N. Puppis (1942), and many other novae which have also been considered, the associated radio sources should be too faint to have been reported in existing surveys.

An examination of the existing observational data shows that only one radio source has been identified with a nova. Thus Bolton, Stanley and Slee¹⁵ have found a source of intensity 270×10^{-26} watts $m^{-2}(c/s)^{-1}$ near the position of N. Aquila (1918) and they have tentatively identified this source with the expanding shell of the nova. It is interesting to note that the value of observed intensity lies well within the calculated range shown in Table 3. In the case of N. Persei (1901), although no source has been found, it is possible to assign an upper limit of about 50×10^{-26} watts $m^{-2}(c/s)^{-1}$ from a detailed examination of a survey at 160 Mc/s. Thus a comparison of the calculations with the observational data is inconclusive since surveys of sufficient sensitivity are not yet available, nevertheless, the detection of a radio source in the position of N. Aquila (1918) supports the suggestion that a similar non-thermal process may occur in the shells of both novae and supernovae.

Finally it is interesting to estimate the contribution which the remnants of supernovae might make to the total radio emission from the Galaxy, and this has also been done by Baade and Minkowski.³ In their estimate they assumed that the lifetime of the associated radio source is 20,000 years and that the sources radiate with the same power as the Crab Nebula ($\sim 5 \times 10^{32}$ ergs $sec.^{-1}$). Thus the total power radiated by a source is about 3×10^{44} ergs and, if the frequency of supernovae in the Galaxy is 1 per 200 years, the total emission from these is about 5×10^{34} ergs. $sec.^{-1}$. Since the radiation from the Galaxy is about 10^{37} ergs. $sec.^{-1}$ the contribution of these sources represents only a few tenths of one per cent of the total.

A corresponding estimate has been made from the model of a supernova remnant given above. If the initial mass and velocity of the expanding shell is taken as $15 M_{\odot}$'s and 1000 kms. $sec.^{-1}$ and if 2×10^{-5} of the kinetic energy of expansion is converted into radio emission, then the total radio energy produced by each supernova is about 3×10^{45} ergs, about ten times that estimated above. Thus, if supernovae occur with a frequency of 1 per 200 years, the total power radiated by their remnants is 5×10^{35} ergs. $sec.^{-1}$ or about 5 per cent of the total radiation observed from the Galaxy in the metre-wave domain.

It must be noted that this latter estimate is very uncertain; not only are the values assumed in the model approximate but the value taken

† Shklovsky has considered the possibility that radio energy is generated in novae and supernovae by the acceleration of relativistic particles, and has suggested that N. Aquila (1918) might be a radio source of intensity 2×10^{-22} watts. $m^{-2}(c/s)^{-1}$.

for the frequency of supernovae is also open to question. If it is accepted that the model is substantially correct, then in principle it is possible to establish more precise values for its parameters by a detailed comparison of the model with the observed sources. The number of these sources is small and their distances are uncertain, hence there is a considerable range of values over which the model will give reasonable agreement with

TABLE III

<i>Nova</i>	<i>Velocity of shell</i> <i>Kms. sec.⁻¹</i>	<i>Distance</i> <i>(parsecs)</i>	<i>Calculated flux density at 100 Mc/s</i> <i>watts m⁻²(c/s)⁻¹</i>	
			$\rho = 0.1 \text{ atoms cm}^{-3}$	$\rho = 1 \text{ atom cm}^{-3}$
Aquila (1918)	1700	430	70×10^{-26}	700×10^{-26}
Persei (1901)	1200	480	20×10^{-26}	200×10^{-26}
Lacerta (1936)	1600	1350	1×10^{-26}	10×10^{-26}
Puppis (1942)	1000	500 or 2000	2×10^{-27} or 1×10^{-28}	2×10^{-26} or 1×10^{-27}

the observational data. A rough analysis shows that the corresponding values of the total radio energy emitted by a supernova remnant may lie anywhere between about 10^{45} and 10^{46} ergs. Therefore, if the frequency of supernovae is 1 per 200 years, the calculated emission from the remnants of supernovae may have any value between about 1.5 and 15 per cent of the total radiation from the Galaxy.

The estimate made by Baade and Minkowski, together with the estimate given above, show that the remnants of supernovae are unlikely to account for more than a minor fraction of the total radiation observed if the frequency of supernovae in the Galaxy is 1 per 200 years. However, several authors have argued that the true frequency must be considerably higher. For example, Opik¹⁰ has concluded that a fair estimate is 1 per 30 years, while Shklovsky¹⁴ has argued that the true frequency must be of the order of 1 per 20—30 years. These latter estimates are difficult to reconcile with observations of extra-galactic nebulae given by Zwicky¹⁷; nevertheless the possibility that the frequency of supernovae is significantly higher than 1 per 200 years cannot be dismissed on the present evidence, and there is a corresponding uncertainty in the estimates of the total radiation from their remnants. For example, if the total radio energy emitted by a supernova remnant is as great as 10^{46} ergs, then the total radiation from the Galaxy might be due to these remnants if the frequency of supernovae is as high as 1 per 30 years. Thus, if the uncertainties in the model and in the frequency of supernovae are taken into account, the possibility cannot be excluded that the remnants of supernovae are responsible for a substantial fraction of the total radiation from the Galaxy at metre-wavelengths.

To summarise the discussion, it has been shown in the present paper that, if certain speculative assumptions are made about the non-thermal generation of radio energy, then the population of discrete sources observed in the Galaxy at metre-wavelengths may possibly be explained in

terms of the remnants of supernovae. It follows that, on the basis of the present evidence, it is not imperative to invoke some unknown type of celestial body to explain these sources. A reliable estimate of the contribution of these sources to the total radiation from the Galaxy cannot be made. However, it has been shown that, if the frequency of supernovae is significantly higher than 1 per 200 years, then the possibility cannot be excluded that their remnants are responsible for a substantial fraction of the radiation observed from the Galaxy at metre-wavelengths. The analysis has been based on the suggestion that radio energy is generated by some non-thermal process which occurs in the collision of gas at high velocity. The idea that some such process is a common phenomenon in the universe is of considerable interest, since it may not be restricted to variable stars but may take place on a large scale in the interstellar gas; furthermore it is also possible that a similar process takes place in the interaction of galaxies and is responsible for part of the extra-galactic component of the total radio flux incident on the Earth.

Acknowledgments.

The author would like to thank Professor Z. Kopal and Professor A. C. B. Lovell for their interest in the paper.

University of Manchester,
Jodrell Bank Experimental Station,
Lower Withington, Cheshire.
1954 August.

References

- (1) Mills, B. Y., *Austr. J. Sci. Res.*, (A), **5**, 266, 1952.
- (2) Baade, W., and Minkowski, R., *Ap. J.*, **119**, 206, 1954.
- (3) Baade, W., and Minkowski, R., *Ap. J.*, **119**, 215, 1954.
- (4) Minkowski, R., Reported in *J. Geophys. Res.*, **59**, 149, 1954.
- (5) Hanbury Brown, R., Palmer, H. P., and Thompson, A. R., *Nature*, **173**, 945, 1954.
- (6) Baldwin, J. E., and Dewhirst, D. W., *Nature*, **173**, 164, 1954.
- (7) Hanbury Brown, R., and Hazard, C. H., *Nature*, **170**, 364, 1952.
- (8) Kahn, F. D., *M.N.*, **112**, 514, 1952.
- (9) Oort, J. H., *M.N.*, **106**, 159, 1946.
- (10) Opik, E. J., *Irish Astr. J.*, **2**, 219, 1953.
- (11) Hanbury Brown, R., and Hazard, C. H., *M.N.*, **113**, 123, 1953.
- (12) Greenstein, J. L., and Minkowski, R., *Ap. J.*, **118**, 1, 1953.
- (13) Shklovsky, I. S., and Parenago, P. P., *Astron. Circ. Acad. Sci., U.S.S.R.*, No. **131**, 1952.
- (14) Shklovsky, I. S., *C.R. Acad. Sci. U.S.S.R.*, **94**, 417, 1954.
- (15) Bolton, J. G., Stanley, G. J., and Slee, O. B., *Austr. J. Phys.*, **7**, 110, 1954.
- (16) Shklovsky, I. S., *Mem. Soc. Roy. Sci. Liege, Quatrième Série*, **14**, 515, 1954.
- (17) Zwicky, F., *Ap. J.*, **96**, 28, 1942.

APPARENT ANGULAR SIZES OF DISCRETE RADIO SOURCES

Observations at Jodrell Bank, Manchester

THE existence of discrete sources of extra-terrestrial radio-frequency radiation is now well established^{1,2} and the positions of more than one hundred sources have been published³⁻⁵. Attempts to identify these sources with any particular class of visual object have so far failed, and the origin of the radiation remains unexplained. One of the fundamental requirements in the study of these sources is a knowledge of their apparent angular size, and although attempts to make this measurement have been made by several observers¹⁻³, it has proved to be beyond the resolving power of their equipment. The present communication gives a preliminary account of a successful attempt to measure the angular size of the two most intense sources the positions⁶ and intensities⁴ of which are given in Table 1.

Table 1. CO-ORDINATES AND INTENSITY OF THE TWO MOST INTENSE RADIO SOURCES

Source	Right Ascension epoch 1950	Declination epoch 1950	Intensity* at 81 Mc./s. (watts/sq.m./ c.p.s.)
Cygnus Cassio- peia	19h. 57m. 45.3s. ± 1 s.	N 40° 35.0' $\pm 1'$	13.5 $\times 10^{-23}$
	23h. 21m. 12.0s. ± 1 s.	N 58° 32.1' $\pm 0.7'$	22.0 $\times 10^{-23}$

* The intensity given is twice that observed in one plane of polarization.

The co-ordinates are those given by Smith (ref. 6), and the intensities are those given by Ryle, Smith and Elsmore (ref. 4).

Previous measurements have been made with interferometers. Bolton and Stanley¹, using an interferometer mounted on a cliff and operating in a manner analogous to 'Lloyd's mirror', have shown that the apparent size of the source in Cygnus is less than 8 minutes of arc. More recently, Stanley and Slee³, using a similar instrument, claim to have reduced this limit to $1\frac{1}{2}$ minutes of arc. Ryle and Smith², using an instrument analogous to Michelson's stellar interferometer and with a baseline of 500 metres, have shown that the source in Cassiopeia has an angular size of less than 6 minutes of arc.

The resolving power of an interferometer depends primarily on the ratio of the wave-length to the

base-line, and the limits quoted above represented the best performance obtained with the instruments. These limits cannot be reduced significantly without a corresponding extension of the base-line.

In 1950 it was decided at Jodrell Bank to attempt to measure the angular size of the two sources shown in Table 1, or at least to reduce the upper limits given for their size. It was assumed that this angular size might lie anywhere between the limit of a few minutes of arc and the diameter of the visible stars, and an instrument of the highest possible resolving power was therefore sought. While it appeared to be possible to extend the base-lines of existing interferometers to lengths of the order of 10-50 km., it was considered that for much longer base-lines the problem of maintaining an adequate stability of phase in the transmission of signals along the base-line would prove to be difficult. For this reason an interferometer of completely new design was developed.

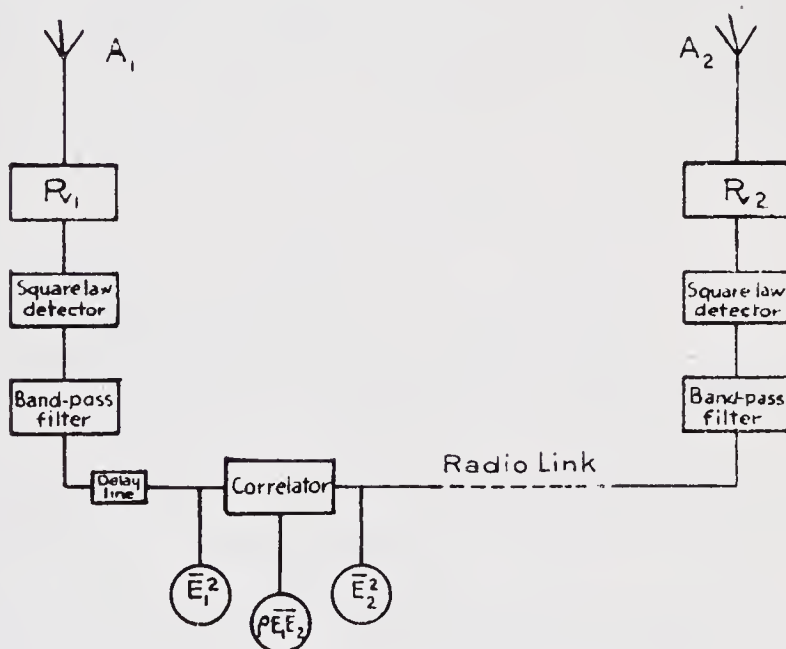


Fig. 1. Schematic diagram of the equipment

Fig. 1 shows a simplified block diagram of the instrument. Two aerial systems A_1 and A_2 , each with an aperture of 500 square metres, are connected to two independent superheterodyne receivers R_1 and R_2 . These receivers are both tuned to 125 Mc./s. and have a band-width of 200 kc./s. The intermediate frequency output of receiver R_1 is rectified in a square-law detector and is fed to a low-frequency filter the pass-band of which extends from 1 to 2 kc./s. The output from receiver R_2 is treated in an identical manner and the two low-frequency outputs are then

Table 2. EXPERIMENTAL RESULTS

Base-line		Cygnus		Cassiopeia	
Length* (km.)	Bearing†	Correlation coefficient	Angular width of equivalent strip	Correlation coefficient	Angular width of equivalent strip
A 0.30	349.5°	0.99 ± 0.10	< 5'	0.96 ± 0.09	3' 40" (< 5' 50")
B 2.16	113.0°	0.30 ± 0.03	2' 10" ± 4"	0.08 ± 0.02	2' 55" ± 10"
C 2.16	235.5°	0.79 ± 0.08	1' 10" ± 7"	< 0.01	< 3' 30"
D 3.99	177.0°	0.79 ± 0.07	0' 34" ± 8"	0.07 ± 0.01**	

* The value given is the actual distance between the two stations. The effective length of the base-line is calculated from the elevation of the source and the orientation of the base-line.

† The bearing is measured east from north, and is the relative bearing of the base-line from the fixed station at Jodrell Bank.

** This value is not taken into account in Fig. 3, since the other results indicate that the point may lie on a secondary maximum of the curve relating correlation coefficient to base-line.

multiplied together in a correlator' and their 'cross-correlation coefficient' is obtained. When a long base-line is used, one low-frequency output is transmitted over a radio-link by modulating a high-frequency carrier. The time of arrival of the two low-frequency outputs at the 'correlator' is equalized by inserting in one output a delay equal to the time of transmission along the base-line. It is essential that all the components should preserve the relative phase of the two low-frequency signals. In practice, this problem is considerably simpler than the corresponding one of preserving the relative phase of the radio-frequency signals in a conventional interferometer, and hence it should be easier to use the new type of instrument with long base-lines.

In operation, the two aerials (A_1 and A_2) are fixed in azimuth (due north or south) and at an elevation corresponding to the declination of the source. As the source transits the aerial beam, the increase in the mean square value of the two low-frequency outputs ($\overline{\epsilon_1^2}$ and $\overline{\epsilon_2^2}$) is recorded together with their product ($\rho \epsilon_1 \epsilon_2$). The value of the 'cross-correlation coefficient' (ρ) is then found from an analysis of the three records.

The theory of the instrument is involved, and it will be given in detail elsewhere⁷. It can be shown that the value of the cross-correlation coefficient (ρ) is given by an expression similar to that for the visibility of the fringes in a Michelson stellar interferometer :

$$\rho = \frac{\sin^2(\pi\alpha b/\lambda)}{(\pi\alpha b/\lambda)^2}, \quad (1)$$

where α is the angular width of an equivalent rectangular source of constant surface intensity; b is

the effective length of the base-line ; and λ is wavelength.

Equation (1) shows that by a suitable choice of the base-line it is possible to obtain a value for the angular width of an equivalent rectangular source of constant surface intensity. The shape and angular width of the actual source, together with the distribution of brightness across its disk, can only be found from a large number of observations made with base-lines of different length and orientation.

A model of the instrument, built in 1950, was used to measure the apparent diameter of the sun at 125 Mc./s. As the results of this test were satisfactory, a full-scale instrument was built in 1951, and this has since been applied to the two sources shown in Table 1. Measurements have so far been made on both sources with four different base-lines and the results are given in Table 2. The length and orientation of the base-lines are given in the table, together with the observed values of the cross-correlation coefficient (ρ). The angular size of the equivalent

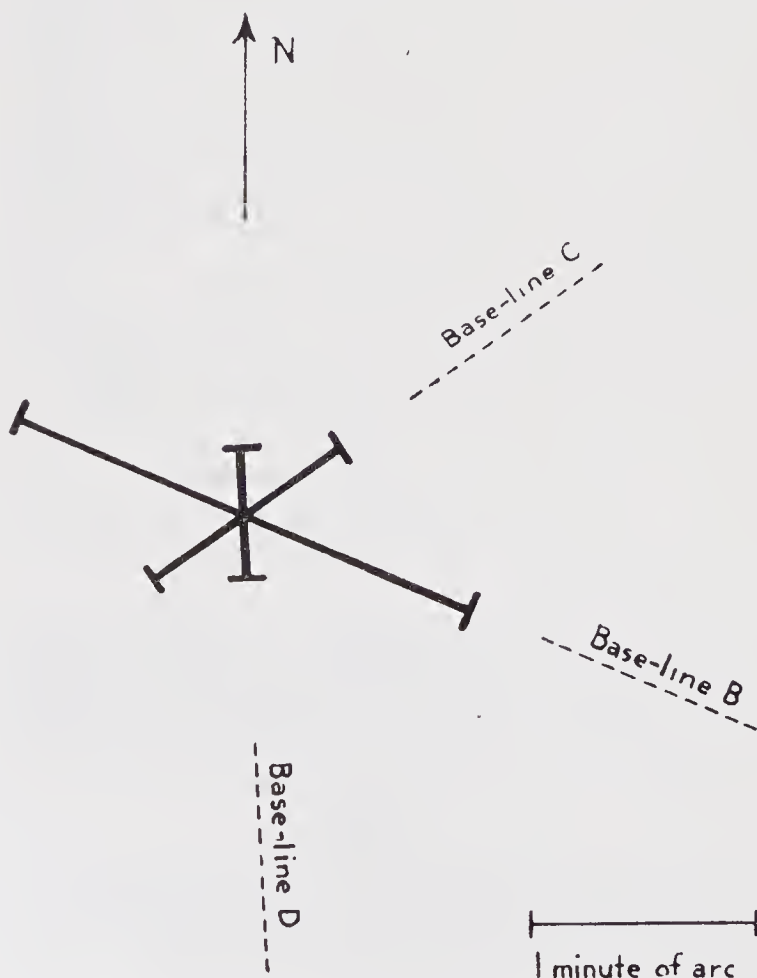


Fig. 2. Equivalent angular width of the source in Cygnus observed from different base-lines. The value shown is the width of an equivalent rectangular strip of constant surface intensity.

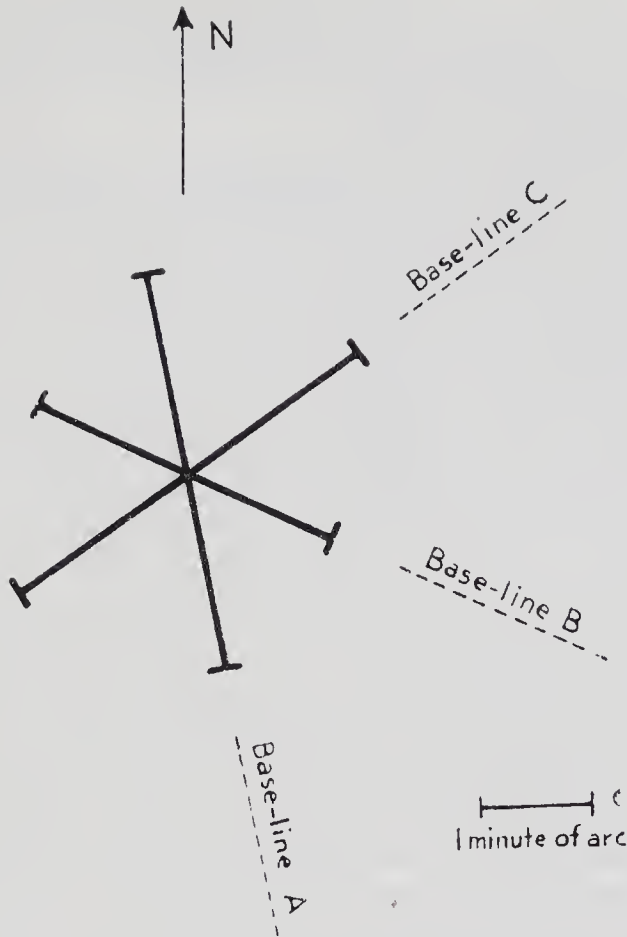


Fig. 3. Equivalent angular width of the source in Cassiopeia observed from different base-lines. The value shown is the width of an equivalent rectangular strip of constant surface intensity

rectangular strip has been calculated for each base-line and the results are also shown in Table 2.

The interpretation of these results in terms of the precise actual size and shape of the sources must be treated with caution, since the three extended base-lines differed in length; and until more results are available it is uncertain what effect variations in the length of the base-line may have on the equivalent angular size of the source.

Figs. 2 and 3 show a plot of the measurements given in Table 2. Fig. 2 shows clearly that the source in Cygnus exhibits a pronounced asymmetry. The value of its equivalent angular size varies from $35''$ to $2' 10''$ of arc with the orientation of the base-line, and the major axis of the source appears to be inclined at an angle of between 90° and 120° to the celestial meridian. A preliminary analysis indicates that the results are incompatible with a source of simple elliptical shape and constant surface intensity, and that a more complicated model must be used. Further progress in this analysis must await more

observations. The results in Fig. 3 suggest that the source in Cassiopeia is not markedly asymmetrical. The equivalent angular size of the source appears to be about 4' of arc.

These preliminary measurements establish two major points. First, the apparent angular size of the two most intense radio sources is thousands of times greater than that of the visible stars and is of the order of a few minutes of arc. Secondly, the source in Cygnus exhibits a pronounced asymmetry in angular size, whereas the source in Cassiopeia appears to be roughly symmetrical. The measurements are not yet adequate to define satisfactorily the shape of the sources or the distribution of intensity across their disks. Further observations are now being made with the present apparatus using different base-lines, and the results will be published later.

The work was carried out at the Jodrell Bank Experimental Station of the University of Manchester. The construction of the apparatus was made possible by a grant from the Department of Scientific and Industrial Research. We wish to thank Dr. R. Q. Twiss for his assistance with the mathematical theory, and Prof. A. C. B. Lovell for making the necessary facilities available and for his interest in the investigation. One of us (R. H. B.) is indebted to Messrs. Imperial Chemical Industries for a fellowship, and one (M. K. D. G.) to the Government of India for a scholarship and to the Department of Scientific and Industrial Research for a maintenance grant.

R. HANBURY BROWN
R. C. JENNISON
M. K. DAS GUPTA

Jodrell Bank Experimental Station,
Holmes Chapel,
Cheshire.

¹ Bolton, J. G., and Stanley, G. J., *Nature*, **161**, 312 (1948).

² Ryle, M., and Smith, F. G., *Nature*, **162**, 462 (1948).

³ Stanley, G. J., and Slee, O. B., *Aust. J. Sci. Res.*, A, **3**, 234 (1950).

⁴ Ryle, M., Smith, F. G., and Elsmore, B., *Mon. Not. Roy. Astro. Soc.*, **110**, 508 (1950).

⁵ Mills, B. Y., *Aust. J. Sci. Res.*, A, **5**, 266 (1952).

⁶ Smith, F. G., *Nature*, **168**, 555 (1951).

⁷ Hanbury Brown, R., and Twiss, R. Q. (in preparation).

Galactic Radio Sources of Large Angular Diameter

THE survey of extra-terrestrial radiation, made at 1.89 m. with the 218-ft. paraboloid at Jodrell Bank, gave the position and intensity of 23 localized sources¹ between declinations N. 38° and N. 68°. The distribution of the intense sources showed a marked concentration close to the galactic plane, and it was concluded that they represented a class of rare objects in the Galaxy. A similar concentration has been found by Mills² from observations in the southern hemisphere. An attempt has now been made to measure the apparent angular width of these sources, and the present communication gives the preliminary results.

The measurements have been made at 1.89 m. using the 218-ft. paraboloid as an interferometer in conjunction with a small mobile aerial of 35 sq. m. aperture. The small aerial was placed at various distances along an east-west base-line from the fixed paraboloid, and in each position the amplitude of the interference pattern in the receiver output was recorded as the sources were in transit. The apparent angular size of each source was found from the change in the amplitude of the pattern with aerial spacing by using the well-known relation³ between the amplitude and the distribution of intensity across the source. The effects of systematic errors and long-

Table 1

Reference No. ¹	Galactic longitude (deg.)	Galactic latitude (deg.)	Intensity* at 1.89 m. (watt. m. ⁻² (c./s.) ⁻¹ × 10 ⁻²⁶)	Apparent angular width	Remarks
1	87.5	+2.1	170	—	Not measured
3	100.5	+2.1	80	>1.5°, <3°	
7	111.8	-0.3	60	>1.5°, <3°	
8	121	-1.5	50	>1.5°, <3°	
9	128.3	+3.8	80	1.4° ± 0.4°	
19	43.6	+4.9	5,700	2' 10" × 35" (ref. 5)	Identified with nebulosity in Fig. 2
20	45.9	+0.8	300	1° or 2° (ref. 9)	Identified as extra-galactic (ref. 10) Cygnus X
21	56.5	+4.1	200	1.5° ± 0.4°	Not measured
22	66.4	+2.9	50	—	
23	79.6	-2.0	9,250	5' × 4' (refs. 4, 5, 6)	

* The intensity given is the maximum intensity observed¹ in a 2° beam. It has not been corrected for the finite size of the source.

period changes in the calibration of the equipment were minimized by daily observation of the transit of the intense source in Cassiopeia (No. 23) for which the intensity¹ and angular diameter is already known^{4,5}.

The original survey¹ listed ten sources within $\pm 5^\circ$ of the galactic plane, as shown in Table 1, all of which were classified as intense ($> 50 \times 10^{-26}$ watt. m.⁻² (c./s.)⁻¹). The present observations have been restricted to five of these sources (Nos. 3, 7, 8, 9 and 21) and the measured values of their angular sizes are shown in Table 1. The angular sizes of sources 19, 20 and 23 have been quoted from previous observations^{4-6,9}. Measurements could not be carried out on Nos. 1 and 22, since serious interference was experienced in their positions from the reception of nearby intense sources in side-lobes of the aerial system.

The variation in the amplitude of the interference pattern observed at different aerial spacings for source 9 is shown in Fig. 1. The results for source 21 were almost identical. In both cases the width of the equivalent strip source is about $1\frac{1}{2}$ deg. Sources 3, 7 and 8 were found to be even greater in size and it was only possible to assign an approximate lower limit of about $1\frac{1}{2}$ –2 deg. to their equivalent widths, since the minimum spacing between the two aerials was restricted to about 20λ by the size of the fixed paraboloid. An upper limit to the size of these three sources of about 3 deg. has been established by inspection of the records obtained in the original survey¹.

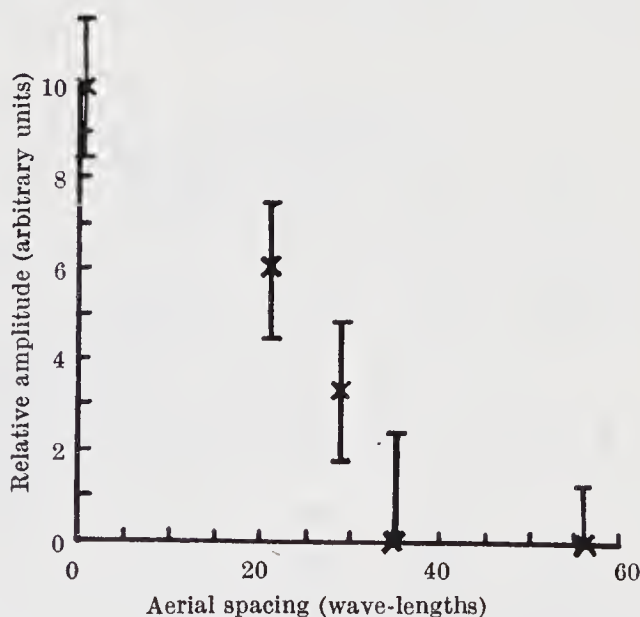


Fig. 1. The relative amplitude of the interference pattern observed from source 9. The value given for zero base-line is derived from the original survey (see ref. 1)

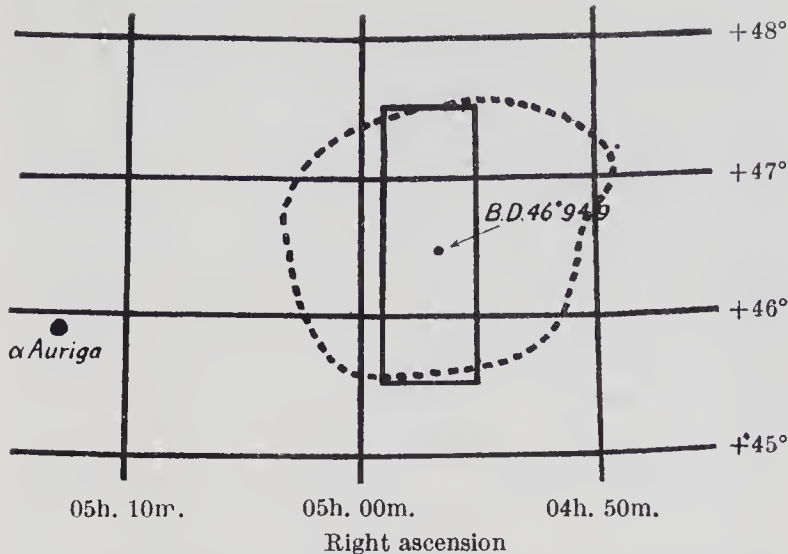


Fig. 2. A faint nebulousity in Auriga. The broken line shows the outline of the nebulousity. The position, and associated errors, of the radio source are given by the rectangle. The positions of α -Auriga and B.D. 46° 949 are shown for reference

An examination of the sky in the position of source 9 has been made by Minkowski⁷ using plates taken during the National Geographic Survey with the 48-in. Schmidt telescope of the Mount Wilson and Palomar Observatories. He has found that in the approximate position of the source there is a faint nebulousity the outline of which is sketched in Fig. 2. The sketch has been made from an exposure taken in red light; only faint traces of the object can be seen in the blue. The nebulousity contains some faint filaments which are most prominent at the western edge. The co-ordinates of the radio source agree closely with the centre of the nebulousity, and the width of the equivalent source (1.4 ± 0.4 deg.) is comparable with the extension of the nebulousity in an east-west direction (~ 2 deg.). In view of this agreement, source 9 may be provisionally identified with the nebulousity.

In addition to the sources listed in Table 1 three other intense sources with large angular diameters have been reported close to the galactic plane in regions outside the field of view of the present equipment. Thus Mills² has observed two intense sources with angular diameters greater than half a degree at $l = 229^\circ$, $b = 0^\circ$ and $l = 330^\circ$, $b = 4^\circ$. Bolton¹¹ has reported that the former of these two sources, in Puppis, has an angular diameter of about 1° . More recently, Baldwin and Dewhirst⁸ have observed a source in Gemini with an angular width of about one degree associated with the nebulousity I.C.443. Bolton¹¹ has also reported the presence of extended patches of radiation in the galactic plane, nearer to

the galactic centre, which may result from the presence of several of these extended sources.

Thus, by combining the data in Table 1 with observations made in other parts of the sky, a total of at least nine intense sources with diameters of the order of a degree have been found close to the galactic plane; furthermore, at wave-lengths of about two or three metres, the apparent surface temperatures of these sources are all of the order of a few hundred degrees K. The similarity between these sources is striking and suggests that they represent a definite class of object in the Galaxy.

At the present time, only five objects in the Galaxy have been identified with radio sources. These are the Crab Nebula in Taurus¹², the nebulosities in Cassiopeia^{10,13}, Puppis^{2,11} and Gemini⁸ (I.C.443) and the nebulosity in Auriga shown in Fig. 2. The radio sources associated with the Crab Nebula and with the nebulosity in Cassiopeia (source 23) appear superficially to be different in character from each other and from the remaining three. They have angular diameters of a few minutes of arc and their apparent surface temperatures are of the order of thousands and millions of degrees respectively. The remaining three radio sources, which have been included among the nine sources already discussed, appear to be similar. Their associated nebulosities all show the presence of filaments but do not resemble each other exactly; nevertheless, the association of these three sources with nebulosities, together with their similarity to the other six unidentified sources of large diameter, indicate that the origin of this class of intense radio source is to be found in extended nebulosities of low photographic brightness.

We wish to thank Prof. A. C. B. Lovell and Prof. Z. Kopal for their interest in the investigation. We also wish to thank Dr. R. Minkowski for his generous co-operation. One of us (A. R. T.) is indebted to the Department of Scientific and Industrial Research for a maintenance grant.

R. HANBURY BROWN
H. P. PALMER
A. R. THOMPSON

University of Manchester,
Jodrell Bank Experimental Station,
Lower Withington, Cheshire.
April 13.

¹ Hanbury Brown, R., and Hazard, C., *Mon. Not. Roy. Astro. Soc.*, **113**, 123 (1953).

² Mills, B. Y., *Aust. J. Sci. Res. A*, **5** 266 (1952).

³ McCready, L. L., Pawsey, J. L., and Payne-Scott, R., *Proc. Roy. Soc., A*, **190**, 357 (1947).

- ⁴ Smith, F. G., *Nature*, **170**, 1065 (1952).
- ⁵ Hanbury Brown, R., Jennison, R. C., and Das Gupta, M. K. *Nature*, **170**, 1061 (1952).
- ⁶ Mills, B. Y., *Nature*, **170**, 1063 (1952).
- ⁷ Minkowski, R. (private communication).
- ⁸ Baldwin, J. E., and Dewhirst, D. W., *Nature*, **173**, 164 (1954).
- ⁹ Piddington, J. H., and Minnett, H. C. *Aust. J. Sci. Res.*, A, **5**, 17 (1952).
- ¹⁰ Minkowski, R., reported by Hanbury Brown, R., *Observatory*, **73**, 185 (1953).
- ¹¹ Bolton, J. G., reported at Tenth General Assembly of the U.R.S.I. (1952).
- ¹² Bolton, J. G., Stanley, G. J., and Slee, O. B., *Nature*, **164**, 101 (1949).
- ¹³ Ryle, M., and Smith, F. G., *Nature*, **162**, 462 (1948).

AN ANALYSIS OF THE ANGULAR SIZES OF RADIO SOURCES

L. R. Allen, R. Hanbury Brown and H. P. Palmer

(Received 1962 July 18)*

Summary

An analysis has been made of the fringe visibilities of 133 sources observed at four baselines between 2200 λ and 61100 λ . It is shown that, in this group of sources with flux density $S \geq 12 \times 10^{-26} \text{ w.m}^{-2} (\text{c/s})^{-1}$ and galactic latitude $|b^l| \geq 12^\circ$, 50 per cent are resolved at a baseline greater than about 4000 λ and 90 per cent are resolved at a baseline greater than about 30000 λ . These results establish the general scale of the angular size distribution among the hundred brightest sources in the Cambridge 3C catalogue.

The results from long baseline observations have been combined with those obtained at the California Institute of Technology with several baselines up to 1560 λ . It is found that at least 40 per cent of the sources must consist of at least two major separated radiating components. An attempt has been made to estimate the characteristic linear size, surface brightness, luminosity and distance of the sources in terms of two cosmological models.

1. *Introduction.*—During the last two years the long baseline interferometer at Jodrell Bank has been used to investigate the angular size of 324 of the radio sources listed in the Cambridge 3C catalogue (Edge *et al.* 1959) and of 60 sources from the list of Mills, Slee and Hill (1958).

The principal objective of this work was to establish, at least approximately, the distribution of angular sizes among as many radio sources as possible. It is clearly important to establish the general scale of this distribution at an early stage; not only is this knowledge of considerable astronomical interest, but it is essential to the planning of more comprehensive investigations of radio sources in the future.

The apparatus has been described by Elgaroy, Morris and Rowson (1962, subsequently referred to as Paper I). The results have been published in Paper II (Allen, Anderson, Conway, Palmer, Reddish and Rowson 1962).

In the first part of this paper the general distribution of the observations is outlined, and an attempt is made to interpret it in terms of simple models of source structure. In the second part these observations are combined with short baseline results due to Moffet (1961) and Maltby (1961), and the characteristic structure, dimensions and luminosity of a radio source are discussed.

* Received in original form 1962 March 9.

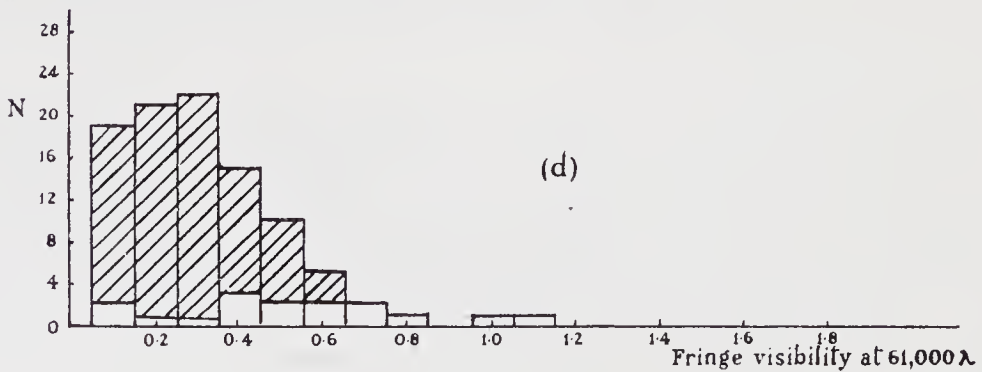
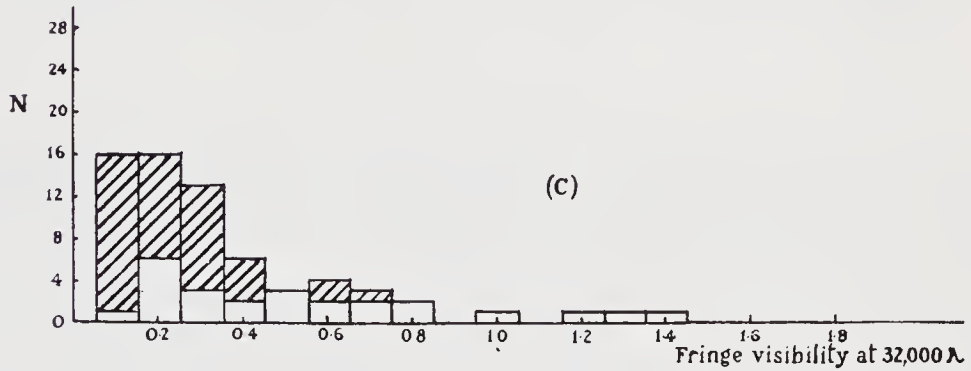
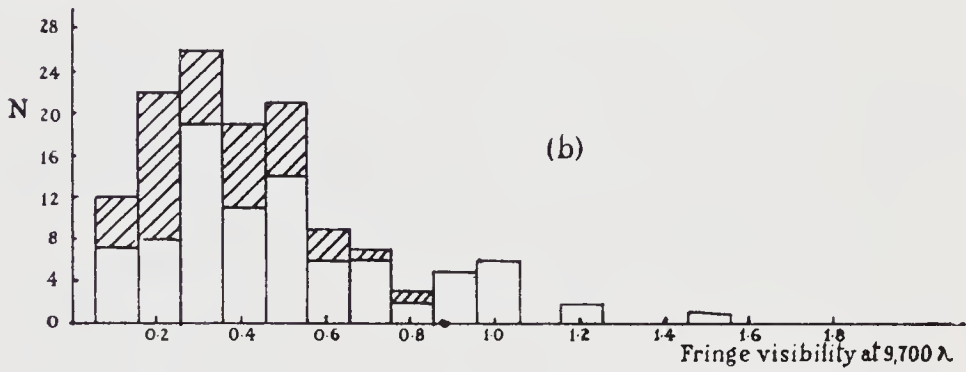
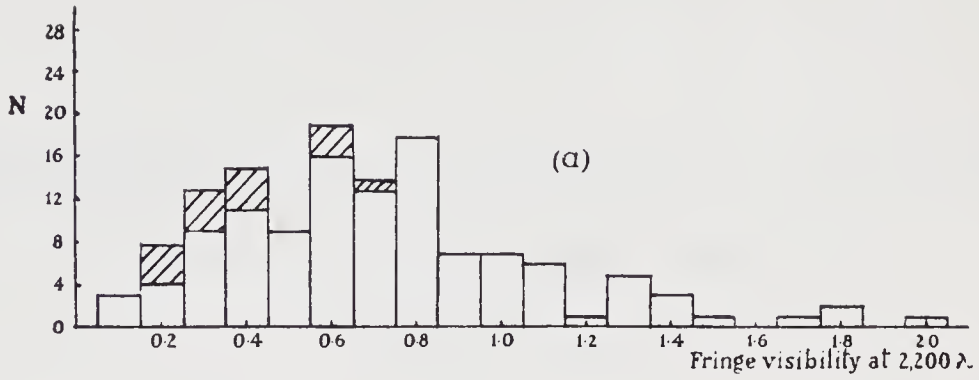


FIG. 1.—The distribution of fringe visibilities observed at four baselines, for a set of 133 sources having flux density $S \geq 12$ f.u. and galactic latitude $|b^l| \geq 12^\circ$.

2. *The observations.*—A detailed description of the apparatus has already been given in Paper I. It is sufficient to mention here that the observations were made at a frequency of 158.5 Mc/s (wave-length $\lambda = 1.89$ m) using four baselines of 2 200 λ , 9 700 λ , 32 000 λ and 61 100 λ at azimuths within $\pm 12^\circ$ of East–West.

The results obtained at these baselines have been given in Tables III and IV of Paper II. They are expressed as the observed fringe amplitude D (in flux units of 10^{-26} w.m $^{-2}$ (c/s) $^{-1}$) and also as the fringe visibility γ where

$$\gamma = D/S \quad (1)$$

and S is the flux density of the source given in the Cambridge 3C catalogue.

TABLE I

Total number of sources observed at each baseline

Baseline in wave-lengths	2 200	9 700	32 000	61 100
Number of 3C sources	274	305	121	187
Number of MSH sources	40	55

The number of sources observed at each baseline is given in Table I. For instrumental reasons the observations at 32 000 λ were not completed. The sources observed at this baseline were selected from the list of those which gave a measurable fringe amplitude when observed previously at the baseline of 9 700 λ . Similarly, all the sources which gave a measurable fringe amplitude at 32 000 λ were subsequently observed at the longest baseline of 61 100 λ .

Because the observational programme did not allow all the sources to be observed at each baseline, the analysis in this paper has been restricted to 133 sources listed in the 3C catalogue with a flux density greater than 12×10^{-26} w.m $^{-2}$ (c/s) $^{-1}$ and galactic latitude $|b^l| \geq 12^\circ$. The data given in the 3C catalogue for all these sources have since been shown to be reliable by later observations (Ryle 1962). Within these limits the observations at 2 200 λ and 9 700 λ are almost complete, the observations at 32 000 λ are 50 per cent complete and at 61 100 λ they are 73 per cent complete.

3. *The distribution of fringe visibilities*

3.1. *The general distribution.*—The distributions of fringe visibilities observed at the four baselines are shown in Fig. 1. In each case where no measurable fringe was observed an upper limit to the fringe visibility has been estimated and the distribution of these limits is shown by the shaded parts of the histograms.

A comparison of the four distributions shows that as the length of the baseline is increased an increasing percentage of the sources is resolved. This effect is illustrated more clearly in Fig. 2 which shows the percentage P of sources which have a fringe visibility $\gamma \geq 0.5$ for each of the four baselines. The vertical lines through each point are estimates of the standard errors, which are asymmetrical in some cases because they were computed from the histograms of Fig. 1. It should be noted that, strictly speaking, the values of P for the

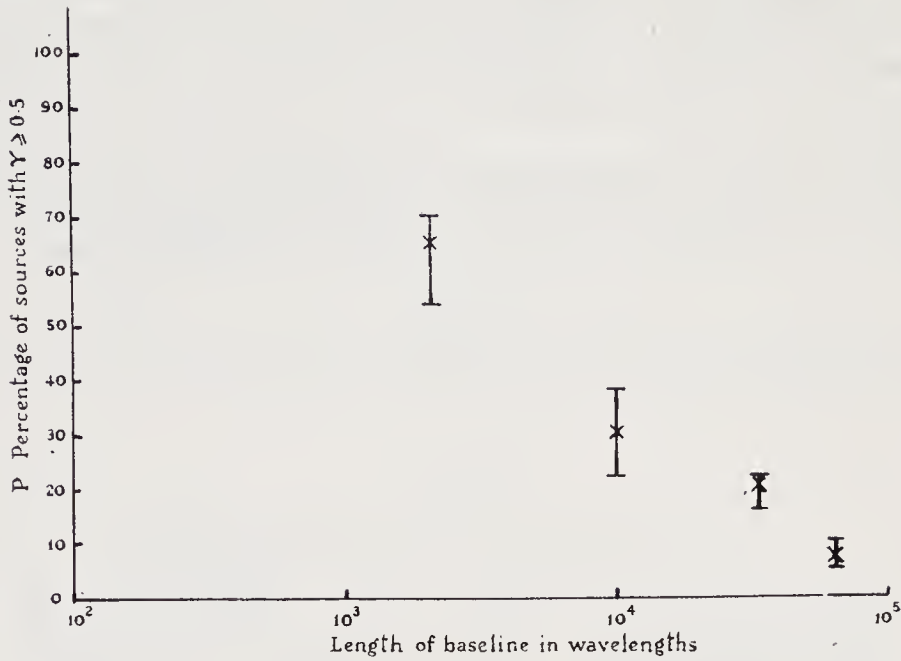


FIG. 2.—The percentage P of sources with fringe visibility $\gamma \geq 0.5$ at four baselines for the set of 133 sources.

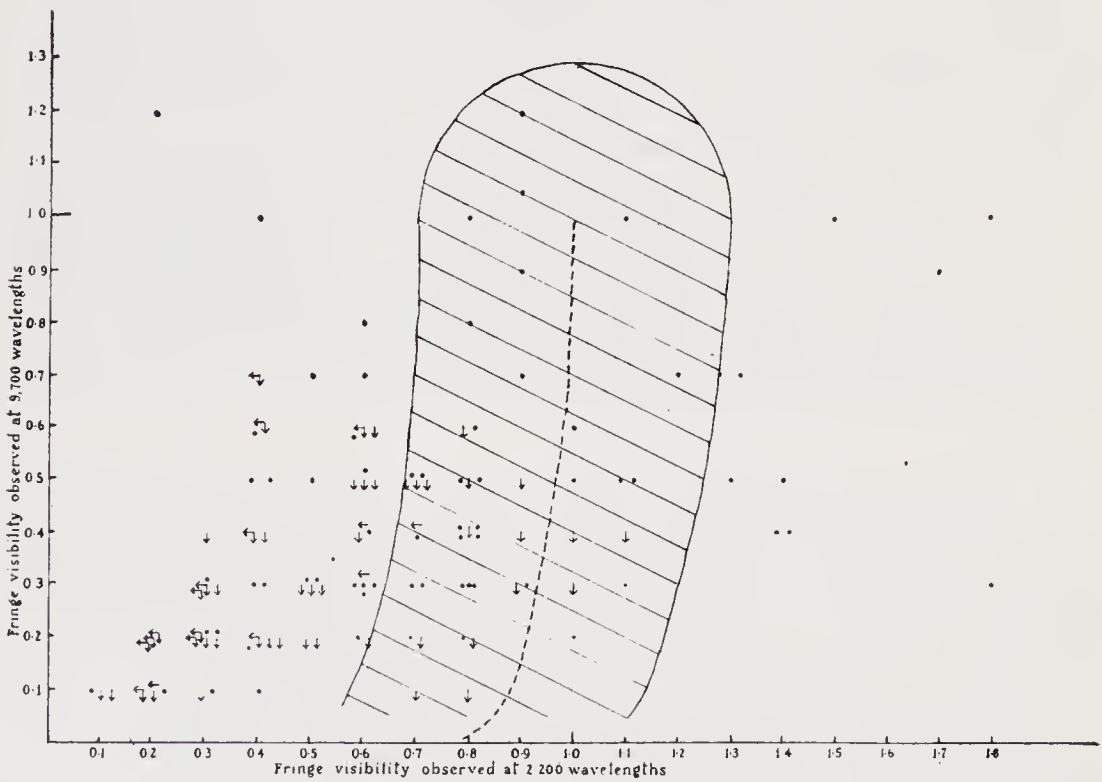


FIG. 3.—The relation between the fringe visibilities observed at two baselines for sources of flux density $S \geq 12$ f.u. and $|b^1| \geq 12^\circ$. The dashed line is the locus of points for a simple gaussian source model. For a population of such sources the errors of observation would cause only one-third of the points to lie outside the shaded area.

two longest baselines are upper limits, because the sources observed at these baselines were selected as most likely to have measurable fringe amplitudes; this selection was made on the basis of observations at the shorter baselines.

The results in Fig. 1 establish the rough scale of the distribution of fringe visibilities. They show that in a group of sources with $S \geq 12 \times 10^{-26} \text{ w.m}^{-2} (\text{c/s})^{-1}$ and $|b^1| \geq 12^\circ$ about 50 per cent are significantly resolved ($\gamma < 0.5$) at baselines greater than about 4000λ ; while at least 90 per cent are resolved at baselines greater than about 30000λ . If these results are interpreted in terms of single circular gaussian sources, then about 50 per cent of these sources have angular sizes $\theta \geq 23''$ (measured between points of half-intensity), and 90 per cent have angular size $\theta \geq 3''$.

3.2. *The variation of fringe visibility with baseline.*—An examination of the fringe visibilities observed at the four baselines shows that, for a substantial fraction of the sources, the variation of fringe visibility with baseline cannot be the type of visibility function expected for single sources as shown in Fig. 4 (a).

This conclusion is illustrated by Fig. 3 in which the fringe visibility for each of the 133 sources at 2200λ is plotted against the fringe visibility at 9700λ . The locus of points expected for a population of single gaussian sources is shown by the broken line. If the observational errors discussed in Paper II are taken into account, then it can be shown that the observed points should cluster about the broken line and that more than two-thirds of them should lie within the shaded area.

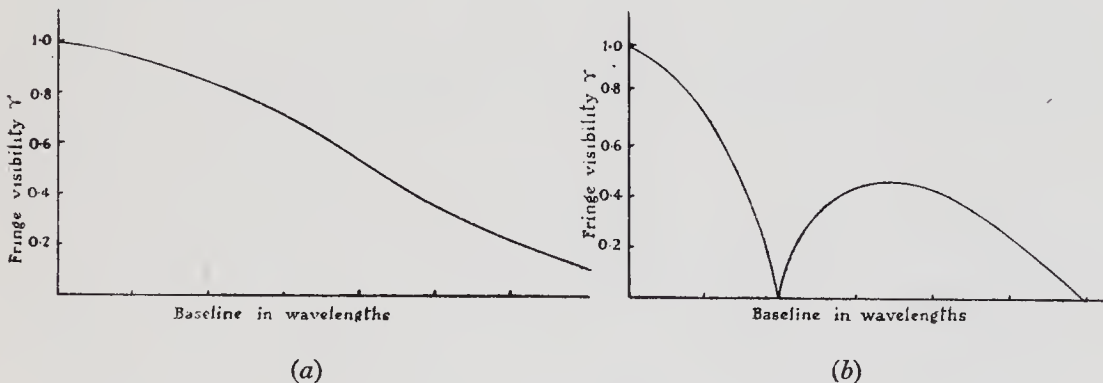


FIG. 4.—The visibility functions of two source models. (a) A single circular source with a radial distribution of surface brightness which is gaussian. (b) A double source, with two identical circular gaussian components.

It is clear from Fig. 3 that the observed points do not cluster about the broken line and that only a minority of them, less than 40 per cent, lie inside the shaded area. It follows that a single gaussian component is not an adequate model of the typical radio source: This conclusion also holds for other single models such as, for example, a uniform disk.

There are many sources in Fig. 3 which exhibit a substantially higher fringe visibility at 9700λ than at 2200λ . After making due allowance for the effects of observational errors, the distribution suggests that a significant number are multiple, that is to say, they have more than one major radiating component. For example, if we attempt to explain the distribution in terms of a mixed population of single and double sources having the fringe visibility functions

in Fig. 4, then it can be shown that at least 30 per cent of the sources must be double. In making this calculation it has been assumed that the orientation of the sources in space is random, that the angular separation of most of the components is large compared with the resolution at $2\,200\lambda$, that the angular size of the components is small compared with the resolution at $9\,700\lambda$, and that the components of a double source do not differ in absolute magnitude by more than one magnitude.

It is, of course, possible to analyse the fringe visibilities in Fig. 3 further and to test a variety of models of the typical structure of sources. However, it is clear that these observations are not sufficient, by themselves, to reveal this structure; observations at many more baselines are required. In the next section an attempt is therefore made to combine these data with some other measurements made at shorter baselines.

4. The typical structure of a radio source

4.1. *Introductory remarks.*—Moffet (1961) and Maltby (1961) have measured the fringe visibility of a large number of sources at 960 Mc/s. They used a number of different 'baselines, both NS and EW, with a maximum length of $1\,560\lambda$. By combining their observations with those reported in Paper II,

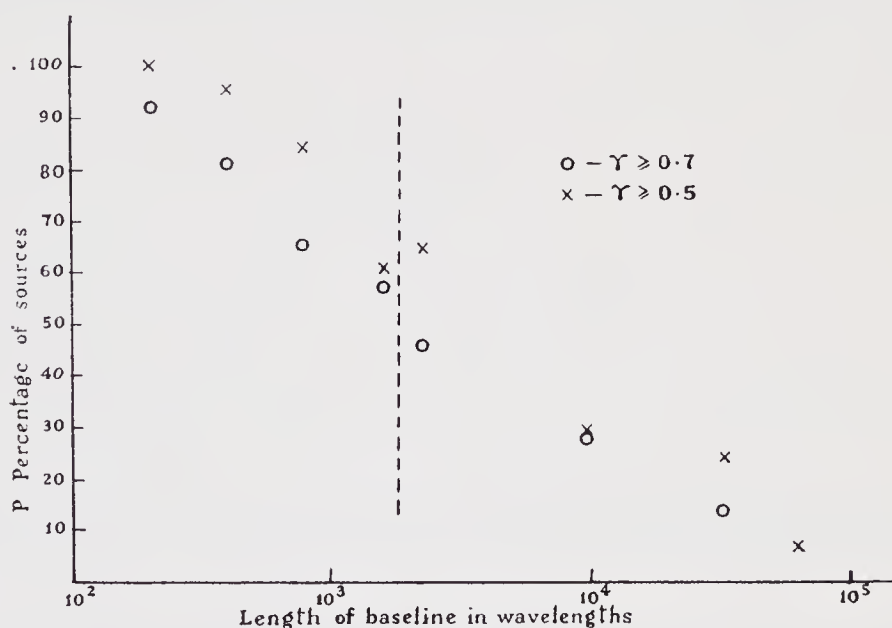


FIG. 5.—Data from Moffet (1961) and Allen *et al.* (1962) have been used to find the percentage P of sources with fringe visibility (a) $\gamma \geq 0.7$ and (b) $\gamma \geq 0.5$. These observations refer to the restricted group (described in the text) of 55 sources. The points derived from Moffet's data lie to the left of the dashed line.

it is possible to select a list of 55 sources which satisfy the following conditions. The sources are all listed in the Cambridge 3C catalogue as having a flux density $S \geq 12 \times 10^{-26} \text{ w.m}^{-2} (\text{c/s})^{-1}$ and all have a galactic latitude $|b^1| \geq 12^\circ$; furthermore they have been studied with both NS and EW baselines by Moffet and Maltby and also with at least two baselines by Allen *et al.* (Paper II).

Fig. 5 shows a statistical comparison of the fringe visibilities for these 55 sources given by the two different sets of data. The percentage P of sources which give values of fringe visibility greater than 0.5 and 0.7 is shown for the various baselines; it can be seen that the two sets of data form a reasonably smooth curve which resembles that of Fig. 2. A more detailed comparison of the two lists, taking individual sources, shows that the two lists are in good agreement in spite of the difference in observing frequency. We shall therefore assume in the subsequent analysis that these 55 sources are a representative sample of the larger group of 133 sources discussed in the previous section.

4.2. *Evidence for multiple sources.*—An examination of the fringe visibilities given by Moffet and Maltby for the 55 sources shows that 17 are probably multiple; that is to say, their fringe visibility passes through a significant minimum at a baseline shorter than $1\ 560\ \lambda$. For these sources observations are available in two position angles, and all the multiple sources with projected angular separations greater than $60''$ should have been recognized. It is also to be expected that a fraction of the multiple sources will have been overlooked because their axes of separation are parallel to the line of sight; however, a rough estimate shows that this fraction is unlikely to exceed about 20 per cent if the ratio of true spacing to component size is as low as 2 : 1, and is even less for greater ratios.

When the data of Moffet and Maltby are combined with the observations at the four long baselines, an additional 6 sources in the list of 55 are shown to be multiple. These sources have angular separations less than about $40''$ and the data from the long baselines refer only to their separation in position angle 90° . It is therefore likely that a greater fraction of multiple sources with small angular separations has been overlooked because of the very few long baselines which have been used.

To summarize, there is direct evidence that 23 of the 55 sources in the combined set are multiple, and it is likely that at least an additional 20 per cent have multiple structure not revealed by these measurements. It follows that approximately two-thirds of the sources in this group of 55 are multiple; the projected angular separation between their components lies in the range $10''$ to $600''$.

4.3. *Models of a source.*—The data in the previous section show that the majority of sources are multiple and have more than one major separated component. Furthermore, an examination of their visibility functions shows that many of them cannot be represented by a simple model of two identical disks with a uniform or gaussian intensity distribution. The data are insufficient to define any model closely, but they do suggest that in many of the sources there are major components which differ considerably in angular size.

An examination of the data for single sources, that is to say sources for which the fringe visibility decreases monotonically with baseline, suggests that very few can be represented by simple uniform or gaussian disks. For most of these sources, the distribution of intensity is markedly non-uniform and they appear to have bright regions which are small compared with the whole disk.

An attempt has been made by Palmer (1961) to represent these data in terms of a typical radio source. His model, which is illustrated in Fig. 6, consists of two separated components which may be of different size and surface brightness.

Each component has a bright central region which is surrounded by a more extensive disk of lower brightness. The distribution of brightness across both the extended disks and the bright central regions or cores is assumed to be gaussian. The associated visibility function, for the symmetrical case where the two components are identical, and with each core in the centre of its extended disk, is shown in Fig. 6.

Although this model is obviously of limited use, it does embody, in the simplest form, the two major features which are suggested by the observed visibility functions; namely, that most sources are multiple and that many have small bright regions. The number of parameters characterizing such a model is obviously too large to be defined by the present data; thus for each source there is one angle of orientation, five angular dimensions, and four values of surface brightness. Nevertheless, in the next section we shall discuss, bearing this general model in mind, what rough parameters for a typical radio source are consistent with the available data.

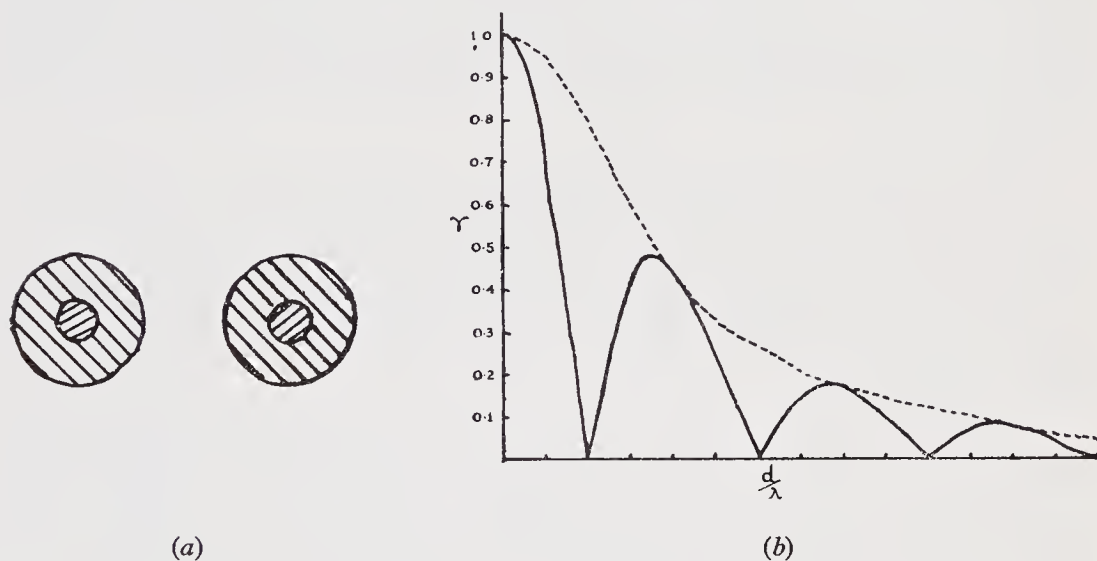


FIG. 6.—An example of the proposed model of radio source structure which has two identical separated components, each of which has a bright core in the centre of an extended disk of lower surface brightness. The visibility function for such a source has the form shown in (b) where the dotted line, showing the envelope of the function, is the visibility function of an isolated component of this type.

5. *The angular dimensions of the sources.*—The fringe visibilities for the 55 sources have been analysed to find the angular sizes of the radiating components and of the separations between the components. This analysis has been carried out by two different methods, neither of which is completely objective. In Method I an idealized visibility function was fitted to the observed values of γ ; two examples are shown in Fig. 7. Bearing in mind the general model in Fig. 6 an estimate was then made, from the *envelope* of this function, of the largest angular size which could be associated with a major component of the source. The angular size associated with the component separation was estimated by noting the position of the first significant minimum in the visibility function.

In Method II the smallest angular size which could be associated with any major component of the source was estimated from the longest baseline at which the fringe visibility $\gamma \geq 0.4$.

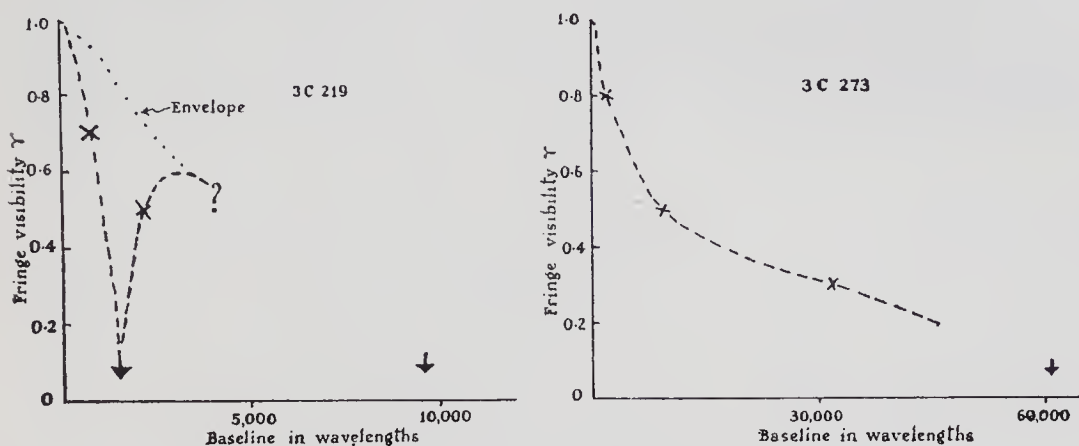


FIG. 7.—The observed values of fringe visibility for two sources. The dashed lines show possible forms of the visibility functions.

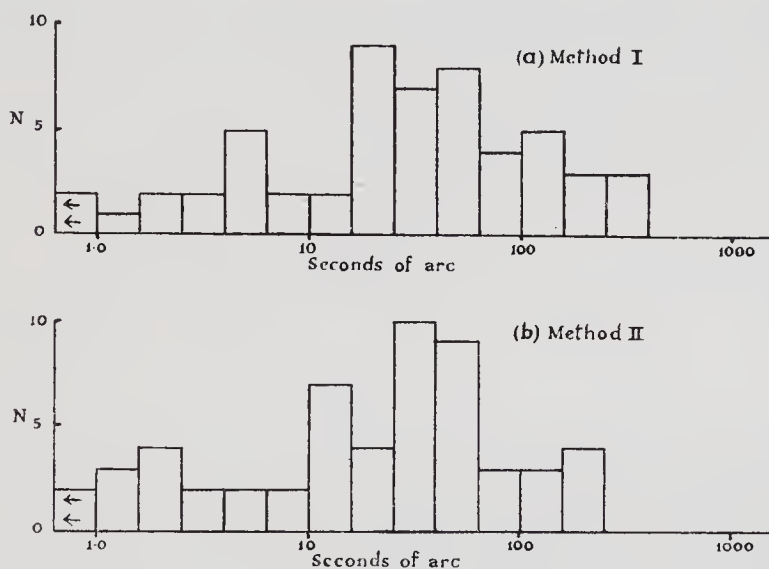


FIG. 8.—The two distributions of the angular dimensions of the major radiating areas of 55 sources derived by the Methods I and II described in the text.

Fig. 8 shows the results of these analyses. As expected, Method I yields a distribution of angular sizes which are somewhat greater than those given by Method II. In individual cases where a source has a bright small core, there are substantial differences between the component diameters given by the two methods. Nevertheless, the two methods yield similar general distributions, and we may conclude that the major components of these 55 sources have angular sizes dispersed over a range of at least 100:1 with a median value of about 30".

The angular separation between the components of these sources which could be clearly recognized as multiple are dispersed over the range $10''$ – $600''$ as shown in Fig. 9.

These sources are seen in projection, so that the median value of $120''$ should be increased by a factor of $\pi/2$ for Moffet and Maltby's data, and of 2.0 for the data from Paper II (for which the baselines were all close to East–West). On the other hand, a number of double sources were probably not recognized

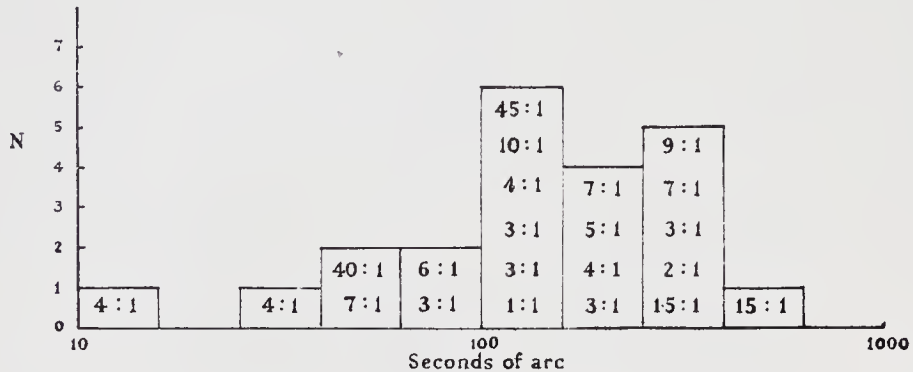


FIG. 9.—The distribution of the angular separations of the components of those sources, from the set of 55, in which double structure has been detected. The figures give the ratios of angular separation to component angular size (Method II, $\gamma \geq 0.4$).

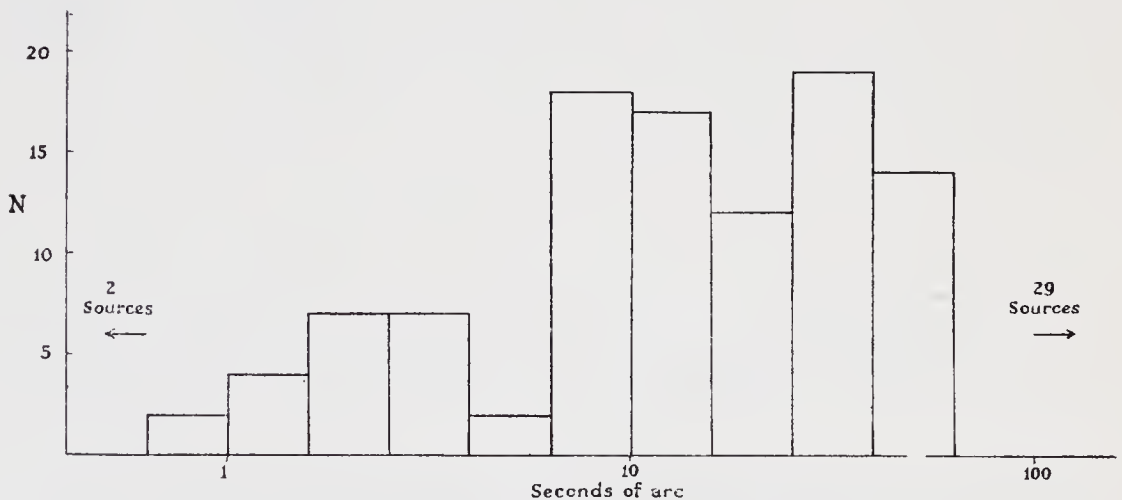


FIG. 10.—The distribution of angular dimensions (in position angle 90°) derived by Method II for a set of 133 sources having $S \geq 12$ f.u. and $|b^I| \geq 12^\circ$. Arrows indicate those sources which were completely unresolved or so much resolved that the value of fringe visibility γ did not exceed 0.4 at any of the long baselines.

in the observations of Paper II, and these additional cases, with small values, of angular separation, would reduce the median value. Until more complete data are available, $120''$ probably represents the best value which can be assigned to the median proper angular separation of double sources in this flux range. The ratio of median separation to median component size is therefore about

4 : 1. It is interesting to note that these ratios are not so widely dispersed as either the values of separation or component size, and this dispersion would probably be reduced by the corrections for projection.

In addition the angular sizes of the 133 sources measured by Allen *et al.* (Paper II) have been estimated. Since only four baselines were used it is not practicable to fit an idealized visibility function as in Method I and for this larger group, therefore, the results have been analysed by Method II. The resulting distribution is shown in Fig. 10 and is reasonably consistent with the distributions in Fig. 8 derived for the 55 sources. It must be remembered that the distribution for the 133 sources refers only to position angle 90° .

6. *The linear size of radio sources.*—For the small number of sources which have been identified photographically the linear size can be estimated from the red-shift of the associated Galaxy and the angular size of the radio source. Estimates of the linear size of 12 sources are shown in Table II. The red-shift data have been taken from the list given by Bolton (1960); the angular size θ of the sources has been derived from the fringe visibilities, as measured by Moffet (1961) and Maltby (1961) and by Allen *et al.* (Paper II), following the two methods described in the previous section. The tabulated values of the linear size W have been calculated from the distance and the angular size assuming a simple Euclidean universe in which the distance is directly proportional to the red-shift and $H = 100 \text{ km sec}^{-1} \text{ Mpc}^{-1}$. The red-shifts are so small that these simple assumptions are valid for all the principal cosmological models, except for the case of 3C295.

Table II shows that the linear sizes of almost all the sources lie in the range 5 kpc to 45 kpc and that their mean value is 27 kpc for Method I and 24 kpc for Method II. This result suggests that the average size of a component of a radio source is comparable with the average size of a Galaxy.

TABLE II
Component diameters and linear sizes of 12 identified radio sources

Radio source 3C No.	$v = \frac{cd\lambda}{\lambda}$	$z = \frac{d\lambda}{\lambda}$	Method I		Method II	
	km sec ⁻¹		θ_1''	W_1	θ_2''	W_2
				kpc		kpc
40	5325*	0.018	115	30	115	30
66	6450*	0.021	140	43	175	55
71	1030	0.003	9	0.45	9	0.45
75	7220*	0.024	115	41	47	16
84	5430	0.018	46	12	35	9
218	15900	0.053	54	42	60	46
270	1136	0.004	230	13	426	23
274	1136	0.004	330	18	70	4
278	4205	0.014	130	25	120	23
295	140000	0.467	5	35	3	20
338	8800	0.029	70	30	70	30
405	17100	0.057	42	35	42	35

* Revised red-shift data (Minkowski 1962).

Taking the mean ratio of separation to component diameter 4 : 1 as given in the previous section, the typical spacing between the components of double source models must be about 100 kpc.

7. *The distances and luminosities of the sources.*—At the present time the distances of the majority of radio sources are unknown, and the only sources for which the distances are established are the few which have been identified photographically. In view of the importance of this problem, particularly in relation to current discussions of cosmology, we shall now explore what general scale of distance is consistent with the available data on angular sizes.

In principle, the distance of a source, which we shall express in terms of the red-shift, can be determined from its apparent angular size if we know its proper linear dimensions. For very remote objects the theoretical relations between the apparent metric angular size θ , the flux density S , the red-shift z , and the power P (per unit bandwidth) radiated by the source depend upon the cosmological model. Following Mattig (1959) and Davidson (1959) we have evaluated these relations for the Einstein-de Sitter ($q_0 = +\frac{1}{2}$) and the steady-state ($q_0 = -1$) models as follows.

Einstein-de Sitter:

The observed flux density

$$S \propto \frac{P(1+z)^x}{((1+z)^{1/2}-1)^2}. \quad (2)$$

The metric angular diameter

$$\theta \propto \frac{W(1+z)^2}{(1+z-(1+z)^{1/2})}. \quad (3)$$

Steady-state:

$$S \propto \frac{P}{z^2(1+z)^{1-x}} \quad (4)$$

and

$$\theta \propto \frac{W(1+z)}{z} \quad (5)$$

where W is the linear size and x is the spectral index ($S \propto \nu^x$) of the source.

In Fig. 11 the observed angular sizes and flux densities of 133 sources are shown as a distribution of points. The angular sizes have been estimated by Method II from the data of Allen *et al.* (Paper II), and the flux densities are from the Cambridge 3C catalogue. The full lines show the theoretical relations for a steady-state model (equations (4) and (5)) for sources with luminosities of 10^{23} , 10^{26} and 10^{29} watts $(c/s)^{-1}$ ster $^{-1}$ at 160 Mc/s assuming a linear size for the radiating disks of 25 kpc. These values of luminosity correspond to absolute radio magnitudes (M_R) of -23.5 ; -31 and -38.5 and to central brightness temperatures of 3×10^4 , 3×10^7 and 3×10^{10} °K, assuming a gaussian distribution of intensity across the disk of the source. The broken lines show how the relationship is modified in an Einstein-de Sitter model (equations (2) and (3)).

Values of distance are also marked on the curves and are expressed as the red-shift parameter z .

It has been assumed in these calculations that the spectral index of the sources is -0.6 and that $H = 100$ km sec $^{-1}$ Mpc $^{-1}$. The absolute radio

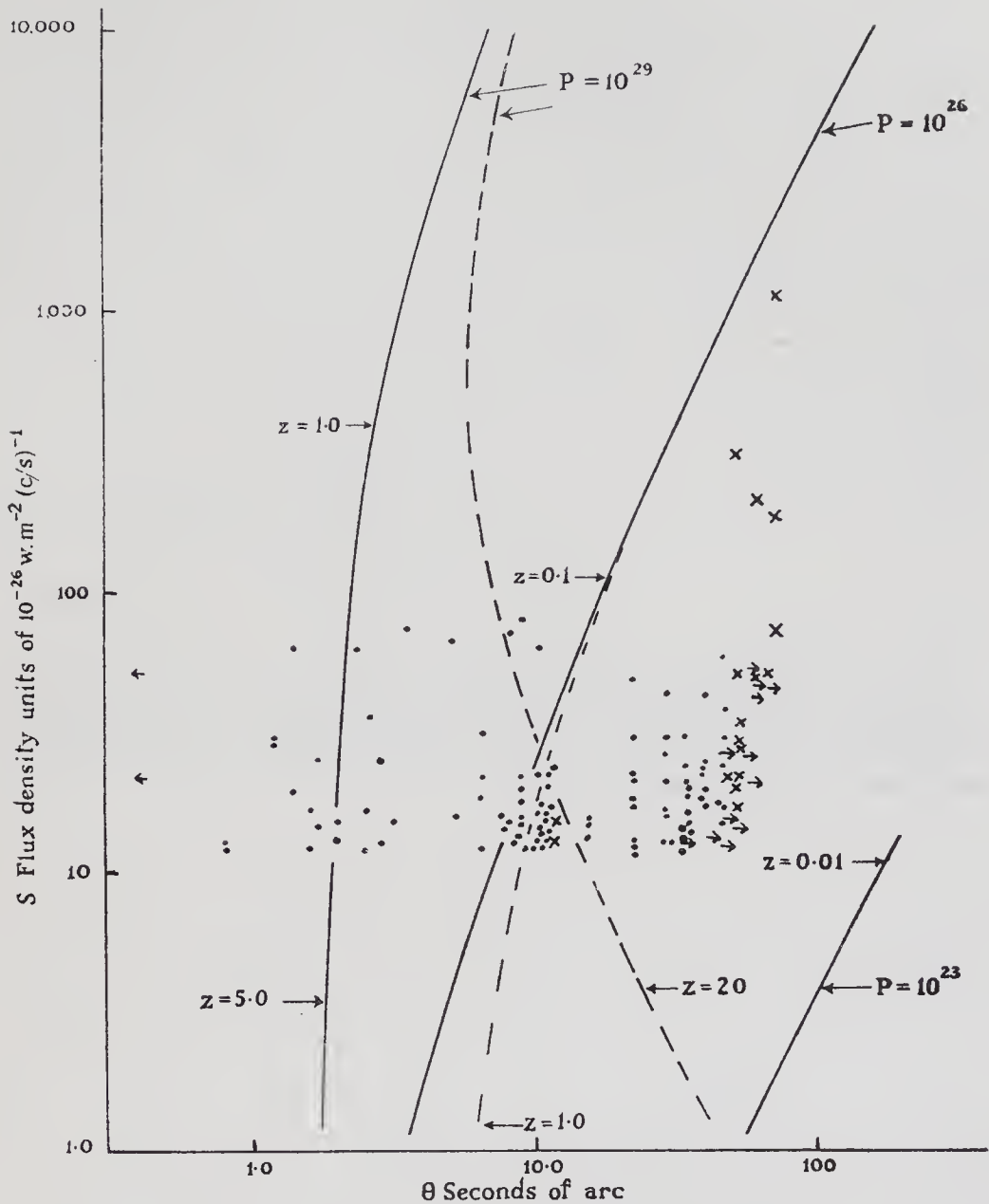


FIG. 11.—The observed angular sizes θ (derived by Method II) plotted against the values of flux density S from the 3C catalogue for 133 sources having $S \geq 12$ f.u. and $|b^l| \geq 12^\circ$. The full lines show the calculated relations for the steady-state cosmology for three values of absolute luminosity P , assuming a source component of linear size equal to 25 kpc. The dotted lines give the equivalent relations for the Einstein-de Sitter cosmology.

The crosses represent those sources for which a fringe pattern was seen but $\gamma < 0.4$ at all our baselines.

The arrows on the right of the diagram represent the sources for which no fringe pattern was seen at any of our baselines, while the arrows on the left represent those sources which were not resolved at any of our baselines.

magnitude of the sources is given at a frequency of 158 Mc/s, and has been derived from the apparent radio magnitude m_r as defined by the usual equation

$$m_r = -53.4 - 2.5 \log S_{158}$$

where S_{158} is the flux density of the source at 158 Mc/s.

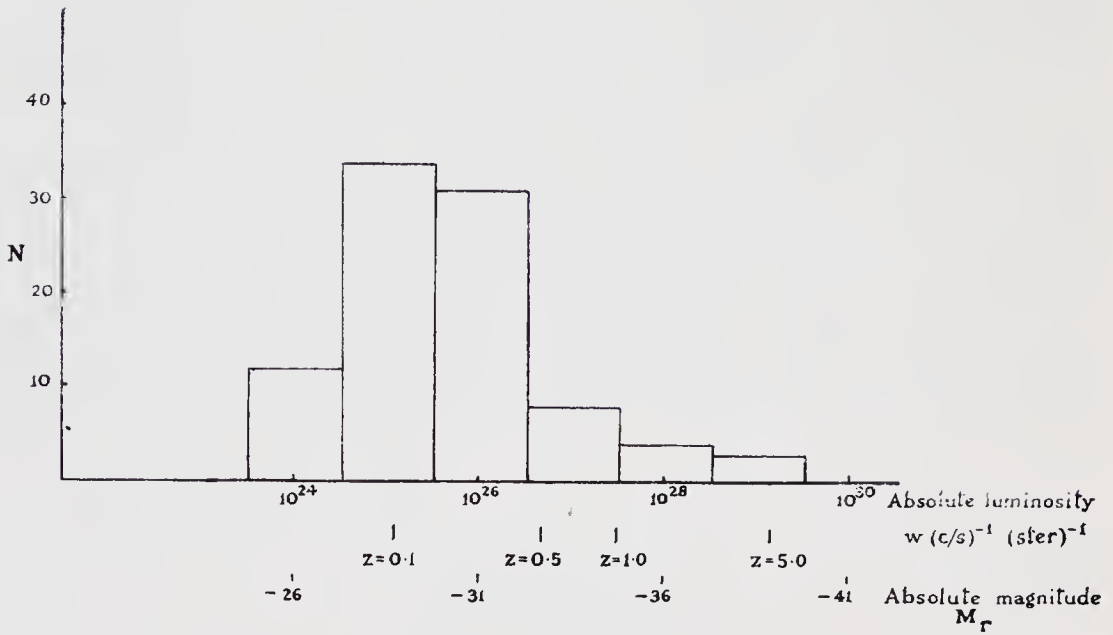


FIG. 12.—The distribution of absolute luminosities, assuming a steady-state model universe. Of the 39 sources which have been omitted from this diagram, 29 gave no observed value of fringe visibility greater than 0.4 at any baseline, while 10 had diameters less than the calculated asymptotic diameter for a source component of linear size equal to 25 kpc. The scale of red-shift z refers to sources having the limiting flux density $S=12$ f.u.

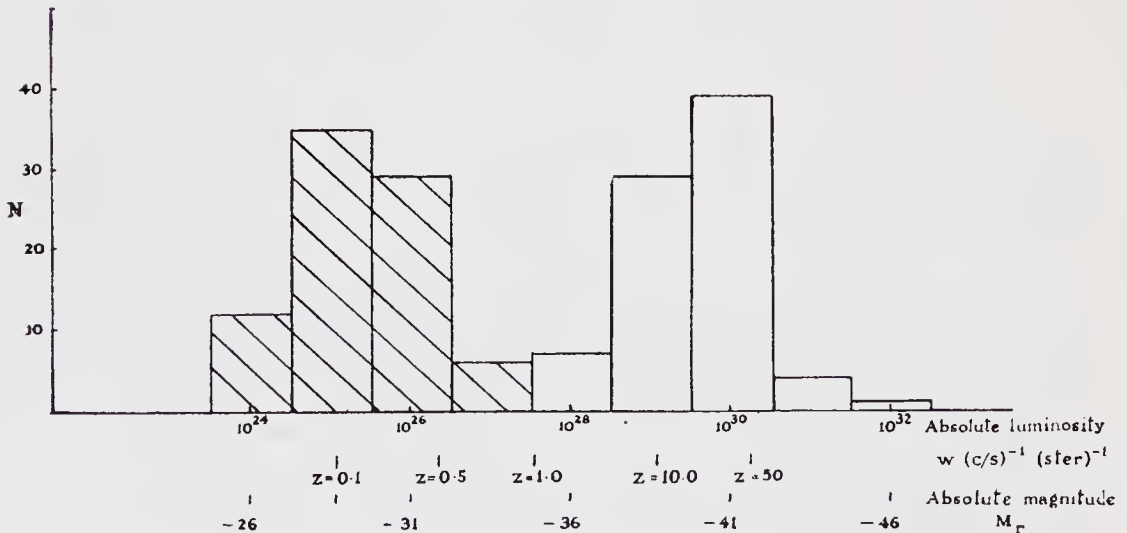


FIG. 13.—Two possible distributions of absolute luminosity assuming an Einstein-de Sitter model universe. There are two values of P and red-shift z , associated with each observed component angular diameter greater than $5''.5$. The absolute luminosities calculated from the lower value ($z < 1.25$) are plotted in the shaded area of the diagram and the absolute luminosities calculated for the higher value ($z > 1.25$) are plotted in the unshaded part. The scale of red-shift z refers to sources having the limiting flux density $S=12$ f.u.

A comparison of the observed distributions with the theoretical curves suggests that the luminosities of the majority of sources lie between 10^{24} and 10^{27} and that the majority have a red-shift $z < 1$. The most frequent value of luminosity is about 10^{25} ($M_R \sim -28$) corresponding to a central brightness temperature for a gaussian disk of 3×10^6 °K. In making this estimate it has been assumed, as discussed later, that the majority of the sources do not lie beyond the equator of the Einstein-de Sitter model.

These conclusions are illustrated in Fig. 12 for the case of the steady-state model. The histogram shows the distribution of luminosities and distances among the 133 sources. The distribution was calculated from equations (4) and (5) taking the linear size of the sources to be 25 kpc, the angular size θ to be that given by the fringe visibilities in Paper II as analysed by Method II, the flux density S to be that given in the Cambridge 3C catalogue and the spectral index α to be -0.6 . The scale of luminosity is shown in terms of the power P radiated by the source in watts $(\text{c/s})^{-1} \text{ster}^{-1}$ at 15^3 Mc/s, and also the absolute radio magnitude M_R . The scale of red-shift z refers to sources having the limiting flux density $S = 12$ f.u.

Fig. 13 shows the distribution of luminosities and distances calculated for the Einstein-de Sitter model from equations (2) and (3). Since in this model the apparent angular size of a source passes through a minimum at the equator there are two possible values for the distance and luminosity of each source. The shaded part of the histogram corresponds to the assumption that all the sources are closer to the observer than the equator, while the unshaded distribution corresponds to the assumption that they all lie beyond. The scale of red-shift z refers to sources having the limiting flux density $S = 12$ f.u.

8. *Discussion.*—A marked feature of the distributions in Figs. 12 and 13 is the sharp cut-off at a value of $P = 10^{24}$ watts $(\text{c/s})^{-1} \text{ster}^{-1}$, which is probably caused by observational selection. The sources studied by Allen *et al.* (Paper II) were taken from the Cambridge 3C catalogue. However the angular sizes θ were derived by Method II so that no values greater than $47''$ have been used to calculate absolute luminosities ($47''$ corresponds to a fringe visibility $\gamma = 0.4$ at 2200λ). Of the group of 133 sources, 14 gave no fringe pattern at any baseline. The lower limits to their angular sizes are indicated by arrows in Fig. 11. These sources, and fifteen others for which no value of $\gamma \geq 0.4$ was observed at any baseline, have been omitted from Figs. 12 and 13. There is a corresponding cut-off in the distributions of absolute magnitude shown in Figs. 12 and 13 at about 10^{24} watts $(\text{c/s})^{-1} \text{ster}^{-1}$.

We may therefore conclude, tentatively, that the typical luminosity among radio sources observed with flux density $S \geq 12$ f.u. is less than 10^{26} watts $(\text{c/s})^{-1} \text{ster}^{-1}$ ($M_r = -31$), and probably lies lower than 10^{25} watts $(\text{c/s})^{-1} \text{ster}^{-1}$. This latter luminosity corresponds roughly to $1/300$ of the value for Cygnus A. These luminosities have been calculated for sources of mean linear size 25 kpc. If this mean value were increased by a factor of 3 the minimum angular diameter expected would be increased by the same factor in both cosmologies. On Fig. 12 the scale of P would be moved towards higher values by approximately one decade except for the minority of sources with $P \geq 10^{26}$ watts $(\text{c/s})^{-1} \text{ster}^{-1}$ where the factor would be greater than 10. In an Einstein-de Sitter universe (Fig. 13) sources would be interpreted as nearer the equator ($z = 1.25$), and a larger fraction would be observed to have angular

sizes smaller than the expected minimum. A decrease in the mean linear size would have the opposite effect.

This conclusion is compatible with limiting the luminosity function shown in Fig. 14 (a) derived by Ryle and Clarke (1961) from radio data alone. However, it is markedly inconsistent with previous attempts to derive the radio luminosity function by combining the radio and photographic data. Thus Minkowski (1960), Bolton (1960), Long and Marks (1961) and Ryle and Clarke (1961) have concluded that the typical radio luminosity of a source is much greater than the value suggested above. For example, Ryle and Clarke conclude that the typical luminosity of radio sources with $S \geq 2$ f.u. lies in the range 10^{24} to 10^{27} and they have used a (presumably "typical") value of 2×10^{26} in theoretical examples. This is at least 20 times the value 10^{25} watts $(\text{c/s})^{-1} \text{ster}^{-1}$ suggested above.

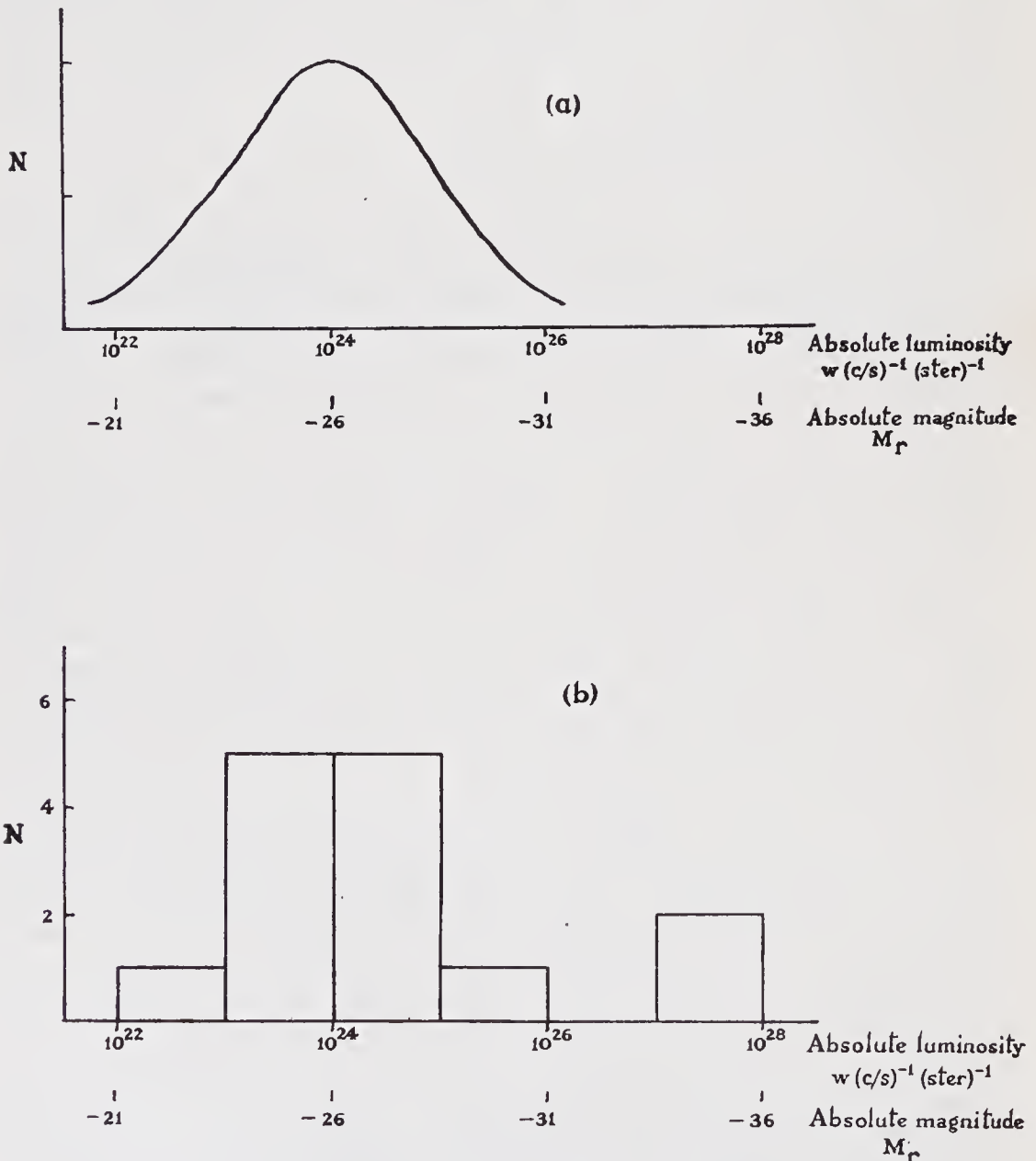


FIG. 14.—(a) The limiting distribution of absolute radio magnitude derived by Ryle and Clarke (1961). (b) The distribution of absolute radio magnitude for the 14 identified radio sources for which a red-shift measurement is available.

It is not clear why there should be this serious discrepancy between these two lines of enquiry; however, it must be noted that they both depend heavily on the observed properties of the very few identified sources and it is possible that they are seriously affected by observational selection. A discussion of this problem is too lengthy for the present paper and has therefore been given in a companion paper (Hanbury Brown 1962).

Finally, there are two more interesting questions raised by Figs. 11, 12 and 13. The first of these concerns the two histograms in Fig. 13 for the Einstein-de-Sitter model. The ambiguity in distance and luminosity shown by this model is, of course, characteristic of all the simple relativistic models with $q_0 \geq \frac{1}{2}$. Clarke (1962) has also discussed this ambiguity, and has concluded that, because of the small number of identifications so far made, most of the extragalactic radio sources are in fact beyond the equator of this cosmology, with typical luminosities of $P \simeq 3 \times 10^{29}$ watts $(c/s)^{-1} \text{ster}^{-1}$. However, at the present time the information about the identified sources shown in Fig. 14 (b) suggests that we should accept the "nearby" interpretation of the radio data. We must therefore look for some other explanation for the difficulty of making identifications, such as the lower value of mean absolute photographic magnitude $M_p \simeq -18$, suggested by Hanbury Brown (1962), or a marked difference between the optical and radio sizes and structures, which is already apparent for the few sources which have been identified. We cannot, of course, exclude the possibility that some of the sources may be of extremely high luminosity and that for them the "distant" solution is correct.

The second question concerns the few sources with very small diameters. For example, in Fig. 10 there are 10 which have an angular size less than the asymptotic limit ($1''.7$) for objects of size 25 kpc in the steady-state model, and there are 22 with a diameter less than the minimum value ($5''$) in an Einstein-de Sitter model. If there were no dispersion in the linear size of radio sources or if we knew this dispersion precisely, then it would be possible to discriminate between certain cosmological models on the basis of data about angular size. In particular we might be able to rule out a range of models simply by observing the apparent cut-off in the angular size distribution for small diameters. However, this cannot yet be done because of the uncertainty about the dispersion in linear sizes, and also because we cannot be sure that our source population does not include some small diameter sources of a radically different type. For example, source 3C48, which has an angular size of less than $1''$, has been provisionally identified with a peculiar star in the Galaxy, and it is not known how many other small diameter sources are of the same type.

9. *Conclusions.*—The analysis presented above shows that, if we consider sources with $S \geq 12 \times 10^{-26}$ w.m $^{-2}$ $(c/s)^{-1}$, about 90 per cent of these sources can be resolved with a baseline of $30\,000 \lambda$ and the median angular size of their radiating disks is about $30''$. The majority of sources appear to be complex and many have more than one radiating centre. There appears to be a considerable dispersion, at least 10 : 1, in their linear size and a much greater dispersion, at least 10^4 : 1, in their luminosity.

A tentative analysis of the data indicates that the majority of these sources lie at distances where the red-shift parameter $z < 1$, and that they have luminosities which are less than 10^{25} watts $(c/s)^{-1} \text{ster}^{-1}$ (i.e. less than $0.003 P_{\text{Cyg}}$). This result is markedly inconsistent with the conclusions reached in other work which is

based on a combination of radio and photographic data. It is clear that the chief weakness in all discussions of the radio luminosity function is the lack of optical identifications, and it is of considerable importance that the work of "identifying" radio sources should be pursued.

Finally, there is an urgent need for more comprehensive radio data. The complexity of the fringe visibility functions makes it impossible to draw any firm conclusions about the structure, types and characteristic parameters of sources from observations carried out at a few baselines. It is therefore important that the angular distribution of intensity across a considerable number of sources should be measured in detail, which can only be done with a large number of baselines of different lengths and orientations.

*Nuffield Radio Astronomy Laboratories,
Jodrell Bank,
Macclesfield,
Cheshire:*
1962 July 17.

References

- Allen, L. R., Anderson, B., Conway, R. G., Palmer, H. P., Reddish, V. C., and Rowson, B., 1962, *M.N.*, **124**, 477.
 Bolton, J. G., 1960, 13th General Assembly, U.R.S.I., London.
 Brown, R. Hanbury, 1962, *M.N.*, **124**, 35.
 Clarke, R. W., 1962, *Nature*, **194**, 171.
 Davidson, W., 1959, *M.N.*, **119**, 54.
 Edge, D. O., Shakeshaft, J. R., McAdam, W. B., Baldwin, J. E., and Archer, S., 1959, *Mem. R.A.S.*, **68**, 37.
 Elgaroy, O., Morris, D., and Rowson, B., 1962, *M.N.*, **124**, 395.
 Long, R. J., and Marks, V. B., 1961, *M.N.*, **122**, 61.
 Maltby, P., 1961, *Observations of the California Institute of Technology Radio Observatory*.
 Moffet, A. T., 1961, *Observations of the California Institute of Technology Radio Observatory*.
 Mattig, W., 1959, *A.N.*, **285**, 1.
 Mills, B. Y., Slee, O. B., and Hill, E. R., 1958, *Austr. J. Phys.*, **11**, 360.
 Minkowski, R., 1960, *Proceedings of the 4th Symposium on Mathematical Statistics and Probability*, Berkeley.
 Minkowski, R., 1962, private communication.
 Palmer, H. P., 1961, I.A.U. Symposium No. 15 on *Problems of Extra-Galactic Research*.
 Ryle, M., 1962, private communication.
 Ryle, M., and Clarke, R. W., 1961, *M.N.*, **122**, 349.

A New Type of Interferometer for Use in Radio Astronomy

By R. HANBURY BROWN

Jodrell Bank Experimental Station, Cheshire

and

R. Q. TWISS

Services Electronics Research Laboratory, Baldock, Herts.*

[Received March 20, 1954]

SUMMARY

A new type of interferometer for measuring the diameter of discrete radio sources is described and its mathematical theory is given. The principle of the instrument is based upon the correlation between the rectified outputs of two independent receivers at each end of a baseline, and it is shown that the cross-correlation coefficient between these outputs is proportional to the square of the amplitude of the Fourier transform of the intensity distribution across the source. The analysis shows that it should be possible to operate the new instrument with extremely long baselines and that it should be almost unaffected by ionospheric irregularities.

§1. INTRODUCTION

At the present time more than one hundred discrete sources of extra-terrestrial radio-frequency radiation have been observed, and it is to be expected that this number will increase rapidly as the sensitivity and resolving power of current equipment is improved. A knowledge of the angular sizes of the discrete sources is fundamental to their general study and is of particular importance to their identification with objects observed photographically.

The first attempts to measure the angular size of the two most intense sources were unsuccessful since they proved to be below the resolving power of the instruments then available. Thus Bolton and Stanley (1948), using a 'Lloyds Mirror' interferometer mounted on a cliff, showed that the apparent diameter of the intense source in Cygnus is less than 8 minutes of arc; while Ryle and Smith (1948), using a 'Michelson' interferometer with a baseline of 500 m, showed that the intense sources in Cygnus and in Cassiopeia both have angular diameters less than 6 minutes of arc. Stanley and Slee (1950), using a similar equipment to that used by Bolton and Stanley, gave a limit of 1.5 minutes of arc for the angular diameter of the source in Cygnus.

The problem of improving upon the resolving power used in these previous measurements was reviewed in 1949, and an examination of the

* Communicated by Professor A. C. B. Lovell.

existing instruments suggested that a considerable improvement could readily be made by extending the baseline of the 'Michelson' type of interferometer. It was estimated, as discussed in § 2, that the baseline might be extended to about 50 km without great difficulty, but that an extension to distances of 100 km or more would involve elaborate equipment. Since at that time it was assumed that the angular sizes of the discrete sources might be comparable with those of the visible stars, the maximum resolving power was sought and a new type of interferometer for use with extremely long baselines was proposed by one of the authors (R.H.B.).

The present paper discusses only the principle and mathematical theory of the new interferometer; a preliminary account of the experimental results has already been published (Hanbury Brown, Jennison and Das Gupta 1952), and a more detailed discussion of these results and of the apparatus will be given elsewhere (Jennison and Das Gupta, in preparation).

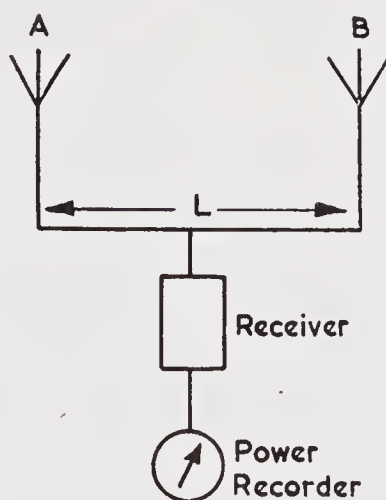
§ 2. THE 'MICHELSON' INTERFEROMETER

The application of the 'Michelson' interferometer to radio astronomy has been discussed by McCready, Pawsey and Payne-Scott (1947) and also by Ryle (1950). A brief description of its theory will be given here for comparison with that of the new instrument described in § 3.

2.1. *The Theory of the 'Michelson' Interferometer*

A simplified diagram of a 'Michelson' interferometer is shown in fig. 1. Two aerials A and B, separated by a horizontal baseline of length L , are joined by a cable; the centre of the cable is connected to a receiver, the

Fig. 1



The 'Michelson' type of radio interferometer.

output of which is recorded. When a discrete source transits the plane normal to the baseline the receiver output exhibits oscillations, as shown in fig. 2, which correspond to the fringes observed in a stellar interferometer. The amplitude and phase of these oscillations will be calculated

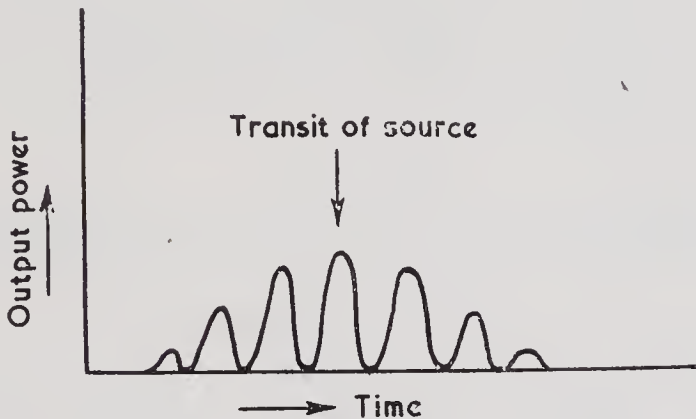
for the simple case shown in fig. 3, where the source is a narrow strip FG coplanar with the baseline of the interferometer AB. Since the distance of the source is much greater than the length of the baseline, the relative phase of the voltages received by the two aerials from a radiating element *E* at an angle θ from the line CD, is

$$(\omega_0 L/c) \sin (\theta + \theta_0),$$

where ω_0 is the angular frequency to which the receiver is tuned, and θ_0 is the angle between CD and a plane normal to the baseline. If the receiver output is linearly proportional to the input power, the interaction of these two voltages produces a term in the receiver output proportional to

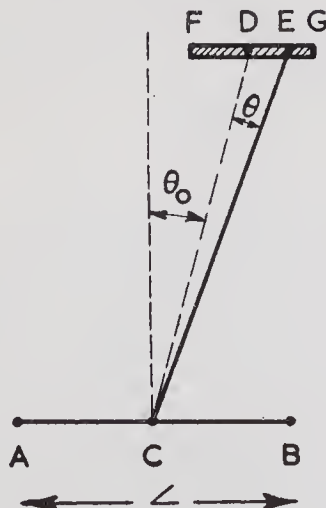
$$P(\theta) \cos [(\omega_0 L/c) \sin \overline{\theta_0 + \theta}] d\theta,$$

Fig. 2



The variation of output power during the transit of a source, as observed with a 'Michelson' type interferometer.

Fig. 3



The geometry of the 'Michelson' type interferometer.

where $P(\theta) d\theta$ is the power received from the element *E* at angular frequency ω_0 . The receiver output due to the signal from the whole source is given by

$$K \sim \int_{-\alpha/2}^{\alpha/2} P(\theta) \cos [(\omega_0 L/c) \sin \overline{\theta_0 + \theta}] d\theta, \quad . . . (1)$$

where α is the maximum angular extension of the source. If $\alpha \ll 1$, so that $\sin \theta \simeq \theta$ and $\cos \theta \simeq 1$ for $|\theta| < \alpha$, eqn. (1) may be expanded to give

$$K(l) = F_{\cos} \left(\frac{\omega_0 l}{c} \right) \cdot \cos \left(\frac{\omega_0 l \tan \theta_0}{c} \right) - F_{\sin} \left(\frac{\omega_0 l}{c} \right) \cdot \sin \left(\frac{\omega_0 l \tan \theta_0}{c} \right), \dots \quad (2)$$

where l is the length of the baseline projected on to the plane perpendicular to CD and where

$$l = L \cos \theta_0, \dots \dots \dots \quad (3)$$

$$\left. \begin{aligned} F_{\cos} \left(\frac{\omega_0 l}{c} \right) &= \int_{-\alpha/2}^{\alpha/2} P(\theta) \cos \left(\frac{\omega_0 l \theta}{c} \right) d\theta, \\ F_{\sin} \left(\frac{\omega_0 l}{c} \right) &= \int_{-\alpha/2}^{\alpha/2} P(\theta) \sin \left(\frac{\omega_0 l \theta}{c} \right) d\theta. \end{aligned} \right\} \dots \dots \quad (4)$$

Equation (2) shows that the output of the receiver oscillates sinusoidally as the angle θ_0 varies, and that the relative amplitude and phase of the oscillations observed with different baselines is given by the Fourier transform of the angular distribution of intensity across the source. For a baseline of zero length,

$$K(0) = F_{\cos}(0), \dots \dots \dots \quad (5)$$

and $K(0)$ is proportional to the total power received from the source.

The modulus of the ratio $K(l)/K(0)$ is called the *correlation coefficient* $\rho(l)$, where*

$$\rho(l) = \frac{[F_{\cos}^2(\omega_0 l/c) + F_{\sin}^2(\omega_0 l/c)]^{1/2}}{F_{\cos}(0)} \dots \dots \dots \quad (6)$$

In principle it is possible to determine the shape of the distribution of intensity across the source by measuring the relative amplitude and phase of the oscillations with different baselines ; however, the measurement of the relative phase presents considerable experimental difficulty and so far has not been attempted. If the relative amplitude only and not the phase of the oscillations is measured, it is no longer possible to determine the distribution across the source uniquely and some *a priori* assumptions about its general shape must be made.

2.2. The Resolving Power of a ' Michelson ' Interferometer

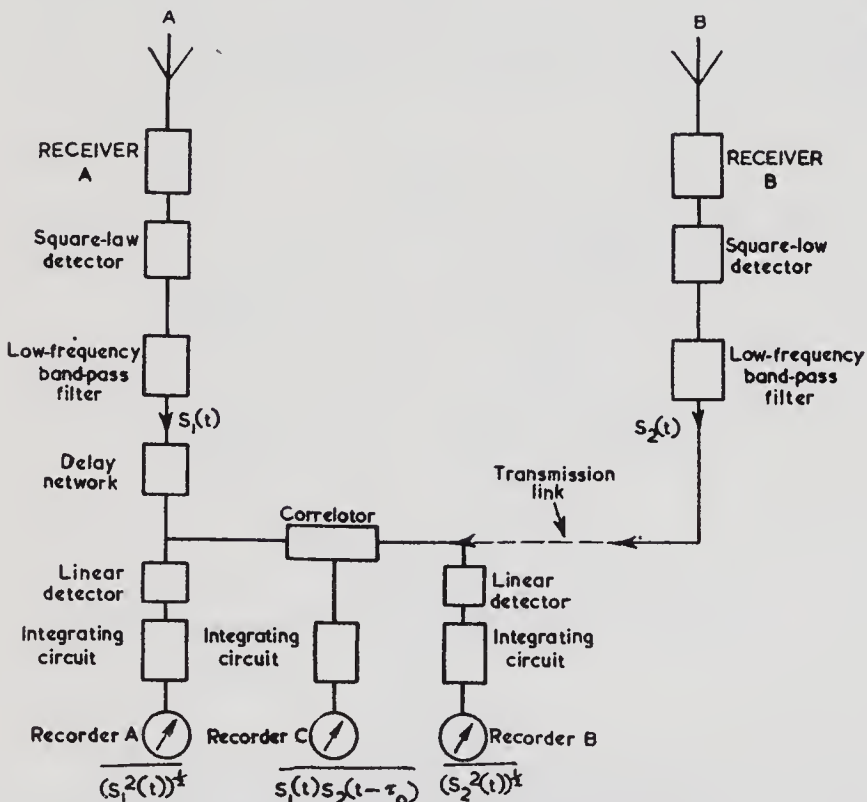
The resolving power of an interferometer is of the order of (λ/l) and can therefore be improved either by extending the baseline or by decreasing the wavelength. At the time the problem was reviewed a substantial improvement in resolving power by the use of shorter wavelengths was not regarded as practicable, since the intensity of the discrete sources was known to decrease with wavelength while the construction of large aerials and sensitive receivers becomes increasingly difficult as the wavelength is decreased ; furthermore it is desirable to know the effective diameter of a source as a function of frequency. The alternative possibility of extending

* This result has been derived for a single frequency and only applies to a practical interferometer if the fractional radio-frequency bandwidth is sufficiently small.

the baseline was therefore considered; initially in relation to the 'Michelson' interferometer.

The baseline of the simple instrument shown in fig. 1 is limited to a few hundred metres by attenuation in the cable between the aerials. This can be overcome by a variety of techniques of which the simplest is the use of radio-frequency amplifiers at both ends of the cable; however, for baselines exceeding about 1 km a cable is both cumbersome and expensive and may advantageously be replaced by a radio link. It is difficult to estimate the maximum length of baseline over which such a link may be used since it depends on the location of the equipment and on details of the installation; nevertheless, it seems likely that in practice the maximum length

Fig. 4



Block diagram of new type of interferometer.

would be limited by instability of phase in the transmission. If the diameter of a source is to be measured reliably, any variations introduced by the equipment into the relative phase of the signals must be slow compared with the period of oscillation of the receiver output, and the published data on short wave propagation suggest that rapid and significant changes of phase may be expected with baselines exceeding 25-50 km unless the equipment is restricted to special sites and operating times. For this reason it was decided to adopt a new technique, specifically designed to reduce the requirements for phase stability in the link, which promised simple and reliable operation with baselines considerably in excess of 25-50 km.

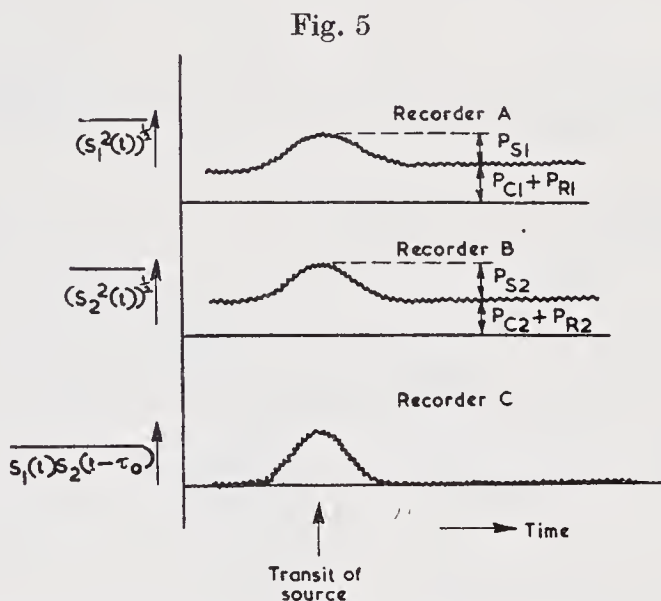
§ 3. DESCRIPTION OF THE NEW TYPE OF INTERFEROMETER

A simplified diagram of the equipment is given in fig. 4. Two aerials, A and B, feed two independent receivers tuned to the same frequency with identical band-pass characteristics. The output of each receiver is rectified in a *square-law* detector and is fed to a low-frequency band-pass filter. The outputs $S_1(t)$, $S_2(t)$ of these filters are combined in a correlator the output of which is passed, via an integrating circuit of bandwidth b_I , to a pen recording the time-dependent signal

$$K(t) = \overline{S_1(t) \cdot S_2(t - \tau_0)}, \quad (7)$$

where τ_0 is a delay time, discussed later, and the bar denotes the averaging process in the integrating circuit.

The outputs of the two filters are also rectified in *linear detectors* and passed, via integrating circuits also of bandwidth b_I , to two additional pens recording the values of $[S_1^2(t)]^{1/2}$ and $[S_2^2(t)]^{1/2}$.



The type of records obtained with the new type of interferometer during the transit of a source.

The appearance of the records obtained from a discrete source is shown in fig. 5. The envelopes of the three curves correspond to the variation of the power received as the source passes through the polar diagram of the aerials, and it can be seen that none of the records exhibit the oscillations observed with a 'Michelson' interferometer. The output of each receiver is proportional to the sum of the signal power received from the source P_S , the noise power generated by the receiver itself P_R , and the cosmic noise power P_C due to the general radiation from the area of sky covered by the aerial beam. The two latter components have been represented in fig. 5 as a steady displacement of the records of $[S_1^2(t)]^{1/2}$ and $[S_2^2(t)]^{1/2}$

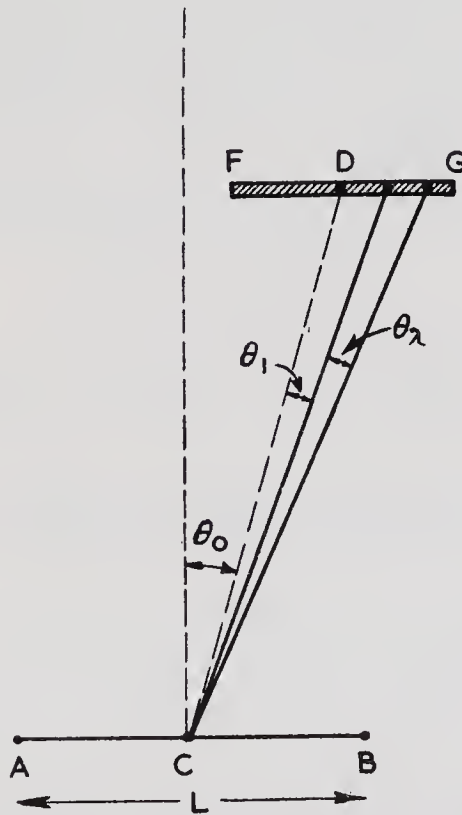
since, for the purpose of the diagram, it has been assumed that both the cosmic and receiver noise remain constant during the observation. The mean deflection of the record of $S_1(t) \cdot S_2(t-\tau_0)$ is due to the radiation from the source alone since the receiver noise in the two channels is independent and the cosmic noise, for most practical values of the baseline, is effectively uncorrelated.

From the three records of the transit of a source the *normalized correlator output*,

$$c(l, t) \equiv \frac{S_1(t) \cdot S_2(t-\tau_0)}{\{[S_1^2(t)]^{1/2} - P_{N1}\} \{[S_2^2(t)]^{1/2} - P_{N2}\}}, \quad \dots (8)$$

is calculated at any time t where P_{N1}, P_{N2} are the average values of the

Fig. 6



The geometry of the new type of interferometer.

low-frequency filter outputs observed when the source is outside the aerial beam. $C(l)$ the mean value of $c(l, t)$ is found by averaging over an arbitrarily large number of complete transits of the source. The measurements are then repeated with a number of different lengths of the baseline and the resulting values are used to determine the angular distribution of intensity across the source by means of eqn. (32).

The first equipment of this type has two aerials each with an aperture of 500 m², the receivers are tuned to 125 Mc/s with a pre-detector bandwidth of 200 kc/s and the band-pass of the low-frequency filters extends

from 1–2.5 kc/s. The correlator is sited for convenience at one end of the baseline and the low-frequency signals from the remote station are transmitted along the baseline as amplitude modulation of the carrier of a radio link. To compensate for the time taken for the signals to travel along the baseline and for the difference in the time of arrival of the signals at the two aerials when the direction of the source is not normal to the baseline, an adjustable delay is inserted between one equipment and the correlator.

§ 4. THE PRINCIPLE OF THE NEW INTERFEROMETER

It was shown in § 2 that the ‘ Michelson ’ interferometer can be analysed by considering the radiation at a *single* frequency from a *single* point in the source. The interaction of radiation from different points in the source or of signals at different frequencies can be neglected, since, as long as they are uncorrelated, they contribute nothing to the average value of the output. In an equivalent analysis of the new type of interferometer it is necessary to consider signals of *different* frequencies ω , ω' emitted by *different* points in directions θ_ν , θ_λ respectively.

The contribution to the output of the square-law detector at A due to the interaction of these two components is proportional to

$$\cos (\overline{\omega-\omega'} \cdot t - \Psi_1),$$

and the phase Ψ_1 of this beat-frequency is given by

$$\Psi_1 = \phi_\nu(\omega) - \phi_\lambda(\omega') + \frac{R_0}{c} \left[\overline{\omega-\omega'} \left(1 + \frac{L \sin \theta_0}{2R_0} \right) + \frac{L \cos \theta_0}{2R_0} (\theta_\nu \omega - \theta_\lambda \omega') \right] \quad (9)$$

where $\phi_\nu(\omega)$, $\phi_\lambda(\omega')$ are the radio-frequency phases at the source and R_0 is the distance from the midpoint of the baseline to a fixed point in the source.

Similarly the output of the detector at B contains a beat-frequency proportional to $\cos (\overline{\omega-\omega'} \cdot t - \Psi_2)$, where the phase Ψ_2 is given by

$$\Psi_2 = \phi_\nu(\omega) - \phi_\lambda(\omega') + \frac{R_0}{c} \left[\overline{\omega-\omega'} \left(1 - \frac{L \sin \theta_0}{2R_0} \right) - \frac{L \cos \theta_0}{2R_0} (\theta_\nu \omega - \theta_\lambda \omega') \right] \quad (10)$$

The difference in phase $\Delta\Psi$ between these two beat-frequencies is given by

$$\Delta\Psi = \overline{\omega-\omega'} \frac{L \sin \theta_0}{c} + \frac{L \cos \theta_0}{c} (\omega \theta_\nu - \omega' \theta_\lambda). \quad (11)$$

The first term in eqn. (11) represents the difference in the time of arrival of the signals at the two aerials. In principle it can be made zero by inserting a compensating delay $\tau_0 = L \sin \theta_0 / c$ in the appropriate receiver channel. In this case the difference in phase between the two beat-frequencies may be written

$$\Delta\Psi = l/c [\omega \theta_\nu - \omega' \theta_\lambda], \quad (12)$$

where l , defined in eqn. (3), is the projected length of the baseline normal to the direction of the source.

Equation (12) shows that the difference in phase between the two beat-frequency components at the detectors is equal to the difference between the relative phase of the two radio-frequency components in each aerial. Thus, although the use of two independent receivers destroys all information about the absolute phase in either aerial of any single radio-frequency component, information about the angular size of the source is preserved by the relative phase of corresponding beat-frequencies in the detector outputs.

If their frequency ($\omega - \omega'$) lies within the bandwidth of the low-frequency filters, the two beat-frequencies are transmitted to the correlator where they are multiplied together and form a direct current output proportional to the cosine of their phase difference. It is shown in the next section that the total direct current output from the correlator is the sum of the outputs due to all the beat-frequencies produced by the interaction of all pairs of points in the source. It is further shown that the correlator output, when suitably normalized, is equal to the square of the correlation coefficient measured by the 'Michelson' interferometer. Hence, by measuring the normalized correlator output with different lengths of baseline, it is possible to obtain information about the distribution of intensity across an equivalent line source coplanar with the baseline.

§ 5. MATHEMATICAL THEORY

5.1. *A Model Radio Source*

It is assumed that a discrete radio source can be divided into a system of regions each very small compared with the resolving power of the interferometer, yet large enough to ensure that the total radio-frequency power generated in any one region has the overall characteristics of thermal radiation and is independent of the power generated in any other region.* As long as the baseline of the interferometer is fixed in space and provided that the angular dimensions of the source are not too large, the actual three-dimensional distribution of intensity in the source cannot be distinguished from that of an equivalent line source coplanar with the baseline. For simplicity we shall consider this idealized case and shall use a Cartesian system of coordinates in which the equivalent line source is parallel to the x axis and the z axis lies along the line joining a fixed point in the source to the midpoint of the baseline. The coordinates of the receiving aerials A, B are then $(-l/2, 0, -l \tan \theta_0/2)$ and $(l/2, 0, l \tan \theta_0/2)$ respectively, where l is related to the baseline length L by eqn. (3).

The field radiated by a region at an angle θ from the axis has components which may be represented by the stationary time series,

$$\sum_{r=0}^{\infty} \frac{c_r(\theta)}{R} \cos \left[\frac{2\pi r t}{T} - \phi_r(\theta) \right]_{t-R/c},$$

* This assumption does not exclude the possibility that the radio-frequency power is generated by plasma oscillations provided that such oscillations are not coherent over volumes comparable with the resolving power of the interferometer.

where R is the distance from the radiating region to the point at which the field is measured, T is the observation time, $\phi_r(\theta)$ is a random variable distributed with uniform probability between 0 and 2π so that there is zero correlation between the phases of different frequencies and between the radiation from different regions, and $c_r(\theta)$ is a quantity proportional to

$$[2p_r(\theta) d\theta/T]^{1/2},$$

where $p_r(\theta) d\theta$ is the power radiated from the region of angular width $d\theta$ at the frequency r/T . As has been shown by Rice (1944) representations of this kind are equivalent to the more familiar representations introduced into radiation theory by Einstein (1915) and by von Laue (1915).

5.2. *The Correlator Output in the Absence of Receiver and Aerial Noise*

The voltages $V_1(t)$, $V_2(t)$ developed across the inputs to the square-law detectors in the two receivers by the signals received from the source are given by

$$\left. \begin{aligned} V_1(t) &\sim \int d\theta_l \sum_{r=0}^{\infty} \frac{A_{1r}}{R_1(\theta_l)} c_r(\theta_l) \cos \left[\frac{2\pi r}{T} \left(t - \frac{R_1(\theta_l)}{c} \right) - \phi_r(\theta_l) - \psi_{1r} \right], \\ V_2(t) &\sim \int d\theta_{l'} \sum_{r'=0}^{\infty} \frac{A_{2r'}}{R_2(\theta_{l'})} c_{r'}(\theta_{l'}) \cos \left[\frac{2\pi r'}{T} \left(t - \frac{R_2(\theta_{l'})}{c} \right) - \phi_{r'}(\theta_{l'}) - \psi_{2r'} \right], \\ &\dots \dots \dots \end{aligned} \right\} \dots \dots \dots (13)$$

where to the first order in $\theta_l, \theta_{l'}$,

$$\left. \begin{aligned} R_1(\theta_l) &= [R_0^2 + (L^2/4) + R_0 l \tan \theta_0 - R_0 l \theta_l]^{1/2}, \\ R_2(\theta_{l'}) &= [R_0^2 + (L^2/4) - R_0 l \tan \theta_0 + R_0 l \theta_{l'}]^{1/2}, \end{aligned} \right\} \dots \dots (14)$$

and where A_r, ψ_r are the amplitude and phase characteristics of the pre-detector amplifiers.*

In the present case, where the fractional pre-detector bandwidth is small compared with unity, the output of the low-frequency filters following the square-law detectors is given by

$$\begin{aligned} S_1(t) &\sim \int d\theta_l \int d\theta_\lambda \sum_{r,s=0}^{\infty} \frac{A_{1r} A_{1s} c_r(\theta_l) c_s(\theta_\lambda)}{R_1(\theta_l) \cdot R_1(\theta_\lambda)} \\ &\quad \times G_1 \left(\frac{2\pi \cdot \overline{r-s}}{T} \right) \cos \left\{ \frac{2\pi t}{T} \overline{r-s} - \left[\frac{rR_1(\theta_l)}{c} - \frac{sR_1(\theta_\lambda)}{c} \right] \frac{1}{T} \right. \\ &\quad \left. - \overline{\psi_{1r} - \psi_{1s} - \phi_{1r}(\theta_l) - \phi_{1s}(\theta_\lambda)} - \chi_1 \left(\frac{2\pi \cdot \overline{r-s}}{T} \right) \right\}, \dots (15) \end{aligned}$$

* The aerial gains and any time-independent phase and amplitude distortions introduced by the ionosphere should also be included in A_r, ψ_r . It is assumed that the angular dimensions of the source are very small compared with the angular width of the aerial beams: the extension to the general case can easily be made by suitably modifying the definition of $c_r(\theta_l)$.

together with a similar expression for $S_2(t)$ where $G(\omega) \exp[-i\chi(\omega)]$, the steady state response of the low-frequency filter, is zero both for direct current and for radio-frequencies.

The outputs of the two low-frequency filters are multiplied together in the correlator the output of which is proportional to

$$S_1(t) \cdot S_2(t-\tau_0),$$

where τ_0 is the delay inserted to compensate for the difference in the time of arrival of the signals at the two aerials.

A typical term in the time-independent part of $S_1(t) \cdot S_2(t-\tau_0)$ is proportional to

$$\begin{aligned} \cos [(2\pi/cT)\{r \cdot \overline{R_1(\theta_l) - R_2(\theta_l')} - s \cdot \overline{R_1(\theta_\lambda) - R_2(\theta_\lambda')}\} \\ + \overline{\phi_r(\theta_l) - \phi_r(\theta_l')} - \overline{\phi_s(\theta_\lambda) - \phi_s(\theta_\lambda')} - (2\pi/T) \cdot \overline{r-s}\tau_0 \\ + \Theta_1(r, s) - \Theta_2(r, s)], \end{aligned} \quad (16)$$

where $\Theta(r, s) = \psi_r - \psi_s + \chi[\overline{r-s} \cdot (2\pi/T)].$

To find the average value of $S_1(t) \cdot S_2(t-\tau_0)$ as $T \rightarrow \infty$ use is made of the fact that the noise radiation is expressible by a *stationary* time series. In this case the distinction between a time and an ensemble average disappears so that the time-averaged value of $S_1(t) \cdot S_2(t-\tau_0)$ is equal to the mean value of $S_1(t) \cdot S_2(t-\tau_0)$ averaged over N different measurements, each of duration T , where $N \rightarrow \infty$. Accordingly an average is taken over the independent random phase angles $\phi_r(\theta_l)$ etc. and the only terms which contribute to $\langle S_1(t) \cdot S_2(t-\tau_0) \rangle_{AV}$ are those for which $\theta_l = \theta_l'$ and $\theta_\lambda = \theta_\lambda'$. Since the angular dimensions of this source are small $\theta_\lambda \ll 1$ and $R_1(\theta_l) - R_2(\theta_l)$ may be expanded by the binomial theorem to give

$$\frac{R_1(\theta_l) - R_2(\theta_l)}{R_0} = \frac{l \tan \theta_0}{R_0} - \frac{l\theta_l}{R_0}, \quad (17)$$

where $R_1(\theta_l), R_2(\theta_l)$ are given by eqn. (14).

If the analysis is restricted to the case where the phase characteristics of the two channels are linear, but have different slopes, then

$$\Psi(r, s) = (2\pi/T)\overline{r-s}[\tau_0 - (l \tan \theta_0/c)] + \Theta_1(r, s) - \Theta_2(r, s), \quad (18)$$

which may be written

$$\Psi(r, s) = (2\pi/T)\overline{r-s} t_0, \quad (19)$$

where t_0 is equivalent to a differential time delay.

In the limiting case where $T \rightarrow \infty$ one may put

$$2\pi r/T = \omega, \quad 2\pi s/T = \omega', \quad (20)$$

and then,

$$\begin{aligned} \langle S_1(t) \cdot S_2(t-\tau_0) \rangle_{AV} \sim \int_{-\alpha/2}^{\alpha/2} d\theta_l \int_{-\alpha/2}^{\alpha/2} d\theta_\lambda \int_0^\infty d\omega \int_0^\infty d\omega' P(\omega, \theta_l) P(\omega', \theta_\lambda) \\ \times A_1(\omega) A_2(\omega) A_1(\omega') A_2(\omega') G_1(\omega - \omega') G_2(\omega - \omega') \\ \times \cos [-(l/c)\overline{\omega\theta_l - \omega'\theta_\lambda - \omega - \omega'} \cdot t_0], \end{aligned} \quad (21)$$

where $P(\omega, \theta_l)$ is the power at an angular frequency ω in unit angular frequency bandwidth received from the region of width $d\theta_l$. If it is

assumed that $P(\omega, \theta_i)$ does not change with frequency over the receiver bandwidth and if the low-frequency filter amplitude characteristic is expressed by the integral

$$G_1(\omega - \omega')G_2(\omega - \omega') = \int_0^\infty G_1(\sigma)G_2(\sigma)[\delta(\omega - \omega' - \sigma) + \delta(\omega - \omega' + \sigma)] d\sigma, \quad (22)$$

where δ is the Dirac delta-function, then

$$\begin{aligned} \langle S_1(t) \cdot S_2(t - \tau_0) \rangle_{AV} \sim & \int_{-\alpha/2}^{\alpha/2} P(\omega_0, \theta_i) d\theta_i \int_{-\alpha/2}^{\alpha/2} P(\omega_0, \theta_\lambda) d\theta_\lambda \\ & \times \int_0^\infty G_1(\sigma)G_2(\sigma) d\sigma \int_0^\infty A_1(\omega)A_2(\omega)A_1(\omega - \sigma)A_2(\omega - \sigma)d\omega \\ & \times \{ \cos [-(l\omega/c)\overline{\theta_i - \theta_\lambda} - (l\theta_i/c) + t_0 \cdot \sigma] \\ & + \cos [-(l\omega/c)\overline{\theta_i - \theta_\lambda} + (l\theta_\lambda/c) + t_0 \cdot \sigma] \}. \quad (23) \end{aligned}$$

This expression is valid whatever the form of $A(\omega)$ and $G(\omega)$; but in the only case considered here the pre-detector and low-frequency filter bandwidths both have rectangular amplitude characteristics such that

$$\left. \begin{aligned} A_1(\omega) \cdot A_2(\omega) &= A^2 \text{ when } \omega_0 - \pi B_R < \omega < \omega_0 + \pi B_R \\ A_1(\omega) \cdot A_2(\omega) &= 0 \text{ when } \omega < \omega_0 - \pi B_R; \omega > \omega_0 + \pi B_R \end{aligned} \right\}, \quad (24)$$

$$\left. \begin{aligned} G_1(\sigma) \cdot G_2(\sigma) &= G^2 \text{ when } \Omega_0 - \pi b_V < \sigma < \Omega_0 + \pi b_V \\ G_1(\sigma) \cdot G_2(\sigma) &= 0 \text{ when } \sigma < \Omega_0 - \pi b_V; \sigma > \Omega_0 + \pi b_V \end{aligned} \right\}. \quad (25)$$

It must be noted that B_R is the width of the pre-detector band common to both receivers, which in general will be less than the pre-detector bandwidth of either receiver separately.

Integrating first over ω and then over σ , and assuming that $b_V \ll B_R$,

$$\begin{aligned} \langle S_1(t) \cdot S_2(t - \tau_0) \rangle_{AV} \sim & \int_{-\alpha/2}^{\alpha/2} P(\omega_0, \theta_i) d\theta_i \int_{-\alpha/2}^{\alpha/2} P(\omega_0, \theta_\lambda) d\theta_\lambda B_R b_V A^4 G^2 \\ & \times \cos \left(\frac{\omega_0 l \cdot \overline{\theta_i - \theta_\lambda}}{c} \right) \frac{\sin [(\pi B_R l \cdot \overline{\theta_i - \theta_\lambda})/c]}{\pi B_R l \cdot \overline{\theta_i - \theta_\lambda}/c} \\ & \times \cos \Omega_0 \left(t_0 + \frac{l \cdot \overline{\theta_i + \theta_\lambda}}{2c} \right) \frac{\sin \pi b_V [t_0 + (l \cdot \overline{\theta_i + \theta_\lambda}/2c)]}{\pi b_V [(l \cdot \overline{\theta_i + \theta_\lambda}/2c) + t_0]}. \quad (26) \end{aligned}$$

If the bandwidths B_R and b_V and the time delay t_0 are restricted so that

$$\frac{\pi B_R l \alpha}{c} \ll 1, \quad (27)$$

$$\frac{\pi b_V l \alpha}{2c} \ll 1, \quad (28)$$

$$(\pi b_V + \Omega_0)(t_0 + l\alpha/2c) \ll 1, \quad (29)$$

where α is the maximum angular extension of the source, then the correlator output given by eqn. (26) is

$$\begin{aligned} \langle S_1(t) \cdot S_2(t - \tau_0) \rangle_{AV} \sim & \int_{-\alpha/2}^{\alpha/2} P(\omega_0, \theta_i) d\theta_i \int_{-\alpha/2}^{\alpha/2} P(\omega_0, \theta_\lambda) d\theta_\lambda \\ & \times B_R b_V A^4 G^2 \cos \left(\frac{\omega_0 l \cdot \overline{\theta_i - \theta_\lambda}}{c} \right), \quad (30) \end{aligned}$$

which may be written

$$\langle S_1(t) \cdot S_2(t - \tau_0) \rangle_{AV} \sim B_R b_V A^4 G^2 [F_{\cos}^2(\omega_0 l/c) + F_{\sin}^2(\omega_0 l/c)], \quad (31)$$

where $F_{\cos}(\omega_0 l/c)$ and $F_{\sin}(\omega_0 l/c)$ are defined by eqn. (4).

The output of the correlator may be normalized by dividing by the product of the r.m.s. filter outputs due to the radiation from the source alone. Since each of these outputs is proportional to the total input power to each aerial it follows that their product is proportional to $B_R b_V A^4 G^2 F_{\cos}^2(0)$ and hence $c(l, t)$ the *normalized correlator output* is given by

$$c(l, t) \equiv \frac{[S_1(t) \cdot S_2(t - \tau_0)]}{\{[S_1^2(t)]^{1/2} - P_{N1}\} \{[S_2^2(t)]^{1/2} - P_{N2}\}} = \frac{F_{\cos}^2(\omega_0 l/c) + F_{\sin}^2(\omega_0 l/c)}{F_{\cos}^2(0)}. \quad (32)$$

Comparison of eqns. (32) and (6) shows that, subject to the inequalities (27), (28) and (29), the normalized correlator output is equal to the square of the correlation coefficient $\rho^2(l)$ measured by an ideal 'Michelson' interferometer of zero bandwidth.

§6. THE EFFECTS OF FINITE BANDWIDTHS AND DIFFERENTIAL TIME DELAYS

6.1. The Pre-Detector Bandwidth

The principal effect of the finite pre-detector bandwidth is to introduce a dispersion into the relative phase of the signals from a source of finite size and thereby to reduce the output of the correlator, but this effect is negligible if the inequality (27) is satisfied. It can be shown that this is equivalent to the requirement that the fractional radio-frequency bandwidth shall be small compared with $1/\pi$.

It is also important that the pre-detector characteristics of the two receiving channels should be identical, since any difference in the width of the pass bands will introduce uncorrelated components of the signal and the normalized value of the correlator output will be correspondingly reduced. It also follows that any difference between the frequencies of the local oscillators of the two receivers must be small compared with the pre-detector bandwidths.

6.2. Differential Time Delays and the Bandwidth of the Low-Frequency Filters

It is shown in §7 that fluctuations in the measured value of the normalized correlator output are proportional to $(b_V)^{-1/2}$ and thus to obtain the best signal to noise ratio the bandwidth of the low-frequency filters must be kept as wide as possible. A theoretical upper limit to this bandwidth is set by the inequalities (28,) (29), but in practice the bandwidth is restricted to a much lower value by a variety of factors of which the more important are the frequency response of the baseline transmission link and the presence of differential time delays in the two channels.

Since the relative amplitude and phase of the low-frequency components in the two channels must be preserved, any amplitude or phase distortion in the transmission link must be kept to a negligible value.

A difference in the time delays associated with the two channels will introduce a dispersion of the relative phase of corresponding low-frequency components at the correlator, and it follows from eqn. (26) that, in the case of a point source ($\alpha=0$), the presence of a differential time delay t_0 will reduce the correlator output by a factor

$$\cos \Omega_0 t_0 \frac{\sin \pi b_V t_0}{\pi b_V t_0},$$

if it is assumed that the bandwidths are rectangular in shape. The error introduced by a differential time delay t_0 is negligible provided that

$$(\pi b_V + \Omega_0) t_0 \ll 1,$$

as is shown by inequality (29) in the case where $\alpha=0$. The total differential time delay for a point source is given by

$$t_0 = \Delta T_D + \Delta T_B + \Delta T_C, \quad (33)$$

where $\Delta T_D = [\tau_0 - (L \sin \theta_0 / c)]$ is the error in compensating for the time delay introduced by the length of the baseline projected in the direction of the source, ΔT_B is the difference in the time delays in the two receiving channels and ΔT_C is the error in compensating for the time delay introduced by the transmission along the baseline. ΔT_D , which depends upon the direction of the source relative to the baseline, is discussed in § 9. ΔT_B , which depends upon the accuracy with which the two receivers are matched, can in practice be made negligibly small. ΔT_C , which depends upon the length of the baseline, is only likely to prove important for very long baselines where there are uncertainties in the time of transmission along the link; however, even for extremely long baselines, it is unlikely that the low-frequency bandwidth would be restricted by the presence of differential time delays to less than about 1 kc/s.

In the above discussion it has been assumed that the source is a point and the dispersion introduced by its finite angular diameter has been neglected. It follows from eqn. (26) that this dispersion may be represented by an additional differential time delay of the order of $l\alpha/2c$ and this is negligible when inequality (27) is satisfied since $b_V \ll B_R$.

It is also essential that the phase and amplitude characteristics of the low-frequency filters should be identical, since any difference in the width of the two pass-bands will introduce uncorrelated low-frequency components and will reduce the observed value of the normalized correlator output. This requirement is similar to that stated previously for matching the two pre-detector bandwidths.

6.3. *The Bandwidth of the Integrating Circuits*

It is shown in § 7 that the overall signal to noise ratio is independent of the bandwidth of the integrating circuit b_I for a given total time of observation. However, the number of separate readings may be reduced

by restricting b_I , and the theoretical limit is set by the requirement that the outputs of the three recorders shall follow the rate of variation of the total power received from the source as it transits the aerial beams. In practice the minimum bandwidth is much greater than this, being determined by the need to recognize such effects as the scintillation of the source or short bursts of interference. These requirements have been found by experience to limit the minimum bandwidth of the integrating circuits to between 1 and 0.1 c.p.s.

§ 7. THE EFFECTS OF RECEIVER AND AERIAL NOISE

The noise generated in the two receivers is completely uncorrelated and hence contributes nothing to the direct current output from the correlator.

It is difficult to calculate the contribution from the ‘background radiation’ in the general case when the effective temperature in the aerial side-lobes is different from that in the main beam. However when the effective background temperature of the sky is uniform, it can be shown by thermodynamical reasoning that the associated contribution to the correlator direct-current output is proportional to the real part of the mutual aerial impedance and to the effective temperature of the sky. This contribution falls rapidly to zero as the length of the baseline becomes large compared with the aperture of the aerials,* and since the majority of observations are made under these conditions, it will be assumed that the cosmic noise contributes nothing to the direct current output from the correlator.

However, both the receiver and cosmic noise will contribute to the fluctuations in the measured value of the normalized correlator output and also to the r.m.s. outputs of the low-frequency filters.

7.1. *Fluctuations in the Normalized Correlator Output*

If the pre-detector bandwidth B_R is large compared with the bandwidth b_V of the low-frequency filters, the noise outputs from the latter will have a normal distribution with r.m.s. amplitudes proportional to the sum of the noise powers due to the cosmic noise P_C , the receiver noise P_R and the source P_S .

The calculation of the fluctuations in $K(l, t)$, the correlator output, is complicated by the presence in each channel of partially correlated components from the source, but it can be shown by a straightforward extension of the analysis in § 5 that the r.m.s. fluctuations in the correlator output $[K(l, t)]$ are given by

$$\frac{[K^2(l, t) - \langle K(l, t)^2 \rangle_{AV}]^{1/2}}{\langle K(l, t) \rangle_{AV}} = \left[\frac{b_I}{b_V} \right]^{1/2} \frac{[1 + C(l) + (P_{N1}/P_{S1})][1 + C(l) + (P_{N2}/P_{S2})]}{C(l)}, \dots \quad (34)$$

* The contribution of the cosmic noise to the correlator output is completely negligible as long as the aerial separation exceeds ten times the aerial aperture.

where $P_{N1}=P_{C1}+P_{R1}$, $P_{N2}=P_{C2}+P_{R2}$ and all the band-pass amplitude characteristics are rectangular in shape. However, it is the fluctuations in $c(l, t)$, the *normalized* correlator output, which are of primary interest and these are extremely difficult to evaluate rigorously especially as the three quantities $[S_1(t)S_2(t-\tau_0)]$, $[(\overline{S_1^2(t)})^{1/2}-P_{N1}]$ and $[(\overline{S_2^2(t)})^{1/2}-P_{N2}]$ are not independent. Indeed, when the contribution from the receiver and cosmic noise are small compared with the signal from the source and when the source is unresolved, the correlation between the fluctuations in these quantities is nearly unity, and hence the associated fluctuations in the normalized correlator output are very small. An upper limit to these fluctuations, which is approached asymptotically as $P_N/P_S \rightarrow \infty$, can be found by assuming that the fluctuations in the three records are uncorrelated. In this case the fluctuations in $c(l, t)$ have an approximately normal distribution as long as $b_I \ll b_V$ and their r.m.s. value is given by

$$\frac{\langle c^2(l, t) - C^2(l) \rangle_{AV}^{1/2}}{C(l)} = \left(\frac{b_I}{b_V}\right)^{1/2} \frac{\{[1+C(l)+(P_N/P_S)]^4 + 2[1+(P_N/P_S)^4]\}^{1/2}}{C(l)} \quad \dots \quad (35)$$

in the special case when the receiver gains and noise factors are the same. For $P_N \equiv P_G + P_C \gg P_S$ this expression reduces to

$$\frac{\langle c^2(l, t) - C^2(l) \rangle_{AV}^{1/2}}{C(l)} \sim \sqrt{\left(\frac{3b_I}{b_V}\right) \cdot \frac{P_N^2}{P_S^2 C(l)}} \quad \dots \quad (36)$$

In practice the r.m.s. fluctuations will always be appreciably less than the upper limit given in eqn. (35) since, for all practical values of the signal to noise ratio, there will be a marked correlation between the fluctuations of the three records.

If the normalized correlator output is measured by taking a large number N of independent observations over a period T_0 , where $N \simeq 2b_I T_0$, then the r.m.s. error in the result is reduced by the factor $N^{-1/2} = [2b_I T_0]^{-1/2}$. It is therefore independent of the bandwidth of the integrating circuits and depends only upon the length of the observation time.

§ 8. THE EFFECTS OF THE IONOSPHERE

Observations of the scintillation of the discrete sources have shown that there are minor irregularities in the ionosphere which introduce irregular changes in the intensity of the radiation received at the earth's surface. It is to be expected that the use of very long baselines will be further complicated by major differences in the characteristics of the ionized layers above the two receiving sites. An idea of the order of magnitude of these effects can be derived from the following simple analysis.

It is assumed, for simplicity, that the down-coming waves from the source are propagated in a direction *parallel* to the earth's magnetic

field through a uniform ionosphere of thickness H . Under these conditions the propagation constant k for a circularly polarized wave may be written

$$k \simeq \frac{\omega}{c} \left[1 - \frac{\omega_c^2}{2\omega^2} \left(1 \pm \frac{\omega_H}{\omega} \right) \right], \quad \dots \dots \dots (37)$$

where ω_c is the critical angular frequency, ω_H is the gyro angular frequency, ω is the angular frequency of the incident wave, and it is assumed that $\omega \gg \omega_H$ and $\omega^2 \gg \omega_c^2$. The choice of sign in (37) depends upon the direction of the rotation of the polarization of the circularly polarized wave. The total change in phase $\Delta\phi$ of a circularly polarized wave crossing the ionosphere, relative to a similar wave in free space is, therefore,

$$\Delta\phi = \frac{H\omega}{c} \left(\frac{\omega_c^2}{2\omega^2} \right) \left(1 \pm \frac{\omega_H}{\omega} \right) \text{ radians.} \quad \dots \dots \dots (38)$$

Substituting very approximate values for the F region ($\omega_c = 2\pi \times 6 \times 10^6$, $\omega_H = 2\pi \times 10^6$, $H = 2 \times 10^5$ m) the total phase shift relative to propagation in free space is about 750 radians at 100 Mc/s, which represents a time delay of 1.2 microseconds. Since in practice the bandwidth of the low-frequency filters is limited to a few kilocycles, it follows from the analysis in §6 that the effects of the maximum differential delay which can be introduced by the ionosphere are negligible at this frequency.

A more serious source of error with long baselines is likely to be the rotation of the polarization of the down-coming waves due to the earth's magnetic field. It follows directly from eqn. (38) that the polarization of a plane wave in the ionosphere is rotated relative to that of a similar wave in free space by

$$\frac{H}{c} \frac{\omega_c^2 \omega_H}{\omega^2} \text{ radians,}$$

and, substituting the parameters of the ionosphere assumed previously, the polarization at 100 Mc/s is rotated by about 15 radians. Since the radiation emitted by the discrete sources is unpolarized, a difference of ϕ radians in the polarization of the received signals at each end of the baseline will reduce the normalized correlator output by a factor $\cos^2 \phi$. For short baselines this effect should be negligible, but it may prove to be serious for very long baselines. The rotation of the polarization is proportional to $(\omega)^{-2}$ and thus may be reduced by using higher frequencies, but with very long baselines it may be necessary to make use of aerials sensitive to both planes of polarization.

Finally there are the random time-dependent changes in the relative amplitude and phase of the signals at the two receiving sites which are produced by minor irregularities in the ionosphere (Smith 1950, Little and Lovell 1950). At 100 Mc/s these irregularities introduce random changes in phase of the order of one or two radians with corresponding fluctuations of intensity which may be as great as 100%.

It has already been shown that the large phase shift introduced by the whole ionosphere may be neglected if the low-frequency filter bandwidth is suitably restricted, and it follows that the effects of these comparatively small changes of phase will be negligible. The associated amplitude fluctuations will not affect the instantaneous value of the *normalized* correlator output provided that their period is long compared with the response time of the integrating circuits. However, a detailed analysis shows that errors will be introduced if the amplitude fluctuations at the two receiving stations are partially correlated and if their period is comparable with, or shorter than, the response time of the integrating circuits. Since the period of the ionospheric 'scintillations' is normally of the order of 30 seconds (Maxwell and Little 1952) and since the response time of the integrating circuits is chosen in practice to lie between about 0.1 and 1.0 second, it follows that the new type of interferometer is virtually unaffected by ionospheric 'scintillations'.

§9. THE EFFECTS OF THE ROTATION OF THE EARTH

Due to the rotation of the earth both the difference in the time of arrival of corresponding signals at the two aerials ($L \sin \theta_0/c$) and the effective length of the baseline ($L \cos \theta_0$) will vary with time.

The rate of change of $L \cos \theta_0$ is a maximum for an east-west baseline and for a source of zero declination, and in that case it is simple to show that the change in the effective length of the baseline may be limited to 1% by restricting the total period of observation to about one hour.

It can also be shown that, for the same direction of the baseline, the effect of the variable time delay is negligible provided that the product of the total period of observation (T_0) in seconds and the low-frequency filter bandwidth (b_V) in c.p.s. is restricted so that

$$b_V T_0 \ll \frac{c}{\pi^2} \frac{T_S}{L \cos \delta}$$

where T_S is the length of a sidereal day in seconds and δ is the declination of the source. For example, for a source of zero declination, a baseline of 100 km and a filter bandwidth of 1 kc/s, the period of observation should not exceed about 1 hour.

§10. DISCUSSION

The new type of interferometer described in this paper differs radically from the 'Michelson' type of instrument. In principle the latter can measure both the phase and amplitude of the Fourier transform of the intensity distribution across the source, whereas the new instrument gives information about the amplitude alone and therefore cannot yield a unique solution to the intensity distribution. It should however be noted that it is not clear how significant this loss of information will prove in practice.

A more important disadvantage of the new instrument is that it is relatively insensitive to weak sources. Thus eqn. (36) shows that, if the power from a source (P_S) is small compared with the sum of the receiver and cosmic noise powers (P_R+P_C), the signal to noise ratio at the correlator output $\propto [P_S/(P_C+P_R)]^2$. Under equivalent conditions the signal to noise ratio of a 'Michelson' interferometer $\propto [P_S/(P_C+P_R)]$ and hence the new instrument is relatively insensitive when $P_S < P_C+P_R$.

The most obvious advantage of the new instrument is that the technical problem of combining the signals from two widely spaced receivers is relatively simple, since there is no need to maintain the high degree of phase stability in the link which is required if the radio-frequency phase of the signals must be preserved. The simplicity of operation and the reliability of the instrument have been shown by an extensive series of measurements of the distribution of intensity across the intense sources in Cygnus and Cassiopeia using baselines of between 300 m and 15 km at 125 Mc/s (Hanbury Brown, Jennison and Das Gupta 1952, Jennison and Das Gupta 1953), and there appears to be no practical reason why the baseline should not be extended further. Indeed it should be possible to eliminate the transmission link altogether and to record the low-frequency outputs of the two receivers on, say, magnetic tape. The records could be compared subsequently in a correlator and it seems that by the use of this technique a baseline of indefinite length could be used.

A second important advantage of the new instrument is that its accuracy should be independent of scintillations caused by the ionosphere so long as the bandwidth of the integrating circuits is not made too small, and this property should prove particularly valuable when operating at the longer wavelengths. Practical experience with the instrument on short baselines has already confirmed that it will operate satisfactorily in the presence of large fluctuations introduced by the ionosphere, even when these fluctuations are partially correlated at the two receiving sites.

The rotation of the polarization of the radiation from the source due to the ionosphere introduces an additional complication into the use of very long baselines. This effect, as has been pointed out in § 8, can be reduced by decreasing the wavelength or by using aerials which accept both planes of polarization.

The use of the 'Michelson' interferometer at radio wavelengths is a logical extension of optical practice and it is interesting to enquire whether the principle of the new type of interferometer can in turn be applied to visual astronomy, since in this way it might be possible to increase the resolving power and mitigate the effects of atmospheric turbulence. A preliminary examination of this question, which will be discussed in a later communication, suggests that the technique cannot be applied to optical wavelengths and that it breaks down due to the limitations imposed by 'photon noise'.

REFERENCES

- BOLTON, J. G., and STANLEY, G. J., 1948, *Nature, Lond.*, **161**, 312.
EINSTEIN, A., 1915, *Ann. d. Physik*, **47**, 879.
HANBURY BROWN, R., JENNISON, R. C., and DAS GUPTA, M. K., 1952, *Nature, Lond.*, **170**, 1061.
JENNISON, R. C., and DAS GUPTA, M. K., 1953, *Nature, Lond.*, **172**, 996.
JENNISON, R. C., and DAS GUPTA, M. K., in preparation.
LITTLE, C. G., and LOVELL, A. C. B., 1950, *Nature, Lond.*, **165**, 422.
MAXWELL, A., and LITTLE, C. G., 1952, *Nature, Lond.*, **169**, 746.
MCCREADY, L. L., PAWSEY, J. L., and PAYNE-SCOTT, R., 1947, *Proc. Roy. Soc. A*, **190**, 357.
RICE, S. O., 1944, *Bell Syst. Tech. J.*, **24**, 306.
RYLE, M., and SMITH, F. G., 1948, *Nature, Lond.*, **162**, 462.
RYLE, M., 1950, *Rep. Prog. Phys.*, **13**, 184 (London : Physical Society).
SMITH, F. G., 1950, *Nature, Lond.*, **165**, 422.
STANLEY, G. J., and SLEE, O. B., 1950, *Aust. J. Sci. Res. A*, **3**, 234.
VON LAUE, M., 1915, *Ann. d. Physik*, **47**, 668.

*A Rotating-Lobe Interferometer and its Application to
Radio Astronomy*

By R. HANBURY BROWN, H. P. PALMER and A. R. THOMPSON
Jodrell Bank Experimental Station, Lower Withington, Macclesfield,
Cheshire*

[Received November 20, 1954 ; revised April 3, 1955]

ABSTRACT

An interferometer, operating on the rotating-lobe principle, is described. It is shown how the frequency of the interference patterns observed from discrete radio sources may be controlled and made independent of the baseline length and direction. The application of the instrument to observations with a short north-south baseline and a long (630 λ) baseline is illustrated by experimental results. It is pointed out that the use of this technique is of particular value for the observation of weak sources with long baselines.

§ 1. INTRODUCTION

AN important experimental problem in radio astronomy is to measure the apparent angular diameter and the distribution of intensity across the discrete sources. In general this measurement demands a high resolving power which can only be obtained by the use of an interferometer. It is the purpose of the present paper to describe an instrument which has been developed for this type of work and which has been termed a rotating-lobe interferometer. It is shown that the use of this instrument offers certain advantages over previous methods.

§ 2. THE PRINCIPLE OF A ROTATING-LOBE INTERFEROMETER

The principle of a rotating-lobe interferometer can be explained simply in terms of the effective polar diagram of the aerial system. Figure 1 represents two aerials A and B which are separated by a baseline of length d and are connected by identical cables to a multiplier. In one of the two cables there is a continuously variable phase-shifter. If radiation from a distant point source is incident on the aerial system at an angle θ_0 to the normal to the baseline, for any given value of the phase-shift ϕ , the time-average of the multiplier output will be proportional to

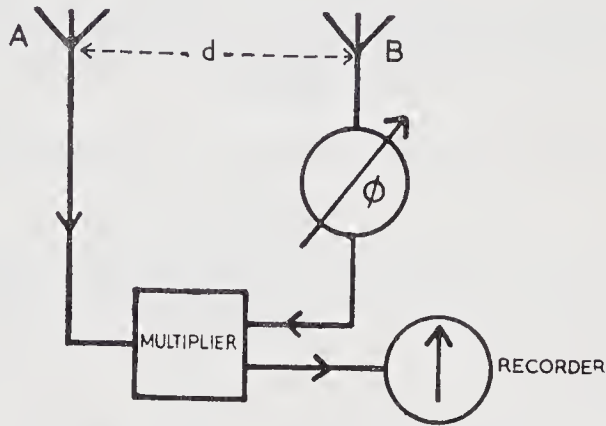
$$P_s [g_A(\theta_0) g_B(\theta_0)]^{1/2} \cos \left[\frac{2\pi d}{\lambda} \sin \theta_0 + \phi \right] \dots \dots \dots (1)$$

where P_s represents the flux from the source and $g_A(\theta_0)$, $g_B(\theta_0)$ represent the power gains of the two aerials. The response of the whole system to a

* Communicated by Professor A. C. B. Lovell.

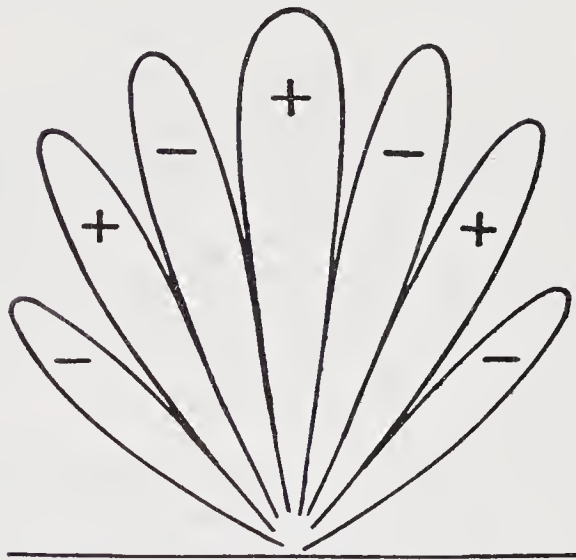
point source at any angle may therefore be represented as a polar diagram of lobes of alternate polarity as shown in fig. 2, the angular position of the central lobe of the pattern with respect to the normal being determined by the value of the phase-shift ϕ .

Fig. 1



A simple form of interferometer.

Fig. 2



The effective polar diagram of reception of the simple interferometer shown in fig. 1.

As a discrete source transits the normal to the baseline, it will produce an interference pattern on the recorder with an apparent frequency f_s given by

$$f_s \simeq \frac{1}{2\pi} \left[\omega_E \cdot \frac{d}{\lambda} \cdot \cos \delta \cos \alpha \right] \dots \dots \dots (2)$$

where ω_E radians sec^{-1} is the rate of angular rotation of the earth, λ is the wavelength, δ is the declination of the source and α is the angle between

the direction of the base-line and a line east-west. If the value of ϕ is now made to vary slowly with time at a rate ω_ϕ radians sec^{-1} , then the lobes of the polar diagram will appear to rotate, while the envelope of their maxima remains stationary. Under these conditions the frequency of the output pattern is modified and becomes

$$f_s' \simeq \frac{1}{2\pi} \left[\omega_E \frac{d}{\lambda} \cos \delta \cos \alpha \pm \omega_\phi \right] \quad (3)$$

where the choice of sign depends upon the direction of rotation of the phase-shifter. It is therefore possible, by controlling both the speed and direction of the phase-shifter, to vary at will the frequency of the output pattern. Thus, by rotating the lobes in the same direction as the apparent angular motion of the source, the frequency of the pattern may be reduced indefinitely, while by rotating the lobes in the opposite direction, or more rapidly in the same direction, the frequency can be increased to any desired value. As discussed later this facility is of particular value when it is necessary to operate an interferometer with very short or very long baselines, or when the baselines are in a direction close to north-south.

§ 3. DESCRIPTION OF A PRACTICAL EQUIPMENT

3.1. *A Simplified Outline*

A rotating-lobe interferometer can be constructed from a number of different circuit arrangements, since there are many ways* in which the relative phase of the signals from the two aerials may be varied. The choice of any particular arrangement must necessarily depend upon the use for which the instrument is intended. The instrument described here has been designed specifically to measure the distribution of intensity across both weak and intense sources, using baselines which may be of widely different lengths and oriented in any direction.

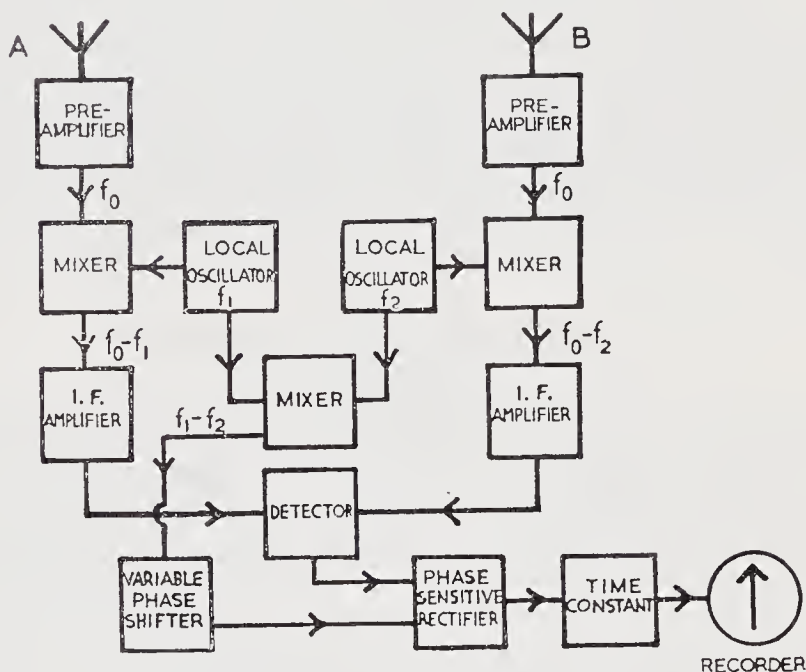
A simplified block diagram of the instrument is shown in fig. 3. A and B represent the two aerials which are connected by cables to separate receiving channels. The output from aerial A is amplified at the signal-frequency f_0 and fed to a mixer, where it is heterodyned by a local oscillator of frequency f_1 . The output from aerial B is treated in the same way, except that the frequency of the local oscillator is f_2 and therefore differs from that used in the other channel. The outputs of the two mixers are amplified at intermediate-frequencies $(f_0 - f_1)$, $(f_0 - f_2)$, and are combined in a detector to form a beat-frequency $(f_1 - f_2)$. This beat-frequency is amplified and rectified in a phase-sensitive rectifier. The reference voltage of the phase-sensitive rectifier is generated by combining the two local

* An interferometer using a rotating phase-shifter in one aerial, but no phase-sensitive rectifier, has been described by Little and Payne-Scott (1951). Also Bolton and Slee (1954) have used an interferometer in which the relative phase of the local oscillator at two mixers was varied slowly to produce a moving lobe-pattern.

oscillators in a mixer; the beat-frequency, between the oscillators is then fed through a continuously variable phase-shifter to operate the rectifier. The output of the phase-sensitive rectifier is passed through a time-constant and is displayed in the usual way on a pen recorder.

Following the method used above it is convenient to discuss the operation of this system in terms of its effective polar diagram of reception. The use of two local oscillators of different frequency may be regarded as a method of introducing a continuous variation of $2\pi (f_1 - f_2)$ radians sec^{-1} into the relative phase of the signals from the two aerials. Thus the lobes of the

Fig. 3



A simplified block diagram of the interferometer.

polar diagram appear to rotate at $\lambda/d (f_1 - f_2)$ radians sec^{-1} , and a discrete source in transit will produce an alternating component in the output of the detector given by

$$P_s [g_A(\theta_0) g_B(\theta_0) G_A G_B]^{1/2} \cos \left[\omega_E \frac{d}{\lambda} \cdot \cos \delta \cos \alpha \pm 2\pi (f_1 - f_2) \right] t \quad . \quad (4)$$

where G_A, G_B are the power gains of the two channels.

The output of the phase-sensitive rectifier is proportional to the amplitude of the input wave and to the cosine of the phase-angle between this wave and the reference voltage. It therefore consists of an alternating component of low-frequency given by

$$P_s [g_A(\theta_0) g_B(\theta_0) G_A G_B]^{1/2} \cos \left[\omega_E \frac{d}{\lambda} \cdot \cos \delta \cos \alpha \pm \omega_\phi \right] t \quad . \quad (5)$$

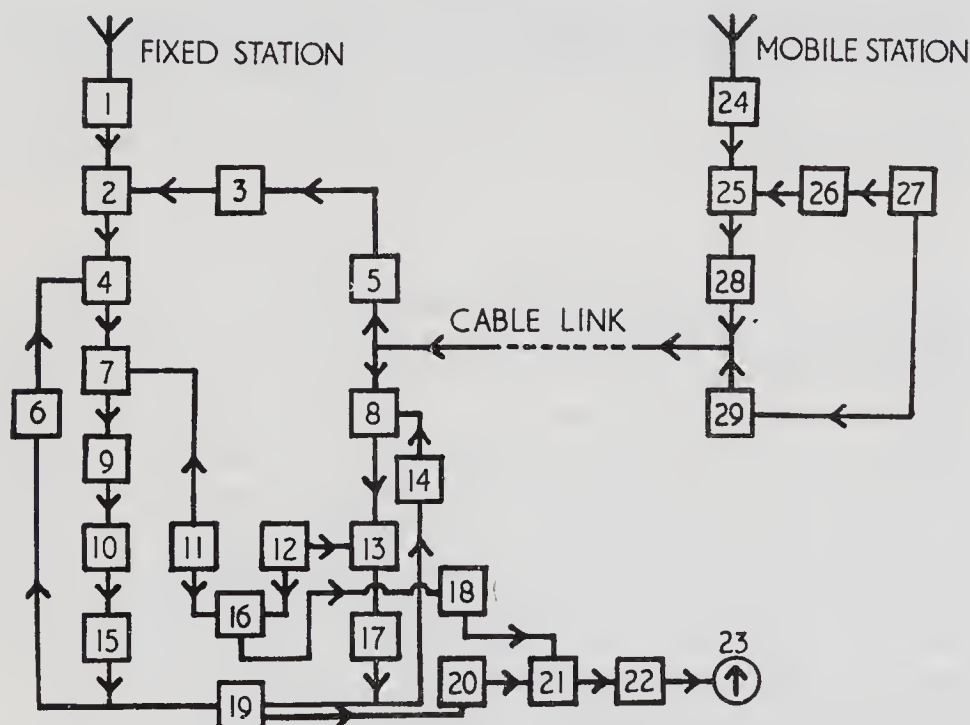
where ω_ϕ is the rate of change of the phase of the reference voltage and the choice of sign depends upon the direction of the phase-shifter.

A comparison of eqns. (4) and (5) shows that the use of a phase-sensitive rectifier brings the rotating lobes apparently to rest, and that the frequency of the interference pattern is determined in the usual way by the rotation of the earth if the phase-shifter is stationary. If, however, the phase-shifter is varied, then the angular frequency of the pattern is changed by the same amount. Thus it follows from eqns (3) and (5) that the phase-shifter shown in fig. 3 may be used to control the frequency of the interference pattern in precisely the same way as a phase-shifter is one aerial cable (fig. 1).

3.2. Some Details of the Apparatus

A schematic diagram of the complete apparatus is shown in fig. 4; although it differs in detail from the simple scheme in fig. 3, the principle

Fig. 4



A complete block diagram of the interferometer.

- (1) Preamplifier (158.2 Mc/s); (2) First mixer; (3) Frequency multiplier ($\times 12$); (4) Intermediate frequency amplifier (10 Mc/s); (5) Amplifier (14.02 Mc/s); (6) Automatic gain control; (7) Second mixer; (8) Intermediate frequency amplifier (10 Mc/s); (9) Intermediate frequency amplifier (3.76 Mc/s); (10) Delay cable; (11) Crystal oscillator (6.240 Mc/s); (12) Crystal oscillator (6.241 Mc/s); (13) Second mixer; (14) Automatic gain control; (15) Intermediate frequency amplifier (3.76 Mc/s); (16) Mixer; (17) Intermediate frequency amplifier (3.76 Mc/s); (18) Magslip phase-shifter driven by velodyne; (19) Multiplier; (20) Selective amplifier (1000 c/s); (21) Phase-sensitive rectifier; (22) Time-constant; (23) Recorder; (24) Preamplifier (158.2 Mc/s); (25) First mixer; (26) Frequency multiplier ($\times 12$); (27) Crystal oscillator (14.02 Mc/s); (28) Intermediate frequency amplifier (10 Mc/s); (29) Amplifier (14.02 Mc/s).

of operation is unchanged. The equipment is divided into a fixed and a mobile station. The signal received at the mobile station is heterodyned to a convenient intermediate frequency (10 Mc/s) and is transmitted over a coaxial cable together with the fundamental frequency of the local oscillator. At the fixed station this signal is amplified at 10 Mc/s and fed to a second mixer; the local-oscillator fundamental is multiplied and used to heterodyne the signal received by the aerial at the fixed station. This latter signal is also amplified at 10 Mc/s and fed to a second mixer. The frequency difference between the two channels is introduced at the second mixers by the use of two second local oscillators which differ in frequency by about 1000 c/s. The signals are then amplified at the second intermediate frequency and are combined in a multiplier. The signal from the fixed aerial is delayed in the second intermediate frequency amplifier to compensate for the delay in the signal from the mobile aerial. The output of the multiplier contains a beat-frequency of 1000 c/s which is amplified in a selective amplifier and applied to a phase-sensitive rectifier. The beat-frequency between the two second local-oscillators is formed in a separate mixer and is fed to the phase-sensitive rectifier through a rotating magflip phase-shifter driven at an adjustable speed by a velodyne motor.

§ 4. THE EQUIPMENT IN OPERATION

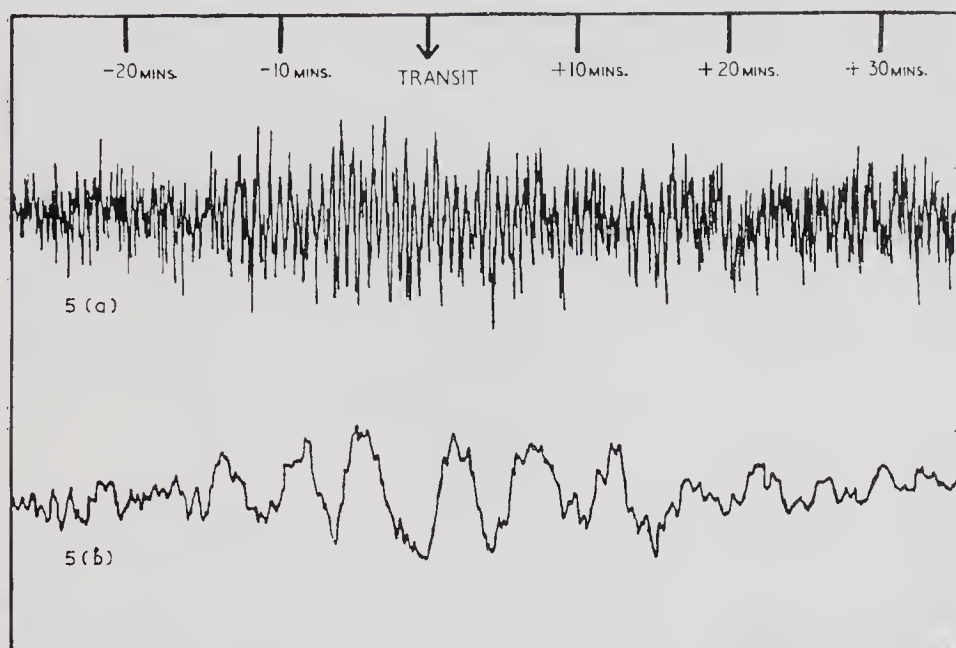
The instrument described above was designed to measure the apparent angular diameter of the discrete sources observed in a previous survey with the large fixed paraboloid (218 ft.) at Jodrell Bank. For the present purpose the large paraboloid was used as the fixed aerial of the interferometer and the mobile aerial usually consisted of a small array of about 35 m² aperture; however, for observations of the most powerful sources the mobile aerial was occasionally a single dipole. The measurements were carried out by observing the sources with baselines of different length and direction as they transited the meridian, and their apparent angular diameter was found from the well-known relation between the distribution of intensity across a source and the relative amplitude of the interference pattern at different aerial spacings.

The results of the first series of measurements have already been reported (Hanbury Brown, Palmer and Thompson 1954). It was found that several of the intense sources have angular diameters of the order of one or two degrees, hence these sources were completely resolved with baselines of less than about 60 λ . On the other hand a number of the sources, particularly those at high galactic latitudes, showed little trace of being resolved with a baseline of 500 λ .

These preliminary measurements illustrate clearly the need for an interferometer which will operate over a wide variety of baseline lengths; furthermore since the sources may not be radially symmetrical, as in the case of the intense source in Cygnus, it is essential that the instrument should operate with a baseline in any direction. Equation (2) shows that,

if the frequency of the pattern is determined only by the rotation of the earth, then it is proportional to the length of the baseline and to the cosine of the angle between the baseline and a line east-west. Thus for very short baselines, or for baselines close to north-south, the frequency of the pattern is low. If the baseline is comparable in length with the aperture of either of the aerials, it becomes difficult in practice to measure the amplitude of the interference pattern during the transit of the source

Fig. 5



The use of a rotating lobe interferometer to decrease the frequency of an interference pattern.

- (a) Record of a weak source observed with a baseline of 630λ in a direction east and west, taken with the phase-shifter stationary. The output time constant is 4 seconds.
- (b) Record of the same source taken under identical conditions but with the phase-shifter rotating and decreasing the frequency of the pattern, and the output time constant increased to 30 seconds.

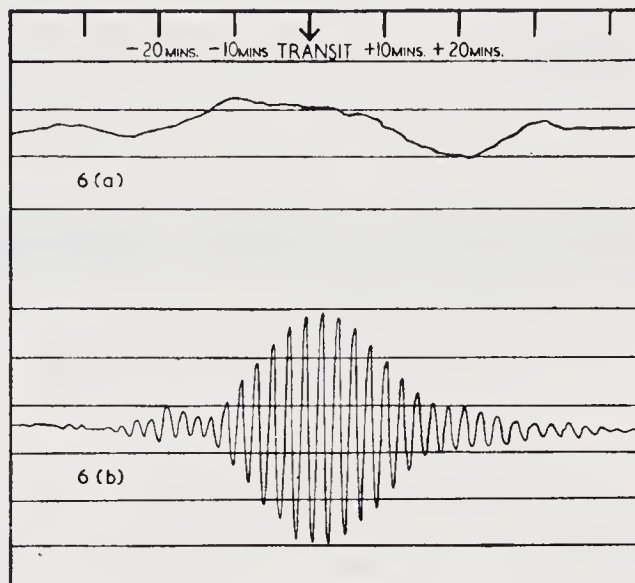
N.B. For both these records the 218 ft. paraboloid was used as one aerial of the interferometer. At a frequency of 158.2 Mc/s. the beam is narrow and the interference pattern is therefore restricted to about 10 minutes on either side of transit.

through the aerial beam. Conversely, if the baseline is long, the frequency of the pattern becomes inconveniently high and it is necessary to reduce the time-constant of the receiver output. Since the signal-to-noise is proportional to the square-root of the time-constant, it follows that, for long baselines, the overall sensitivity of the equipment will be reduced.

Practical experience shows that the difficulties outlined above can be substantially reduced by the use of the equipment described in the present

paper. Observations* have been made with baselines in several directions and with a variety of lengths between 21λ and 630λ . It was found that, with the exception of very short baselines as mentioned later, it was always possible to bring the frequency of the interference pattern to a convenient standard value by adjusting the speed and direction of the phase-shifter. As an example fig. 5 shows a record of a weak source

Fig. 6



The use of a rotating lobe interferometer to increase the frequency of an interference pattern.

- (a) A record of an intense source taken with a baseline 50λ in a direction north-south and with the phase-shifter at rest in an arbitrary position.
- (b) A record taken under identical conditions but with the phase-shifter rotating and increasing the frequency of the interference pattern.

observed with a baseline of 480λ and with the phase-shifter stopped; while fig. 5 (b) shows a record of the same source, taken under identical conditions, but with the phase-shifter adjusted to slow down the interference pattern to a convenient value, and a greater output time constant. It is clear that a considerable increase in the effective signal-to-noise ratio has been gained by the use of this technique.

As an example of the reverse operation, namely the speeding up of a pattern, fig. 6 (a) shows a record of the transit of the intense source in Cassiopeia made with a baseline of 50λ oriented north-south and with the phase-shifter at rest in an arbitrary position. The amplitude of this pattern varies with the position of the phase-shifter and in the example shown it happens to be small. Figure 6 (b) shows a record of the same source made under identical conditions, but with the phase-shifter rotating at a speed chosen to give a pattern of convenient frequency.

* For observations with baselines exceeding 500λ the cable was replaced by a radio link.

Although the equipment operated satisfactorily under nearly all conditions, some difficulty was experienced when the phase-shifter was used to increase the frequency of patterns from weak sources observed with very short baselines. Thus, when the aerials were separated by a distance of less than about 40λ , approximately the diameter of the large paraboloid, a small and almost constant output was observed from the multiplier even in the absence of a source. If the phase-shifter was stationary, this output represented a small displacement of the zero of the records and was unimportant; however, with the phase-shifter rotating, the output was converted to a sine-wave and tended to confuse the records of weak sources. It is to be expected that, when the baseline is comparable with the dimensions of the aerials, there should be an output due partly to receiver noise cross-coupled between the aerials and partly to the background radiation from the sky. This problem has not yet been investigated completely; however it appears that in the present equipment the limitation is set by the considerable mutual impedance which exists, at close aerial spacings, between the mobile aerial and the elevated primary feed of the fixed paraboloid. The extent to which the performance at short baselines can be improved by reduction of this mutual impedance remains to be investigated.

§ 5. DISCUSSION

In the simplest form of interferometer the output powers of two spaced aerials are added together, either before or after amplification, and the total power is recorded. Thus, in addition to the interference pattern produced by a discrete source, the output contains components proportional to the receiver noise and to the background radiation. The presence of these large components imposes serious limitations on the observation of weak sources and a considerable gain in effective sensitivity results from their removal. In principle this can be accomplished by the use of the simple system shown in fig. 1 in which the outputs of the two aerials are multiplied rather than added. But in practice this method is not attractive since the design of a satisfactory multiplier is difficult when the signal is very small compared with the noise.

An effective way of overcoming this difficulty has been developed by Ryle (1952) and is termed 'phase-switching'. In this system the phase of one of the spaced aerials is reversed periodically by a mechanical switch and therefore, when the outputs of the two aerials are combined, signals which are mutually coherent in the two aerials produce switch-frequency components in the amplitude of the combined output. These components are selected from the output of the receiver and are rectified in a phase-sensitive rectifier operated in synchronism with the phase-reversing switch. It has been shown (Ryle 1952) that this system removes the mean value of the receiver noise and background radiation from the output of the phase-sensitive rectifier. It can also be shown that the effective polar diagram of the aerial system is a series of alternate positive and negative lobes similar to that shown in fig. 2.

The interferometer described in the present paper also eliminates the mean value of the unwanted components from the output. In fact the principles of operation of the present system and the phase-switching system are similar, and the latter may be regarded as a special form of rotating-lobe interferometer in which the lobes are rotated in discrete jumps rather than continuously. A comparison of the two systems suggests that, in general, the phase-switching technique is preferable for the precise measurement of the celestial coordinates of discrete sources. For this type of measurement it is essential to know the relative phase of the signals in the two aerials and, if the baseline is not too long, this can be best achieved by connecting the aerials to a common receiver through identical cables. Under these conditions phase-switching has the considerable practical advantage that it is much simpler to introduce a phase-reversing switch into one of the cables than a continuously variable phase-shifter. On the other hand, if the baseline is so long that separate amplifiers must be used for each aerial, or if a precise knowledge of the relative phase of the signals is unimportant, then the technique described in the present paper has certain advantages. For example the use of two local oscillators of different frequency is reasonably simple and avoids the use of a mechanical phase-reversing switch; furthermore the frequency difference between these oscillators, which corresponds to the phase-switching frequency, is not limited by mechanical considerations.

The most interesting property of the present instrument, and one which offers the greatest potential advantage over previous methods, is the simplicity with which the frequency of the interference patterns can be controlled. This property is likely to prove useful for interferometers working on long wavelengths with restricted baselines, for the measurement of the intensity distribution across sources using baselines close to north-south, and for observations of weak sources, or the detailed structure of intense sources, with long baselines. The last of these applications, namely the use of long baselines, is of particular interest. Thus it follows from the analysis given above that, by the proper use of lobe-rotation technique, the resolving power of an interferometer can be increased without loss of sensitivity until the limit is set by other factors such as the instability of propagation.

ACKNOWLEDGMENTS

The authors wish to thank Professor A. C. B. Lovell for his interest in this investigation. One of us (A. R. T.) is indebted to the Department of Scientific and Industrial Research for a maintenance grant.

REFERENCES

- BOLTON, J. G., and SLEE, O. B., 1954, Reported in *Special Report No. 3*, p. 44 (U.R.S.I. Brussels).
HANBURY BROWN, R., PALMER, H. P., and THOMPSON, A. R., 1954, *Nature, Lond.*, **173**, 945.
LITTLE, A. G., and PAYNE-SCOTT, R., 1951, *Aust. J. Sci. Res. A*, **4**, 489.
RYLE, M., 1952, *Proc. Roy. Soc. A*, **211**, 351.

CORRELATION BETWEEN PHOTONS IN TWO COHERENT BEAMS OF LIGHT

By R. HANBURY BROWN

University of Manchester, Jodrell Bank Experimental Station
AND

R. Q. TWISS

Services Electronics Research Laboratory, Baldock

IN an earlier paper¹, we have described a new type of interferometer which has been used to measure the angular diameter of radio stars². In this instrument the signals from two aerials A_1 and A_2 (Fig. 1a) are detected independently and the correlation between the low-frequency outputs of the detectors is recorded. The relative phases of the two radio signals are therefore lost, and only the correlation in their intensity fluctuations is measured; so that the principle differs radically from that of the familiar Michelson interferometer where the signals are combined before detection and where their relative phase must be preserved.

This new system was developed for use with very long base-lines, and experimentally it has proved to be largely free of the effects of ionospheric scintillation³. These advantages led us to suggest¹ that the principle might be applied to the measurement of the angular diameter of visual stars. Thus one could replace the two aerials by two mirrors M_1 , M_2 (Fig. 1b) and the radio-frequency detectors by photoelectric cells C_1 , C_2 , and measure, as a function of the separation of the mirrors, the correlation between the fluctuations in the currents from the cells when illuminated by a star.

It is, of course, essential to the operation of such a system that the time of arrival of photons at the two photocathodes should be correlated when the light beams incident upon the two mirrors are coherent. However, so far as we know, this fundamental effect has never been directly observed with light, and indeed its very existence has been questioned. Furthermore, it was by no means certain that the correlation would be fully preserved in the process of photoelectric emission. For these reasons a laboratory experiment was carried out as described below.

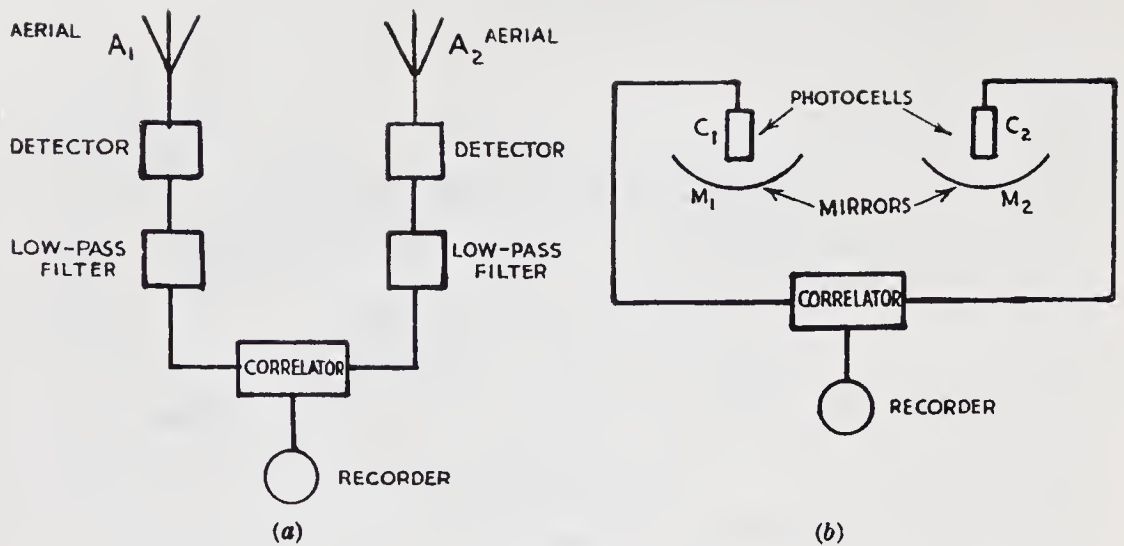


Fig. 1. A new type of radio interferometer (a), together with its analogue (b) at optical wave-lengths

The apparatus is shown in outline in Fig. 2. A light source was formed by a small rectangular aperture, 0.13 mm. \times 0.15 mm. in cross-section, on which the image of a high-pressure mercury arc was focused. The 4358 A. line was isolated by a system of filters, and the beam was divided by the half-silvered mirror M to illuminate the cathodes of the photomultipliers C_1 , C_2 . The two cathodes were at a distance of 2.65 m. from the source and their areas were limited by identical rectangular apertures O_1 , O_2 , 9.0 mm. \times 8.5 mm. in cross-section. (It can be shown that for this type of instrument the two cathodes need not be located at precisely equal distances from the source. In the present case their

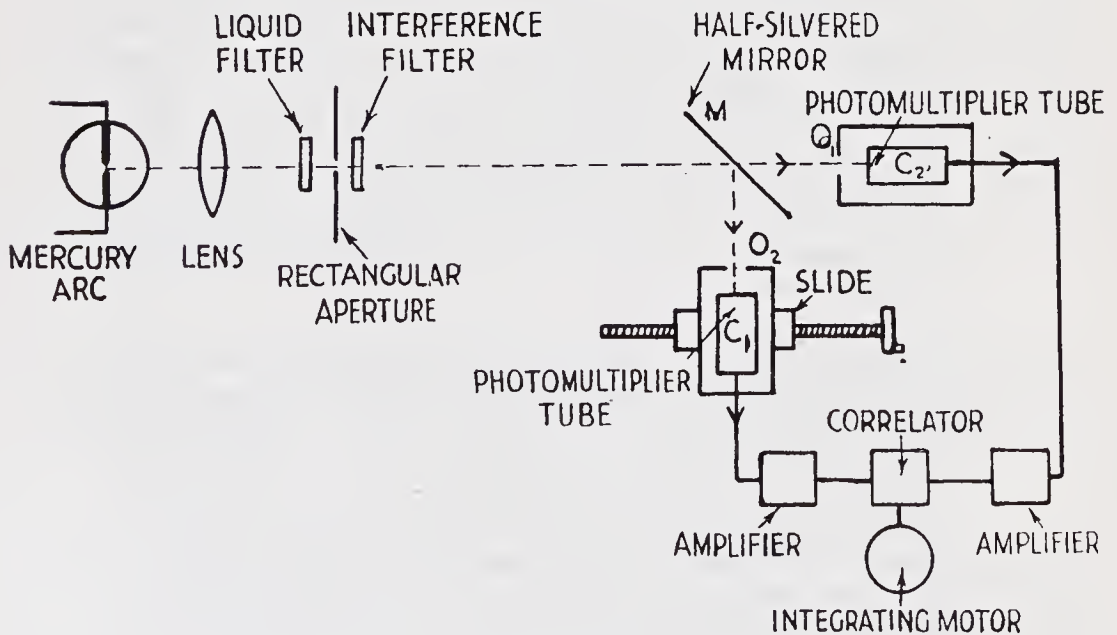


Fig. 2. Simplified diagram of the apparatus

distances were adjusted to be roughly equal to an accuracy of about 1 cm.) In order that the degree of coherence of the two light beams might be varied at will, the photomultiplier C_1 was mounted on a horizontal slide which could be traversed normal to the incident light. The two cathode apertures, as viewed from the source, could thus be superimposed or separated by any amount up to about three times their own width. The fluctuations in the output currents from the photomultipliers were amplified over the band 3–27 Mc./s. and multiplied together in a linear mixer. The average value of the product, which was recorded on the revolution counter of an integrating motor, gave a measure of the correlation in the fluctuations. To obtain a significant result it was necessary to integrate for periods of the order of one hour, so very great care had to be taken in the design of the electronic equipment to eliminate the effects of drift, of interference and of amplifier noise.

Assuming that the probability of emission of a photoelectron is proportional to the square of the amplitude of the incident light, one can use classical electromagnetic wave theory to calculate the correlation between the fluctuations in the current from the two cathodes. On this assumption it can be shown that, with the two cathodes superimposed, the correlation $S(0)$ is given by :

$$S(0) = A.T.b_v.f\left(\frac{a_1\theta_1\pi}{\lambda_0}\right).f\left(\frac{a_2\theta_2\pi}{\lambda_0}\right)\int\alpha^2(\nu).n_0^2(\nu).d\nu \quad (1)$$

It can also be shown that the associated root-mean-square fluctuations N are given by :

$$N = A.T.\frac{2m^*}{m-1}.b_v(b_vT)^{-\frac{1}{2}}\int\alpha(\nu).n_0(\nu).d\nu \quad (2)$$

where A is a constant of proportionality depending on the amplifier gain, etc. ; T is the time of observation ; $\alpha(\nu)$ is the quantum efficiency of the photocathodes at a frequency ν ; $n_0(\nu)$ is the number of quanta incident on a photocathode per second, per cycle bandwidth ; b_v is the bandwidth of the amplifiers ; $m/(m-1)$ is the familiar excess noise introduced by secondary multiplication ; a_1, a_2 are the horizontal and vertical dimensions of the photocathode apertures ; θ_1, θ_2 are the angular dimensions of the source as viewed from the photocathodes ; and λ_0 is the mean wave-length of the light. The integrals are taken over the complete optical spectrum and the phototubes are assumed to be identical. The factor $f\left(\frac{a\theta\pi}{\lambda_0}\right)$ is determined by the dimensionless parameter η defined by

$$\eta = a\theta/\lambda_0 \quad (3)$$

which is a measure of the degree to which the light is coherent over a photocathode. When $\eta \ll 1$, as for a point source, $f(\eta)$ is effectively unity; however, in the laboratory experiment it proved convenient to make η_1, η_2 of the order of unity in order to increase the light incident on the cathodes and thereby improve the ratio of signal to noise. The corresponding values of $f(\eta_1), f(\eta_2)$ were 0.62 and 0.69 respectively.

When the centres of the cathodes, as viewed from the source, are displaced horizontally by a distance d , the theoretical value of the correlation decreases in a manner dependent upon the dimensionless parameters, η_1 and d/a_1 . In the simple case where $\eta_1 \ll 1$, which would apply to an experiment on a visual star, it can be shown that $S(d)$, the correlation as a function of d , is proportional to the square of the Fourier transform of the intensity distribution across the equivalent line source. However, when $\eta \gg 1$, as in the present experiment, the correlation is determined effectively by the apparent overlap of the cathodes and does not depend critically on the actual width of the source. For this reason no attempt was made in the present experiment to measure the apparent angular size of the source.

The initial observations were taken with the photocathodes effectively superimposed ($d=0$) and with varying intensities of illumination. In all cases a positive correlation was observed which completely disappeared, as expected, when the separation of the photocathodes was large. In these first experiments the quantum efficiency of the photocathodes was too low to give a satisfactory ratio of signal to noise. However, when an improved type of photomultiplier became available with an appreciably higher quantum efficiency, it was possible to make a quantitative test of the theory.

A set of four runs, each of 90 min. duration, was made with the cathodes superimposed ($d=0$), the counter readings being recorded at 5-min. intervals. From these readings an estimate was made of N_e , the root mean square deviation in the final reading $S(0)$ of the counter, and the observed values of $S_e(0)/N_e$ are shown in column 2 of Table 1. The results are given as a ratio in order to eliminate the factor A in equations (1) and (2), which is affected by changes in the gain of the equipment. For each run the factor

$$\frac{m-1}{m} \int \alpha^2(\nu) n_0^2(\nu) d\nu \bigg/ \int \alpha(\nu) n_0(\nu) d\nu$$

was determined from measurements of the spectrum of the incident light and of the d.c. current, gain and

Table 1. COMPARISON BETWEEN THE THEORETICAL AND EXPERIMENTAL VALUES OF THE CORRELATION

Cathodes superimposed ($d = 0$)		Cathodes separated ($d = 2a = 1.8$ cm.)	
Experimental ratio of correlation to r.m.s. deviation $S_e(0)/N_e$	Theoretical ratio of correlation to r.m.s. deviation $S(0)/N$	Experimental ratio of correlation to r.m.s. deviation $S_e(d)/N_e$	Theoretical ratio of correlation to r.m.s. deviation $S(d)/N$
1 + 7.4	+ 8.4	- 0.4	~ 0
2 + 6.6	+ 8.0	+ 0.5	~ 0
3 + 7.6	+ 8.4	+ 1.7	~ 0
4 + 4.2	+ 5.2	- 0.3	~ 0

output noise of the photomultipliers; the corresponding theoretical values of $S(0)/N$ are shown in the second column of Table 1. In a typical case, the photomultiplier gain was 3×10^5 , the output current was 140 μ amp., the quantum efficiency $\alpha(\nu_0)$ was of the order of 15 per cent and $n_0(\nu_0)$ was of the order of 3×10^{-3} . After each run a comparison run was taken with the centres of the photocathodes, as viewed from the source, separated by twice their width ($d=2a$), in which position the theoretical correlation is virtually zero. The ratio of $S_e(d)$, the counter reading after 90 minutes, to N_e , the root mean square deviation, is shown in the third column of Table 1.

The results shown in Table 1 confirm that correlation is observed when the cathodes are superimposed but not when they are widely separated. However, it may be noted that the correlations observed with $d=0$ are consistently lower than those predicted theoretically. The discrepancy may not be significant but, if it is real, it was possibly caused by defects in the optical system. In particular, the image of the arc showed striations due to imperfections in the glass bulb of the lamp; this implies that unwanted differential phase-shifts were being introduced which would tend to reduce the observed correlation.

This experiment shows beyond question that the photons in two coherent beams of light are correlated, and that this correlation is preserved in the process of photoelectric emission. Furthermore, the quantitative results are in fair agreement with those predicted by classical electromagnetic wave theory and the correspondence principle. It follows that the fundamental principle of the interferometer represented in Fig. 1b is sound, and it is proposed to examine in further detail its application to visual astronomy. The basic mathematical theory together with a description of the electronic apparatus used in the laboratory experiment will be given later.

We thank the Director of Jodrell Bank for making available the necessary facilities, the Superintendent of the Services Electronics Research Laboratory for the loan of equipment, and Mr. J. Rodda, of the Ediswan Co., for the use of two experimental phototubes. One of us wishes to thank the Admiralty for permission to submit this communication for publication.

[Oct. 5

¹ Hanbury Brown, R., and Twiss, R. Q., *Phil. Mag.*, **45**, 663 (1954).

² Jennison, R. C., and Das Gupta, M. K., *Phil. Mag.*, (in the press).

CORRELATION BETWEEN PHOTONS, IN COHERENT BEAMS OF LIGHT, DETECTED BY A COINCIDENCE COUNTING TECHNIQUE

By R. Q. TWISS and A. G. LITTLE

Division of Radiophysics, Commonwealth Scientific and
Industrial Research Organization, Sydney

AND

R. HANBURY BROWN

University of Manchester Jodrell Bank Experimental Station

THERE has recently been a controversy¹⁻⁴ in the columns of *Nature* on the existence of a correlation between photons in coherent beams of light. In the initial communication¹, by Hanbury Brown and Twiss, an experiment was described in which light from a pinhole source was split, by a semi-transparent mirror, into two separate beams which then illuminated the cathodes of two separate phototubes. As long as the two light beams were partially coherent a correlation was observed between the fluctuations in the anode currents of the two phototubes and it was argued that this proved that the arrival times of light quanta at different points illuminated by coherent beams of light were correlated.

This experiment was criticized by Brannen and Ferguson², who had themselves carried out a somewhat different test, in which the simultaneous emission of photoelectrons at the two photocathodes were recorded by a coincidence counter, and in which no significant difference was observed in the number of counts with coherent or incoherent light. Furthermore, these authors suggested that the results obtained by Hanbury Brown and Twiss were due, not to a true correlation between the arrival times of quanta, but to some other cause such as an intensity fluctuation in the light source.

In reply it was pointed out by Purcell³ and by Hanbury Brown and Twiss⁴ that there was no real disagreement between the results of these two tests, since the experiment of Brannen and Ferguson², and the similar experiment of Adám, Janossy and Varga⁵, were far too insensitive to detect the effect. In addition, the reality of the phenomenon has been confirmed by observations⁶ on Sirius; also the experiment of Hanbury Brown and Twiss has been repeated under precisely controlled conditions, when the observed correlation, with various degrees of optical superimposition of the photocathodes, agreed within a few per cent with the predictions of theory (unpublished work).

However, to make assurance doubly sure, we have repeated the experiment of Brannen and Ferguson, under conditions which permit the detection of the effect, and have obtained a positive result, in reasonable agreement with theory, as described below.

If a correlation between photons is to be detected in a convenient time by the coincidence counter technique it can be shown, not only that the light source must be brilliant, but also that the light reaching the photocathodes must be confined to a very narrow band. This immediately suggests the use of an isotope lamp and, in the present experiment, the light source was an electrodeless radio-frequency discharge in mercury-198 vapour, cooled by a forced air draught, to which the radio-frequency oscillator delivered $1\frac{1}{2}$ watts of power at a frequency of 800 Mc./s. In other respects the experimental arrangement was very similar to that of Brannen and Ferguson², employing 1P21 phototubes, the coincidence circuit being that of Bell, Graham and Petch⁷, with a resolution time of 3.5×10^{-9} sec.

The light source was limited by a pinhole 0.360 mm. in diameter; the photocathodes, at a distance of 1.25 metres, were limited by square apertures, 2 mm. \times 2 mm., and the 5461 A. line was isolated by an optical filter. Both phototubes were mounted on movable slides so that, as seen by the source, they could be optically superimposed or separated by a distance of 5 mm. transverse to the line of sight; at the latter distance the pinhole source was completely resolved so that the incident light beams were effectively uncorrelated. The photon counts could also be uncorrelated by inserting a length of cable in one channel of the coincidence counter circuit with a delay of 15 μ sec., about four times the resolution time of the coincidence circuit.

The measurements were carried out as follows.

The photocathodes were optically superimposed for two minutes and the number of coincidences n_{1r} observed in this interval was recorded. One or other of the photocathodes was then moved to the displaced position, and n_{2r} , the number of coincidences in a two-minute period, was also recorded. This procedure was repeated ten times in a run in which the total observation time was 40 min. and the difference

$$\Delta n_c = \sum_{r=1}^{10} (n_{1r} - n_{2r}) \quad (1)$$

was measured. In order to eliminate the effect of any difference in the light intensity reaching the two different positions of the photocathode, an identical comparison run was then made with the extra cable inserted in one arm of the coincidence circuit and the difference

$$\Delta n'_c = \sum_{r=1}^{10} (n'_{1r} - n'_{2r}) \quad (2)$$

between the coincidences observed with the photocathodes superimposed and displaced was recorded. The quantity $N_c = (\Delta n_c - \Delta n'_c)$ was then taken as a measure of the number of correlated photoelectrons emitted in coincidence during a 20-min. interval.

A total of six such tests, with an overall observation time of 480 min., were performed, and the results are shown in Table 1. Combining all the measurements, we conclude that the ratio ρ of the correlated to the random counts is given by

$$\rho_{\text{exp.}} = 0.0193 \pm 0.0017 \text{ (probable error)} \quad (3)$$

The probability that this result is a random noise fluctuation is quite negligible, being less than 1 in 10^{15} ; in addition, the possibility that it was significantly affected by drifts was eliminated by stabilizing the light intensity and the power supplies to the phototubes, with the result that any such drifts in the counting rate in a 40-min. run were too small, compared with the random fluctuation, to be detected.

A seventh run was then taken with the isotope light source replaced by a tungsten filament lamp, under which conditions no significant correlation is to be expected. As may be seen from Table 1, no significant correlation was in fact observed.

The experimental results have been compared with theory as follows. It has been shown by Purcell³ that

Table 1. RATIO OF CORRELATED TO RANDOM COINCIDENCES

Run No.	Observed number of coincidences in 20 min.* (N_T)	Observed number of correlated coincidences in 20 min. (N_c)	Percentage ratio of correlated to total coincidences ($\rho \times 100$)	Ratio of correlated coincidences to r.m.s. uncertainty in random coincidences† ($N_c/2(N_T)^{1/2}$)
1	136,941	2,986	2.18	4.03
2	130,067	2,190	1.68	3.04
3	137,435	2,369	1.72	3.2
4	100,732	2,185	2.18	3.43
5	97,258	1,864	1.93	3.0
6	94,739	1,761	1.86	2.8
7	81,576	185	0.22	0.33‡

* The average number of photoelectrons emitted in a 20 min. interval was of the order of 10^8 .

† In deriving the root-mean-square uncertainty in the number of random coincidences it was assumed that they obeyed a Poisson distribution. The root-mean-square uncertainty for any one run is twice the square root of the number of coincidences observed in 20 min. since, as explained in the text, each run consisted of four 20 min. observation periods.

‡ Run No. 7 was taken with a broad bandwidth light source, a tungsten filament lamp, for which no significant correlation was expected.

the theoretical ratio ρ of the correlated to the random coincidences is given by

$$\rho_{\text{theor.}} = \frac{\tau_0}{4\tau_c} \quad (4)$$

in the idealized case of a point source and unpolarized light. In this expression τ_c is the resolving time of the coincidence counter, and $c\tau_0$ is the 'coherence length' of the light when τ_0 , which is approximately equal to the reciprocal light bandwidth, is defined by

$$\tau_0 = \int_{-\infty}^{\infty} |g^2(t)| dt \quad (5)$$

and $g(t)$, the Fourier transform of $f(\nu - \nu_0)$, the normalized spectral density of the incident light centred on frequency ν_0 , is defined by

$$g(t) = \int_{-\infty}^{\infty} f(\nu) \exp(2\pi i\nu t) d\nu \quad (6)$$

The resolving time τ_c of the coincidence counter was measured to be 3.5×10^{-9} sec. under the conditions of the present experiment. The value of τ_0 for the mercury isotope lamp was measured by observing the visibility of fringes in a Michelson interferometer as a function of mirror spacing, and was found to be 0.73×10^{-9} sec.; this is somewhat

smaller than the ideal value to be expected from a lamp of this kind with an atomic temperature of $\sim 300^\circ \text{K.}$, but the decrease is caused by self-absorption at the centre of the line.

In applying equation (4) to the present equipment it is necessary to reduce the theoretical value of ρ by a factor $\Delta(\nu_0)\gamma$; where $\Delta(\nu_0)$ is the 'partial coherence' factor which allows for the fact that the source is of finite angular size and is therefore partially resolved by the individual photocathodes, and γ takes into account the polarization introduced by the semi-transparent mirror and the false counts due to dark current in the phototubes. The value of $\Delta(\nu_0)$ was calculated to be 0.475, and γ was measured to be 0.86.

With the numerical values given above, the theoretical value for ρ is

$$\rho_{\text{theor.}} = \Delta(\nu_0)\gamma \frac{\tau_0}{4\tau_c} = 0.0207 \quad (7)$$

The error in this value is unlikely to exceed ± 0.002 and is principally caused by uncertainties in the value of τ_c , which in turn depends, in a complex manner, upon the amplitude distribution of the pulses from the phototubes.

A comparison of equations (3) and (7) shows that the experimental and theoretical values for the fraction of photoelectrons which are correlated and emitted in time coincidence are in satisfactory agreement, the discrepancy being less than the probable error in the measurement or the uncertainty in the theoretical value. Thus the present experiment confirms the conclusions drawn from the earlier test¹, and shows in a very direct manner that the arrival times of photons at different points are correlated when these points are illuminated by coherent beams of light.

We should like to thank Prof. R. E. Bell for very helpful advice on the operating conditions of the coincidence circuit, and the Division of Electrotechnology of the Commonwealth Scientific and Industrial Research Organization for the use of its high-speed counter. A detailed discussion of this and allied experiments will be submitted for publication in the *Australian Journal of Physics*.

¹ Hanbury Brown, R., and Twiss, R. Q., *Nature*, **177**, 27 (1956).

² Brannen, E., and Ferguson, H. I. S., *Nature*, **178**, 481 (1956).

³ Purcell, E. M., *Nature*, **178**, 1449 (1956).

⁴ Hanbury Brown, R., and Twiss, R. Q., *Nature*, **178**, 1447 (1956).

⁵ Adam, A., Jánossy, L., and Varga, P., *Acta Hungarica*, **4**, 301 (1955).

⁶ Hanbury Brown, R., and Twiss, R. Q., *Nature*, **178**, 1046 (1956).

⁷ Bell, R. E., Graham, R. L., and Petch, H. E., *Canad. J. Phys.*, **30**, 35 (1952).

A TEST OF A NEW TYPE OF STELLAR INTERFEROMETER ON SIRIUS

By R. HANBURY BROWN

Jodrell Bank Experimental Station, University of Manchester

AND

DR. R. Q. TWISS

Services Electronics Research Laboratory, Baldock

WE have recently described¹ a laboratory experiment which established that the time of arrival of photons in coherent beams of light is correlated, and we pointed out that this phenomenon might be utilized in an interferometer to measure the apparent angular diameter of bright visual stars.

The astronomical value of such an instrument, which might be called an 'intensity' interferometer, lies in its great potential resolving power, the maximum usable base-line being governed by the limitations of electronic rather than of optical technique. In particular, it should be possible to use it with base-lines of hundreds, if not thousands of feet, which are needed to resolve even the nearest of the *W*-, *O*- and *B*-type stars. It is for these stars that the measurements would be of particular interest since the theoretical estimates of their diameters are the most uncertain.

The first test of the new technique was made on Sirius (α Canis Majoris A), since this was the only star bright enough to give a workable signal-to-noise ratio with our preliminary equipment.

The basic equipment of the interferometer is shown schematically in Fig. 1. It consisted of two mirrors M_1 , M_2 , which focused light on to the cathodes of the photomultipliers P_1 , P_2 and which were guided manually on to the star by means of an optical sight mounted on a remote-control column. The intensity fluctuations in the anode currents of the photomultipliers were amplified over the band 5-45 Mc./s., which excluded the scintillation frequencies, and a suitable delay was inserted into one or other of the amplifiers to compensate for the difference in the time of arrival of the light from the star at the two mirrors. The outputs from these amplifiers were multiplied together in a linear mixer and, after further amplification in a system where special pre-

cautions were taken to eliminate the effects of drift ; the average value of the product was recorded on the revolution counter of an integrating motor. The readings of this counter gave a direct measure of the correlation between the intensity fluctuations in the light received at the two mirrors ; however, the magnitude of the readings depended upon the gain of the equipment, and for this reason the r.m.s. value of the fluctuations at the input to the correlation motor was also recorded by a second motor. Since the readings of both revolution counters depend in the same manner upon the gain, it was possible to eliminate the effects of changes in amplification by expressing all results as the ratio of the integrated correlation to the r.m.s. fluctuations, or uncertainty in the final value. The same procedure was also followed in the laboratory experiment described in a previous communication¹.

There is no necessity in an 'intensity' interferometer to form a good optical image of the star. It is essential only that the mirrors should focus the light from the star on to a small area, so that the photocathodes may be stopped down by diaphragms to the point where the background light from the night sky is relatively insignificant. In the present case, the two mirrors were the reflectors of two standard searchlights, 156 cm. in diameter and 65 cm. in focal length, which focused the light into an area 8 mm. in diameter. However, for observations of Sirius, the circular diaphragms limiting the cathode areas of the photomultipliers (*R.C.A.* type 6342) were made as large as possible, namely, 2.5 cm. in diameter, thereby reducing the precision with which the mirrors had to be guided.

The first series of observations was made with the shortest possible base-line. The searchlights were placed north and south, 6.1 metres apart, and observations were made while Sirius was within 2 hr. of transit. Since the experiments were all

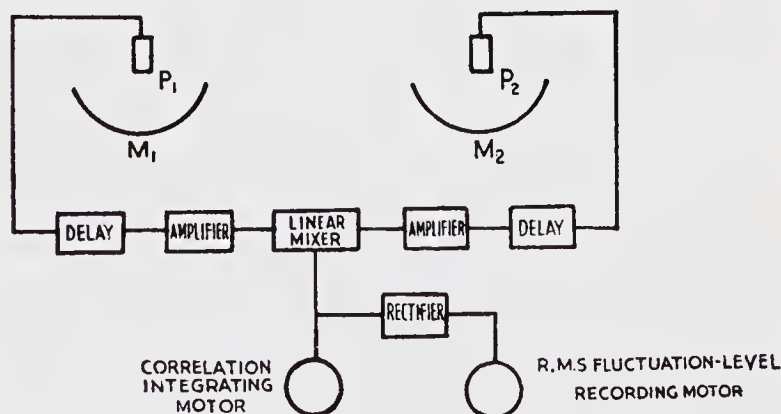


Fig. 1. Simplified diagram of the apparatus

Table 1. COMPARISON BETWEEN THEORETICAL AND OBSERVED CORRELATION

1. Base-line in metres	2.5 (N.S.)	5.54 (E.W.)	7.27 (E.W.)	9.20 (E.W.)
2. Observing time (min.)	345	285	280	170
3. Observed ratio of integrated correlation to r.m.s. deviation: $C(d)$	+8.50	+3.59	+2.65	+0.83
4. Theoretical ratio of integrated correlation to r.m.s. deviation, assuming star has an angular diameter of 0.0063": $C(d)$	+9.35	+4.11	+2.89	+1.67
5. Theoretical ratio of integrated correlation to r.m.s. deviation, assuming star is a point source: $C(o)$	+10.15	+5.63	+5.06	+4.40
6. Theoretical normalized correlation coefficient for star of diameter 0.0063": $\Gamma^2(d)$	0.92	0.73	0.57	0.38
7. Observed normalized correlation coefficient with associated probable errors: $\Gamma^2(d)$	0.84 ± 0.07	0.64 ± 0.12	0.52 ± 0.13	0.19 ± 0.15

carried out at Jodrell Bank, lat. 53° 14' N., the elevation of the star varied between 15½° and 20°, and the average length of the base-line projected normal to the star was 2.5 metres; at this short distance Sirius should not be appreciably resolved.

Throughout the observations the average d.c. current in each photomultiplier was recorded every 5 min., together with the readings of the revolution counters on both the integrating motors. The small contributions to the photomultiplier currents due to the night-sky background were measured at the beginning and end of each run. The gains of the photomultipliers were also measured and were found to remain practically constant over periods of several hours.

In order to ensure that any correlation observed was not due to internal drifts in the equipment, or to coupling between the photomultipliers or amplifier systems, dummy runs of several hours duration were made before and after every observation; for these runs the photomultiplier in each mirror was illuminated by a small lamp mounted inside a detachable cap over the photocathode. In no case was any significant correlation observed.

In this initial stage of the experiment, observations were attempted on every night in the first, and last

quarters of the Moon in the months of November and December 1955; the period around the full moon was avoided because the background light was then too high. During these months a total observation time of 5 hr. 45 min. was obtained, an approximately equal period being lost due to failure of the searchlight control equipment. The experimental value for the integrated correlation $C(d)$ at the end of the observations is given in the line 3 of Table 1. The value of $C(d)$ is the ratio of the change in the reading of the counter on the correlation motor to the associated r.m.s. uncertainty in this reading.

In the second stage of the experiment the spacing between the mirrors was increased and observations were carried out with east-west base-lines of 5.6, 7.3 and 9.2 metres. These measurements were made on all possible nights during the period January-March 1956, and a total observing time of 12½ hr. was obtained. The observed values of the integrated correlation $C(d)$ are shown in line 3 of Table 1.

As a final check that there was no significant contribution to the observed correlation from any other source of light in the sky, such as the Čerenkov component from cosmic rays², a series of observations was made with the mirrors close together and exposed to the night sky alone. No significant correlation was observed over a period of several hours.

The results have been used to derive an experimental value for the apparent angular diameter of Sirius. The four measured values of $C(d)$ were compared with theoretical values for uniformly illuminated disks of different angular sizes, and the best fit to the observations was found by minimizing the sum of the squares of the residuals weighted by the observational error at each point. In making this comparison, both the angular diameter of the disk and the value of $C(o)$, the correlation at zero base-line, were assumed to be unknown, and account was taken of the different light flux and observing time for each point. Thus the final experimental value for the diameter depends only on the relative values of $C(d)$ at the different base-lines, and rests on the assumption that these relative values are independent of systematic errors in the equipment or in the method of computing $C(d)$ for the models. The best fit to the observations was given by a disk of angular diameter 0.0068" with a probable error of ± 0.0005 ".

The angular diameter of Sirius, which is a star of spectral type A1 and photovisual magnitude -1.43, has never been measured directly; but if we assume that the star radiates like a uniform disk and that the effective black body temperature^{3,4} and bolo-

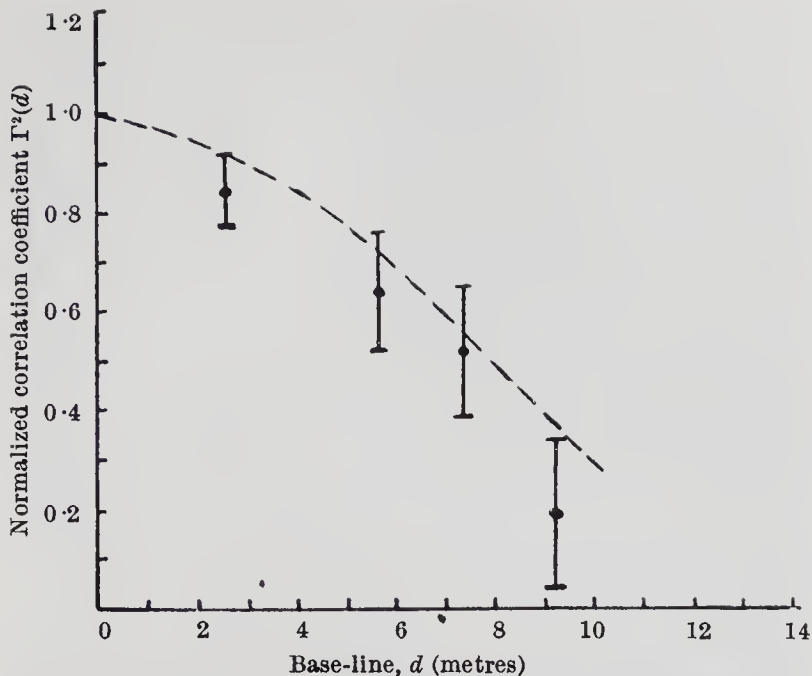


Fig. 2. Comparison between the values of the normalized correlation coefficient $\Gamma^2(d)$ observed from Sirius and the theoretical values for a star of angular diameter $0.0063''$. The errors shown are the probable errors of the observations

metric correction are $10,300^\circ$ K. and -0.60 , respectively, it can be shown that the apparent angular diameter is $0.0063''$, a result not likely to be in error by more than 10 per cent. (In this calculation the effective temperature, bolometric magnitude and apparent angular diameter of the Sun were taken as $5,785^\circ$ K., -26.95 , and $1,919''$, respectively.) Thus it follows that the experimental value for the angular diameter given above does not differ significantly from the value predicted from astrophysical theory.

A detailed comparison of the absolute values of the observed correlation with those expected theoretically has also been made, and the results are given in Table 1 and in Fig. 2. In making this comparison, it is convenient to define a normalized correlation coefficient $\Gamma^2(d)$, which is independent of observing time, light flux and the characteristics of the equipment, where $\Gamma^2(d) = C(d)/C(o)$ and $C(d)$ is the correlation with a base-line of length d , and $C(o)$ is the correlation which would be observed with zero base-line under the same conditions of light flux and observing time. The theoretical values of $\Gamma^2(d)$ for a uniformly illuminated disk of diameter $0.0063''$ are shown in line 6 of Table 1. For monochromatic radiation it is simple to evaluate $\Gamma^2(d)$, since it can be shown⁵ that it is proportional to the square of the Fourier transform of the intensity distribution across

the equivalent strip source ; however, in the present case, where the light band-width is large, the values of $\Gamma^2(d)$ were calculated by numerical integration.

The theoretical values of $C(o)$, given in line 5, were calculated for the conditions of light flux and observing time appropriate to each base-line by means of equations (1) and (2) of our previous communication¹ (though in the present experiment the r.m.s. fluctuations were smaller by a factor $1/\sqrt{2}$ than the value given in the previous paper, which refers to an alternative electronic technique). The most important quantities in this calculation are the gains and output currents of the photomultipliers and the band-widths of the amplifiers ; but it is also necessary to make a small correction for the combined spectral characteristics of the photocathodes, the atmospheric attenuation, the star and the mirrors. Finally, in line 4 of Table 1 the theoretical values of the correlation $C(d)$ are shown ; they were calculated from the theoretical values of $C(o)$ and $\Gamma^2(d)$ by means of the relation given above.

The correlation observed at the shortest base-line (2.5 m.) can be used as a rough test of the effects of atmospheric scintillation on the equipment, since the corresponding theoretical value depends only on well-known quantities and is almost independent of the angular diameter of the star. Throughout the observations Sirius was seen to be scintillating violently, although the corresponding fluctuations in the d.c. anode currents of the photomultiplier tubes, which were smoothed with a time constant of about 0.1 sec., were only of the order of ± 10 per cent, as might be expected with mirrors large by normal telescope standards. Nevertheless, the observed correlation $C(d) = + 8.50$ does not differ significantly from the calculated value of $+ 9.35$, and it follows that it cannot be greatly affected by scintillation.

The experimental values of $C(d)$ obtained at the four base-lines may be compared with the corresponding theoretical values $C(d)$ by means of lines 3 and 4 of Table 1. However, it is more convenient, since these values depend upon the different values of observing time and light flux at each base-line, to normalize the observed values of $C(d)$ by the corresponding values of $C(o)$, so as to give the normalized correlation coefficients $\Gamma^2(d)$ shown in line 7. In Fig. 2 these experimental values of $\Gamma^2(d)$ are shown together with their probable errors, and may be compared with the broken curve, which gives the theoretical values for a uniform disk of 0.0063". It can be seen that both the relative and absolute values of $\Gamma^2(d)$ are in reasonable agreement with theory, and

that within the rather wide limits of this preliminary test there is no significant difference between the correlation predicted and observed.

In assessing the potentialities of the technique described here, it is important to note that, although the measurements took five months to complete, the visibility was so poor that the total observing time was only 18 hr., while in this limited period additional absorption of 0.25–0.75 magnitudes due to haze or thin cloud was often present. If the observations had been made at a latitude where Sirius transits close to the zenith, the improved signal-to-noise ratio, due to decreased atmospheric absorption, would have made it possible to obtain the same data in a total observing time of about four hours.

Thus, despite their tentative nature, the results of this preliminary test show definitely that a practical stellar interferometer could be designed on the principles described above. Admittedly such an instrument would require the use of large mirrors. Judging from the results of this test experiment, where the peak quantum efficiency of the phototubes was about 16 per cent and the overall bandwidth of the amplifiers was about 38 Mc./s., one would need mirrors at least 3 metres in diameter to measure a star, near the zenith, with an apparent photographic magnitude +1.5. Mirrors of at least 6 metres in diameter would be required to measure stars of mag. +3, and an increase in size would also be needed for stars at low elevation because of atmospheric absorption. However, the optical properties of such mirrors need be no better than those of searchlight reflectors, and their diameters could be decreased if the overall band-width of the photomultipliers and the electronic apparatus could be increased, or if photocathodes with higher quantum efficiencies become available. It must also be noted that the technique of using two mirrors, as described here, would probably be restricted to stars of spectral type earlier than *G*, since cooler stars of adequate apparent magnitude would be partially resolved by the individual mirrors.

The results of the present experiment also confirm the theoretical prediction⁶ that an 'intensity' interferometer should be substantially unaffected by atmospheric scintillation. This expectation is also supported by experience with a radio 'intensity' interferometer^{5,7,8} which proved to be virtually independent of ionospheric scintillation. It is also to be expected that the technique should be capable of giving an extremely high resolving power. Without further experience it is impossible to estimate the maximum practical length of the base-line;

however, it is to be expected that the resolving power could be at least one hundred times greater than the highest value so far employed in astronomy, and that almost any star of sufficient apparent magnitude could be resolved.

We thank the Director of Jodrell Bank for making available the necessary facilities, the Superintendent of the Services Electronics Research Laboratory for the loan of much of the equipment, and Dr. J. G. Davies for his assistance with setting up the search-lights. One of us (R. Q. T.) wishes to thank the Admiralty for permission to submit this communication for publication.

¹ Hanbury Brown, R., and Twiss, R. Q., *Nature*, **177**, 27 (1956).

² Galbraith, W., and Jelley, J. V., *J. Atmos. Terr. Phys.*, **6**, 250 (1955).

³ Kuiper, G. P., *Astrophys. J.*, **88**, 429 (1938).

⁴ Keenan, P. C., and Morgan, W. W., "Astrophysics", edit. J. A. Hynek (McGraw-Hill, New York, 1951).

⁵ Hanbury Brown, R., and Twiss, R. Q., *Phil. Mag.*, **45**, 663 (1954).

⁶ Twiss, R. Q., and Hanbury Brown, R. (in preparation).

⁷ Hanbury Brown, R., Jennison, R. C., and Das Gupta, M. K., *Nature*, **170**, 1061 (1952).

⁸ Jennison, R. C., and Das Gupta, M. K., *Phil. Mag.*, **1**, viii, 55 (1956).

Interferometry of the intensity fluctuations in light

I. Basic theory: the correlation between photons in coherent beams of radiation

BY R. HANBURY BROWN

Jodrell Bank Experimental Station, University of Manchester

AND R. Q. TWISS

Division of Radiophysics, C.S.I.R.O., Sydney, Australia

*(Communicated by A. C. B. Lovell, F.R.S.—Received 15 November 1956—
Revised 23 May 1957)*

It is shown by a quantum-mechanical treatment that the emission times of photoelectrons at different points illuminated by a plane wave of light are partially correlated, and identical results are obtained by a classical theory in which the photocathode is regarded as a square-law detector of suitable conversion efficiency. It is argued that the phenomenon exemplifies the wave rather than the particle aspect of light and that it may most easily be interpreted as a correlation between the intensity fluctuations at different points on a wavefront which arise because of interference between different frequency components of the light.

From the point of view of the corpuscular picture the interpretation is much less straightforward but it is shown that the correlation is directly related to the so-called bunching of photons which arises because light quanta are mutually indistinguishable and obey Bose-Einstein statistics. However, it is stressed that the use of the photon concept before the light energy is actually detected is highly misleading since, in an interference experiment, the electromagnetic field behaves in a manner which cannot be explained in terms of classical particles.

The quantitative predictions of the theory have been confirmed by laboratory experiments and the phenomenon has been used, in an interferometer, to measure the apparent angular diameter of Sirius: these results, together with further applications to astronomy, will be discussed in detail in later papers.

It is shown that the classical and quantum treatments give identical results when applied to find the fluctuations in the photoemission current produced by a single light beam, and the connexion between these fluctuations and the correlation between photons in coherent beams is pointed out. The results given here are in full agreement with those obtained by Kahn from an analysis based on quantum statistics: however, they differ from those derived on thermodynamical grounds by Fellgett and by Clark Jones and the reasons for this discrepancy are discussed.

I. INTRODUCTION

In this paper, the first of a series on the interferometry of intensity fluctuations in light, we shall establish theoretically the underlying principle of the technique, which is that the times of emission of photoelectrons at different points illuminated by coherent beams of light are partially correlated. The chief application of this technique is to astronomy, and it has already been successfully tested in a measurement of the angular diameter of Sirius (Hanbury Brown & Twiss 1956*b*). The existence of a correlation between photons has been denied by some authors (Brannen & Ferguson 1956) who have stated, in our view wrongly, that it is contrary to the laws of quantum mechanics. The error appears to have arisen because of a too literal reliance on the corpuscular picture of light. As Bohr has pointed out, in his

Principle of Complementarity, a particular experiment can exemplify the wave or the particle aspect of light but not both; thus the interpretation is greatly simplified, and indeed is much more likely to be correct, if one confines oneself rigidly to the use of the appropriate language and talks of photons when the energy behaves like a classical particle but otherwise talks only of waves. In the present paper, as we shall show, we are dealing essentially with an interference phenomenon which can be interpreted, on the classical wave picture, as a correlation between intensity fluctuations due to beats between waves of different frequency; the concept of a photon need only be introduced at the stage where energy is extracted from the light beam in the process of photoemission.

This does not mean that one cannot interpret the phenomenon from the corpuscular point of view: one can, but only if one is prepared to endow the photons with properties very different from those of classical particles, and in practice the corpuscular picture is more of a hindrance than a help to an interpretation of the phenomenon. Indeed if photons did behave like independent classical particles, distinguishable one from another and obeying Boltzmann statistics, the correlation between them would be identically zero. However, photons are not independent since only states symmetrical between them can occur in nature; thus they obey Bose-Einstein statistics and must be regarded as mutually indistinguishable.

The connexion between the fact that photons are bosons and the existence of a correlation between light quanta may be illustrated by the familiar example of a cavity filled with thermal radiation. In this case, as is well known, the r.m.s. fluctuations in the number of photons in an elementary cell in phase space are greater than those predicted by the classical Boltzmann statistics; as Einstein (1909) pointed out, this excess noise is essentially a wave interference effect, but it can be interpreted in the corpuscular picture as the so-called 'bunching' of photons (Clark Jones 1953).

In principle this 'bunching' of photons could be measured directly if a single photocathode were illuminated by a coherent beam of light, since the fluctuations in the photoemission current should be slightly greater than the pure noise fluctuations which would arise if the photoelectrons were emitted completely independently. In practice the difference between photon and shot noise, which we have called the excess photon noise, is too small to be detected conveniently with one photocathode (Fürth & MacDonald 1947), being swamped by effects such as space-charge smoothing in the photocell or fluctuations in the multiplication process in a photomultiplier. However, the 'bunching' can be measured with two separate phototubes, the cathodes of which lie in the same cell in phase space or, in other words, are illuminated by coherent beams of light.† In this arrangement the shot noise currents, the space-charge smoothing effects and the multiplication noise in the two phototubes are uncorrelated, and thus the small correlation between the fluctuations in the two currents can be detected if the observations are carried out over a sufficiently long time. This correlation can only arise if there is a corresponding correlation in the

† The connexion between the extent, in real space, of an elementary cell in phase space and the volume over which a light beam may be regarded as coherent is not perhaps self-evident and it is therefore examined in appendix I.

time of emission of photoelectrons from the two cathodes, and it follows that this latter phenomenon is related to the fact that photons obey Bose-Einstein statistics. It is of course possible, by means of quantum statistics, to develop the theory given in this paper entirely in terms of the particle picture, as has been done by Kahn (1957); however, we have chosen an alternative approach which emphasizes that the correlation between photons is essentially an interference effect related to the wave picture rather than to the corpuscular aspect of light.

Experiments to measure directly the correlation in the arrival times of photons with coincidence counters have been carried out by *Ádám, Jánosy & Varga* (1955) and, with more sensitive equipment, by *Brannen & Ferguson* (1956), but with a negative result. However, as we have pointed out elsewhere (*Hanbury Brown & Twiss 1956c*), under the conditions of these experiments the expected correlation would have been far too small to be detected. We have carried out independently (*Hanbury Brown & Twiss 1956a*) a similar experiment in which we measured the correlation between fluctuations in the emission currents† of two phototubes, under conditions where the expected signal to noise ratio was of the order 10 to 1, and we have obtained a positive result in satisfactory quantitative agreement with theory. However, the detailed interpretation of this experiment will be left to a later paper of this series since the analysis is complicated by the fact that the light beam was not fully coherent over the surfaces of the photocathodes. In the present paper we shall consider only the idealized case of a plane wave of linearly polarized light in order to present the basic theory in the simplest form.

The phenomenon we are discussing is a general characteristic of an electromagnetic radiation field and will therefore occur not only at optical but also at radio wavelengths. The existence of the effect in the latter case has been demonstrated, implicitly, by experiments with an 'intensity' interferometer which has been used to measure the angular diameter of discrete radio sources (*Hanbury Brown, Jennison & Das Gupta 1952*). In these experiments energy was extracted from the electromagnetic field by two separate aeriels, corresponding to the apertures of the phototubes in the optical experiment, and was then rectified by two square law detectors which correspond to the two photoelectric cathodes. The correlation between the fluctuations in the output currents of the two detectors was measured and was found to be equal to the theoretical value as calculated by classical electromagnetic theory.

The general theory of this radio interferometer has been given elsewhere (*Hanbury Brown & Twiss 1954*), but in the rather complex form required for practical applications to radio-astronomy. To bring out the connexion between the radio and the optical case we shall first develop a simple classical theory for the correlation between the intensity fluctuations at different points in space for the idealized case where the incident radiation field is a plane wave of radio frequency.

† The correlation was measured in this way, and not with a coincidence counter as in the experiments of *Ádám et al.* (1955), because the latter technique is not practical for the measurements on stars to which our work was primarily directed.

2. THE CLASSICAL THEORY OF THE INTENSITY FLUCTUATIONS
IN A PLANE ELECTROMAGNETIC WAVE

(a) *The intensity fluctuations in a plane wave*

Let us assume that the frequency components of the incident electromagnetic plane wave are confined to a limited region of the radio-frequency spectrum defined by

$$\nu_1 < \nu < \nu_2,$$

such that

$$\nu_1 > \nu_2 - \nu_1.$$

If the voltage induced by this radiation field in an aerial of aperture A is rectified in a square-law detector, then the low-frequency fluctuations in the output current of the detector can be expressed as a sum of the beats between the different radio-frequency components of the electromagnetic wave and correspond to the intensity fluctuations in the incident radiation. It is obvious that the amplitude and phase of these low-frequency fluctuations in the detector output current are the same at any point on the wavefront of a plane wave: so if signals are picked up by two separate aeriels and rectified in separate square-law detectors, the low-frequency fluctuations in the two output currents will be perfectly correlated so long as the effects of shot noise in the detector current can be neglected. The fact that this correlation is equally to be expected, on a classical theory, at optical wavelengths appears to have been overlooked.

To develop this argument in a quantitative form, which will later be compared with the results obtained by a quantum theory, we proceed as follows. By a suitable choice of gauge a linearly polarized wave of electromagnetic radiation can be completely described by a vector potential \mathfrak{A} with a single component perpendicular to the direction of propagation. If the observation is of duration T , this component can be represented by a Fourier series,

$$\mathfrak{A} = \sum_{r=1}^{\infty} q_r \exp \left[\frac{2\pi i r}{T} (t + \mathbf{k} \cdot \mathbf{x}) \right] + q_r^* \exp \left[- \frac{2\pi i r}{T} (t + \mathbf{k} \cdot \mathbf{x}) \right], \quad (2.1)$$

where q_r, q_r^* are quantities determining the amplitude and phase of the r th Fourier component, and the sign of $\mathbf{k} \cdot \mathbf{x}$ is that appropriate to an inward travelling wave. In the present case we are assuming that q_r is zero except when $\nu_1 T < r < \nu_2 T$.

In a classical theory q_r is a complex number such that

$$q_r q_r^* = \left(\frac{p_r}{8\pi^2 \nu_r^2 T} \sqrt{\frac{\mu_0}{\epsilon_0}} \right) \quad (2.2)$$

where p_r/T is the power flow across unit area perpendicular to the direction of propagation associated with the r th Fourier component of frequency ν_r , where

$$\nu_r = r/T, \quad (2.3)$$

and where $(\mu_0/\epsilon_0)^{1/2}$ is the characteristic impedance of free space. If we define a quantity n_r by the equation

$$n_r h \nu_r = p_r, \quad (2.4)$$

then n_r/T may formally be identified with the average number of quanta of energy $h\nu_r$ crossing unit area in unit time, and we may put

$$q_r = \left(\frac{h}{8\pi^2\nu_r\sqrt{\epsilon_0}} \right)^{\frac{1}{2}} n_r^{\frac{1}{2}} \exp i\phi_r, \tag{2.5}$$

where ϕ_r is the phase of the r th Fourier component of the vector potential at the wavefront defined by

$$t + \mathbf{k} \cdot \mathbf{x} = 0. \tag{2.6}$$

In the limiting case as $T \rightarrow \infty$, n_r is the average number of quanta per unit frequency bandwidth.

In what follows we shall assume that the phases of the different Fourier components are quite uncorrelated so that we may take the values of ϕ_r to be a set of independent random variables distributed with uniform probability over the range $0 < \phi_r < 2\pi$. This assumption is certainly valid as long as the radiation can be described by a stationary time series. Even when this is not the case, as when the electromagnetic energy is produced in bursts, the phases of the Fourier components of the radiation received by the observer will be effectively uncorrelated as long as the region of the source over which the intensity fluctuation is coherent is sufficiently small.

The voltage $V(t)$ produced across the input terminals to the square law detector by the vector potential defined by (2.1) will be of the form

$$V(t) = \sum_{r=1}^{\infty} \beta_r q_r \exp \left[\frac{2\pi i r}{T} (t + \mathbf{k} \cdot \mathbf{x}_1) \right] + \beta_r^* q_r^* \exp \left[- \frac{2\pi i r}{T} (t + \mathbf{k} \cdot \mathbf{x}_1) \right], \tag{2.7}$$

where \mathbf{x}_1 are the co-ordinates of the phase reference point and β_r is a complex quantity such that $\beta_r \beta_r^*$ is linearly proportional to the aerial aperture A and to the aerial efficiency at frequency r/T .

If we substitute from (2.5) and (2.7) in the equation

$$i(t) = b V^2(t), \tag{2.8}$$

then the low-frequency components in the output current of the square-law detector are given by an expression of the general form,

$$i(t) = eA \sum_{r=1}^{\infty} \frac{\alpha_r n_r}{T} + 2eA \sum_{r>s}^{\infty} \sum_{s=1}^{\infty} \left(\frac{\alpha_r \alpha_s n_r n_s}{T^2} \right)^{\frac{1}{2}} \cos \left[\frac{2\pi}{T} (r-s) (t + \mathbf{k} \cdot \mathbf{x}_1) + \phi_r - \phi_s \right], \tag{2.9}$$

where e is the electronic charge and α_r is defined by the equation

$$\alpha_r = \frac{\beta_r \beta_r^*}{eA} \frac{h}{4\pi^2\nu_r} \sqrt{\left(\frac{\mu_0}{\epsilon_0} \right)} b. \tag{2.10}$$

This unconventional and somewhat clumsy symbolism has been adopted so that a direct comparison may be made with the quantum treatment of the optical case in which the symbol α_r will correspond to the photocathode quantum efficiency.

Let us now suppose that the a.c. fluctuations in the detector output are passed through a filter, with a frequency response $F(f)$ which does not transmit d.c. so that

$$F(0) = 0, \tag{2.11}$$

then $J(t)$ the output current of this filter may be written

$$J(t) = A \sum_{r>s}^{\infty} \sum_{s=1}^{\infty} \left(\frac{\alpha_r \alpha_s n_r n_s}{T^2} \right)^{\frac{1}{2}} \left\{ F \left(\frac{r-s}{T} \right) \exp i \left[\frac{2\pi(r-s)}{T} (t + \mathbf{k} \cdot \mathbf{x}_1) + (\phi_r - \phi_s) \right] + F^* \left(\frac{r-s}{T} \right) \exp -i \left[\frac{2\pi(r-s)}{T} (t + \mathbf{k} \cdot \mathbf{x}_1) + (\phi_r - \phi_s) \right] \right\}. \quad (2.12)$$

This expression may be simplified if the filter bandwidth is so narrow that $\alpha_r n_r \simeq \alpha_s n_s$ for all values of r and s for which the frequency $(r-s)/T$ lies in the filter passband. In this case if we introduce two new indices l, m defined by

$$\frac{1}{2}(r+s) = l, \quad r-s = m, \quad (2.13)$$

we have that

$$J(t) = A \sum_{m=1}^M \sum_{l=T\nu_1}^{T\nu_2} \frac{a_l n_l}{T} \left\{ F \left(\frac{m}{T} \right) \exp i \left[\frac{2\pi m}{T} (t + \mathbf{k} \cdot \mathbf{x}_1) + (\phi_r - \phi_s) \right] + F^* \left(\frac{m}{T} \right) \exp -i \left[\frac{2\pi m}{T} (t + \mathbf{k} \cdot \mathbf{x}_1) + (\phi_r - \phi_s) \right] \right\}, \quad (2.14)$$

where M/T , the highest beat frequency passed by the filter, is very much less than $\nu_2 - \nu_1$, the bandwidth of the incident radiation, and where ϕ_r, ϕ_s are independent random variables distributed with uniform probability over the range

$$0 < \phi_r < 2\pi; \quad 0 < \phi_s < 2\pi.$$

This result will now be used to derive expressions for the correlation between intensity fluctuations at different points on the wavefront and for the mean square value of the intensity fluctuations at a single point.

(b) *The correlation between intensity fluctuations at different points on the wavefront*

Let us consider the case where the plane electromagnetic wave is incident on two aerials with apertures A_1, A_2 and phase reference points $\mathbf{x}_1, \mathbf{x}_2$ respectively. If $J_1(t), J_2(t)$ are the a.c. output currents of the two low frequency filters, which we shall assume to have identical characteristics, the correlation $C(T_0)$ between these two currents, averaged over a time interval T_0 , is given by

$$C(T_0) = \frac{1}{T_0} \int_0^{T_0} J_1(t-t_0) J_2(t) dt, \quad (2.15)$$

where

$$t_0 = \mathbf{k} \cdot (\mathbf{x}_1 - \mathbf{x}_2) \quad (2.16)$$

is the difference in time between the arrival of the incident radiation at the two aerials, and where T_0 may have any value less than T .

For our present purposes the quantity of interest is C , the ensemble average of $C(T_0)$ taken over an infinite number of independent time intervals each of length T_0 , which is equal to the time average

$$\lim_{T_0 \rightarrow \infty} C(T_0)$$

in the present case where the fluctuations are determined by a stationary time series.

For the classical radio case this calculation is very straightforward, since it is only necessary to average over the random radio-frequency phases. Terms in $C(T_0)$ which depend on ϕ_r, ϕ_s will average to zero and so we have immediately that

$$\bar{C} = 2e^2 A_1 A_2 \sum_{l=\nu_1 T}^{\nu_2 T} \frac{\alpha_l^2 n_l^2}{T} \sum_{m=1}^M \frac{|F(m/T)|^2}{T}, \tag{2.17}$$

which, as one would expect, is independent of T_0 .

In the limiting case $T \rightarrow \infty$, so we may replace the sums in (2.17) by integrals on putting $1/T = d\nu$ when we have that

$$\bar{C} = 2e^2 \int_{\nu_1}^{\nu_2} A_1 A_2 \alpha^2(\nu) n^2(\nu) d\nu \int_0^\infty F^2(f) df. \tag{2.18}$$

(c) *The mean square value of the intensity fluctuations*

If, for the moment, we ignore the effects of shot noise in the current of the square-law detector, the mean square fluctuations \bar{j}_C^2 in the output current of the filter may be defined as the ensemble average of

$$\frac{1}{T_0} \int_0^{T_0} J^2(t) dt,$$

where $J(t)$ is given by (2.14). Accordingly, \bar{j}_C^2 is given by (2.18) with $A_1 = A_2 = A$.

If a current I_0 flows in the detector circuit the mean square fluctuations are increased by the shot noise term \bar{j}_N^2 which, in the absence of space-charge smoothing (Rice 1944), is given by

$$\bar{j}_N^2 = 2eI_0 \int_0^\infty |F(f)|^2 df. \tag{2.19}$$

Now from (2.9) the incident radiation field increases the average current I_0 in the square-law detector by J_0 , where

$$J_0 = eA \sum_{r=1}^\infty \alpha_r n_r / T, \tag{2.20}$$

so, in the limiting case, as $T \rightarrow \infty$,

$$J_0 = e \int_0^\infty A \alpha(\nu) n(\nu) d\nu. \tag{2.21}$$

The total mean square fluctuations $\bar{J}^2(t)$ in the filtered output current of the square-law detector due to the incident radiation field are therefore given by

$$\bar{J}^2(t) = \bar{j}_N^2 + \bar{j}_C^2 = 2e^2 \left[\int_0^\infty A \alpha(\nu) n(\nu) d\nu + \int_0^\infty A^2 \alpha^2(\nu) n^2(\nu) d\nu \right] \int_0^\infty |F(f)|^2 df, \tag{2.22}$$

since the noise currents j_N and j_C are uncorrelated.

The first term in (2.22) represents the *shot-noise* term due to the discrete nature of the particles carrying the detector current, while the second term, which is due to beats between the different Fourier components of the incident radiation field, may be called the *wave interaction* noise.

In a typical radio case $An(\nu)$, which is effectively equal to the number of quanta extracted from the radiation field by the aerial in unit time and unit bandwidth, is of

the order of 10^5 , while $\alpha(\nu)$, which is effectively equal to the average number of electrons transported from cathode to anode of the square-law detector by the incidence of a single photon, might be of the order of 10^6 . Under these conditions $\overline{j_C^2}$ exceeds $\overline{j_N^2}$ by a factor of 10^{11} , so that the contribution of the latter is completely negligible.

However, at optical wavelengths $An(\nu)$ is of the order of 10^{-4} in a typical case, while $\alpha(\nu)$, the quantum efficiency of the photocathode, is of the order of 10^{-1} . Under these conditions everything is reversed and the classical theory would lead one to expect that $\overline{j_C^2}$ would be smaller than $\overline{j_N^2}$ by a factor $\sim 10^{-5}$. Admittedly it is not obvious that the quantitative predictions of a classical and determinist wave theory will be valid for the optical case, but it is shown below that indeed they are and that the wave interaction noise is simply another name for the excess photon noise, due on the corpuscular picture to the fact that photons obey Bose-Einstein statistics.

3. THE FLUCTUATIONS IN THE PHOTOELECTRIC EMISSION DUE TO A PLANE WAVE OF LIGHT

(a) *The probability of photoelectric emission by a plane wave of light*

In order to calculate the correlation between the times of emission of photoelectrons at different points of a wavefront and to find the mean square fluctuations in the photoemission current from a given photocathode, we shall first obtain an expression for the probability of photoemission in terms of the observables of the incident beam of light.

In a quantum theory one must regard the quantities q_r, q_r^* , which occur in (2.1), as operators rather than as numbers, and the quantities $n_r, \exp i\phi_r$, which correspond to the action and angle variables of the equivalent harmonic oscillator, are also operators satisfying commutation relations of the form (Heitler 1954),

$$n_r \exp(i\phi_s) - \exp(i\phi_s) n_r = \delta_{rs} \exp(i\phi_s), \quad (3.1)$$

$$n_r \exp(-i\phi_s) - \exp(-i\phi_s) n_r = -\delta_{rs} \exp(-i\phi_s), \quad (3.2)$$

where δ_{rs} is the familiar Kronecker symbol and (3.2) is the complex conjugate of (3.1).

In the standard treatment of the interaction between the matter and radiation fields, as given by Dirac (1947), one calculates the probability of a transition in which a photon is absorbed from a specific Fourier component of the radiation field so that the number of quanta associated with this component changes by unity. However, this procedure can clearly not be used to analyse an experiment in which we measure the correlation between the times of arrival of photons at different points of a wavefront, since, if the time of arrival of a photon is known to an accuracy Δt , the uncertainty, $\Delta F \equiv h\Delta\nu$, in the energy must satisfy the inequality

$$\Delta E \Delta t = h, \quad (3.3)$$

or

$$\Delta\nu \Delta t = 1. \quad (3.4)$$

If the particular Fourier component with which a specific photon is to be associated is known then $\Delta\nu = 1/T$, where T is the total observing time, and one has no knowledge whatever as to the actual moment, in the observation period, when the photon arrived.

It follows that the action and angle variables of the radiation field are not observables for the conditions under which one would look for a correlation between the arrival times of photons. As we have just shown in the classical analysis of the radio-frequency case the intensity fluctuations depend upon the beat frequencies between the different radio-frequency components of the incident radiation rather than upon the radio-frequency components themselves, while the correlation between the intensity fluctuations is determined by the amplitudes and relative phases of these beat frequencies.

When interpreting interference phenomena according to the corpuscular theory of radiation, it has been emphasized by Dirac (1947) that one must not talk of interference between two different photons, which never occurs, but rather of the interference of a photon with itself. This point was originally made for the case of spatial interference, as in an interferometer, but the arguments on which it is based are equally valid for temporal interference as in the phenomenon of a beat frequency. Accordingly, in the corpuscular theory, one must not interpret a beat frequency as an interference between photons of different energy, but rather as a phenomenon caused by the uncertainty in the energies of the individual photons which may be associated with either of the two Fourier components of the radiation field, the interference of which gives the beat frequency.

It follows that the observables appropriate to the measurement of a beat frequency are the *relative* phases of the two Fourier components and the *total* number of quanta associated with the two components. As is well known (Heitler 1954), these quantities can be measured simultaneously without violating the uncertainty principle since they are characterized by operators of the form

$$n_r + n_s \quad \text{and} \quad \exp i(\phi_r - \phi_s)$$

which commute. To prove this we have from (3.1) and (3.2) that

$$\begin{aligned} (n_r + n_s) \exp i(\phi_r - \phi_s) &= \exp i(\phi_r - \phi_s) n_r + \exp i(\phi_r - \phi_s) \\ &\quad + \exp i(\phi_r - \phi_s) n_s - \exp i(\phi_r - \phi_s) \\ &= \exp i(\phi_r - \phi_s) (n_r + n_s). \end{aligned} \quad (3.5)$$

For the specialized purposes of this paper, in which one is concerned simply with the fluctuations in the cathode currents of photocells, one may therefore discuss the interaction of the radiation field and the photocathode by a simplified theory in which the radiation field is characterized by a set of commuting operators and may therefore be treated classically. This procedure takes no specific account of the fact that the emission of a photoelectron reduces the total number of photons in the radiation field by one, but then there is no *a priori* knowledge of this number, still less of the actual distribution of these photons, with energy: all that is known, from a study of the light source, is the *average* number of photons arriving in unit time in unit bandwidth together with the fact that the fluctuations in the number of incident photons are controlled by Bose-Einstein statistics. It is this indeterminacy, basic to the existence of a correlation between photons, which makes it possible to use a classical treatment for the radiation and impossible to use the standard

quantized field treatment of the photoelectric effect; the latter applies rigorously to an experiment where the energy of the incident photon and the momentum of the emitted electron can both be known to the maximum accuracy permitted by the uncertainty principle.

In what follows we shall assume that Ψ represents the total wave function for the electrons and ions forming the photocathode when acted upon by the incident radiation field. Then Ψ will be a solution of the Schrödinger equation

$$i\hbar \frac{\partial \Psi}{\partial t} = (H_0 + H_1) \Psi, \quad (3.6)$$

where H_0 is the Hamiltonian for the matter field alone, and H_1 , the interaction energy, is of the form

$$H_1 = \sum_l \rho_l \mathbf{v}_l \mathfrak{A}(\mathbf{x}_l), \quad (3.7)$$

where \mathbf{v}_l is a dynamical variable describing the l th particle of charge ρ_l at the point \mathbf{x}_l , and $\mathfrak{A}(\mathbf{x}_l)$ is the vector potential acting on the l th particle.

From (2.1) and (2.5) the expression for H_1 may be written

$$H_1 = \sum_l \rho_l \mathbf{v}_l \sum_{r=1}^{\infty} \left(\frac{\hbar}{4\pi\nu_r T \sqrt{\epsilon_0}} \right)^{\frac{1}{2}} \{ n_r^{\frac{1}{2}} \exp(+i\phi_r) \exp(2\pi i\nu_r(t + \mathbf{k} \cdot \mathbf{x}_l)) + \exp(-i\phi_r) n_r^{\frac{1}{2}} \exp(-2\pi i\nu_r(t + \mathbf{k} \cdot \mathbf{x}_l)) \} \quad (3.8)$$

If the wave function Ψ_0 satisfying the zero-order equation

$$i\hbar \frac{\partial \Psi_0}{\partial t} = H_0 \Psi_0 \quad (3.9)$$

can be found, one can use a perturbation procedure to determine the first-order approximation to the exact solution from the equation

$$i\hbar \frac{\partial \Psi_1}{\partial t} - H_0 \Psi_1 = H_1 \Psi_0. \quad (3.10)$$

For our present purposes there is no need to derive a detailed theory for the photoelectric effect since quantitative data, such as the dependence of quantum efficiency on frequency, or the lower limit to the time delay of photoemission, can be taken from experiment. The important thing to note is that the interaction energy is linearly dependent upon the vector potential of the radiation field as, therefore, is the first-order perturbation in the wave function of the matter field. However, this is no longer the case in the second- and higher-order perturbation terms which describe processes in which several photons are simultaneously emitted or absorbed. Such processes are of two kinds. In the first, several photons are involved in the emission of a single photoelectron, but such events are very rare and can be ignored without significant error. In the second, two or more electrons are emitted in a process, in which each photoemission absorbs a single photon, which is clearly related to the problem of the coherent emission of photoelectrons. In a fully rigorous treatment one would have to use a higher-order perturbation theory to analyze this case but we shall make the simplifying assumption that the combined probability of

obtaining two photoemissions in a very small time interval from areas $A_1 A_2$ of a photocathode is equal to the product of the probability of obtaining a photoemission from each area separately. Clearly this assumption is valid in the physically important case when the areas $A_1 A_2$ belong to quite separate photocathodes illuminated by coherent light beams since the actual processes of photoemission in the two photocathodes are quite independent. The assumption will also be valid for a single photocathode as long as the fractional volume over which appreciable electronic interaction can take place inside the photocathode is very small compared with unity, a condition that will always be met in practice.

The solution for Ψ_1 , corresponding to the *absorption* of a photon by an electron which is then emitted from the photocathode, is of the general form

$$\Psi_1 = \sum_l \sum_{r=1}^{\infty} \eta_{lr} \exp(-i\phi_r) n_r^{\frac{1}{2}} \exp\{-2\pi i\nu_r(t + \mathbf{k} \cdot \mathbf{x}_l)\}, \quad (3.11)$$

where η_{lr} is a complex quantity involving the l th particle of the matter field and the r th component of the radiation field. The terms in H_1 proportional to $\exp\{2\pi i\nu_r(t + \mathbf{k} \cdot \mathbf{x}_l)\}$ do not contribute since they correspond to processes involving the *emission* of a photon by the particles of the photocathode.

The probability of a single photoemission in time dt is then proportional to

$$dt \int \Psi_1^* \Psi_1 d\tau,$$

where the integral is taken over the volume of the photocathode and a summation is made over all the particles of the matter field. If we assume that the photocathode of area A_1 is placed normal to the incident plane light wave so that (\mathbf{x}_1) are the co-ordinates of the midpoint of the cathode, then

$$P(\mathbf{x}_1, t) \equiv \int \Psi_1^* \Psi_1 d\tau \quad (3.12)$$

is given by an expression of the form

$$P(\mathbf{x}_1, t) = \sum_{r=1}^{\infty} A_1 \frac{\alpha_r n_r}{T} + 2A_1 \sum_{r>s}^{\infty} \sum_{s=1}^{\infty} \left(\frac{\alpha_r \alpha_s n_r n_s}{T^2} \right)^{\frac{1}{2}} \times \cos(2\pi(\nu_r - \nu_s)(t + \mathbf{k} \cdot \mathbf{x}_1) + (\phi_r - \phi_s) - (\theta_r - \theta_s)), \quad (3.13)$$

where $\theta_r/\nu_r, \theta_s/\nu_s$ determine the delays in the emission of a photoelectron after the absorption of photons of energy $h\nu_r, h\nu_s$ respectively. As the delay in photoemission is known experimentally (Forrester, Gudmundsen & Johnson 1955) to be much less than 10^{-10} s while, because of the limited amplifier bandwidths and the spread in transit time through the photomultiplier tube, the beat frequencies which are significant in a practical case all lie below 10^8 or 10^9 c/s, we may put

$$\theta_r - \theta_s = 0$$

in (3.13) without introducing significant error.

The quantity α_r is simply the cathode quantum efficiency for a normally incident plane wave of frequency r/T and, as in the analysis for the radio case, we shall assume that α_r is a smoothly changing function of frequency effectively constant over the maximum beat frequency bandwidth that can arise in practice. It would be difficult

to establish this assumption experimentally since the cathode quantum efficiency is normally measured with a light beam of bandwidth large compared to 10^8 c/s and any rapid changes in α_r , with frequency would be smoothed out, but it is almost certainly valid in view of the appreciable energy spread of the electrons inside the photocathode. We shall also assume that the quantity n_r , which represents the average number of quanta of energy crossing unit area in unit time, is a smoothly varying function of frequency effectively constant over the beat frequency bandwidth. As before we now introduce two indices l, m defined by

$$\frac{1}{2}(r+s) = l, \quad r-s = m,$$

when $P(\mathbf{x}_1, t)$ is given by

$$P(\mathbf{x}_1, t) = \sum_{r=1}^{\infty} A_1 \frac{\alpha_r n_r}{T} + 2A_1 \sum_{m=1}^M \sum_{l=L_1}^{L_2} \frac{\alpha_l n_l}{T} \cos \left(\frac{2\pi m}{T} (t + \mathbf{k} \cdot \mathbf{x}_1) + (\phi_r - \phi_s) \right), \quad (3.14)$$

a result that can be compared with (2.9).

(b) *The correlation between fluctuations in the emission currents of two separate photomultipliers*

Let us consider the case where a linearly polarized plane wave of light is normally incident on two separate photocathodes of areas A_1, A_2 centred at $\mathbf{x}_1, \mathbf{x}_2$ respectively. We assume that the photomultipliers are followed by bandpass filters with zero d.c. response, and we shall show that the average value of the correlation between the a.c. fluctuations in the output currents of these filters is identical with that derived above for the radio case by a classical deterministic theory.

As before, we take $J_1(t), J_2(t)$ to be the a.c. output currents of the two filters and we must then calculate \bar{C} the ensemble average of the integrated correlation defined by (2.15) and (2.16).

In this case the calculation is complicated by the necessity of averaging over the number and time of emission of the photoelectrons produced in time T as well as over the radio-frequency phases.

In the development of statistical theory a large number of methods have been evolved for analyzing problems of this kind. The one that we shall use is based on the so-called shot noise representation since, though not perhaps the most elegant procedure, it has the most direct physical interpretation in the present case. This procedure has been extensively studied by Rice (1944) and frequent use will be made of his results.

Following Rice we introduce a normalized probability function $p(t + \mathbf{k} \cdot \mathbf{x}_1)$ such that

$$\int_0^T p(t + \mathbf{k} \cdot \mathbf{x}_1) = 1, \quad (3.15)$$

which is related to $P(\mathbf{x}_1, t)$ by the equation

$$Np(t + \mathbf{k} \cdot \mathbf{x}) = P(\mathbf{x}_1, t), \quad (3.16)$$

where

$$N = \sum_{r=1}^{\infty} A\alpha_r n_r = I_0/e \quad (3.17)$$

and I_0 is the average photoemission current.

We now consider a particular time interval of length T , in which exactly K electrons are emitted from one photocathode and exactly N electrons from the other, so that the output currents of the filters following the photomultipliers may be written

$$J_1(t) = \sum_{k=1}^K e f_k(t-t_k), \tag{3.18}$$

$$J_2(t) = \sum_{n=1}^N e g_n(t-t_n), \tag{3.19}$$

where $e f_k(t-t_k)$, $e g_n(t-t_n)$ are the effects produced in the first and second filters by electrons of charge e emitted at times t_k and t_n respectively.

Since the filters do not pass d.c.

$$\int_{-\infty}^{\infty} f_k(t-t_k) dt = \int_{-\infty}^{\infty} g_n(t-t_n) dt = 0 \tag{3.20}$$

and it will further be assumed that $f_k(t)$, $g_n(t)$ only differ appreciably from zero in an interval Δ which is negligibly small compared with T .

In a complete discussion it would be necessary to note that $f_k(t)$ will vary from one photoemission to another, since it will depend to some extent upon such things as the emission velocities of the photoelectrons and upon the number and momentum distribution of the secondary electrons produced at each stage of the photomultiplication process. For the present, however, we shall ignore these effects, which would considerably complicate the algebra without adding anything significant to a basic understanding of the phenomenon, though they are of real practical importance since they impose a lower limit to the resolving time of the electronic equipment.

Accordingly, we shall assume that

$$\left. \begin{aligned} f_k(t-t_k) &= f(t-t_k), \\ g_n(t-t_n) &= g(t-t_n). \end{aligned} \right\} \tag{3.21}$$

Finally, we shall limit ourselves to the idealized case

$$f(t) \equiv g(t), \tag{3.22}$$

though to begin with it will be more convenient to retain both symbols.

From (2.15), (3.18) and (3.19) we have that

$$C(T_0) = \frac{1}{T_0} \int_0^{T_0} dt \sum_{k=1}^K \sum_{n=1}^N e^2 f(t-t_0-t_{1k}) g(t-t_{2n}). \tag{3.23}$$

To find \bar{C} we must average over the times of emission of the different photoelectrons, over the total number of photoelectrons emitted in a time interval T , and over the phases of the Fourier components of the radiation field so that

$$\bar{C} = \left\langle \frac{1}{T_0} \int_0^{T_0} dt \sum_{K=1}^{\infty} \sum_{N=1}^{\infty} e^2 \rho_1(K) \rho_2(N) \sum_{k=1}^K \sum_{n=1}^N \int_0^T f(t-t_0-t_{1k}) p_1(t_{1k} + \mathbf{k} \cdot \mathbf{x}_1) dt_{1k} \right. \\ \left. \times \int_0^T g(t-t_{2n}) p_2(t_{2n} + \mathbf{k} \cdot \mathbf{x}_2) dt_{2n} \right\rangle_{\text{aver.}}, \tag{3.24}$$

where the angle brackets denote an averaging over the phases of the individual Fourier components of the radiation field. The quantities

$$p_1(t_1 + \mathbf{k} \cdot \mathbf{x}_1), \quad p_2(t_2 + \mathbf{k} \cdot \mathbf{x}_2)$$

are defined by (3.16), (3.17) and (3.14) and differ only in so far as the areas A_1 , A_2 and the position vectors of the photocathodes are not identical. The quantities

$$\rho_1(K), \rho_2(N)$$

are the probabilities that exactly K and N photoelectrons are emitted in time T from the first and second photocathodes respectively. Rice (1944) has discussed the generalization of Campbell's theorem to the case where the probability of a fundamental event varies with time and it can easily be shown, along the lines of his analysis, that

$$\rho_1(K) = \frac{\bar{K}^K \exp(-\bar{K})}{K!}, \quad \rho_2(N) = \frac{\bar{N}^N \exp(-\bar{N})}{N!}, \quad (3.25)$$

where

$$\bar{K} = N_1 T, \quad \bar{N} = N_2 T, \quad (3.26)$$

but this result, which will be needed in the next section, is not essential to the present argument.

If we introduce new time variables τ_{1k}, τ_{2n} defined by

$$\tau_{1k} = t - t_0 - t_{1k}, \quad \tau_{2n} = t - t_{2n} \quad (3.27)$$

in place of t_{1k}, t_{2n} we see that

$$\begin{aligned} \bar{C} = \left\langle \frac{1}{T} \int_0^{T_0} dt \sum_{K=1}^{\infty} \sum_{N=1}^{\infty} e^2 \rho_1(K) \rho_2(N) \sum_{k=1}^K \sum_{n=1}^N \int_{-(t-t_0)}^{T-(t-t_0)} f(\tau_{1k}) p_1(t + \mathbf{k} \cdot \mathbf{x}_1 - \tau_{1k}) d\tau_{1k} \right. \\ \left. \times \int_{-t}^{T-t} g(\tau_{2n}) p_2(t + \mathbf{k} \cdot \mathbf{x}_2 - \tau_{2n}) d\tau_{2n} \right\rangle_{\text{aver.}} \end{aligned} \quad (3.28)$$

As long as $t < T - \Delta$ we may replace the integration limits over the variables τ_{1k}, τ_{2n} by $(-\infty, \infty)$ and since Δ/T is, *ex hypothesi*, negligibly small, the resulting error is also negligible.

From (3.16), (3.17) and (3.22) we get that

$$\bar{C} = \left\langle \int_0^{T_0} \frac{dt}{T_0} e^2 \sum_{K=1}^{\infty} \sum_{N=1}^{\infty} K \rho_1(K) N \rho_2(N) \frac{A_2}{A_1} \left\{ \int_0^{\infty} f(\tau_k) p_1(t + \mathbf{k} \cdot \mathbf{x}_2 - \tau_k) d\tau_k \right\}^2 \right\rangle_{\text{aver.}} \quad (3.29)$$

From (3.20) only the time-dependent part will contribute to \bar{C} , while all the terms explicitly dependent upon the phases of the individual Fourier components of the incident light will average to zero.

Hence, since

$$\left. \begin{aligned} \sum_{K=1}^{\infty} K \rho_1(K) &= \bar{K} = N_1 T = A_1 T \sum_{r=1}^{\infty} \alpha_r n_r, \\ \sum_{N=1}^{\infty} N \rho_2(N) &= \bar{N} = N_2 T = A_2 T \sum_{r=1}^{\infty} \alpha_r n_r, \end{aligned} \right\} \quad (3.30)$$

we have from (3·16), (3·17) and (3·14) that

$$\bar{C} = 2e^2 \sum_{l=L_1}^{L_2} \frac{A_1 A_2 \alpha_l^2 n_l^2}{T} \sum_{m=1}^M \frac{|F(fm)|^2}{T}, \quad (3\cdot31)$$

where

$$F(f) = \int_{-\infty}^{\infty} f(t) \exp[-2\pi ift] dt \quad (3\cdot32)$$

is the Fourier transform of $f(t)$ and satisfies the integral equation

$$f(t) = \int_{-\infty}^{\infty} F(f) \exp[2\pi ift] df \quad (3\cdot33)$$

as long as $\int_{-\infty}^{\infty} |f(t)| dt$ exists: a condition which certainly holds in the present case where $f(t)$ satisfies (3·7) and is zero outside $0 < t < \Delta$.

In the limiting case, as $T \rightarrow \infty$, (3·31) may be written

$$\bar{C} = 2e^2 A_1 A_2 \int_0^{\infty} \alpha^2(\nu) n^2(\nu) d\nu \int_0^{\infty} |F(f)|^2 df, \quad (3\cdot34)$$

which is formally identical with the correlation for the radio case given by (2·18), although the physical interpretation of the symbols $\alpha(\nu)$, $F(f)$ is different in the two cases. Thus in the optical case $\alpha(\nu)$ is simply the quantum efficiency of the photocathode, while in the radio case it depends upon the aerial efficiency and the conversion characteristics of the square law detector; again, in the radio case $F(f)$ is simply the frequency characteristic of the filter, while in the optical case it also depends upon the frequency characteristic of the photomultiplier. However, these are minor points which do not alter the fundamental conclusion that the correlation can be found by a purely classical theory in which the photocathode is regarded as a square law detector of suitable conversion efficiency. It is this result which provides the basis for our claim that the correlation is essentially an interference effect exemplifying the wave rather than the corpuscular aspect of light.

(c) *The mean square fluctuations in the emission current of a phototube*

We have argued above that the excess photon noise and the correlation between photons in coherent beams are closely related, and to bring this out more explicitly we shall derive an expression for the mean square fluctuations in the output current of a bandpass filter following a phototube of cathode area A placed normal to an incident plane wave of light.

Let $J_K(t)$ be the output current in the case when exactly K photoelectrons are emitted in time T , then we may use the same shot noise representation in the previous section and write

$$J_K(t) = \sum_{k=1}^K e f(t-t_k), \quad (3\cdot35)$$

so that

$$J_K^2(t) = \sum_{k=1}^K e^2 f^2(t-t_k) + 2 \sum_{k>n}^K \sum_{n=1}^K e^2 f(t-t_k) f(t-t_n). \quad (3\cdot36)$$

The mean square fluctuations $\bar{J}^2(t)$ can then be found by averaging over the times of emission of different photoelectrons, over the total number of electrons emitted in

time T and over the phases of the Fourier component of the incident light, so that we may write

$$\overline{J^2}(t) = \overline{j_N^2} + \overline{j_C^2}, \quad (3.37)$$

where

$$\overline{j_N^2} = \left\langle \sum_{K=1}^{\infty} e^{2\rho(K)} \int_0^T f^2(t-t_k) p_1(t+\mathbf{k}\cdot\mathbf{x}_1) dt_k \right\rangle_{\text{aver.}} \quad (3.38)$$

$$\overline{j_C^2} = \left\langle 2 \sum_{k>n}^K \sum_{n=1}^K \int_0^T f(t-t_k) p_1(t+\mathbf{k}\cdot\mathbf{x}_1) dt_k \int_0^T f(t-t_n) p_1(t+\mathbf{k}\cdot\mathbf{x}_1) dt_n \right\rangle_{\text{aver.}}, \quad (3.39)$$

where $p(t+\mathbf{k}\cdot\mathbf{x}_1)$ is defined by (3.14) and (3.16) and $\rho(K)$ is given by (3.25).

We shall now show that $\overline{j_N^2}$, the shot noise contribution to the mean square fluctuations, and $\overline{j_C^2}$ the wave interaction noise, are given by expressions formally identical with those derived in §2 for the classical radio case.

Only the time *independent* part of $p(t+\mathbf{k}\cdot\mathbf{x}_1)$ contributes to $\overline{j_N^2}$, since the time dependent part depends linearly on the random phases of the Fourier components of the incident light wave and averages to zero.

As long as $t_k < T - \Delta$ we may replace the limits of integration $(0, T)$ by $(-\infty, \infty)$ and, using Parseval's theorem in the form

$$\int_{-\infty}^{\infty} f^2(t) dt = \int_{-\infty}^{\infty} |F^2(f)| df = 2 \int_0^{\infty} |F^2(f)| df, \quad (3.40)$$

where $f(t)$, $F(\nu)$ are Fourier mates related by (3.32), (3.33), we get that

$$\overline{j_N^2} = 2e^2 A \int_0^{\infty} \alpha(\nu) n(\nu) d\nu \int_0^{\infty} |F(f)|^2 df \quad (3.41)$$

on substituting in (3.39) from (3.14), (3.16) and (3.25).

Since J_0 , the average emission current of the photocell, is given by

$$J_0 = eA \int_0^{\infty} \alpha(\nu) n(\nu) d\nu, \quad (3.42)$$

which is formally identical with (2.20), we see that j_N is indeed the shot noise current, for which

$$\overline{j_N^2} = 2e J_0 \int_0^{\infty} |F(f)|^2 df. \quad (3.43)$$

On the other hand, only the time *dependent* part of $p(t+\mathbf{k}\cdot\mathbf{x}_1)$ contributes to $\overline{j_C^2}$, the contribution from the time-independent part being zero from (3.20). By a discussion along identical lines with that given in the previous section it can be shown that

$$\overline{j_C^2} = 2e^2 \int_0^{\infty} A^2 \alpha^2(\nu) n^2(\nu) d\nu \int_0^{\infty} |F(f)|^2 df \sum_{K=1}^{\infty} \frac{K(K-1)\rho(K)}{K^2} \quad (3.44)$$

But from (3.25) it follows immediately that

$$\sum_{K=1}^{\infty} \frac{K(K-1)\rho(K)}{K^2} = 1, \quad (3.45)$$

so that

$$\overline{j_C^2} = 2e^2 \int_0^{\infty} A^2 \alpha^2(\nu) n^2(\nu) d\nu \int_0^{\infty} |F(f)|^2 df \quad (3.46)$$

If (3.46) is compared with (3.34) it will be seen that the two expressions are identical in the special case $A_1 = A_2$, which establishes the close connexion between the excess photon noise in a coherent beam of light and the correlation between photons in two coherent light beams. It may also be seen that the expression given

by (3.46) is identical with the second term in (2.21) which gives the wave interaction noise for the classical case, so that the excess photon noise due to the so-called 'bunching' of photons is the equivalent, in the corpuscular language, of the wave interaction noise of the undulatory picture. This identification is supported by the analysis of Kahn (1957) who obtains results identical with ours by a treatment based directly on the particle model of the incident light; but quite a different expression for the excess photon noise has been obtained by Fellgett (1949) and by Clark Jones (1953) who relied on thermodynamical arguments. In our view, however, thermodynamical considerations cannot be applied to the photoelectric effect and for this, and other reasons given in appendix II, we consider that their expression for the excess photon noise is wrong. If we may anticipate results which are to be given in a later paper; we may observe that this conclusion is supported by experimental measurements of the correlation between the fluctuations in separate phototubes. These results indicate that the ratio $\overline{j_C^2}/\overline{j_N^2}$ is approximately proportional to α , the quantum efficiency of the photocathodes, which is in accordance with the theory given above, but is incompatible with that of Fellgett (1949) in which $\overline{j_C^2}/\overline{j_N^2}$ should be independent of α .

Ideally, it would be desirable to confirm this conclusion by a direct measurement of the noise in the photoemission current, but this would be very difficult in practice since the excess photon noise is so small by comparison with the shot noise proper. Thus let us consider the case, appropriate to the laboratory experiment reported elsewhere (Hanbury Brown & Twiss 1956*a*), in which the light source is square in shape and subtends an angle θ^2 at the photocathode. Let us assume the idealized conditions in which the radiant energy is linearly polarized and concentrated into a narrow frequency band of rectangular shape centred at 4400 Å with an effective black-body temperature of 7000° K, and that the photocathode has a quantum efficiency of 20 % and a square aperture of width d . If the incident light is to be effectively a plane wave, the source must be so distant that it is not appreciably resolved by the photocathode and this sets an upper limit to the product θd given by the inequality $\theta d < 0.2\lambda$ where $\lambda = 4400$ Å is the mean wavelength of the incident light. The number of quanta n incident on the photocathode in unit frequency bandwidth then obeys the inequality $n < 3.7 \times 10^{-4}$ so that

$$\overline{j_C^2}/\overline{j_N^2} < \alpha n < 0.74 \times 10^{-4}.$$

Since this is appreciably smaller than the uncertainties in the measurement of the shot noise proper, and since we have assumed conditions exceptionally favourable to the observation of the excess photon noise, we can conclude that the contribution of the latter to the total noise current in a phototube is quite negligible in a practical case.

(d) *The signal to noise ratio in a measurement of the correlation*

To complete the fundamental theory we shall calculate the signal to noise ratio in a measurement of the correlation. Thus if S is given by

$$S = \bar{C} = \left\langle \frac{1}{T_0} \int_0^{T_0} J_1(t-t_0) J_2(t) dt \right\rangle_{\text{aver.}}, \quad (3.47)$$

and N is the r.m.s. fluctuation in $C(T)$ defined by

$$N^2 = \left\langle \left\{ \frac{1}{T_0} \int_0^{T_0} J_1(t-t_0) J_2(t) dt \right\}^2 \right\rangle_{\text{aver.}} - \bar{C}^2, \tag{3.48}$$

we shall calculate the ratio S/N .

As we have just seen, the contribution to N^2 due to the excess photon noise is negligible in comparison with the contribution from the shot noise proper, therefore in finding N we can assume that the fluctuations in the emission currents of the two photocathodes are due to independent shot noise currents. To this order of accuracy $J_1(t-t_0), J_2(t)$ may be represented by the Fourier series

$$\left. \begin{aligned} J_1(t-t_0) &= \sum_{n=1}^{\infty} \gamma_n \cos \left(\frac{2\pi n t}{T} - \phi_n \right), \\ J_2(t) &= \sum_{m=1}^{\infty} \eta_m \cos \left(\frac{2\pi m t}{T} - \psi_m \right), \end{aligned} \right\} \tag{3.49}$$

where ϕ_n, ψ_m are independent random variables distributed with uniform probability over the range 0 to 2π .

If the photomultiplying process and the bandpass filters introduce no additional noise it follows immediately from (3.43), with $d\nu = 1/T$ that

$$\left. \begin{aligned} \frac{1}{2} j_N^2 &= 2eI_1 \frac{|F_1^2(f_n)|}{T}, \\ \frac{1}{2} \eta_m^2 &= 2eI_2 \frac{|F_2^2(f_m)|}{T}, \end{aligned} \right\} \tag{3.50}$$

if the amplitude and phase response of the photomultiplier are included in $F(f)$. When the gain M of the photomultiplier is large, the noise introduced by the bandpass filters is normally negligible; but the number of secondary electrons emitted at a given stage of the photomultiplier is itself a fluctuating quantity, and it has been shown by Shockley & Pierce (1938) that this effect increases the output noise power by a term

$$\frac{M\mu - 1}{M(\mu - 1)} \simeq \frac{\mu}{\mu - 1}, \tag{3.51}$$

if $M \gg 1$, where μ is the secondary emission multiplication factor.

It is therefore more realistic to assume that

$$\left. \begin{aligned} \frac{1}{2} j_n^2 &= 2eI_1 \frac{\mu}{\mu - 1} \frac{|F_1(f_n)|^2}{T}, \\ \frac{1}{2} \eta_m^2 &= 2eI_2 \frac{\mu}{\mu - 1} \frac{|F_2(f_m)|^2}{T}. \end{aligned} \right\} \tag{3.52}$$

From (3.49) we have immediately that

$$N^2 = \left\langle \left| \frac{1}{T_0} \int_0^{T_0} dt \sum_{n,m=1}^{\infty} \gamma_n \eta_m \cos(2\pi f_n t - \phi_n) \cos(2\pi f_m t - \psi_m) \right|^2 \right\rangle_{\text{aver.}}, \tag{3.53}$$

where the angle brackets now mean that the expression contained within them is to be averaged over the random variables ϕ_n, ψ_m ; since these phases are all mutually uncorrelated only terms independent of them contribute to N^2 .

Integrating over time we get that

$$N^2 = \left\langle \left| \sum_{n,m=1}^{\infty} \frac{\gamma_n \eta_m}{2T_0} \left[\frac{\sin \{2\pi(f_n - f_m)T_0 - (\phi_n - \psi_m)\} + \sin(\phi_n - \psi_m)}{2\pi(f_n - f_m)} + \frac{\sin \{2\pi(f_n + f_m)T_0 - (\phi_n + \psi_m)\} + \sin(\phi_n + \psi_m)}{2\pi(f_n + f_m)} \right] \right|^2 \right\rangle_{\text{aver.}} \quad (3.54)$$

If we collect the terms independent of the random phases and proceed to the limit in which sums are replaced by integrals we get from (3.40) that

$$N^2 = \left(\frac{2e\sqrt{(I_1 I_2)\mu}}{\mu - 1} \right)^2 \frac{1}{T_0} \int_0^{\infty} |F_1(f_1)|^2 df_1 \int_0^{\infty} |F_2(f_2)|^2 df_2 \times \frac{1}{2} \left[\frac{\sin^2 \pi(f_1 + f_2)T_0}{\pi^2(f_1 + f_2)^2} + \frac{\sin^2 \pi(f_1 - f_2)T_0}{\pi^2(f_1 - f_2)^2} \right], \quad (3.55)$$

a result very similar to that derived, for a somewhat different case, by Rice (1945). The contribution to N^2 from the term proportional to

$$\sin^2(\pi(f_1 + f_2)T_0)/\pi^2(f_1 + f_2)^2$$

is quite negligible in the practical case where the integration time $T_0 > 10^3$ s, and where the lowest frequency passed by the filter following the photomultiplier tube is $> 10^6$ c/s. Furthermore, with $T > 10^3$, then $F(f_1) \simeq F(f_2)$ for values of $f_1 - f_2$ for which $\sin^2(\pi(f_1 - f_2)T_0)/\pi^2(f_1 - f_2)^2$ differs significantly from zero, and in this case N^2 may be written in the simplified form

$$N^2 = \left(\frac{2e\sqrt{(I_1 I_2)\mu}}{\mu - 1} \right)^2 \frac{1}{T_0} \int_0^{\infty} |F_1(f)F_2(f)|^2 df \frac{1}{2\pi} \int_0^{\infty} \frac{\sin^2 X}{X^2} dX. \quad (3.56)$$

The effective bandwidth of the bandpass filters, which we now assume to be identical, may be defined by the expression

$$b_v = \int_0^{\infty} |F(f)|^2 df / F_{\text{max}}^2, \quad (3.57)$$

where

$$|F_1^2(f)| = |F_2^2(f)| = |F(f)|^2$$

and F_{max} is the maximum value of $F(f)$.

If we define a normalized spectral density coefficient η by the relation

$$\eta = \int_0^{\infty} |F^4(f)| df / F_{\text{max}}^2 \int_0^{\infty} |F^2(f)| df, \quad (3.58)$$

then, since

$$\frac{1}{2\pi} \int_{-\infty}^{\infty} \frac{\sin^2 X}{X^2} dX = \frac{1}{2}, \quad (3.59)$$

we get from (2.20), (3.56) and (3.57) that†

$$N = \frac{\sqrt{2e^2\mu}}{\mu-1} (A_1 A_2)^{\frac{1}{2}} (b_c/T_0)^{\frac{1}{2}} \eta^{\frac{1}{2}} |F_{\max}|^2 \int_0^\infty \alpha(\nu) n(\nu) d\nu. \quad (3.60)$$

From (3.34) and (3.60) we have that the signal to noise ratio S/N is given by

$$\left(\frac{S}{N}\right)_{\text{r.m.s.}} = \sqrt{2} (1 - 1/\mu) (A_1 A_2)^{\frac{1}{2}} (b_v T_0)^{\frac{1}{2}} \eta^{-\frac{1}{2}} \int_0^\infty \alpha^2(\nu) n^2(\nu) d\nu / \int_0^\infty \alpha(\nu) n(\nu) d\nu, \quad (3.61)$$

which is independent of $|F_{\max}|^2$ and, therefore, of the gain of the photomultiplier tubes.

This result has been derived for the case where the incident light is linearly polarized. If the light is unpolarized, as is normally the case, the expression for N will be unaltered if the average number of quanta per cycle bandwidth is unaltered. However, the expression for S will be different since there is no correlation between quanta in different states of polarization, and we must decompose the incident beam into two independent components each with $\frac{1}{2}n$ quanta per cycle bandwidth. Since the correlation between coherent beams of polarized light is proportional to the square of the number of quanta per cycle bandwidth, the value for S must be reduced by a factor $\frac{1}{2}$, and the signal to noise ratio for the case of unpolarized light becomes

$$\left(\frac{S}{N}\right)_{\text{r.m.s.}} = (1/\sqrt{2}) (1 - 1/\mu) (A_1 A_2)^{\frac{1}{2}} (b_v T_0)^{\frac{1}{2}} \eta^{-\frac{1}{2}} \int_0^\infty \alpha^2(\nu) n^2(\nu) d\nu / \int_0^\infty \alpha(\nu) n(\nu) d\nu. \quad (3.62)$$

Because of the very small number of quanta received per unit bandwidth from even the hottest sources the signal to noise ratio will only be significant if one integrates for long times and also accepts the intensity fluctuations over the widest possible bandwidth. However, the signal to noise ratio is independent of the bandwidth of the incident light.

4. DISCUSSION

In calculating the correlation between the emission times of photoelectrons at different points on the wavefront of a plane wave of light we have used a quantum theory in which the incident radiation field is treated classically. Such a procedure is justified theoretically by the fact that the relevant observables of the radiation field can be characterized by commuting operators, but it is opposed to one's natural tendency to regard a correlation between the emission times of photoelectrons as essentially a quantum phenomenon for which a classical treatment of the radiation field would only be valid in the limiting case where the number of incident quanta is very large. Accordingly, to make the argument more acceptable from a physical point of view we shall consider the analogous case of a diffraction grating illuminated by monochromatic light to produce an interference pattern on a screen.

In this latter case it is well known that the average distribution of light intensity over the screen can be found by a classical wave theory, even in the limiting case

† This expression for N is smaller by a factor $1/\sqrt{2}$ than that given in an earlier paper (Hanbury Brown & Twiss 1956*a*) which applies when the correlation is measured by a somewhat different technique.

where the light is so weak that one can count the arrival of individual photons. As Born (1945) points out in discussing an essentially similar experiment, things are in no way altered if the screen is replaced by a mosaic of photoelectric elements; the experiment still illustrates the wave aspect of light, since the particle aspect can only really be brought out by observations in which the position of a single quantum is measured at two successive instants of time. If such observations were introduced into the present experiment, the interference pattern would be destroyed.

From the point of view in which light is viewed as a photon stream the appearance of interference effects is closely related to Heisenberg's uncertainty principle; an accurate knowledge of the transverse point of impact of a photon involves a corresponding uncertainty in the transverse momentum, and therefore an uncertainty in the element of the grating from which the photon has come. If we perform an experiment, such as blackening out the rest of the grating to determine the transverse momentum of the photons, then the main interference pattern once more disappears.

This state of affairs is exactly paralleled by the correlation experiment, which is the subject of this paper, if one everywhere substitutes the concepts of time and energy for those of position and momentum. Thus the bandwidth of the light and the length of the observation time in the correlation experiment are the analogues of the width and number of lines per unit length of the grating. The interference pattern in time, the beat phenomenon of the correlation experiment, arises because of the uncertainty in the energy of the photon which produced a specific photoemission, and is the analogue of the interference pattern on the screen which arises because of the uncertainty in the transverse momentum of a photon reaching a specific point on the screen. Both phenomena are to be understood from the particle point of view as being due to an uncertainty in the behaviour of a single photon and not as due to interference between different quanta. Finally, it may be noted, that if one partly removes the uncertainty in the energy of the incident photons in the correlation experiment, by using a highly monochromatic source or by analyzing the light with a prism of very great resolving power, the higher beat frequency components will disappear, just as the analogous components of the interference pattern on the screen will disappear if the angular width of the grating is suitably reduced.

Accordingly, since the radiation field can be treated classically in the case of the diffraction grating, it is only to be expected that it can be treated classically in analyzing the correlation experiment.

In this paper we have considered the idealized case where the two photocathodes lie on the same wavefront of the incident light. However, the emission time of a photoelectron is uncertain within limits determined in practice by the resolving time of the electronic equipment, so the observed correlation will not be affected as long as the difference in the time of arrival of a particular wavefront of the two photocathodes is small compared with this resolving time. This means that the position of the photocathodes need only be controlled to an accuracy determined by the bandwidth of the fluctuations rather than by the wavelength or bandwidth of the incident light.

To simplify the presentation, we have developed the fundamental theory for the case where this incident radiation is a plane wave. However, an arbitrary radiation field can be expressed as a sum of plane waves and, since the operators associated with the observables of one plane wave commute with all the operators associated with the observables of any other, one is equally justified in analyzing this general case by a theory in which the radiation field is treated classically; this will be done in a subsequent paper.

A quantum theory is needed to compute the probability of photoemission which, as we have shown, is proportional to the square of the amplitude of the incident light; but if this probability is known from experiment, one can calculate the correlation between the fluctuations in the photoemission currents at two separate phototubes by a fully classical theory in which the photoelectrodes are regarded as square law detectors of a suitable conversion efficiency. This emphasizes the fact that the theory is equally valid if the phototubes are replaced by true energy detectors such as bolometers or thermistors, though for reasons of signal to noise ratio these latter alternatives could not be used in a practical correlation experiment.

A purely classical theory can also be used to calculate the mean square fluctuations in the emission current of a single phototube. As we have shown these fluctuations can be represented as the sum of two terms, a *shot noise* term due to the discrete nature of the electrons carrying the photocurrent, and a term which we have called the *wave interaction noise* because in the classical theory it arises from the beats between the different Fourier components of the radiation field. The expressions for these terms are identical with those derived by Kahn (1957) in a treatment based directly on quantum statistics, and two conclusions can be drawn from this. First, that the shot noise is a consequence of the corpuscular nature of the electrons, it does not depend at all on the fact that the radiation field is also quantized; secondly, that the wave interaction noise is identical with the excess photon noise which is interpreted, in the language of the corpuscular theory, as due to the so-called 'bunching' of photons and which is essentially a consequence of the fact that light quanta obey Bose-Einstein statistics. This so-called 'bunching' is, of course, in no way dependent upon the actual mechanism by which the light energy was originally generated; still less does it imply that the photons must have been injected coherently into the radiation field. On the contrary, if one wishes to picture the electromagnetic field as a stream of photons, one has to imagine that the light quanta redistribute themselves over the wavefront, as the radiation field, which may be quite incoherent in origin, is focused and collimated into beams capable of mutual interference; thus the correlation between photons is determined solely by the energy distribution and coherence of the light reaching the photon detectors.

APPENDIX I. COHERENT INTERFERENCE AND THE EXTENT IN REAL SPACE OF AN ELEMENTARY CELL IN PHASE SPACE

When one is dealing with particles such as gas molecules the dimensions, in real space, of an elementary cell of volume L^3 in phase space are likely to be very small. Thus, in the extreme case of a hydrogen gas in which the uncertainties in the momenta are those appropriate to a thermal spread of 1°K , the dimensions, in real

space, of the elementary cell are of the order of 10 \AA cube and these will be correspondingly reduced for heavier gases or for larger uncertainties in the momenta of the individual molecules.

However, things are quite different in the case of light if the angular size of the source is very small. Thus, when light is received from a star, the volume in real space of an elementary cell can be many cubic metres, and we shall prove the general result that as long as two points are close enough together to permit virtually complete interference between the light rays reaching them, which implies that their separation is insufficient to resolve the star, then they lie in the same elementary cell in phase space.

For simplicity let us consider a very distant source of square angular aperture $\theta \times \theta$, where θ is very small, and two observing points on the earth with relative coordinates $(\Delta x, \Delta y, \Delta z)$ such that the light source lies on the z axis. Let us further suppose that the light is concentrated with a narrow frequency band of width $\Delta\nu$.

Then, since the volume of an elementary cell in phase space is h^3 we have that

$$\Delta p_x \Delta p_y \Delta p_z \Delta q_x \Delta q_y \Delta q_z = h^3, \quad (\text{A } 1)$$

where Δp , Δq are the uncertainties in the momentum and position respectively.

In the present case

$$\Delta p_x = \Delta p_y = \frac{h\nu}{c} \theta, \quad (\text{A } 2)$$

while if θ^2 is negligible compared with $\Delta\nu/\nu$

$$\Delta p_z = h\Delta\nu/c. \quad (\text{A } 3)$$

Substituting from (A 2) and (A 3) in (A 1) we get that

$$\theta^2 \frac{\Delta q_x \Delta q_y \Delta q_z}{\lambda^2} \Delta\nu = 1, \quad (\text{A } 4)$$

where $\lambda = c/\nu$.

Now if the interference fringes obtained from two coherent beams of light bandwidth $\Delta\nu$ are not to be appreciably weakened, the difference in the path length of the two beams must not exceed a wavelength of a frequency $\Delta\nu$ so that we must have

$$\Delta\nu\Delta z/c < 1. \quad (\text{A } 5)$$

Furthermore, if the transverse separation of the two points is to be so small that they do not resolve the source, one must certainly have

$$\theta\Delta x/\lambda < 1, \quad \theta\Delta y/\lambda < 1. \quad (\text{A } 6)$$

Combining the inequalities (A 5) and (A 6) with (A 4) one gets

$$\Delta x \Delta y \Delta z < \Delta q_x \Delta q_y \Delta q_z, \quad (\text{A } 7)$$

and since $\Delta q_x \Delta q_y \Delta q_z$ is the spatial volume of the elementary cell in phase space we have proved the required result.

The importance of this argument from the theoretical point of view is that it brings out the connexion between the wave and particle interpretations of the phenomenon intensity interference. Thus, on the classical picture one would expect

the intensity fluctuations in the light at two different points in space to be correlated as long as the light rays reaching these two points were capable of mutual interference; while on the quantum picture one would expect a correlation between the arrival times of quanta at different points as long as these lie in the same cell in phase space, and the above discussion shows that if the latter condition is satisfied then so is the former.

APPENDIX II. ON THE EXCESS PHOTON NOISE OF LIGHT DETECTORS

In the text we derived an expression for the noise in a photoemission current from first principles, and noted that an identical result has been obtained by Kahn (1957) with the aid of quantum statistics. However, a quite different result has been given by Fellgett (1949) and also by Clark Jones (1953) from thermodynamical arguments, and in this appendix we give the reasons for rejecting their procedure.

The thermodynamical argument depends in the first place on an analysis of a thermal detector in thermal equilibrium with a blackbody enclosure at temperature T . The discussion given by Clark Jones is based on a general theorem by Callen & Welton (1951) which enables one to find the fluctuations associated with a linear dissipation process, and which represents a powerful generalization of Nyquist's theorem (1928) to cover any case where the underlying physical process can be characterized by a generalized impedance. The treatment by Fellgett is more specific in that the equivalent electrical circuit is explicitly derived for a given detector, but it is identical in essentials. Both writers assume that the fluctuations in the thermal detector output are equal to the energy fluctuations in the thermal radiation field, half being due to the absorbed and half to the emitted radiation. In the case of the photocell the emitted stream of radiation does not exist so, it is argued, the fluctuations in this case will be reduced by one-half.

Two objections to this treatment are immediately apparent. In the first place the theorem of Callen & Welton does not apply, since the dissipation process of a thermal detector is non-linear, the equivalent resistance being itself a function of the temperature. Admittedly if the temperature fluctuations are very small compared with T the error is also small, but then so is the contribution of the excess photon noise. If we consider the analogous case of a radio antenna in a blackbody of temperature T , then the voltage fluctuations across the output terminals of the antenna can be found from Nyquist's theorem by taking the radiation resistance of the antenna to be at temperature T . However, if a square-law detector were placed between the antenna and the output terminals, one could not use a generalized Nyquist's theorem to find the energy fluctuations in the incident field or the fluctuations across the output terminals of the square-law detector, since this would ignore the presence of beats between different components of the radiation field.

The second and more serious objection is that one cannot in general equate the fluctuations in the output of a thermal or photon detector to the energy fluctuations in the thermal radiation field; the principle of detailed balancing applies to the average flow of energy but not to the fluctuations themselves. It is essentially for

this reason that the analysis for the thermal detector cannot be applied to the photo-cell and that the estimate of the excess photon noise given by Fellgett and Clark Jones is linearly proportional to the quantum efficiency rather than quadratically proportional as found by Kahn and by the present writers.

We thank Professor Rosenfeld for many helpful criticisms of this paper. We are also indebted to Dr Kahn for showing us his results before publication and for his valuable comments on our own approach. We also thank Dr Wolf and Professor le Couteur for their useful criticism.

REFERENCES

- Ádam, A., Jánossy, L. & Varga, P. 1955 *Acta Phys. Hung.* **4**, 301.
 Born, M. 1945 *Atomic physics*. Glasgow: Blackie and Son.
 Brannen, E. & Ferguson, H. I. S. 1956 *Nature, Lond.*, **178**, 481.
 Callen, H. B. & Welton, T. A. 1951 *Phys. Rev.* **83**, 34.
 Clark Jones, R. 1953 *Advances in electronics*, **5**. New York: Academic Press Inc.
 Dirac, P. A. M. 1947 *The principles of quantum mechanics*, 3rd ed. Oxford: Clarendon Press.
 Einstein, A. 1909 *Phys. Z.* **10**, 185.
 Fellgett, P. B. 1949 *J. Opt. Soc. Amer.* **39**, 970.
 Forrester, A. T., Gudmundsen, R. A. & Johnson, P. O. 1955 *Phys. Rev.* **99**, 1691.
 Fürth, R. & MacDonald, D. K. C. 1947 *Nature, Lond.*, **159**, 608.
 Hanbury Brown, R., Jennison, R. C. & Das Gupta, M. K. 1952 *Nature, Lond.*, **170**, 1061.
 Hanbury Brown, R. & Twiss, R. Q. 1954 *Phil. Mag.* **45**, 663.
 Hanbury Brown, R. & Twiss, R. Q. 1956a *Nature, Lond.*, **177**, 27.
 Hanbury Brown, R. & Twiss, R. Q. 1956b *Nature, Lond.*, **178**, 1046.
 Hanbury Brown, R. & Twiss, R. Q. 1956c *Nature, Lond.*, **178**, 1447.
 Heitler, W. 1954 *The quantum theory of radiation*, 3rd ed. Oxford: Clarendon Press.
 Jennison, R. C. & Das Gupta, M. K. 1956 *Phil. Mag.* (8), **1**, 55.
 Kahn, F. 1957 In preparation.
 Nyquist, H. 1928 *Phys. Rev.* **32**, 110.
 Rice, S. O. 1944 *Bell. Syst. Tech. J.* **23**, 294.
 Rice, S. O. 1945 *Bell. Syst. Tech. J.* **25**, 87.
 Shockley, W. & Pierce, J. R. 1938 *Proc. Inst. Rad. Engrs*, **26**, 321.

Interferometry of the intensity fluctuations in light

II. An experimental test of the theory for partially coherent light

BY R. HANBURY BROWN

Jodrell Bank Experimental Station, University of Manchester

AND R. Q. TWISS

Division of Radiophysics, C.S.I.R.O., Sydney, Australia

(Communicated by A. C. B. Lovell, F.R.S.—Received 20 June 1957)

A theoretical analysis is given of the correlation to be expected between the fluctuations in the outputs of two photoelectric detectors when these detectors are illuminated with partially coherent light. It is shown how this correlation depends upon the parameters of the equipment and upon the geometry of the experiment.

The correlation may be detected either by linear multiplication of the fluctuations in the two outputs or by a coincidence counter which counts the simultaneous arrival of photons at the detectors. The theory is given for both these techniques and it is shown that they are closely equivalent.

A laboratory test is described in which two photomultipliers were illuminated with partially coherent light and the correlation between the fluctuations in their outputs measured as a function of the degree of coherence. The results of this experiment are compared with the theory and it is shown that they agree within the limits of accuracy of the test; it is concluded that if there is any systematic error in the theory it is unlikely to exceed a few parts per cent.

1. INTRODUCTION

The basic principles of intensity interferometry, that is interferometry based on correlating the fluctuations of intensity in two beams of radiation, were presented in part I of this paper (Hanbury Brown & Twiss 1957). We showed there that the intensity fluctuations in two coherent beams are correlated and that, in the optical case, this correlation should be preserved in the process of photoemission so that the fluctuations in the anode currents of two phototubes should be partially coherent when they are illuminated by coherent beams of light.

We have already described (Hanbury Brown & Twiss 1956*a*) a preliminary test which established the existence of this correlation; however, this test was not designed to yield a precise quantitative result. It seemed desirable, especially in view of the considerable controversy about the principles involved, that a more exact check of the theory should be carried out, and so we have recently repeated the experiment with improved apparatus operating under more carefully controlled conditions. The results are reported below together with the necessary theoretical treatment of partially coherent light.

The principles of an intensity interferometer can be presented either in the classical terms of wave interference, or in terms of the relative times of arrival of photons. These two ways of looking at the phenomenon suggest two different experimental techniques for testing the correlation. The first technique, which may conveniently be regarded as illustrating the wave picture, consists in finding the correlation

between the fluctuations in the anode currents of two light detectors by means of a linear multiplier which takes the time average of their cross-product. The second technique, which illustrates the corpuscular nature of light, makes use of a coincidence counter to detect individual events in which photoelectrons are emitted simultaneously from the cathodes of two light detectors.

At first sight, the second of these techniques appears more attractive since, by the use of coincidence counters, it should be possible to circumvent the major technical difficulty in the design of an extremely sensitive correlator, namely the elimination of random drifts in the apparatus. However, it is shown below that, with present-day counters and photomultipliers, the use of a coincidence counter demands a highly monochromatic and brilliant light source if significant results are to be obtained in a reasonable observing time. The apparatus used in the present experiment was also intended for use in a stellar interferometer, and it was not considered practicable to restrict the spectrum of the starlight to an extremely narrow band. It was therefore decided to employ a system based on a linear multiplier, since such a system can be used with light of arbitrarily broad bandwidth and significant correlation can be obtained in periods of a few minutes using a standard arc lamp as a source of light.

Although the present paper deals only with an experiment using a linear multiplier we also give in an appendix a short theoretical treatment of the results to be expected with a coincidence counter. This treatment demonstrates the equivalence of the two techniques and the results can be used to interpret the experimental data of other experimenters who have attempted to detect correlation using coincidence counters.

2. THE CORRELATION EXPECTED BETWEEN THE OUTPUTS OF TWO PHOTO-ELECTRIC LIGHT DETECTORS ILLUMINATED BY PARTIALLY COHERENT LIGHT

In this section we shall consider theoretically the behaviour of the system shown in simple outline in figure 1. Two phototubes P_1P_2 are illuminated from a single source of light. The fluctuations in their anode currents are amplified by the amplifiers B_1B_2 and are multiplied together by the linear multiplier C . The time average of the multiplier output is proportional to the correlation and is measured by the integrating device M_1 .

The expressions given in part I of this paper for the average value of the correlation between the fluctuations in the anode currents of two separate phototubes were calculated for the idealized case in which the incident radiation was a plane wave. However, we also showed that the extension to the general case, where the light source and the apertures of the photocathodes are of arbitrary size, could be made entirely within the framework of a classical theory in which the photocathodes are regarded as square law detectors of suitable conversion efficiency.

2.1. *Light detectors with small aperture*

Under the conditions where the apertures of the individual photocathodes are too small to resolve the source appreciably, we can apply to the optical problem a similar analysis to that we have given elsewhere for a radio interferometer based on

the same principle (Hanbury Brown & Twiss 1954), and this is given in the course of the general discussion in appendix A.

When the incident radiation is approximately monochromatic we show in appendix A that $\overline{C(d)}$, the average value of the correlation when the apertures of the radiation detectors are separated by a distance d , is related to $\overline{C(0)}$ the correlation observed with zero separation, by the equation

$$\overline{C(d)} = \Gamma^2(\nu_0, d) \overline{C(0)}, \tag{2.1}$$

where ν_0 is the midband frequency of the incident radiation and where $\Gamma^2(\nu_0, d)$, the normalized correlation factor, is equal to the square of the modulus of the Fourier transform of the intensity across the equivalent line source. As we have pointed out in analyzing the radio case, this normalized correlation factor is related to the square

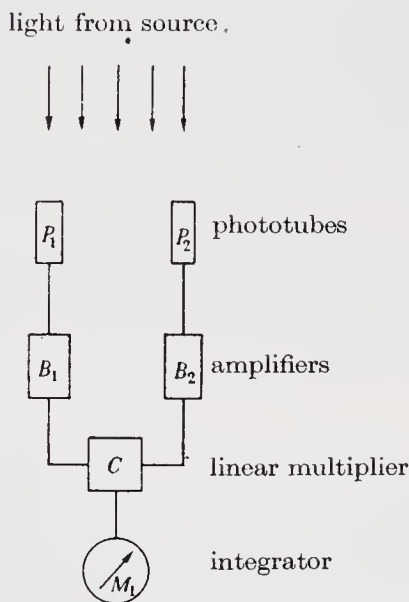


FIGURE 1. A simplified outline of an intensity interferometer.

of the visibility of the fringes that would be observed by a Michelson interferometer with the same baseline; it is also related to the square of the so-called *degree of coherence* (Zernike 1938) and the modulus of the *coherence phase factor* (Hopkins 1951).

Equation (2.1) is only valid when the fractional light bandwidth is very small and, when this is not the case, one must integrate over the light spectrum to find $\overline{C(d)}$. Thus, it was shown in part I that, if the incident light is a linearly polarized plane wave,

$$\overline{C(0)} = 2e^2 A_1 A_2 \int_0^\infty \alpha^2(\nu) n_0^2(\nu) d\nu \int_0^\infty |F(f)|^2 df, \tag{2.2}$$

where A_1, A_2 are the areas of the photocathode apertures; $\alpha(\nu)$ is the cathode quantum efficiency; $n_0(\nu)$ is the number of quanta incident on unit area in unit bandwidth; $F(f)$ is the combined frequency response of the photomultipliers and of the amplifiers. This equation is equally valid when the light source is of finite

angular size, provided that the photocathode apertures are themselves small, and hence we may write

$$\overline{C(d)} = 2e^2 A_1 A_2 \int_0^\infty \Gamma^2(\nu, d) \alpha^2(\nu) n_0^2(\nu) d\nu \int_0^\infty |F(f)|^2 df. \quad (2.3)$$

The assumptions underlying equation (2.3) are, however, too idealized for it to be applicable to a practical case even when the apertures of the light detectors are very small. It is necessary to take account of the fact that the quantum efficiency and spectral response may be different at the two photocathodes, and that the light may not be linearly polarized; furthermore, the electrical frequency response of the photomultipliers and amplifiers may not be identical in the two channels and there will inevitably be a slight loss of correlation in the correlator system. To take account of these factors equation (2.3) may be written in the convenient form

$$\overline{C(d)} = e^2 \epsilon A_1 A_2 \beta_0 \overline{\Gamma^2(d)} \alpha^2(\nu_0) n_0^2(\nu_0) \sigma B_0 b_v |F_{\max.}|^2, \quad (2.4)$$

where $(1 - \epsilon)$ is the fraction of the correlation lost in the correlator circuits; B_0 is the effective bandwidth of the light defined by

$$B_0 = \left[\int_0^\infty \alpha_1(\nu) n_1(\nu) d\nu \int_0^\infty \alpha_2(\nu) n_2(\nu) d\nu \right]^{\frac{1}{2}} / \alpha(\nu_0) n_0(\nu_0) \quad (2.5)$$

and

$$\left. \begin{aligned} n_1(\nu) &= n_{1a}(\nu) + n_{1b}(\nu), & n_2(\nu) &= n_{2a}(\nu) + n_{2b}(\nu), \\ \alpha^2(\nu_0) n_0^2(\nu_0) &= \alpha_1(\nu_0) \alpha_2(\nu_0) n_1(\nu_0) n_2(\nu_0) \end{aligned} \right\} \quad (2.6)$$

and the subscripts a, b refer to two orthogonal directions of polarization; where σ , the spectral density, is defined by

$$\sigma = \int_0^\infty \alpha_1(\nu) \alpha_2(\nu) n_1(\nu) n_2(\nu) d\nu / B_0 \alpha^2(\nu_0) n_0^2(\nu_0) \quad (2.7)$$

and the polarization factor β_0 is defined by

$$\beta_0 = 2[n_{1a}(\nu) n_{2a}(\nu) + n_{1b}(\nu) n_{2b}(\nu)] / n_1(\nu) n_2(\nu), \quad (2.8)$$

so that $\beta_0 = 1$ when $n_a(\nu) = n_b(\nu)$ as in the case of randomly polarized light. The mean value $\overline{\Gamma^2(d)}$ of the normalized correlation factor is defined by

$$\overline{\Gamma^2(d)} = \frac{\int_0^\infty \Gamma^2(\nu, d) \alpha_1(\nu) \alpha_2(\nu) [n_{1a}(\nu) n_{2a}(\nu) + n_{1b}(\nu) n_{2b}(\nu)] d\nu}{\int_0^\infty \alpha_1(\nu) \alpha_2(\nu) [n_{1a}(\nu) n_{2a}(\nu) + n_{1b}(\nu) n_{2b}(\nu)] d\nu} \quad (2.9)$$

and b_v , the effective cross-correlation bandwidth of the amplifiers, is defined by

$$|F_{\max.}|^2 b_v = \frac{1}{2} \int_0^\infty [F_1(f) F_2^*(f) + F_1^*(f) F_2(f)] df, \quad (2.10)$$

where $|F_{\max.}|$ is the maximum value of $\frac{1}{2}[F_1(f) F_2^*(f) + F_1^*(f) F_2(f)]$.

We shall use equation (2.4) in a later part of this paper to interpret some observations on Sirius which have been briefly reported elsewhere (Hanbury Brown & Twiss 1956*b*). However, it cannot be applied to the experiment analyzed in the

present paper in which the apertures of the light detectors were so large that they partially resolved the source. In this case the light cannot be regarded as coherent over the whole aperture of the light detectors and the correlation given by equation (2.4) must be reduced by the *partial coherence factor* $\bar{\Delta}$, where the bar denotes that the factor has been found by averaging over the frequency spectrum. The value of $\overline{\Gamma^2(d)}$, the normalized *correlation factor*, is now a function of both the angular size of the source and aperture of the light detectors.

2.2. Light detectors with large apertures

If no restrictions are placed upon the spectrum of the light or the intensity distribution over the source or the shape of the photocathodes, the general expression for the expected correlation is impracticably complex. However, for the purposes of the present paper we have greatly simplified the analysis by making the assumptions: (i) the intensity is uniform over the source of light, which is taken to be either circular or rectangular; (ii) the two photocathodes have identical rectangular apertures and the quantum efficiency is constant over each cathode; (iii) the quantum efficiency and the number of quanta received per unit bandwidth do not vary significantly

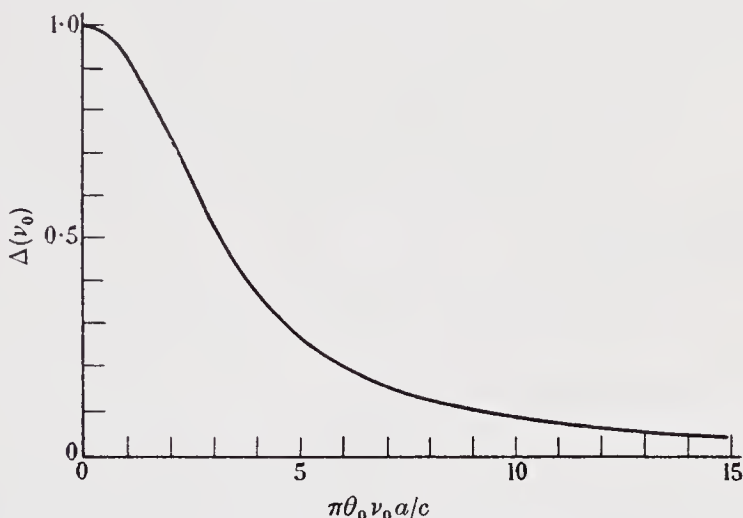


FIGURE 2. The variation of the partial coherence factor, $\Delta(\nu_0)$, with the parameter $\pi\theta_0\nu_0 a/c$, calculated for a circular source of angular diameter θ_0 viewed by two identical light detectors with square apertures $a \times a$.

over a frequency range equal to the bandwidth of the correlator. On the other hand, it will be assumed that the spectral width of the light is so narrow that both $\Gamma^2(\nu_0, d)$ and $\Delta(\nu_0)$ may be taken as constant over the light bandwidth, and that we may put

$$\overline{\Delta\Gamma^2(d)} \simeq \Delta(\nu_0) \Gamma^2(\nu_0, d).$$

The expressions for $\Gamma^2(\nu_0, d)$ and $\Delta(\nu_0)$, based on the assumptions stated above, have been derived in appendix A. The numerical values for the case of a circular source viewed by two square cathodes of identical size have been calculated from equations (A25) and (A26) by means of the Manchester University Electronic Computing Machine. Figure 2 shows the partial coherence factor $\Delta(\nu_0)$ as a function of $\pi\theta_0\nu_0 a/c$, where θ_0 is the apparent angular diameter of the source and a is the

width of the photocathode apertures. Figure 3 shows the normalized correlation factor $\Gamma^2(\nu_0, d)$ as a function of $\pi\theta_0\nu_0 d/c$, where d is the cathode separation and $\pi\theta_0\nu_0 a/c$ has the value 3.06 which is appropriate to the present experiment.

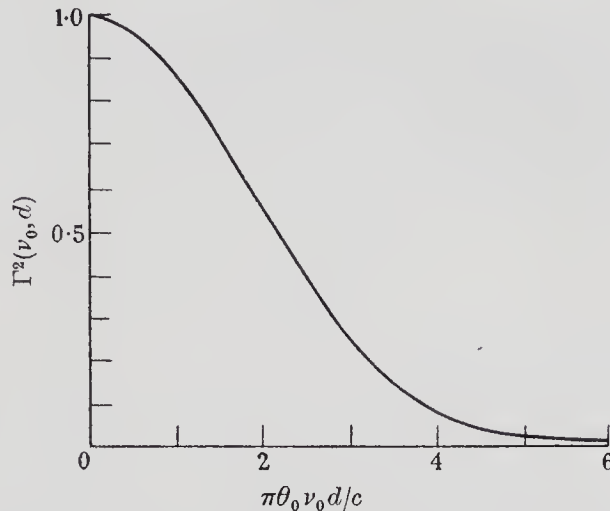


FIGURE 3. The variation of the normalized correlation factor $\Gamma^2(\nu_0, d)$ with the parameter $\pi\theta_0\nu_0 d/c$, calculated for a circular source of angular diameter θ_0 viewed by two identical light detectors with square apertures $a \times a$, where $\pi\theta_0\nu_0 a/c = 3.06$.

2.3. The expected signal to noise ratio

We proved in part I that the r.m.s. uncertainty $N(T_0)$ in the correlation measured over an observing time T_0 depends, in a practical case, only upon the magnitude of the photomission current, since the excess photon noise is negligible with any known light source. This enables us to write $N(T_0)$ immediately in the form

$$N(T_0) = \frac{e^2\mu}{\mu-1} (1+a)(1+\delta) (A_1 A_2)^{\frac{1}{2}} \left(\frac{2b_v \eta}{T_0} \right)^{\frac{1}{2}} |F_{\max.}|^2 \alpha(\nu_0) n_0(\nu_0) B_0, \quad (2.11)$$

which differs from equation (3.60) in part I by the two factors $(1+a)$ and $(1+\delta)$. The first factor has been introduced to allow for the presence of stray light, so that $(1+a)$ is the ratio of the total incident light to that from the source alone. The second factor has been introduced to allow for the presence of excess noise produced in the correlator, so that $(1+\delta)$ is the ratio of the total r.m.s. uncertainty in the reading of the integrating motor M_1 to the r.m.s. uncertainty due to fluctuations in the output of the photomultiplier tubes. In addition the quantity η , which is the normalized spectral density of the cross-correlation frequency response of the amplifiers following the phototubes, must be defined by

$$\eta = \int_0^\infty |F_1^2(f) F_2^2(f)| df/b_v |F_{\max.}|^4 \quad (2.12)$$

in the practical case where the individual frequency responses of the two amplifiers are *not* identical, rather than by equation (3.58) of part I.

The only other quantity which has not previously been defined in the present paper is the factor $\mu/(\mu-1)$ which represents the excess noise introduced by the

photomultiplier chain. It is known (Shockley & Pierce 1938) that μ is equal to the multiplication factor of the first stage, at least as long as this is not too great.

If we compare equations (2.4) and (2.11) it will be seen that both the correlation $\overline{C(d)}$ and the uncertainty, or noise, in the output are linearly proportional to $|F_{\max.}|^2$. It follows that their ratio is independent of the gain of the equipment. We have therefore adopted the practice in the present papers of expressing both the observed and theoretical values of correlation as *signal to noise ratios* S/N . The theoretical value of this ratio, from equations (2.4) and (2.11) is

$$\frac{S}{N} = \frac{\overline{C(d)}}{N(T_0)} = \epsilon\beta_0 \frac{\mu-1}{\mu} \frac{(A_1 A_2)^{\frac{1}{2}}}{(1+a)(1+\delta)} \alpha(\nu_0) n_0(\nu_0) \left(\frac{b_\nu T_0}{2\eta}\right)^{\frac{1}{2}} \sigma\Delta(\nu_0) \Gamma^2(\nu_0, d), \quad (2.13)$$

where the factor $\Delta(\nu_0) \Gamma^2(\nu_0, d)$ has been substituted for $\Gamma^2(d)$ to allow for the finite size of the photocathode apertures.

To compare the theory with experiment we need to develop equation (2.13) to give the signal to noise ratio in the practical case where successive measurements may be made with different values of light flux. Let us suppose that, in the r th measurement, of duration T_r , the number of quanta incident in unit bandwidth at frequency ν_0 is $n_r(\nu_0)$. If the gain of the equipment has been kept the same for all the observations, the average value of the final reading of the integrating motor is proportional to $\Sigma n_r^2(\nu_0) T_r$; while the r.m.s. uncertainty in the value of a given reading can be found by adding the individual fluctuations incoherently, so that it is proportional to $(\Sigma n_r^2(\nu_0) T_r)^{\frac{1}{2}}$. The theoretical value of the signal to noise ratio, in a convenient form for comparison with experiment, may therefore be written,

$$\frac{S}{N} = \frac{\overline{C(d)}}{N(\Sigma T_r)} = \epsilon\beta_0 \frac{\mu-1}{\mu} \frac{(A_1 A_2)^{\frac{1}{2}}}{(1+a)(1+\delta)} \alpha(\nu_0) \left(\frac{b_\nu}{2\eta}\right)^{\frac{1}{2}} \sigma\Delta(\nu_0, d) \frac{\sum_{r=1}^M n_r^2(\nu_0) T_r}{\left[\sum_{r=1}^M n_r^2(\nu_0) T_r\right]^{\frac{1}{2}}} \quad (2.14)$$

2.4. *The limiting signal to noise ratio for an arbitrarily large source*

In the limiting case where the source is completely resolved by an individual photocathode, the signal to noise ratio, with the cathodes optically superimposed, tends monotonically to a value determined simply by the effective black-body temperature of the source at the received wavelength, and this limit is independent of the source shape. To show this we consider first the case where the source is of arbitrary rectangular shape with an apparent angular width θ_1, θ_2 . Then, in the limit,

$$A\theta_1\theta_2\nu_0^2/c^2 \rightarrow \infty \quad (2.15)$$

and we have from equations (2.13, A 23) that the signal to noise ratio tends to the limiting value

$$\lim_{\theta \rightarrow \infty} \left(\frac{S}{N}\right) = K_1 \frac{\alpha(\nu_0) n_0(\nu_0) c^2}{\nu_0^2 \theta_1 \theta_2}, \quad (2.16)$$

where K_1 is a constant of proportionality given by

$$K_1 = \frac{\epsilon\beta_0\sigma}{(1+a)(1+\delta)} \frac{\mu-1}{\mu} \left(\frac{b_\nu T_0}{2\eta}\right)^{\frac{1}{2}}, \quad (2.17)$$

which depends solely on the parameters of the electronic system and upon the spectral density of the light.

It may be noted that

$$Q_0 = \frac{2\gamma_0 n_0(\nu_0)}{\theta_1 \theta_2} \quad (2.18)$$

is the number of quanta of both polarizations emitted from an area of the source in unit bandwidth and unit solid angle. The factor 2 is included to allow for the fact that in practice the light beam must be split in order to superimpose the photocathodes, and the factor γ_0 takes account of any loss of light in the optical system. If the black-body temperature of the source at a frequency ν_0 is Θ_0 , then

$$Q_0 = \frac{2\nu_0^2}{c^2} [\exp(h\nu_0/k\Theta_0) - 1]^{-1} \quad (2.19)$$

and substituting in equation (2.16) the maximum signal to noise ratio from a rectangular source, however large, is given by

$$\left(\frac{S}{N}\right)_{\max.} = K_1 \frac{\alpha(\nu_0)}{\gamma_0} [\exp(h\nu_0/k\Theta_0) - 1]^{-1}. \quad (2.20)$$

This limit will clearly apply whatever the shape of the source, so long as it can be approximated by a series of rectangles or its area can be defined by a Riemann integral. It is interesting to note that under these conditions the signal to noise ratio depends upon the temperature but not upon the shape of the source; thus, effectively the equipment operates as pyrometer.

3. DESCRIPTION OF THE APPARATUS

3.1. *The optical equipment*

A simplified outline of the optical equipment is shown in figure 4. A secondary light source was formed by a circular pinhole 0.19 mm in diameter on which the image of a mercury arc was focused by a lens. The image of the arc in the plane of the pinhole was approximately 5 cm in length and its position was adjusted so that the pinhole lay in the relatively bright part of the arc close to one of the electrodes. The arc lamp, Mazda type ME/D 250 W was supplied by a direct current of approximately 4 A and the 4358 Å line of the mercury spectrum was isolated by means of a liquid filter with a transmission of 82% at 4358 Å. The beam of light from the pinhole was divided by a semi-transparent mirror to illuminate the cathode of the photomultipliers P_1 , P_2 . The mirror surface was formed by evaporating pure aluminium on to glass, the reverse side being bloomed with cryolite to reduce unwanted internal reflexions. The area of each cathode exposed to the light was limited by a square aperture of 5 × 5 mm, and the distance from the pinhole to each cathode was adjusted to be 2.24 m with an accuracy of about 2 mm.

The photomultipliers were a matched pair, R.C.A. type 6342, with flat end-on cathodes and ten stages of multiplication. The photocathode surfaces had a maximum response at about 4000 Å. Tests at the National Physical Laboratory showed that the quantum efficiencies of the two cathodes, measured at 4000 Å, were 16.9 and 14.6% and that the shapes of the spectral response curves were almost

identical. The type 6342 photomultiplier has a small spread in electron transit time, particularly when the photocathode aperture is limited, and the effective bandwidth of the secondary emission amplification considerably exceeds the limit of 45 Mc/s set by the amplifiers in the correlator.

In order that the degree of coherence between the light on the two cathodes might be varied at will, one of the photomultipliers (P_2) was mounted on a horizontal slide which could be traversed normal to the incident light. Thus the cathode apertures, as viewed from the pinhole, could be superimposed or separated by any amount up to several times their width.

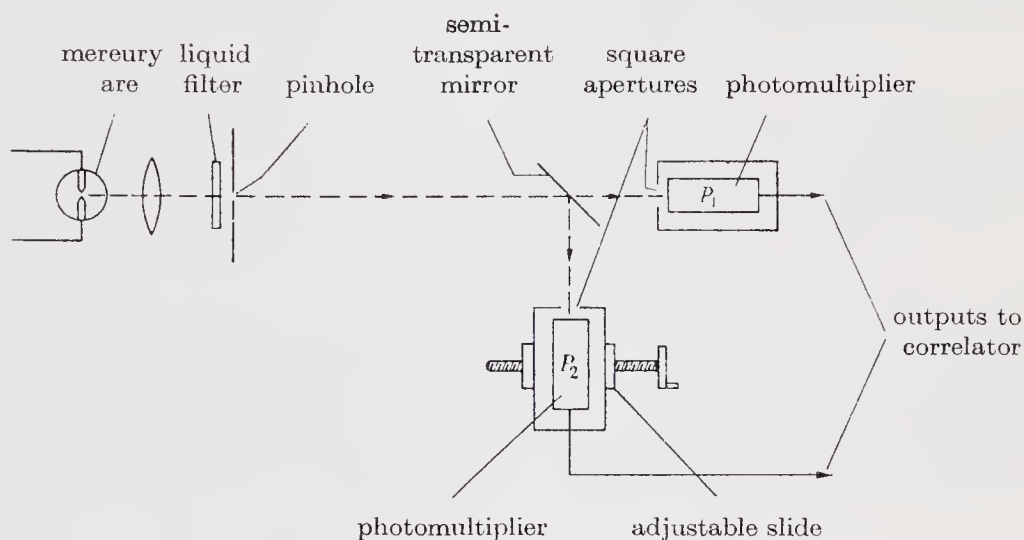


FIGURE 4. A simplified outline of the optical system.

The fluctuations in the anode currents of the photomultipliers were transmitted to the correlator through coaxial cables of equal length. In each case a simple high-pass filter was inserted between the anode and the input to the cable to remove the direct current component.

3.2. *The correlator*

A simplified diagram of the correlator is shown in figure 5. The cable from each of the photomultipliers was terminated in a matched load and the voltage fluctuations across this load were applied to one of the two input channels of the correlator. Both channels consisted of a phase-reversing switch followed by a wide-band amplifier. The switch (S_1) in channel 1 was electronic and reversed the phase of the input voltage 10000 times per second in response to a 5 kc/s square wave from the generator G_1 . It is essential to reduce amplitude modulation of the signal by this switch to an extremely low level in order to prevent spurious drifts in the equipment; for this reason the gain of the switch was equalized in both positions by means of an automatic balancing circuit comprising a detector, a selective 5 kc/s amplifier B_3 and a synchronous rectifier R_1 . The phase-reversing switch S_2 in channel 2 consisted of a relay-operated coaxial switch which reversed the phase of the input every 10 s in response to a 0.05 c/s square wave from the generator G_2 .

The wide-band amplifiers B_1 , B_2 were identical in construction, their gain was substantially constant (± 1 db) from about 5 to 45 Mc/s and decreased rapidly outside this band. The outputs of these amplifiers were multiplied together in the multiplier C , which consisted of a balanced arrangement of two pentode valves with their anodes in push-pull. The output of the multiplier was then amplified by a high-gain selective amplifier B_4 tuned to 5 kc/s with a bandwidth of 70 c/s. The output of B_4 was applied to the synchronous rectifier R_2 which was of the conventional

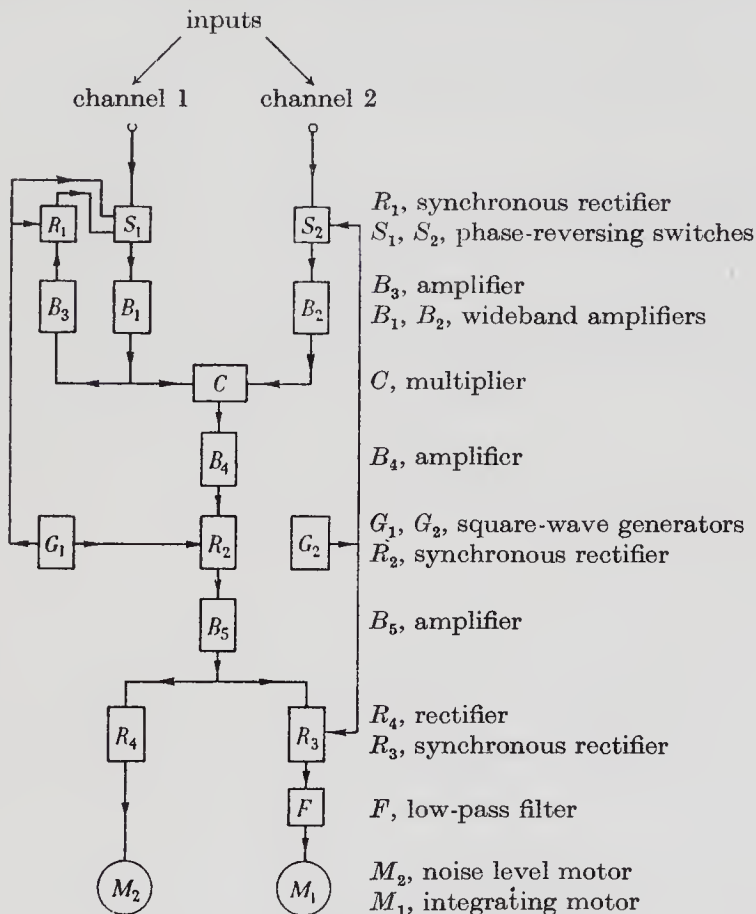


FIGURE 5. An outline of the correlator.

type using a ring of four diodes synchronized by the 5 kc/s switching wave generated by G_1 . The rectifier R_2 was followed by the 0.05 c/s amplifier B_5 which was relatively broadband and passed frequencies from about 0.01 to 0.25 c/s. The final synchronous rectifier R_3 consists of a relay-operated switch which, in response to the 0.05 c/s square wave from G_2 , periodically reversed the connexions between the output of the amplifier B_5 and the integrating motor M_1 . A low-pass filter, containing only passive elements, was inserted between the output of R_3 and the motor to restrict the bandwidth of the signal to the range 0 to 0.01 c/s. The motor itself was a miniature integrating motor coupled through a reduction gear to a revolution counter; it was capable of rotation in either direction and tests showed the relation between speed and input voltage to be linear to better than 1%. An additional integrating motor M_2 was provided to monitor the r.m.s. level of the output voltage from the amplifier B_5 .

If the photomultipliers are illuminated with uncorrelated beams of light then the inputs to the correlator are mutually incoherent random noise voltages. Under these conditions the output of the multiplier is random noise with a spectral density which has a maximum around zero frequency and which decreases to zero at about 40 Mc/s. The corresponding output from the 5 kc/s amplifier B_4 is random noise centred about 5 kc/s with a bandwidth of 70 c/s. After passing through the synchronous rectifier R_2 the spectrum extends from 0 to 35 c/s, and after passing through amplifier B_5 and the second synchronous rectifier R_3 it is reduced to a band extending from about 0 to 0.25 c/s. The low-pass filter following the rectifier R_3 finally restricts the bandwidth to the range 0 to 0.01 c/s. Under the influence of this noise the motor spins in either direction at random and the reading of the revolution counter remains close to zero. However, if there is any correlation between the output voltage of the photomultipliers a 5 kc/s component appears at the anode of the multiplier; this component is coherent with the 5 kc/s switching wave and reverses in phase every 10 s in synchronism with the 0.05 c/s switching wave. After amplification by the selective amplifier B_4 the 5 kc/s component produces a 0.05 c/s square wave in the output of the synchronous rectifier R_2 , which in turn is amplified by B_5 and rectified synchronously by R_3 to produce a direct current component in the voltage applied to the integrating motor M_1 . Thus, when there is correlation between the input voltages, the integrating motor revolves more in one direction than the other and the reading on the revolution counter increases with time.

The principal difficulty in designing the correlator was to reduce the random drifts in the output to an acceptable value. It was desirable that any drift should be less than the r.m.s. deviation of the integrating motor M_1 , due to noise alone, in a period of several hours. This requirement sets an unusually stringent limit to the tolerable level of any spurious signals in the correlator or to any drift in the synchronous rectifiers. For example a 5 kc/s signal, coherent with the switching wave frequency, will produce an output equal to the r.m.s. deviation of the output counter in 1 h if it is greater than 120 db below noise at the output of the multiplier. In a simple system employing a phase-reversing switch in only one channel, it is difficult to reduce random drifts to an acceptable value; however, by the use of two reversing switches and two synchronous rectifiers in cascade it was found possible to reduce the drift by several orders of magnitude without the use of precisely balanced circuits. It was also necessary to ensure that there was no electrical coupling between the inputs to the correlator, and that these circuits did not pick up signals from external sources. For this reason the photomultipliers were heavily screened and all their supply leads were thoroughly decoupled. Any coupling between the two channels which takes place after the phase-reversing switches does not give rise to spurious correlation, and therefore the switches were put as close as possible to the input terminals of the equipment. Apart from these precautions the equipment was mounted in enclosed racks to improve the screening and to help in stabilizing the temperature; all supplies to the equipment were stabilized.

Extensive tests of the correlator, using independent light sources to illuminate the photomultipliers, have shown that over a period of several hours the drift in the

output is less than the r.m.s. uncertainty in the counter readings due to noise alone. However, a more detailed examination of the counter readings shows that over periods of a few minutes there are occasional deviations which are unexpectedly large, and it is believed that this effect is due to short-term drifts in the correlator. For the purposes of the present experiment these short-term drifts are unimportant since tests show that their average effect on the counter readings is not significant when readings are taken over periods of $\frac{1}{2}$ h or more.

4. EXPERIMENTAL PROCEDURE AND RESULTS

4.1 Calibration of the equipment

The first step in calibrating the equipment was to measure the various parameters which are involved in the theoretical expression for the correlation in equation (2.14).

The combined spectral response of the arc lamp, lens, liquid filter and photocathodes was measured with a spectrograph with a resolving power of about 5 \AA , and the result is shown in figure 6. The response has been plotted in terms of the frequency of the light and corresponds to the quantity $\alpha(\nu) n_0(\nu)/\alpha(\nu_0) n_0(\nu_0)$. From this curve the effective bandwidth B_0 and the normalized spectral density σ were found to be

$$\left. \begin{aligned} B_0 &= 0.85 \times 10^{13} \text{ c/s,} \\ \sigma &= 0.451, \end{aligned} \right\} \quad (4.1)$$

where B_0 is defined by equation (2.5), $\lambda_0 = c/\nu_0 = 4358 \text{ \AA}$, and σ is defined by equation (2.7).

The frequency response curves $|F_1^2(f)|$, $|F_2^2(f)|$ of the two amplifiers, B_1 and B_2 in figure 5 were measured directly with a signal generator. The cross-correlation frequency response $\frac{1}{2}[F_1(f)F_2^*(f) + F_1^*(f)F_2(f)]$ was measured by feeding a signal of variable frequency and constant amplitude into the inputs of the correlator in parallel and observing the output of the multiplier. From these results the bandwidth of the correlator b_v (equation (2.10)), and the spectral density factor η (equation (2.12)) were found to be

$$\left. \begin{aligned} b_v &= 38 \text{ Mc/s,} \\ \eta &= 0.98. \end{aligned} \right\} \quad (4.2)$$

The excess noise introduced by the correlator and by the stray light reaching the photocathodes is represented in equation (2.14) by the factors $(1+a)$ and $(1+\delta)$, respectively. Measurements showed that there was a small noise contribution from the correlator, mainly due to shot noise in the multiplier which was about 6% of the total noise, but that stray light was negligible; the two factors therefore have the values

$$\left. \begin{aligned} 1 + \delta &= 1.06, \\ 1 + a &= 1. \end{aligned} \right\} \quad (4.3)$$

It is also necessary, in order to evaluate equation (2.14) to know the value of $G\mu/(\mu-1)$ for each photomultiplier, where G is the overall current gain and μ is the gain of the first stage. As a preliminary test $G\mu/(\mu-1)$ was measured in two different ways. In the first method the current gains G and μ were measured directly.

by observing the ratio of the respective currents. In the second method the noise voltage across the anode load of each photomultiplier was compared with the noise generated across the same load by a temperature-limited tungsten-filament diode, this comparison being made at the output of the amplifiers B_1 and B_2 to ensure that the noise bandwidth was the same as that used in the actual tests. The quantity $G\mu/(\mu - 1)$ for each photomultiplier was then calculated from the simple relation

$$G\mu/(\mu - 1) = I_D/I_A, \tag{4.4}$$

where I_D, I_A are the anode currents of the diode and the photomultiplier, respectively, when their noise outputs are adjusted to be equal. The values obtained by the two methods described above agreed within the limits of experimental error.

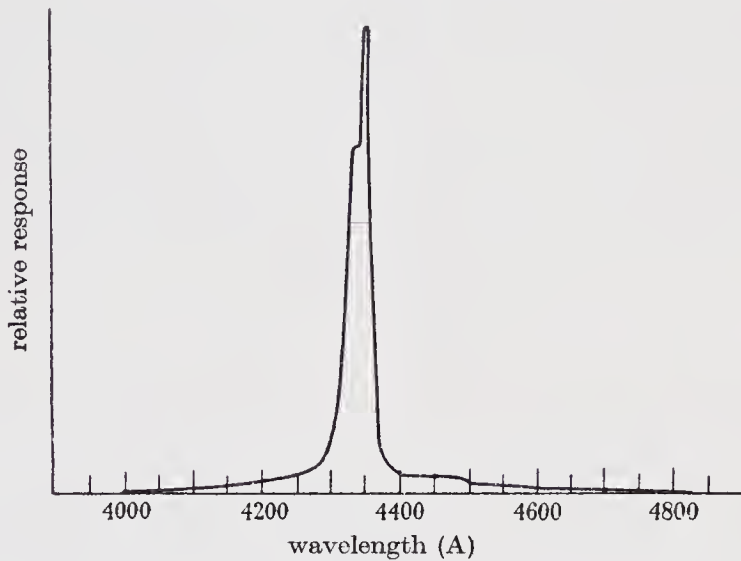


FIGURE 6. Combined spectral response of the arc lamp, optical system, filter and photocathodes.

It was therefore decided to use the second method, employing a noise diode, because it yields the value of $G\mu/(\mu - 1)$ directly from a simple observation of the ratio of two currents, and the final theoretical value of the correlation is obtained without an independent measurement of the excess noise introduced by the multiplication process in the phototube. The measured values of $G\mu/(\mu - 1)$, under the conditions of the experiment, were found to be 3.43×10^5 and 4.63×10^5 for the two photomultipliers, respectively.

Loss of correlation can occur both in the optical and in the electronic part of the equipment. In the present equipment the loss in the optical equipment arises because of polarization produced by the semi-transparent mirror and this is allowed for, in equation (2.14) by the factor β_0 defined by equation (2.8). For the optical system described here it was found that

$$\beta_0 = 0.96. \tag{4.5}$$

The loss of correlation in the electronic equipment occurs almost entirely at the synchronous rectifiers. Ideally, the amplifiers before these rectifiers should pass all the harmonics of the square-wave switching waveform if there is to be no loss of

sensitivity. However, in the present equipment it was necessary, in order to reduce the level at the input to the synchronous rectifier R_2 (figure 5) to a convenient value, to restrict the bandwidth of the amplifier B_4 to the fundamental of the phase-switching frequency of 5 kc/s. Under these conditions it can be shown (Dicke 1946) that the signal to noise ratio is reduced by the factor $\sqrt{8/\pi} \simeq 0.90$. The frequency of the second phase-switch was only 0.05 c/s and it was possible to reduce the loss at the second synchronous rectifier R_3 to a factor 0.955. The overall loss of correlation in the electronic part of the equipment therefore reduced the signal to noise ratio by the factor

$$\epsilon = 0.90 \times 0.955 = 0.86. \quad (4.6)$$

The final step in calibrating the equipment was to relate the r.m.s. fluctuations in the readings of the signal motor M_1 (figure 5) to the rate of revolution of the noise level motor M_2 . This calibration was performed as follows. (a) Noise from two independent generators was fed into the inputs of the correlator and the output N_1, N_2 of the amplifiers B_1 and B_2 were adjusted so that the noise motor M_2 was turning at the arbitrarily chosen rate of 14 rev in 5 min. (b) The two noise generators were replaced by a single generator which was fed into both inputs in parallel, and the power output of this generator was adjusted to give levels N_1, N_2 , as before, at the output of the amplifiers, the signal motor M_1 being disconnected to avoid overloading. (c) The power output of the single source was then reduced by a factor ρ^2 by means of a precision attenuator. The signal motor was reconnected and the change in output reading C_0 in a time of 5 min was recorded for various values of ρ^2 .

It can be shown that the r.m.s. uncertainty $N(T)$ in the reading of the signal motor after a time T is

$$N(T) = \frac{C_0}{\rho^2} \left(\frac{1 + \delta}{\epsilon} \right) \left(\frac{\eta}{2b_v T} \right)^{\frac{1}{2}}, \quad (4.7)$$

where $\delta, \epsilon, \eta, b_v$ are parameters of the equipment defined previously. In the present case it was found that $C_0 = 131$ rev, $T = 5$ min, $\rho^2 = 1.34 \times 10^4$, and substituting the appropriate numerical values for the other parameters, we get that,

$$N(5 \text{ min}) = N_0 = 14.7 \text{ rev}, \quad (4.8)$$

where N_0 is defined as the r.m.s. uncertainty in the signal motor reading in a period of 5 min when the noise level motor is revolving at 14 rev in 5 min.

It is interesting to note that the factor $\frac{1 + \delta}{\epsilon} \left(\frac{\eta}{2b_v T} \right)^{\frac{1}{2}}$ in equation (4.7) also appears in the theoretical expression for the signal to noise ratio equation (2.14). Therefore provided the measurement of N_0 is carried out by the method described here, a comparison of the theoretical and experimental signal to noise ratios is independent of the constants ϵ, δ, η and b_v .

4.2. Experimental procedure

The measurements were carried out as follows. The two photocathodes, as viewed from the light source, were superimposed by adjusting the position of the photomultiplier P_2 (figure 4). Readings were then taken every 5 min, for a total period of 4 h, of the revolution counters on the integrating motors M_1 and M_2 and also of the

anode currents of the photomultipliers. The centres of the two photocathodes, as seen from the light source, were then separated by 1.25, 2.50, 3.75, 5.0 and 10.0 mm. In each of these positions readings were taken at 5 min intervals for about 30 min, the readings were then repeated with the cathodes separated by the same distances but in the opposite direction.

Throughout the experiment the gain of the amplifier B_4 (figure 5) was controlled to keep the output noise from the correlator approximately constant at a level such that the noise motor M_2 was recording 14 rev in 5 min. The gains of the two photomultipliers were measured before and after every run by comparison with a noise diode, as described in §4.1. In practice the gains of the two photomultipliers, which were operated at an anode current of about $100\mu\text{A}$, remained constant throughout the experiment.

4.3. *Experimental results*

A marked correlation was observed in the first run with the cathodes superimposed; the total change in the reading of the integrating motor M_1 after 4 h was 1832 rev which, taking the value of N_0 given in equation (4.8), corresponds to an r.m.s. signal to noise ratio of about 18/1. This correlation was progressively reduced as the cathodes were separated until, when their centres were 10 mm apart, no significant correlation was observed.

TABLE 1. THE EXPERIMENTAL AND THEORETICAL CORRELATION BETWEEN THE FLUCTUATIONS IN THE OUTPUTS OF TWO PHOTOELECTRIC DETECTORS ILLUMINATED WITH PARTIALLY COHERENT LIGHT

run no.	duration (h)	cathode separation (mm) d	observed correla- tion (r.m.s. signal to noise ratio) (S/N)	theoretical correla- tion (r.m.s. signal to noise ratio) (S/N)
1	4	0	+ 17.55	+ 17.10
2	1	1.25	+ 8.25	+ 8.51
3	1	2.50	+ 5.75	+ 6.33
4	1	3.75	+ 3.59	+ 4.19
5	1	5.00	+ 2.97	+ 2.22
6	1	10.00	+ 0.90	+ 0.13

The actual readings of the counters and the associated anode currents, etc., taken every 5 min, have not been reproduced here; instead the experimental results have been given in the more convenient form of r.m.s. signal to noise ratios, which are shown for each separation of the photocathodes in column 4 of table 1.

The experimental signal to noise ratios shown in table 1 were calculated from the original readings of the counters by the following method. Each 5 min interval was characterized by readings of the integrated correlation C_r recorded by the signal motor M_1 , the noise level N_r recorded by the noise motor M_2 , and the anode currents I_{1r} , I_{2r} of the photomultipliers. As they stood these results could not be added to give the final signal to noise ratios, because the gain of the correlator had been frequently altered during each run in an attempt to keep the noise level roughly constant and independent of the inevitable small changes in light flux from the arc lamp. However,

it can be shown simply that the final signal to noise ratios, formed by combining the observations from M equal intervals, is independent of the correlator gain in each interval if the readings are weighted and added according to the formula

$$\frac{S}{N} = \frac{1}{N_0} \frac{\sum_{r=1}^M \frac{I_{1r} I_{2r}}{\bar{I}_1 \bar{I}_2} C_r \frac{\bar{N}}{N_r}}{\left[\sum_{r=1}^M \left(\frac{I_{1r} I_{2r}}{\bar{I}_1 \bar{I}_2} \right) \right]^{\frac{1}{2}}}, \quad (4.9)$$

where N_0 is the r.m.s. uncertainty in the correlation recorded in one interval for a standard noise level \bar{N} , and \bar{I}_1, \bar{I}_2 are averaged over all the intervals. The experimental signal to noise ratios shown in table 1 were therefore calculated for each position of the photocathodes by summing the individual readings taken every 5 min according to equation (4.9) using the experimental value of $N_0 = 14.7$ rev given in equation (4.8).

5. COMPARISON BETWEEN THEORY AND EXPERIMENT

The theoretical values of the expected correlation for each cathode separation were calculated as follows. For every 5 min interval the quantity

$$\frac{\mu - 1}{\mu} \alpha(\nu_0) n_r(\nu_0) (A_1 A_2)^{\frac{1}{2}}$$

was derived from the observed anode currents I_{1r}, I_{2r} of the photomultipliers by the relation

$$\frac{(I_{1r} I_{2r})^{\frac{1}{2}}}{eB_0 \{G_1 G_2 \mu_1 \mu_2 / (\mu_1 - 1)(\mu_2 - 1)\}^{\frac{1}{2}}} = \frac{\mu - 1}{\mu} \alpha(\nu_0) n_r(\nu_0) (A_1 A_2)^{\frac{1}{2}}, \quad (5.1)$$

using the values of B_0 and $G\mu/(\mu - 1)$ given in § 4.3. In a typical 5 min interval

$$(I_{1r} I_{2r})^{\frac{1}{2}} = 104 \times 10^{-6} \text{ A} \quad \text{and} \quad \frac{\mu - 1}{\mu} \alpha(\nu_0) n_r(\nu_0) (A_1 A_2)^{\frac{1}{2}} = 1.92 \times 10^{-4}.$$

Since $(1 - 1/\mu)\alpha(\nu_0)$ had a value of about 0.12, a typical value for the number of quanta per second incident on each photocathode in unit bandwidth at the centre of the emission line was 1.6×10^{-3} . Following equation (2.14), the results for each interval were then added together to give the theoretical signal to noise ratio, taking $T_r = 300$ s and assuming the values for the various parameters of the equipment given in § 4. The partial coherence factor $\Delta(\nu_0)$ for the present equipment, where $\pi\theta_0 a\nu_0/c = \pi\theta_0 b\nu_0/c = 3.06$, was calculated from equation (A 25) to be 0.52; the normalized correlation factor $\Gamma^2(\nu_0, d)$ was computed from equation (A 26) and the values are shown in column 6 of table 2. The final theoretical values for the correlation are shown in column 5 of table 1 where they may be compared with the experimental results in column 4.

The results have also been displayed in table 2 and in figure 7 in a form which is intended to show clearly how the correlation decreased with cathode spacing. To allow for the fact that the photomultiplier currents and the observation times were not the same for every cathode spacing, the observed value of the signal to noise

ratio at each spacing has been normalized by the corresponding theoretical value calculated for zero cathode spacing, and for the appropriate values of incident light flux and observing time. Effectively, this procedure yields experimental values for the normalized correlation factor, and the results are shown in column 5 of table 2 where they can be compared directly with the theoretical values in column 6. The

TABLE 2. THE EXPERIMENTAL AND THEORETICAL VALUES FOR THE NORMALIZED CORRELATION FACTOR FOR DIFFERENT CATHODE SPACINGS

run no.	cathode separation (mm) d	observed correlation (r.m.s. signal to noise ratio) (S/N)	theoretical correlation assuming cathodes superimposed (r.m.s. signal to noise ratio) $(S/N)'$	experimental value of normalized correlation factor $\Gamma^2(\nu_0, d) = \frac{(S/N)}{(S/N)'}$	theoretical value of the normalized correlation factor $\Gamma^2(\nu_0, d)$
1	0	+ 17.55	+ 17.10	1.03 ± 0.04 (p.e.)	1.00
2	1.25	+ 8.25	+ 9.27	0.89 ± 0.07	0.928
3	2.50	+ 5.75	+ 8.85	0.65 ± 0.08	0.713
4	3.75	+ 3.59	+ 8.99	0.40 ± 0.07	0.461
5	5.00	+ 2.97	+ 9.00	0.33 ± 0.07	0.244
6	10.00	+ 0.90	+ 8.17	0.11 ± 0.08	0.015

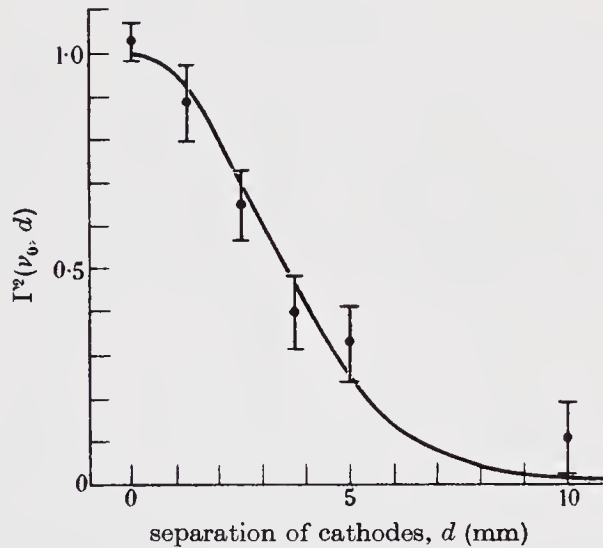


FIGURE 7. The experimental and theoretical values of the normalized correlation factor $\Gamma^2(\nu_0, d)$ for different values of separation between the photocathodes. The full line is the theoretical curve and the experimental results are plotted as points with their associated probable errors.

experimental results have also been plotted in figure 7 for comparison with the theoretical values shown as a solid curve.

A comparison between the theoretical and the experimental values of the correlation given in table 1 and also of the normalized correlation factor given in table 2 and figure 7 shows that, for all cathode spacings, the experimental results are in agreement with theory within the accuracy set by the statistical fluctuations in the measurements. It is true that the difference between theory and experiment is

a little greater than the probable error in the case of the widest spacing, but this difference is not significant. The probable error is itself so small a fraction of the observed correlation that the probability that the agreement is due to chance fluctuation and that no real effect is being measured is negligibly small. The probability that the effect is due to some quite different cause, such as fluctuations in the source intensity, is rendered extremely unlikely by the closeness of the agreement between theory and experiment not only with the cathodes superimposed but also with five different cathode spacings.

There remains the possibility that the effect is real, but that its magnitude is not accurately predicted by our theory. This suggestion has been advanced by Fellgett (1957) who has argued on thermodynamical grounds that the excess photon noise, and therefore also the cross-correlation between the fluctuations in different phototubes, should be larger by a factor $\alpha^{-1}(\nu_0)$ than that which we have calculated. We have stated our theoretical objections to Fellgett's analysis in part I of this paper; in addition, his formula is quite incompatible with experimental results reported above, since it would require the correlation to have been about six times greater than that actually observed. In fact, significant disagreement with experiment would arise if the theoretical magnitude of the correlation at every cathode spacing, were increased or decreased† by more than about 12 or 10 %, respectively. However, it must be noted that a systematic error smaller than these limits could not be detected by the present measurements.

In principle, the accuracy of the experiment could be increased indefinitely by increasing the time of observation, since this would reduce the errors due to statistical fluctuations in the correlator output. However, in practice, it is to be expected that the accuracy would soon prove to be limited by errors in the calibration of the equipment or by errors in measurements of such parameters as the spectral density of the light, the cross-correlation frequency bandwidth and the incident light flux, which are probably of the order of 2 or 3 %; furthermore, the theoretical treatment was based on a number of simplifying assumptions, for example, that the quantum efficiency is constant over the photocathodes, and these approximations would also prevent any substantial increase in the precision of the comparison between theory and experiment.

6. DISCUSSION

The experimental results given in the present paper confirm the results of our earlier test (Hanbury Brown & Twiss 1956*a*) and show that the fluctuations of intensity in two coherent beams of light are correlated. They also show that, for the general case of partially coherent light, the observed value of the correlation agrees, within the limits of accuracy of the measurements, with that calculated from a simple classical theory. If there is any systematic error in our calculation of the correlation, for example, due to some quantum effect which has been ignored, it is

† If the theoretical values of the correlation are all increased by the factor a , it can be shown that the best fit with the experimental data, found by minimizing the sum of the weighted squares of the residuals, occurs when $a = 1.0137$. The standard deviation of a can be shown to be 0.037 and, if a significant disagreement is defined as three times the standard deviation, we get the result quoted above.

less than 10 %, since any greater error would have produced a significant disagreement with experiment.

Our earlier test has been criticized (Brannen & Ferguson 1956) on the grounds that the observed correlation might have been due to some effect which was modulating the intensity of the light source at frequencies within the passband of the correlator. This suggestion cannot, however, explain the observed decrease of correlation as the separation between the photoathodes is increased, which we have shown here to be in accordance with theory. Admittedly, it has also been suggested, by the same authors, that the decrease in correlation might have been due to light reaching the two photoathodes from different parts of the source as their separation was increased. However, in designing and adjusting the equipment used in both experiments we have taken considerable care to exclude this possibility, and even at the maximum separation of the photoathodes at least 95 % of the incident light came from regions of the source visible to both photoathodes.

The results of our preliminary demonstrations have also been criticized on the grounds that they do not agree with two other experiments which have failed to detect correlation. These experiments were carried out by Ádám, Jánossy & Varga (1955) and by Brannen & Ferguson (1956). In both cases an attempt was made to detect the correlation between the arrival times of photons in two coherent beams of light by means of a coincidence counter. Analyses of these experiments, which have been published elsewhere (Purcell 1956; Hanbury Brown & Twiss 1956*c*), show that they were both too insensitive, by several orders of magnitude, to detect any correlation. In appendix B of the present paper we show the equivalence of the techniques using a coincidence counter and a linear multiplier, but we have also shown that for practical reasons the use of a coincidence counter demands a highly monochromatic, as well as brilliant, source of light. Calculations show that, while it is not feasible to use a standard high-pressure mercury arc, it should be quite practicable to detect correlation with a coincidence counter using a low-pressure mercury isotope lamp. (Since the present paper was written a successful measurement of the correlation between photons using a low-pressure isotope lamp and a coincidence counter has been reported by Twiss, Little & Hanbury Brown (1957).)

It is possible that the principles described here will find practical application in the laboratory. For example, an intensity interferometer can be made to give an extremely high angular resolving power; alternatively, it might perhaps be applied to the measurement of the width and profile of extremely narrow spectral lines. An interesting property, which might have some practical use, was described in §2.4, where it was shown that, when the source of light is completely resolved, the correlation is a function of the blackbody temperature of the source and effectively the equipment behaves as a pyrometer.

Although we have not considered any of these laboratory applications in detail, we have made a fairly thorough analysis of the application of an intensity interferometer to the measurement of the apparent angular sizes of the visible stars which is given in a later part of this paper. We have also reported briefly a test of the method on Sirius (Hanbury Brown & Twiss 1956*b*). A more detailed account of this work will also be given in a later part of this paper.

We thank the Director of Jodrell Bank Experimental Station for making available the necessary facilities, the Superintendent of the Services Electronic Research Laboratory for the loan of much of the equipment, Dr J. G. Davies for making the numerical computations shown in figures 2 and 3, and Dr A. Burawoy for developing the liquid optical filter.

APPENDIX A. THE THEORETICAL VALUE OF THE CORRELATION FACTOR
AND PARTIAL COHERENCE FACTOR FOR PARTIALLY COHERENT LIGHT

A 1. *The general formula for the correlation between partially coherent fields*

To calculate the correlation, in the general case, where the two light detectors are illuminated with partially coherent light, we shall follow a similar method to that used previously in analyzing a radio interferometer which operated on the same principle (Hanbury Brown & Twiss 1954).

To obtain a quantitative expression for the correlation factor $\Gamma^2(\nu_0, d)$ and the partial coherence factor $\Delta(\nu_0)$ in the case of the simple arrangement shown in figure 1, we shall consider a system of rectangular Cartesian co-ordinates such that the origin lies midway between the centres of the two light detectors, both of which lie in the x axis, and such that the z axis passes through the centre of the light source. We shall assume that the surface of the light source, distant R_0 from the plane containing the photocathodes, can be divided up into elementary areas $d\xi = d\xi d\eta$ centred on the points (ξ, η, R_0) . It has been shown by Kahn (1957) that the elementary area must be greater than $\lambda^2/2\pi$, where λ is the wavelength of the emitted radiation, but we shall assume here that the area of the source is so large that the error involved in replacing finite summations by integrals is negligible.

Consider the light emitted with a specific polarization from a particular elementary area in a time T . The vector potential at a point distant from the area may be represented by a Fourier series of the form

$$\sum_{r=0}^{\infty} h_r(\xi) \cos \left[\frac{2\pi r}{T} \left(t - \frac{R(\xi, \mathbf{x})}{c} \right) - \chi_r(\xi) \right], \quad (\text{A } 1)$$

where $\chi_r(\xi)$ is a random phase variable distributed with uniform probability between 0 and 2π such that

$$\chi_r(\xi) \chi_s(\xi') = \delta_{rs} \delta(\xi - \xi')$$

and $h_r^2(\xi) d\xi$ is proportional to the number of quanta, incident on unit area at distance R_0 , which are emitted with energy h_r/T from an elementary area $d\xi$ of the source. In what follows we shall assume that the source is so far distant that its apparent angular size at the photocathodes is very small compared with unity.

If we assume that the photocathodes behave like square-law detectors with a conversion efficiency proportional to the quantum efficiency, it follows that the low-frequency fluctuations in one of the photoemission currents due to the intensity fluctuations in the incident light are proportional to

$$\int d\xi \cdot d\xi' \sum_{r>s} \sum_{s=1}^{\infty} \int d\mathbf{x} \frac{2e(\alpha_{1r} \alpha_{1s} n_{1r} n_{1s})^{\frac{1}{2}}}{T} \\ \times \cos \left[\frac{2\pi(r-s)t}{T} - \frac{2\pi}{cT} \{rR(\xi, \mathbf{x}) - sR(\xi', \mathbf{x})\} - \{\chi_r(\xi) - \chi_s(\xi')\} \right],$$

where $n_r(\xi) \sim h_r^2(\xi)$ is the number of quanta, emitted by unit area of the source, incident on unit area of the photocathode; e is the charge on the electron; ξ, ξ' are the co-ordinates of arbitrary points on the surface of the source; $\mathbf{x} = (x, y, 0)$ are the co-ordinates of an arbitrary point on one of the photocathodes which we shall take to be rectangular in shape and defined by the inequalities

$$\left. \begin{aligned} -\frac{1}{2}b < y < \frac{1}{2}b, & \quad -\frac{1}{2}d - \frac{1}{2}a < x < -\frac{1}{2}d + \frac{1}{2}a, \\ -\frac{1}{2}b < y < \frac{1}{2}b, & \quad \frac{1}{2}d - \frac{1}{2}a < x < \frac{1}{2}d + \frac{1}{2}a, \end{aligned} \right\} \quad (\text{A } 2)$$

respectively.

These fluctuations are amplified by a secondary emission multiplier and an amplifier with a combined complex frequency response $F_1(f)$, and at the output of the amplifier they are proportional to

$$\iint d\xi d\xi' \sum_{r>s} \sum_{s=1}^{\infty} \int d\mathbf{x} \frac{2e(\alpha_{1r}\alpha_{1s}n_{1r}n_{1s})^{\frac{1}{2}}}{T} \times \mathcal{R} \left\{ F_1 \left(\frac{r-s}{T} \right) \exp i \left[\frac{2\pi}{T} \left((r-s)t - \frac{rR(\xi, \mathbf{x}) - sR(\xi', \mathbf{x})}{c} \right) - (\chi_r(\xi) - \chi_s(\xi')) \right] \right\}.$$

To the second order in R_0^{-1} we may write

$$\frac{R(\xi, \mathbf{x})}{R_0} = 1 - \frac{\mathbf{x} \cdot \xi}{R_0^2} + \frac{\xi^2 + \mathbf{x}^2}{2R_0^2},$$

so that

$$\frac{rR(\xi, \mathbf{x}) - sR(\xi', \mathbf{x})}{cT} = \frac{1}{cT} \left\{ (r-s)R_0 - \mathbf{x}(r\xi - s\xi') + \frac{r\xi^2 - s\xi'^2}{2R_0} - \frac{(r-s)\mathbf{x}^2}{2R_0} \right\}. \quad (\text{A } 3)$$

In a practical case the last term in equation (A 3) is quite negligible for all values of r, s for which $F_1((r-s)/T)$ differs significantly from zero. Accordingly, the ensemble averaged correlation between the fluctuations in the outputs of the two amplifiers with complex response $F_1(f), F_2(f)$ respectively is proportional to

$$\iiint d\xi d\xi' d\mathbf{x} d\mathbf{x}' \sum_{r>s} \sum_{s=1}^{\infty} \frac{2e^2}{T} (\alpha_{1r}\alpha_{1s}n_{1r}n_{1s}\alpha_{2r}\alpha_{2s}n_{2r}n_{2s})^{\frac{1}{2}} \frac{1}{2} \left\{ F_1 \left(\frac{r-s}{T} \right) \times F_2^* \left(\frac{r-s}{T} \right) + F_1^* \left(\frac{r-s}{T} \right) F_2 \left(\frac{r-s}{T} \right) \right\} \cos \left[\frac{2\pi}{cTR_0} \{ r(\mathbf{x} - \mathbf{x}') \xi - s(\mathbf{x} - \mathbf{x}') \xi' \} \right],$$

where \mathbf{x}, \mathbf{x}' are the co-ordinates of typical points on the first and second photocathodes, respectively. We shall assume that $\alpha_{1r}n_{1r} \simeq \alpha_{1s}n_{1s}$ and $\alpha_{2r}n_{2r} \simeq \alpha_{2s}n_{2s}$ for all values of r, s for which $F((r-s)/T)$ differs significantly from zero, and also that the angular size of the source is sufficiently small to ensure that,

$$\cos \left\{ \frac{2\pi}{cTR_0} \left(r(\mathbf{x} - \mathbf{x}') \xi - s(\mathbf{x} - \mathbf{x}') \xi' \right) \right\} \simeq \cos \left\{ \frac{2\pi(r+s)}{2cTR_0} (\mathbf{x} - \mathbf{x}') (\xi - \xi') \right\}. \quad (\text{A } 4)$$

In this case we can introduce new frequency variables f, ν such that

$$f = (r-s)/T, \quad \nu = (r+s)/2T. \quad (\text{A } 5)$$

Then in the limit as $T \rightarrow \infty$ we have that, with the cathodes at a spacing d , the ensemble average $\overline{C(d)}$ of the correlation is given by

$$\overline{C(d)} = 2e^2 \iiint \int d\xi d\xi' d\mathbf{x} d\mathbf{x}' \int_0^\infty d\nu \alpha_1(\nu) \alpha_2(\nu) [n_1(\nu, \xi) n_2(\nu, \xi) n_1(\nu, \xi') n_2(\nu, \xi')]^{\frac{1}{2}} \times \cos \left\{ \frac{2\pi\nu}{cR_0} (\mathbf{x} - \mathbf{x}') \cdot (\xi - \xi') \right\} \int_0^\infty df \frac{1}{2} (F_1(f) F_2^*(f) + F_1^*(f) F_2(f)), \quad (\text{A } 6)$$

where the integrals are taken over the surfaces of both photocathodes, twice over the surface of the source, over the frequency spectrum of the incident light and over the cross-correlation frequency response of the amplifiers following the photomultiplier tubes.

A 2. The correlation when the apertures of the light detectors are small

In the simple case where the apertures of the two photocathodes are too small to resolve the source appreciably and where the bandwidth of the light is small, we may replace $(\mathbf{x} - \mathbf{x}') \cdot (\xi - \xi')$ in equation (A 6) by $d(\xi - \xi')$ and write

$$\overline{C(d)} = \Gamma^2(\nu_0, d) \overline{C(0)}, \quad (\text{A } 7)$$

where ν_0 is the midband frequency of the light; $\overline{C(0)}$ is the correlation with zero spacing between the photocathodes; $\Gamma^2(\nu_0, d)$ is the normalized correlation factor. It follows from equation (A 6) that

$$\Gamma^2(\nu_0, d) = \frac{\iint d\xi d\xi' h^2(\xi) h^2(\xi') \cos \left\{ \frac{2\pi\nu_0}{cR_0} d(\xi - \xi') \right\}}{\iint d\xi d\xi' h^2(\xi) h^2(\xi')}, \quad (\text{A } 8)$$

where $h^2(\xi) \sim [n_1(\nu_0, \xi) n_2(\nu_0, \xi)]^{\frac{1}{2}}$.

Alternatively, we may write

$$\Gamma^2(\nu_0, d) = H(\nu_0, d) H^*(\nu_0, d), \quad (\text{A } 9)$$

where $H(\nu_0, d)$ is defined by

$$H(\nu_0, d) = \int_{-\infty}^{\infty} d\xi \exp \left(\frac{-2\pi i \xi \nu_0 d}{cR_0} \right) \int_{-\infty}^{\infty} d\eta h^2(\xi, \eta) / \int_{-\infty}^{\infty} d\xi \int_{-\infty}^{\infty} d\eta h^2(\xi, \eta), \quad (\text{A } 10)$$

Now $h^2(\xi) = \int_{-\infty}^{\infty} d\eta h^2(\xi, \eta)$

is the intensity distribution over the equivalent line source projected parallel to the x axis and $H(\nu_0, d)$ is the normalized Fourier transform of this quantity. It follows, as stated in the text, that $\Gamma^2(\nu_0, d)$ is the square of the amplitude of this normalized Fourier transform.

A 3. The correlation when the apertures of the light detectors are large

A 3.1. The general formula

In the case where the aperture of the two photocathodes are so large that they appreciably resolve the source, the correlation with zero spacing is reduced by the *partial coherence factor* $\Delta(\nu_0)$ while $\Gamma^2(\nu_0, d)$, the *correlation factor* is now a function of the apertures of the photocathodes as well as of the angular size of the source.

If we assume (see § 2.2) that the light intensity may be taken as uniform over the source and that the quantum efficiency is constant over each photocathode, then from equation (A 6) the correlation is

$$\begin{aligned} \overline{C(d)} = & 2e^2 \iiint \int d\xi d\xi' d\mathbf{x} d\mathbf{x}' \cos \left[\frac{2\pi\nu_0}{cR_0} (\mathbf{x} - \mathbf{x}') (\xi - \xi') \right] \\ & \times \int_0^\infty \alpha_1(\nu) \alpha_2(\nu) n_1(\nu) n_2(\nu) d\nu \int_0^\infty \frac{1}{2} \{ F_1^*(f) F_2^*(f) + F_1^*(f) F_2(f) \} df \quad (\text{A } 11) \end{aligned}$$

and it has been assumed that the light bandwidth is so narrow that

$$\cos \left[\frac{2\pi\nu}{cR_0} (\mathbf{x} - \mathbf{x}') (\xi - \xi') \right]$$

does not change significantly over the bandwidth for which $\alpha_1(\nu) \alpha_2(\nu) n_1(\nu) n_2(\nu)$ differs appreciably from zero.

From the definition of $\Delta(\nu_0)$ and $\Gamma^2(\nu_0, d)$ in § 2.2, it follows simply from equation (A 11) that

$$\Delta(\nu_0) \Gamma^2(\nu_0, d) = \frac{1}{\Omega_0^2 A_1 A_2} \iiint \int \frac{d\xi d\xi' d\mathbf{x} d\mathbf{x}'}{R_0^4} \cos \left\{ \frac{2\pi\nu_0 (\mathbf{x} - \mathbf{x}') (\xi - \xi')}{cR_0} \right\}, \quad (\text{A } 12)$$

where the areas A_1, A_2 of the photocathodes and the solid angle subtended by the source at the photocathodes are given by

$$A_1 = \int d\mathbf{x}, \quad A_2 = \int d\mathbf{x}', \quad \Omega_0 = \int \frac{d\xi}{R_0^2} = \int \frac{d\xi'}{R_0^2}. \quad (\text{A } 13)$$

A 3.2. A rectangular source viewed by two light detectors with rectangular apertures

When the source is rectangular in shape with angular dimensions θ_1, θ_2 , where $\theta_1 \theta_2 = \Omega_0$, it is best to evaluate equation (A 12) by integrating initially over the variables \mathbf{x}, \mathbf{x}' to get

$$\begin{aligned} \Delta(\nu_0) \Gamma^2(\nu_0, d) = & \frac{1}{A_1 A_2 (\theta_1 \theta_2)^2} \iint \frac{d\eta d\eta'}{R_0^2} \left[\frac{\sin(\pi(\eta - \eta') b \nu_0 / c R_0)}{\pi(\eta - \eta') \nu_0 / c R_0} \right] \iint \frac{d\xi d\xi'}{R_0^2} \\ & \times \left[\frac{\sin(\pi(\xi - \xi') a \nu_0 / c R_0)}{\pi(\xi - \xi') \nu_0 / c R_0} \right]^2 \cos \left[\frac{2\pi\nu_0 d(\xi - \xi')}{cR_0} \right], \quad (\text{A } 14) \end{aligned}$$

where (A 15)

$$A_1 = A_2 = ab.$$

We now introduce new variables defined by,

$$\left. \begin{aligned} \phi &= \frac{\pi a \nu_0}{c R_0} (\xi - \xi'), & \phi' &= \frac{\pi a \nu_0}{c R_0} \left(\frac{\xi + \xi'}{2} \right), \\ \psi &= \frac{\pi b \nu_0}{c R_0} (\eta - \eta'), & \psi' &= \frac{\pi b \nu_0}{c R_0} \left(\frac{\eta + \eta'}{2} \right), \end{aligned} \right\} \quad (\text{A } 16)$$

and integrate over ϕ', ψ' subject to the inequalities

$$\phi' < \left| \frac{\pi a \theta_1 \nu_0}{c} - \phi \right|, \quad \psi' < \left| \frac{\pi b \theta_2 \nu_0}{c} - \psi \right| \quad (\text{A } 17)$$

We then get that

$$\Delta(\nu_0)\Gamma^2(\nu_0, d) = \left(\frac{c^2}{\pi^2\nu_0^2\theta_1\theta_2}\right)^2 \frac{1}{A_1A_2} \times \int_0^\Phi \frac{2\sin^2\phi}{\phi^2} (\Phi - \phi) \cos\left(\frac{2d\phi}{a}\right) d\phi \int_0^\Psi \frac{2\sin^2\psi}{\psi^2} (\Psi - \psi) d\psi, \quad (\text{A } 18)$$

where θ_1, θ_2 , the angular dimensions of the source, are defined by

$$\theta_1 = |\xi_1 - \xi_2|_{\max}/R_0, \quad \theta_2 = |\eta_1 - \eta_2|_{\max}/R_0, \quad (\text{A } 19)$$

and
$$\Phi = \frac{\pi a \theta_1 \nu_0}{c}, \quad \Psi = \frac{\pi b \theta_2 \nu_0}{c} \quad (\text{A } 20)$$

Equation (A 18) involves integrals of the form

$$\mathfrak{J}(\Phi) = \int_0^\Phi \frac{2\sin^2\phi}{\phi^2} (\Phi - \phi) d\phi \quad (\text{A } 21)$$

and, in the case where the source is not appreciably resolved by the individual photocathode apertures ($\Phi \ll 1$), we may write

$$\mathfrak{J}(\Phi) = \Phi^2 = \frac{\pi^2\theta_1^2 a^2 \nu_0^2}{c^2}, \quad (\text{A } 22)$$

so that in this case $\Delta(\nu_0) = 1$, as indeed it must be by definition.

For the opposite extremes, where the source is completely resolved by the individual photocathode apertures ($\Phi \rightarrow \infty$), then $\mathfrak{J}(\Phi) \rightarrow \pi\Phi$ and hence,

$$\Delta(\nu_0) \rightarrow \frac{c^2}{\nu_0^2\theta_1\theta_2} (A_1A_2)^{-\frac{1}{2}}. \quad (\text{A } 23)$$

For intermediate values of Φ , $\mathfrak{J}(\Phi)$ may be expressed conveniently in terms of tabulated functions

$$\mathfrak{J}(\Phi) = 2\Phi \text{Si}(2\Phi) - (1 - \cos 2\Phi) + \ln(\gamma\Phi) - \text{Ci}(2\Phi), \quad (\text{A } 24)$$

where γ is Euler's constant given approximately by $\ln(\gamma) = 0.5772$, and this result was used in computing the partial coherence factor for the case of the preliminary experiment that we have described elsewhere (Hanbury Brown & Twiss 1956*a*).

A 3.3. A circular source viewed by two light detectors with rectangular apertures

When the light source is circular the quantities $\Delta(\nu_0)$ and $\Gamma^2(\nu_0, d)$ can be derived more simply, since the distribution of intensity over the equivalent line source is independent of the direction of the line joining points on the two photocathodes. Thus, the correlation between the fluctuations in the currents emitted from points $(x_1, y_1, 0)$ and $(x_2, y_2, 0)$ on the two photocathodes is proportional to

$$\frac{4J_1^2\{(\pi\theta_0\nu_0/c) \cdot ((x_1 - x_2)^2 + (y_1 - y_2)^2)^{\frac{1}{2}}\}}{(\pi\theta_0\nu_0/c)^2 ((x_1 - x_2)^2 + (y_1 - y_2)^2)},$$

where J_1 is a Bessel function of the first order, and θ_0 is the angular diameter of the source.

Thus from equation (A 12) the partial coherence factor $\Delta(\nu_0)$ is given by

$$\Delta(\nu_0) = \frac{1}{A_1 A_2} \int_{-\frac{1}{2}b}^{\frac{1}{2}b} dy_1 \int_{-\frac{1}{2}b}^{\frac{1}{2}b} dy_2 \int_{-\frac{1}{2}a}^{\frac{1}{2}a} dx_1 \int_{-\frac{1}{2}a}^{\frac{1}{2}a} dx_2 \frac{4J_1^2\{(\pi\theta_0\nu_0/c)((x_1-x_2)^2+(y_1-y_2)^2)^{\frac{1}{2}}\}}{(\pi\theta_0\nu_0/c)^2((x_1-x_2)^2+(y_1-y_2)^2)} \quad (\text{A } 25)$$

and the normalized correlation factor $\Gamma^2(\nu_0, d)$ is given by

$$\Gamma^2(\nu_0, d) = \frac{1}{A_1 A_2 \Delta(\nu_0)} \int_{-\frac{1}{2}b}^{\frac{1}{2}b} dy_1 \int_{-\frac{1}{2}b}^{\frac{1}{2}b} dy_2 \int_{-\frac{1}{2}(d-a)}^{-\frac{1}{2}(d-a)} dx_1 \int_{\frac{1}{2}(d-a)}^{\frac{1}{2}(d+a)} dx_2 \times \frac{4J_1^2\{(\pi\theta_0\nu_0/c)((x_1-x_2)^2+(y_1-y_2)^2)^{\frac{1}{2}}\}}{(\pi\theta_0\nu_0/c)^2((x_1-x_2)^2+(y_1-y_2)^2)}. \quad (\text{A } 26)$$

These last two results have been used to analyze the experiment described in the text.

APPENDIX B. THE CORRELATION BETWEEN PHOTONS MEASURED WITH A COINCIDENCE COUNTER

We shall consider here an extremely simple system consisting of two photo-multiplier tubes and a coincidence counter, and shall discuss briefly the idealized case in which a coincidence will be recorded if, and only if, two photoelectrons are emitted from the two photocathodes with a time difference less than the resolving time of the coincidence counter. We shall assume initially that the incident light is a linearly polarized plane wave; the extension to the general case of an arbitrarily polarized and partially coherent beam can then be made along identical lines to those developed in §2 of the text.

B 1. *Mathematical theory*

If $P(t_n) dt$ is the probability that a photoelectron be emitted from a photocathode in the time interval

$$t_n \leq t < t_n + dt, \quad (\text{B } 1)$$

then we showed in equation (3·14) of part I that

$$P(t_n) = \sum_{r=0}^{\infty} \frac{\alpha_r n_r A}{T} + 2 \sum_{r>s} \sum_{s=1}^{\infty} \frac{A}{T} (\alpha_r \alpha_s n_r n_s)^{\frac{1}{2}} \cos \left\{ \frac{2\pi}{T} (r-s)t_n + \phi_r - \phi_s \right\}, \quad (\text{B } 2)$$

where T is an arbitrary time interval not less than the observation time of the experiment; α_r is the cathode quantum efficiency at frequency r/T ; n_r is the number of linearly polarized quanta of frequency r/T incident in unit time on unit area of the photocathode; A is the area of the photocathode; ϕ_r, ϕ_s are independent random variables distributed with uniform probability over the range $0 \rightarrow 2\pi$.

It follows that $P(\tau_c, t_n)$, the probability that *one* electron be emitted in the time interval

$$t_n - \tau_c < t < t_n + \tau_c, \quad (\text{B } 3)$$

is given by

$$P(\tau_c, t_n) = \sum_{r=1}^{\infty} \frac{A}{T} \alpha_r n_r 2\tau_c + 2 \sum_{r>s} \sum_{s=1}^{\infty} \frac{A}{T} (\alpha_r \alpha_s n_r n_s)^{\frac{1}{2}} \times \frac{2 \sin(2\pi(r-s)\tau_c/T)}{2\pi(r-s)/T} \cos \left[\frac{2\pi}{T} (r-s)t_n + \phi_r - \phi_s \right], \quad (\text{B } 4)$$

provided that τ_c is so small that one can neglect the probability that two or more electrons will be emitted in a time interval of duration $2\tau_c$. This last limitation is obviously essential to the use of a coincidence counter technique.

The ensemble average of the joint probability $P_1(\tau_c, t_n)$ that an electron be emitted from one photocathode in the interval given by the inequality (B 1) while an electron is emitted from the other photocathode in the interval given by the inequality (B 3), may be written

$$\overline{P_1(\tau_c, t_n) P_2(t_n)} dt = dt \left\{ \left(\sum_{r=1}^{\infty} \frac{A_1}{T} \alpha_{1r} n_{1r} \right) \left(\sum_{s=1}^{\infty} \frac{A_2}{T} \alpha_{2s} n_{2s} \right) 2\tau_c + 4 \sum_{r>s=1}^{\infty} \frac{A_1 A_2}{T^2} (\alpha_{1r} \alpha_{2r} n_{1r} n_{2r}) \frac{\sin(2\pi(r-s)\tau_c/T)}{2\pi(r-s)/T} \right\}, \quad (\text{B } 5)$$

since all the terms which depend explicitly on ϕ_r, ϕ_s average to zero.

In the simple case where $A_1 \alpha_1 n_1 = A_2 \alpha_2 n_2 = A \alpha(\nu) n(\nu)$ the ensemble average $\overline{C(T_0)}$ of the number of coincidences in time T_0 , is given by

$$\overline{C(T_0)} = 2\tau_c T_0 \left(\int_0^{\infty} A \alpha(\nu) n(\nu) d\nu \right)^2 + 4T_0 \int_{\nu_r}^{\infty} d\nu_r \int_0^{\infty} d\nu_s A^2 \alpha(\nu_r) \alpha(\nu_s) n(\nu_r) n(\nu_s) \frac{\sin(2\pi(\nu_r - \nu_s)\tau_c)}{2\pi(\nu_r - \nu_s)}, \quad (\text{B } 6)$$

where we have let $T \rightarrow \infty$.

If the light bandwidth is so large compared with $1/\tau_c$ the reciprocal resolving time of the coincidence counter, that $\alpha(\nu) n(\nu)$ does not vary appreciably over the frequency band for which $\sin(2\pi(\nu_r - \nu_s)\tau_c)/2\pi(\nu_r - \nu_s)$ differs significantly from zero, we have that

$$\overline{C(T_0)} = 2\tau_c T_0 \left(\int_0^{\infty} A \alpha(\nu) n(\nu) d\nu \right)^2 + T_0 \int_0^{\infty} A^2 \alpha^2(\nu) n^2(\nu) d\nu, \quad (\text{B } 7)$$

which may be written

$$\overline{C(T_0)} = \overline{C_R(T_0)} + \overline{C_c(T_0)} = 2\tau_c T_0 N_p^2 + \tau_0 T_0 N_p^2, \quad (\text{B } 8)$$

where N_p , the average number of photoelectrons emitted by either photocathode in unit time, is

$$N_p = \int_0^{\infty} A \alpha(\nu) n_0(\nu) d\nu \quad (\text{B } 9)$$

and $c\tau_0$ is the 'coherence length' of the light (Born 1933) which, in the general case where the light bandwidth is of arbitrary shape, may be defined by

$$c\tau_0 = \frac{c\sigma}{B_0}, \quad (\text{B } 10)$$

where σ , and B_0 are defined by equations (2.7) and (2.5).

In equation (B 8) $\overline{C_R(T_0)}$ is the average number of coincidences which would occur by chance if the emission of photoelectrons by the two photocathodes was completely random, and is given by

$$\overline{C_R(T_0)} = 2\tau_c T_0 N_p^2, \quad (\text{B } 11)$$

where it is assumed that $\tau_c \gg \tau_0$ and that $N_p \tau_c \ll 1$, while $\overline{C_c(T_0)}$ is the average number of excess coincidences due to the so-called 'bunching' of photons, and is given by

$$\overline{C_c(T_0)} = \tau_0 T_0 N_p^2. \tag{B 12}$$

If the incident light is randomly polarized and if N_0 is now the total average number of photoelectrons emitted in unit time from either photocathode, then the average number of excess coincidences is given by

$$\overline{C_c(T_0)} = \frac{1}{2} \tau_0 T_0 N_0^2. \tag{B 13}$$

since there is no correlation between quanta with mutually orthogonal polarizations. The random coincidences, on the other hand, depend only upon the total number of incident quanta so that,

$$\overline{C_R(T_0)} = 2\tau_c T_0 N_0^2 \tag{B 14}$$

as long as

$$\left. \begin{aligned} \tau_c &\gg \tau_0, \\ N_0 \tau_c &\ll 1. \end{aligned} \right\} \tag{B 15}$$

When the incident light is only partially coherent over the individual photocathode apertures and when the centres of the latter are separated by a distance d , the number of excess coincidences will be reduced by a factor $\overline{\Delta \Gamma^2(d)}$, where $\overline{\Delta}$ the *partial coherence factor* and $\overline{\Gamma^2(d)}$ the *normalized correlation factor* are defined in §2. Thus, in this more general case, the correlation between the photons arriving at the two photocathodes increases the number of coincidences over the random rate by a factor

$$1 + \rho_c = 1 + \overline{\Delta \Gamma^2(d)} \frac{\tau_0}{4\tau_c}, \tag{B 16}$$

which is independent of the quantum efficiency and of the intensity of the incident light.

The random coincidences obey a Poisson distribution so that the r.m.s. fluctuation in their number is given by,

$$\{\langle C_R(T_0) - \overline{C_R(T_0)} \rangle_{\text{aver.}}^2\}^{\frac{1}{2}} = \overline{C_R(T_0)}^{\frac{1}{2}} = 2N_0(\tau_c T_0)^{\frac{1}{2}}. \tag{B 17}$$

Therefore the *signal to noise ratio*, defined as the ratio of the average number of excess coincidences to the r.m.s. fluctuation in the random coincidence rate, is

$$\frac{S}{N} = \frac{\overline{C_c(T_0)}}{\overline{C_R(T_0)}^{\frac{1}{2}}} = \frac{\overline{\Delta \Gamma^2(d)} N_0 \tau_0}{2} \left(\frac{T_0}{2\tau_c} \right)^{\frac{1}{2}}, \tag{B 18}$$

which from equations (2.3) (2.6) and (B 10) may be written in the equivalent form

$$\frac{S}{N} = \overline{\Delta \Gamma^2(d)} A \alpha(\nu_0) n_0(\nu_0) \sigma \left(\frac{T_0}{4\sqrt{2}\tau_c} \right)^{\frac{1}{2}}. \tag{B 19}$$

The results given above have been quoted elsewhere (Hanbury Brown & Twiss 1956c) for the special case $\overline{\Gamma^2(d)} = 1$; an exactly similar result has been derived by Purcell (1956) for the case $\overline{\Delta \Gamma^2(d)} = 1$ by an analysis based upon the auto-correlation function for the intensity fluctuations in the incident light. The present analysis, is, in effect, the Fourier transform dual to that of Purcell and it is simple to show that τ_0 as defined in (B 10) is identical with the τ_0 used by Purcell.

B2. *Comparison with the alternative technique*

If equation (B19) is compared with equation (2.13) which gives the signal to noise ratio for the linear multiplier technique, we see that the two expressions are the same if we put

$$\frac{b_v}{\eta} = \frac{1}{4\tau_c} \quad (\text{B20})$$

and assume that both equipments have an ideal performance

$$\text{(i.e. } \epsilon\gamma_0(\mu - 1)/\{\mu(1 + a)(1 + \delta)\} = 1).$$

Now b_v/η is roughly the response time of the amplifiers in the linear multiplier system, or alternatively is roughly the effective bandwidth of the coincidence counter. It is therefore clear that in the ideal case both techniques, coincidence counting of photoelectrons or linear multiplication of intensity fluctuations, give about the same signal to noise ratio provided that the effective bandwidth of their circuits, the spectral distribution of the incident light, and the primary photoemission currents are the same in both cases.

However, in a practical case there are considerable difficulties in meeting the condition that the primary photoemission currents should be the same for both techniques. Thus the need to satisfy the inequalities defined in equation (B15) severely limits the maximum photoemission current when the resolving time of coincidence counter is fixed, and in practice it is difficult to let N_0 , the average number of photoelectrons emitted per second, rise much above 10^6 when one is using the coincidence-counter technique. As we have shown above the signal to noise ratio, which is by far the most important limitation of an 'intensity' interferometer, is determined by the number of incident quanta per cycle bandwidth rather than by the total incident light flux, and to ensure a workable signal to noise ratio, the average number of photoelectrons produced per second, by quanta in a frequency band of 1 c/s, must be of the order† of 10^{-5} or greater. This latter requirement can only be satisfied by a source of high equivalent temperature, especially if the source is to be negligibly resolved by the apertures of the photocathodes. For example, if $N_0 < 10^6$ this means that the light bandwidth must be less than 10^{11} c/s, which corresponds to a bandwidth of about 0.5 \AA at a wavelength of 4000 \AA .

In the laboratory these conditions can easily be met by using a low-pressure electrodeless isotope lamp. Thus a source described by Forrester, Gudmundsen & Johnson (1955) had a bandwidth of only $8 \cdot 10^8$ cycles, centred on the 5461 green line of ^{198}Hg , with an output flux of $0.004 \text{ W cm}^{-2} \text{ sterad}^{-1}$ which corresponds to an effective black-body temperature at the centre of the line of 6750° K .

However, in the case of a measurement on a star, where the incident light is spread over the whole visible spectrum, narrow bandwidths can only be obtained by means of interference filters (Ring 1956) which introduce appreciable attenuation and demand well collimated beams of light. For these and other technical reasons the coincidence-counting technique has not been seriously considered for astronomical applications.

† With practical values for the parameters of equation (2.14) and an amplifier bandwidth of 100 Mc/s one would get a signal to noise ratio of 3 to 1 in 1 h with $\sqrt{(A_1 A_2)} \alpha(\nu_0) n_0(\nu_0) = 10^{-5}$ and this is about the lowest sensitivity with which one could work comfortably.

B3. The limiting case of arbitrarily small resolving time

We have, so far, only considered the case in which τ_c , the resolving time of the coincidence counter is very much greater than τ_0 , where $c\tau_0$ is the 'coherence length' of the incident light. However, if the light source is, for example, a low-pressure isotope lamp this condition is not necessarily valid and a brief discussion of the more general case is needed.

In the limiting case $\tau_c/\tau_0 \rightarrow 0$ it follows immediately from equation (B5) that

$$C(T_0) \rightarrow 2\tau_c T_0 \left(\int_0^\infty A\alpha(\nu) n(\nu) d\nu \right)^2 + 2\tau_c T_0 \left(\int_0^\infty A\alpha(\nu) n(\nu) d\nu \right)^2, \quad (\text{B21})$$

when
$$\overline{C_c(T_0)} \rightarrow \overline{C_R(T_0)} = 2\tau_c T_0 N_p^2 \quad (\text{B22})$$

in the idealized case of a linearly polarized plane wave of light. The average number of excess coincidences is therefore equal to the number of purely random coincidences which would arise from completely incoherent light beams, a result which is independent of the spectral distribution of the incident light.

In the general case, when τ_c/τ_0 is finite and non-zero, it can be shown from equation (B5) that

$$C_R(T_0) = \tau_0 T_0 N_p^2 \operatorname{erf} \left(\frac{\sqrt{\pi} \tau_c}{\tau_0} \right), \quad (\text{B23})$$

assuming that the spectral distribution of the incident light is Gaussian, as will be approximately the case when the line broadening is due to Doppler effect. The signal to noise ratio is therefore reduced by the factor

$$\operatorname{erf}(\sqrt{\pi} \tau_c/\tau_0),$$

which tends to zero as $\tau_c \rightarrow 0$, and this result emphasizes that the correlated photons are not in perfect time coincidence. There is a fundamental uncertainty in their arrival time which is of the order of the reciprocal of the bandwidth of the incident light, a result which can be deduced directly from the uncertainty principle.

REFERENCES

- Ádám, A, Jánossy, L. & Varga, P. 1955 *Acta Phys. Hungar.* **4**, 301.
 Born, M. 1933 *Optik*. Berlin: Springer.
 Brannen, E. & Ferguson, H. I. S. 1956 *Nature, Lond.* **178**, 481.
 Dicke, R. H. 1946 *Rev. Sci. Instrum.* **17**, 268.
 Fellgett, P. B. 1957 *Nature, Lond.* **179**, 956.
 Forrester, A. T., Gudmundsen, R. A. & Johnson, P. O. 1955 *Phys. Rev.* **99**, 1691.
 Hanbury Brown, R. & Twiss, R. Q. 1954 *Phil. Mag.* **45**, 663.
 Hanbury Brown, R. & Twiss, R. Q. 1956a *Nature, Lond.* **177**, 27.
 Hanbury Brown, R. & Twiss, R. Q. 1956b *Nature, Lond.* **178**, 1046.
 Hanbury Brown, R. & Twiss, R. Q. 1956c *Nature, Lond.* **178**, 1447.
 Hanbury Brown, R. & Twiss, R. Q. 1957 *Proc. Roy. Soc. A*, **242**, 300.
 Hopkins, H. H. 1951 *Proc. Roy. Soc. A*, **208**, 263.
 Kahn, F. D. *In preparation*.
 Purcell, E. M. 1956 *Nature, Lond.* **178**, 1449.
 Ring, J. 1956 *Astronomical optics* (ed. Z. Kopal). Amsterdam: North Holland Publ. Co.
 Shockley, W. & Pierce, J. R. 1938 *Proc. Inst. Rad. Engn.* **26**, 321.
 Twiss, R. Q., Little, A. G. & Hanbury Brown, R. 1957 *Nature, Lond.* **180**, 324.
 Zernike, F. 1938 *Physica*, **5**, 785.

Interferometry of the intensity fluctuations in light

III. Applications to astronomy

BY R. HANBURY BROWN

Jodrell Bank Experimental Station, University of Manchester

AND R. Q. TWISS

Division of Radiophysics, C.S.I.R.O., Sydney, Australia

(Communicated by A. C. B. Lovell, F.R.S.—Received 10 April 1958)

A theoretical analysis is given of the application of an intensity interferometer to the measurement of the angular diameters of stars and the performance of such an instrument is calculated for representative parameters of the apparatus.

It is shown that observations with an intensity interferometer are probably limited by the inherently low sensitivity of the technique to the stars visible to the naked eye, but that the resolving power, which is determined by the limitations of radio rather than of optical technique, should be great enough to measure any star, however hot, of sufficient apparent brightness; furthermore, the operation should be substantially unaffected by atmospheric scintillation.

Very cool stars of adequate apparent brightness would be completely resolved by the individual mirrors of an intensity interferometer and this fact limits the technique to stars of spectral type earlier than about *K5*. However, a modified form of interferometer using a single main mirror should enable this limit to be extended to bright stars of spectral type as late as *M5*.

Some applications of an intensity interferometer to measurements of both single and double stars are discussed briefly and it is concluded that such an instrument might be of value in astronomy.

1. INTRODUCTION

In parts I and II of the present series of papers (Hanbury Brown & Twiss 1957 *a, b*) we showed that the fluctuations in the outputs of two photoelectric detectors, illuminated with mutually coherent beams of light, are correlated, and we showed how this correlation depends upon the parameters of the equipment and upon the apparent angular distribution of intensity over the source of light. We also pointed out that it should be possible to apply this effect to optical astronomy in measurements of the angular diameters of the bright stars. In the present part of the paper we shall examine this proposal from a theoretical point of view, and in part IV we shall describe an experimental test of the technique on Sirius (α Can. Maj. *A*).

The idea of applying interferometric methods to astronomy was advanced by Fizeau (1868), but the first direct measurement of the angular diameter of a star did not take place until 1920 when Michelson & Pease (1921) determined the angular diameter of Betelgeuse (α Ori) with a 20 ft. interferometer mounted on the 100 in. telescope at Mount Wilson. In the course of the next 10 years Pease reported measurements on six more stars all of which were giants or supergiants of late spectral type ranging from *K0* to *M8*; their angular diameters all lay in the range 0.047 to 0.020 sec of arc and the mirror separations needed to resolve them varied from 3.0 to 7.3 m.

However, although the interferometer has proved to be a valuable tool in the study of visual binaries, its use on single stars has been abandoned largely because of the great practical difficulties of increasing the resolving power beyond that of the original 20 ft. model. For example, the requirement that the optical paths from the two mirrors to the observer should be equal with an accuracy of the order of the wavelength of light, imposes extremely severe requirements on the precision and rigidity of the component parts: the effects of atmospheric scintillation have also proved to be very serious, especially at the larger mirror spacings. A less important objection to the original type of instrument was that it was necessary to use white light in order to get adequate sensitivity; this meant that the effective wavelength, from which the angular diameter of the star was calculated, was always rather uncertain owing, among other factors, to the variable effects of atmospheric extinction. The practical difficulties of extending the technique are perhaps best illustrated by the fact that the 50 ft. interferometer, which was also constructed at Mount Wilson, never seems to have given reliable results.

In recent years a great deal of progress has been made in the application of photoelectric detectors and optical filters to astronomy, and it has been suggested that these techniques might be used to extend the resolving power of Michelson's stellar interferometer. However, in considering the potentialities of these proposals the importance of angular diameter measurements must be viewed against a different background from that prevailing in the year 1920. Thus, the subsequent developments of astrophysical theory, the spectroscopic measurements of effective temperature, the observations of eclipsing binaries and the lunar occultation of a few bright stars have all contributed to our knowledge of the size of the stars, and it is now believed possible to estimate the dimensions of many types of star, especially main sequence stars in the spectral range *A* to *K*, with reasonable accuracy. It would of course, be valuable to check these estimates by direct observation; however, it must be remembered that the greatest uncertainties concern the dimensions and temperatures of the hotter stars of type *W*, *O* and *B*, particularly in the giant and supergiant class. It is for this reason that a new type of stellar interferometer should, if possible, be designed to measure some of the very hot stars.

To accomplish such measurements requires an instrument with extremely high resolving power. For example, it is to be expected that a baseline of at least 400 m would be required to resolve fully the brightest *O* star in the sky (ζ Puppis); while the brightest *W* star, the nucleus of the Wolf-Rayet component of γ Velorum, might possibly require a baseline of 2 km or more. It is our opinion that baselines of this length cannot be achieved with any foreseeable improvements to Michelson's stellar interferometer, but that they should be within the reach of an intensity interferometer of the type discussed in the present paper.

2. OUTLINE OF AN INTENSITY INTERFEROMETER

The main optical equipment of an intensity interferometer consists of two large mirrors A_1 , A_2 separated by a baseline d as shown in figure 1. These mirrors are directed at the star to be measured and focus its light on to the photocathodes of the two photomultipliers P_1 , P_2 through optical filters. The bandwidths of these

filters must be narrow and, in general, it is desirable that they should be of the order of 100 Å. The fluctuations in the output currents of the two photomultipliers are amplified by the amplifiers B_1 , B_2 which have bandwidths of about 100 Mc/s. The low-frequency cut-off of these amplifiers is about 1 Mc/s in order to prevent direct amplification of atmospheric scintillation frequencies. An adjustable time delay τ is inserted in the appropriate channel to compensate for any difference in the times of arrival of the light from the star at the two mirrors.

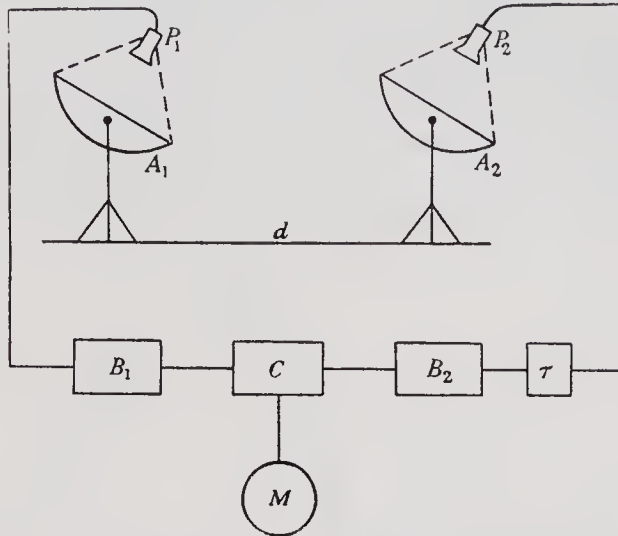


FIGURE 1. Schematic diagram of an intensity interferometer. A, mirrors; B, amplifiers; C, multiplier; M, integrator; P, phototubes; τ , delay.

The outputs from the two amplifiers are multiplied together in a linear multiplier C and their product, averaged over a period of several seconds, drives the integrating device M . In any given period of observation the change in the reading of M is therefore linearly proportional to the correlation between the fluctuations in the two phototubes. A more detailed description of a suitable type of correlator was given in part II.

3. THE MEASUREMENT OF ANGULAR SIZE

In operation, the two mirrors are separated by a sequence of different baselines and in each position the correlation is measured for a sufficiently long period to give a satisfactory signal-to-noise ratio (see § 4). If $C(d)$ is the measured value of the correlation with a baseline d , then for each length of baseline the *normalized correlation factor* $\overline{\Gamma^2(d)}$ is calculated from the equation

$$\overline{\Gamma^2(d)} = C(d)/C(0), \tag{3.1}$$

where $C(0)$ is the correlation with zero baseline under identical conditions of light flux and observing time. The value of $C(0)$ can, in principle, be derived directly from measurements with the mirrors at very close spacing or indirectly from measurements of the light flux during the observations of $C(d)$.

The values of $\overline{\Gamma^2(d)}$ obtained in this way give a measure of the angular size of the star. In the ideal case, where the transmission band of the optical filters is so

narrow that the light may be treated as monochromatic and where the angular size of the star is so small that it is not appreciably resolved by the individual mirrors, it was shown in part II that $\overline{\Gamma^2(d)}$ is simply proportional to the square of the Fourier transform of the angular distribution of intensity across the equivalent line source. For example, if we consider the case of a uniform disk of angular diameter θ_0 observed in monochromatic light of frequency ν_0 then

$$\overline{\Gamma^2(d)} = \Gamma^2(\nu_0, d) = \left[\frac{2J_1(\pi\nu_0\theta_0 d/c)}{(\pi\nu_0\theta_0 d/c)} \right]^2 \quad (3.2)$$

and it is relatively simple to find the value of θ_0 which gives the best fit with the observed values of $\overline{\Gamma^2(d)}$. In practice, the problem will obviously arise of finding the best model of a star. The measured values of $\overline{\Gamma^2(d)}$ do not disclose the relative phase of the components of the Fourier transform, and so it will usually be necessary to assume a centro-symmetric distribution unless there is auxiliary information.

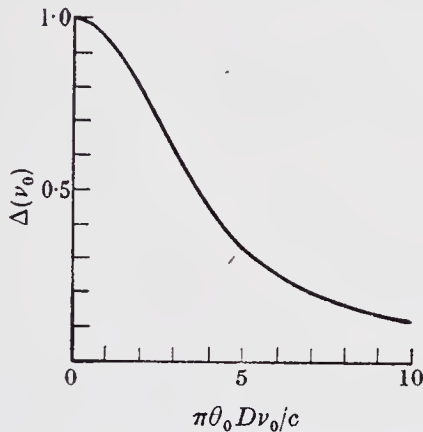


FIGURE 2a. The variation of the partial coherence factor $\Delta(\nu_0)$ with the parameter $\pi\theta_0 D\nu_0/c$, calculated for a circular source of angular diameter θ_0 viewed by two identical mirrors with circular apertures of diameter D .

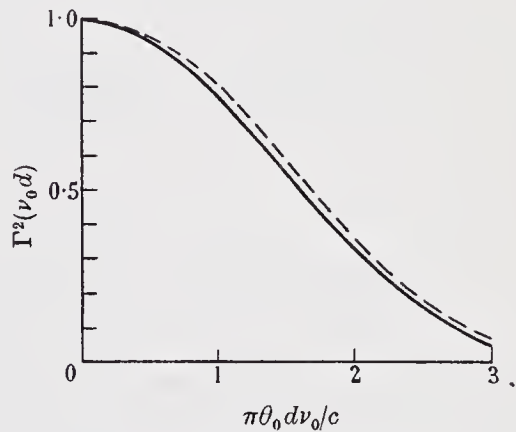


FIGURE 2b. The variation of the normalized correlation factor $\Gamma^2(\nu_0, d)$ with the parameter $\pi\theta_0 d\nu_0/c$, calculated for a circular source of angular diameter θ_0 viewed by two identical mirrors with circular apertures of diameter $\theta_0 D = 0$ (—) and $\theta_0 D = c/\pi\nu_0$ (----).

If the transmission band of the optical filters is wide, or if the observations are carried out in white light, then $\overline{\Gamma^2(d)}$ must be found from $\Gamma^2(\nu, d)$ by integrating over the light spectrum. This procedure is discussed in part II and is carried out for a practical case in part IV.

In the complicated case where the star is partially resolved by the individual mirrors it was shown in part II that the correlation with zero baseline is reduced, relative to that from a point star giving the same light flux, by the *partial coherence factor* $\bar{\Delta}$. The value of $\bar{\Delta}$ depends upon the angular size and shape of the star and upon the size and shape of the mirrors; furthermore, under these conditions the normalized correlation factor $\overline{\Gamma^2(d)}$ also becomes a function of the mirror parameters. As an example we have considered the case of a star which radiates like a

circular disk of uniform brightness and which is observed by two identical mirrors with uniform cross-section and uniform reflectivity. In figure 2a we have plotted $\Delta(\nu_0)$ as a function of the dimensionless parameter $\pi\theta_0 D\nu_0/c$, where θ_0 is the angular diameter of the star and D is the diameter of the mirrors. In figure 2b we have plotted $\Gamma^2(\nu_0, d)$ as a function of the mirror separation d for the two values 0 and 1 of the parameter $\pi\theta_0 D\nu_0/c$ which correspond respectively to the condition that the star is (a) unresolved, and (b) partially resolved, by the individual mirrors. These curves were calculated by means of an electronic digital computer, following the general principles laid down in appendix A of part II. They show that the dependence of $\Gamma^2(\nu_0, d)$ on d is closely similar in the two cases considered, and therefore the correction which must be applied to find the diameter of the star when it is partially resolved by the individual mirrors is small.

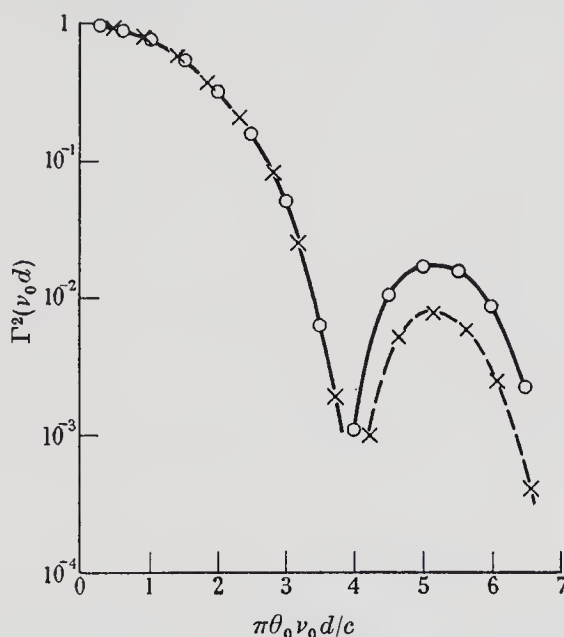


FIGURE 3. The effect of limb-darkening on the variation of correlation with baseline length d . The curves show the variation of the *normalized correlation factor* $\Gamma^2(\nu_0, d)$ with the parameter $\pi\theta_0\nu_0d/c$ for a star with a circular disk and two different degrees of limb-darkening viewed by two mirrors of small diameter. \times --- \times --- \times , complete limb-darkening ($u_\lambda = 1.0$); \circ — \circ — \circ , no limb-darkening ($u_\lambda = 0$).

3.1. The effects of radial limb-darkening

An important weakness of an intensity interferometer is that the observed correlation is proportional to the *square* of the amplitude of the Fourier transform of the intensity distribution across the stellar disk, in contrast to the Michelson stellar interferometer in which the visibility of the fringes is *linearly* proportional to the amplitude of the Fourier transform. In consequence, unless the star is very bright the details of the distribution, which are carried by the Fourier components of high order and small relative amplitude, are likely to be lost since their signal-to-noise ratio will be correspondingly low. To illustrate this point we have shown in figure 3 the theoretical curves of the normalized correlation factor $\Gamma^2(\nu_0, d)$ for a star with a uniform disk of angular diameter θ_0 and also for a star of angular

diameter θ_1 with complete radial limb-darkening according to the law $(1 - \theta^2/\theta_1^2)^{\frac{1}{2}}$. The ratio θ_0/θ_1 has been chosen so that the two curves osculate at the origin and, as may be seen, they do not differ thereafter by more than 0.01 even at extreme values of the baseline d .

It follows that these two cases of zero and complete limb-darkening cannot be distinguished unless the signal-to-noise ratio is of the order of 100 to 1 with the minimum usable baseline. With practical equipment and reasonable observation times this sensitivity could only be achieved on a few of the brightest stars; so, for most stars, it can be stated that an intensity interferometer gives a measure of the apparent angular diameter of the equivalent uniform disk rather than the detailed angular distribution of intensity over the stellar surface. The equivalent uniform disk is defined here as a disk which radiates the same total light flux as the actual star and has a Fourier transform, for the equivalent line source, which osculates at zero baseline with that of the actual star.

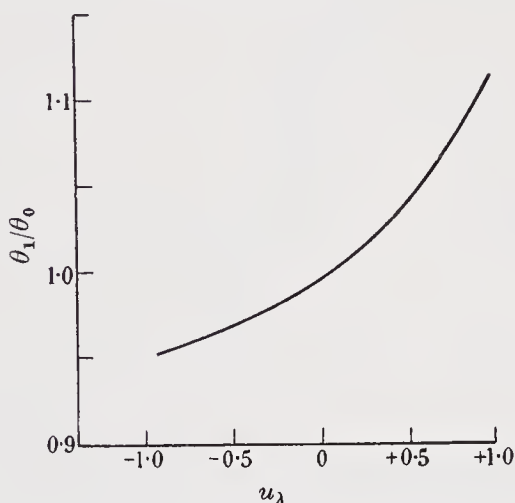


FIGURE 4. The effect of the limb-darkening coefficient u_λ on the apparent angular diameter of a star. The curve shows the ratio θ_1/θ_0 as a function of u_λ , where θ_1 is the true angular diameter of the star and θ_0 is the diameter of the equivalent disk as defined in the text.

However, it should be noted that the difference between the true angular diameter of the star and the angular diameter of the equivalent disk is not large, even in the extreme case of complete limb-darkening. Thus let us consider the case where the limb-darkening of the actual star at a given wavelength can be expressed by the approximate law

$$I_\lambda(\theta) = I_\lambda(0) [1 - u_\lambda(1 - (1 - \theta^2/\theta_1^2)^{\frac{1}{2}})], \quad (3.3)$$

where θ_1 is the true angular diameter of the star. Then it can easily be shown that θ_1 is related to θ_0 the angular diameter of the equivalent uniform disk by the equation

$$\frac{\theta_1}{\theta_0} = \left[\frac{1 - u_\lambda/3}{1 - 7u_\lambda/15} \right]^{\frac{1}{2}}, \quad (3.4)$$

which has been plotted in figure 4 as a function of u_λ ; the negative values of u_λ correspond to limb-brightening. The curve shows that for the assumed law the maximum possible error in the angular diameter is 5.6% if we assume that $u_\lambda = 0.6$

in all cases of limb-darkening, and this error can be considerably reduced in a practical case when an approximate estimate of the limb-darkening can be obtained from astrophysical theory.

3.2. Double stars

Although the intensity interferometer is insensitive to the details of the intensity distribution over the surface of a single star, it should be able to distinguish single from multiple stars as long as the ratio of the intensities of the individual components is not too large.

As an illustration let us consider the simple case of a binary star with an angular separation $\bar{\theta}$, which is too small to be resolved by the individual mirrors of the intensity interferometer. If the line joining the two components of the star makes an angle ψ_1 with the baseline joining the two mirrors of the interferometer, then the correlation observed as a function of the mirror separation d is proportional to

$$I_1^2 + I_2^2 + 2I_1 I_2 \cos \{(2\pi\bar{\theta}d\nu_0 \cos \psi_1)/c\},$$

where I_1, I_2 are the intensities of the two components, and it is assumed that the mirror separation is not large enough to resolve the individual components of the binary. Under these conditions the observed correlation will oscillate between the values $(I_1 + I_2)^2$ and $(I_1 - I_2)^2$ as the length of the baseline or the position angle of axis of the binary varies. If the star is just bright enough to lie within the working range of the interferometer, the minimum fractional variation of correlation which can be measured reliably is roughly of the order of 0.33. Even in this limiting case it follows that the binary nature of the star will be detected provided that the two components do not differ by more than about 2.5 magnitudes, and this critical magnitude difference would be appreciably larger for stars for which the signal-to-noise ratio is much above the workable minimum.

4. THE SIGNAL-TO-NOISE RATIO

The faintest star which can be observed, and also the precision with which the correlation can be measured for any given star and position of the mirrors, will be determined predominantly by the inevitable statistical fluctuations in the output of the correlator. It was shown in parts I and II that the major fraction of these fluctuations is inherent in the received light itself and that the contribution from the apparatus can be made almost negligible. For convenience we have termed the ratio of the observed correlation to the r.m.s. value of these fluctuations the *signal-to-noise ratio*. It follows* from equation (2.14) of part II that, in the case where the light is unpolarized, the general expression for the signal-to-noise ratio $(S/N)(T_0)$ for an observing time T_0 is

$$\frac{S}{N}(T_0) = \epsilon\gamma(\nu_0) \frac{\mu - 1}{\mu} \frac{(A_1 A_2)^{\frac{1}{2}}}{(1 + \delta)} \alpha(\nu_0) n_0(\nu_0) \left(\frac{b_v}{2\eta}\right)^{\frac{1}{2}} \Gamma^2(\nu_0, d) \Delta(\nu_0) \times \frac{\sum_{r=1}^m T_r \rho_r^{2 \text{sec} \zeta_r}(\nu_0) \sigma_r}{\left[\sum_{r=1}^m T_r \rho_r^{2 \text{sec} \zeta_r}(\nu_0) (1 + a_r)^2 \right]^{\frac{1}{2}}}, \tag{4.1}$$

* There is an error in equation (2.14) in part II. The factor $\Delta(\nu_0, d)$ is a misprint and should read $\Delta(\nu_0) \Gamma^2(\nu_0, d)$ as in (2.13).

where

- $\alpha(\nu_0)$ is the geometric mean of the quantum efficiencies of the photocathodes for light of frequency ν_0 ;
- $n_0(\nu_0)$ is the number of quanta $m^{-2}s^{-1}(c/s)^{-1}$ incident normally on the top of the atmosphere at a frequency ν_0 ;
- $T_0 = \sum_{r=1}^m T_r$ is the total observation time, where T_r is an interval which is so short that the factors $\rho_r^{2\text{sec } \zeta_r}(\nu_0)$ and $(1+a_r)$ do not vary appreciably during it;
- $\rho_r(\nu_0)$ is the average value of the atmospheric transmission for light of frequency ν_0 at vertical incidence on the atmosphere in the r th time interval;
- ζ_r is the average value of the zenith angle of the star in the r th time interval;
- $(1+a_r)$ is the ratio of the total light flux at each photocathode from the star plus the night sky to that due to the star alone;
- $\gamma(\nu_0)$ is the product of the transmission factor of the optical filter and the reflectivity of the mirror at a frequency ν_0 ;
- ϵ is the combined loss of correlation in the optical and electronic equipment (see part II);
- $(1+\delta)$ is the excess noise produced in the electronic equipment;
- $\mu/(\mu-1)$ is the excess noise introduced by a photomultiplier;
- A_1, A_2 are the mirror apertures;
- b_v is the cross-correlation bandwidth of the two channels defined by

$$b_v = \int_0^\infty \frac{1}{2} [F_1(f) F_2^*(f) + F_1^*(f) F_2(f)] df / F_{\text{max}}^2, \quad (4.2)$$

where

- $F_1(f), F_2(f)$ are the complex frequency characteristics of the two channels;
- η is the normalized spectral density of the fluctuations at the outputs of the two amplifiers defined by

$$\eta = \int_0^\infty |F_1^2(f) F_2^2(f)| df / (b_v F_{\text{max}}^4), \quad (4.3)$$

- σ_r is the normalized spectral density of the light incident on the photocathodes defined by

$$\sigma_r = \frac{\int_0^\infty \alpha^2(\nu) \gamma^2(\nu) \rho_r^{2\text{sec } \zeta_r}(\nu) n_0^2(\nu) d\nu}{\left[\alpha(\nu_0) \gamma(\nu_0) \rho_r^{\text{sec } \zeta_r}(\nu_0) n_0(\nu_0) \int_0^\infty \alpha(\nu) \gamma(\nu) \rho_r^{\text{sec } \zeta_r}(\nu) n_0(\nu) d\nu \right]}. \quad (4.4)$$

The performance of a practical stellar interferometer has been estimated from equation (4.1) as follows. From experience of a test of the method on Sirius and from the known limitations of photoelectric and optical technique, the following values for the parameters of the equipment have been assumed

$$\left. \begin{aligned} b_v/\eta &= 10^8 \text{ c/s}, & \epsilon &= 1.0, & (\mu-1)/\mu &= 0.8, \\ \sigma &= 0.8, & \gamma(\nu_0) &= 0.7, & (1+\delta) &= 1.0. \end{aligned} \right\} \quad (4.5)$$

The quantum efficiency of the photocathodes has been taken as $\alpha(\nu_0) = 0.20$ at 4300 Å, and 0.10 at 5400 Å, since this performance can be readily achieved with multi-alkali photocathodes (Sommer 1956).

The contribution to the output fluctuations due to light from the night sky, represented by the term $(1 + a_r)$ depends upon the position of the star and also upon the optical quality of the mirrors. As a typical value it has been assumed that the light from the night sky is equivalent to one-fourth magnitude star per square degree, and that the optical quality of the mirrors is such that their field of view can be satisfactorily limited to a cone with a half angle of about 6 min of arc. The values for $\rho_0(\nu_0)$ the atmospheric extinction, will be taken as those appropriate to clear sky conditions. On these assumptions it follows that

$$\left. \begin{aligned} 1 + a_r &= 1 + 10^{(-3+0.4m)}, \\ \rho(\nu_0) &= 0.70 \quad \text{for } \lambda_0 = 4300 \text{ Å}, \\ \rho(\nu_0) &= 0.82 \quad \text{for } \lambda_0 = 5400 \text{ Å}, \end{aligned} \right\} \quad (4.6)$$

where m is the apparent magnitude of the star under observation.

The value of $n_0(\nu_0)$ for any given star can be derived from well-known formulae (see, for example, Woolley & Stibbs 1953), and for stars in the spectral range M to B it is sufficiently accurate to write

$$\left. \begin{aligned} n_0(\nu_0) &= 9.3 \times 10^{(-5.0-0.4m_{pv})} \quad \text{for } \lambda_0 = 5400 \text{ Å}, \\ n_0(\nu_0) &= 6.67 \times 10^{(-5.0-0.4m_{pg})} \quad \text{for } \lambda_0 = 4300 \text{ Å}, \end{aligned} \right\} \quad (4.7)$$

where m_{pv} , m_{pg} are the photovisual and photographic magnitudes, respectively.

Substituting the numerical values given above in equation (4.1) the r.m.s. signal-to-noise ratio obtainable on a given star after an observation time of 1 h is

$$\frac{S}{N}(5400 \text{ Å}, 1 \text{ h}) = \frac{1.14D^2 10^{-0.4m_{pv}}}{1 + 10^{(-3+0.4m_{pv})}} 0.82^{(\sec \zeta - 1)} \Gamma^2(\nu_0, d) \Delta(\nu_0) \quad (4.8)$$

and
$$\frac{S}{N}(4300 \text{ Å}, 1 \text{ h}) = \frac{1.39D^2 10^{-0.4m_{pg}}}{1 + 10^{(-3+0.4m_{pg})}} 0.70^{(\sec \zeta - 1)} \Gamma^2(\nu_0, d) \Delta(\nu_0), \quad (4.9)$$

where D is the diameter of the mirrors and ζ is the average value of the zenith angle of the star during the observation.

From equations (4.1), (4.8) and (4.9) it can be seen that the signal-to-noise ratio for a given star varies as the square root of the observing time and as the square of the mirror diameter. Thus, assuming that all the other parameters remain fixed, we can increase the signal-to-noise ratio on a given star, or alternatively extend the measurements to fainter stars, either by increasing the time of observation or by using larger mirrors. Our limited experience with the preliminary equipment used in the observations on Sirius, described in part IV, suggests that it is desirable that the r.m.s. signal-to-noise ratio after 1 h observation should be at least 3 to 1 with the minimum mirror separation. On this basis we have plotted, in figure 5, the mirror diameter D as a function of the apparent magnitude of the faintest star which can be satisfactorily measured. The curve is given for a wavelength of 4300 Å and it has been assumed that the star is unresolved and in the zenith.

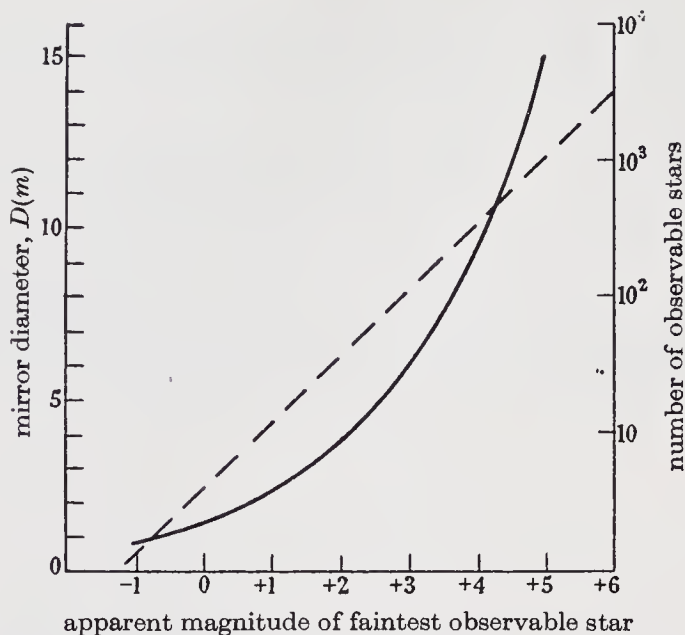


FIGURE 5. The minimum mirror diameter necessary to achieve a signal-to-noise ratio of 3/1 in a period of 1 h as a function of the apparent magnitude of the faintest star which can be observed ($\lambda = 4300 \text{ \AA}$). The broken line shows the total number of stars, including both hemispheres, brighter than the limiting magnitude.

5. THE PROBLEM OF MEASURING COOL STARS

5.1. *The limitations of a two-mirror interferometer*

In the preceding section the size of the mirrors required to achieve a workable signal-to-noise ratio was calculated as a function of apparent magnitude on the assumptions that the star is not significantly resolved by the individual mirrors so that $\Delta(\nu_0) \simeq 1$, and also that the baseline could be reduced to a sufficiently short value so that $\Gamma^2(\nu_0, d_{\text{min.}}) \simeq 1$. While these assumptions are valid for hot stars, they are not justified for the cooler stars of late spectral type. As stars of lower temperature are observed, assuming that their apparent angular diameter remains the same, the size of the mirrors must be increased to maintain a given signal-to-noise ratio: eventually the size and separation of the mirrors becomes so large that the star is significantly resolved even with the two mirrors so close together that they touch, that is when $d_{\text{min.}} = D$. Under these circumstances the factor $\Gamma^2(\nu_0, d_{\text{min.}}) \Delta(\nu_0)$ is appreciably less than unity, and it can be shown that the factor $D^2 \Gamma^2(\nu_0, D) \Delta(\nu_0)$ which determines the variation of the signal-to-noise with diameter, as given by equations (4.8) and (4.9), has a maximum value when

$$\pi \theta_0 D \nu_0 / c \simeq 2, \quad (5.1)$$

where θ_0 is the angular diameter of the star. Hence, with a given electronic equipment it is impossible to obtain a workable signal-to-noise ratio from a star below a certain temperature, and this limit applies no matter how bright the star or how large the mirrors.

This effect is illustrated in figure 6 which shows the maximum possible signal-to-noise ratio which can be obtained in an observation of 1 h as a function of the

brightness temperature of the star. It has been assumed in these calculations that, (i) the observations are made with the optimum size of mirrors for each temperature, (ii) the mirrors are circular and mounted with their centres separated by their diameter, (iii) the star radiates as a uniform disk and is observed in the zenith, the background light from the sky being negligible, (iv) the wavelength of observation is 5400 \AA and the electronic equipment has the parameters given in § 4.

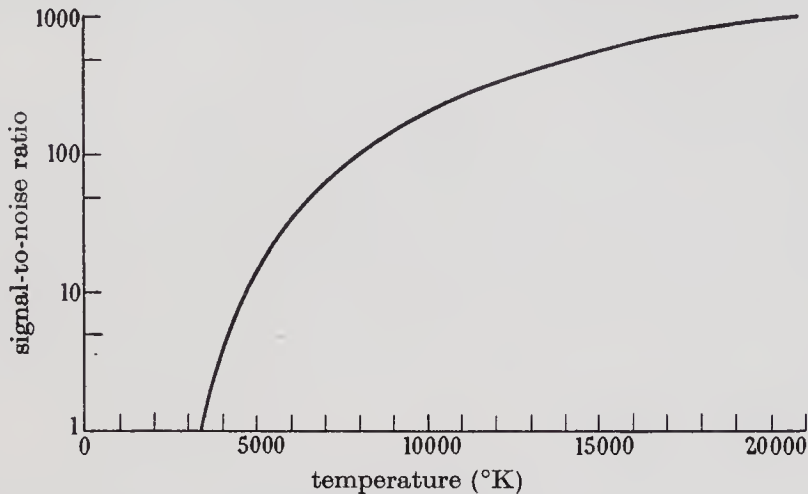


FIGURE 6. The maximum possible signal-to-noise ratio which can be obtained with a two-mirror interferometer in an observation lasting for 1 h as a function of the brightness temperature of the star ($\lambda = 5400 \text{ \AA}$).

It is reasonable to assume that, for satisfactory measurements of angular diameter, the signal-to-noise ratio with the star unresolved must approach 10/1 for an observation carried out on one night. The signal-to-noise ratio in a period of 1 h must therefore exceed about 3/1, and the curve in figure 6 shows that this can only be achieved if the brightness temperature of the star is greater than about $4000 \text{ }^\circ\text{K}$. We have already shown that measurements of the detailed distribution across a star, such as limb-darkening, can only be carried out if the signal-to-noise ratio approaches 100/1, that is to say if it has a value of at least 30/1 in 1 h, and it follows from figure 6 that these detailed measurements are only possible on stars with a temperature exceeding about $6000 \text{ }^\circ\text{K}$.

Thus it follows from this analysis that a two-mirror interferometer of the type described here cannot be used to measure the angular size of stars with a spectral type later than about *K7* (main sequence), and that measurements of limb-darkening cannot be carried out on stars with a spectral type later than about *G0*.

5.2. *The possibility of using a single mirror*

The limitations described above might partially be overcome by replacing the two mirrors by a single mirror in which the light is split to illuminate two separate phototubes. This can be accomplished either by mounting a semi-transparent mirror to divide the light near the focus, or by constructing the surface of the single mirror of a very large number of small mirrors which can be focused individually on either of two phototubes. In effect this arrangement reduces the baseline of the interferometer to zero, and the star would then be resolved only by the mirror itself.

To find the angular diameter θ_0 of a star one would need to measure not only the correlation between the fluctuations in the outputs of the two phototubes but also the total incident light flux. Since the correlation for a partially resolved star is less by the partial coherence factor Δ than that for a point source producing the same incident light flux, these measurements would yield a value of Δ from which one could estimate the angular size of the star with an accuracy that was linearly proportional to $\delta\Delta/\delta\theta_0$. Additional information about the intensity distribution over the star's disk could, in principle, be obtained by measuring Δ for different values of mirror diameter.

The signal-to-noise ratio with a single mirror of diameter D would differ by a factor $1/(2\Gamma^2(\nu_0, D))$ from that with two mirrors of diameter D mounted with their centres separated by their diameter; the factor $\frac{1}{2}$ represents the loss of sensitivity due to the need to divide the light between the two photocathodes. A detailed analysis of the variation of this factor with stellar temperature and mirror size shows that it should be possible, by the single-mirror technique, to measure stars which are about 1000 °K cooler than those which can be measured by the two-mirror method, thereby extending the observations to stars with a brightness temperature of about 3000 °K.

It must be noted, however, that the range of stellar temperatures over which the single-mirror technique could be used is limited by the requirement that $\delta\Delta/\delta\theta_0$ should be large enough to yield a reasonably accurate result. Thus if the value of Δ is too close to unity or to zero, then only upper or lower limits can be found for the angular diameter of the star. It can be shown that in effect this requirement limits the use of the single-mirror technique to stars whose brightness temperature lies between about 3000 and 5500 °K, corresponding approximately to the spectral range *M5* to *K0*.

6. THE EFFECTS OF ATMOSPHERIC SCINTILLATION

There is no generally accepted theory of atmospheric scintillation. In particular, there is still argument as to the relative importance of refraction, which can be adequately analyzed by a ray theory, and of diffraction which involves a complete wave theory. For this reason we shall not attempt a precise quantitative analysis of the effects of scintillation on an intensity interferometer, but shall show that these effects are likely to be negligible even if, in each case, the least favourable assumptions are made.

To analyze the general case in which both refraction and diffraction may be involved let us first consider the effects of scintillation in the case of an unresolved star, which may be regarded as an infinitely distant point source. Under these conditions the light incident upon the top of the earth's atmosphere can be represented by a set of plane waves which can be decomposed into two independent and orthogonally polarized components. The electric vector in one of these components can be represented by a Fourier series of the form

$$E(t) = \sum_{r=1}^{\infty} E_r \cos \left[\frac{2\pi r}{T} \left(t - \frac{(z-z_0)}{c} \right) - \phi_r \right], \quad (6.1)$$

where the Z -axis is taken along the line joining the observer and the star and where z_0 is the length of the equivalent vacuum path from the observer to the top of the atmosphere.

At the bottom of the atmosphere an incident plane wave will appear as a continuum of plane waves produced by refraction and diffraction at atmospheric irregularities so that the electric field at a particular point $(x_1, y_1, 0, t)$ will have components along all three spatial axes, the l th component being of the general form

$$E_{lr}(1 + \rho_{lr}(\mathbf{x}_1, t)) \cos \left[\frac{2\pi r t}{T} - \phi_r - \psi_{lr}(\mathbf{x}_1, t) \right], \quad (6.2)$$

where $\rho_{lr}(\mathbf{x}_1, t)$, $\psi_{lr}(\mathbf{x}_1, t)$ are the fluctuating amplitude and phase variables, respectively, which determine the scintillation at the point (\mathbf{x}_1, t) .

If (\mathbf{x}_1) represents a point on the photocathode of one of the phototubes then $p(\mathbf{x}_1, t)$, the probability of the emission of a photoelectron, is proportional to the square of the amplitude of the electric field, and following the treatment given in part I may be written

$$\begin{aligned} p(\mathbf{x}_1, t) \sim \sum_{l=1}^3 \left\{ \sum_{r=1}^{\infty} \frac{1}{2} \alpha_r E_{lr}^2 [1 + \rho_{lr}(\mathbf{x}_1, t)]^2 \right. \\ \left. + \sum_{r=s}^{\infty} \sum_{s=1}^{\infty} (\alpha_r \alpha_s)^{\frac{1}{2}} E_{lr} E_{ls} (1 + \rho_{lr}(\mathbf{x}_1, t)) (1 + \rho_{ls}(\mathbf{x}_1, t)) \right. \\ \left. \times \cos \left[\frac{2\pi(r-s)t}{T} - (\phi_r - \phi_s) - (\psi_{lr}(\mathbf{x}_1, t) - \psi_{ls}(\mathbf{x}_1, t)) \right] \right\}, \quad (6.3) \end{aligned}$$

where α_r is the quantum efficiency of the photocathode at a frequency r/T . To find the probability $P_1(t)$ that a photoelectron will be emitted when the light is focused on to the photocathode by a parabolic mirror of aperture A , one must integrate \mathbf{x}_1 over the area of aperture so that

$$P_1(t) = \int_A p(\mathbf{x}_1, t) d\mathbf{x}_1. \quad (6.4)$$

The fluctuations in the anode current of the phototube are amplified over a band of frequencies, with a low-frequency cut-off which is chosen to exclude scintillation frequencies, and they are then correlated with the fluctuations in the anode current of the phototube at the focus of the second mirror. As we have already shown in part I the observed correlation is proportional to the time average of the joint probability of photoemission at the two photocathodes.

Consideration of equation (6.3) suggests that the correlation observed from a point source may be affected by atmospheric scintillation in at least two ways; first, there will be additional phase shifts introduced into the light reaching each photocathode, and these phase shifts may not be the same in each channel; secondly, the amplitude of the fluctuations in the outputs of the phototubes will be amplitude modulated by the scintillations. We shall consider these two effects in turn.

6.1. Phase scintillation

We shall assume that atmospheric scintillation is caused by three-dimensional irregularities of refractive index, and that the local deviations of refractive index are small compared with the average value. This case of a thick medium with weak

irregularities has been treated by Bramley (1955) and also by Fejer (1953). Bramley's procedure for finding the phase of the emerging wavefront at a given point is essentially a ray treatment, since he equates the fluctuating phase shift to $1/\lambda$ times the change in optical path length along a line drawn in the direction of the star. In effect he assumes that

$$\psi(\mathbf{x}_1, t) = \int_0^L (\mu - \mu_{av.}) dz = \int_0^L \delta\mu dz, \quad (6.5)$$

where μ , $\mu_{av.}$ are the instantaneous and average values of the refractive index, respectively. Some of the atmospheric irregularities will increase and some will decrease the optical path length, so that the effect is that of a random walk and, on plausible assumptions, Bramley shows that the phase of the emergent wave is randomly distributed with a standard deviation given by

$$\delta\psi_m(\mathbf{x}_1, t) = \frac{2\pi}{\lambda} (lL)^{\frac{1}{2}} \delta\mu_m, \quad (6.6)$$

where $\delta\mu_m$ is the standard deviation of the refractive index; L is the total path length through the atmosphere; l is the 'size' of a typical irregularity; λ is the wavelength of the light. The validity of this analysis is supported by the fact that it leads to identical results to those obtained by Fejer who supposed the thick medium to be divided into a series of thin slabs which successively diffract the light waves.

If for the moment we neglect the effects of dispersion, then the phase scintillation given by equations (6.5) and (6.6) can conveniently be represented as a scintillating time delay τ_m which is introduced into the light path by the atmosphere. The r.m.s. value of τ_m is given by

$$(\overline{\tau_m^2})^{\frac{1}{2}} = \frac{\delta\mu_m}{c} (lL)^{\frac{1}{2}}. \quad (6.7)$$

Assuming the scale height of the atmosphere to be about 10^4 m, the size of the irregularities to be about 1 m, and taking $\delta\mu \simeq 10^{-6}$, which corresponds to local temperature fluctuations of about 1 °K, then $(\overline{\tau_m^2})^{\frac{1}{2}} \simeq 3 \times 10^{-13}$ s.

The effect of inserting a time delay in the light reaching one mirror of an intensity interferometer is to reduce the correlation. Thus if the correlated components in the outputs of the two phototubes are delayed with respect to each other by a time $\delta\tau$, then it is simple to show (e.g. by the Wiener-Kintchine theorem) that the observed correlation will be reduced by a factor

$$\frac{1}{B} \int_0^B \cos(2\pi f\delta\tau) df \simeq 1 - \frac{1}{6}(2\pi B\delta\tau)^2, \quad (6.8)$$

where B is the bandwidth of the amplifiers which is assumed to be rectangular for simplicity. In practice B will be of the order of 10^8 c/s and therefore the loss of correlation will be less than 1 % provided that $\delta\tau < 3.9 \times 10^{-11}$ s.

It follows that the random time delays introduced by atmospheric scintillation are two orders of magnitude less than those which would produce a significant loss of correlation. Furthermore, there is evidence to suggest that the value of 1 m,

which we have assumed for the size of the irregularities is too great, and that the scintillations are produced predominantly in a thin layer rather than throughout the entire atmosphere. If this is correct the effects of scintillation will be even smaller still.

In the analysis given above the effects of dispersion have been neglected, since it can be shown that they are negligible as follows. The correlated components in the outputs of the two phototubes can be regarded, as we have shown in part I, as beat frequencies formed by intermodulation of frequencies present in the original light wave at the photocathodes. If the bandwidth of the amplifiers following the phototubes is restricted to frequencies less than 100 Mc/s, then phase dispersion in the atmosphere can only affect the correlation if it introduces significantly different phase shifts into components of the light which differ in frequency by only 100 Mc/s; furthermore, the amount of this phase dispersion must be different at the two mirrors. Taking the usual formula for the refractive index of air, it is simple to show that the difference in phase introduced by the entire atmosphere into light waves which are 100 Mc/s apart in frequency is only about 0.5 rad at 4000 Å. It is clear that any differential phase dispersion produced at two points on the earth's surface by minor irregularities in the atmosphere will be very much less than 0.5 rad and therefore its effect on the observed correlation will be negligible.

6.2. *Amplitude scintillation*

The effects of amplitude scintillation can be deduced from equation (6.3). The discussion can be simplified appreciably by the assumption that the amplitude scintillations of two light frequencies received at a given point are fully coherent if these frequencies are separated by not more than 100 Mc/s. Plausible theoretical arguments can be found to justify this assumption, and it is also supported by experimental evidence, for example, by the observations of Mikesell, Hoag & Hall (1951). Under these conditions it is permissible to write

$$1 + \rho_{lr}(\mathbf{x}_1, t) = 1 + \rho_{ls}(\mathbf{x}_1, t)$$

in equation (6.3), and the effects of amplitude scintillation can be represented by assuming that the probability that photoelectron is produced by light incident at any point of one mirror varies with time as $1 + g_1(t)$, where

$$g_1(t) = \frac{\sum_{r=1}^{\infty} \sum_{l=1}^3 \int_{A_1} [(1 + \rho_{lr}(\mathbf{x}_1, t))^2 - 1] d\mathbf{x}_1 \alpha_r E_{lr}^2}{\sum_{r=1}^{\infty} \sum_{l=1}^3 \alpha_r E_{lr}^2 A_1} \tag{6.9}$$

and where A_1 is the aperture of one of the mirrors.

The quantity $g_1(t)$ is an irregularly fluctuating quantity with zero mean value and with a power spectrum which in practice seldom extends above about 1000 c/s. The r.m.s. value of $g_1(t)$ depends upon the mirror aperture and upon the zenith angle of the star, but with mirrors of the order of 3 m in diameter or more and for stars at zenith angles less than 45° we estimate that it will not exceed about 0.03 even under conditions of bad seeing.

Now the time-averaged correlation between the fluctuations in the outputs of the two phototubes will be increased by the factor

$$\langle (1 + g_1(t)) (1 + g_2(t)) \rangle_{av.} = 1 + \langle g_1(t) g_2(t) \rangle_{av.} \quad (6.10)$$

when amplitude scintillation is present. Thus, even in the extreme case when the amplitude scintillations are completely correlated at the two mirrors and when $[\overline{g_1^2(t)}]^{\frac{1}{2}} = 0.03$, the correlation will be increased by less than 1 part in 10^3 . In practice the amplitude scintillations at two mirrors separated by a few metres will be almost uncorrelated, and hence we are justified in neglecting entirely the effects of amplitude scintillation on an intensity interferometer.

6.3. Angular scintillation

In the previous analysis it has been assumed that the star is a point source and that the light incident on the top of the atmosphere can be represented by a system of plane waves. It remains to consider a star with a finite angular size; in this case the correlation may be altered if atmospheric scintillation introduces appreciable differential phase shifts into light waves reaching a point on the earth from different points on the star. Such differential shifts might be introduced if rays from different points on the source traverse different irregularities. However, simple considerations show that this effect cannot be significant if the two points at which the rays traverse the irregularities are so close that they lie in the same Fresnel zone as viewed from the receiving point. For example, if the angular diameter of the star is 0.01 sec of arc and the irregularities are at any height up to say 10^4 m, then the maximum separation between two rays from the extremities of the star cannot be greater than about 0.5 cm. At a wavelength of 4000 Å the diameter of the first Fresnel zone on a plane at a height of 10^4 m, as seen from a point on the earth, is of the order of 5 cm. It follows that the effects of these differential phase shifts are unlikely to be significant.

A second way in which differential phase shifts could arise is through angular scintillation. Thus it is known from experiment that, for a specific point on the mirror, the instantaneous direction of the incident light can fluctuate by as much as 3 sec around the mean with a standard deviation of about 1 sec under conditions of rather poor 'seeing'. In the most unfavourable case, where the scattering occurs in a single thin layer, the differential phase shifts introduced by this effect into light emitted by different points on the star are just those which would arise if the observing point on the earth were to be translated horizontally by a distance

$$\xi = \chi H \sec \zeta, \quad (6.11)$$

where χ is the scattering angle, H is the height of the scintillation layer, ζ is the zenith angle of the star. Thus if $H \sec \zeta$ has the extreme value of 5×10^4 m and the standard deviation of χ is taken as 1 sec, then the standard deviation of ξ is about 25 cm.

Experience with large mirrors shows that the correlation between angular scintillation at points more than about 30 cm apart is usually small. Hence, the effect of angular scintillation on an intensity interferometer can be analyzed on

the assumption that elements of the mirror aperture, of the order of 30 cm in size, are randomly displaced with respect to one another by distances of the order of 25 cm. This movement would effectively change the shape and area of the aperture and randomly displace the optical centre by an amount which is appreciably smaller than the displacement of a single element. For mirrors of 3 m or more in size this random apparent displacement of the optical centre would probably be less by an order of magnitude than 25 cm; furthermore, the direction of this displacement would itself be random and its mean value would tend to zero over a long period. It is clear that, for measurements which involve baselines of the order of several metres, the effect of this random apparent displacement of the optical centres of the mirrors by angular scintillation would be negligible. It can also be shown that any random changes in the effective shape and aperture of the mirrors are unlikely to produce significant effects.

7. THE EFFECT OF THE COSMIC RAY COMPONENT IN THE NIGHT SKY

The principle underlying the intensity stellar interferometer is the existence of a partial correlation between the arrival times at the two spaced mirrors of the light quanta emitted by the star. Hence, the presence of any other source of time—correlated light quanta in the night sky will alter the correlation observed at a particular mirror spacing and, unless this effect is eliminated or corrected, it will lead to erroneous estimates of the angular size of the star. Such a light source is provided by the high-energy electrons, and to a much smaller extent by the other charged particles, in a cosmic-ray shower (Blackett 1948). This phenomenon has been studied experimentally by Galbraith & Jelley (1955) who concluded that the principal cause of the emitted light was probably Čerenkov radiation from the fast electrons rather than Bremsstrahlung or recombination radiation, and they have shown that the light quanta reaching a particular point on the earth's surface arrive spread over a time interval of approximately 10^{-8} s. On theoretical grounds they estimate that a cosmic-ray shower will produce a pool of light on the ground with a radius of the order of magnitude of 100 m, so both mirrors of the intensity interferometer might lie in the light pool and would reflect correlated light pulses into the cathodes of the phototubes, as long as the light was produced at points within the acceptance cones of both the mirrors.

In appendix I we have derived an upper limit δC_{max} to the fractional increase, due to this cosmic ray effect, in the correlation to be expected in measurements on unresolved stars of photovisual magnitude m_{pv} . In this calculation we have relied as much as possible on the experimental data and any simplifying assumptions have been biased on the pessimistic side; on this basis we have shown that

$$\delta C_{\text{max}} \simeq 0.18 \Omega_0 B^{0.8} 10^{(-9-0.72m_{pv})} \left[\left(\frac{\pi D^2 \alpha \gamma}{4} \right)^{-0.2} \sigma^{-1} \rho_0^{-1.8 \sec \xi} \cos^l \zeta \right], \quad (7.1)$$

where Ω_0 is the solid angle of the field of view of the mirror, l is a number between 2 and 3 and the remaining symbols have been defined in § 4 above.

With typical values of D and ζ the term in square brackets in equation (7.1) may be taken as equal to or less than unity. If we assume, as in § 4, that the field of view

of the mirrors is limited to a cone with a half angle of 6 min of arc, so that $\Omega_0 \simeq 10^{-5}$, and if the bandwidth of the optical filter is 100 Å centred on 5400 Å, then $\delta C_{\max.} < 1\%$ if the photovisual magnitude of the star is brighter than +3.2. For a star of fifth magnitude it would appear from equation (7.1) that the correlation due to Čerenkov radiation in the earth's atmosphere would be comparable with that due to the light quanta emitted by the star. However, for the reasons pointed out in appendix I, the experimental value of the Čerenkov contribution may be appreciably smaller than $\delta C_{\max.}$, especially with the larger baselines required for measurements of the fainter stars; it is therefore possible that the operation of an intensity stellar interferometer will, in practice, never be seriously affected by the light pulses from cosmic-ray showers as long as the light bandwidth and the acceptance cone of the mirrors can be made sufficiently small. If this hope is not fulfilled, it may prove necessary, for observations of faint stars, to develop suitable circuits to paralyze the receivers in the interferometer whenever a Čerenkov light pulse appears.

8. DISCUSSION

8.1. *Technique*

It follows from the detailed analysis of the sensitivity of the intensity interferometer, which is given in §4, that very large mirrors would be required if the instrument is to be of astronomical value; for example, mirrors 4.6 m in diameter would be needed to observe stars of apparent photographic magnitude +2.5 and their diameter must be doubled to observe stars of +4. However, although such mirrors are extremely large by any standard they are not required to form an image of the star but only to direct the light on to the cathodes of the phototubes. Indeed, there is no fundamental reason why a single main mirror should not be split up into a bank of smaller mirrors, each with its own phototube, as long as the time delays in the different channels were properly equalized. The optical quality of the mirrors is determined principally by the need to maintain a high ratio between the light received from the star and the background light from the night sky. It is important that this ratio should be large for two reasons; first, because the effect of background light is to increase the fluctuations in the outputs of the phototubes and hence reduce the signal-to-noise ratio, and secondly, because the cosmic ray component in the night sky may produce spurious correlation. Thus, if the mirror is to be used to observe a star of magnitude +5 and the tolerable increase in noise due to background light is about 10%, then the mirrors must not accept light outside a cone of half angle approximately equal to 6 min of arc. If the spurious correlation introduced by Čerenkov radiation is also to be negligible in measurements on a star of magnitude +5, it is possible that more stringent tolerances must be imposed upon the design of the mirrors; but in any case their optical accuracy, which is comparable with that of searchlight reflectors, need not approach that of conventional telescopes.

At the present time there is not sufficient practical experience in the construction of very large but crude optical mirrors on which to base reliable estimates of the maximum feasible size. It is fairly certain that an instrument of reasonable cost

could be built to work on stars with apparent magnitudes less than +2.5, and it seems that it might be possible eventually to reach stars of magnitude +5 to +6, that is to say stars which can be seen with the naked eye. However, the difficulties of reaching even fainter stars are very great since, not only must the diameters of the mirrors be increased to give adequate sensitivity, but their optical quality must be improved at the same time.

It is interesting to estimate the accuracy with which an intensity interferometer would measure stellar diameters. In general this accuracy would probably be limited by the effect of fluctuations or, on other words, by the signal-to-noise ratio. For example, if the signal-to-noise ratio for a given star is 3 to 1 in 1 h when the star is unresolved, then simple considerations suggest that it should be possible to measure the angular diameter with a probable error of $\pm 10\%$ in about 8 h of observation; with ten times this sensitivity the error would be decreased to $\pm 1\%$, and it should be possible to achieve this accuracy with mirrors of a few metres in diameter on a few of the brightest stars. However, it seems unlikely that the accuracy could be increased substantially beyond 1%, since further improvement would probably be limited by a number of small systematic errors.

Another interesting question is what maximum resolving power would be possible. It seems likely that the limits to the maximum length of baseline would be set by the practical difficulties of ensuring that the fluctuations received in the two channels are not significantly displaced in time with respect to each other at the correlator. If the bandwidth of the amplifiers is about 10^8 c/s, then the maximum displacement which can be tolerated without serious loss of correlation is about 10^{-9} s which corresponds to a free-space path difference of about 30 cm. At very long baselines two obvious difficulties arise in maintaining this small path difference. First, the changing direction of the star introduced a path difference which varies with time, and this must be compensated either electrically or by moving the mirrors; secondly, the relative electrical lengths of the cables connecting the two mirrors to the correlator must remain sufficiently stable. Without further practical experience it is difficult to assess the limits set by these two requirements; nevertheless, experience with radio interferometers suggests that the baseline might perhaps be extended to distances of about 1 or 2 km, and under those conditions the interferometer would resolve a star with an angular diameter of about 4×10^{-5} s of arc.

8.2. *Measurements of double stars*

One possible use of an interferometer with great resolving power is to detect double stars which lie in the range between spectroscopic and visual binaries. Such stars might have an angular diameter too small to permit visual observation, say less than 0.1 sec of arc, but might not be detected spectroscopically, either because the separation of the components is too large or because the inclination of the orbit is too small.

Valuable information might also be obtained with an interferometer from observations on bright spectroscopic binaries. With an interferometer using two mutually perpendicular baselines it is possible, in principle, to determine the angular dimensions of the binary orbit projected on a plane perpendicular to the

line of sight: the spectroscopic data give the apparent orbit projected on a plane through the line of sight in absolute units. By combining those two sets of data one might find all the kinematical parameters of the system, together with the distance, with an accuracy which is independent of the degree of light absorption in interstellar space or of the absolute value of the trigonometrical parallax.

8.3. *Measurements on single stars*

We have shown in §5 that, assuming reasonable parameters for the electronic equipment, a two-mirror intensity interferometer should be able to measure the angular size of single stars provided that their brightness temperature exceeds about 4000 °K. By means of a single mirror with a split beam it should be possible to lower this minimum temperature to about 3000 °K. This latter technique would be very limited in application and its practical value is doubtful; nevertheless, it is interesting to note that it would extend the range of the intensity interferometer to embrace all but two of the stars measured by Pease with a Michelson interferometer, thereby permitting a direct comparison of the results obtained with the two different types of instrument.

A disadvantage of the intensity interferometer is that its use would be confined to bright stars. Nevertheless, the calculations presented in figure 5 show that, taking representative values for the performance of modern phototubes, a considerable number of stars should be within reach of an instrument of reasonable size. For example, mirrors of 6 m diameter would permit observations of stars of $m_{pg} + 3.0$ and, including multiple systems and stars of all temperatures, there are at least 100 stars brighter than this limit.

It should be possible, by measuring their angular size, to establish the brightness temperature of a large number of these stars. This information would be especially valuable in the case of the *O* and *B* stars and the supergiants of spectral type earlier than *F*, whose position on the temperature scale is uncertain. Furthermore, for those stars whose parallax is known, it would be possible to find absolute dimensions.

We have already shown that a direct measurement of limb-darkening would only be possible on a limited number of very bright stars with a temperature exceeding 6000 °K. There is, however, the possibility that indirect evidence of limb-darkening might be obtained on a greater range of stars by comparing their apparent angular size at different wavelengths.

There are, of course, a number of particularly interesting objects which could be studied with an interferometer of high resolving power and sufficient size. For example, there are a few classical Cepheids brighter than $m_{pg} + 5$. On present astrophysical theory the light variation of these stars is connected with a radial pulsation. It might be possible to measure the variation in angular size of some of these stars directly and use these data, in conjunction with spectroscopic observations, to establish their parallax and absolute magnitude.

Another class of interesting objects is that of the emission line stars of which outstanding examples are the Wolf-Rayet stars. The sensitivity of an intensity interferometer in which the light from the star is passed through a narrow band-filter depends upon the peak intensity and spectral distribution of the filtered light,

but it is independent of the actual width of the pass band. Hence, if the filter can be centred on an emission line in which the intensity per eyelet bandwidth is E times that of the neighbouring continuum, then the sensitivity can also be increased by a factor E if the insertion loss of the filter can be held sufficiently low, and if its spectral pass band can be matched to or made narrower than that of the emission line. A considerable fraction of the ideal increase in sensitivity should be possible in the case of the Wolf-Rayet stars in which the helium emission lines are from 20 to 60 Å wide, and since the peak intensity in these lines may be anything from 3 to 100 times that in the neighbouring continuum the potential gain in sensitivity is very large. The emission lines are believed to be produced not at the surface of the star but in a surrounding envelope, and it is the angular size of this envelope that would be measured if the light reaching the phototubes came only from the emission lines. To measure the angular diameter of the star itself it would be necessary to exclude light frequencies in the emission bands.

8.4. *Comparison with other techniques*

The angular diameters of stars have been derived from observations of eclipsing binaries and also from lunar occultations. By comparison with either of these methods the technique of measurement with an interferometer is clearly more flexible, particularly in respect of the choice of stars. For example, the majority of the results obtained from eclipsing binaries are complicated by the fact that a large number of these systems exhibit mutual tides and other distortions, whereas an interferometer can be used to study either multiple stars or isolated stars. The method of observing lunar occultations can be applied to single stars, but is clearly extremely restricted in the choice of stars and also in the periods at which any given star can be observed.

A comparison of the intensity interferometer with Michelson's stellar interferometer suggests that the former has two outstanding advantages. First, it should be capable of achieving a far higher resolving power and of reaching the performance necessary to resolve the hottest stars; secondly, it should be comparatively immune to the disturbing effects of atmospheric scintillation.

9. CONCLUSIONS

The analysis presented in this paper suggests that an interferometer based on correlating the fluctuations in the intensity of the light received from a star at separated points on the earth's surface might profitably be applied to astronomy. This conclusion contradicts the tentative suggestion made by us in an earlier paper (Hanbury Brown & Twiss 1954) that an intensity interferometer could be applied in radio but not in optical astronomy. However, at that time we had not appreciated the fact that the large mirrors required by an intensity stellar interferometer need not form an image of the star and could therefore be relatively crude in construction.

The use of an intensity interferometer is limited by its inherent lack of sensitivity, rather than by any lack of resolving power, so it should be possible to apply it to any star, however hot, of adequate apparent brightness. With practical sizes of mirrors the intensity interferometer would probably be restricted to the stars visible to the naked eye and then only to those of spectral type earlier than about $M5$.

Since the intensity interferometer should not be affected by atmospheric scintillation its use would not be limited to nights of good 'seeing'. To a limited extent this last conclusion is supported by measurements of the angular size of Sirius (α Can. Maj. A) which are described in part IV of this series of papers.

APPENDIX I. THE EFFECTS OF THE COSMIC RAY CONTRIBUTION TO THE NIGHT SKY

Let us suppose that the light incident upon the phototubes at the foci of the mirrors of the intensity interferometer be passed through a filter with a bandwidth B so narrow that the spectrum of the filtered light does not depend upon the spectral response of the star or of the light radiated from the cosmic-ray shower.

Let $p(n_c)dn_c dt d\Omega$ be the probability that a cosmic ray event occurs in time dt such that n_c photons reach unit area of the mirror in unit frequency bandwidth from solid angle $d\Omega$ of the sky, and let us make the unfavourable assumption that any such event at one mirror is automatically accompanied by an identical and simultaneous event at the other.

Let us assume that the light quanta arrive in a time interval τ_c such that $\tau_c b_v \gg 1$, where b_v , the bandwidth of the electronic equipment, is approximately rectangular in shape, and that the response of the electronic equipment to a burst of N photoelectrons, emitted in time τ_c , is linear for $N < N_{\max.}$ and independent of N for $N > N_{\max.}$ Under these conditions it can be shown that the contribution C_c to the time-averaged value of the correlation from the totality of such events is given by

$$C_c = \Omega_0 \left[\int_0^{n_{c \max.}} \left(\frac{\alpha \gamma B \pi D^2}{4} \right)^2 p(n_c) dn_c + \int_{n_{c \max.}}^{\infty} N_{\max.}^2 p(n_c) dn_c \right] e^2 | F_{\max.}^2 | \tau_c^{-1}, \quad (\text{A } 1)$$

where Ω_0 is the solid angle of the field of view, $N = \pi D^2 \alpha \gamma B n_c / 4$ is the number of primary photoelectrons produced by a burst of $B n_c$ photons incident on unit area and where the other symbols have been defined in the text.

It is known from the results of Jelley & Galbraith (1955) that

$$p(n_c) = K_0 n_c^{-2.6} \cos^l \zeta, \quad (\text{A } 2)$$

where 1 is a number between 2 and 3 and ζ is the angle between the zenith and the axis of the mirror, and from the parameters of their equipment it can be shown with reasonable assumptions as to the spectral response of their phototube that

$$K_0 \simeq 10^{-16}.$$

Accordingly, we have that

$$C_c \simeq 3 \Omega_0 e^2 | F_{\max.}^2 | 10^{-16} \left(\frac{\pi D^2 \alpha \gamma B}{4} \right)^{1.6} N_{\max.}^{0.4} \tau_c^{-1} \propto_{C \text{ vs } S} \xi \quad (\text{A } 3)$$

Now from equations (4.1) and (4.7) in the text combined with equation (3.34) in part I it can be shown that C_s , the correlation expected from an unresolved star of photovisual magnitude m_{pv} at a wavelength centred on 5400 \AA , is given by

$$C_s \simeq 86.5 \times 10^{-10} \left(\frac{\pi D^2 \alpha \gamma}{4} \right)^2 B \sigma 10^{-0.8 m_{pv}} e^2 b_v | F_{\max.}^2 | \rho_0^2 \sec^2 \xi. \quad (\text{A } 4)$$

If the light pulse from the cosmic-ray shower be limited at the level where its peak value is approximately 10 times greater than the r.m.s. noise due to the light from the star, it can be shown that

$$N_{\max.} \simeq 1.36\tau_c 10^{(-2-0.2m_{pv})} \left[b_v \frac{\pi D^2 \alpha \gamma}{4} \rho_0^{\sec \zeta} B \right]^{\frac{1}{2}}, \quad (\text{A } 5)$$

and in the case $b_v = \tau_c^{-1} = 10^{-8}$ we have that

$$\delta C_{\max.} \simeq 0.18\Omega_0 B^{0.8} 10^{(-9-0.72m_{pv})} \left[\left(\frac{\pi D^2 \alpha \gamma}{4} \right)^{-0.2} \sigma^{-1} \rho_0^{-1.8 \sec \zeta} \cos^l \zeta \right]. \quad (\text{A } 6)$$

This result, which is quoted in the text, is likely to be an overestimate of the contribution from the cosmic ray component especially in observations on the fainter stars when the mirror separation will normally be relatively large. For example, it is not certain that the power-spectrum law given by (A 2) will still be valid for values of n_c much smaller than those at which it was confirmed by Jelley & Galbraith; but a more important point is that it does not necessarily follow that, if a light pulse is picked up by one mirror, then a similar pulse will simultaneously be picked up by the other. For example, in the case when the mirror separation is 200 ft. and the half angle of the mirror acceptance cone is 6 min of arc, the two acceptance cones only intersect at heights more than 10 miles above the surface of the earth. Furthermore, it is now known (Brennan 1957) that some of the light pulses picked up by mirrors directed at the zenith come from cosmic-ray showers entering the earth's atmosphere at appreciable zenith angles; in this case, if light pulses are picked up by both mirrors, one will be delayed behind the other by many times the resolving time of the electronic equipment described in the text and the two pulses will therefore be effectively decorrelated.

We thank Dr S. C. B. Gascoigne for helpful criticism of this paper and Dr J. G. Davies for his assistance in computing the results given in figures 2 and 3.

REFERENCES

- Blackett, P. M. S. 1948 *Gassiot Committee Report*, p. 34. Phys. Soc. Lond.
 Bramley, E. N. 1955 *Proc. Instn Elec. Engrs*, B, **102**, 533.
 Brennan, M. H. 1957 Ph.D. Thesis, University of Sydney.
 Fejer, J. A. 1953 *Proc. Roy. Soc. A*, **220**, 455.
 Fizeau, H. I. 1868 *C.R. Acad. Sci., Paris*, **66**, 934.
 Galbraith, W. & Jelley, J. V. 1955 *J. Atmos. Terr. Phys.* **6**, 250.
 Hanbury Brown, R. & Twiss, R. Q. 1954 *Phil. Mag.* **45**, 663.
 Hanbury Brown, R. & Twiss, R. Q. 1957*a* *Proc. Roy. Soc. A*, **242**, 300 (part I).
 Hanbury Brown, R. & Twiss, R. Q. 1957*b* *Proc. Roy. Soc. A*, **243**, 291 (part II).
 Jelley, J. V. & Galbraith, W. 1955 *J. Atmos. Terr. Phys.* **6**, 304.
 Michelson, A. A. & Pease, F. G. 1921 *Astrophys. J.* **53**, 249.
 Mikesell, A. H., Hoag, A. A. & Hall, J. S. 1951 *J. Opt. Soc. Amer.* **41**, 689.
 Sommer, A. H. 1956 *Inst. Rad. Engrs Trans. Nuclear Sci.* Scintillation Counter Symposium.
 Woolley, R. v. d. R. & Stibbs, D. W. N. 1953 *Outer layers of a star*. Oxford University Press.

Interferometry of the intensity fluctuations in light IV. A test of an intensity interferometer on Sirius A

BY R. HANBURY BROWN

Jodrell Bank Experimental Station, University of Manchester

AND R. Q. TWISS

Division of Radiophysics, C.S.I.R.O., Sydney, Australia

(Communicated by A. C. B. Lovell, F.R.S.—Received 10 April 1958)

An experimental intensity interferometer has been constructed with two searchlight mirrors and tested on Sirius.

The correlation observed with the two mirrors close together was found to be in good agreement with that expected theoretically. This result supports the prediction, made in part III of the present series, that the performance of an intensity interferometer should not be significantly affected by atmospheric scintillation.

Observations of Sirius were carried out with four different baselines and the decrease of correlation with increasing baseline length was found to be consistent with theory. The observed results have been used to derive an experimental value for the angular diameter of Sirius which is in good agreement with the value given by astrophysical theory.

The results of this preliminary experiment confirm, to a considerable extent, the general conclusions reached in part III.

I. INTRODUCTION

In part III of this series of papers (Hanbury Brown & Twiss 1958) we gave a theoretical discussion of a stellar interferometer based on the principle of correlating the fluctuations in the outputs of two photoelectric detectors illuminated by partially coherent beams of light. We showed that it should be possible to make an instrument with a far higher resolving power than has been attained previously, and we argued that its operation would not be significantly disturbed by atmospheric scintillation.

In the present part of the paper we shall describe a preliminary experiment which was designed to test these predictions. In the first part of this experiment we were concerned to test the effect of atmospheric scintillations. Accordingly, two photoelectric detectors, with their associated mirrors, were mounted as close together as possible and were directed at the bright star Sirius (α Can. Maj. *A*). The correlation between the fluctuations in the two outputs was then measured under conditions of severe atmospheric scintillation, and was compared with the theoretical value derived on the assumption that the effects of scintillation could be ignored. In the second part of the experiment, the correlation was measured as a function of the separation between the two detectors and the results were used to derive an experimental value for the angular diameter of Sirius. This result was then compared with the value predicted by astrophysical theory.

2. DESCRIPTION OF THE APPARATUS

A simplified diagram of the apparatus is shown in figure 1. The optical system consisted of two mirrors A_1 , A_2 which focused light on to the cathodes of the photomultipliers P_1 , P_2 . The two mirrors were the reflectors of standard Army search-

lights, they consisted of back-silvered paraboloids of borosilicate glass 156 cm in diameter and 65 cm in focal length; tests showed them to be capable of focusing light from a star into an area about 8 mm in diameter. The mirrors were supported in their standard searchlight barrels on alt-azimuth mounts. For the purpose of these experiments the front glass of each searchlight was removed and the barrel itself was extended with aluminium sheet to a total length of about 6 ft. in order to exclude extraneous light and to minimize the formation of dew on the mirrors. Experience showed that on cold nights there was considerable condensation and even ice on the mirrors; to prevent this and to keep the photomultipliers dry, a 1 kW electric heater was maintained permanently in operation in each barrel.

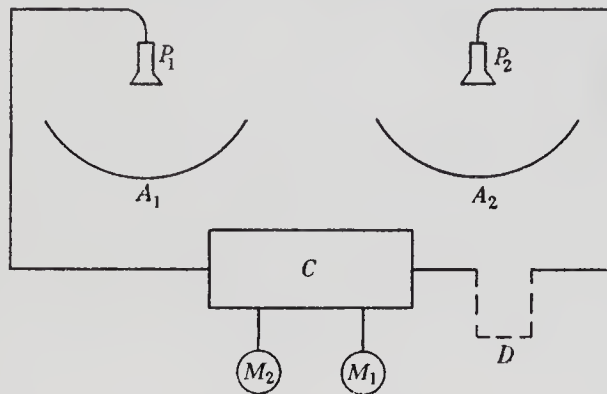


FIGURE 1. Simplified diagram of the interferometer. A description of the correlator was given in part II of this series of papers. *A*, mirrors; *C*, correlator; *D*, adjustable cable delay; *M*₁, signal motor; *M*₂, noise motor; *P*, phototubes.

The azimuth and elevation of the searchlights were controlled manually from a standard Army control pillar carrying a small optical sight; but, in order to reduce the work of guiding on a star, an electric motor was provided to rotate the pillar at approximately the correct rate in azimuth.

A photomultiplier was mounted in a box at the focus of each mirror on an adjustable carriage, the boxes being very thoroughly screened to prevent the reception of radio interference. The photocathodes were exposed through circular apertures 2.5 cm in diameter, and when observations were not in progress, they were covered by detachable caps carrying small lamps. The photomultipliers were of R.C.A. type 6342 with flat semi-transparent cathodes and ten stages of multiplication. The cathodes had a spectral response with a maximum sensitivity at about 4000 Å; tests at the National Physical Laboratory showed that their quantum efficiencies were 16.9 and 14.6 %, respectively, at 4000 Å and that their spectral response curves were substantially identical in shape. The anodes of the photomultipliers were connected by about 100 ft. of high-frequency coaxial cable to an electronic correlator in the laboratory. Provision was made to monitor the anode currents of the photomultipliers both in the laboratory and at the searchlight control pillar.

In the laboratory the two cables were brought to a panel where their delay could be equalized with an accuracy better than 0.002 μs by means of a set of cables which could be inserted rapidly into either channel; thus throughout the observations it

was possible to compensate for the difference in the times of arrival of the light from the star at the two mirrors.

After the delays had been equalized the cables from the photomultipliers were terminated in matched loads, and connected to the input channels of a correlator which measured the correlation between the fluctuations in the voltages across the loads. The correlator has been described in part II (Hanbury Brown & Twiss 1957) so only a brief description of it will be given here. The fluctuations were amplified in the band 5 to 45 Mc/s and, by means of a system of phase-reversing switches, amplifiers and synchronous rectifiers, the two signals were multiplied together and their product was found. The average value of this product, which is a direct measure of the correlation between the intensity fluctuations of the light incident upon the two photocathodes, was recorded on the revolution counter of the 'signal' integrating motor M_1 (figure 1). The root-mean-square amplitude of the fluctuations in the output of the correlator was recorded by the 'noise' integrating motor M_2 . Since the readings of both counters depend in the same way upon the gain of the equipment, it was possible to eliminate the effects of changes in amplification by expressing all results as a signal to noise ratio, that is to say as the ratio of the time-averaged value of the correlation to the r.m.s. uncertainty in the final value. This is the same procedure as that which was used in the laboratory experiment described in part II and, as shown below, the theoretical analysis given there can readily be adapted to cover the case of the present observations.

3. EXPERIMENTAL PROCEDURE

A series of observations was made at Jodrell Bank with the two searchlights separated by different distances. In each case the searchlights were manoeuvred into the required positions on the ground with an accuracy in plan of about ± 3 in. They were then supported on adjustable jacks and levelled, the centres of the two mirrors being brought into the same horizontal plane by observing them with a theodolite.

The searchlights were guided on Sirius, and every 5 min readings were taken of the revolution counters of the two integrating motors M_1 and M_2 (figure 1), and of the anode currents of the two photomultipliers. The gain of the amplifiers in the correlator was controlled manually so that its r.m.s. output, as recorded by the motor M_2 remained roughly constant. Measurements were also made at convenient intervals throughout each run of the relative contributions to the total photomultiplier currents of the light from the night sky and of the light from Sirius alone.

Before and after every run the correlator was checked for sensitivity and drift. The sensitivity was found by applying a known voltage from a signal generator to the two inputs in parallel and noting the output. The absence of drift was checked by illuminating the two photomultipliers by small lamps, mounted in detachable caps over the photocathodes, and noting the output of the correlator over a period of 2 or 3 h. Since, in this latter test, the light on the two photocathodes was completely uncorrelated, any significant deviation of the output from zero would have established the existence of a long period drift. No evidence of such a drift was obtained throughout the whole series of observations.

In addition to these checks the gains of the two photomultipliers were measured on every occasion by observing the r.m.s. value of the fluctuations in their anode currents when they were illuminated by the two small lamps; this procedure has already been analyzed in part II.

4. RESULTS

Observations of Sirius were made on all possible occasions between November 1955 and March 1956. Approximately half of the nights in this period were excluded since the background light from the moon would then have been excessive. The observing time was further restricted by the low elevation of Sirius which reaches a maximum value of about 20° at the latitude of Jodrell Bank. It was therefore necessary, in order to avoid the excessive atmospheric extinction at low angles, to limit the observations to within 2 h of transit; even so, experience showed that at 20° elevation the extinction was very variable, being often prohibitively great when the sky appeared reasonably clear in the zenith. If the extinction as calculated from the measured currents and gains of the photomultiplier tubes exceeded the value for a normal clear sky by more than about 0.75 magnitudes the observations were rejected. Furthermore, in order to minimize the effects of the short-period drifts in the correlator, the existence of which was noted in part II, no observations were accepted unless they formed part of a continuous series extending over a period of at least 30 min.

The total observing time during which the conditions given above were satisfied, proved to be 18 h over the period of 5 months. In addition about 6 h were lost owing to failure of the searchlight controls.

4.1. *Observations with a short baseline*

The first set of observations was designed to check the magnitude of the correlation with the shortest practical baseline, when the comparison with theory would be as independent as possible of the actual angular diameter of Sirius. The construction of the searchlights made it impossible to place the two mirrors in contact on an east-west baseline, accordingly they were positioned on a north-south baseline 6.1 m apart. In this way the length of the effective baseline, defined as the projection of the line joining the two mirrors in a plane normal to the light from the star, varied from 2.10 m at transit to 3.35 m at 2 h from transit, the average baseline length in the 4 h period being 2.56 m. The differential time delay introduced by the north-south separation was compensated by a fixed length of cable in the channel of the south mirror, the variation in time delay, over a period within 2 h of transit, being quite negligible ($< 2 \times 10^{-3} \mu\text{s}$).

Observations were carried out during November and December 1955 with the searchlights in this position and a total of 345 min of satisfactory observing time was obtained; an approximately equal time was lost due to failure of the searchlight controls.

As an example of the results all the readings taken on the night of 12/13 December 1955 are shown in figure 2. The first curve shows the readings ΣC_r on the revolution

counter of the signal motor M_1 ; a marked positive correlation was recorded throughout this run. The second curve shows the number of revolutions N_r of the noise motor M_2 in each period of 5 min; this curve shows that the output noise level of the correlator varied considerably throughout the run. The third curve gives the geometric mean $(I_{1r}I_{2r})^{1/2}$ of the anode currents in microamperes of the two photomultipliers. The increase in current during the first 90 min of the run corresponds to an increase in the elevation of the star as it approached transit. The only other observed quantities are the gains of the two photomultipliers G_1, G_2 which on this occasion were 0.71×10^5 and 0.97×10^5 , respectively.

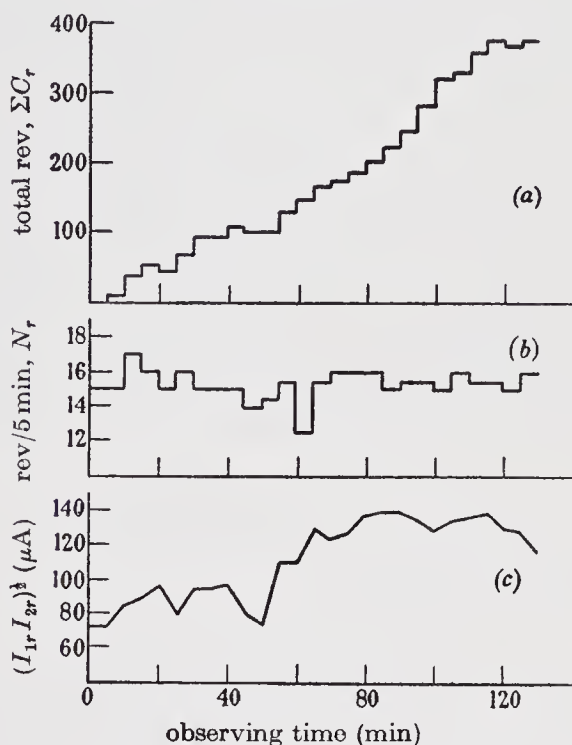


FIGURE 2. Observations of Sirius recorded on the night of 12/13 December 1955. (a) The total number of revolutions of the signal motor M_1 (ΣC_r). (b) The speed of the noise motor M_2 in revolutions per 5 min (N_r). (c) The geometric mean of the two phototube anode currents $(I_{1r}I_{2r})^{1/2}$.

The calculation of the final signal-to-noise ratio was complicated by the fact that the gain of the electronic equipment was frequently varied in order to maintain the noise output of the correlator roughly constant and independent of the light flux incident on the photocathode. However, a similar complication was encountered in the laboratory experiment described in part II and, following the procedure given there, the overall 'signal-to-noise' ratio for the set of observations was written

$$\frac{S}{N}(T_0) = \frac{\sum_{r=1}^M \left[\frac{I_{1r}I_{2r}\bar{N}}{\bar{I}_1\bar{I}_2N_r} C_r \right]}{N_0 \left[\sum_{r=1}^M \left(\frac{I_{1r}I_{2r}}{\bar{I}_1\bar{I}_2} \right)^2 T_r \right]^{1/2}}, \quad (4.1)$$

where T_r is the duration of the r th time interval and was taken to be 300 s; C_r is the change in the reading of the correlation motor M_1 in the r th time interval;

N_r is the change in the reading of the noise motor M_2 in the r th time interval; I_{1r}, I_{2r} , are the anode currents of the photomultipliers averaged over the r th interval and \bar{I}_1, \bar{I}_2 are these anode currents averaged over the entire period of observation; N_0 is the standard deviation of the reading of the signal motor M_1 at the end of a 5 min period during which the noise motor M_2 turns at the rate of \bar{N} revolutions in 5 min.

To evaluate $(S/N)(T_0)$, as defined by equation (4.1), it was also necessary to determine the ratio N_0/\bar{N} . In part II we described a method of measuring this ratio by feeding both channels of the correlator from a common source of broad-band noise; unfortunately, this technique was not developed at the time of the present experiment, and the value of N_0/\bar{N} was established by the relatively laborious method of analyzing the first-order differences in the readings of the signal motor. A preliminary analysis of these differences showed that their distribution was not rigorously normal, there being an excess of large deviations. In order to minimize the effect of these large deviations the first-order differences D_r^{r+1} were calculated from the formula

$$D_r^{r+1} = \frac{\bar{N}C_{r+1}}{N_{r+1}} - \frac{\bar{N}C_r}{N_r} \quad (4.2)$$

and the median value D_0 of these differences was found. The value of N_0/\bar{N} was then calculated from the relation

$$\frac{N_0}{\bar{N}} = \frac{1}{\sqrt{2}} (1.483 D_0) \quad (4.3)$$

which is rigorously valid only when the differences are distributed normally. An analysis of all the available data, including the dummy runs with lamps illuminating the phototubes, gave the value

$$\frac{N_0}{\bar{N}} = 0.867 \pm 0.43 \text{ (p.e.)}, \quad (4.4)$$

where the probable error has been estimated on the assumption that the differences were normally distributed. A subsequent comparison of this method of finding N_0/\bar{N} with the superior method described in part II showed that the results obtained were in satisfactory agreement.

The final signal-to-noise ratio was calculated by substituting all the observed readings in equation (4.1), using the value of N_0/\bar{N} given in equation (4.4). For a baseline of average length 2.56 m and a total time of 345 min the total observed correlation, expressed as an r.m.s. signal-to-noise ratio, was +8.50. This result is shown in the first column of table 1.

4.2. *Observations with extended baselines*

Throughout January 1956 attempts were made to increase the number of observations with the searchlights in their initial positions, but no results were obtained because of cloud, and it was decided to use the remaining time to measure the correlation with longer baselines and thus to find an experimental value for the angular diameter of Sirius. Accordingly, the searchlights were placed on an east-

west line at spacings of 5.54, 7.27 and 9.20 m and a total observing time of $12\frac{1}{4}$ h was obtained during the months of February and March. Observations were not practical after the end of March because Sirius was then in transit during daylight.

The results were analyzed by the method described above and the values of the correlation measured at each mirror spacing are given in table 1 as signal-to-noise ratios. From these results it may be seen that the correlation decreased as the mirror separation increased, and that at an east-west separation of 9.20 m the observed value was comparable with the probable uncertainty in the measurement.

TABLE 1. COMPARISON BETWEEN THEORETICAL AND EXPERIMENTAL CORRELATION

mirror separation (m)	6.1	5.54	7.27	9.20
	(north-south)	(east-west)	(east-west)	(east-west)
average length of baseline projected normal to direction of star d (m)	2.56	5.35	6.98	8.93
observed ratio of integrated correlation to r.m.s. deviation of correlator output (r.m.s. signal-to-noise ratio) with associated probable error	$+8.50 \pm 0.67$	$+3.59 \pm 0.67$	$+2.65 \pm 0.67$	$+0.83 \pm 0.67$
theoretical ratio of integrated correlation to r.m.s. deviation of correlator output (r.m.s. signal-to-noise ratio)	+9.58	+3.60	+2.69	+1.59

To confirm that the observed correlation was not significantly affected by light pulses from cosmic ray showers or by any other coherent source of light in the night sky, the two searchlights were placed as close together as possible with an east-west separation of 4.6 m. In this position they were exposed to the night sky alone, at an elevation of 25° , and the equipment was operated at the normal gain used for observations of Sirius. No significant correlation was recorded over a period of 3 h.

5. THEORETICAL ANALYSIS

5.1. *The theoretical value of the correlation with a short baseline*

In equation (4.1) of part III we gave a formula for the signal-to-noise ratio $(S/N)(T_0)$, where S is the correlation between the fluctuations in the outputs of two photoelectric detectors averaged over an observation of duration T_0 and N is the r.m.s. associated uncertainty. This expression was derived on the assumption that the light reaching the detectors passed through a narrow-band filter and could be treated as effectively monochromatic. Although it is clearly desirable that the bandwidth of the light should be restricted in this way, it was not practicable in the present preliminary tests to use a narrow-band filter and the overall spectral response was determined by the combined spectra of the star, the atmospheric transmission, the reflectivity of the mirrors and the quantum efficiencies of the photoelectric detectors. In consequence the overall response had a bandwidth of the

order of 1000 Å, and to allow for this it is necessary to make certain modifications to the formula given in part III.

The effect of using a wide spectrum is to complicate the analysis very considerably. For example, if we consider first the simple case when the star is not appreciably resolved, the correlation observed with a given light flux is proportional to the spectral density of the overall spectral response, and this must be calculated as a function of the zenith angle to take account of changes in the spectral characteristics of the atmospheric transmission.

In the case when the star is appreciably resolved the analysis is even more complicated, since it must also take account of the variation of the coherence of the light at the two detectors with frequency. Thus if the two mirrors have a diameter D and are separated by a distance d , we showed in part II that the correlation is decreased by a factor $\bar{\Delta}\bar{\Gamma}^2(d)$, where the partial coherence factor $\bar{\Delta}$ is the ratio of the correlation expected with zero baseline to that which would be observed if the star were a true point source, the normalized correlation factor $\bar{\Gamma}^2(d)$ is the ratio of the correlation expected with a baseline d to that which would be observed at zero baseline with an identical light flux, and the bar over these factors denotes averaging over the light spectrum. It is shown below that when Sirius is observed with 156 cm mirrors the value of the partial coherence factor is so close to unity that no significant error is introduced by taking $\bar{\Delta} = \Delta(\nu_0)$, where ν_0 is the frequency at which the overall spectral response, under typical conditions of the atmospheric transmission, is a maximum. However, a similar approximation cannot be made in the case of the normalized correlation factor $\bar{\Gamma}^2(d)$, and to calculate this factor it is necessary to take into account the shape of the overall spectral response at each zenith angle as shown in equation (5.1) below.

A simple extension of the analysis in part III shows that, for the purposes of the present experiment, the effect of the wide spectral band of the light can be taken into account if equation (4.1) of part III is rewritten

$$\frac{S}{N}(T_0) = \frac{\pi D^2}{4} \alpha(\nu_0) n_0(\nu_0) \frac{\mu - 1}{\mu} \frac{\gamma(\nu_0) \epsilon}{1 + \delta} \left(\frac{b_v}{2\eta}\right)^{\frac{1}{2}} \Delta(\nu_0) \times \sum_{r=1}^M \sigma_r(\zeta_r) \rho_r^{2 \sec \zeta_r}(\nu_0) T_r \bar{\Gamma}_r^2(d) \left/ \left[\sum_{r=1}^M (1 + a_r^2) \rho_r^{2 \sec \zeta_r}(\nu_0) T_r \right]^{\frac{1}{2}} \right., \quad (5.1)$$

where $(S/N)(T_0)$ is the ratio of the correlation averaged over the interval T_0 to the associated r.m.s. uncertainty; D is the diameter of the two identical mirrors; $\alpha(\nu)$ is the geometric mean of the quantum efficiencies of the two photocathodes at a frequency ν ; $n_0(\nu)$ is the number of quanta per unit bandwidth from the star incident normally on unit area at the top of the atmosphere; $\mu/(\mu - 1)$ is the excess noise introduced by the photomultipliers; $\gamma(\nu)$ is the reflexion efficiency of the two mirrors; $1 + \delta$ is the excess noise introduced by the correlator; ϵ is the loss of correlation in the correlator; b_v is the cross-correlation bandwidth of the amplifiers and η is the spectral density function of their response as defined in equation (4.3) of part III; $\sigma_r(\zeta_r)$ is the spectral density function of the overall response of the apparatus to light from the star at a zenith angle ζ , and is defined by equation (4.4) of part III, and ζ_r is the zenith angle in the r th interval of observation; $\rho_r(\nu)$ is the atmospheric

transmission in the zenith at a frequency ν ; T_r is the duration of the r th interval, which is taken to be so short that ζ_r does not vary appreciably; M is the number of intervals into which the total observing period T_0 is divided; $1 + a_r$ is the ratio of the light from the star plus background to the light from the star alone; $\Delta(\nu_0)$ is the partial coherence factor for a frequency ν_0 and mirror size D ; $\overline{\Gamma_r^2(d)}$ is the normalized correlation factor for a baseline d and is calculated for the spectral distribution of light appropriate to the r th interval by the formula

$$\overline{\Gamma_r^2(d)} = \frac{\int_0^\infty \alpha^2(\nu) n_0^2(\nu) \rho_r^{2\text{sec}} \zeta_r(\nu) \gamma^2(\nu) \Gamma^2(\nu, d) d\nu}{\int_0^\infty \alpha^2(\nu) n_0^2(\nu) \rho_r^{2\text{sec}} \zeta_r(\nu) \gamma^2(\nu) d\nu} \quad (5.2)$$

5.2. *The theoretical variation of correlation with baseline length*

In order to predict the variation of correlation with the length of the baseline it is first necessary to make an independent estimate of the angular diameter of Sirius. The most accurate procedure would be to construct a model atmosphere to fit the observational spectroscopic data and hence derive the monochromatic flux, but the accuracy of the present experiment is too low to justify an elaborate theoretical comparison, and instead we have followed the classical analysis in which one compares the apparent bolometric magnitude and effective black-body temperature of Sirius with those of the sun. Thus from Stefan's law one has immediately that

$$\log_{10} \theta_S = \log_{10} \theta_\odot - 2(\log_{10} \Theta_S - \log_{10} \Theta_\odot) + 0.2(m_{\text{bol},\odot} - m_{\text{bol},S}), \quad (5.3)$$

where θ , Θ and m_{bol} denote the angular diameter, effective black-body temperature and bolometric magnitude, respectively.

The value of θ_\odot at the mean sun-earth distance is known with considerable accuracy and we have adopted the value given by Auwers (1891) of 1919.3 sec. The temperature Θ_\odot of the sun refers to the uniform black-body temperature to which the disk of the sun would have to be raised to produce the energy flux received at the earth. We have adopted the value given by Unsöld (1955) and Allen (1955) of 5785 °K. The effective temperature of Sirius is much less certain since so much of the energy radiated by an A1 star lies at wavelengths which are cut off by the earth's atmosphere, but we have assumed a value of 10 300 °K on the basis of the spectral classification A1 v and the corresponding temperature scale given by Morgan, Keenan & Kellmann (1943). The bolometric magnitudes have been computed from the bolometric corrections given by Kuiper (1938), which are also rather uncertain for A1 stars, and from the apparent magnitudes.

There is a considerable variation in the published values for the apparent magnitude of both Sirius and the sun, but recent advances in photoelectric photometry have reduced the likelihood of significant systematic errors in the measurements. Accordingly, instead of using a weighted mean of all the available data we have adopted the values obtained in the most recent photoelectric measurements which correspond on the international photovisual scale to an apparent magnitude of -1.47 ± 0.015 (Johnson & Knuckles 1957) for Sirius and an apparent magnitude of -26.73 ± 0.03 (Stebbins & Kron 1957) for the sun. The bolometric correction for

the sun has been taken as 0.09 from the data given by Allen (1955) and for Sirius as 0.63 from the tables given by Kuiper (1938).

Substituting these figures in equation (5.4) and assuming that the probable errors in Θ_S and in $(m_{\text{bol.}\odot} - m_{\text{bol.}S})$ are $\pm 300^\circ\text{K}$ and ± 0.1 mag. respectively, the expected value for the angular diameter of Sirius is

$$\theta_S = 0.0069 \pm 0.0004 \text{ sec (p.e.)}. \quad (5.4)$$

This value is about 8% greater than that we have previously estimated (Hanbury Brown & Twiss 1956), the difference being due to the revised values for the photo-visual magnitudes of Sirius and of the sun.

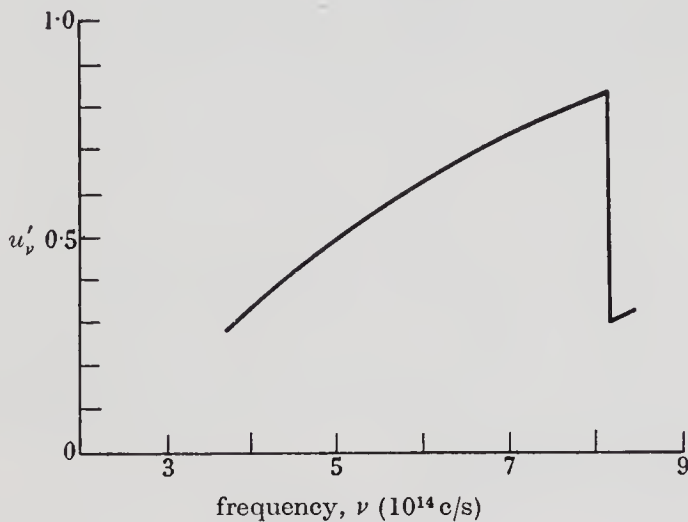


FIGURE 3. The limb-darkening coefficient u'_ν as a function of the frequency of the light, calculated for a star of spectral type $A1v$.

It is also necessary to take into account the effect of limb-darkening. As we have shown in §3.1 of part III this can be allowed for, with an accuracy more than adequate for our present purposes, by assuming that the star radiates like a uniform disk of angular diameter $\theta'_S(\nu) < \theta_S$, where the ratio $\theta'_S(\nu)/\theta$ is determined by the limb-darkening law and by the magnitude of the limb-darkening coefficients. The actual limb-darkening law for Sirius is not known, but since we are discussing a correction of the order of 5% to the apparent angular diameter it will be quite accurate enough for our present purposes to assume the simple approximate law

$$I_\nu(\theta) = I_\nu(0) \left[1 - u'(\nu) \left(1 - \frac{\theta^2}{\theta_S^2} \right)^{\frac{1}{2}} \right], \quad (5.5)$$

where $I_\nu(0)$ is the intensity at frequency ν at the centre of the star and $I_\nu(\theta)$ is the intensity at an angular distance $\frac{1}{2}\theta$ from the centre. The value of $u'(\nu)$ in this equation has been calculated following the analysis of Chandrasekhar (1950) as a function of ν for a star of spectral type $A1v$ and the results are shown in figure 3.

As derived in equation (3.4) of part III, we have that

$$\frac{\theta'_S(\nu)}{\theta_S} = \left[\left(1 - \frac{7u'(\nu)}{15} \right) / \left(1 - \frac{u'(\nu)}{3} \right) \right]^{\frac{1}{2}} \quad (5.6)$$

and, as shown in part III, the correlation at a frequency ν and with a baseline d is proportional to $\Gamma^2(\nu, d)$ where

$$\Gamma^2(\nu, d) = [2J_1(\pi\theta'_S(\nu)\nu d/c)/(\pi\theta'_S(\nu)\nu d/c)]^2 \quad (5.7)$$

in the present case in which the individual mirrors do not appreciably resolve the star.

The final theoretical variation of correlation with baseline length for the present equipment under representative conditions of atmospheric extinction was calculated from equations (5.2) and (5.6) and (5.7) assuming that the true angular diameter of Sirius was 0.0069 sec, as given by equation (5.4), and that the limb darkening coefficient was given as a function of frequency by figure 3. The overall spectral characteristics of the star atmosphere and apparatus were taken from the data in figure 4. The results of these calculations are shown by the full line in figure 5 where the theoretical value of $\overline{\Gamma^2(d)}$ has been plotted as a function of d the separation of the mirrors projected on a plane normal to the direction of the star.

5.3. *The effects of light pulses emitted by cosmic-ray showers*

In equation (7.1) of part III we gave a theoretical expression for δC_{\max} , the upper limit to the fractional increase in correlation which might be caused by light pulses emitted by cosmic-ray showers when observing an unresolved star of a given magnitude. If we substitute in this equation the parameters of the equipment given in § 6, and take representative values of B , σ , $\rho(\nu_0)$, ζ to be 2.2×10^{14} c/s, 0.75, 0.8 and 70° , respectively, then for Sirius

$$\delta C_{\max} \simeq 1.2 \times 10^{-3}.$$

In making this calculation we have taken the field of view of the mirrors to be 10^{-3} sterad, and have made the pessimistic assumption that the probability of receiving a light pulse of given amplitude varies with the zenith angle as $\cos^2 \zeta$.

The value of δC_{\max} , calculated above is far too small to be significant in the present experiment where the signal-to-noise ratio was of the order of 10 to 1.

6. COMPARISON BETWEEN THEORY AND EXPERIMENT

6.1. *The correlation observed with a short baseline*

The correlation observed with a baseline of projected length 2.56 m was compared with theory by substituting the appropriate numerical values in equation (5.1).

The parameters of the electrical equipment were measured in the laboratory and are almost identical with those given for the experiment described in part II. Thus, using the symbols of equation (5.1), $\mu = 5$, $\epsilon = 0.85$, $1 + \delta = 1.06$, $b_v = 38$ Mc/s, $\eta = 0.98$.

The parameters of the optical equipment are D , $\alpha(\nu_0)$, $\gamma(\nu_0)$; where D the diameter of the mirrors was 156 cm; $\alpha(\nu_0)$ the geometric mean of the quantum efficiencies of the two photocathodes, was measured to be 0.123 at $\nu_0 = 6 \times 10^{14}$ c/s (5000 Å); $\gamma(\nu_0)$ the fraction of the incident light reflected by the mirrors on to the photocathodes at 5000 Å was 0.9.

The light flux and spectrum of the star were calculated as follows. The colour temperature of Sirius was assumed to be 14 000 °K in the range 6500 to 4900 Å, 14 500 °K between 4900 and 3700 Å, 10 000 °K between 3700 and 3200 Å (Barbier & Chalonge 1941), and the Balmer discontinuity was taken as 0.47 (Barbier, Chalonge & Canavaggia 1947). These values were used to compute $n_0(\nu)$ the number of quanta per unit bandwidth at a frequency ν incident normally on unit area at the top of the atmosphere. The presence of the absorption lines of the Balmer series was neglected as a more detailed analysis showed that their effect on the final calculations would be insignificant.

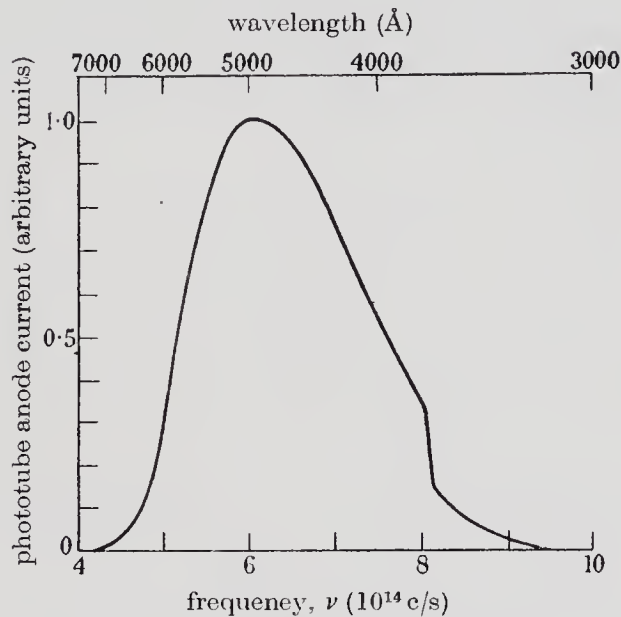


FIGURE 4. The overall spectral response. The curve includes the spectral characteristics of the star (Sirius), the atmosphere, the mirrors, and the photocathodes. The spectral transmission of the atmosphere corresponds to a zenith angle of 70° and 'fairly clear conditions' (Allen 1955).

The atmospheric transmission was estimated as follows. The observations were divided into 5 min intervals ($T_r = 300$ s) and from the measured gains and anode currents of the phototubes the received light flux in each interval was calculated and used to find an approximate value for the atmospheric transmission. The frequency dependence of this transmission, which must be known to calculate the overall spectral response, was found from the data given by Allen (1955); it was assumed that observed variations in transmission were related to changes in the dust content of the atmosphere, and that changes in water vapour were small since all the observations were carried out with the air temperature close to freezing point.

The overall spectral response for each 5 min interval was found approximately by combining the spectral characteristics of the atmosphere with those of the star, the mirrors and the photocathodes. Figure 4 shows the response for a typical interval in which the atmosphere is assumed to be fairly clear (Allen 1955) and the zenith angle of the star is 70°. These data were used to calculate the spectral density factor σ_r for each interval.

The time-dependent factor $(1 + a_r)$, which takes into account the effect of background light from the night sky, was found for each 5 min interval by interpolating between observations of this factor carried out at various stages during each night.

The value of $\Delta(\nu_0)$ the partial coherence factor was calculated from the data presented in figure 2a of part III. For circular mirrors of diameter 156 cm and for the theoretical diameter of Sirius given in the previous section it was found that $\Delta(\nu_0) = 0.99$, where $\nu_0 = 6 \times 10^{14}$ c/s (5000 Å) is a frequency close to the centre of the overall spectral response. This value of $\Delta(\nu_0)$ is so nearly unity that its variation with frequency can be neglected and the approximation $\bar{\Delta} = \Delta(\nu_0) = 0.99$ was therefore made in evaluating equation (5.1). The value of the normalized correlation factor $\bar{\Gamma}_r^2(\bar{d})$ was calculated for each 5 min interval from equation (5.3), taking into account the overall spectral distribution of the light and using the theoretical diameter of the equivalent uniform disk of Sirius which was calculated as a function of frequency from equations (5.2) and (5.7).

The final results of this calculation are shown in table 1. For a projected baseline length of 2.56 m, a total observing time of 345 min and for the actual conditions of light flux and atmospheric extinction of the experiment, the theoretical signal-to-noise ratio was +9.58, while the observed value was +8.50. Thus it follows that, within the rather wide limits set by the limitations of this preliminary test, the observed correlation did not differ significantly from that expected theoretically.

6.2. *The variation of correlation with baseline length*

The theoretical values of the correlation were calculated for the observations with baselines of 5.35, 6.98 and 8.93 m by exactly the same procedure as that described above; the results are shown in table 1. A comparison of these values* with the corresponding observed signal-to-noise ratios shows that there is no significant difference between theory and experiment.

As they stand the experimental results given in table 1 cannot be compared conveniently with each other to give the variation of correlation with baseline length because the observing conditions were not identical for each baseline; they have therefore been normalized as follows. For each baseline the observed correlation was adjusted, using the relations contained in equation (5.1), to standard conditions of atmospheric transmission and observing time; the standard atmospheric transmission was that assumed in calculating figure 4. The results were then divided by the absolute value of correlation to be expected theoretically under the standard observing conditions and with zero baseline. This procedure converts the observed absolute values of correlation into dimensionless fractions of the correlation to be expected at zero baseline, and in this form they can be compared directly with the theoretical values of $\bar{\Gamma}_r^2(\bar{d})$ the normalized correlation factor.

The experimental results, normalized by the procedure described above, have been plotted in figure 5 as points with their associated probable errors. A comparison

* The theoretical values given in table 1 are not identical with those given in an earlier account of the experiment (Hanbury Brown & Twiss 1956). This is because we have given here a more elaborate analysis of the effects of limb-darkening and changes in the spectral characteristics of the atmosphere. The difference between the two sets of theoretical results is less than the probable error in the associated experimental signal-to-noise ratios.

of these points with the full line, which gives the corresponding theoretical values of $\Gamma^2(d)$, shows that within the rather wide limits set by the observational errors the correlation observed from Sirius decreased with increasing baseline in a way which is consistent with that expected theoretically.

6.3. *An experimental value for the angular diameter of Sirius*

An experimental value for the angular diameter of Sirius was calculated from the values of correlation observed with the four different baselines as follows. Using the procedure developed in § 5.1 the theoretical value for the signal-to-noise ratio at each mirror spacing was calculated for a range of values of θ_S the angular diameter of Sirius, assuming that the law of limb-darkening is that given by equation (5.6).

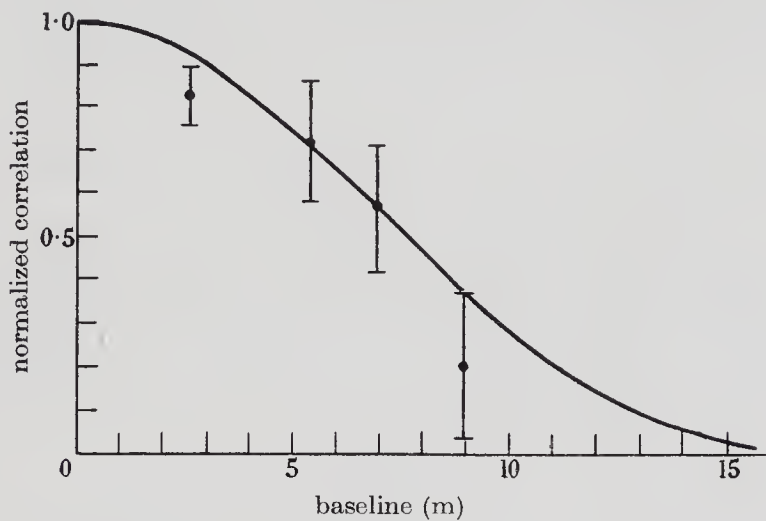


FIGURE 5. The variation of correlation with baseline length. The full line shows the theoretical variation of the *normalized correlation factor* $\Gamma^2(d)$ calculated for Sirius for the standard conditions specified in the text and taking the theoretical angular diameter of Sirius to be 0.0069 sec. The points represent the experimental results normalized to the standard conditions; each point is shown with its associated probable error.

In order to allow for possible errors in the calibration procedure or in measuring the various parameters of the equipment, the experimental values were all multiplied by a factor $F(\theta_S)$; for each value of θ_S the best value of $F(\theta_S)$ was then found by minimizing the sum of the squares of the differences between the experimental and theoretical values of the correlation at each mirror spacing, the difference being weighted by the associated mean square uncertainty for each observation.

The best fit to the experimental results is given by $F(\theta_S) = 1.096 \pm 0.11$, and by

$$\theta_S = 0.0071 \pm 0.00055 \text{ sec (p.e.)}, \tag{6.1}$$

where the probable error $\delta\theta_S$ was found from

$$\frac{1}{\delta\theta_S} = \left[\sum_{m=1}^4 \frac{1}{\delta\theta_{Sm}} \right]^{\frac{1}{2}}, \tag{6.2}$$

where $\delta\theta_{Sm}$ is the change in the optimum value of θ_S when the experimental value of the correlation at the m th mirror spacing is changed by the probable error.

The experimental value* for the true angular diameter of Sirius of 0.0071 ± 0.00055 sec may be compared with the theoretical value of 0.0069 ± 0.00044 sec derived in § 5.2. The difference between these two values is less than the associated probable errors and is therefore not significant. If we take the trigonometrical parallax of Sirius to be 0.375 sec (Allen 1955), then the associated value of the diameter of Sirius is 2.04 times that of the sun.

7. DISCUSSION AND CONCLUSIONS

The observations reported in the present paper show that the experimental values of correlation, both with short and extended baselines, do not differ significantly from those calculated from an idealized theory in which the effects of scintillation have been ignored. Unfortunately, the limited signal-to-noise ratios which were achieved in this preliminary experiment do not permit the comparison between theory and experiment to be made with satisfactory precision; nevertheless, the results are a confirmation, necessarily tentative, of the theoretical prediction made in part III that the performance of an intensity interferometer should not be significantly affected by atmospheric scintillation.

We have shown theoretically that the contribution to the observed correlation due to light pulses from cosmic ray showers should be negligible in measurements on Sirius, and this expectation is confirmed by the absence of correlation from the night sky found in the present tests. This result supports the conclusion, reached in part III, that any spurious correlation should be insignificant in measurements of the brighter stars.

Finally, the measured value of the angular diameter of Sirius is in reasonable agreement with that to be expected from astrophysical theory and this result confirms the conclusion, reached in part III, that the technique of intensity interferometry could be applied to measurements of the angular diameters of the bright stars. Although practical experience revealed a number of minor faults in the equipment, no serious difficulties in the technique were encountered.

One obvious weakness of the experiment described here is that the effect of scintillation was not tested directly by comparing the correlation observed during scintillation with that during conditions of steady seeing. However, under the conditions of this preliminary experiment it was not possible to make such a test; whenever Sirius, which was never more than 20° above the horizon, was observed without excessive atmospheric extinction it was found to be scintillating violently.

A second objection to the experiment is that no positive check could be made that the observed decrease in correlation with increasing baseline was due to the finite angular size of Sirius and not to some instrumental effect. In principle, such a check could have been made by observing a comparison star of smaller angular diameter; however, in the present case, the size of the mirrors was not sufficiently great for any suitable star to be observed. A great deal of care was taken to ensure

* The experimental value of 0.0067 sec given in an earlier account of this experiment (Hanbury Brown & Twiss 1956) differs from the value given here largely because it refers to the equivalent uniform disk and not to the true angular diameter; under the conditions of the present experiment one would expect the latter to be larger than the former by a factor $\simeq 1.05$.

that there should be no loss of correlation due to the equipment, and the reasonable agreement between theory and experiment is a powerful confirmation that the observed decrease in correlation was not spurious.

A third objection to the experiment is the great complexity introduced into the analysis by the use of wide-band light. In future equipment these difficulties can be overcome by the use of a narrow-band filter with a bandwidth, for example, of about 100 Å. Such a filter would permit a much simpler analysis based on the assumption of substantially monochromatic light and, except for a small transmission loss in the filter, would not entail any loss of sensitivity.

We thank the Director of Jodrell Bank Experimental Station for making available the necessary facilities, the Superintendent of the Services Electronic Research Laboratory for the loan of some of the equipment, and Dr S. C. B. Gascoigne for helpful discussions.

REFERENCES

- Allen, C. W. 1955 *Astrophysical quantities*. London: Athlone Press.
 Auwers, G. F. 1891 *Astron. Nachr.* **128**, 367.
 Barbier, D. & Chalonge, D. 1941 *Ann. Astrophys.* **4**, 30.
 Barbier, D., Chalonge, D. & Canavaggia, R. 1947 *Ann. Astrophys.* **10**, 195.
 Chandrasekhar, S. 1950 *Radiative transfer*. Oxford: Clarendon Press.
 Hanbury Brown, R. & Twiss, R. Q. 1956 *Nature, Lond.* **178**, 1046.
 Hanbury Brown, R. & Twiss, R. Q. 1957 *Proc. Roy. Soc. A*, **243**, 291 (part II).
 Hanbury Brown, R. & Twiss, R. Q. 1958 *Proc. Roy. Soc. A*, **248**, 199 (part III).
 Johnson, H. L. & Knuckles, C. F. 1957 *Astrophys. J.* **126**, 113.
 Kopal, Z. & Treuenfels, C. G. 1951 Harvard Circular 457.
 Kuiper, G. P. 1938 *Astrophys. J.* **88**, 429.
 Morgan, W. W., Keenan, P. C. & Kellman, E. 1943 *Atlas of stellar spectra*. Chicago University Press.
 Stebbins, J. & Kron, G. E. 1957 *Astrophys. J.* **126**, 266.
 Unsöld, A. 1955 *Physik der Sternatmosphären*. Berlin: Springer.

THE STELLAR INTERFEROMETER AT
NARRABRI OBSERVATORY—I

A DESCRIPTION OF THE INSTRUMENT AND THE OBSERVATIONAL PROCEDURE

R. Hanbury Brown, J. Davis and L. R. Allen

(Received 1967 July 18)

Summary

A stellar intensity interferometer has been installed at Narrabri Observatory in New South Wales, and is being used to measure the angular diameters of bright stars in the spectral range O to F. This paper describes the instrument and the observational procedure. Experience has shown that the performance is in reasonable agreement with theory and it is concluded that the measurements of angular diameter given in Paper II are reliable.

1. *Introduction.* The stellar interferometer at Narrabri Observatory is an *intensity* interferometer. It correlates the fluctuations in the intensity of the light received by two spaced photoelectric detectors. This novel principle was first applied (1) to a radio interferometer which was used to measure the apparent angular diameters of the two major radio sources in Cygnus and Cassiopeia. Subsequently, two laboratory experiments (2), (3) were carried out to verify that the technique could be applied to light, and a pilot model of a stellar interferometer was built and used in 1956 to measure the angular diameter of Sirius (4). The results of these experiments, together with a theoretical treatment of the technique, have been published by Hanbury Brown & Twiss (5)–(8).

It has been shown that, for certain specific applications, the use of an intensity interferometer has two valuable advantages. Firstly, it offers the possibility of achieving a very high resolving power without meeting the extreme technical difficulties which limit the extension of Michelson's interferometer. Secondly, it is not significantly affected by atmospheric scintillations which impose severe limitations on the use of conventional instruments. The interferometer at Narrabri was built to exploit these advantages by making direct measurements of the angular diameters of stars of early spectral type. Specifically, it was designed to measure the angular diameters of all stars brighter than $B = +2.5$ of spectral type earlier than F₀. This represents an extension of the work of Michelson & Pease (9) who succeeded in measuring the angular diameters of seven stars in the spectral range K to M.

The interferometer was built as a joint project of the Universities of Manchester and Sydney and was installed at Narrabri. The Observatory is in pastoral country about 700 feet above sea level and roughly 300 miles north of Sydney in New South Wales. The site was chosen largely because it has clear skies on about 60 per cent of all nights and, for most of the time, the surface wind is very low. The interferometer itself was made in Great Britain and arrived at Narrabri in January 1962. It is a complex instrument and took roughly two years to install; the first full-scale test was made in July 1963 when it was used to make a preliminary measurement

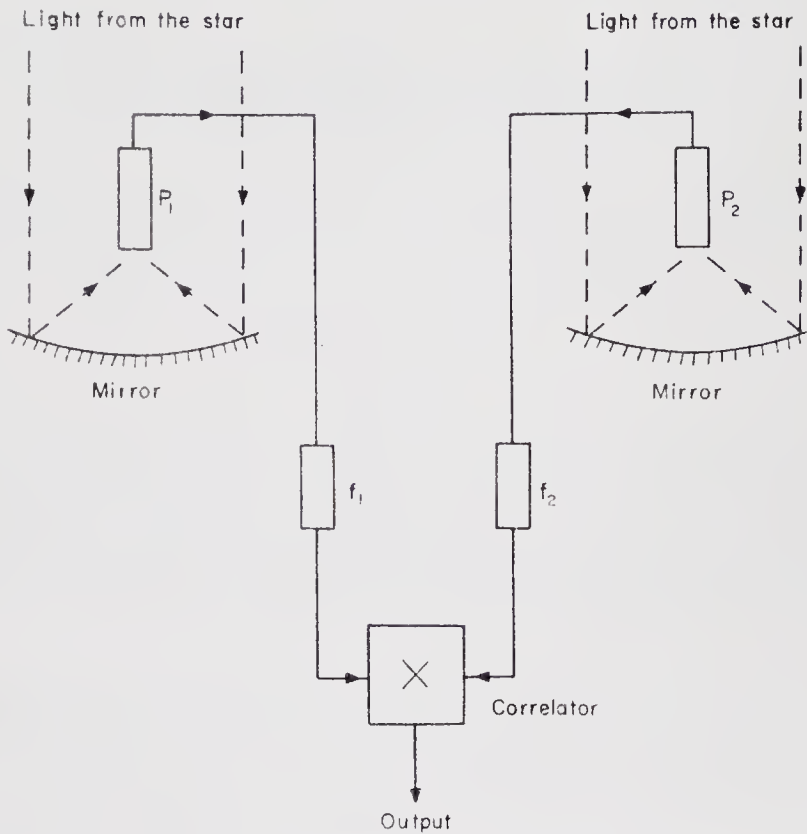


FIG. 1. A simplified diagram of an intensity interferometer.

of the angular diameter of Vega (10). Following this trial a few modifications were made and it was tested again in a more extensive programme on four stars in 1964. Further minor modifications were then introduced and the main observing programme was started in February 1965. The present paper describes the interferometer, and Paper II presents the results of the first two years of operation.

2. Description of the installation

2.1 General layout. A simplified diagram of an intensity interferometer is shown in Fig. 1. Light from a star is received by two photoelectric detectors P_1 , P_2 . The output currents of these detectors fluctuate partly due to fluctuations in the intensity of the incident starlight and partly due to the random statistical fluctuations (shot noise) in the currents themselves. Two identical wideband filters f_1 , f_2 select a band of frequencies from these fluctuations and their outputs are fed to a correlator. The correlator multiplies the two sets of fluctuations together and measures their cross-product averaged over some arbitrary time interval. This product, or correlation, is then measured as a function of the spacing between the detectors, and from these measurements it is possible, as discussed later, to find the angular diameter of the star.

The general layout of the interferometer at Narrabri is shown in Fig. 2. The photoelectric detectors are mounted at the focus of two large reflectors carried on trucks which run on a 5.5 m gauge railway track laid in a circle 188 m in diameter. In the centre of this track there is a control building which houses the

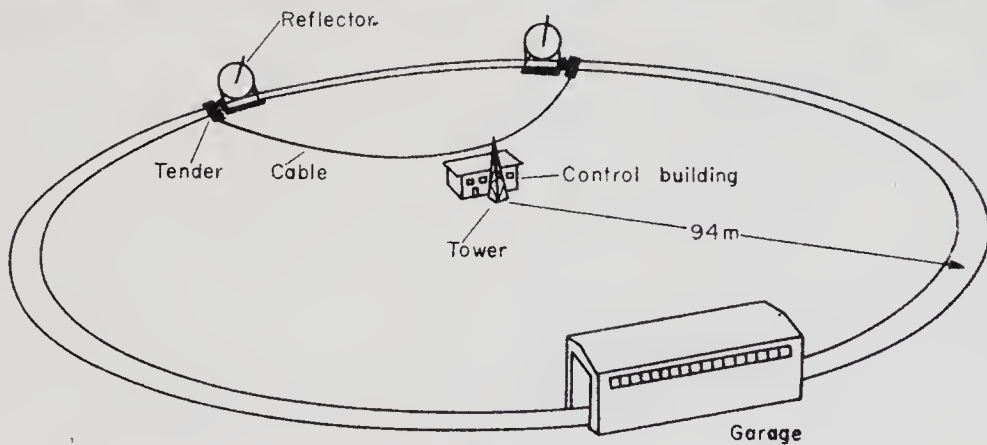
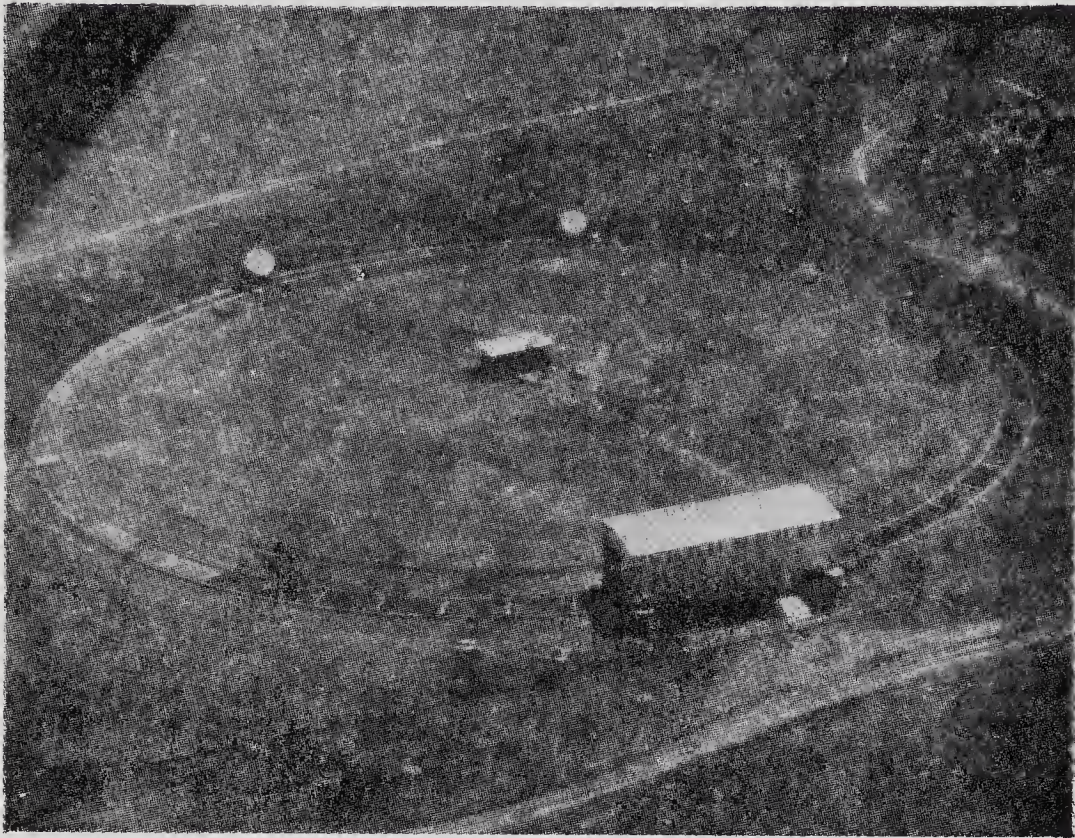


FIG. 2. *The general layout of the interferometer at Narrabri Observatory.*

main control desk and the electronic correlator. Each of the two moving trucks is connected to the control building by cables suspended from a steel catenary cable. At the centre of the track these catenary cables are attached to a bearing at the top of a tower; at the reflectors they are attached to a small tender towed by each truck. When not in use the reflectors are housed in a garage which is built over the track in the southern sector. A valuable, but expensive feature of this garage is that the trucks can be parked inside without detaching the catenary cables and disturbing the electrical connections; this is achieved by a slot which runs almost the full length of the wall of the garage.

2.2 *The reflectors.* Each reflector is roughly 6.5 m in diameter. The framework is made of light alloy and is paraboloidal so that all the light incident on the reflector reaches the focus at the same time. The phototubes at the focus are mounted on a steel tube about 11 m long which projects from the centre of the mirror. It is guyed by stainless steel rods which are themselves attached to a simple framework of steel beams which is not coupled directly to the framework supporting the mirrors.

The reflectors are mounted on turntables which are carried by the trucks, and are capable of three independent motions. They can move around the circular track, tilt in elevation about a horizontal axis and rotate about a vertical axis on their turntables. These three motions are driven by electro-hydraulic motors which are controlled through servo amplifiers. The wheels of the trucks are all conical in profile and their axles are aligned on the centre of the track. The small tenders, towed by the trucks, take the radial pull of the catenary cable and to do this they are equipped with sidethrust wheels which run on the sides of the rails. The tenders also carry auxiliary electronic equipment and a manual control console which is used when driving the reflectors in and out of the garage.

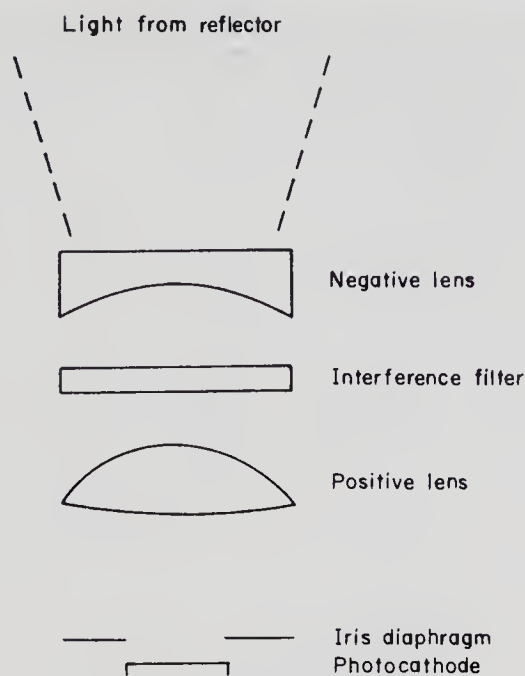
Since the reflectors are remotely controlled and cannot be seen by the operator at night, there is an elaborate system of safety devices which prevents accidental damage. For example, there are long probes which extend in front of the trucks to prevent collisions, and there is a system of interlocks which prevents the reflectors from fouling each other or the garage doors.

2.3 *The optical system.* The surface of each reflector is formed by a mosaic of 252 hexagonal glass mirrors each approximately 38 cm between opposite sides and 2 cm thick. Since it is not necessary to form a conventional image, the mirrors need not be figured to a high precision. All the mirrors are therefore spherical in curvature and after preliminary tests it was specified that they should focus substantially all the light from a distant point source within a circle 1 cm in diameter at the nominal focal length of 11 m. For the sake of economy, the mirrors were all made to the same nominal focal length (11 m) with an overall tolerance of ± 15 cm. The resulting range of focal lengths, which were all measured, has allowed us to distribute the mirrors over each reflector so that their combined optical performance approximates to that of a paraboloidal surface. The mirrors are front-aluminized and have a protective coating of silicon oxide. Each mirror is mounted on a three point suspension and can be adjusted in orientation from the back. An electrical heating pad cemented to the back of each mirror prevents the formation of dew.

The optical system at the focus of each reflector is illustrated in Fig. 3. The converging beam is collimated by a negative lens with a diameter of 9 cm and is passed through an interference filter. It is then focused by a positive lens, through an iris diaphragm, on to the cathode of a photomultiplier. The cathode has a maximum useful diameter of 42 mm.

In order to avoid a loss of correlation, the filters in the two channels must be uniform over their whole surface and closely matched. We have aimed to keep any non-uniformities or differences between the two filters to less than about 5 per cent of their passband.

When the instrument was first tested the mirror assembly was aligned on a distant light to give the minimum possible image size which corresponds to a roughly circular patch 13 mm in diameter. The image was then checked under working conditions by photographing the image of Jupiter over a wide range of elevations.

FIG. 3. *The optical system.*

These tests showed that the size of the image varied greatly with elevation; at its worst it deformed into an ellipse measuring 60×25 mm. Following a detailed investigation of this effect it was found that the reflector framework is distorted by a deflection of the main steel tube which carries the mirror assembly. By means of a television camera at the focus the movements of the individual mirrors were measured and a system of aligning the mirrors was developed which partially compensates for the distortion so that, over most of the working range of elevation, the image of a star is roughly 25×25 mm. This size can be accommodated on the photo-cathode which has a diameter of 42 mm, and it corresponds to an angular resolution in the sky of about $8' \times 8'$; the corresponding angular field of view of the whole photocathode is about $15'$.

The optical components illustrated in Fig. 3 are mounted at the focus in a light-tight fibre-glass box which is shielded both electrically and magnetically. The front of this box is closed by a shutter which can be operated remotely from the central control desk. There is also a small lamp mounted inside the box which is used to illuminate the photocathode when the shutter is closed.

2.4 Guiding and control. The movements of the two reflectors are controlled by an analogue computer which, given the sidereal time, the declination and right ascension, and the latitude of the Observatory, calculates the azimuth and elevation of the chosen star. To follow the star in azimuth the reflectors move around the track, and to follow it in elevation they tilt about a horizontal axis. At all times the line joining the two reflectors, which we shall call the baseline, is held at right angles to the direction of the star; this is essential, not only to preserve a constant resolving power, but also to ensure that the light reaches the two reflectors simultaneously. The length of the baseline can be varied from a minimum value of about 10 m to a maximum of 188 m. To make the two reflectors look in the same direction they are rotated on their turntables through half the angle subtended by the baseline

at the centre of the track. To follow a star which transits north of the zenith the reflectors look outwards from the centre of the track, and to follow a star south of the zenith they look inwards. This arrangement is necessary because the garage obstructs the extreme southern sector of the track.

On entering and leaving the garage the reflectors are controlled manually from a console on each tender. When they are clear of the garage a rail-operated switch allows them to be controlled from the main desk in the control building.

The computed values of azimuth and elevation have a standard error of about $\pm 2\frac{1}{2}'$. However, these errors are usually small compared with the uncertainty in the pointing of the reflectors due to irregularities in the track which can introduce random errors of up to $20'$. The combined effect of both these errors is removed by the use of an automatic photoelectric star-guiding system which employs a second phototube mounted at the focus of each reflector. This auxiliary phototube, which makes use of one mirror of the mosaic, views the star through a rotating shutter and provides error signals corresponding to the azimuth and elevation of the star with respect to the optical axis of the reflector. These error signals are then used to correct the elevation and turntable angles transmitted by the computer to the appropriate reflector. It must be noted that the azimuth corrections are applied to the turntable motion and not to the position of the reflector on the track. Apart from considerations of dynamical stability, it is essential that the corrections should not alter the positions of the reflectors on the track since the baseline must always be constant in length and normal to the direction of the star. Although the irregularities in the track disturb the pointing of the reflectors, they do not significantly alter the length and orientation of the baseline. The performance of the star-guiding system has been monitored by a television camera at the focus of each reflector. It was found that the pointing accuracy depends on the speed of the trucks and on the local condition of the track. The maximum error is about $\pm 3'$ and the r.m.s. error is close to $\pm 1'$ and, in practice, once the reflectors are 'locked', they will track the star without any further attention. Finally, it is interesting to note that, because the star-guiding phototubes are mounted at the foci together with the main phototubes, they automatically compensate for the pointing errors due to sag of the long focal poles; this has made possible the use of a light and economical method of supporting the equipment at the foci.

2.5 The correlator. Light from the star is focused by the optical system on to the cathodes of photomultiplier tubes. These tubes have a quantum efficiency of about 20 per cent at a wavelength of 4400 \AA and are adjusted in gain to give anode currents of about $100 \mu\text{A}$. The anode current of each photomultiplier fluctuates about the d.c. value and the correlator multiplies the fluctuations in the two channels together so that the correlation appears as a unidirectional output superimposed on random noise. The r.m.s. signal to noise ratio at the output of the multiplier is extremely low (about 1 in 10^5 even for a bright unresolved star) so it is necessary to integrate the output of the multiplier for several hours to obtain the required precision. This low signal to noise ratio and the long integration time set very stringent limits to any instability in the correlator.

The correlator is shown in schematic form in Fig. 4. The fluctuations in the anode currents of the photomultipliers are carried by high-frequency coaxial cables to the control building. Here they are amplified by wide band (10–110 Mc/s) amplifiers, and combined in the multiplier. In order to avoid the well known

problems of stability associated with high gain d.c. amplifiers, the output of the multiplier is converted into an a.c. form by inverting the phase of the signal in one channel at a rate of 5000 times a second. The correlation signal now appears at the output of the multiplier as a 5 kc/s square wave superimposed on random noise.

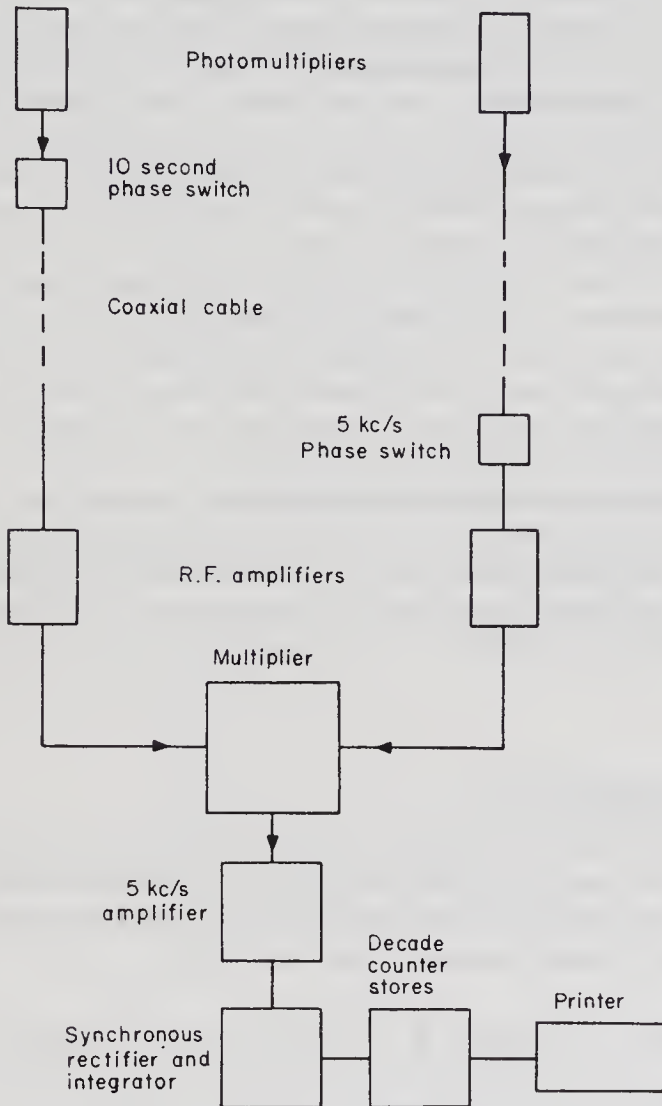


FIG. 4. *Block diagram of the correlator.*

The output of the multiplier is amplified in a high gain 5 kc/s amplifier which is tuned to the phase-inverting frequency. The signal is then rectified synchronously and passed to an integrator.

To minimize the effect of drift in the synchronous rectifier and integrator circuits, phase-switching is introduced into the second channel so that the sign of the integrated correlation is changed every 10 s. The correlation in successive 10 s periods is then added by reversing the sign of alternate periods in the data-handling system; this process cancels out the majority of the drift.

One of the most difficult problems encountered during the installation of the

correlator was to reduce the electrical coupling between the two channels to an acceptable level. Extreme precautions had to be taken to double-screen all the cables carrying radio-frequencies and to double-screen particular units inside the correlator. As a final precaution the 10 s phase-switch was mounted next to the photomultiplier at the focus of one of the reflectors. This ensures that any false correlation due to coupling of circuits after the phase-switch is cancelled in the same way as the drift in the synchronous rectifier and integrator circuits.

The output of the correlation integrator is read every 10 s and stored in two decade counters corresponding to the two states of the phase-switch. The form of the final data output is as follows. Every 100 s a printer records 5 numbers. The first two represent the contents of the two decade counters. The printer automatically takes the difference between these two numbers—thus adding the true correlation and cancelling the drift—and adds this difference to the contents of a sub-total register. As the third number it then prints the sub-total which is the integral of the correlation received since the observing run began. The fourth and fifth numbers are the outputs of integrators which measure the mean phototube anode currents averaged over a period of 100 s. The timing of the various operations of phase-switching, data storage etc. is controlled by a sequence-timer which is initiated by pulses from a crystal-controlled clock.

All the apparatus associated with the correlator is operated from a mains supply which is stabilized to better than 1 per cent; some sections of the correlator use supply voltages stabilized to better than 1 part in 1000. The whole apparatus is housed in an air-conditioned room and the temperature is held constant to within 2°C . A more detailed description of the correlator has been published elsewhere (11).

3. Theoretical considerations

3.1 *The expected value of correlation.* It can be shown, following Refs (5) and (6), that the time average $\overline{c(d)}$ of the correlation expected between the fluctuations in the outputs of two identical photoelectric detectors, when separated by a distance d and exposed to a common source of light is given by,

$$\overline{c(d)} = \Delta_\lambda \Gamma_\lambda^2(d) e^2 A^2 \int_0^\infty \gamma^2(\nu) \alpha^2(\nu) n^2(\nu) d\nu \epsilon \int_0^\infty |F(f)|^2 df \quad (1)$$

where $\Delta_\lambda \Gamma_\lambda^2(d)$ is a factor representing the partial coherence of the light at the two detectors and is discussed further in the next section; e is the charge on the electron; A is the area of each detector; $\alpha(\nu)$ is the effective quantum efficiency of the photocathodes for light of frequency ν and includes the collection efficiency of the photomultipliers; $\gamma(\nu)$ is the overall transmission efficiency of the optical system in front of the detectors; $n(\nu)$ is the number of photons per unit time, per unit area and per unit bandwidth received from the source; ϵ is the efficiency of the whole electronic correlator including the photomultipliers and is defined so that $(1 - \epsilon)$ is the fraction of the correlation lost; $F(f)$ is the gain of each channel at an electrical frequency f and includes the gain of the photomultipliers.

For the purpose of calculating the performance of a practical instrument it is convenient to rewrite equation (1) so that the various parameters of the equipment and the observed output currents from the phototubes can be clearly separated.

Also it is necessary to take account of differences between the two channels. In this case, following the discussion in Ref. (6), equation (1) may be rewritten

$$\overline{c(d)} = \Delta_\lambda \Gamma_\lambda^2(d) i_1 i_2 \frac{\sigma}{B_0} \epsilon b_\nu \frac{|F_{\max}|^2}{G_1 G_2} \tag{2}$$

where i_1, i_2 are the d.c. components of the output currents of the two phototubes; B_0 and σ are respectively the optical bandwidth and the cross-spectral density of the light reaching the photocathodes and are defined by,

$$B_0 = \frac{\left[\int_0^\infty \gamma_1(\nu) \alpha_1(\nu) n_1(\nu) d\nu \cdot \int_0^\infty \gamma_2(\nu) \alpha_2(\nu) n_2(\nu) d\nu \right]^{1/2}}{\gamma(\nu_0) \alpha(\nu_0) n(\nu_0)} \tag{3}$$

and

$$\sigma = \frac{\int_0^\infty \gamma_1(\nu) \alpha_1(\nu) n_1(\nu) \gamma_2(\nu) \alpha_2(\nu) n_2(\nu) d\nu}{B_0 \gamma^2(\nu_0) \alpha^2(\nu_0) n^2(\nu_0)} \tag{4}$$

where

$$\gamma^2(\nu_0) \alpha^2(\nu_0) n^2(\nu_0) = \gamma_1(\nu_0) \alpha_1(\nu_0) n_1(\nu_0) \gamma_2(\nu_0) \alpha_2(\nu_0) n_2(\nu_0) \tag{5}$$

and ν_0 is the midband frequency of the light reaching the photocathodes. The electronic parameters are represented by the cross-correlation bandwidth b_ν defined by,

$$b_\nu = \frac{1}{2 |F_{\max}|^2} \int_0^\infty [F_1(f) F_2^*(f) + F_1^*(f) F_2(f)] df \tag{6}$$

where $|F_{\max}|^2$ is the maximum value of,

$$\frac{1}{2} [F_1(f) F_2^*(f) + F_1^*(f) F_2(f)] \tag{7}$$

and G_1, G_2 are the d.c. gains of the two photomultipliers defined by the relation,

$$G = i/eA \int_0^\infty \gamma(\nu) \alpha(\nu) n(\nu) d\nu \tag{8}$$

and throughout the subscripts 1 and 2 refer to the two channels of the interferometer.

3.2 The measurement of angular diameter. Equation (1) shows that the correlation observed with a baseline d is proportional to $\Delta_\lambda \Gamma_\lambda^2(d)$, where these two factors represent the mutual coherence of the light fluctuations at the two detectors. Following Hanbury Brown & Twiss (6) we shall call Δ_λ the *partial coherence factor*, and $\Gamma_\lambda^2(d)$ the *correlation factor*.

The partial coherence factor, Δ_λ , takes account of the finite size of the two reflectors which are so large that the light fluctuations are not fully correlated over their apertures. The numerical value of Δ_λ depends upon the size and shape of the reflectors and the angular diameter of the star. In calculating this factor we have used the general formulae given in Ref. (6). For most of the stars on the programme $\Delta_\lambda \sim 1$, but for a few stars (e.g. α CMa, α Car) it is substantially less than unity.

The correlation factor, $\Gamma_\lambda^2(d)$, is a function of the angular size of the star and of the separation between the two detectors. In the simple case, where the aperture

of the reflectors is small compared with the baseline necessary to resolve the star ($\Delta_\lambda \sim 1$), it can be shown that $\Gamma_\lambda^2(d)$ is proportional to the square of the modulus of the Fourier Transform of the intensity distribution across the light source when it is reduced to an equivalent line parallel to the baseline. This result implies that $\Gamma_\lambda^2(d)$ is simply proportional to the *square of the fringe visibility* in a Michelson interferometer with the same baseline.

It follows that, if we measure the correlation $c(d)$ as a function of the separation between the detectors and suitably normalize the results (as discussed in Paper II), we can find the distribution of intensity across the light source and hence its angular size. This statement is, however, subject to two restrictions. Firstly we cannot find the phase of the Fourier transform and so the observations do not yield a unique solution; it is therefore necessary to assume that the source is symmetrical. Secondly, the finer details of the distribution, for example the law of limb darkening, are contained in the wings of the Fourier transform which, due to practical limitations of signal to noise ratio, are almost impossible to measure with sufficient accuracy.

In the simple case where a star has a circular disc of uniform intensity it is simple to show that

$$\Gamma_\lambda^2(d) = \left| \frac{2J_1(\pi\theta_{UD}d/\lambda_0)}{\pi\theta_{UD}d/\lambda_0} \right|^2 \quad (9)$$

where θ_{UD} is the angular diameter of the star, λ_0 is the mid-band wavelength of the light and it is assumed that the fractional bandwidth is small. This function is illustrated in Fig. 5.

If the distribution over the disc is radially symmetrical but non-uniform due, for example, to limb-darkening, then the variation of $\Gamma_\lambda^2(d)$ with d can be found

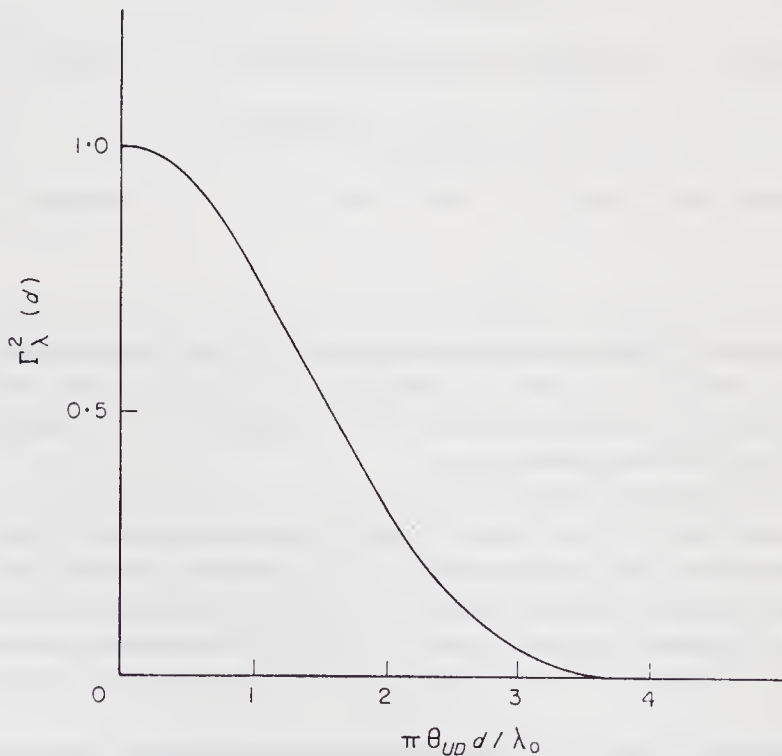


FIG. 5. The variation of the correlation factor with baseline for a uniform disc.

by taking the appropriate Fourier transform. A comparison of the curve for a uniform disc with those for extreme cases of limb-darkening shows that out to the first minimum they are very similar in shape; they differ of course in width, but the only significant differences are in the relative amplitudes of the secondary maxima with which we are not concerned. It is therefore convenient to derive from the observations the *equivalent uniform disc* θ_{UD} of a star and to interpret this in terms of the actual diameter θ_{LD} by computing the ratio θ_{UD}/θ_{LD} for various models of limb-darkening. An example of such a calculation for a simple limb-darkening law is given in Ref. (7). In more complicated cases, for example where the star is multiple, $\Gamma_\lambda^2(d)$ departs from the general shape shown in Fig. 5 and the effects are discussed briefly in Paper II.

A more complex, but important, case occurs when the ratio of the angular diameter of the star to the size of the detectors is such that the individual reflectors are large enough to resolve the star partially ($\Delta_\lambda < 1$). This problem has been explored in Ref. (6) where the general formulae are given; it is also discussed briefly in Paper II.

Finally, we must consider how the optimum baselines and observing times are chosen for a particular star. This choice is particularly important with the present instrument where the observing times are very long, and it is essential to minimize the total time required to achieve the desired precision in the final result. It is clear that if we assume that $\Gamma_\lambda^2(d)$ is of the form given by equation (9) and Fig. 5, then the angular diameter of the star can be found from measurements at only two baselines; furthermore, it can be shown that for a given total observing time, the use of only two baselines yields the highest precision in the diameter θ . Ideally, one of these two baselines should be as short as possible which, in our present instrument, leads to a choice of about 10 m. The optimum length of the second baseline, together with the optimum ratio of observing times at the two baselines, can be calculated in terms of the expected angular diameter of the star. As an example, if the angular diameter of the star is such that $\pi\theta d_1/\lambda = 0.5$, where d_1 is the length of the first baseline, the highest precision in θ is obtained when the second baseline corresponds to $d_2 = 2.25d_1$, and the corresponding optimum ratio of observing times is given by $T_2/T_1 = 4$.

In practice, calculations such as these are a useful guide to planning the observations, but there are other considerations to be taken into account. For example, it is desirable to minimize the effects of possible systematic errors by interleaving alternate observations at the two baselines, and usually this leads to a choice of the ratio T_2/T_1 which is closer to unity than the theoretical optimum. Furthermore, if it is suspected, either from the observations themselves or from spectroscopic evidence, that the star is multiple, for example a close binary, it cannot be assumed that $\Gamma_\lambda^2(d)$ follows the simple curve shown in Fig. 5 and it is then desirable to observe at more than two baselines. This problem is discussed further in Paper II.

3.3 *The effects of differential time delays and atmospheric scintillations.* In equation (1) the expected correlation is given on the assumption that the overall time delays from the light source to the inputs of the multiplier are equal. However, in practice it is inevitable that there will be some differential time delay, and the correlation will be reduced by an amount which depends both on the delay and the electrical bandwidth, but not on the bandwidth of light. It can be shown (e.g. by the Wiener-Kintchine Theorem) that the correlation $c(d, \tau)$, observed with a

differential delay τ is reduced by the factor,

$$c(d, \tau)/c(d, 0) = \int_0^\infty S(f) \cos 2\pi f\tau df \quad (10)$$

where $S(f)$ is the normalized cross-power spectrum of the two channels. In the simple case where the two channels are identical and have a rectangular bandwidth extending from zero frequency to f_{\max} the correlation will therefore be reduced by,

$$c(d, \tau)/c(d, 0) = \frac{\sin(2\pi f_{\max}\tau)}{2\pi f_{\max}\tau} \simeq 1 - \frac{1}{6}(2\pi f_{\max}\tau)^2. \quad (11)$$

Taking a rough value of $f_{\max} = 10^8$ c/s for the correlator, the observed correlation will be reduced by about 10 per cent for a differential time delay of 1 nano-second. This calculation applies to delays both in the arrival of the light at the two detectors and in the electrical paths from the detectors to the input of the multiplier. At short baselines differential optical delays are relatively easy to eliminate, but at long baselines this becomes more difficult. For example, at the maximum baseline of 188 m a differential delay of 1 ns corresponds to a misalignment of the baseline with respect to the star of about $\pm 5\frac{1}{2}$ min of arc. Correspondingly, in the electrical circuits it is necessary to equalize the delays in the phototubes, in the cables and in the amplifiers of the correlator with an accuracy better than 1 ns.

The fact that an intensity interferometer can tolerate comparatively large differential delays makes it practicable to construct instruments with very long baselines and correspondingly high resolving power. Furthermore, this unusual property allows an intensity interferometer to work, without significant loss of precision, through atmospheric scintillations. This latter statement is based on the theoretical analysis given in Ref. (7) and also by further observations reported in Paper II. Briefly, it is shown in Ref. (7) that the effects of angular and amplitude scintillation on the observed correlation must be insignificant. The largest effects are to be expected from phase scintillation, or in other words, from random variations in the relative time of arrival of the light at the two detectors. However, it is argued that these differential delays in the atmosphere are unlikely to exceed 10^{-13} s and therefore their effects on the observed correlation will be negligible because they are small compared with the reciprocal of the electrical bandwidth ($\sim 10^{-8}$ s).

3.4 *The expected signal to noise ratio.* In this section we consider the theoretical limits set to the measurement of correlation (signal) by the statistical fluctuations (noise) in the output of the correlator. Following the analysis in Ref. (6) the r.m.s. uncertainty $N(T_0)$ in the correlation observed over a time T_0 is given by,

$$N(T_0) = e^2 \frac{\mu}{(\mu - 1)} (1 + a)(1 + \delta) \left(\frac{2b_v\eta}{T_0}\right)^{1/2} |F_{\max}|^2 (A_1 A_2)^{1/2} \left[\int_0^\infty \gamma_1(\nu)\alpha_1(\nu)n_1(\nu)d\nu \int_0^\infty \gamma_2(\nu)\alpha_2(\nu)n_2(\nu)d\nu \right]^{1/2} \quad (12)$$

where $\mu/(\mu - 1)$ is the excess noise due to the phototubes; $(1 + a)$ is the excess noise introduced by stray light from the sky or by moonlight; $(1 + \delta)$ is the excess noise introduced by the electronic correlator; η is the normalized spectral density of the

cross-correlation frequency response of the two electronic channels and is defined by

$$\eta = \int_0^{\infty} F_1^2(f)F_2^2(f)df/b_v|F_{\max}|^4 \quad (13)$$

and the other symbols have the same meanings as defined above. To correspond more closely with equation (2), we can rewrite equation (12) in the form,

$$N(T_0) = e^{(i_1 i_2)^{1/2}} \frac{\mu}{(\mu-1)} (1+a)(1+\delta) \left(\frac{2b_v \eta}{T_0}\right)^{1/2} \frac{|F_{\max}|^2}{G_1 G_2}. \quad (14)$$

Combining equations (1) and (12), we can write the r.m.s. signal/noise ratio as,

$$\frac{c(d)}{N(T_0)} = \epsilon \frac{(\mu-1)}{\mu} \frac{1}{(1+a)} \frac{1}{(1+\delta)} \left(\frac{b_v T_0}{2\eta}\right)^{1/2} \sigma \Delta_\lambda \Gamma_\lambda^2(d) (A_1 A_2)^{1/2} \\ (\gamma_1(\nu_0)\alpha_1(\nu_0)\gamma_2(\nu_0)\alpha_2(\nu_0)n_1(\nu_0)n_2(\nu_0))^{1/2} \quad (15)$$

It is interesting to note that, assuming $n_1(\nu) = n_2(\nu)$, the signal/noise ratio is linearly proportional to the number of quanta *in unit light bandwidth* in unit time. While it does depend upon the spectral distribution σ of the light, it is *independent* of the total light bandwidth B_0 provided that this bandwidth is large compared with the electrical bandwidth of the correlator.

4. Observational technique

4.1 *Measurement of correlator drift rate and gain.* It can be shown, following the discussions on signal to noise ratio in the last section, that, even for a bright star, integration times of several hours are required to reduce the statistical uncertainty in the measured correlation to an acceptable value. For a faint star this time can extend up to 50 hours and be spread over several weeks. During this period the sensitivity of the correlator must be maintained and, in particular, a careful check must be made on any systematic errors which can appear as false correlation in the recorded output. In practice we have found that the correlator does produce a small false correlation component which causes the recorded output to drift away from zero, even when the two input signals are completely uncorrelated.

To obtain a sufficiently precise indication of this drift, the correlator is kept running continuously between the stellar observations. During these control runs the phototubes are illuminated by small lamps whose brilliance can be adjusted to give exactly the same phototube anode currents as the star. The light from these lamps is completely uncorrelated and the correlator output therefore gives a true indication of any false correlation generated by the instrument. This output may be used to correct the stellar observations provided that the drift rate does not vary. Experience shows that the rate does not change significantly (compared with the statistical uncertainty) over a period of three days, hence, the stellar observations are corrected by an amount equal to the mean drift rate for the period extending $1\frac{1}{2}$ days before and after each observation. The use of this three day running mean has the advantage that the total integration time spent in measuring the drift is some six times larger than the time for the stellar observations, and therefore the drift correction does not increase the statistical uncertainty in the observations appreciably.

With an apparatus as complex as the correlator it is inevitable that small changes

in electrical gain should occur due, for example, to ageing and replacement of components. While such changes do not affect the overall signal to noise ratio they do change the scale of the recorded correlation. Therefore in order to relate and compare observations made at different times it is necessary to measure the gain of the correlator and to normalize the data to some standard gain. The gain is measured with a standard source of wideband noise which is applied to both channels simultaneously. This standard source is a saturated diode which is mounted in the garage so that it can be connected to both channels in place of the outputs from the two phototubes. The signals in the two channels are completely correlated and give a high value of correlation with a high signal to noise ratio. In this way the gain of the correlator is measured with an accuracy better than 1 per cent in a few minutes, and this is always done immediately before and after every observation of a star.

4.2 *Measurement of the light flux from a star.* The correlation observed from a star is proportional to the product of the light intensities at the two detectors which is itself proportional to the product of the mean anode currents of the two phototubes. Because long integration times are required, it is necessary to observe a star over an appreciable range of elevation and hence of atmospheric extinction. Also, observations of a particular star at various baselines extend over several weeks and have to be made under varying conditions of extinction and moonlight. It is therefore necessary to monitor the light flux from the star continuously and to normalize the observed correlation to a standard value as discussed in Paper II.

During the stellar observations the recorded anode currents measure the total light falling on the phototubes which includes a contribution from the night sky. To measure this component the automatic star guiding system is switched off and the reflectors are pointed to a part of the sky near the star but clear of any other bright stars. The anode currents are then integrated and recorded for several periods of 100 s and afterwards the reflectors are reset to follow the star. On those nights when the Moon is near full, the sky brightness can change significantly with changes in the elevation of the Moon. In this case the current due to the sky background is measured at two-hourly intervals and a smoothed value is used in the normalization procedure. Since the background current increases the noise level in the correlator, but does not contribute to the correlation, observations are not made when it is greater than 10 per cent of the current due to the star. In practice this means that observations are not usually made on the two nights on either side of the full Moon.

A further limitation has been imposed because observations made when the extinction is high have a correspondingly low weight (cf. Section 2.3, Paper II). We have therefore usually restricted the observations of a star to a range of elevations such that the product of the two phototube anode currents is at least 70 per cent of the maximum value observed at upper culmination.

4.3 *Orientation of the baseline and equalization of the time delays.* We have shown in Section 3.3 that the differential delay between the arrival time of the two signals at the correlator must not exceed 1 ns if they are not to be partially decorrelated. The paths of the two signals from the star to the point where they are actually combined in the multiplier comprise the light paths from the star to the photocathode, the paths of the electron stream through the photomultiplier,

the cables connecting the photomultipliers to the correlator, and the amplifiers prior to the multiplier.

The differential delay between the arrival of the light at the two photocathodes depends upon the orientation of the baseline with respect to the line of sight to the star, and hence upon the positions of the two reflectors on the track. The required precision in the azimuth positions of the reflectors, quoted in Section 3.3, is $\pm 5\frac{1}{2}'$ for the maximum possible baseline of 188 m; normally much shorter baselines are used and hence the permissible error is correspondingly greater. In practice the errors in position are due partly to errors in the computed azimuth and partly to discrepancies between the computed and actual position of the reflectors. Usually both these errors are less than $\pm 2\frac{1}{2}'$ and thus their combined effect is less than the permissible error even for the longest baseline.

The transit times through the two photomultipliers are not necessarily the same, due to small differences in construction. Before installing the phototubes on the reflectors these transit times were measured in the laboratory using a luminescent avalanche diode which gives a pulse of light with a rise time of less than 1 ns. When the phototubes were installed on the reflectors the measured difference in transit time was compensated by an extra length of cable in one channel.

The delays in the cable system and the correlator were equalized by adjusting the delay in one channel for maximum correlation from the standard noise source.

As a final check on the whole system the optimum adjustment was confirmed by observing a bright star which gave a high signal to noise ratio. When the adjustment is correct, the introduction of short lengths of delay cable into either channel reduces the correlation symmetrically.

4.4 *The length of the baseline.* The measurement of the angular diameter of a star always involves observations made at the shortest possible baseline which is about 10 m. For stars which are already significantly resolved at 10 m the observed correlation depends critically on the exact length of the baseline. To obtain an accurate and consistent length at these short baselines the separation of the reflectors is checked frequently with a tape measure.

If the baseline is greater than 18 m it is not convenient to measure the separation of the moving reflectors in this way. However, these longer baselines can be set from the control desk with an overall accuracy better than 1 per cent.

4.5 *Observational procedure.* The reflectors are parked in the garage during the daylight hours to shield them from direct sunlight and protect them from the weather. About one hour before sunset the correlator gain is calibrated and the reflectors are driven out of the garage, using the controls on the tenders, until they are clear of the garage. From this position they can be moved using the controls on the central control desk. Meanwhile, in the control room, the appropriate adjustments are made to the right ascension, declination and baseline settings of the computer so that the reflectors can be controlled automatically to follow the star with the required separation.

The reflectors are now driven to an accurate azimuth mark on the track near to the required starting position and the indicated azimuth at the control desk is checked and corrected if necessary. The turntable, elevation and azimuth positions of each reflector are now adjusted to coincide with the positions demanded by the computer and they are then locked on automatic control. When it is sufficiently

dark the shutters of the phototubes are opened and the star-guiding system is brought into operation. During the course of the observations a continuous check is kept on the magnitude of the star-guiding errors to ensure that the guiding and control system is working satisfactorily.

When the observations are completed the reflectors are driven back into the garage, the correlator gain is calibrated, and the control run is started. The control run is continued until the following mid-day, when it is interrupted for routine maintenance.

5. *Tests of the performance.* Since its original installation at Narrabri a continuous effort has been made to investigate and to improve the performance of the interferometer. During the past three years improvements have been made to the phototubes, optical filters, electronic multiplier and data handling system. As a consequence both the signal to noise ratio and the reliability of the installation have been materially increased. The instrument has now reached a point where major improvements in the performance cannot be made without substantial modifications.

The most satisfactory test of the whole instrument would be to measure the angular diameter of a star already known from independent observations. However, this cannot be done since there are no stars in that category, and we must therefore rely on the evidence of a number of detailed tests; a brief account of the most important of these follows.

As a first check of the overall performance the following comparison has been made between the signal to noise ratio observed on four stars and the theoretical value predicted by equation (15). Representative parameters of the equipment in this equation are, $\epsilon = 0.90$, $(\mu - 1)/\mu = 0.75$, $(1 + a) = 1.01$ $(1 + \delta) = 1.10$, $b_v = 70 \times 10^6$ c/s, $\eta = 0.74$, $\sigma = 0.84$, $(A_1 A_2)^{1/2} = 29.5$ m². The factors $\gamma_1(\nu_0)$ and $\gamma_2(\nu_0)$ are the products of the reflectivity of the mirrors (0.75), the transmission of the lenses (0.80) and of the interference and blocking filters (0.70), and therefore $\gamma_1(\nu_0) = \gamma_2(\nu_0) = 0.42$. The values of $\alpha_1(\nu_0)$ and $\alpha_2(\nu_0)$ are the products of the quantum efficiency and collection efficiency of the phototubes and we shall put $|\alpha_1(\nu_0)\alpha_2(\nu_0)|^{1/2} = 0.20$. Finally, we shall take $n_1(\nu_0) = n_2(\nu_0) = 0.62 \times 10^{-4}$ photons m⁻² s⁻¹ (c/s)⁻¹ at 4385 Å, corresponding to a star with $B = 0$ observed in the zenith on a reasonably clear night with an atmospheric extinction of 0.4 magnitude. Substituting these values in equation (15), the expected signal to noise ratio is,

$$\frac{c(d)}{N(T_0)} = 0.52\sqrt{T_0} \cdot \Delta_\lambda \Gamma_\lambda^2(d) \quad (16)$$

where T_0 is the observing time in seconds. Many of the parameters which we have used are rather uncertain; a rough estimate suggests that the overall uncertainty in the theoretical signal to noise ratio given by equation (16), is at least ± 20 per cent.

Table I shows the signal to noise ratio observed on four stars; the values shown correspond to $T_0 = 100$ s and they have been reduced to the zenith and to $\Delta_\lambda \Gamma_\lambda^2(d) = 1$. The corresponding theoretical values, from equation (16), are also given and a comparison shows that there is reasonable agreement. The observed signal to noise ratios are consistently lower than expected by about 20 per cent; nevertheless, the discrepancy is comparable with the uncertainty in the theoretical result and cannot be regarded as very significant.

TABLE I

Star	Apparent magnitude B	Theoretical signal to noise	Observed signal to noise
α CMa	-1.46	$20 \pm 4^*$	16.0 ± 1.1
α Lyr	0.00	5 ± 1	4.0 ± 0.3
α PsA	+1.24	1.5 ± 0.3	1.2 ± 0.1
α Gru	+1.63	1.2 ± 0.2	0.9 ± 0.1

* The uncertainty in the theoretical value has been estimated as ± 20 per cent as stated in the text.

A second series of tests was made to find whether correlation is produced by any source other than the star under observation. For example, we had in mind Cerenkov radiation from cosmic rays and also the possibility that the phototubes might pick up interfering radio signals when the reflectors are outside the garage. Although neither of these sources is expected to be significant, it is important to set upper limits to spurious correlation from any source. In the first of these tests the star β Cru was observed for 55 hours with a baseline of 154 m. At such a long baseline the correlation due to the star is negligibly small and any correlation observed must be due to other sources. No significant correlation was observed. A further two tests were carried out at a baseline of 10 m with the phototubes exposed for several hours to a region of the sky without a bright star. Again no significant correlation was observed. The numerical limits set by these tests are given in Section 5.1 of Paper II.

A third test was designed to measure whether there is any spurious correlation due to coupling between the phototube circuits external to the electronic correlator. Such correlation, if it exists, might possibly introduce a systematic error which would change with baseline. A stringent test for this coupling was therefore carried out by operating one phototube only at a high signal level, and using the correlator to detect any coupled component in the other channel. These experiments were carried out in both channels firstly with the reflectors close together in the garage, and then with them widely separated on the track. No significant coupling was observed and the numerical limits set by this test are given in Section 5.1 of Paper II.

A fourth important test of the theory was to check the prediction (c.f. Section 3.3) that the observed correlation is not significantly affected by atmospheric scintillation. An analysis of the observations confirms that there are no significant effects and the results are discussed in Section 3.2 of Paper II.

As a final overall check of the reliability of the observations, the angular diameters of seven stars were measured twice and the results compared. Not only were the pairs of observations made in successive years, but in the interval some critical components of the interferometer (e.g. phototubes, optical filters, electronic multiplier) were changed. The results of these tests are given in Section 7.1 of Paper II, and they demonstrate that the measurements can be repeated satisfactorily and do not depend on the individual characteristics of some of the critical components of the system.

6. *Conclusions.* The interferometer is, by conventional astronomical standards, very complicated both electrically and mechanically. In practice it has proved relatively easy to operate but difficult to maintain. Thus, although less than 15

per cent of the possible observing time has been lost due to breakdowns, this performance has been achieved at the cost of a great deal of maintenance work. The principal difficulty has been to maintain the correlator; nevertheless, this problem is being rapidly overcome by the use of improved equipment and we look forward to more reliable operation in the future.

Experience shows that the interferometer is about 0.5 magnitude less sensitive than originally proposed. Roughly speaking, if one takes 50 hours as the maximum convenient exposure on a star and $\pm 7\frac{1}{2}$ per cent as the largest acceptable standard error in the measured diameter, then the limiting stellar apparent magnitude is +2.0. The original design envisaged a limit of +2.5, but it is now clear that it was based on optimistic assumptions about the optical system. Nevertheless it is likely that the existing sensitivity can be raised by about 0.5 magnitude, to the value originally planned, by minor improvements to the components. Further increases would require considerable modifications and in particular it would be necessary to improve the whole optical system including the rigidity of the parabolic reflectors.

To sum up, the interferometer has worked satisfactorily for the past two years, and all the tests which have been carried out confirm that its performance is in reasonable agreement with theory. We are therefore confident that the results presented in Paper II are reliable values for the angular diameters of the hot stars.

Acknowledgments. The interferometer was sponsored jointly by the School of Physics of Sydney University and by Manchester University. The construction was financed by the Department of Scientific and Industrial Research (U.K.), the Science Foundation for Research in Physics within the University of Sydney and by the Air Force Office of Scientific Research (Office of Aerospace Research) of the United States Air Force. The project has been supported by further grants from the United States Air Force (AF-AFOSR-302-63/66) and from the Australian Research Grants Committee. The detailed design was carried out by Messrs. Dunford and Elliott (Sheffield) and by the Research Laboratory of Mullard Limited. The authors thank Professor H. Messel for his help in establishing and running the project, and Dr R. Q. Twiss, Professor E. P. Ney, Dr D. M. Popper, Mr M. J. Yerbury, Mr J. M. Rome and Mr R. H. Frater for their assistance.

*Cornell-Sydney University Astronomy Centre,
School of Physics,
University of Sydney,
Australia.*

1967 July.

References

- (1) Hanbury Brown, R., Jennison, R. C. & Das Gupta, M. K., 1952. *Nature, Lond.*, **170**, 1061.
- (2) Hanbury Brown, R. & Twiss, R. Q., 1956. *Nature, Lond.*, **177**, 27.
- (3) Twiss, R. Q., Little, A. G. & Hanbury Brown, R., 1957. *Nature, Lond.*, **180**, 324.
- (4) Hanbury Brown, R. & Twiss, R. Q., 1956. *Nature, Lond.*, **178**, 1046.
- (5) Hanbury Brown, R. & Twiss, R. Q., 1957. *Proc. R. Soc.*, **A242**, 300.
- (6) Hanbury Brown, R. & Twiss, R. Q., 1957. *Proc. R. Soc.*, **A243**, 291.
- (7) Hanbury Brown, R. & Twiss, R. Q., 1958. *Proc. R. Soc.*, **A248**, 199.
- (8) Hanbury Brown, R. & Twiss, R. Q., 1958. *Proc. R. Soc.*, **A248**, 222.
- (9) Pease, F. G., 1931. *Ergebn. exact. Naturw.*, **10**, 84.
- (10) Hanbury Brown, R., Hazard, C., Davis, J. & Allen, L. R. 1964. *Nature, Lond.*, **201**, 1111.
- (11) Hanbury Brown, R. & Browne, A., 1966. *Philips tech. Rev.*, **27**, 141.

THE STELLAR INTERFEROMETER AT
NARRABRI OBSERVATORY—II

THE ANGULAR DIAMETERS OF 15 STARS

R. Hanbury Brown, J. Davis, L. R. Allen and J. M. Rome

(Received 1967 July 18)

Summary

The results of the first observational programme of the stellar intensity interferometer at Narrabri are presented. The measurements are analysed to yield the angular diameters of 15 stars. The results are used to derive the absolute monochromatic flux (F_λ) at the surface of these stars. These values of F_λ are then used to calibrate the line blanketed theoretical model stellar atmospheres of Mihalas to find the effective temperatures (T_e). A scale of effective temperature for stars in the spectral range B0 to G2, excluding supergiants, is derived. It is believed that this scale represents an improvement on previous temperature scales.

1. *Introduction.* In Paper I we described the stellar interferometer at Narrabri and outlined the observational procedure. In this paper, we report the results of the first observational programme which was completed in February 1967. These results comprise the measured angular diameters of 15 bright stars with spectral types ranging from B0 to F5. In view of the novelty of the technique we have included a fairly thorough discussion of the methods used to analyse the observations and to estimate the errors. On the other hand, since we plan to measure several more stars, we have given only a brief discussion of the astrophysical interpretation of the results.

2. *Data reduction*

2.1 *The observational data.* The form in which the observational data are obtained has been described in Section 2.5 of Paper I. Briefly, the printed output from the correlator includes the cumulative total of the observed correlation, which is given every 100 s, together with the two phototube anode currents averaged over the preceding 100 s.

2.2 *Correction for correlator zero drift.* The first step in the reduction of the data is to correct the observed correlation for the zero drift of the correlator. The method used to find this drift was described in Section 4.1 of Paper I. A 3-day mean for the zero drift \bar{D} is found, and this is subtracted from the average correlator output $\overline{c(d)}$ when observing the star with a baseline d , to give the mean observed correlation from the star, $\overline{c_0(d)}$, and so

$$\overline{c_0(d)} = \overline{c(d)} - \bar{D} \quad (1)$$

In practice the zero drift is small but not negligible; the average value of \bar{D} for a period of 2 years is about 4 per cent of the zero-baseline correlation from a star of magnitude $B = +1$.

2.3 *Normalization for flux and gain variations.* It was shown in equation (1) of Paper I that the correlation observed from a star is proportional to the product of the light intensities at the two detectors and also to the gain of the correlator. Before the observational data can be combined it is therefore necessary to normalize them in order to remove the effects of variations in these parameters.

(a) *Flux variations.* As explained in Section 4.2 of Paper I, the effects of variation in light flux during the course of a single night, and also from night to night, can be eliminated if the observed correlation is normalized by the product of the phototube anode currents. Since this normalization should be by the stellar flux alone, the anode currents are first corrected for sky and moon contributions. Near new moon these corrections are of the order of 1 per cent for a star with $B = +1$; they have not been allowed to exceed 10 per cent of the total anode current for any of the observations.

The signal to noise ratio of the instrument is proportional to the light flux received from the star and as this varies during the course of a series of observations so does the weight of the data obtained. Thus, in computing the mean normalized correlation for an observational run, each 100 s cycle is given an appropriate weight as follows. Let i_{T_1} and i_{T_2} be the total observed photomultiplier anode currents, and i_{S_1} and i_{S_2} the components of these currents due to the star alone. Then $c_0(d)$ the observed correlation is

$$c_0(d) \pm K\sqrt{i_{T_1}i_{T_2}}$$

where K is a constant, and $c_n(d)$ the correlation normalized to standard photomultiplier anode currents is

$$c_n(d) = \frac{c_0(d)}{i_{S_1}i_{S_2}} \pm \frac{K\sqrt{i_{T_1}i_{T_2}}}{i_{S_1}i_{S_2}} \quad (2)$$

The weight w of a single cycle is therefore

$$w = \left[\frac{i_{S_1}i_{S_2}}{K\sqrt{i_{T_1}i_{T_2}}} \right]^2 \quad (3)$$

and $\overline{c_n(d)}$, the weighted mean correlation for an observational run of p cycles, is

$$\overline{c_n(d)} = \frac{\sum_p w c_n(d)}{\sum_p w} = \frac{\sum_p [c_0(d)i_{S_1}i_{S_2}/i_{T_1}i_{T_2}]}{\sum_p [(i_{S_1}i_{S_2})^2/i_{T_1}i_{T_2}]} \quad (4)$$

where \sum_p is the sum of the individual values for p cycles.

If, for the purposes of weighting alone, it is assumed that $i_{T_1} = i_{S_1}$ and $i_{T_2} = i_{S_2}$ then

$$\overline{c_n(d)} = \frac{\sum_p c_0(d)}{\sum_p i_{S_1}i_{S_2}} = \frac{\sum_p c_0(d)/p}{\sum_p i_{S_1}i_{S_2}/p} \quad (5)$$

which can be written

$$\overline{c_n(d)} = \overline{c_0(d)/i_{S_1}i_{S_2}} \quad (6)$$

Thus the weighted mean correlation, normalized for flux variations, is simply equal to the mean observed correlation divided by the mean phototube anode current product due to the star. It should be noted that equation (6) contains the implicit assumption that \overline{D} is independent of the phototube anode currents;

it is known from experiment that this assumption is valid with sufficient accuracy for our present purposes.

(b) *Correlator gain variations.* Gain variations of the correlator are generally of long period and are relatively small, but they must be taken into account when combining observations of a star made over a period of several days or weeks. This is accomplished by normalizing the weighted mean correlation, $\overline{c_n(d)}$, to a standard gain, using the gain calibration factor determined as described in Section 4.1 of Paper I.

Thus

$$\overline{c_N(d)} = \overline{c_n(d)} / \text{CAL} \tag{7}$$

where $\overline{c_N(d)}$ is the normalized, weighted mean correlation from the star, and CAL is the gain calibration factor.

3. Uncertainty in the normalized correlation

3.1 *Statistical uncertainty in the mean correlation from a star.* The primary source of uncertainty in the normalized values of correlation is the statistical fluctuation (noise) in the output of the correlator (cf. Section 3.4, Paper I). A simple statistical analysis of the fluctuations during long control runs, and also during runs on the star, gives the r.m.s. uncertainty σ_{obs} in a single 100 s cycle of the correlator output. It is simple to show that

$$\sigma_{\text{obs}} \propto \sqrt{i_{T_1} i_{T_2}} \text{CAL} \tag{8}$$

and hence we can define a normalized or 'standard uncertainty' σ_{std} , which is independent of the light flux falling on the phototubes and of the gain of the correlator, as

$$\sigma_{\text{std}} = \frac{\sigma_{\text{obs}}}{\sqrt{i_{T_1} i_{T_2}} \text{CAL}} \tag{9}$$

This 'standard uncertainty' is a constant for the observations of a star and only changes when equipment parameters, such as phototube gains, are changed in order to observe a star of different brightness. In practice the value of σ_{std} used for each star is the mean value obtained from the analysis of several runs.

It follows that the r.m.s. uncertainty in the mean correlator output $\overline{c(d)}$ from p periods of 100 s is

$$\frac{\sigma_{\text{std}} \sqrt{i_{T_1} i_{T_2}} \text{CAL}}{\sqrt{p}} \tag{10}$$

Similarly the r.m.s. uncertainty in the mean correlator zero drift (\overline{D}) determined from q periods is

$$\frac{\sigma_{\text{std}} \sqrt{i_1 i_2} \text{CAL}}{\sqrt{q}} \tag{11}$$

where i_1 and i_2 are the phototube anode currents used during the control runs. The r.m.s. uncertainty in the mean observed correlation from the star $\overline{c_0(d)}$ is given by the combination of these two uncertainties.

3.2 *The effects of atmospheric scintillation.* A theoretical analysis (c.f. Section 3.3, Paper I) predicts that the effects of atmospheric scintillation on the correlation should be negligibly small. To confirm this prediction we have made two tests.

Firstly, since it is to be expected that these effects would vary with elevation, we have analysed our observations of α CMa to test for a variation of normalized correlation with elevation. Measurements taken on six different nights in 1966 and 1967 show that any such variation was less than 10 per cent over a very wide range (75° to 15°) of elevation angles. Secondly, since it is to be expected that the effects would vary from night to night, we have looked for a variation in the normalized correlation $\overline{c_N(d)}$ observed on different nights. We have compared the dispersion in $\overline{c_N(d)}$ with the dispersion expected due to statistical fluctuations in the correlator output, the magnitude of the fluctuations being established largely by control runs with the reflectors in the garage. Taking observations on 126 different nights the observed dispersion in $\overline{c_N(d)}$ is 0.99 ± 0.06 of the expected value and therefore shows no evidence of any effect due to scintillations. These tests, although not exhaustive, confirm that any effects due to scintillation are small and are unlikely to have a significant influence on the accuracy of our measurements.

Since the observational programme was planned before these tests were made some precautions were included to reduce the possible effects of scintillation. Thus, for any given star, all the observations at different baselines are carried out over the same range of elevation angles. Again, for any given star, the observations at different baselines are interleaved in order to minimize any possible effects due to slow changes in the atmospheric conditions.

3.3 *Additional sources of uncertainty in the correlation.* Two additional sources of uncertainty in the observed correlation should be mentioned. Firstly, there are small and variable differential delays in the arrival of the signals at the correlator due to misalignment of the baseline.¹ These are discussed in Section 4.3 of Paper I and we estimate that, in the worst case, they introduce an uncertainty of ± 1 per cent in the measured correlation. Secondly, there are uncertainties in the zero level of the correlator output due to possible spurious correlation as discussed in Section 5 of Paper I. The numerical values are given later in Section 5.1.

Finally, there are small additional uncertainties introduced into the normalized correlation by the normalizing factors, namely, the phototube anode currents and the gain calibration. The uncertainty in the phototube anode current product is a function of the linearity, calibration, and zero level of the two current integrators. We estimate that the total uncertainty in the product of the anode currents is less than ± 1 per cent. The uncertainty in the gain calibration of the correlator is principally due to changes in the ambient temperature of the cables which carry the signals to the correlator, and we estimate that for each night the uncertainty in the mean calibration is less than $\pm 1\frac{1}{2}$ per cent.

These small sources of uncertainty are taken into account when estimating the overall uncertainty in the angular diameters as discussed in Section 7.

4. *Angular diameter determination.* The values obtained on r different nights for the mean normalized correlation, $\overline{c_N(d)}_r$, at a baseline d , are combined to give a weighted mean as follows

$$\overline{c_N(d)} = \frac{\sum_r \frac{1}{\sigma_r^2} \overline{c_N(d)}_r}{\sum_r \frac{1}{\sigma_r^2}} \quad (12)$$

where σ_r is the uncertainty in $\overline{c_N(d)}_r$ on the r th night. The r.m.s. uncertainty in this weighted mean value is

$$\sigma = \frac{1}{\sqrt{\sum_r \frac{1}{\sigma_r^2}}} \quad (13)$$

As described in Section 3.2 of Paper I, the correlation at a baseline d is proportional to $\Delta_\lambda \Gamma_\lambda^2(d)$. In the case of a circular source of uniform intensity and angular diameter θ_{UD} , observed by reflectors which do not appreciably resolve the source ($\Delta_\lambda \simeq 1$), the function

$$\Gamma_\lambda^2(d) = \left[\frac{2J_1(x)}{x} \right]^2 \quad (14)$$

gives the shape of the curve relating correlation to baseline where $x = \pi d \theta_{UD} / \lambda_0$ and λ_0 is the effective wavelength of the interferometer. For a real, limb darkened star, the shape of the curve is not significantly altered although the scale is changed. As explained in Section 3.2 of Paper I, it is convenient to fit a curve of the shape given by equation (14) to the observations to obtain the equivalent uniform disc diameter θ_{UD} , and then to interpret this result in terms of the actual limb darkened diameter θ_{LD} by computing the ratio $\theta_{LD} / \theta_{UD}$ for various models of limb darkening.

The least-squares fitting of the curve for a uniform disc to the observations is carried out by an iterative process using a computer. Initial values are assumed for $\overline{c_N(0)}$ (the normalized correlation at zero baseline) and θ_{UD} , and corrections $d\overline{c_N(0)}$ and $d\theta_{UD}$ are computed which minimize the weighted squared differences between the observational data and the theoretical curve. The r.m.s. uncertainties in $\overline{c_N(0)}$ and θ_{UD} are also computed. The calculation is then repeated, using the initial values $[\overline{c_N(0)} + d\overline{c_N(0)}]$ and $[\theta_{UD} + d\theta_{UD}]$ and the iteration is continued until $d\theta_{UD} / \theta_{UD} < 10^{-3}$.

If the angular diameter of a star is large enough to be partially resolved by the individual reflectors, the shape of the curve relating correlation to baseline is altered, and the correlation at zero baseline is reduced by the partial coherence factor Δ_λ . This problem has been discussed by Hanbury Brown & Twiss (1), (2). Following their analysis, if (x_1, y_1) and (x_2, y_2) represent points on the two reflectors, whose centres are separated by a distance d , the shape of the curve for a uniform disc is given by

$$\Delta_\lambda \Gamma_\lambda^2(d) = \frac{1}{A^2} \iiint \left[\frac{2J_1(\xi)}{\xi} \right]^2 dx_1 dx_2 dy_1 dy_2 \quad (15)$$

where

$$\xi = \frac{\pi \theta_{UD}}{\lambda_0} [(x_1 - x_2)^2 + (y_1 - y_2)^2]^{1/2} \quad (16)$$

and the integral is taken over the areas of the reflectors and A is the area of each reflector. In this case, the least-squares fit is again carried out using the computer, but the numerical integration of the above expression at each baseline appreciably increases the computing time.

The effect of the finite size of the reflectors is to smooth out, or flatten, the curve and to give lower values of $\overline{c_N(0)}$. As an example, Fig. 1 shows the curve calculated for $\Delta_\lambda = 0.90$, which corresponds to observations of α CMa ($\theta_{UD} = 5.85 \times 10^{-3}$ s of arc) with the reflectors at Narrabri. For comparison the curve is also shown for

the case where the reflectors are very small ($\Delta_\lambda = 1$). In the present programme most of the stars have angular diameters $\theta_{UD} < 2 \times 10^{-3}$ s of arc, which corresponds to $\Delta_\lambda > 0.99$, and for them the effects of partial resolution are very small.

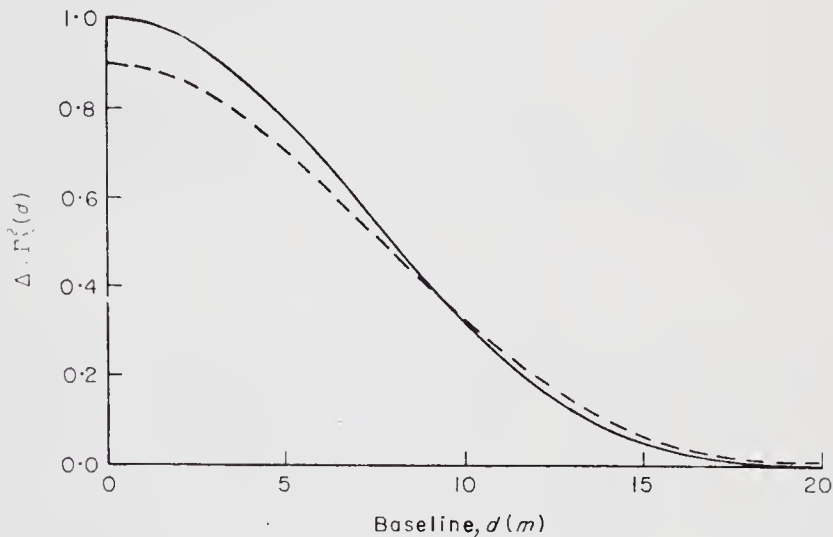


FIG. 1. The variation of normalized correlation with baseline for a star with $\theta_{UD} = 5.85 \times 10^{-3}$ seconds of arc for small reflectors ($\Delta_\lambda = 1$, full line) and for large reflectors ($\Delta_\lambda = 0.90$, broken line).

5. Uncertainties in curve fitting

5.1 *The zero level of correlation.* As already described in Section 5 of Paper I several tests were carried out to find whether the true zero level of the correlator output is disturbed by any source of spurious correlation. No significant correlation was observed; nevertheless, we have assumed that there is an uncertainty in the zero level corresponding to the upper limits to spurious correlation set by these tests. It can be shown that, in our normalized data, this uncertainty depends upon the brightness of the star under observation. We have therefore summarized the results of these tests in Fig. 2 where the combined uncertainty in the zero level

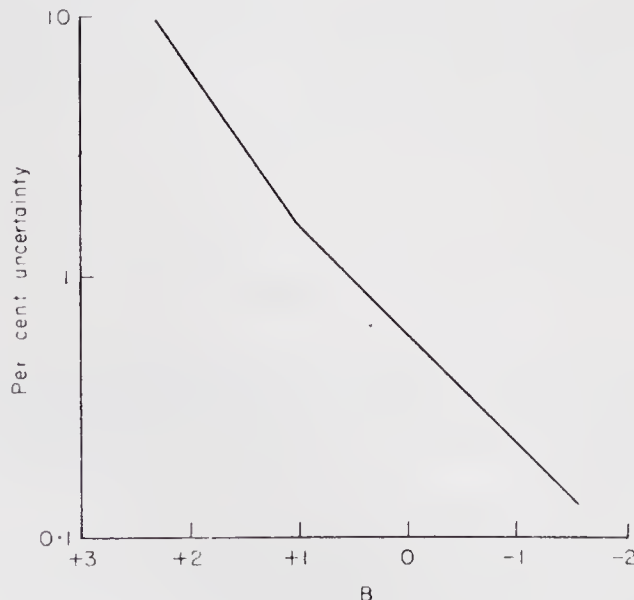


FIG. 2. The uncertainty in the zero level correlation as a function of stellar magnitude.

is shown as a function of the brightness of the star under observation; it is expressed, for convenience, as a percentage of the zero baseline correlation expected from the star.

The effect of these uncertainties is to produce corresponding small uncertainties in the final measured parameters of the star; they have therefore been included in estimating the overall r.m.s. uncertainty in the measured values of the zero baseline correlation, $\overline{c_N(0)}$, and of the angular diameter, θ_{UD} .

5.2 *The effect of binary stars.* In the present programme it is important that we should deal, as far as possible, with single stars and that the interpretation of the data should not be complicated by binaries. It is, of course, possible to reject many unwanted binaries on the basis of optical evidence alone. However, the interferometer is capable of resolving the separation of a wide range of close binaries and it is possible that some of these may not have been detected by other methods. It is therefore important that the results for each star should be examined to check whether or not they are consistent with a single star.

Let us first consider the case when the interferometer is observing a binary system in which the components have an angular separation $\bar{\theta}$, which is too small to be resolved by the individual reflectors of the interferometer. If the line joining the two components makes an angle ψ with the baseline, the shape of the curve relating correlation to baseline is given by

$$\Gamma^2(d) = \frac{I}{(I_1 + I_2)^2} \left[I_1^2 \Gamma_1^2(d) + I_2^2 \Gamma_2^2(d) + 2I_1 I_2 |\Gamma_1(d)| |\Gamma_2(d)| \cos \left\{ \frac{2\pi \bar{\theta} d \cos \psi}{\lambda} \right\} \right] \quad (17)$$

where I_1 and I_2 are the intensities of the two components, both of which are assumed to be too small to be resolved by the individual reflectors. This curve is modulated at a frequency determined by $\bar{\theta} \cos \psi$, and the observed correlation oscillates between values which are proportional to

$$[I_1 |\Gamma_1(d)| + I_2 |\Gamma_2(d)|]^2 \text{ and } [I_1 |\Gamma_1(d)| - I_2 |\Gamma_2(d)|]^2.$$

Since $\bar{\theta} \cos \psi$ varies with time as the position angle of the system changes, the correlation observed at a given baseline also varies with time and has a mean value which lies between these extremes; it is therefore less than the correlation expected from a single star giving the same light flux.

In the more complicated case where the angular separation of the binary is significantly resolved by the individual reflectors the modulation of $\Gamma^2(d)$ is reduced. A full discussion of this case is not justified here and is not important in the present context.

In principle it is therefore possible to distinguish a binary from a single star either by observing that the correlation is less than expected from a single star of the same brightness, or by noting that the correlation factor $\Gamma^2(d)$ varies with time, or with baseline, in a way which is inconsistent with a single star. As an example, consider the case where the separation of the binary $\bar{\theta}$ is such that it is completely resolved at the shortest baseline ($d_{\min} \gg \lambda/2\bar{\theta}$). Then the correlation factor, averaged over a wide range of position angles, is given by

$$\Gamma^2(d) = \frac{I}{(I_1^2 + I_2^2)} [I_1^2 \Gamma_1^2(d) + I_2^2 \Gamma_2^2(d)]. \quad (18)$$

Thus, in this simple case, the interferometer treats the two stars as separate entities and the observed correlation is the sum of the correlation due to each star separately. It follows that at short baselines, where neither of the component stars are individually resolved, the correlation will be reduced, relative to a single star, by the factor

$$\frac{I_1^2 + I_2^2}{(I_1 + I_2)^2} \quad (19)$$

and we can distinguish a binary from a single star by measuring $\overline{c_N(0)}$, the normalized zero baseline correlation, and comparing it with the value for a single star.

A more complicated case is where the binary is very close, and the separation $\bar{\theta}$ is not resolved at the shortest baseline ($d_{\min} \ll \lambda/2\bar{\theta}$). In this case the correlation at short baselines is not reduced relative to a single star and therefore we cannot rely wholly on detecting all binaries by measuring $\overline{c_N(0)}$. The best method of detecting these very close binaries is to make observations at several baselines and to compare the observed variation of $\Gamma^2(d)$ with the curve expected for a single star. However, this method is very time-consuming and for the stars in the present programme we use the following procedure.

The first measurements of each star are always made at the shortest possible baseline of about 10 m. If the observed correlation is less than we expect, and will obviously lead to a significantly low value of $\overline{c_N(0)}$, we delete the star from the present programme. The criterion adopted is that if the star gives less than 80 per cent of the expected correlation it is rejected (see Section 7.2); this implies that, if any of the stars which remain on our programme are binary, then their companions are at least 2.2 magnitudes fainter than the primary components. As a further safeguard against very close binaries, we review the optical and spectroscopic data on each star and, wherever there is a suspicion that the star may be a binary, we make observations at three or more baselines and compare the ratios of the correlations at the baselines with those expected from a single star. As a test of these methods we have confirmed that they lead to the rejection of the spectroscopic binaries λ Sco and α Vir.

5.3 The effects of stellar rotation. The most obvious effect of rotation on a star is to change its shape, increasing the equatorial diameter relative to the polar diameter. If the star were to remain uniformly bright these changes would appear directly as changes in the apparent angular diameter. However, the situation is complicated by the fact that the variation in surface gravity leads to a significantly higher luminosity at the poles compared with the equator. The overall effect of rotation on measurements of angular diameter therefore depends on the orientation of the rotation axis relative to the baseline of an interferometer.

In order to establish approximate limits to these effects, we have used the rapidly rotating model of a star (equatorial velocity of 350 km s^{-1}) given by Ireland (3) and have considered only three particular orientations of the rotation axis. Thus, when the rotation axis of the star is parallel to the baseline, numerical integration of the brightness distribution shows that the equivalent strip source is both narrower and limb brightened as compared with that for a uniform disc with a radius equal to the mean of the polar and equatorial radii. But the Fourier transform of this distribution is almost identical to that of the uniform disc, at least out to the first minimum in the transform, and it follows that the measured angular diameter is

almost unchanged by rotation. This rather remarkable result is due to the fact that the changes produced in the Fourier transform by the reduction in polar diameter are in the opposite sense to those produced by the polar brightening and to a first order they cancel one another.

Further consideration of Ireland's model shows that when the star is viewed equator-on, with the rotational axis perpendicular to the baseline, the apparent angular diameter will be approximately 8 per cent greater than for the equivalent uniform disc. When seen pole-on the apparent angular diameter will be about 5 per cent greater than for the equivalent uniform disc.

It follows that if observations are averaged over an appreciable range of position angles the resulting apparent angular diameters may be as much as 6–7 per cent higher, in the extreme case, than the equivalent uniform disc for Ireland's model. This extreme corresponds to a very rapidly rotating star seen equator-on and with the range of position angles centred about the equator of the star.

It must be noted that the model is based on elementary assumptions about the effects of rotation on a star and we have used it simply to give a rough upper limit to the effects of very rapid rotation on our measurements; for most stars, the observational effects will be considerably less. The observations of known rapidly rotating stars are discussed in Section 7.3.

6. *Observational data.* Table I is a summary of the observational data for 15 stars. The stars are listed in chronological order of observation; 7 of them have been measured twice. For each star we show the lengths of the baselines used, the normalized weighted mean correlation $\overline{c_N(d)}$ observed at each baseline with its associated r.m.s. uncertainty σ , the observing time at each baseline, and finally the effective wavelength of the optical system. The values of $\overline{c_N(d)}$ are in arbitrary units which are not the same for every star because several modifications have been made to the equipment at various stages of the programme to improve the signal to noise ratio. These modifications to the equipment are listed at the foot of Table I. It is important to note that they do not affect the measurements of angular diameter because they were all made between programmes on different stars. On the other hand they do affect the arbitrary scale on which the correlation $\overline{c_N(d)}$ is measured. In principle the effect of these changes on $\overline{c_N(d)}$ can be removed by normalizing the results by the relevant equipment parameters such as B_0 , σ and ϵ (see Section 3 of Paper I); however, not all these factors are known with sufficient accuracy and therefore the correlation is given in arbitrary units.

The uncertainty σ associated with $\overline{c_N(d)}$ represents the statistical fluctuations in the correlator output due to noise as discussed in Section 3.1.

7. *Results.* Theoretical curves for uniform discs have been fitted, as described in Section 4, to the observed values of correlation $\overline{c_N(d)}$ in Table I. This calculation gives the zero-baseline correlation C and the angular diameter θ_{UD} of the equivalent uniform disc, together with their uncertainties, for the curve of best fit. The results are shown in Table II. Examples of the fitted curves are shown in Fig. 3 for three stars of widely different angular diameter.

Several of the stars have been measured twice and, with the exception of α CMa, the second measurement was made with improved sensitivity and therefore has a

TABLE I

Observational data

1	2	3	4	5	6	7	8
Star	Epoch of observations	Baseline (m)	$\overline{cN(d)} \pm \sigma^*$ Arbitrary units†		Observing time (h)	Wavelength of observations (Å)	Equipment configuration
α Lyr	1963 July– August	9.85	323	50	5.6	4385	(a)
		13.15	266	70	2.6		
		16.42	220	50	4.9		
		19.68	110	50	6.4		
α Aql	1964 June– August	23.0	-9	40	8.2	4608	(b)
		9.85	95	14	10.7		
		14.79	64	13	12.2		
		19.68	39	18	10.9		
α Gru	1964 August– September	24.6	42	16	12.7	4608	(b)
		29.5	-4	14	14.4		
		9.85	111	22	11.3		
		26.2	111	25	11.4		
α PsA	1964 September– October	42.4	70	28	11.3	4608	(b)
		58.2	32	28	11.9		
		73.6	36	26	11.9		
		9.85	101	17	12.4		
α Eri	1964 October– November	16.42	74	21	11.0	4385	(a)
		23.0	58	18	11.3		
		29.5	57	20	11.0		
		35.9	41	22	12.6		
β Cru	1965 May–July	42.4	22	17	12.2	4385	(c)
		9.85	460	40	13.4		
		18.04	304	49	11.3		
		26.2	223	47	12.7		
α Aql	1965 June– August	34.3	115	48	11.3	4385	(a)
		42.4	11	45	11.3		
		79.6	-30	98	2.8		
		9.85	286	12	20.1		
α Lyr	1965 July– August	32.7	194	19	6.9	4385	(c)
		48.8	184	18	7.5		
		64.4	126	19	7.0		
		79.6	119	11.5	24.5		
α Gru	1965 August– September	94.2	67	17	10.4	4385	(c)
		114.7	20	22	6.5		
		133.2	-8	19	7.3		
		154.3	4.5	7.7	53.9		
α Lyr	1965 July– August	9.85	241	10	29.8	4385	(c)
		19.68	114	11	29.6		
		24.6	66	15	14.4		
		9.85	251	8	21.5		
α Gru	1965 August– September	19.68	88	8	22.6	4385	(c)
		9.85	361	27	18.4		
		58.2	126	17	45.8		
		9.85	361	27	18.4		

TABLE I—*continued*

1	2	3	4	5	6	7	8
Star	Epoch of observations	Baseline (m)	$\overline{c_N(d)} \pm \sigma^*$ Arbitrary units†		Observing time (h)	Wavelength of observations (Å)	Equipment configuration
α PsA	1965	9.85	319	24	16.2	4385	(c)
	September	35.9	51	15	41.5		
α Eri	1965	9.85	283	12	11.4	4385	(c)
	October	32.7	96	9	32.1		
β Ori	1965	9.85	251	15	4.6	4385	(c)
	October	23.0	97	9.5	10.7		
α Car	1965	9.58	84	4	14.9	4385	(c)
	October–	13.85	20	5	12.6		
	November	14.46	10	6	5.1		
α CMa	1966	9.58	122.2	1.6	15.9	4385	(c)
	February–	12.96	49.9	1.8	8.5		
	March	18.20	3.3	2.0	8.7		
ε Leo	1966	9.97	346	19	16.2	4385	(c)
	March–	45.5	140	22	12.7		
	April	55.0	40	14	27.9		
β Cru	1966	9.97	211	10	11.7	4430	(d)
	April	91.2	49	7.5	22.9		
α Pav	1966	9.97	248	15	20.6	4430	(d)
	August	32.7	177	18	15.4		
		82.5	67	12	38.2		
		100.0	19	36	3.5		
γ Ori	1966	9.97	164.0	9.6	15.6	4430	(e)
	November	82.5	48.7	7.3	28.6		
ε Ori	1966	9.97	138.2	9.5	17.7	4430	(e)
	December	99.8	26.2	6.4	38.3		
α CMa	1967	9.56	59.8	1.1	8.6	4430	(e)
	January	12.93	24.6	1.1	11.4		
ε CMa	1967	9.97	142.5	9.1	17.6	4430	(e)
	January	67.5	60.4	6.5	42.7		
α CMi	1967	9.51	72.2	6.3	13.9	4430	(e)
	February	15.40	16.7	3.5	40.4	4430	(e)

* $\overline{c_N(d)}$ is the normalized, weighted mean correlation from the star in arbitrary units for a reflector separation d . All the observations have been reduced to the same standard interval. σ is the r.m.s. uncertainty in $\overline{c_N(d)}$.

† $\overline{c_N(d)}$ is in arbitrary units which depend on the parameters of the equipment in use the time. Over the period covered by the observations several modifications were made to the equipment which altered the scale of $\overline{c_N(d)}$ (see Section 6). There were five principal configurations of the equipment which are shown by the letters (a)–(e) in column 8. These letters correspond to the use of the following major components:

- (a) R.C.A. type 7046 phototubes, 4385 ± 40 Å filters.
- (b) R.C.A. type 7046 phototubes, 4608 ± 150 Å filters.
- (c) R.C.A. type dev. C31011 phototubes, 4385 ± 40 Å filters. Mark I transistorized multiplier.
- (d) R.C.A. type dev. C31011 phototubes, 4430 ± 50 Å filters.
- (e) R.C.A. type 8575 phototubes, 4430 ± 50 Å filters. Mark II transistorized multiplier.

higher accuracy. Within the quoted uncertainties of the measurements there is satisfactory agreement between the independent determinations of angular diameter.

7.1 *Angular diameters of equivalent uniform discs.* The values of θ_{UD} given in column 9 of Table II are the angular diameters of the equivalent uniform discs for each set of observations; the values of $\bar{\theta}_{UD}$ in column 11 give the weighted mean of all the sets of observations for each star on the assumption that the angular diameter is independent of wavelength over the range 4385–4608 Å. The associated

TABLE II
The angular diameters of the equivalent uniform discs for 15 stars

1	2	3	4	5	6	7	8	9	10	11	12
Star	Year	Wave-length (Å)	$C \pm \sigma$ (Arbitrary units)		$C_N \pm \sigma$ (Normalized)		Δ_λ	$\theta_{UD} \pm \sigma$ (10^{-3} seconds of arc)		$\bar{\theta}_{UD} \pm \sigma$ (10^{-3} seconds of arc)	
β Cru	1965	4385	276	13	0.87	0.04	0.998	0.689	0.033		
	1966	4430	215	12	0.93	0.07	0.998	0.726	0.038	0.705	0.025
γ Ori	1966	4430	167	11	1.11	0.12	0.998	0.74	0.05	0.74	0.05
ϵ CMa	1967	4430	145	10	0.96	0.11	0.998	0.78	0.04	0.78	0.05
α Pav	1966	4430	241	16	1.06	0.09	0.998	0.77	0.06	0.77	0.06
ϵ Ori	1966	4430	140	11	0.93	0.11	0.998	0.70	0.05	0.70	0.05
α Eri	1964	4385	521	49	—	—	0.988	2.01	0.18		
	1965	4385	319	16	0.98	0.05	0.990	1.83	0.08	1.86	0.07
α Gru	1964	4608	119	19	1.03	0.17	0.997	0.97	0.20		
	1965	4385	374	32	1.13	0.10	0.997	0.98	0.07	0.98	0.07
α Leo	1966	4385	373	23	1.12	0.07	0.994	1.33	0.07	1.33	0.07
β Ori	1965	4385	318	24	0.99	0.08	0.980	2.57	0.14	2.57	0.14
α CMa	1966	4385	385	17	1.10	0.05	0.901	5.83	0.13		
	1967	4430	187	10	1.24	0.12	0.900	5.87	0.16	5.85	0.10
α Lyr	1963	4385	544	103	—	—	0.961	3.56	0.40		
	1965	4385	367	21	1.05	0.06	0.968	3.26	0.16	3.31	0.15
α PsA	1964	4608	103	16	0.89	0.14	0.990	1.65	0.28		
	1965	4385	373	31	1.08	0.09	0.987	2.07	0.15	1.98	0.13
α Car	1965	4385	345	55	1.08	0.17	0.880	6.48	0.39	6.48	0.39
α Aql	1964	4608	124	22	1.08	0.19	0.973	2.98	0.43		
	1965	4385	317	18	0.96	0.06	0.976	2.77	0.15	2.79	0.14
α CMi	1967	4430	182	28	1.21	0.21	0.917	5.31	0.36	5.31	0.36

r.m.s. uncertainties ($\pm \sigma$) are largely determined by the uncertainties in the corresponding values of $\overline{c_N(d)}$ given in Table I which are themselves due to statistical fluctuations in the correlator output. But they also include the uncertainty in the zero of the correlation which varies with the brightness of the star (Fig. 2 and Section 5.1), the small (± 1 per cent) uncertainty due to differential delays (Section 3.3) and the small uncertainties in the normalizing factors for the photomultiplier anode currents (± 1 per cent) and correlator gain ($\pm 1\frac{1}{2}$ per cent) as discussed in Section 3.3. In estimating the overall uncertainty ($\pm \sigma$) these contributions have been taken as random and statistically independent.

7.2 *Zero-baseline correlation.* The values of C in column 4 of Table II give the zero-baseline correlation for the curve of best fit corrected for partial resolution so that

$$C = \overline{c_N(0)}/\Delta_\lambda \quad (20)$$

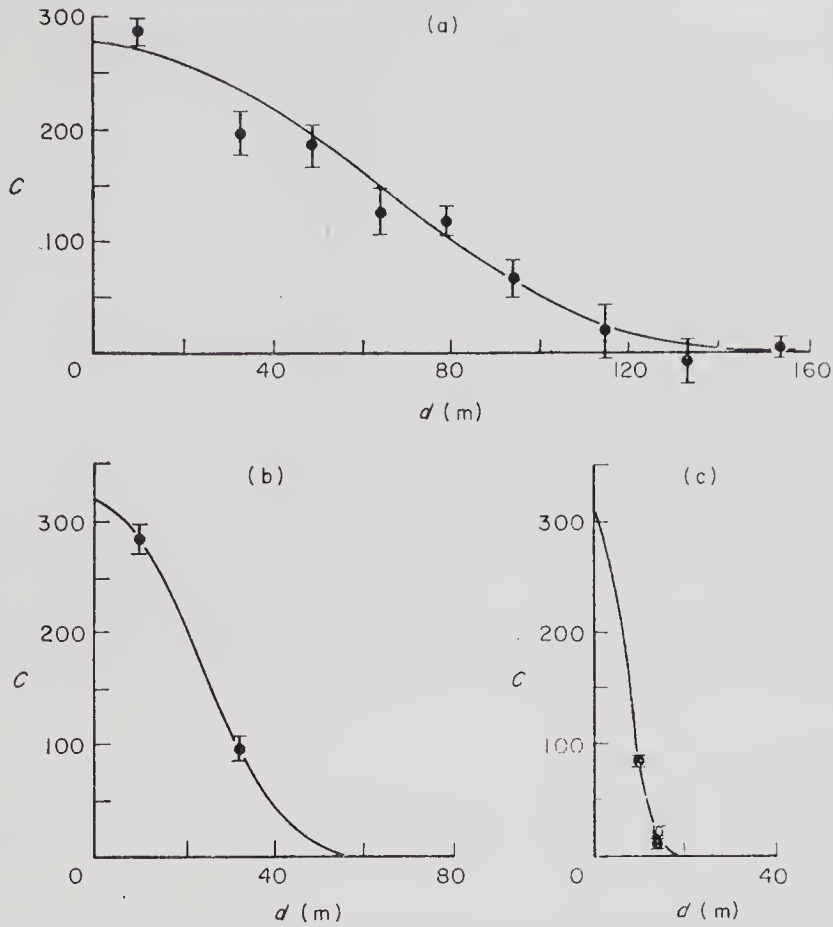


FIG. 3. Examples of the observed variation of correlation with baseline for three stars. (a) β Cru (1965); (b) α Eri (1965); (c) α Car (1965).

where Δ_λ is the partial resolution factor corresponding to θ_{UD} and is shown in column 8. For each set of observations the value of C is expressed in the same arbitrary units as the associated values of $\overline{c_N(d)}$ in Table I, and they *can only be used* in conjunction with that table. It is however, of considerable value in the detection of binaries to compare the values of C for different stars; but, before this can be done, they must all be reduced to the same scale as discussed in the following paragraphs.

The longest series of observations without a change in the equipment was made between May 1965 and April 1966 during which 10 stars were measured. Examination of the values of C obtained during this period reveals a large scatter in the data with the values for main sequence stars of spectral type A being consistently high. This phenomenon is due to an unfortunate first choice of optical filter characteristics. These filters have a bandwidth of 80 Å centred on a wavelength of 4385 Å and their central wavelength is sufficiently close to the H_γ line of the Balmer series of hydrogen for the long wavelength wing of the line profile to extend into the filter bandwidth for A and late B type stars. Thus the spectral distribution of the light reaching the photocathodes is changed and the parameters σ and B_0 (see equation (2), Paper I) vary from star to star as a function of the H_γ profile. An analysis shows that the effect of H_γ is to increase the normalized correlation $\overline{c_N(d)}$, and that this increase reaches a maximum of about 9 per cent for A0V stars and falls to about 2 per cent for types F0V and B5V. Correction of the 1965-6

data was therefore carried out by calculating the effect of $H\gamma$ for each star and by adjusting the values of C in Table II to remove these effects.

In addition the values of C must be adjusted to take account of the modifications to the equipment. This cannot be done for stars observed in 1963 and 1964 with the equipment configuration (a) in Table I, because the necessary scaling factors were not measured. However, the other observations can be reduced to the same scale by means of factors derived from special 'transfer' observations of α Eri made at a short baseline both before and after the modifications were carried out. The observations made after April 1966 (configurations (d) and (e)) do not need correction for the effects of $H\gamma$ because they were carried out with optical filters with a bandwidth of 100 Å centred on 4430 Å. The final values of C , corrected for $H\gamma$ and adjusted to the same scale, are shown as C_N in column 6 of Table II; for convenience they have been normalized to a mean value of unity.

It is to be expected that for single stars the values of C_N will not depart significantly from unity, and this condition is satisfied by the 15 stars in the Table. The average uncertainty in a single value of C_N is about ± 9 per cent and we have therefore adopted the rough criterion, stated in Section 5.2, that a star is rejected from our list as being a possible binary if the zero-baseline correlation is less than 80 per cent of the mean value shown by single stars.

7.3 Notes on individual stars

α Leo. This star is rotating very rapidly and has a value of 350 km s^{-1} for $v \sin i$ where v is the equatorial velocity and i is the angle between the equatorial plane of the star and the sky plane. The very high value of $v \sin i$ implies that α Leo must be seen nearly equator-on.

The observations at three baselines each covered 90° in the position angle of the star. Hence the measured angular diameter will be an average value lying somewhere between that of the mean equivalent uniform disc and a value 6-7 per cent larger which corresponds to the extreme case discussed in Section 5.3. In view of this uncertainty, the measured angular diameter has not been corrected for the effects of rotation. This must be borne in mind in any discussion of the implications of the measured angular diameter of α Leo.

α CMa. The two measurements of α CMa given in Table II were independent and made with comparable sensitivity. The agreement obtained between the two results is excellent (< 0.7 per cent difference) and it should be noted that several major changes were made to the equipment between the two sets of observations. These changes included the installation of new optical filters, new photomultipliers and a new multiplier in the correlator.

The present mean result is apparently in poor agreement with the original measurement by Hanbury Brown & Twiss (4), and gives a value for the angular diameter of the equivalent uniform disc which is lower by 14 per cent. The r.m.s. uncertainty of the earlier result was estimated to be ± 11 per cent (5) but a least-squares fit carried out with the computer programme used for the present data shows that the uncertainty due to statistical errors alone was ± 18 per cent. In the light of this revised figure we can conclude that the difference between the two series of measurements is not significant. Inclusion of the 1955 value for the angular diameter of α CMa in the weighted mean value given in Table II would not change the latter appreciably because of the very low weight of the earlier value.

α Lyr. The 1963 measurement of α Lyr was published in a preliminary note (6) with an estimated r.m.s. uncertainty of ± 8 per cent. A subsequent computer fit to the data shows that this estimate was optimistic and that the accuracy is only ± 11 per cent.

α Aql. This star is rotating rapidly with $v \sin i$ equal to 240 km s^{-1} . The observations for this star covered a range of 90° in position angle for each baseline so that the measured angular diameter will be an average value as for α Leo. In this case, however, the measured angular diameter may be increased by rotation by up to 4 per cent (Section 5.3). The measured angular diameter has not been corrected for the effects of rotation.

8. *Interpretation of results.* A knowledge of the angular diameter and the absolute monochromatic flux received from a star (f_λ) allows the absolute monochromatic flux at the surface of the star (F_λ) to be calculated. F_λ is an important parameter of the stellar surface and provides a valuable observational check on the theoretical models of stellar atmospheres.

Since F_λ is a function of the effective temperature of the stellar atmosphere it is possible to use the data to derive a scale of effective temperatures for stars of early spectral type. The linear diameters of stars of known parallax may also be found.

Table III contains a list of the 15 stars which have been measured, and gives the photometric data, angular diameters, fluxes and temperatures. A detailed discussion of the data in the table is given in the following sections.

8.1 *Angular diameters.* The true angular diameter θ_{LD} of a star is related to the angular diameter of the equivalent uniform disc θ_{UD} by a limb darkening law. A cosine law has been adopted here and, as discussed by Hanbury Brown & Twiss (2), this leads to the relationship

$$\frac{\theta_{LD}}{\theta_{UD}} = \left[\frac{1 - U_\lambda/3}{1 - 7U_\lambda/15} \right]^{1/2} \quad (21)$$

where U_λ is the limb darkening coefficient.

A wavelength of 4425 \AA has been chosen, for reasons given in Section 8.2, and the values of U_{4425} (except for α CMi) have been obtained from the model atmosphere data given by Grygar (10) and Gingerich (11). Grygar lists limb darkening coefficients which are cosine approximations to the actual law given by the models of various authors, and we have made similar approximations to the data given by Gingerich. The values of U_{4425} listed in Table III have been obtained from a smooth curve drawn through the interpolated values at 4425 \AA plotted against B-V. The value of U_{4425} for α CMi has been derived from the model atmospheres calculated for this star by Edmonds (12).

The correction applied to θ_{UD} to give θ_{LD} is small, with an average value $\theta_{LD}/\theta_{UD} = 1.045$, and is relatively insensitive to changes in the limb darkening coefficient. For example, an uncertainty of ± 20 per cent in U_{4425} leads, on the average, to an uncertainty of only ± 0.5 per cent in θ_{LD} . Any error introduced in correcting from θ_{UD} to θ_{LD} is therefore small compared with the observational uncertainty for main sequence stars. However, for supergiants the cosine law may be a poor approximation, particularly in the case of α Car, and some additional

TABLE III
The angular diameters, monochromatic absolute fluxes and effective temperatures for 15 stars

1	2	3	4	5	6	7	8	9	10	11	12	13	14
B.S.	Name	Sp.	Lum.	B	B-V	U-B	$\theta_{UD} \pm \sigma$ (10^{-3} seconds of arc)	U_{4425}	$\theta_{LD} \pm \sigma$ (10^{-3} seconds of arc)	f_{4425} (10^{-11} erg $cm^{-2} s^{-1} \text{Å}^{-1}$)	$F_{4425} \pm \sigma$ (10^6 erg $cm^{-2} s^{-1} \text{Å}^{-1}$)	$T_{4425} \pm \sigma$ (°K)	$T_e \pm \sigma$ (°K)
4853	β Cru	B0.5	IV	+1.02	-0.23	-0.98	0.705	0.40	0.728	240	770	24 100	26 600
1790	γ Ori	B2	III	+1.42	-0.22	-0.88	0.74	0.41	0.76	166	490	19 100	21 000
2618	ϵ CMa	B2	II	+1.29	-0.21	-0.92	0.78	0.42	0.81	188	490	19 100	21 000
7790	α Pav	B3	IV	+1.74	-0.20	-0.71	0.77	0.42	0.80	124	330	15 900	17 100
1903	ϵ Ori	B0	Ia	+1.51	-0.18	-1.03	0.70	0.43	0.72	151	495	19 200	21 100
472	α Eri	B5	IV	+0.32*	-0.15	-0.67*	1.86	0.45	1.93	471	214	13 400	14 000
8425	α Gru	B5	V	+1.61	-0.13	-0.47	0.98	0.46	1.02	144	235	13 900	14 600
3982	α Leo	B7	V	+1.24	-0.11	-0.36	1.33	0.47	1.38	205	184	12 700	13 000
1713	β Ori	B8	Ia	+0.10	-0.03	-0.65	2.57	0.52	2.69	576	135	11 400	11 200
2491	α CMa	A1	V	-1.46	0.00	-0.04	5.85	0.54	6.12	2560	116	10 850	10 380
7001	α Lyr	A0	V	+0.03	0.00	0.00	3.31	0.54	3.47	647	91	10 050	9500
8728	α PsA	A3	V	+1.25	+0.09	+0.06	1.98	0.59	2.09	219	85	9850	400
2326	α Car	F0	Ib-II	-0.60	+0.15	+0.04*	6.48	0.63	6.86	1120	41.1	8150	7510
7557	α Aql	A7	IV, V	+0.98	+0.22	+0.08	2.79	0.67	2.97	275	53.1	8650	250
2943	α CMi	F5	IV-V.	+0.79	+0.42	+0.03	5.31	0.76	5.71	327	17.1	6700	200

Column

- 1. Number of star in the *Catalogue of Bright Stars* (7);
- 2. Name of star;
- 3.† Spectral type;
- 4.† Luminosity class;
- 5-7.† Photometric data;
- 8.† Angular diameter of equivalent uniform disc (from Table II);
- 9. Assumed limb darkening coefficient;
- 10.† Angular diameter of star (limb darkened);
- 11. Flux received from star outside the Earth's atmosphere at a wavelength of 4425 Å;
- 12.† Flux at the surface of star at a wavelength of 4425 Å;
- 13.† Brightness temperature at a wavelength of 4425 Å;
- 14.† Effective temperature.

* Values for α Eri and α Car not listed by Johnson *et al.*; they are from *Photometric Observations of 244 Bright Stars*, by Hogg (9).

† From *UBVRJKL Photometry of Bright Stars* by Johnson, Mitchell, Iriarte & Wisniewski (8).

‡ In each case σ is the associated r.m.s. uncertainty.

uncertainty may be present in θ_{LD} ; we have not made any allowance for it in Table III.

8.2 *Absolute monochromatic fluxes.* The absolute monochromatic flux at the surface of a star (F_λ) is related to the absolute monochromatic flux received outside the Earth's atmosphere (f_λ) by

$$F_\lambda = \frac{4f_\lambda}{\theta_{LD}^2} \quad (22)$$

The values of f_λ in Table III have been derived from the comprehensive table of absolute monochromatic fluxes published by Willstrop (13) and the V magnitudes of Johnson *et al.* (8). The primary source of uncertainty in Willstrop's data lies in the absolute calibration (14) rather than in the relative spectral energy measurements (13) and it follows that the uncertainty in his *absolute* fluxes varies very little over the wavelength range from 4000 Å to 6000 Å. We have therefore chosen a wavelength of 4425 Å, as close as possible to that at which the angular diameter measurements were made, in order to calculate F_λ in equation (22); a wavelength of 4425 Å has been selected, rather than 4400 Å, so that the fluxes are completely free from the effects of the long wavelength wing of the $H\gamma$ line.

The values of f_{4425} in Willstrop's table (given for $V = 0.00$) form a fairly smooth function of $B-V$ for luminosity classes II–V inclusive. Main sequence stars show an r.m.s. scatter of the order of ± 1 per cent in f_{4425} for a given $B-V$, while stars of higher luminosity show a slightly greater scatter although the data are fewer. Since α Eri and α PsA were measured by Willstrop, the values of f_{4425} for these stars have been taken directly from his table. For the remaining stars in Table III (including α Car), except for two luminous supergiants ϵ Ori and β Ori, the values of f_{4425} have been obtained from a plot of f_{4425} against $B-V$. The overall uncertainty in these absolute values is in the range 3 to 3.5 per cent depending on the luminosity class. Reduction of the values of f_{4425} from $V = 0.00$ has been achieved using the V magnitudes of Johnson *et al.* (8).

There are no luminous supergiants comparable with ϵ Ori and β Ori in Willstrop's list although the indications are that their fluxes at 4425 Å are lower than for main sequence stars with the same $B-V$. Monochromatic magnitudes (m_λ) relative to m_{5556} have been given by Oke (15) for ϵ Ori and by Code (16) for β Ori. The values of ($m_{4425} - m_{5556}$) have been interpolated from these data for the two stars. Willstrop's fluxes are normalized to $V = 0.00$ and inspection of his data shows that the scatter in f_{5556} is very small (~ 1 per cent) for a given $B-V$ and almost independent of the luminosity class. We have therefore taken the mean values of f_{5556} corresponding to the $B-V$ of ϵ Ori and β Ori from his data and converted them to the required wavelength (f_{4425}) by the appropriate values of ($m_{4425} - m_{5556}$). The uncertainty in the final values of f_{4425} found in this way is less than ± 3.5 per cent and is comparable with that for the main sequence stars.

The values of F_{4425} calculated from equation (22) are shown in Table III together with their uncertainties σ . The values of σ have been calculated on the assumption that the stars in the list are single. Although we have taken great care to avoid binary stars, as already discussed in Section 5.2, it cannot be excluded that some of the stars in our list are unsuspected close binaries with companions fainter by at least 2.2 magnitudes. Briefly, in the most general case, the interferometer measures the angular diameter of the primary component, while the light flux f_λ is the total light from both components. Thus, in the worst possible case, where the star has a companion which is 2.2 magnitudes fainter, the value of F_λ could

be as much as 13 per cent too high. On the other hand the average value of this error, taken over many stars, is certainly very much lower and we estimate that it is small compared with the observational errors. The values of the uncertainty in F_{4425} shown in the table are therefore wholly observational; they are the combined uncertainties in the measured values of the angular diameter (θ_{LD}) as shown in column 10, and the uncertainties in the measured flux (f_{4425}) which we have discussed above.

For convenience the values of F_{4425} have also been expressed as brightness temperatures (T_{4425}), and are shown in column 13 of the table.

In Fig. 4 the values of F_{4425} are plotted against $B-V$ together with the value for the Sun (17). It should be stressed that the values of F_{4425} presented here are fundamental; apart from a minor correction for limb darkening, they are independent of theoretical model stellar atmospheres, and depend only on the measurements of angular diameter and absolute flux.

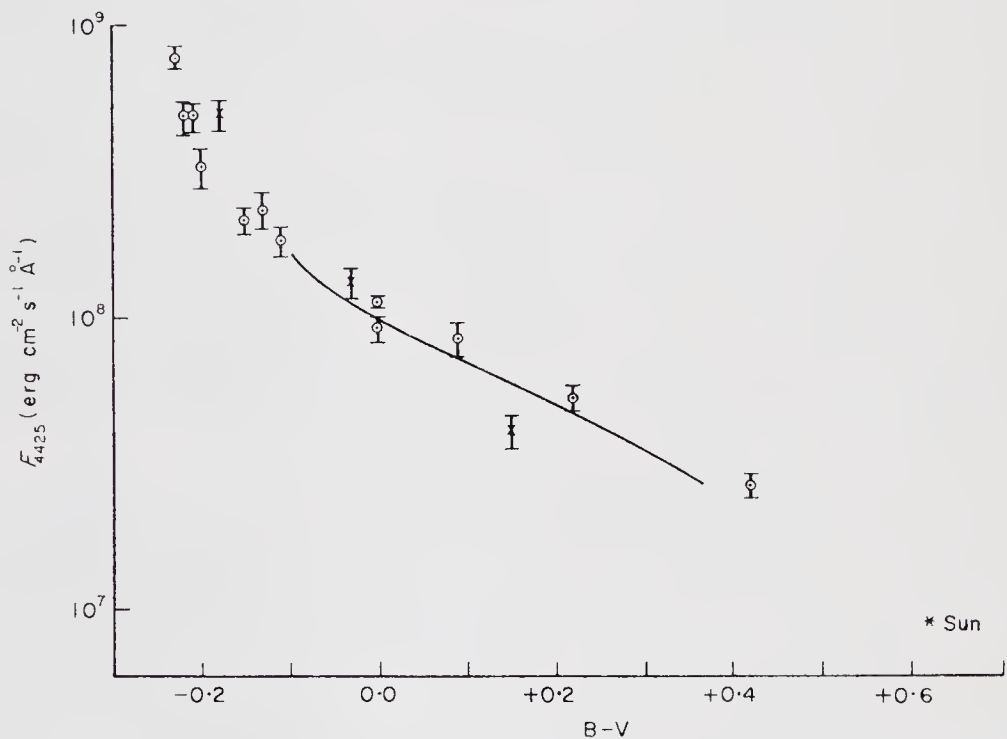


FIG. 4. The absolute monochromatic fluxes at the surfaces of 16 stars including the Sun. ○ Luminosity classes II-V, × Luminosity class I, — Mihalas' line blanketed models.

It is interesting to compare these values of F_{4425} with the Balmer-line blanketed model atmospheres computed by Mihalas (18) which represent the most advanced models available at present. Mihalas has derived $B-V$ values for the models corresponding most closely to main sequence stars ($\log g = 4$) and, in addition to accounting for the effects of the Balmer lines, he has included corrections to $B-V$ for metal-line blanketing. The relationship between F_{4425} and $B-V$ for his models with $\log g = 4$ is shown, together with our observational data, in Fig. 4. It can be seen that the theoretical curve is in reasonable agreement with our observational data. For the supergiant α Car ($B-V = +0.15$) the observed flux is significantly below the results for main sequence stars, but this difference is predicted by the corresponding models for lower surface gravities.

Although it is to be expected that theoretical models will be improved by the inclusion of non-LTE effects, Fig. 4 shows that there is already close agreement between the line blanketed LTE models and observation. This agreement justifies our use of Mihalas' models in the next section to estimate the effective temperatures of the stars.

8.3 *Effective temperatures.* The effective temperature (T_e) of a stellar atmosphere is defined by

$$\int_0^{\infty} F_{\lambda} d\lambda = \sigma T_e^4 \quad (23)$$

where σ is Stefan's constant.

Equation (23) implies that the absolute flux distribution throughout the spectrum must be known in order to determine T_e . Unfortunately, for the relatively hot stars measured by the intensity interferometer, much of the energy is in the ultraviolet region of the spectrum and is absorbed by the Earth's atmosphere. For stars cooler than about 9000°K a sufficient fraction of the energy reaches the Earth for a bolometric magnitude to be determined with reasonable precision. This allows the effective temperatures to be found from the angular diameters by comparison with the known parameters of the Sun. On the other hand, for stars hotter than about 9000°K, it is necessary to resort to model atmospheres which predict the absolute spectral energy distribution as a function of effective temperature.

Grids of model atmospheres covering a range of effective temperature and surface gravity have been published by Mihalas (18), (19) and by Strom & Avrett (20). Given F_{λ} , and assuming a value for the surface gravity, it is possible to interpolate in these grids to obtain the corresponding value of T_e . It is important to appreciate that, apart from the uncertainty in F_{λ} , the value of T_e obtained in this manner is only as good as the model. If the relative energy distribution given by the model is incorrect, then T_e will be in error. Only the later models of Mihalas (18) include the significant effects of line blanketing and, following the discussion in Section 8.2, they will be used in conjunction with the present results.

The effective temperature range from 7200°K to 12 500°K is covered by Mihalas' grid of models with $\log g = 4$. In addition Mihalas & Morton (21) have published a line blanketed model with $\log g = 4$ and $T_e = 21\ 914^{\circ}\text{K}$, Adams & Morton (22) a line blanketed model with $\log g = 4$ and $T_e = 16\ 800^{\circ}\text{K}$, and Hickok & Morton (23) line blanketed models with $\log g = 4$ and $T_e = 28\ 640^{\circ}\text{K}$ and $37\ 450^{\circ}\text{K}$. The effective temperatures of 12 of the stars in Table III have been obtained from these models. For stars hotter than 12 500°K there is some uncertainty in the interpolation of the model data. This has been taken into account in the r.m.s. uncertainties given with the effective temperatures in Table III, although the major source of uncertainty is still in the angular diameter measurements.

The effective temperatures of the remaining 3 stars in Table III have been found as follows. For β Ori and α Car a value of $\log g = 2.5$ has been adopted (17) and an interpolation between the Mihalas line blanketed models for $\log g = 3$ and $\log g = 2$ has been made. In the case of α CMi, which is appreciably cooler than Mihalas' models, interpolation has been made between the models published by Edmonds (12). These models have effective temperatures of 6385°K and 6685°K and were constructed specifically for α CMi. Since we have used a fixed wavelength

(4425 Å) in computing the values of F_λ , the relative accuracy of the effective temperatures derived from the models will be a function of temperature. Thus, although the total flux varies as T_e^4 , the monochromatic flux varies as T_e^n where n decreases with increasing T_e . For example, considering the line blanketed models, $n = 5$ for $T_e \sim 7800^\circ\text{K}$ and decreases to $n = 2$ for $T_e \sim 20\,000^\circ\text{K}$. Thus, in comparing the accuracies of the angular diameters with those of the temperatures in Table III, this must be borne in mind, and is the explanation for the relatively greater accuracy of the lower temperatures.

A check on the effective temperatures determined from the models can be carried out by comparison with the Sun for the two relatively cool stars, namely α Aql and α CMi, for which bolometric corrections (B.C.) are known with reasonable precision. In determining the effective temperatures from the bolometric corrections, the following data were assumed: for the Sun, $\theta_{\text{LD}} = 1919$ sec of arc, $V = -26.78$, B.C. = -0.07 , and $T_e = 5800^\circ\text{K}$; for the stars, the angular diameters and V magnitudes as given in Table III. The bolometric corrections assumed for the stars (24) are given in Table IV together with the effective temperatures derived from them. For comparison, the table includes the effective temperatures determined for these stars from the models of Mihalas and Edmonds. The agreement between the effective temperatures obtained by the two methods for these cooler stars is good and this fact increases confidence in the use of the models to obtain effective temperatures. It is important to note that although the measured angular diameter of α Aql may be affected by rotation (Section 7.3) this would not invalidate the comparison of effective temperatures determined from the models and from the bolometric corrections. The value of F_{4425} is closely proportional to T_e^4 for α Aql and so for both methods $T_e \propto \theta_{\text{LD}}^{-1/2}$ and any error in θ_{LD} will affect both determinations of T_e by the same amount and in the same sense.

TABLE IV

A comparison of the effective temperatures derived from bolometric corrections and from models for two stars

Star	Spectral type	Luminosity class	$B-V$	Bolometric correction	$T_e \pm \sigma$ ($^\circ\text{K}$)	
					from B.C.	from models
α Aql	A ₇	IV, V	+0.22	-0.11	8290 210	8250 180
α CMi	F ₅	IV-V	+0.42	-0.03	6420 220	6450 190

A further check is afforded by the value of T_e for α Lyr deduced by Mihalas (18) who compared the observed energy distribution and H γ profile with his models. He found good agreement with $T_e = 9600^\circ\text{K}$ and $\log g = 4$. This result agrees well with the temperature of α Lyr ($9500 \pm 300^\circ\text{K}$) shown in Table III.

The effective temperatures of α Lyr and α CMa in Table III require some comment. The temperature of α Lyr (9500°K) is higher than the value (9200°K) given by Hanbury Brown, Hazard, Davis & Allen (6) in 1963. This increase corresponds to the difference between the angular diameter given in Table III ($3''.47 \times 10^{-3}$) and the preliminary value ($3''.7 \times 10^{-3}$) used in their calculations. The temperature of α CMa ($10\,380^\circ\text{K}$) is substantially higher than the value (9400°K) quoted by Hanbury Brown *et al.* (6). Again the angular diameter given in Table III is $6''.12 \times 10^{-3}$ as compared with the earlier value of $7''.1 \times 10^{-3}$ (5)

used in their calculations. The large increase of 10 per cent in the temperature of α CMa, due to a decrease of only 14 per cent in the angular size, is explained by the rapid rate of change of T_e with F_{4425} in this temperature range as already noted above. It should be noted that the precision of both these earlier measurements was over-estimated as discussed in Section 7.3.

Recently, Strom, Gingerich & Strom (25) have also made a study of α CMa and α Lyr in connection with their model atmospheres. These authors conclude that the effective temperature of both stars is $9000 \pm 500^\circ\text{K}$ which is substantially lower than the values in Table III. The monochromatic fluxes at 4425 \AA , predicted by their models for various values of surface gravity and chemical composition, all lie within 4 per cent of the flux predicted by Mihalas' line blanketed models at a given effective temperature. Therefore, if the models of Strom *et al.* are used in conjunction with the empirical fluxes in Table III to find effective temperatures, the results obtained agree within about 1 per cent of those in Table III from Mihalas' models. It follows that their estimates of effective temperature are not compatible with the observed fluxes. Furthermore, the smaller Balmer discontinuity observed for α CMa can be explained, at least partially, by the higher effective temperature of this star compared to α Lyr, and the discrepancy found by the above authors between theory and the earlier directly determined effective temperatures (6) is removed. The higher metal abundance of α CMa found by Strom *et al.* (25) would explain why α CMa (A₁ V) has a later spectral classification than α Lyr (A₀ V) in spite of its higher effective temperature.

Fig. 5 shows the values of T_e plotted against $B-V$. It can be seen that, with the exception of the two supergiants ϵ Ori and α Car, the results lie on a smooth curve. We have therefore excluded the three supergiants (ϵ Ori, β Ori, α Car) and

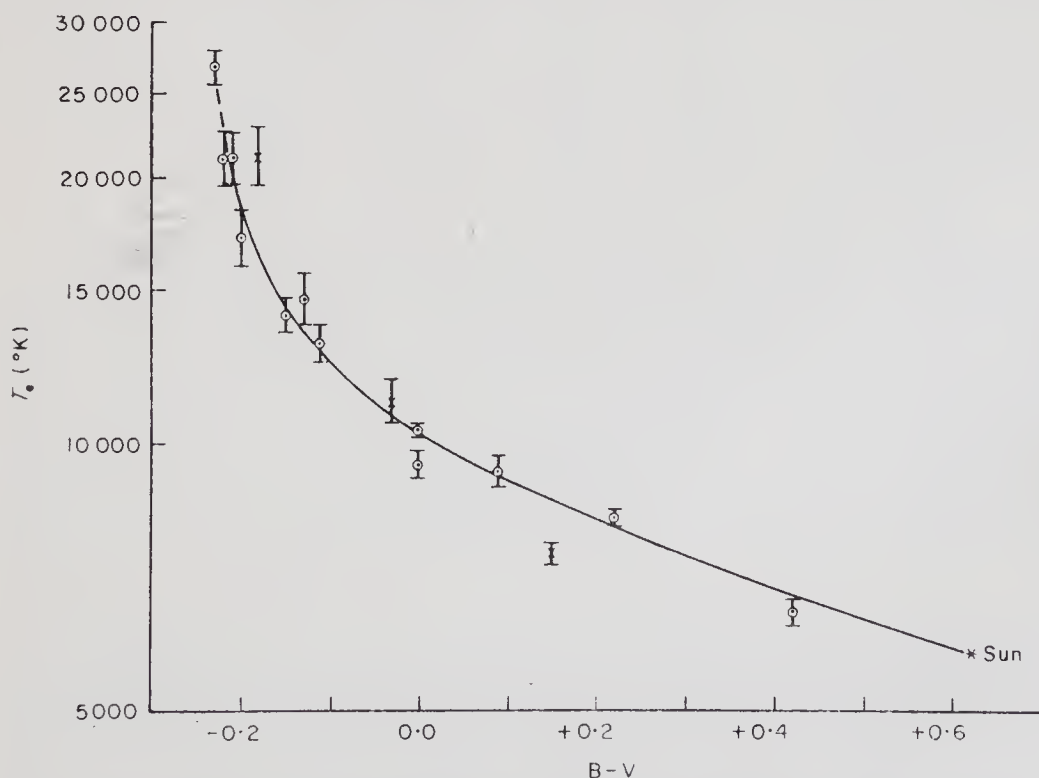


FIG. 5. The effective temperatures of 16 stars including the Sun. \odot Luminosity classes II-V, \times Luminosity class I, — Curve fitted to data for luminosity classes II-V (see text).

fitted a curve to the remaining 12 stars and the Sun (17); the curve was approximated by three overlapping quadratic expressions and was fitted to the data by the method of least-squares using a computer. Thus, the curve in Fig. 5 represents the scale of effective temperature for stars, excluding supergiants, in the spectral range B0 to G2, as determined from our measurements of angular diameter, Willstrop's flux measurements and the line blanketed model atmospheres (18),

TABLE V

The scale of effective temperature derived from the measurements of angular diameter

<i>B-V</i>	T_e (°K)	<i>B-V</i>	T_e (°K)
-0.23	(26600)	+0.10	9100
-0.22	22900	+0.15	8650
-0.20	18600	+0.20	8250
-0.15	14250	+0.25	7850
-0.10	12400	+0.30	7500
-0.05	11150	+0.40	6850
0.00	10250	+0.50	6325
+0.05	9600	+0.60	5875

(21)-(23). For convenience we have also given this temperature scale in numerical form in Table V. Above 21 000°K the scale is based on only one star (β Cru) and must be regarded as tentative. This is indicated by the broken section at the high temperature end of the curve in Fig. 5.

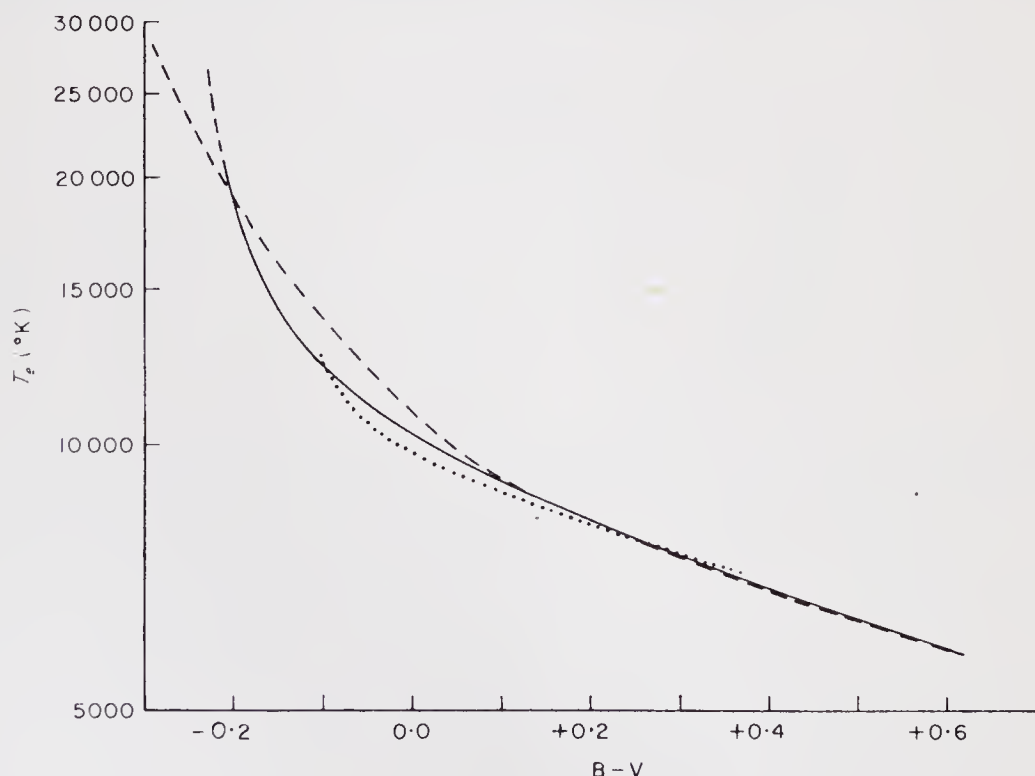


FIG. 6. A comparison of three scales of effective temperature. — The scale derived in this paper, - - - Harris (26), ····· Mihalas (18).

A comparison of the effective temperature scale given in Table V with the scales published by Harris (26) and Mihalas (18) is shown in Fig. 6. For $B-V > +0.10$ the new scale is in good agreement with Harris' scale but for $+0.10 > B-V > -0.20$ Harris' scale is apparently too high with a maximum difference of about 1600°K at $B-V = -0.12$. On the other hand, for $B-V < -0.20$, Harris' scale is too low and departs from the curve presented here. We believe that the new scale derived from the angular diameter results represents an improvement over Harris' effective temperature scale. It is interesting to note that μ_1 Sco, the star used by Harris as the only observational point for $T_e > 10\,500^\circ\text{K}$, lies much closer to the new curve than to Harris' curve. However, as Harris pointed out, the temperature of $27\,500^\circ\text{K}$ ($B-V = -0.22$) for μ_1 Sco must be regarded 'as very uncertain because of the critical dependence of the calculated value on the parallax used in the reduction'. The theoretically based curve computed by Mihalas covers only part of the range in $B-V$ and, as might be expected, shows better agreement on average with the revised scale than with Harris' scale.

8.4 *Stellar diameters.* The linear diameter of a star can be found from its angular diameter if the parallax is known. Six of the stars in Table III have parallaxes which are known to better than ± 30 per cent (27), (28). These six stars are listed in Table VI with their radii expressed in terms of the solar radius. Clearly there are too few stars in the table to establish the general run of stellar radii for main sequence stars.

TABLE VI
The radii of six stars

Star	Parallax $\pm \sigma$		Radius $\pm \sigma$	
	(seconds of arc)		(Sun = 1)	
α Leo	0.039	0.010	3.8	1.0
α CMa	0.374	0.006	1.76	0.04
α Lyr	0.123	0.007	3.03	0.22
α PsA	0.144	0.010	1.56	0.15
α Aql	0.194	0.006	1.65	0.10
α CMi	0.283	0.006	2.17	0.15

It is interesting to note that, from the radii given in Table VI and the temperatures in Table III, α Lyr is 1.7 times larger and 0.8 magnitudes (bolometric) more luminous than α CMa. As an explanation it has been suggested by Petrie (29) that α Lyr may be a double star with two components of comparable brightness. If this explanation is correct, then it is to be expected that the normalized zero baseline correlation C_N would be significantly less than unity. But reference to Table II shows that $C_N = 1.05 \pm 0.06$, and it follows that the star appears as a single object and than any secondary component is at least 3 magnitudes fainter than the primary.

9. *Conclusions.* The first observational programme of the stellar intensity interferometer has yielded measurements of the angular diameters of 15 stars of spectral type B0 to F5. By combining these results with photometric data we have derived the absolute monochromatic fluxes (F_{4425}) at the surfaces of the stars. If these empirical values of F_{4425} are used to provide an absolute calibration of observed relative spectral energy distributions then the *absolute* spectral energy

distributions at the surfaces of the stars, and hence their effective temperatures, can be found.

At the present time reliable relative energy distributions are only available for wavelengths $> 3400 \text{ \AA}$. Since much of the energy emitted by the hot stars observed in the present programme lies in the UV region of the spectrum and is absorbed by the Earth's atmosphere, only a very limited section of the total spectral energy curve is available to us for these stars. For this reason it is necessary to adopt the relative energy distributions predicted by theoretical models for stars hotter than about 9000°K , until such time as reliable measurements are made in the UV from above the Earth's atmosphere. For the 15 stars measured by the interferometer, 12 of which are hotter than 9000°K , we have therefore used our results to calibrate theoretical models and to derive values of the effective temperature. Excluding the three supergiants in our list, we have derived a scale of effective temperature for the remaining stars over the spectral range B0 to G2. We believe that this scale, because it is based on the empirical fluxes (F_{4425}) for 12 stars and on line blanketed models, represents an improvement over previous scales. It seems likely that any substantial improvement of this scale must depend upon making observations of the early-type stars from above the Earth's atmosphere.

Acknowledgments. The observational programme of the interferometer has been supported by the Air Force Office of Scientific Research (Office of Aerospace Research) of the United States Air Force under grants (AF-AFOSR-302-63/66), the Australian Research Grants Committee, the Research Grants Committee of the University of Sydney and the Science Foundation for Research in Physics within the University of Sydney. We thank Professor H. Messel for his support in running the project and Mr R. K. Outhred for his assistance with the observational programme. We are indebted to Dr D. M. Popper for his contributions to the methods of analysis of the interferometer data and for helping to make some of the observations during an extended visit to Sydney and Narrabri in 1965.

*Cornell-Sydney University Astronomy Centre,
School of Physics,
University of Sydney,
Australia.
1967 July.*

Note added in press

The effect of interstellar extinction is expected to be small compared with the observational uncertainty for all but one of the stars whose angular diameters have been measured. Only for β Cru is the effect likely to be significant and even for this star it will be small and uncertain. No corrections for the effects of interstellar extinction have been made to the data presented in this paper.

References

- (1) Hanbury Brown, R. & Twiss, R. Q., 1957. *Proc. R. Soc.* **A243**, 291.
- (2) Hanbury Brown, R. & Twiss, R. Q., 1958. *Proc. R. Soc.* **A248**, 199.
- (3) Ireland, J. G., 1966. *Publ. R. Obs. Edinb.*, **5**, No. 5, 63.
- (4) Hanbury Brown, R. & Twiss, R. Q., 1956. *Nature, Lond.*, **178**, 1046.
- (5) Hanbury Brown, R. & Twiss, R. Q., 1958. *Proc. R. Soc.* **A248**, 222.
- (6) Hanbury Brown, R., Hazard, C., Davis, J. & Allen, L. R., 1964. *Nature, Lond.*, **201**,

- (7) Hoffleit, D., 1964. *Catalogue of Bright Stars*, Yale University Observatory.
- (8) Johnson, H. L., Mitchell, R. I., Iriarte, B. & Wisniewski, W. Z., 1966. *Communs. lunar planet. Lab.*, 4, 99.
- (9) Hogg, A. R., 1958. *Photometric Measurements of 244 Bright Stars*. Mount Stromlo.
- (10) Grygar, J., 1965. *Bull. astr. Instr. Csl.*, 16, 195.
- (11) Gingerich, O., 1966. *Astrophys. J.*, 144, 1213.
- (12) Edmonds, F. N., 1964. *Astrophys. J.*, 140, 902.
- (13) Willstrop, R. V., 1965. *Mcm. R. astr. Soc.*, 69, 83.
- (14) Willstrop, R. V., 1960. *Mon. Not. R. astr. Soc.*, 121, 17.
- (15) Oke, J. B., 1964. *Astrophys. J.*, 140, 689.
- (16) Code, A. D., 1960. *Stellar Atmospheres*, ed. by J. L. Greenstein, University of Chicago Press.
- (17) Allen, C. W., 1963. *Astrophysical Quantities*, 2nd edn., Athlone Press, London.
- (18) Mihalas, D., 1966. *Astrophys. J., Suppl. Ser.*, 13, 1.
- (19) Mihalas, D., 1965. *Astrophys. J., Suppl. Ser.*, 11, 321.
- (20) Strom, S. E. & Avrett, E. H., 1965. *Astrophys. J., Suppl. Ser.*, 12, 1.
- (21) Mihalas, D. & Morton, D. C., 1965. *Astrophys. J.*, 142, 253.
- (22) Adams, T. F. & Morton, D. C., private communication.
- (23) Hickok, F. & Morton, D. C., private communication.
- (24) Popper, D. M., private communication.
- (25) Strom, S. E., Gingerich, O. & Strom, K. M., 1966. *Astrophys. J.*, 146, 880.
- (26) Harris, D. L., 1963. *Basic Astronomical Data*, ed. by K. Aa. Strand, University of Chicago Press.
- (27) Jenkins, L. F., 1952. *General Catalogue of Trigonometric Stellar Parallaxes*, Yale University Observatory.
- (28) Jenkins, L. F., 1963. *Supplement to the General Catalogue of Trigonometric Stellar Parallaxes*, Yale University Observatory.
- (29) Petrie, R. M., 1965. *Publs astr. Soc. Pacif.*, 77, 97.

THE ANGULAR DIAMETERS OF 32 STARS

R. Hanbury Brown, J. Davis and L. R. Allen

(Received 1973 November 5)

SUMMARY

The complete results of the observational programme on single stars carried out with the stellar intensity interferometer at Narrabri are presented. The measurements are analysed to yield the angular diameters of 32 stars in the spectral range O5f to F8. Information is also presented on nine multiple stars.

1. INTRODUCTION

The stellar interferometer at Narrabri Observatory has been used to measure the apparent angular diameters of 32 stars. This programme was started in 1964 June and completed in 1972 February. In a previous paper (1) referred to as Paper I, we described the instrument and the observational procedure; in Paper II (2) we reported the first results on 15 stars. The present paper gives a complete list of the results including those reported in Paper II with the exception of a preliminary observation (3) of α Lyr in 1963.

2. EQUIPMENT

The installation at Narrabri Observatory was described in Paper I. Briefly it consists of two large mosaic reflectors (6.7 m in diameter) mounted on trucks which move around a circular railway track 188 m in diameter. The reflectors are controlled by a computer, assisted by automatic photoelectric guiding, and follow a star in azimuth by moving around the track and in elevation by tilting about a horizontal axis. The separation between the reflectors, the baseline, can be pre-set anywhere within the range 10–188 m and the reflectors move so that this baseline is constant in length and always normal to the direction of the star. At the focus of each reflector the light from the star passes through a narrow-band interference filter and is then focused on to the cathode of a photomultiplier. High-frequency fluctuations (10–100 MHz) in the anode currents of these photomultipliers are carried by cables to a central control building where the time-average of their cross-product, or correlation, is measured in an electronic correlator. The angular diameter of a star is found by measuring this correlation as a function of baseline length.

The installation described in Paper I has remained substantially unchanged throughout the whole programme. However, we have, at various times, introduced improved types of phototube and also modified the circuits of the correlator. As a result the limiting magnitude of the interferometer was increased from $B = +1.5$ in 1964 to $+2.5$ in 1971 and the stability and reliability of the correlator were greatly improved. A complete list of the various configurations of the equipment is given in the notes to Table I. As noted in Paper II, all these modifications were

TABLE I
Observational data

1	2	3	4	5	6	7	
Star	Epoch of observations	Base-line (m)	$\overline{c_N(d)} \pm \sigma^*$ (Arbitrary units†)	Ob-serving time (h)	Wave-length (Å)	Equip-ment	
α Aql	1964 July	9·85	95	14	10·7	4608	b
		14·79	64	13	12·2		
		19·68	39	18	10·9		
		24·6	42	16	12·7		
		29·5	-4	13	14·4		
α Gru	1964 August	9·85	113	22	11·3	4608	b
		26·2	113	25	11·4		
		42·4	72	28	11·3		
		58·2	32	28	11·9		
		73·6	36	26	11·9		
α PsA	1964 September	9·85	103	17	12·4	4608	b
		16·42	76	21	11·0		
		23·0	60	18	11·3		
		29·5	59	20	11·0		
		35·9	42	22	12·6		
α Eri	1964 October	9·85	468	40	13·4	4385	a
		18·04	310	49	11·3		
		26·2	226	47	12·7		
		34·3	116	48	11·3		
		42·4	11	45	11·3		
β Cru	1965 June	9·85	286	12	20·1	4385	c
		32·7	194	19	6·9		
		48·8	184	18	7·5		
		64·4	127	19	7·0		
		79·6	120	11·5	24·5		
		94·2	67	17	10·4		
		114·7	20	22	6·5		
		133·2	-8	19	7·3		
154·3	4·5	7·7	53·9				
α Aql	1965 July	9·85	241	10	29·8	4385	c
		19·68	115	11	29·6		
		24·6	66	15	14·4		
α Lyr	1965 July	9·85	251	8	21·5	4385	c
		19·68	88	8	22·6		
α Gru	1965 August	9·85	361	27	18·4	4385	c
		58·2	128	17	45·8		
α PsA	1965 September	9·85	319	24	16·2	4385	c
		35·9	51	15	41·5		
α Eri	1965 October	9·85	283	12	11·4	4385	c
		32·7	97	9	32·1		
β Ori	1965 October	9·85	252	15	4·6	4385	c
		23·0	98	9·5	10·7		

TABLE I—continued

1	2	3	4	5	6	7	
Star	Epoch of observations	Base-line (m)	$\overline{c_N(d)} \pm \sigma^*$ (Arbitrary units†)	Ob-serving time (h)	Wave-length (Å)	Equip-ment	
α Car	1865 October	9.58	77	7	5.7	4385	c
		13.85	24	9	4.3		
		14.46	11	10	2.3		
α CMa	1966 February	9.58	129.3	2.6	6.1	4385	c
		12.96	57.9	3.1	3.0		
		18.20	1.7	3.3	3.0		
α Leo	1966 March	9.97	347	19	16.2	4385	c
		45.5	146	22	12.7		
		55.0	42	14	27.9		
β Cru	1966 April	9.97	211	10	11.7	4430	d
		91.2	49	7.5	22.9		
α Pav	1966 August	9.97	248	15	20.6	4430	d
		32.7	177	18	15.4		
		82.5	67	12	38.2		
		100.0	19	36	3.5		
γ Ori	1966 November	9.97	165.0	9.6	15.6	4430	e
		82.5	57.4	7.3	28.6		
ϵ Ori	1966 December	9.97	139.0	9.5	17.7	4430	e
		99.8	31.4	6.4	38.3		
α CMa	1967 January	9.56	59.7	1.8	2.7	4430	e
		12.93	25.0	1.7	3.7		
ϵ CMa	1967 January	9.97	142.5	9.1	17.6	4430	e
		67.5	60.8	6.5	42.7		
α CMi	1967 February	9.51	72.6	6.3	13.9	4430	e
		15.40	16.8	3.5	40.4		
ϵ Sgr	1967 July	9.94	557	42	24.8	4430	f
		42.4	273	72	8.0		
		45.6	110	41	28.3		
		48.8	32	49	17.3		
β CMa	1967 November	9.90	729	43	21.4	4430	f
		121.1	202	58	11.1		
		126.0	354	91	5.0		
		130.9	132	55	12.7		
		135.5	135	69	9.0		
		144.3	145	90	5.1		
κ Ori	1967 December	9.90	811	50	24.7	4430	f
		113.4	216	97	6.4		
		130.9	305	42	36.1		
ζ Ori	1968 December	9.93	366	37	10.5	4430	g
		108.0	235	46	6.5		
		123.6	102	25	21.0		
γ Gem	1969 January	9.93	686	46	17.9	4430	g
		48.8	180	34	31.6		

TABLE I—continued

1	2	3	4	5	6	7	
Star	Epoch of observations	Base-line (m)	$\overline{c_N(d)} \pm \sigma^*$ (Arbitrary units†)	Ob-serving time (h)	Wave-length (Å)	Equip-ment	
ζ Pup	1969 February	9·97	650	44	19·6	4430	g
		133·2	217	39	24·1		
		144·3	251	48	19·8		
β Leo	1969 April	9·92	694	49	29·2	4430	g
		48·8	214	34	58·8		
ε Cen	1969 May	9·92	633	41	33·8	4430	g
		144·3	130	29	64·2		
ε Sgr	1969 June	9·91	686	42	18·4	4430	g
		43·2	257	26	47·0		
α CMa	1969 December	9·54	205·9	3·6	5·4	4430	h
		13·07	89·9	2·3	5·6		
η CMa	1970 February	9·88	600	45	25·8	4430	h
		87·0	168	32	55·1		
β Car	1970 March	9·93	586	28	17·9	4430	h
		41·6	171	21	28·5		
γ Crv	1970 May	9·90	612	47	37·5	4430	h
		76·6	285	49	32·5		
		94·2	101	42	44·3		
α Oph	1970 June	9·90	565	47	20·4	4430	h
		42·4	148	30	52·6		
α CMa	1970 December	9·53	257·7	3·3	6·0	4430	h
		13·07	113·4	6·1	1·0		
δ Sco	1971 April	9·90	479	53	15·7	4430	h
		48·8	562	52	23·8		
		121·1	228	31	64·6		
		163·1	—3	65	11·0		
ζ Oph	1971 June	9·90	752	68	29·3	4430	h
		133·2	173	36	88·0		
α Lyr	1971 July	9·62	569	16	7·1	4430	h
		19·59	241	14	9·4		
α Lyr	1971 August	9·95	550	27	3·3	4430	h
		19·59	228	14	11·4		
β Ori	1971 November	9·95	1069	33	19·0	4430	‡
		19·69	631	11	47·6		
α CMi	1972 January	9·56	384	14	12·5	4430	h
		14·81	126	10	25·2		
δ CMa	1972 January	9·62	567	67	16·4	4430	h
		19·77	204	58	23·2		
		26·2	20	83	11·2		

introduced in the intervals between programmes on particular stars and therefore did not affect the measurements of angular size which depend only on the ratio of the correlations at different baselines. On the other hand they did affect the arbitrary scale on which correlation was measured, and to relate one scale to another we made transfer observations on standard stars as discussed in Section 7.2.

3. OBSERVATIONAL PROGRAMME

The interferometer is limited by considerations of signal-to-noise ratio to measuring stars of spectral type earlier than G0 and brighter than $B = +2.5$; furthermore, for this particular programme, it was planned to restrict the measurements to single stars or stars with companions at least 2 mag⁰fainter. We therefore chose 34 stars which apparently satisfied these criteria and at the same time represented a reasonable sample of the different spectral types and luminosity classes. Subsequently, our measurements at Narrabri disclosed that seven of the stars (Table IV) are not single and that four of these (β Cen, λ Sco, σ Sgr, δ Vel) have companions which are too bright for our purpose. These four stars were therefore excluded from the programme but we have added to the list the primary stars of two binary systems (α Vir, γ^2 Vel) to make the total 32. These two binaries were observed in separate programmes which have been described elsewhere (4, 5).

It would have been desirable to measure many more stars and this could have been done by increasing the exposures beyond 100 hr to reach stars fainter than $B = +2.5$. However, we decided not to work on fainter stars; not only would the exposures have become impracticably long, but there would have been an increasing risk that at very low signal-to-noise ratios minor systematic errors might introduce significant errors into the measured values of angular size.

4. OBSERVATIONAL PROCEDURE

For all the results reported in this paper the observational procedure was the same as that described in detail in Paper I. For convenience we shall summarize here some of the more important features.

Footnotes to Table I

* $\overline{c_N(d)}$ is the normalized, weighted mean correlation from the star in arbitrary units, for a reflector separation d . All the observations have been reduced to the same standard interval. σ is the rms uncertainty in $\overline{c_N(d)}$.

† $\overline{c_N(d)}$ is in arbitrary units which depend on the parameters of the equipment in use at the time. Over the period covered by the observations several modifications were made to the equipment which altered the scale $\overline{c_N(d)}$ (Section 6). There were eight principal configurations of the equipment which are shown by the letters (a)–(h) in column 7. These letters correspond to the use of the following major components:

- (a) RCA type 7046 phototubes, 4385 ± 40 Å filters.
- (b) RCA type 7046 phototubes, 4608 ± 150 Å filters.
- (c) RCA type dev. C 31011 phototubes, 4385 ± 40 Å filters.
Mark I transistorized multiplier.
- (d) RCA type dev. C 31011 phototubes, 4430 ± 50 Å filters.
- (e) RCA type 8575 phototubes, 4430 ± 50 Å filters.
Mark II transistorized multiplier.
- (f) RCA type 8575 phototubes, 4430 ± 50 Å filters.
Mark II transistorized multiplier plus synchronous integrator.
- (g) As (f) but with RCA type dev. C 31000 phototubes.
- (h) As (f) but with RCA type 8850 phototubes.
- (‡) As (h) but with polaroid in front of phototubes.

Before each observing session the delays in the two arms of the interferometer were equalized by measurements on the phototubes, cables and amplifiers. A final check on the whole system was made by observing a bright star and adjusting the relative delay in the two arms of the interferometer to give the maximum signal-to-noise ratio.

Throughout the programme a close check was kept on the gain and zero-drift of the correlator. The correlator was kept running continuously night and day and, between runs on a star, the two phototubes were illuminated by small pea-lamps adjusted in brightness to give the same phototube anode currents as the star. The gain was measured at least once per day and immediately before and after every run on a star. The zero-drift was found by taking a three-day running mean of the correlation recorded with the phototubes illuminated by the pea-lamps.

During observations routine checks were made on the length and orientation of the baseline. As a first precaution we checked, at least once every night, that the actual position of the reflectors on the track agreed with that shown on the control desk; this was done by driving the reflectors to calibrated marks on the track. As a further check the length of short baselines, which are critical for partially resolved stars, were measured directly with a tape measure. Errors in the orientation of the baselines, which introduce differential delays into the light reaching the reflectors, were monitored by recording the indicated azimuths of the two reflectors at least every half hour and comparing them with the true azimuth of the star.

Great care was taken to minimize the effects of any possible systematic errors on the ratio of the correlations observed with different baselines since they might introduce errors into the final values of angular size. For example, to reduce errors which might depend on azimuth and elevation, we carried out the observations of any given star over the same range of hour angles at all baselines. To minimize possible effects due to slow changes in the equipment or in the observing conditions we interleaved measurements at long and short baselines and rejected all observations made when the atmospheric extinction was significantly (~ 0.2 mag) higher than normal.

5. DATA REDUCTION

The form in which the observational data are obtained and the method of data reduction have been described in detail in Papers I and II. Briefly, the printed output from the correlator shows the cumulative total of the correlation every 100 s together with the two phototube anode currents averaged over the preceding 100 s.

The first step in reducing the data was to correct the recorded correlation for any zero-drift in the output of the correlator thereby finding the true mean correlation $\overline{c_0(d)}$ from the star when observed with a baseline d . The next step was to normalize this correlation to take account of variations in the light flux received from the star and in the gain of the correlator. Following Paper II, $\overline{c_N(d)}$ the mean normalized correlation per 100 s cycle of the correlator was found from,

$$\overline{c_N(d)} = \overline{c_0(d)} / \text{CAL}(i_{S1} \cdot i_{S2}) \quad (1)$$

where i_{S1} , i_{S2} are the components of the phototube anode currents due to the star alone found by subtracting from the total currents the contributions due to the night sky and moonlight, CAL is the gain of the correlator and all the quantities are averaged over the whole night's run. The rms uncertainty σ in $\overline{c_N(d)}$ is compounded of the uncertainty due to noise in the correlator output and the uncertainty

in the zero-drift and, following Paper II, was found from

$$\sigma = \text{CAL. } \sigma_{\text{STD}}[(i_{T1}i_{T2}/p) + (i_1i_2/q)]^{1/2} \quad (2)$$

where i_{T1} , i_{T2} are the total phototube anode currents averaged over the whole run of p cycles of the correlator on the star; i_1 , i_2 are the phototube anode currents averaged over q cycles of the control runs on the pea-lamps; σ_{STD} is the normalized uncertainty in one cycle of the correlator output derived from an analysis of the output fluctuations over very many runs.

The next step was to combine the normalized correlations found on different nights. They are weighted by the inverse square of their uncertainty, so that

$$\overline{c_N(d)} = \frac{\sum_r (\overline{c_N(d)}_r / \sigma_r^2)}{\sum_r 1 / \sigma_r^2} \quad (3)$$

where $\overline{c_N(d)}_r \pm \sigma_r$ represents the normalized correlation observed on the r th night. The uncertainty σ in this final value is given by,

$$\sigma = 1 / \sqrt{\sum_r 1 / \sigma_r^2}. \quad (4)$$

The final step was to correct the values of mean normalized correlation for the loss of correlation due to errors in the orientation of the baseline which, as noted in Section 4, were recorded every half-hour during observations of a star. From these records the differential time delay in the arrival of the light at the two reflectors was calculated for each star and baseline. A corresponding loss factor was computed as a function of hour angle; the relation between time delay and loss factor was found from measurements on bright stars and differed for each configuration of the equipment. The correlation observed at each baseline was then corrected by a weighted mean loss factor based on the distribution of observing time with hour angle. It should be noted that these corrections were small, only a few per cent, and do not contribute significantly to the overall uncertainty in the final values of correlation.

6. OBSERVATIONAL DATA

Table I is a summary of the observational data on 32 stars listed in chronological order of observation; 10 of the stars have been measured at least twice. Columns 1–3 show the star name, epoch of observation and the baselines in metres; column 4 shows $\overline{c_N(d)}$ the weighted mean normalized correlation (equation (3)) observed at each baseline, with its associated rms uncertainty (equation (4)), expressed in arbitrary units which are not the same for every star since they depend on the particular configuration of the equipment as noted in Section 4; columns 5–6 show the observing time at each baseline and the effective wavelength of the optical system; finally, column 7 shows which of eight different configurations of the equipment were used.

It should be noted that there are some small differences between the values of $\overline{c_N(d)}$ in Table I and those published previously in Paper II. For all the stars, except two (α CMa, α Car), these differences represent minor corrections for errors in the orientation of the baseline (Section 5) which were not taken into account in Paper II. However, for α CMa and α Car the differences are due to the fact that we have restricted the observational data to a narrow range of elevation angles

(35–55°), whereas in Paper II we used data from all elevations. Both these very bright stars have such large angular diameters that they are significantly resolved at a baseline comparable in length with the diameter of the reflectors. As a consequence the normalized correlation at very short baselines depends upon the relative contributions to the total light at the photomultipliers from different parts of the reflectors. Unfortunately, the structure supporting the reflectors is insufficiently rigid and the contributions from different parts of the reflectors changes appreciably with elevation. It follows that the normalized correlation from α CMa and α Car varies with elevation and that at very short baselines this variation may itself be a function of the baseline length. Such a variation would not, of course, be a significant source of error in the final values of angular diameter if it were independent of baseline since the observations at all baselines are carried out over the same range of elevation angles; but for α CMa and α Car the dependence of the effect on baseline might perhaps introduce significant errors and we have therefore restricted the data to a small range of elevations. We have chosen the range (35–55°) because the reflector is adjusted to give its optimum optical performance at 45° and there is experimental evidence to show that there is no significant change of normalized correlation over a range of $\pm 10^\circ$ about this optimum angle.

7. RESULTS

7.1 Introduction

It was shown by Hanbury Brown & Twiss (6) that the normalized correlation $\overline{c_N(d)}$ varies with baseline d as,

$$\overline{c_N(d)} \propto \Delta_\lambda \Gamma_\lambda^2(d) \quad (5)$$

where Δ_λ is the *partial coherence factor* and $\Gamma_\lambda^2(d)$ is the *correlation factor*.

The partial coherence factor Δ_λ takes account of the finite size of the two reflectors which are so large that they partially resolve some of the stars and reduce the correlation at short baselines. In the simple case where the aperture of the reflectors is small compared with the baseline necessary to resolve the star ($\Delta_\lambda \sim 1$) the correlation factor $\Gamma_\lambda^2(d)$ is simply proportional to the square of the modulus of the Fourier transform of the intensity distribution across the light source when it is reduced to an equivalent strip distribution parallel to the baseline (6). In the case where a star has a circular disc of uniform intensity it follows that:

$$\Gamma_\lambda^2(d) = \left[\frac{2J_1(\pi\theta_{UD} d/\lambda_0)}{\pi\theta_{UD} d/\lambda_0} \right]^2 \quad (6)$$

where θ_{UD} is the angular diameter of the uniform disc, λ_0 is the mid-band wavelength of the light and it is assumed that the light is, in effect, monochromatic. In the more general case where the angular diameter of a star is large enough to be partially resolved by the individual reflectors, it has been shown (6) that,

$$\Delta_\lambda \Gamma_\lambda^2(d) = \frac{1}{A^2} \iiint \left[\frac{2J_1(\xi)}{\xi} \right]^2 dx_1 dx_2 dy_1 dy_2 \quad (7)$$

where

$$\xi = \frac{\pi\theta_{UD}}{\lambda_0} [(x_1 - x_2)^2 + (y_1 - y_2)^2]^{1/2} \quad (8)$$

and (x_1, y_1) , (x_2, y_2) represent points on the two reflectors and the integral is taken over the area (A) of each reflector.

The normalized correlation also depends upon whether a star is single or multiple. It was shown in Paper II that, if a star is binary and the angular separation of the two components is completely resolved by the interferometer at the shortest baseline, then the normalized zero-baseline correlation $\overline{c_N(o)'} / \overline{c_N(o)}$ averaged over a range of position angles is reduced relative to a single star $c_N(o)$ by the factor,

$$\overline{c_N(o)'} / \overline{c_N(o)} = (I_1^2 + I_2^2) / (I_1 + I_2)^2 \quad (9)$$

where I_1, I_2 are the brightness of the two components. It is simple to extend this analysis to a multiple star with n components and to show that, if the angular separation between all the components is resolved, the zero-baseline correlation is reduced relative to a single star by the factor,

$$\overline{c_N(o)'} / \overline{c_N(o)} = \sum_n I^2 / \left(\sum_n I \right)^2. \quad (10)$$

It follows that if a star yields a correlation which is significantly less than that expected from a single star, then it must be multiple.

7.2 *Method of analysis*

For each star in Table I the angular diameter of the equivalent uniform disc was found by fitting to the observed values of normalized correlation the theoretical curve for $\Delta_\lambda \Gamma_\lambda^2(d)$ given in equation (7). The curve was fitted to the observations by the method of least squares using an iterative computer program. Reasonable initial values were taken for C and θ_{UD} , where C is the normalized correlation at zero-baseline assuming no partial resolution ($\Delta_\lambda = 1$), so that

$$C = \overline{c_N(o)} / \Delta_\lambda \quad (11)$$

and corrections δC and $\delta \theta_{UD}$ were computed to find values of C and θ_{UD} which minimized the weighted squared residuals between the observations and the theoretical curve. The calculation was then repeated using corrected initial values until both $\delta C / C$ and $\delta \theta_{UD} / \theta_{UD}$ were $< 10^{-4}$. The results are shown in Table II.

In estimating the uncertainties in C and θ_{UD} we have taken into account not only the statistical uncertainties in fitting a curve to the normalized correlations but also the possibility that the zero level of the correlator might be systematically displaced by some unknown source of spurious correlation. In Papers I and II we described a variety of special tests which failed to show any spurious correlation, nevertheless, we have used the results of these tests to set upper limits to any such effect. Since writing Papers I and II more tests have been carried out and have lowered the limits significantly. They are now given by

$$\log(\sigma/C) \leq -2.71 + 0.41 B + 0.07 B^2 \quad (12)$$

where σ is the uncertainty in the zero-level of the correlator, C is the zero-baseline correlation from the star and B is its apparent blue magnitude. For each star in Table II we have therefore computed the uncertainty in C and θ_{UD} corresponding to an uncertainty in the zero level of the correlator given by equation (12) and combined this with the conventional statistical uncertainty in fitting a theoretical

curve to the observations. The final uncertainties in C and θ_{UD} are shown in Table II.

As they stand the values of C in Table II cannot be interpreted readily because they are in arbitrary units which vary in scale with the different configurations of the equipment. We have therefore reduced them all to the same scale and normalized them by the zero-baseline correlation expected from a single unresolved star. They were first reduced to the same scale by computing from a network of transfer observations a set of scale factors which yielded the best overall agreement between the values of C measured for the same stars but with different configurations. The correlation expected from a single unresolved star was then found by taking the weighted mean \bar{C} for all the stars in Table II and expressing the deviation of each star from this mean in terms of its rms uncertainty σ . All stars with deviations exceeding 3σ were then excluded and the process was repeated until the distribution of the remaining deviations was roughly normal about the weighted mean \bar{C} . This value of \bar{C} was then taken to be the best value for the correlation from a single unresolved star and was used to find C_N for each star in the list, where

$$C_N = C'/\bar{C} \quad (13)$$

and C' is the measured value of C in Table II expressed on a common scale, and C_N is the zero-baseline correlation without partial resolution ($\Delta_\lambda = 1$) normalized by the zero-baseline correlation expected from a single unresolved star. The values of C_N found in this way are shown in column 4 of Table III.

The ratio of the true angular diameter of a star (θ_{LD}) to the angular diameter of its equivalent uniform disc (θ_{UD}) depends on the limb darkening law for its atmosphere. The angular diameters of the equivalent uniform discs of the stars listed in Table II must therefore be corrected to find their true angular diameters.

At present limb darkening corrections can only be based on model atmospheres. In Paper I (1) a cosine law was adopted and, with appropriate values for the limb darkening coefficient u_λ derived from model atmospheres, the angular diameters were corrected using the relationship between θ_{LD}/θ_{UD} and u_λ given by Hanbury Brown & Twiss (7). In fact limb darkening is non-linear and, while the cosine law is a reasonable approximation, a more realistic method of correction is used in this paper. The squared modulus of the Fourier transform of the equivalent line intensity distribution across a star as predicted by various model atmospheres was compared with the same function for a uniform disc to find values of θ_{LD}/θ_{UD} directly in terms of the parameters T_e and $\log g$ of the model. From these results the ratio θ_{LD}/θ_{UD} was obtained for each star in Table II using values of $(B-V)_0$ and $\log g$ appropriate to their spectral type and luminosity class. The necessary transformations between T_e and $(B-V)$ were those given by Webb (8); the intensity distribution across the star was taken from the model atmospheres computed by Carbon, Gingerich & Kurucz (9) except for the F8 Ia star δ CMa for which the models computed by Parsons (10) were used.

The resulting values of θ_{LD} , the true angular diameters of the stars, are shown in column 6 of Table III. It should be noted that the correction factor from equivalent uniform disc to true angular diameter is small and has a mean value $\theta_{LD}/\theta_{UD} = 1.044$. The uncertainties in the adopted values of $\log g$ and in the transformation between T_e and $(B-V)_0$ introduce a maximum additional uncertainty, for the adopted models, of $\sim \pm 0.5$ per cent into the true angular diameters. In most cases the additional uncertainty is less than this and, in all cases, is negligible compared with the uncertainty in the measurement of θ_{UD} .

7.3 Explanation of Tables II, III and IV

In Table II, columns 1-4 show the *Bright star catalogue* (II) number, the name of the star, the date and wavelength of observation. Columns 5-8 show the results of fitting a theoretical curve to the observations as described above. Column 5 shows C the normalized correlation at zero-baseline, with the effect of partial resolution removed by putting $\Delta_\lambda = 1$ in equation (9), together with its rms uncertainty; column 6 shows Δ_λ the partial resolution factor; column 7 shows θ_{UD} the angular diameter of the equivalent uniform disc for each observation together with its rms uncertainty; column 8 shows $\bar{\theta}_{UD}$ the weighted mean value of the angular diameter of the equivalent uniform disc for all observations of the star together with its associated rms uncertainty.

Table III summarizes the results of the whole programme. Columns 1-3 give the *Bright star catalogue* (II) number, the name of the star and its spectral classification. Column 4 gives C_N the zero-baseline correlation corrected for partial resolution ($\Delta_\lambda = 1$) and normalized by the value expected from a single unresolved

TABLE II

The angular diameters of the equivalent uniform discs and zero-baseline correlations for 30 stars

1	2	3	4	5	6	7	8
B.S.	Name	Year	Wave-length (Å)	$C \pm \sigma$ (Arbitrary units)	Δ_λ	$\theta_{UD} \pm \sigma$ (10^{-3} seconds of arc)	$\bar{\theta}_{UD} \pm \sigma$ (10^{-3} seconds of arc)
472	α Eri	1964	4385	523 ± 48	0.987	2.02 ± 0.18	1.85 ± 0.07
		1965	4385	315 ± 15	0.989	1.82 ± 0.08	
1713	β Ori	1965	4385	312 ± 23	0.979	2.56 ± 0.14	2.43 ± 0.05
		1971	4430	1291 ± 46	0.982	2.41 ± 0.05	
1790	γ Ori	1966	4430	168 ± 10	0.998	0.70 ± 0.04	0.70 ± 0.04
1903	ϵ Ori	1966	4430	141 ± 10	0.999	0.67 ± 0.04	0.67 ± 0.04
1948-9	ζ Ori	1968	4430	374 ± 37	0.999	0.47 ± 0.04	0.47 ± 0.04
2004	κ Ori	1967	4430	811 ± 52	0.999	0.44 ± 0.03	0.44 ± 0.03
2294	β CMa	1967	4430	735 ± 46	0.999	0.50 ± 0.03	0.50 ± 0.03
2326	α Car	1965	4385	240 ± 71	0.890	6.1 ± 0.7	6.1 ± 0.7
2421	γ Gem	1968	4430	726 ± 53	0.994	1.32 ± 0.09	1.32 ± 0.09
2491	α CMa	1966	4385	344 ± 23	0.905	5.65 ± 0.17	$5.60 \pm 0.15^*$
		1967	4430	166 ± 16	0.899	5.84 ± 0.23	
		1969	4430	519 ± 22	0.908	5.57 ± 0.09	
		1970	4430	642 ± 38	0.909	5.54 ± 0.17	
2618	ϵ CMa	1967	4430	145 ± 9	0.998	0.77 ± 0.05	0.77 ± 0.05
2693	δ CMa	1972	4430	793 ± 132	0.966	3.29 ± 0.46	3.29 ± 0.46
2827	η CMa	1970	4430	610 ± 53	0.998	0.72 ± 0.06	0.72 ± 0.06

TABLE II—continued

1	2	3	4	5	6	7	8
B.S.	Name	Year	Wave-length (Å)	$C \pm \sigma$ (Arbitrary units)	Δ_λ	$\theta_{UD} \pm \sigma$ (10^{-3} seconds of arc)	$\bar{\theta}_{UD} \pm \sigma$ (10^{-3} seconds of arc)
2943	α CMi	1967	4430	168 ± 28	0.915	5.32 ± 0.36	
		1972	4430	825 ± 62	0.923	5.05 ± 0.18	5.10 ± 0.16
3165	ζ Pup	1969	4430	651 ± 47	1.000	0.41 ± 0.03	0.41 ± 0.03
3685	β Car	1970	4430	631 ± 33	0.993	1.51 ± 0.07	1.51 ± 0.07
3982	α Leo	1966	4385	371 ± 21	0.994	1.32 ± 0.06	1.32 ± 0.06
4534	β Leo	1969	4430	730 ± 59	0.995	1.25 ± 0.09	1.25 ± 0.09
4662	γ Crv	1970	4430	629 ± 58	0.998	0.72 ± 0.06	0.72 ± 0.06
4853	β Cru	1965	4385	275 ± 11	0.998	0.685 ± 0.029	
		1966	4430	215 ± 10	0.998	0.726 ± 0.034	0.702 ± 0.022
5132	ϵ Cen	1969	4430	638 ± 45	0.999	0.47 ± 0.03	0.47 ± 0.03
5953	δ Sco	1971	4430	556 ± 46	0.999	0.45 ± 0.04	0.45 ± 0.04
6175	ζ Oph	1971	4430	758 ± 84	0.999	0.50 ± 0.05	0.50 ± 0.05
6556	α Oph	1970	4430	609 ± 57	0.992	1.53 ± 0.12	1.53 ± 0.12
6879	ϵ Sgr	1967	4430	604 ± 48	0.993	1.52 ± 0.11	
		1969	4430	725 ± 49	0.995	1.31 ± 0.07	1.37 ± 0.06
7001	α Lyr	1965	4385	355 ± 17	0.966	3.26 ± 0.13	
		1971	4430	751 ± 30	0.972	3.01 ± 0.10	
		1971	4430	728 ± 48	0.971	3.04 ± 0.12	3.08 ± 0.07
7557	α Aql	1964	4608	120 ± 22	0.975	2.96 ± 0.43	
		1965	4385	308 ± 17	0.976	2.76 ± 0.14	2.78 ± 0.13
7790	α Pav	1966	4430	241 ± 14	0.998	0.77 ± 0.05	0.77 ± 0.05
8425	α Gru	1964	4608	121 ± 19	0.997	0.97 ± 0.20	
		1965	4385	372 ± 29	0.997	0.98 ± 0.07	0.98 ± 0.07
8728	α PsA	1964	4608	104 ± 16	0.992	1.63 ± 0.28	
		1965	4385	367 ± 30	0.996	2.07 ± 0.14	1.98 ± 0.13

* The formal statistical uncertainty in θ_{UD} for α CMa is ± 0.07 (± 1.2 per cent). We cannot be certain that all possible systematic effects have been completely eliminated at this level of precision and to cover this we have increased the uncertainty in $\bar{\theta}_{UD}$ for α CMa to ± 0.15 .

Column 1, number of star in *Catalogue of bright stars* (11); column 2, name of star; column 3, year of observation; column 4, effective wavelength of observation; column 5, normalized zero-baseline correlation with no partial resolution ($\Delta_\lambda = 1$) in arbitrary units; column 6, partial resolution factor; column 7, equivalent uniform disc angular diameter with rms uncertainty; column 8, weighted mean equivalent uniform disc angular diameter with rms uncertainty.

TABLE III

The uniform disc angular diameters, true angular diameters and normalized zero-baseline correlations for 32 stars

1	2	3	4	5	6
B.S.	Name	MK	$C_N \pm \sigma$ (normalized)	$\bar{\theta}_{UD} \pm \sigma$ (10^{-3} seconds of arc)	$\theta_{LD} \pm \sigma$ (10^{-3} seconds of arc)
472	α Eri	‡B ₃ Vp	0.98 ± 0.05	1.85 ± 0.07	1.92 ± 0.07
1713	β Ori	†B ₈ Ia	0.98 ± 0.08	2.43 ± 0.05	2.55 ± 0.05
1790	γ Ori	†B ₂ III	1.03 ± 0.07	0.70 ± 0.04	0.72 ± 0.04
1903	ϵ Ori	†B ₀ Ia	0.86 ± 0.07	0.67 ± 0.04	0.69 ± 0.04
1948	ζ Ori	**O _{9.5} Ib	0.60 ± 0.06	0.47 ± 0.04	0.48 ± 0.04
2004	κ Ori	†B _{0.5} Ia	1.18 ± 0.09	0.44 ± 0.03	0.45 ± 0.03
2294	β CMa	*B ₁ II-III	1.07 ± 0.08	0.50 ± 0.03	0.52 ± 0.03
2326	α Car	F ₀ Ib-II	0.75 ± 0.22	6.1 ± 0.7	6.6 ± 0.8
2421	γ Gem	**A ₀ IV	1.17 ± 0.09	1.32 ± 0.09	1.39 ± 0.09
2491	α CMa	A ₁ V	0.91 ± 0.06	5.60 ± 0.15	5.89 ± 0.16
2618	ϵ CMa	**B ₂ II	0.89 ± 0.06	0.77 ± 0.05	0.80 ± 0.05
2693	δ CMa	**F ₈ Ia	0.93 ± 0.18	3.29 ± 0.46	3.60 ± 0.50
2827	η CMa	†B ₅ Ia	0.99 ± 0.09	0.72 ± 0.06	0.75 ± 0.06
2943	α CMi	F ₅ IV-V	0.98 ± 0.10	5.10 ± 0.16	5.50 ± 0.17
3165	ζ Pup	†O ₅ f	1.04 ± 0.08	0.41 ± 0.03	0.42 ± 0.03
3207	γ^2 Vel	§WC8 + O ₉ I	—	0.43 ± 0.05	0.44 ± 0.05
3685	β Car	A ₁ IV	1.01 ± 0.06	1.51 ± 0.07	1.59 ± 0.07
3982	α Leo	**B ₇ V	1.12 ± 0.07	1.32 ± 0.06	1.37 ± 0.06
4534	β Leo	**A ₃ V	1.17 ± 0.10	1.25 ± 0.09	1.33 ± 0.10
4662	γ Crv	B ₈ III	0.97 ± 0.10	0.72 ± 0.06	0.75 ± 0.06
4853	β Cru	‡B _{0.5} III	0.88 ± 0.03	0.702 ± 0.022	0.722 ± 0.023
5056	α Vir	*B ₁ IV	—	0.85 ± 0.04	0.87 ± 0.04
5132	ϵ Cen	‡B ₁ III	1.02 ± 0.07	0.47 ± 0.03	0.48 ± 0.03
5953	δ Sco	†B _{0.5} IV	0.75 ± 0.07	0.45 ± 0.04	0.46 ± 0.04
6175	ζ Oph	**O _{9.5} V	1.01 ± 0.12	0.50 ± 0.05	0.51 ± 0.05
6556	α Oph	**A ₅ III	0.94 ± 0.09	1.53 ± 0.12	1.63 ± 0.13
6879	ϵ Sgr	A ₀ V	1.02 ± 0.06	1.37 ± 0.06	1.44 ± 0.06
7001	α Lyr	†A ₀ V	0.99 ± 0.04	3.08 ± 0.07	3.24 ± 0.07
7557	α Aql	A ₇ IV, V	0.94 ± 0.06	2.78 ± 0.13	2.98 ± 0.14
7790	α Pav	‡B _{2.5} V	1.01 ± 0.07	0.77 ± 0.05	0.80 ± 0.05
8425	α Gru	‡B ₇ IV	1.11 ± 0.08	0.98 ± 0.07	1.02 ± 0.07
8728	α PsA	†A ₃ V	1.02 ± 0.08	1.98 ± 0.13	2.10 ± 0.14

References for MK Spectral Types in order of preference

- † Morgan, W. W. & Keenan, P. C., 1973. *A. Rev. Astr. Astrophys.*, in press.
 ** Johnson, H. L. & Morgan, W. W., 1953. *Astrophys. J.*, **117**, 313.
 ‡ Hiltner, W. A., Garrison, R. F. & Schild, R. E., 1969. *Astrophys. J.*, **157**, 313.
 § Conti, P. S. & Smith, L. F., 1972. *Astrophys. J.*, **172**, 623.
 * Lesh, J. R., 1968. *Astrophys. J. Suppl. Ser.*, **17**, 371.

Remainder from Johnson, H. L., Mitchell, R. I., Iriarte, B. & Wiśniewski, W. Z., 1966. *Communs. lunar planet Lab.*, **4**, 99.

Column 1, number of star in *Catalogue of bright stars* (11); column 2, name of star; column 3, MK spectral classification; column 4, zero-baseline correlation with no partial resolution ($\Delta_\lambda = 1$) normalized by the value expected from a single unresolved star; column 5, weighted mean equivalent uniform disc angular diameter with rms uncertainty; column 6, true angular diameter allowing for effects of limb darkening (see Section 7.2).

TABLE IV
Multiple stars

B.S.	Name	$C_N \pm \sigma^*$	Remarks
1948/9	ζ Ori	0.60 ± 0.06	
3207	γ^2 Vel	—	See (5)
3485	δ Vel	0.65 ± 0.06	
4853	β Cru	0.88 ± 0.03	
5056	α Vir	—	See (4)
5267	β Cen	0.47 ± 0.02	
5953	δ Sco	0.75 ± 0.07	
6527	λ Sco	0.48 ± 0.08	
7121	σ Sgr	0.54 ± 0.07	

* Zero-baseline correlation with effects of partial resolution removed ($\Delta\lambda = 1$) normalized by value expected from a single unresolved star.

star; σ is the rms uncertainty and includes the uncertainty in the original measurements, the uncertainty in the scale factor used to reduce this measurement to a common scale and the uncertainty in the correlation expected from a single star. Column 5 is reproduced from Table II and gives θ_{UD} the weighted mean angular diameter of the equivalent uniform disc. Column 6 gives θ_{LD} the true angular diameter of the star allowing for the effects of limb darkening (Section 7.2). We have included in Table III the angular diameters of the primary components of two binary systems (α Vir, γ^2 Vel) which were measured in comparatively elaborate programmes reported previously (4, 5). In the original analysis of these two stars no account was taken of the effects of minor errors in the orientation of the baseline. We have therefore reviewed this analysis and find that in both cases the only significant effect is to change the angular diameter of the primary star by a few per cent; the values shown for the primary components of α Vir and γ^2 Vel in Table III include this correction and therefore differ slightly from the previously published (4, 5) values.

Table IV is a list of stars which we have found to give significantly less correlation than expected from a single star and they must therefore be multiple. Columns 1–2 give the *Bright star catalogue* (11) number and name of the star; column 3 gives C_N the zero-baseline correlation corrected for partial resolution ($\Delta\lambda = 1$) and normalized by the value expected from a single unresolved star.

8. DISCUSSION

The results of the whole programme of measuring the angular diameters of single stars are summarized in Table III. For 27 of the stars the measured value of C_N does not differ significantly ($< 3\sigma$) from unity and is therefore consistent with a single star. An upper limit to the brightness of any companion star can be evaluated for each individual star from equations (9) and (10). For most of the stars in the Table $C_N > 0.85$ which means that any companion stars are likely to be at least 2.5 mag fainter. It follows that any correlation due to such a companion would be less than 1 per cent of the correlation from the bright star itself, consequently any error in the angular size of these 27 stars, due to the presence of a companion, would be negligibly small. We are therefore justified in treating the listed values of θ_{LD} for these stars as the angular diameters of single stars.

We note that among the 27 stars in Table III which we have treated as single there are two unresolved astrometric binaries (α Oph and γ Gem). For α Oph the observed value of C_N is 0.94 ± 0.09 and, taking 3σ as the lower limit, it is therefore unlikely that any companion is less than 1.5 mag fainter. The astrometric and spectroscopic data on γ Gem have been discussed by Beardsley (13) who interprets them to show that γ Gem may be a triple system with the two major components forming a binary with a period of 12.9 yr, a maximum angular separation of $0''.3$ and $\Delta m = 1.6$ mag. Our observed value of C_N is 1.17 ± 0.09 which, again taking 3σ as a lower limit, is consistent with a binary star with $\Delta m \geq 3$ mag. Although this result is apparently inconsistent with the model put forward by Beardsley it must be noted that our interpretation of C_N assumes that the angular separation of the components is fully resolved by the interferometer and, at the particular epoch of our observations, this may not have been the case.

However, five of the stars in Table III (ζ Ori, γ^2 Vel, β Cru, α Vir, δ Sco) are clearly not single and have been included in Table IV as multiple stars. ζ Ori is listed (11) as a triple system with a difference of about 2 mag between the brightest components. The observed value of C_N (0.60 ± 0.06) shows that the brightest component of the system is itself a multiple star and the simplest interpretation is that it is a binary star with $\Delta m \simeq 2$ mag. Nevertheless, we may certainly interpret θ_{LD} in Table III as the angular diameter of the brightest single star in ζ Ori because it is simple to show that the contributions of the companion stars to the total correlation are so small that their effects on θ_{LD} are negligible in comparison with the observational uncertainty (σ) shown in the Table. γ^2 Vel and α Vir are well-known multiple stars and have been discussed in detail elsewhere (4, 5); the values of θ_{LD} shown for them represent the angular diameters of their brightest components. The data on β Cru show clearly that it is a multiple star and this has already been pointed out by Popper (14) on the basis of our earlier results; the value of C_N (0.88 ± 0.03) is consistent with a binary star with $\Delta m \simeq 2.9$ mag. Again the measured value of angular diameter refers to the brighter component since it can be shown that any effect due to the companion would be negligibly small. δ Sco has not been listed previously as a multiple star but the observed value of C_N (0.75 ± 0.07) is consistent with a binary star with $\Delta m \simeq 1.9$ mag. Again the angular diameter refers to the brighter component since any effect of the companion on θ_{LD} would be small, much smaller than the observational uncertainty (σ) in Table III. It follows that we are justified in treating all 32 angular diameters in Table III as the angular diameters of single stars.

There are four stars (δ Vel, β Cen, λ Sco, σ Sgr) in Table IV which do not appear in Table III. These stars were possible candidates for our observing list but were rejected because they were found to have bright companions. δ Vel is listed (11) as having a faint double companion, however, the measured value of C_N (0.65 ± 0.06) shows that the bright component must itself be multiple; the simplest interpretation is that it is a binary with $\Delta m \simeq 1.3$ mag and since this would produce an appreciable uncertainty in angular size of the brightest component it was rejected from our list. β Cen is well known to exhibit a variable radial velocity and has been discussed by Breger (15) and also by Shobbrook & Robertson (16). The value of C_N (0.47 ± 0.02) is consistent with a binary star with two equally bright components. λ Sco was reported by Slipher (17) to be a spectroscopic binary and by Shobbrook & Lomb (18) to be a β CMa variable; the value of C_N (0.48 ± 0.08) confirms that it is multiple and indicates that it is a binary with

components of about equal brightness. σ Sgr has not been reported previously as a multiple star but the value of C_N (0.54 ± 0.07) is consistent with a binary star with components of roughly equal brightness ($\Delta m \simeq 0.6$ mag).

ACKNOWLEDGMENTS

The programme of the interferometer has been supported by the Australian Research Grants Committee, the Research Grants Committee of the University of Sydney, the United States Air Force and the Science Foundation for Physics within the University of Sydney. We thank Professor Messel for his support: we thank Dr R. J. Webb, Mr R. J. W. Lake and Mr R. T. Kery for their assistance with the observations and Mr R. J. Thompson for computing the limb darkening corrections.

Chatterton Astronomy Department, School of Physics, University of Sydney, N.S.W. 2006

REFERENCES

- (1) Hanbury Brown, R., Davis, J. & Allen, L. R., 1967. *Mon. Not. R. astr. Soc.*, **137**, 375.
- (2) Hanbury Brown, R., Davis, J., Allen, L. R. & Rome, J. M., 1967. *Mon. Not. R. astr. Soc.*, **137**, 393.
- (3) Hanbury Brown, R., Hazard, C., Davis, J. & Allen, L. R., 1964. *Nature, Lond.*, **201**, 1111.
- (4) Herbison-Evans, D., Hanbury Brown, R., Davis, J. & Allen, L. R., 1971. *Mon. Not. R. astr. Soc.*, **151**, 161.
- (5) Hanbury Brown, R., Davis, J., Herbison-Evans, D. & Allen, L. R., 1970. *Mon. Not. R. astr. Soc.*, **148**, 103.
- (6) Hanbury Brown, R. & Twiss, R. Q., 1957. *Proc. R. Soc. London, Ser. A*, **243**, 291.
- (7) Hanbury Brown, R. & Twiss, R. Q., 1958. *Proc. R. Soc. London, Ser. A*, **248**, 199.
- (8) Webb, R. J., 1971. Ph.D. Thesis, University of Sydney.
- (9) Gingerich, O., 1969. *Theory and observation of normal stellar atmospheres*, M.I.T. Press, Cambridge, Mass., U.S.A.
- (10) Parsons, S. B., 1971. *Astrophys. J.*, **164**, 355.
- (11) Hoffleit, D., 1964. *Catalogue of bright stars*, Yale University Observatory.
- (12) Jenkins, L. F., 1952. *General catalogue of trigonometric parallaxes*, Yale University Observatory.
- (13) Beardsley, W. R., 1967. *I.A.U. Symp. No. 30*, 189, Academic Press, London.
- (14) Popper, D. M., 1968. *Astrophys. J.*, **151**, L51.
- (15) Breger, M., 1967. *Mon. Not. R. astr. Soc.*, **136**, 51.
- (16) Shobbrook, R. R. & Robertson, J. W., 1968. *Proc. astr. Soc. Aust.*, **1**, 82.
- (17) Slipher, V. M., 1903. *Lick Obs. Bull.*, **1**, 23.
- (18) Shobbrook, R. R. & Lomb, N. R., 1972. *Mon. Not. R. astr. Soc.*, **156**, 181.
- (19) Davis, J. Morton, D. C., Allen, L. R. & Hanbury Brown, R., 1970. *Mon. Not. R. astr. Soc.*, **150**, 45.

NOTE ADDED IN PROOF

We omitted to note that the values for ζ Pup in Tables I, II and III differ slightly, but not significantly, from those published previously (19). These differences represent minor corrections for errors in the orientation of the baseline (Section 5).

EMPIRICAL EFFECTIVE TEMPERATURES AND BOLOMETRIC CORRECTIONS FOR EARLY-TYPE STARS

A. D. CODE,* J. DAVIS,† R. C. BLESS,* AND R. HANBURY BROWN†

Received 1975 January 10

ABSTRACT

An empirical effective temperature for a star can be found by measuring its apparent angular diameter and absolute flux distribution. The angular diameters of 32 bright stars in the spectral range O5f to F8 have recently been measured with the stellar interferometer at Narrabri Observatory, and their absolute flux distributions have been found by combining observations of ultraviolet flux from the Orbiting Astronomical Observatory (OAO-2) with ground-based photometry. In this paper these data have been combined to derive empirical effective temperatures and bolometric corrections for these 32 stars.

Subject headings: spectrophotometry — stars: atmospheres — stars: early-type — ultraviolet: general

I. INTRODUCTION

Effective temperatures and bolometric corrections provide the essential link between the observed properties of stars and the results of theoretical calculations on stellar structure and stellar atmospheres. Until recently, however, the determination of main-sequence stellar effective temperatures and bolometric corrections, with the exception of the Sun, has depended upon theoretical arguments for its derivation. This is because a large fraction of the emergent flux for hot stars is in the ultraviolet, and, without measurements in this region of the spectrum, recourse to theoretical extrapolation was necessary. Morton and Adams (1968) have reviewed the history of efforts in this field and at the same time given effective temperature and bolometric correction scales for early-type stars based on theoretical model stellar atmospheres. In the absence of empirical data these scales have been valuable. However, the recent development of two new observational techniques, the Orbiting Astronomical Observatory and the stellar intensity interferometer, has now made it possible, for the first time, to base our knowledge of these fundamental parameters on observational data.

The effective temperature of a star can be found from measurements of its angular diameter and the total absolute flux, integrated over the entire spectrum received from the star above the Earth's atmosphere. The bolometric correction can be found from the flux distribution alone. For 32 stars in the spectral range of O5f to F8 we now know both the angular diameters (at $\lambda 4430$) and the absolute flux longward of $\lambda 1100$. The angular diameters have been measured with the stellar intensity interferometer at Narrabri Observatory (Hanbury Brown *et al.* 1974), and the ultraviolet

fluxes in the range $\lambda 1100$ – 3300 have been measured with the Orbiting Astronomical Observatory (OAO-2) (Bless *et al.* 1976). Fluxes in the range $\lambda 3300$ – 8080 have been found via conventional spectrophotometry (Davis and Webb 1974), while broad-band photometry is available longward of $\lambda 8080$.

In this paper we report the results of combining these data to find the effective temperatures and bolometric corrections, both based on observations for these 32 stars.

II. OBSERVATIONS

a) Angular Diameters

The angular diameters of the equivalent uniform disks (θ_{UD}) for 32 stars in the spectral range O5f to F8 have been measured at Narrabri Observatory (Hanbury Brown *et al.* 1974). The true angular diameters (θ_{LD}) have been derived by Hanbury Brown *et al.* by applying small but significant corrections to the values of θ_{UD} to allow for limb darkening. The corrections were derived from model stellar atmospheres and have been discussed in detail by Hanbury Brown *et al.* (1974). Of the 32 stars measured, five were found to have companions (ζ Ori, γ^2 Vel, β Cru, α Vir, and δ Sco), and the brightness ratio at $\lambda 4430$ of the brighter to the fainter component was found for each with the interferometer. Allowances for the flux contributions of the companions to the total measured flux will be considered in § IVb.

The 32 stars and their angular diameters are listed in Table 1 together with their MK spectral types and photometric data. The MK types have been taken, in order of preference, from Morgan and Keenan (1973), Johnson and Morgan (1952), Hiltner *et al.* (1969), Conti and Smith (1972), Lesh (1968), and Johnson *et al.* (1966), and the photometric data from Johnson *et al.* (1966).

* Washburn Observatory, University of Wisconsin, Madison.

† Chatterton Astronomy Department, School of Physics, University of Sydney, Australia.

TABLE 1

THE PROGRAM STARS

Photometry and Angular Diameters

B.S.	HD	NAME	MK	V	B-V	θ_{LO}		m_{5500}^*	E_{B-V}	Δm^\dagger
						$(10^{-3} \text{ seconds of arc})$				
472	10144	α Eri	B3 Vp	(0 ^m .47)	-0 ^m .15	1.92	± 0.07	+0 ^m .422		
1713	34085	β Ori	B8 Ia	+0.13	-0.03	2.55	0.05	+0.171		
1790	35468	γ Ori	B2 III	+1.64	-0.22	0.72	0.04	+1.607		
1903	37128	ϵ Ori	B0 Ia	+1.69	-0.18	0.69	0.04	+1.684	0 ^m .06	
1948	37742	ζ Ori	09.5 Ib	+1.77	-0.21	0.48	0.04	+1.732	0.04	2 ^m .0
2004	38771	κ Ori	80.5 Ia	+2.05	-0.18	0.45	0.03	+2.052	0.03	
2294	44743	β CMa	B1 II-III	+1.97	-0.24	0.52	0.03	+1.952		
2326	45348	α Car	F0 Ib-II	-0.75	+0.15	6.6	0.8	-0.776		
2421	47105	γ Gem	A0 IV	+1.92	0.00	1.39	0.09	+1.899		
2491	48915	α CMa	A1 V	-1.46	0.00	5.89	0.16	-1.456		
2618	52089	ϵ CMa	B2 II	+1.50	-0.21	0.80	0.05	+1.466		
2693	54605	δ CMa	F8 Ia	+1.84	+0.67	3.60	0.50	+1.779	0.12	
2827	58350	η CMa	B5 Ia	+2.44	-0.09	0.75	0.06	+2.414		
2943	61421	α CMi	F5 IV-V	+0.37	+0.42	5.50	0.17	+0.321		
3165	66811	ζ Pup	O5 V	+2.25	-0.27	0.42	0.03	+2.219	0.04	
3207	68273	γ^2 Vel	WC8 + O9I	+1.83	-0.25	0.44	0.05	+1.877	0.04	1.4
3685	80007	β Car	A1 IV	+1.68	0.00	1.59	0.07	+1.629		
3982	87901	α Leo	B7 V	+1.35	-0.11	1.37	0.06	+1.335		
4534	102647	β Leo	A3 V	+2.14	+0.08	1.33	0.10	+2.091		
4662	106625	γ Crv	B8 III	+2.58	-0.11	0.75	0.06	+2.557		
4853	111123	β Cru	80.5 III	+1.25	-0.23	0.722	0.023	+1.221	0.03	2.9
5056	116658	α Vir	B1 IV	+0.97	-0.23	0.87	0.04	+0.947		2.0
5132	118716	ϵ Cen	B1 III	+2.30	-0.22	0.48	0.03	+2.270	0.03	
5953	143275	δ Sco	80.5 IV	+2.32	-0.12	0.46	0.04	+2.295	0.17	1.9
6175	149757	ζ Oph	09.5 V	+2.56	+0.02	0.51	0.05	+2.532	0.32	
6556	159561	α Oph	A5 III	+2.07	+0.15	1.63	0.13	+2.040		
6879	169022	ϵ Sgr	A0 V	+1.85	-0.03	1.44	0.06	+1.784		
7001	172167	α Lyr	A0 V	+0.03	0.00	3.24	0.07	0.000		
7557	187642	α Aql	A7 IV,V	+0.76	+0.22	2.98	0.14	+0.724		
7790	193924	α Pav	B2.5 V	+1.94	-0.20	0.80	0.05	+1.907		
8425	209952	α Gru	B7 IV	+1.74	-0.13	1.02	0.07	+1.724		
8728	216956	α PsA	A3 V	+1.16	+0.09	2.10	0.14	+1.114		

*Monochromatic magnitudes by Davis (1974)

†Measured with intensity interferometer at $\lambda 4430$ (Hanbury Brown *et al.* 1974) except for γ^2 Vel where listed $\Delta m = \Delta m_V$ (Conti and Smith, 1972)

b) Ultraviolet Fluxes

The reader can find a detailed description of the OAO-2 Wisconsin instrumentation in the paper by Code *et al.* (1970). The ultraviolet observations were made with two objective grating spectrometers, the first sensitive over the region $\lambda\lambda 3500-2000$ (Sp 1), the second from $\lambda\lambda 2000-1100$ (Sp 2), with spectral resolution of about 20 Å and 10 Å, respectively. Generally, two Sp 1 scans were available for each star, whereas about five scans were used to form the average curve in the Sp 2 region. All scans were checked to make certain that the various environmental and instrumental effects possible—scattered sunlight, the South Atlantic anomaly, changes in spacecraft pointing during a scan, etc.—were not affecting the data. The Sp 1 and 2 scans were then averaged and tabulated by computer at 10 Å and 5 Å intervals, respectively, and stored on disk for future use. The dispersion of individual Sp 2 scans about the average was typically only a few percent and never more than 7 percent. Sp 1 scans were similarly constant in their relative sensi-

tivity but show large variations in their absolute level, caused by electronic problems in the payload.

These averaged scans of the program stars were then transformed to absolute energy curves by applying the appropriate calibration corrections determined from an Aerobee rocket flight (Bless *et al.* 1976). In this flight absolute photometric observations in six wavelength bands between $\lambda 1300$ and $\lambda 2900$ were made of α Vir, η UMa, and α Leo. The absolute calibration of the Aerobee telescopes was determined with reference to the well-defined synchrotron radiation from 240 MeV electrons circulating in the University of Wisconsin electron storage ring. This absolute calibration was performed before and after the Aerobee flight; in addition, field calibrations made three days before the flight and one day afterward, as well as comparisons during the laboratory calibrations, confirmed the stability of the calibration. Internal errors amounted to ± 5 percent for the photometers with bandpasses longward of $\lambda 2000$, and ± 10 percent for those shortward of $\lambda 2000$. With these data on OAO-2, calibration was determined as described in the previous paper, and

this calibration was applied to the averaged scans. Sp 2 data were immediately on an absolute energy basis ($\text{ergs cm}^{-2} \text{s}^{-1} \text{\AA}^{-1}$), whereas the longer wavelength scans were only in "relative absolute" terms because of the variations in the overall absolute sensitivity level of this instrument, mentioned earlier.

c) Visual Fluxes

Relative spectrophotometry with 50 Å bandwidths centered on 25 wavelengths in the range $\lambda\lambda 3300\text{--}8080$ for 30 of the 32 stars listed in Table 1 has been carried out by Davis and Webb (1974). The two stars not observed are α Lyr, which was too far north to be observed satisfactorily from Mount Stromlo where the observations were made, and γ^2 Vel, which has bright emission lines making 50 Å band observations difficult to interpret. The spectrophotometric observations for the 30 stars were reduced relative to the Oke secondary standards ϵ Ori and ζ Oph, which are included in the 30 stars, and the results have been presented as magnitudes relative to α Lyr using Oke's (1964) relative spectrophotometry of ϵ Ori, ζ Oph, and α Lyr. Each relative flux distribution was normalized to zero at $\lambda 5556$. For γ^2 Vel, monochromatic magnitudes, based on a continuous spectral scan, have been taken from Aller and Faulkner (1961) in the range $\lambda\lambda 3440\text{--}5850$, and expressed as magnitudes relative to α Lyr.

Hayes (1970) and Oke and Schild (1970) have carried out careful spectrophotometric calibrations of α Lyr in the spectral range $\lambda\lambda 3200\text{--}10870$. The agreement between these two calibrations is excellent for $\lambda\lambda 4000\text{--}6000$, but there are discrepancies shortward of the Balmer jump and longward of the Paschen jump. Oke and Schild also measured the absolute monochromatic flux from α Lyr at $\lambda 5556$. The absolute monochromatic flux from a star with $V = 0.00$ mag at $\lambda 5556$ has been discussed by Code (1960), for $V = 0.00$ mag at $\lambda 5464$ by Davis and Webb (1970), and the integral effective intensity for the V band for $V = 0.00$ mag by Code (1973). But, rather than take some arbitrary average of the spectrophotometric calibrations and of absolute monochromatic flux determinations, the measurements of Oke and Schild have been adopted for the sake of simplicity and consistency. The effects of this arbitrary decision, rather than taking into consideration other spectrophotometric and flux calibrations, including the recent revision by Hayes and Latham (1974) of the Hayes (1970) and Oke and Schild (1970) calibrations, will be discussed in § III d. With the adoption of Oke and Schild's results, their spectrophotometric calibration of α Lyr, which is in fact a relative absolute flux distribution, has been used to convert the relative flux distributions for the other 31 stars in Table 1 into relative absolute flux distributions.

It is obviously preferable to scale the relative absolute flux distribution for each star by a narrow-band measurement to obtain the absolute flux distribution rather than by the broad-band V magnitude. With this in mind, monochromatic magnitudes at $\lambda 5500$ (m_{5500}) for all the stars in Table 1 have been

measured by Davis (1974). The observations were made with a bandwidth of 30 Å centered on $\lambda 5500$ which was defined by an interference filter whose temperature was held constant for the observations. The choice of $\lambda 5500$ for the monochromatic photometry is a compromise between the desire to be close to the adopted effective wavelength of the V band ($\lambda 5480$) and the wavelength chosen by Oke and Schild for their absolute flux measurement of α Lyr ($\lambda 5556$) and, at the same time, to avoid emission lines in the spectra of the night sky and of terrestrial sources. Since α Lyr was included in the observational program, the monochromatic magnitude for each star (m_{5500}) can be expressed relative to $m_{5500} = 0.00$ for α Lyr. These are listed in column (8) of Table 1. The flux from α Lyr at $\lambda 5500$, based on the spectrophotometric calibration and absolute flux measurement of Oke and Schild, was taken as $3.47 \times 10^{-9} \text{ ergs cm}^{-2} \text{ s}^{-1} \text{\AA}^{-1}$. Thus the relative absolute flux distributions were converted to absolute flux distributions by scaling this flux by the intensity ratio corresponding to the normalized values of m_{5500} in Table 1. To facilitate this scaling, $\lambda 5500$ was included as one of the 25 wavelengths in the spectrophotometry of Davis and Webb (1974). The absolute flux distributions have all been computed in units of $\text{ergs cm}^{-2} \text{ s}^{-1} \text{\AA}^{-1}$ rather than per unit frequency interval, in order to correspond to the ultraviolet data which are to be matched to them (§ III a).

d) Infrared Fluxes

To extend the flux curves longward of $\lambda 8080$ use has been made of the narrow band "86," "99," and "110" magnitudes of Mitchell and Johnson (1969), the broad-band I , J , K , and L magnitudes of Johnson *et al.* (1966); and the broad-band M and N magnitudes of Johnson (1965a).

In order that the absolute calibration of the infrared photometry should be consistent with that used in the visual, it has been based on the calibration of α Lyr by Oke and Schild (1970). In the case of the "86," "99," "110," and I bands, this is straightforward, since the Oke and Schild calibration extends to $\lambda 10800$, covering all but the "110" band, for which a small extrapolation is necessary. For the J , K , L , M , and N bands, the calibration was derived via a mean of the Labs and Neckel (1968) and Arvesen *et al.* (1969) solar flux distributions using $V_{\odot} = -26.74$ and the solar colors given by Johnson (1965b) to obtain fluxes corresponding to zero magnitude for each of the bands. The fluxes were finally scaled by the ratio, at $\lambda 5480$, of the Oke and Schild flux for $V = 0.00$ to the mean solar flux reduced to $V = 0.00$, to put them on the same calibration as the "86," "99," "110," and I bands.

Magnitudes are not generally available for all nine photometric bands for the stars in Table 1. In fact, for seven stars the only available infrared photometry is a magnitude for the I band. However, for most of the stars in Table 1 the infrared flux is only a small fraction of the total flux, and sufficient data are available to enable the integrated infrared flux from each

of the stars to be estimated with adequate precision for the present purpose. This will be discussed further in § IIIa.

III. EMPIRICAL FLUX DISTRIBUTION

a) Combining Ultraviolet, Visual, and Infrared Flux Measurements

The calibration of the flux distributions in the middle ultraviolet ($\lambda\lambda 1800\text{--}3800$) is of a relative absolute nature (§ IIb), and, in order to place it on an absolute basis, use must be made of the absolute calibration in either one or both of the adjacent spectral regions. The absolute calibration of the visual fluxes is believed to be more secure than that for the far-ultraviolet ($\lambda\lambda 1100\text{--}1800$), and, for this reason, the absolute calibration of the middle-ultraviolet flux distributions has been based on matching them to the visual data in the overlapping range $\lambda\lambda 3300\text{--}3800$.

The matching was carried out with the aid of an interactive computer program and a storage display unit. The program, written on a Modcomp III computer for the analysis and calibration of OAO-2 scanner data, accepted spectral data in the form of fluxes at wavelengths spaced with a constant interval between them. The simplest way of accommodating the visual data was to interpolate in the data described in § IIc at constant wavelength interval. Thus visual fluxes at wavelengths from $\lambda 3300$ to $\lambda 8100$ inclusive, at 200 Å intervals, were obtained for each star except γ^2 Vel, for which wavelengths from $\lambda 3400$ to $\lambda 6000$ inclusive, at 200 Å intervals, were used.

For each star, in turn, the visual fluxes were displayed on a flux versus wavelength plot on the storage display unit. The middle ultraviolet fluxes were also displayed and scaled by an appropriate factor to give the best fit, judged by eye, to the visual fluxes at $\lambda\lambda 3300$, 3500, and 3700. To facilitate an accurate match, it was possible to select only the overlapping region of interest for display on an expanded scale. After completion of the match, the far-ultraviolet fluxes were also displayed, and the region in the neighborhood of $\lambda 1800$, where they meet the middle-ultraviolet fluxes, was examined. It was found that the agreement between the two ultraviolet flux distributions is in general remarkably good, with a mean difference of only ~ 3 percent, the middle-ultraviolet having higher fluxes on the average than the far-ultraviolet. The rms deviation about the mean is ± 7 percent, which lies well within our estimated uncertainty in the far-ultraviolet calibration (§ III d). As a result, there was no difficulty in deciding how to join the two flux distributions in the neighborhood of $\lambda 1800$. Hence, flux distributions extending over the range $\lambda\lambda 1100\text{--}8100$ have been obtained for all the stars except γ^2 Vel, where the range is $\lambda\lambda 1100\text{--}6000$, and δ CMa and α CMi, where the range is effectively $\lambda\lambda 1800\text{--}8100$. (No far-ultraviolet scans were obtained for these cooler stars, since they have negligible flux in that region of the spectrum as verified by OAO-2 filter photometry.)

The region of the spectrum longward of $\lambda 8100$ was

treated separately. To avoid an infinite tail, the fluxes per unit frequency were plotted against $1/\lambda$. For each star for which infrared photometry was available, a plot, including the red end of the visual flux distributions as well as all the available infrared photometry, was made, and a smooth curve drawn through the points to zero at $1/\lambda = 0$. In this way infrared flux distributions were constructed for 25 out of the 32 stars. For the remaining seven stars, integrated fluxes were obtained by interpolation in the results for the 25 stars (see § III c). Figure 1 shows the combined flux curves for four of the program stars.

b) Corrections for Interstellar Extinction

Interstellar extinction is significant for only 10 of the 32 stars, and the color excesses (E_{B-V}) for these stars are listed in column (9) of Table 1. Table 2 contains the interstellar extinction curve adopted. This curve was constructed by combining the results in the visual and near-infrared of Johnson and Borgman (1963), Boggess and Borgman (1964), and van de Hulst's (1949) theoretical curve number 15. These agree very well with each other except in the region $1.0 < \lambda^{-1} < 1.75$, where a mean was taken. The infrared results ($\lambda^{-1} < 0.5$) were taken from van de Hulst. Toward the ultraviolet the visual curve was joined to the ultraviolet results of Cashdollar and Code (1975) based on the mean values derived from OAO-2 photometry of about 60 stars. This curve is identical to the "average" curve of Bless and Savage (1972) to $\lambda^{-1} \approx 5.5$; shortward of this the extinction based on the much larger sample of stars taken by Cashdollar and Code is about 5–10 percent greater than that derived by Bless and Savage. By $\lambda^{-1} \approx 9$, however, the two curves join again. With the rather large scatter in extinction possible shortward of the $\lambda 2200$ bump and the generally small values of $(B - V)$ color excesses for the program stars discussed here, these differences in the ultraviolet extinction curves are of no importance except for ζ Oph [$E(B - V) = 0.32$ mag]. For this object, extinction corrections were derived from ζ Oph itself by comparing its energy curve with the mean of less reddened stars of similar spectral type.

The computer program used to match the ultraviolet and visual flux distributions (§ III a) has provision for correcting fluxes for the effects of interstellar extinction, and it was therefore used to apply the appropriate corrections before the flux integrations were made. In the case of the infrared fluxes, the corrections were made before the fluxes were plotted against $1/\lambda$.

c) Integration of Fluxes

The empirical flux distributions were integrated in five wavelength bands: (1) $\lambda\lambda 1100\text{--}1300$, (2) $\lambda\lambda 1300\text{--}1800$, (3) $\lambda\lambda 1800\text{--}3300$, (4) $\lambda\lambda 3300\text{--}8100$, and (5) $\lambda\lambda 8100\text{--}\infty$. The division at $\lambda 1300$ was made because the absolute flux calibration is more uncertain shortward of $\lambda 1300$ than for $\lambda\lambda 1300\text{--}1800$. The divisions at $\lambda 1800$ and $\lambda 3300$ mark the boundaries between Sp 1 and Sp 2, and between the ultraviolet and visual

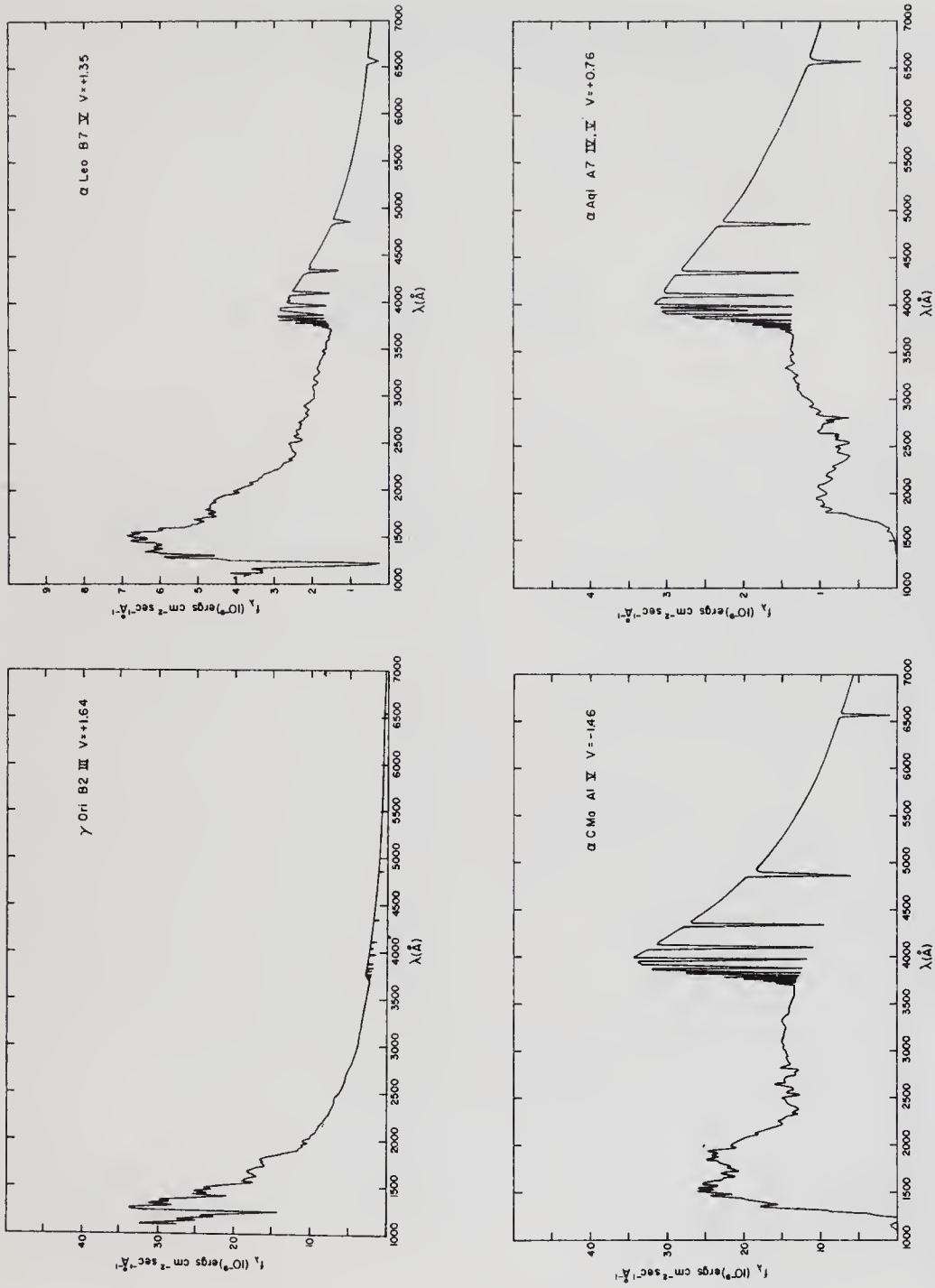


FIG. 1.—The observed energy distribution for the four program stars, γ Ori, α Leo, α CMa, and α Aql, in the spectral interval from 1100 to 7000 Å . The flux received at the Earth is plotted per unit wavelength interval in units of 10^{-9} ergs $\text{cm}^{-2} \text{sec}^{-1} \text{Å}^{-1}$.

TABLE 2

ADOPTED EXTINCTION CURVE
 A_λ/E_{B-V}

Wavelength	A_λ/E_{B-V}	Wavelength	A_λ/E_{B-V}	Wavelength	A_λ/E_{B-V}
1100	11.70	2600	6.82	5500	3.09
1200	10.20	2700	6.41	5700	2.95
1300	9.19	2800	6.10	5900	2.80
1400	8.54	2900	5.85	6100	2.65
1500	8.29	3000	5.65	6300	2.50
1600	8.03	3300	5.16	6500	2.36
1700	7.85	3500	4.92	6700	2.25
1800	7.90	3700	4.70	6900	2.15
1900	8.38	3900	4.51	7100	2.05
2000	9.05	4100	4.35	7300	1.96
2100	9.90	4300	4.14	7500	1.87
2160	10.10	4500	3.94	7700	1.76
2200	9.85	4700	3.76	7900	1.69
2300	8.75	4900	3.57	8100	1.62
2400	7.92	5100	3.40	8300	1.55
2500	7.30	5300	3.24	8500	1.49

measurements, respectively. These boundaries differed slightly for some stars, depending on how the adjoining flux distributions were matched. The flux integrations for the first four bands were carried out in the computer using the trapezoidal approximation, while for the fifth band the integrations of the smooth curves drawn through the fluxes were done graphically. The results of these integrations together with the actual integration boundaries are listed in Table 3. Errors arising from the use of the trapezoidal approximation for $\lambda 3300-8100$ are discussed in § IVa.

For six stars Sp 1 scans were not available, and in each case substitute scans were obtained from stars of similar spectral type. These latter stars are given in the footnote to Table 3. The substitute scans were scaled to fit the visual data for the program stars just as if they had been measured for the stars themselves. In each case, except for δ CMa, the resulting fit near $\lambda 1800$ to the Sp 2 scan was good. For δ CMa there was no Sp 2 scan as explained in § IIIa because the flux in that region of the spectrum is negligible. In fact, less than 2 percent of the flux from δ CMa is radiated shortward of $\lambda 3300$, so the total integrated flux is insensitive to the scan adopted for $\lambda < 3300 \text{ \AA}$.

We believe that the use of substitute scans in the six cases introduces no significant additional uncertainty beyond that discussed in the next section.

In order to obtain integrated infrared fluxes for the seven stars for which such flux measurements were not available (§ IIIa), the following approach was adopted. The integrated infrared fluxes for 21 of the other stars (four binary stars were omitted) were scaled to $V = 0.00$ mag and plotted against $(B - V)_0$. A smooth curve was drawn through the points and integrated fluxes for the seven stars obtained by interpolation, using $(B - V)_0$ and scaling by the V magnitudes of the stars. The uncertainty introduced by this interpolation is discussed in the next section.

d) Uncertainties In Integrated Fluxes

The percentage uncertainties in the integrated fluxes in each of the five bands have been estimated and are listed in Table 4. These percentage uncertainties were applied to the integrated fluxes in each band in order to obtain the uncertainties in the total empirical fluxes as given in Table 3.

Because of the manner in which the estimates were made, the percentage uncertainties in Table 4 represent more nearly the maximum likely error rather than the standard deviation in the flux integrations.

For band (1) the uncertainty estimate is based on a comparison of the OAO calibration (§ IIb) with the calibrations of Stuart (1969), Carruthers (1969), and Henry *et al.* (1975).

In order to estimate the uncertainty for band (2), the uncertainty in the absolute flux at $\lambda 1300$ has been assumed to be ± 30 percent and, at $\lambda 1800$, ± 10 percent, varying linearly between these limits. The largest percentage uncertainty in the *integrated* flux between these limits will occur for the hottest stars, since they give the largest ratios for the flux at $\lambda 1300$ to the flux at $\lambda 1800$. For ζ Pup the uncertainty in the integrated flux in this band was found to be ± 21 percent, and, although this could be regarded as an upper limit, it has been adopted as the uncertainty for band (2). For band (3) the same approach has been used as for band (2), assuming the uncertainty in the absolute flux at $\lambda 1800$ to be ± 10 percent and, at $\lambda 3300$, ± 5 percent with a linear interpolation in between. The uncertainty in the integrated flux for ζ Pup in the band was found to be ± 8.5 percent, and this has been adopted as the uncertainty for band (3). The uncertainty in the visual band (4) has been estimated from the uncertainties in the relative spectrophotometry (Davis and Webb 1974), in the relative spectrophotometry and absolute flux calibration of α Lyr (Oke and Schild

TABLE 3

INTEGRATED STELLAR FLUXES OUTSIDE THE EARTH'S ATMOSPHERE
CORRECTED FOR INTERSTELLAR ABSORPTION

BS	Star	Band	Wavelength Range (Å)	Flux $\pm \sigma$ (10^{-6} erg cm $^{-2}$ s $^{-1}$)	$\frac{100\delta F}{F}$	Total flux $\pm \sigma$ (10^{-6} erg cm $^{-2}$ s $^{-1}$)	
472	α Eri	T	0 - 1100	2.0	0.4	54.4	4.3
		1	1100 - 1300	6.0	2.1		
		2	1300 - 1870	16.5	3.5		
		3	1870 - 3300	15.2	1.3		
		4	3300 - 8100	13.0	0.5		
1713	β Ori	5	8100 - ∞	2.2	0.2	38.5	1.7
		T	0 - 1100	0.13	0.03		
		1	1100 - 1300	0.8	0.3		
		2	1300 - 1810	5.4	1.1		
		3	1810 - 3300	12.5	1.1		
1790	γ Ori	4	3300 - 8100	16.2	0.6	37.6	3.4
		5	8100 - ∞	3.7	0.4		
		T	0 - 1100	6.1	1.2		
		1	1100 - 1300	5.4	1.9		
		2	1300 - 1850	11.3	2.4		
1903	ϵ Ori	3	1850 - 3500	10.0	0.8	60.2	5.4
		4	3500 - 8100	4.4	0.2		
		5	8100 - ∞	0.6	0.1		
		T	0 - 1100	12.5	2.5		
		1	1100 - 1300	8.3	3.1		
1948	ζ Ori	2	1300 - 1800	15.7	3.3	71.4	13.1
		3	1800 - 3300	16.9	1.4		
		4	3300 - 8100	5.9	0.2		
		5	8100 - ∞	0.7	0.1		
		T	0 - 1100	24.3	12.1		
2004	κ Ori	1	1100 - 1300	9.5	3.3	32.7	4.5
		2	1300 - 1820	8.0	1.7		
		3	1820 - 3300	8.8	0.7		
		4	3300 - 8100	3.8	0.2		
		5	8100 - ∞	0.5	0.1		
2294	β CMa	T	0 - 1100	7.6	3.8	36.2	4.9
		1	1100 - 1300	4.2	1.5		
		2	1300 - 1850	10.3	2.2		
		3	1850 - 3500	8.8	0.7		
		4	3500 - 8100	3.3	0.1		
2326	α Car	5	8100 - ∞	0.5	0.1	45.0	1.8
		T	---	---	---		
		1	---	---	---		
		2	1500 - 1850	0.12	0.03		
		3	1850 - 3300	1.8	0.2		
2421	γ Gem	4	3300 - 8100	31.3	1.3	4.73	0.17
		5	8100 - ∞	12.5	1.2		
		T	---	---	---		
		1	1280 - 1300	~0.00	---		
		2	1300 - 1830	0.27	0.06		

TABLE 3 -- Continued

BS	Star	Band	Wavelength Range (Å)	Flux $\pm \sigma$ (10^{-6} erg cm $^{-2}$ s $^{-1}$)		$\frac{100\delta F}{F}$	Total flux $\pm \sigma$ (10^{-6} erg cm $^{-2}$ s $^{-1}$)	
2491	α CMa	T	---	---	---			
		1	1130 - 1300	0.3	0.1			
		2	1300 - 1830	11.3	2.4	2.5	114.3	4.4
		3	1830 - 3300	23.7	2.0			
		4	3300 - 8100	66.7	2.7			
5	8100 - ∞	15.2	1.5					
2618	ϵ CMa	T	0 - 1100	6.5	1.3			
		1	1100 - 1300	5.2	1.8			
		2	1300 - 1810	10.7	2.2	0.5	41.5	3.3
		3	1810 - 3300	12.8	1.1			
		4	3300 - 8100	5.8	0.2			
5	8100 - ∞	0.7	0.1					
2693	δ CMa	T	---	---	---			
		1	---	---				
		2	---	---				
		3	2530 - 3300	0.10	0.01	1.5	6.01	0.27
		4	3300 - 8100	3.69	0.15			
5	8100 - ∞	2.31	0.23					
2827	η CMa	T	0 - 1100	0.10	0.02			
		1	1100 - 1300	0.21	0.07			
		2	1300 - 1860	1.05	0.22	0.5	5.88	0.30
		3	1860 - 3300	1.97	0.17			
		4	3300 - 8100	2.14	0.09			
5	8100 - ∞	0.44	0.04					
2943	α CMi	T	---	---	---			
		1	---	---				
		2	---	---				
		3	2020 - 3300	1.03	0.09	1.0	18.08	0.76
		4	3300 - 8100	11.16	0.45			
5	8100 - ∞	6.07	0.61					
3165	ζ Pup	T	0 - 1100	22.6	11.3			
		1	1100 - 1300	10.7	3.7			
		2	1300 - 1850	16.5	3.5	0.5	65.6	12.4
		3	1850 - 3300	12.0	1.0			
		4	3300 - 8100	3.7	0.1			
5	8100 - ∞	0.36	0.04					
3207	γ^2 Vel	T	0 - 1100	36.1	18.0			
		1	1100 - 1300	13.1	4.6			
		2	1300 - 1810	19.6	4.1	0	91.8	19.1
		3	1800 - 3600	18.5	1.6			
		4	3600 - 6000	3.2	0.1			
5	6000 - ∞	1.3	0.1					
3685	β Car	T	---	---	---			
		1	1125 - 1300	0.10	0.04			
		2	1300 - 1820	0.43	0.09	2.0	6.14	0.22
		3	1820 - 3300	1.02	0.09			
		4	3300 - 8100	3.78	0.15			
5	8100 - ∞	0.94	0.09					
3982	α Leo	T	0 - 1100	0.10	0.02			
		1	1100 - 1300	0.64	0.22			
		2	1300 - 1850	3.08	0.65	1.5	13.94	0.80
		3	1850 - 3300	3.86	0.33			
		4	3300 - 8100	5.39	0.22			
5	8100 - ∞	1.08	0.11					
4534	β Leo	T	---	---	---			
		1	---	---				
		2	1470 - 1820	0.09	0.02	2.5	3.61	0.13
		3	1820 - 3300	0.57	0.05			
		4	3300 - 8100	2.36	0.09			
5	8100 - ∞	0.68	0.07					

TABLE 3 -- Continued

BS	Star	Band	Wavelength Range (Å)	Flux $\pm \sigma$ (10^{-6} erg cm $^{-2}$ s $^{-1}$)	$\frac{100\delta F}{F}$	Total Flux $\pm \sigma$ (10^{-6} erg cm $^{-2}$ s $^{-1}$)		
4662	γ Crv	T	0 - 1100	0.04	0.01	1.0	4.49	0.27
		1	1100 - 1300	0.23	0.08			
		2	1300 - 1830	1.05	0.22			
		3	1830 - 3500	1.22	0.10			
		4	3500 - 8100	1.65	0.07			
5	8100 - ∞	0.35	0.04					
4853	β Cru	T	0 - 1100	23.4	11.7	0.5	102.9	14.9
		1	1100 - 1300	18.1	6.3			
		2	1300 - 1890	31.1	6.5			
		3	1890 - 3300	21.5	1.8			
		4	3300 - 8100	8.4	0.3			
5	8100 - ∞	0.9	0.1					
5056	α Vir	T	0 - 1100	17.2	3.4	0.5	89.9	8.6
		1	1100 - 1300	14.8	5.2			
		2	1300 - 1830	26.9	5.6			
		3	1830 - 3500	22.1	1.9			
		4	3500 - 8100	8.2	0.3			
5	8100 - ∞	1.2	0.1					
5132	ϵ Cen	T	0 - 1100	6.9	3.4	0.5	33.7	4.6
		1	1100 - 1300	5.9	2.1			
		2	1300 - 1850	9.9	2.1			
		3	1850 - 3300	7.7	0.7			
		4	3300 - 8100	3.1	0.1			
5	8100 - ∞	0.36	0.04					
5953	δ Sco	T	0 - 1100	20.6	10.3	0.5	72.7	12.1
		1	1100 - 1300	12.9	4.5			
		2	1300 - 1840	20.2	4.2			
		3	1840 - 3300	14.2	1.2			
		4	3300 - 8100	4.7	0.2			
5	8100 - ∞	0.49	0.05					
6175	ζ Oph	T	0 - 1100	25.7	12.8	0.5	89.8	14.7
		1	1100 - 1300	13.1	4.6			
		2	1300 - 1850	24.7	5.2			
		3	1850 - 3300	20.3	1.7			
		4	3300 - 8100	6.0	0.2			
5	8100 - ∞	0.5	0.1					
6556	α Oph	T	---	---	---	20.0	3.65	0.13
		1	---	---	---			
		2	1610 - 1820	0.03	0.01			
		3	1820 - 3300	0.46	0.04			
		4	3300 - 8100	2.40	0.10			
5	8100 - ∞	0.83	0.08					
6879	ϵ Sgr	T	---	---	---	2.5	5.53	0.22
		1	1145 - 1300	0.05	0.02			
		2	1300 - 2010	0.66	0.14			
		3	2010 - 3300	0.86	0.07			
		4	3300 - 8100	3.33	0.13			
5	8100 - ∞	0.77	0.08					
7001	α Lyr	T	---	---	---	2.5	30.4	1.2
		1	1240 - 1300	0.10	0.04			
		2	1300 - 1820	3.5	0.7			
		3	1820 - 3300	6.4	0.5			
		4	3300 - 8100	16.9	0.7			
5	8100 - ∞	4.3	0.4					
7557	α Aql	T	---	---	---	2.0	12.17	0.46
		1	---	---	---			
		2	1535 - 1830	0.10	0.02			
		3	1830 - 3300	1.43	0.12			
		4	3300 - 8100	7.89	0.32			
5	8100 - ∞	3.00	0.30					

TABLE 3 -- Continued

BS	Star	Band	Wavelength Range (Å)	Flux ± σ ₂ (10 ⁻⁶ erg cm ⁻² s ⁻¹)	100ΔF/F	Total Flux ± σ ₁ (10 ⁻⁶ erg cm ⁻² s ⁻¹)	
7790	α Pav	T	0 - 1100	2.4	0.5	21.8	1.9
		1	1100 - 1300	3.1	1.1		
		2	1300 - 1900	6.8	1.4		
		3	1900 - 3300	5.4	0.5		
		4	3300 - 8100	3.7	0.1		
8425	α Cru	T	0 - 1100	0.4	0.1	13.5	0.9
		1	1100 - 1300	1.0	0.4		
		2	1300 - 1810	3.5	0.7		
		3	1810 - 3300	4.1	0.3		
		4	3300 - 8100	4.0	0.2		
8728	α PsA	T	---	---	---	8.80	0.31
		1	---	---	---		
		2	1465 - 1820	0.18	0.04		
		3	1820 - 3300	1.38	0.12		
		4	3300 - 8100	5.80	0.23		
5	8100 - ∞	1.67	0.17				

Notes for Column 5 (See § IIIc for full explanation)

1. Flux using α Lup for 2618 ε CMa
2. Flux using β Dor for 2693 δ CMa
3. Flux using α PsA for 4534 β Leo
4. Flux using φ Sgr for 4662 γ Crv
5. Flux using β Car for 6879 ε Sgr
6. Flux using ε Lup for 7790 α Pav

1970), and in the monochromatic photometry (Davis 1974). Since the Oke and Schild calibration of α Lyr was adopted arbitrarily (§ IIc), the differences between it and the spectrophotometric calibration by Hayes (1970), as discussed by Hayes and Latham (1975), and other absolute flux calibrations (see Code 1960, Davis and Webb 1970, and Code 1973 for additional discussions of this topic) have also been taken into consideration. The uncertainty in the integrated flux in band (4), taking all the above factors into account, is estimated to be ± 4 percent. The uncertainty in the infrared band (5) is based on the plot of integrated fluxes for V = 0.00 mag against (B - V)₀ (§ IIIc). The rms deviation of the 21 points about the curve drawn through them is ± 6 percent with a maximum deviation in the range used for interpolations of ± 10

percent. Since this is much larger than the uncertainty in the absolute calibration, it is reasonable to assume that the interpolated values lie within ± 10 percent of the true fluxes.

IV. EMERGENT FLUXES AND EFFECTIVE TEMPERATURES

a) Completion of Flux Distributions

The observed flux in the wavelength interval from λ1100 to infinity has been discussed in § III. For the cooler stars in Table 1, the flux emitted shortward of λ1100 is negligible, but for the hotter stars it will be a significant fraction of the total flux. For example, for T_e ≈ 12,500 K the flux for λ < 1100 Å is less than 1 percent of the total flux, whereas for T_e ≈ 25,000 K it is ~20 percent and for T_e ≈ 35,000 K it is ~35 percent of the total flux. Thus, in determining effective temperatures, an allowance must be made for the flux shortward of λ1100 for stars of spectral type about B3 or earlier. Since no flux measurements are available in this region, we must rely entirely on the predictions of model atmospheres. The models used were the LTE, statistically blanketed atmospheres of Kurucz *et al.* (1972) for which the fraction of this radiated flux, ΔF/F, was computed as a function of effective temperature of the model, i.e.,

$$\Delta F/F = \int_0^{1100} F(\lambda)d\lambda / \int_0^\infty F(\lambda)d\lambda.$$

These models were compared with the unblanketed

TABLE 4
ESTIMATED PERCENTAGE UNCERTAINTIES IN THE FIVE EMPIRICAL SPECTRAL BANDS

Band	Wavelength Range (Å)	Adopted Uncertainty (%)
1	1100 - 1300	35.0
2	1300 - 1800	21.0
3	1900 - 3300	8.5
4	3300 - 8100	4.0
5	8100 - ∞	10.0

non-LTE atmospheres computed by Mihalas (1972) which radiate somewhat more energy in the Lyman continuum than do the LTE models. For example, at 30,000 K, $\log g = 4.0$, about 1.5 times as much energy is radiated shortward of $\lambda 912$ by a non-LTE model as by the corresponding LTE atmosphere. Even so, only about 8 percent of the total flux in such a model is in the Lyman continuum. Since for lower temperatures the Lyman continuum radiation contributes a rapidly decreasing fraction of the total flux, we have ignored these non-LTE effects. They may perhaps be significant in determining the line blanketing, but the appropriate models are not available. In any case, for stars hotter than about B0 the effects of atmospheric extension may be significant. That the total energy radiated shortward of $\lambda 1100$ is insensitive to the particular model atmosphere used is indicated by the agreement with models obtained when a blackbody curve of the same effective temperature is used for the flux extrapolation. For example, at $T_e = 25,000$ K, the flux from $0 \leq \lambda \leq 1100$ derived from a blackbody distribution differs by only about 2.5 percent from that predicted by an SAO model. Thus effective temperatures derived here are not model atmosphere dependent. Furthermore, the SAO models generally agree very well with energy distributions of B1 and later-type stars over the entire spectral range for which observations are available. This lends confidence to their use in estimating stellar fluxes shortward of $\lambda 1100$. We also note that, except for seven of the hotter stars, varying the assumed value of the surface gravity has little effect on the value of $\Delta F/F$. Thus, $\log g = 4$ was adopted for all of the stars except β CMa, ϵ CMa, ζ Pup, and γ^2 Vel for which $\log g = 3.5$ was taken, and ϵ Ori, ζ Ori, and κ Ori for which $\log g = 3.0$ was used. A generous estimate of the uncertainty in the flux in the spectral region shortward of $\lambda 1100$ was taken: ± 20 percent for $T_e < 25,000$ K; ± 50 percent for $T_e \geq 25,000$ K.

The appropriate value of $\Delta F/F$ for each star was found as follows. A preliminary estimate of $\Delta F/F$ was made using the "effective temperature" corresponding to the total integrated empirical flux. This total empirical flux was increased by the indicated fraction, and the revised T_e found which was then used to make a revised estimate of $\Delta F/F$. Iteration was continued until $\Delta F/F$ remained unchanged. The process converged rapidly with only 2 or 3 iterations required, usually.

In § IIIc the flux curves for $\lambda\lambda 3300-8100$ were integrated using the trapezoidal approximation. Since the data points were spaced at 200 Å intervals, this procedure will lead to an overestimate of the flux contribution for this wavelength band, since it integrates under the continuum and ignores absorption lines. Allowance must be made for the Balmer lines, particularly for stars of spectral type A. The Balmer jump is also approximated in the integration by a straight line joining the fluxes at $\lambda\lambda 3700$ and 3900. Estimates of the error introduced have been obtained from the theoretical hydrogen line-blanketed model stellar atmospheres of Klinglesmith (1971). The flux

distributions of representative models were plotted, and continuum points corresponding to the wavelengths of the empirical data were joined by straight lines. The difference between the model flux distribution and the straight-line continuum interpolation curves was integrated and expressed as a fraction of the total model flux. This fraction was plotted against the equivalent width of H γ ; a straight line through the points gave a reasonable representation. This plot was used to estimate the corrections to be made to the total flux. For several stars observed, energy curves with a resolution of 10 Å were integrated to determine the fraction of the total flux in the lines. These results agreed with those determined by the above procedure to a few percent.

The total fluxes listed in column (7) of Table 3 are the totals of the fluxes listed in column (5) reduced by the corrections which are listed as percentages $(100\delta F/F)$ in column (6). The corrections are small and have a maximum value of ~ 2.5 percent with an uncertainty ≤ 0.5 percent. This uncertainty corresponds to $\sim \pm 0.1$ percent in T_e which is negligible compared with other sources of uncertainty.

b) Corrections for Companions

Five of the stars in Table 1 are known to be binary or multiple, and corrections must be applied to the fluxes to allow for the contributions from the companions. The magnitude difference between primary and secondary for each of the five stars is given in column (10) of Table 1, but we note that the photometry listed in columns (5), (6), and (8) applies to the combined light for each system. The magnitude differences for ζ Ori, β Cru, δ Sco, and α Vir are from measurements with the intensity interferometer at $\lambda 4430$ (Hanbury Brown *et al.* 1974). For γ^2 Vel the magnitude difference is the value of ΔM_v given by Conti and Smith (1972). In the case of ζ Ori, which is a known binary with $\Delta V = 2.08$ mag (Worley 1969), the intensity interferometer has revealed that the primary itself is a binary. The two companions are apparently of equal brightness, and each is 2.0 magnitudes fainter than the primary at $\lambda 4430$.

In order to allow for the effect of a companion, an assumption must be made concerning its spectrum. From the spectral classification of the primary and the magnitude difference, it is possible to specify in a spectral type-luminosity class array an area in which the secondary may be expected to lie. The resulting range in spectral type and luminosity class can be converted to a corresponding range in flux for the secondary. To facilitate this, the total fluxes (col. [7] of Table 3) for single stars were scaled to correspond to $V = 0.00$ mag and plotted against $(B - V)_0$. For ζ Ori, β Cru, α Vir, and δ Sco, interpolation in these data for spectral type and luminosity class with appropriate $(B - V)_0$ gave a flux range corresponding to $V = 0.00$ mag. Taking the mean of this range and scaling to the visual magnitude of the companion gave what has been adopted as the most likely value of flux for the companion. The mean visual absolute magnitudes for MK luminosity classes by Blaauw (1963) and

TABLE 5

INTEGRATED STELLAR FLUXES OUTSIDE THE EARTH'S
ATMOSPHERE, CORRECTED FOR INTERSTELLAR ABSORPTION,
FOR PRIMARY COMPONENTS OF MULTIPLE SYSTEMS

Star	Total Flux* (10^{-6} erg $\text{cm}^{-2}\text{s}^{-1}$)	Secondary Flux† (10^{-6} erg $\text{cm}^{-2}\text{s}^{-1}$)	Primary Flux (10^{-6} erg $\text{cm}^{-2}\text{s}^{-1}$)
ζ Ori	71.4 ± 13.1	5.0 ± 3.4	61.4 ± 14.0
γ^2 Vel	91.8 ± 19.1	19.8 ± 4.4	72.0 ± 15.2
β Cru	102.9 ± 14.9	2.2 ± 1.6	100.7 ± 15.0
α Vir	89.9 ± 8.6	7.3 ± 2.2	82.6 ± 3.9
δ Sco	72.7 ± 12.1	3.7 ± 2.9	69.0 ± 12.4

*Total flux from Table 3
†See §IVb

the intrinsic colors by Johnson (1963) were used in this analysis. In the case of γ^2 Vel, uncertainty exists concerning the relative temperatures and colors of the O9 I star and the fainter WC8 companion. The approach adopted has been to assume that both stars have the same effective temperature (but different luminosities) and simply divide the total flux between the two components according to their relative brightness. Any error in the primary flux because of the assumption of identical temperatures is likely to be small compared with the uncertainty arising from the uncertainty in the total flux. The fluxes for the primary components of the five multiple stars are listed in Table 5.

c) Emergent Fluxes

The emergent flux at the stellar surface, \mathfrak{F} , is related to the integrated stellar flux outside the Earth's atmosphere, f , by

$$\mathfrak{F} = 4f/\theta_{\text{LD}}^2, \quad (1)$$

where f is free of the effect of interstellar extinction and θ_{LD} is the angular diameter of the star.

Values of f from column (7) of Table 3 for single stars and from Table 5 for the primaries of the five multiple stars have been combined with the angular diameters listed in Table 1 to obtain values of \mathfrak{F} . These emergent or total physical fluxes are given in column (4) of Table 6.

d) Effective Temperatures

The effective temperature of a star (T_e) is defined by

$$T_e = (\mathfrak{F}/\sigma)^{1/4}, \quad (2)$$

where σ is the Stefan-Boltzmann constant.

The effective temperature for each star has been calculated from equation (2) and listed in column (5) of Table 6. We defer discussion of these effective temperatures to the next section.

V. BOLOMETRIC CORRECTIONS

The bolometric correction (B.C.) is, by convention, the correction required to reduce visual magnitudes to

bolometric magnitudes, and is defined by

$$\text{B.C.} = m_{\text{bol}} - V. \quad (3)$$

Equation (3) may be written as

$$\text{B.C.} = -2.5 \log \left(\int_0^\infty f_\lambda d\lambda \right) - V + C_1, \quad (4)$$

or, alternatively, as

$$\text{B.C.} = 2.5 \log \left(\int_0^\infty f_\lambda S_V d\lambda / \int_0^\infty f_\lambda d\lambda \right) + C_2, \quad (5)$$

where f_λ is the flux per unit wavelength interval received outside the atmosphere from a star at wavelength λ , S_V is the sensitivity function of the V magnitude system, and C_1 and C_2 are constants.

Equations (4) and (5) are both completely equivalent to equation (3), and while equation (5) may be used to determine bolometric corrections for any spectral energy distribution irrespective of the units in which f_λ is expressed, equation (4) can be applied only when f_λ is expressed in the units for which the constant C_1 has been determined. However, equation (4) is more closely related to the observed parameters and is the appropriate form of equation (3) to use in evaluating bolometric corrections from the empirical flux distributions presented in this paper.

The constants in equations (4) and (5) are uniquely defined if we adopt a value for the bolometric correction for a specified spectral distribution of f_λ with the addition of the V magnitude in the case of C_1 . In the past, the Sun has been the only star for which f_λ has been sufficiently well known to define the zero point of the bolometric correction scale. It is no longer clear that this is the case, and there might be some advantage in choosing one of the present program stars for this purpose. Nevertheless, for historical reasons, we have used the Sun.

We have, however, chosen not to determine C_1 directly by substituting solar values in equation (4), since solar fluxes are measured quite separately from stellar fluxes and the absolute fluxes are not consistent with the V -magnitude differences. Possible calibration differences plus any error in V_\odot would be reflected as an error in C_1 . Therefore, we have adopted the following procedure. C_2 has been determined by substituting solar fluxes in equation (5), and then, in order to convert C_2 into C_1 , the mean relationship between V and $\int_0^\infty f_\lambda S_V d\lambda$ has been established from the 21 non-reddened single stars in Table 1. This approach gives C_1 independent of the absolute solar flux calibration and effectively gives a mean value derived from 21 separate V magnitudes rather than from just V_\odot . The result is insensitive to the precise form of S_V because of the manner in which it enters for both stars and the Sun.

The choice of a value for the bolometric correction of the Sun is arbitrary and is equivalent to specifying the zero point of the bolometric magnitude scale. Kuiper (1938), Popper (1959), Harris (1963), and

others have adopted a value of B.C. = -0.07 for a star of spectral type G2 V. We will, therefore, adopt -0.07 mag for the bolometric correction of the Sun as did Davis and Webb (1970) in their discussion of empirical bolometric corrections for late B to F main-sequence stars and theoretical bolometric corrections for model stellar atmospheres. We also adopt the sensitivity function S_v , outside the atmosphere, as tabulated by Matthews and Sandage (1963) (their v_0) and the solar spectral energy distribution of Arvesen *et al.* (1969) (their H_λ). With these data, substitution in equation (5) leads to $C_2 = 0.958$ mag. As a check on the effect of using a different spectral energy distribution for the Sun, we have evaluated C_2 using the distribution given by Labs and Neckel (1968) [their $H(\lambda)$]. This gave $C_2 = 0.946$ mag, and while we adopt the value of $C_2 = 0.958$ mag from the Arvesen *et al.* distribution we note that the uncertainty in C_2 is probably of the order of 0.01 mag.

Thus we can write equation (5) as

$$\text{B.C.} = 2.5 \log \left(\int_0^\infty f_\lambda S_v d\lambda / \int_0^\infty f_\lambda d\lambda \right) + 0.958. \quad (6)$$

This equation can be used to evaluate bolometric corrections for any spectral flux distribution irrespective of the units in which it is expressed, and it can therefore be used to determine bolometric corrections

for model atmospheres on the same scale as the empirical bolometric corrections given below.

In order to determine C_1 a linear relationship was fitted to V and $2.5 \int_0^\infty f_\lambda S_v d\lambda$ for the 21 nonreddened single stars in Table 1. This gave a slope of -1 as would be expected, with residuals from the fitted curve consistent with zero dependence on $(B - V)_0$. The fitted relationship gave

$$V = -2.5 \log \left(\int_0^\infty f_\lambda S_v d\lambda \right) - 12.47. \quad (7)$$

Thus a combination of equations (4), (6), and (7) leads to a value of $C_1 = -11.51$ mag. Equation (4) can thus be rewritten as

$$\text{B.C.} = - \left[V + 2.5 \log \left(\int_0^\infty f_\lambda d\lambda \right) + 11.51 \right], \quad (8)$$

and we have used this equation to determine empirical bolometric corrections from the integrated flux distributions. If we solve for the constant C_1 in equation (4) from the Sun alone, by inserting the value of the visual magnitude of the Sun, $V = -26.74$ mag \pm 0.03 mag (Johnson 1965*b*; Code 1973) and the total integrated flux of the Sun, $f = 1.360(\pm 0.014) \times 10^8$ ergs $\text{cm}^{-2} \text{s}^{-1}$ (Duncan 1969; Allen 1973), we obtain

TABLE 6
EMERGENT FLUXES, EFFECTIVE TEMPERATURES
AND BOLOMETRIC CORRECTIONS FOR PROGRAM STARS

Star	V_0	$(10^{-6} \text{ erg cm}^{-2} \text{ s}^{-1})$	$(10^{12} \text{ erg cm}^{-2} \text{ s}^{-1})$	T_e (K^e)	B.C.				
α Eri	(+0.47)	54.4 \pm 4.3	2.51 \pm 0.27	14510 \pm 390	-1. ^m 32 \pm 0. ^m 09				
β Ori	+0.13	38.5	1.01	0.06	11550	170	-0.60	0.05	
γ Ori	+1.64	37.6	3.4	12.3	1.8	21580	790	-2.09	0.10
ϵ Ori	+1.50	60.2	5.4	21.5	3.2	24820	920	-2.46	0.11
ζ Ori*	+1.95	61.4	14.0	45.4	12.8	29910	2110	-2.93	0.29
κ Ori	+1.96	32.7	4.5	27.5	5.3	26390	1270	-2.26	0.15
β CMa	+1.97	36.2	4.9	22.8	4.1	25180	1130	-2.38	0.15
α Car	-0.75	45.0	1.8	0.176	0.043	7460	460	+0.11	0.05
γ Gem	+1.92	4.73	0.17	0.417	0.056	3260	310	-0.12	0.04
α CMa	-1.46	114.3	4.4	0.561	0.037	9970	160	-0.20	0.04
ϵ CMa	+1.50	41.5	3.3	11.0	1.6	20990	760	-2.06	0.09
δ CMa	+1.47	6.01	0.27	0.079	0.022	6110	430	+0.07	0.08
η CMa	+2.44	5.88	0.30	1.78	0.30	13310	560	-0.87	0.06
α CMi	+0.37	18.08	0.76	0.102	0.008	6510	130	-0.02	0.05
ζ Pup	+2.13	65.6	12.4	63.3	15.0	32510	1930	-3.18	0.21
γ^2 Vel*	+1.97	72.0	15.2	63.3	19.6	32510	2520	-3.12	0.23
β Car	+1.68	6.14	0.22	0.413	0.039	9240	220	-0.16	0.04
α Leo	+1.35	13.94	0.80	1.26	0.13	12210	310	-0.72	0.06
β Leo	+2.14	3.61	0.13	0.347	0.054	8850	340	-0.04	0.04
γ Crv	+2.58	4.49	0.27	1.36	0.23	12450	530	-0.72	0.07
β Cru*	+1.23	100.7	15.0	32.9	5.3	27600	1110	-2.75	0.16
α Vir*	+1.14	82.6	8.9	18.6	2.6	23930	840	-2.44	0.12
ϵ Cen	+2.21	33.7	4.6	24.9	4.6	25740	1190	-2.54	0.15
δ Sco*	+1.96	69.0	12.4	55.5	13.9	31460	1970	-3.07	0.22
ζ Oph	+1.57	89.8	14.7	58.8	15.0	31910	2040	-2.96	0.22
α Oph	+2.07	3.65	0.13	0.234	0.038	8020	330	+0.01	0.04
ϵ Sgr	+1.85	5.53	0.22	0.454	0.042	9460	220	-0.22	0.04
α Lyr	+0.03	30.4	1.2	0.493	0.029	9660	140	-0.25	0.04
α Aql	+0.76	12.17	0.46	0.233	0.024	8010	210	+0.02	0.04
α Pav	+1.94	21.8	1.9	5.80	0.88	17880	680	-1.80	0.10
α Gru	+1.74	13.5	0.9	2.21	0.34	14050	540	-1.08	0.07
α PsA	+1.16	8.80	0.31	0.340	0.047	8800	300	-0.03	0.04

*Primary Component

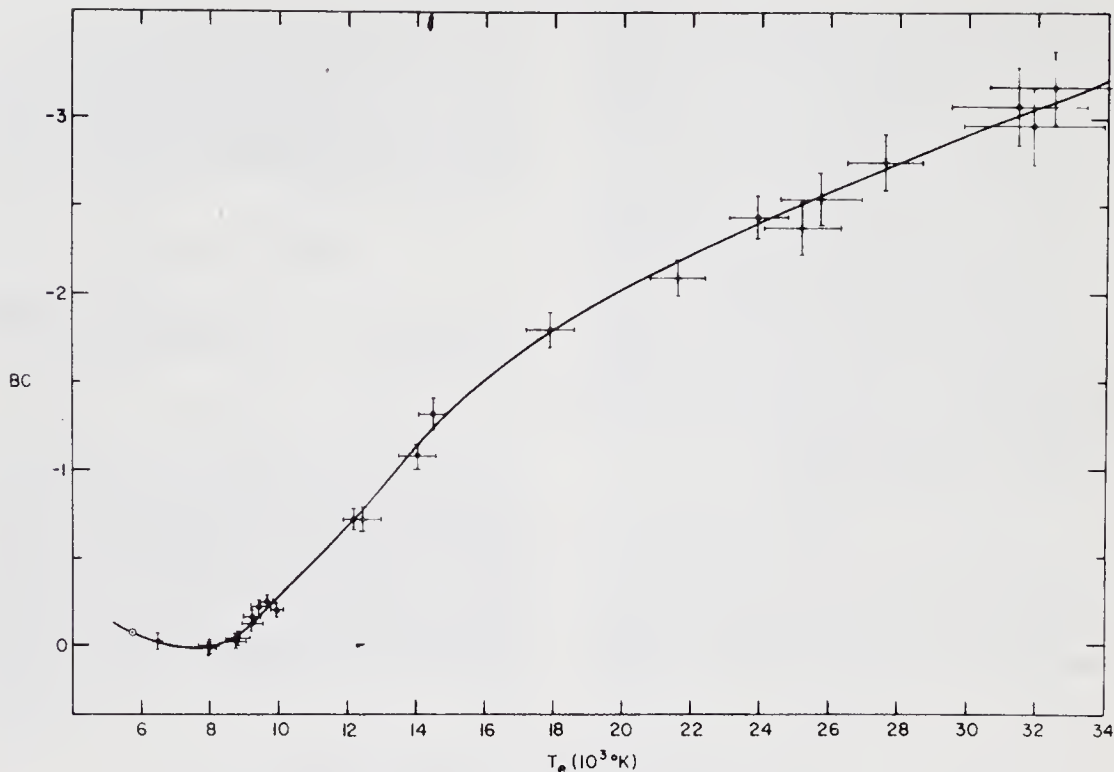


FIG. 2.—The bolometric corrections are shown as a function of T_e for luminosity class IV and V (points) and luminosity class III (crosses). The error bars correspond to the standard deviations given in Table 6. The smooth curve corresponds to the relation tabulated in Table 7.

the value $C_1 = -11.48 \text{ mag} \pm 0.03 \text{ mag}$, which therefore differs by one standard deviation from our adopted value. We prefer to derive C_1 from the mean of the 21 stars, and, moreover, as mentioned above, the procedure provides the recipe for computing bolometric corrections on this scale for model atmosphere fluxes. The bolometric corrections for the 32 stars in Table 6 are tabulated in column (6) based upon the values of V_0 and f given in columns (2) and (3).

The bolometric corrections for main-sequence and luminosity class III stars are plotted versus the empirical effective temperatures in Figure 2. The relation is well determined. The adopted mean relation is shown by the smooth curve and given in Table 7. The supergiants do not deviate substantially from this relation. Usually, a stellar temperature scale is presented in the form of a relation between temperature and the normal colors of stars or in terms of the spectral types. The adoption of the $(B - V)_0$ color is based upon the large number of objects for which this parameter has been measured. Thirty-two stars are not enough to establish a reliable statistical relation between T_e and $(B - V)_0$ for several reasons. For early-type stars, $(B - V)$ is relatively insensitive to a change in temperature or bolometric correction. A

change in $(B - V)$ of 1 mag corresponds to a change of 12 mag in the bolometric correction. The normal colors of stars are in general uncertain by 0.02 mag and, hence, the bolometric correction by one-quarter of a magnitude. $(B - V)_0$ is not an observed quantity for an individual star, and uncertainties in interstellar extinction among our program stars contribute to the errors in determining a mean relation.

With these reservations in mind, however, we have tabulated the mean $(B - V)_0$ corresponding to each temperature in Table 7. In Figure 3 are plotted $\log T_e$ versus $(B - V)_0$ for main-sequence and giant stars. The dashed line corresponds to the adopted relation given in Table 3. For comparison the temperature scale of Morton and Adams (1968) is shown as the solid line. Figure 4 shows the relation between bolometric corrections and $(B - V)_0$. The Morton-Adams scale is shown by the solid line while the relation from Table 3 is shown by the dashed line. While we regard this relation as preliminary, we believe that it is the best currently available in view of the fact that it is based upon empirical data. It would appear that reasonable effective temperatures could be determined from the measurement of bolometric corrections, in the absence of angular diameter determinations. A

TABLE 7

MEAN RELATION BETWEEN EFFECTIVE TEMPERATURE AND BOLOMETRIC CORRECTIONS FOR MAIN SEQUENCE STARS

T_e (K)	B.C.	$(B-V)_0$
34000	-3.21	-0.31
32000	-3.06	-0.30
30000	-2.91	-0.29
28000	-2.75	-0.28
26000	-2.58	-0.26
24000	-2.41	-0.25
22000	-2.23	-0.23
20000	-2.02	-0.21
18000	-1.80	-0.20
16000	-1.52	-0.17
15000	-1.35	-0.16
14000	-1.14	-0.14
13000	-0.90	-0.12
12000	-0.68	-0.10
11000	-0.48	-0.08
10000	-0.28	-0.05
9500	-0.18	0.00
9000	-0.08	+0.07
8500	-0.02	+0.14
8000	+0.01	+0.20
7500	+0.01	+0.27
7000	+0.01	+0.34
6500	-0.02	+0.44
6000	-0.05	+0.56
5780	-0.07	+0.63

program to determine empirical bolometric corrections for a larger sample of stars is currently underway and should provide an improved temperature scale.

VI. STELLAR LUMINOSITIES AND RADII

Of the 32 stars for which effective temperatures and bolometric corrections have been obtained, 12 have reliable trigonometric parallaxes, while Spica's distance is known from the interferometer data. For these 13 stars it is possible to determine luminosities and radii. Table 8 lists these stars along with the derived properties. The trigonometric parallaxes tabulated in column (3) were provided by Van Altena (1974a) and incorporate some recent determinations and his revised corrections to absolute parallax (Van Altena 1974b). The luminosity in solar luminosities is found from the total fluxes tabulated in Table 3 and the parallaxes given here, adopting a solar flux of 3.826×10^{33} ergs s^{-1} corresponding to a solar effective temperature of 5770 K. The radii in solar radii in column (6) follow from the tabulated angular diameters and parallaxes.

The empirical effective temperatures and luminosities make it possible to plot a fundamental $\log L - \log T_e$ diagram based directly on observations. This fundamental H-R diagram is shown in Figure 5. The zero-age main sequence for a chemical composition of

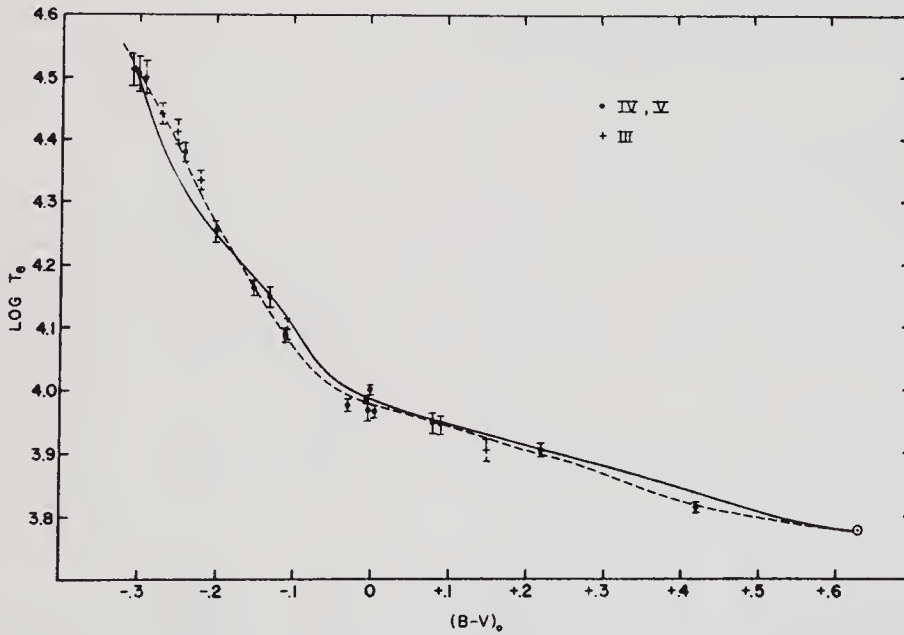


FIG. 3.—The relation between $\log T_e$ and the adopted $(B - V)_0$ for the program stars is shown for luminosity class IV and V (points) and luminosity class III (crosses). The error bars in $\log T_e$ correspond to the standard deviations given in Table 6. The uncertainty in $(B - V)_0$ is probably of the order of 0.02 mag. The solid curve is the relation of Morton and Adams (1968); the dashed line corresponds to the values given in Table 7.

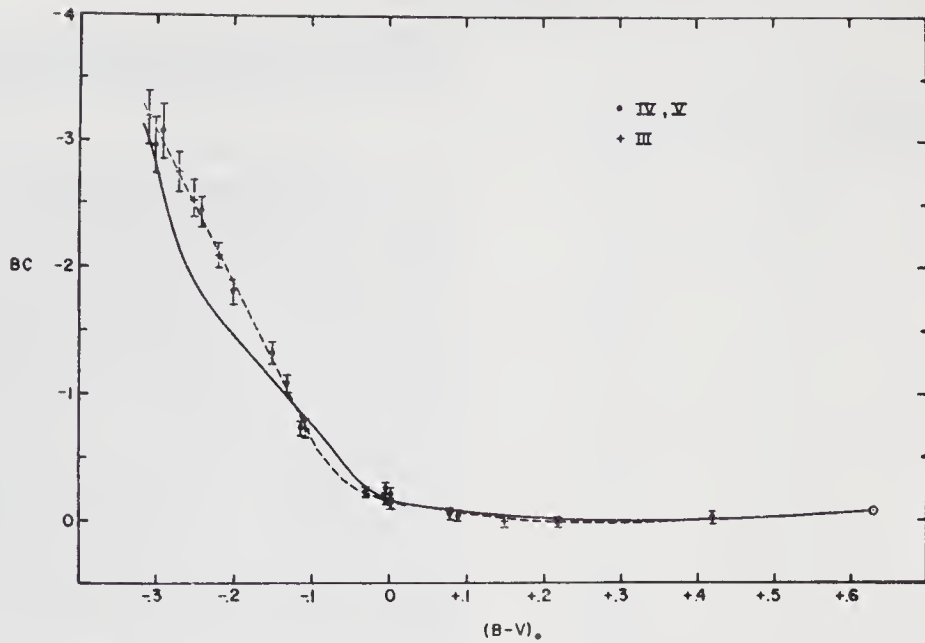


FIG. 4.—The relation between BC and the adopted $(B - V)_0$ for the program stars is shown for luminosity class IV and V (points) and luminosity class III (crosses). The solid curve is the relation of Morton and Adams (1968). The dashed line corresponds to the values given in Table 7.

TABLE 8
LUMINOSITIES AND RADII

HR #	Name	π	$\log T_e$ °K	$\log L/L_\odot$	$\log R/R_\odot$
1	472 α Eri	0 ⁰ .025 ±.017	4.162 ±.012	3.44 ±.59	0.92 ±.30
2	2421 γ Gem	.038 ±.006	3.967 ±.015	2.01 ±.14	0.60 ±.07
3	2491 α CMa	.377 ±.005	3.999 ±.007	1.400 ±.023	0.225 ±.013
4	2943 α CMi	.285 ±.006	3.814 ±.009	0.843 ±.029	0.317 ±.016
5	3685 β Car	.044 ±.015	3.966 ±.010	2.00 ±.30	0.59 ±.15
6	3982 α Leo	.041 ±.010	4.087 ±.011	2.41 ±.21	0.56 ±.11
7	4534 β Leo	.076 ±.007	3.947 ±.017	1.29 ±.08	0.27 ±.05
8	5056 α Vir	.012* ±.001	4.379 ±.015	4.25 ±.06	7.89 ±.04
9	6556 α Oph	.058 ±.005	3.904 ±.018	1.53 ±.08	0.48 ±.05
10	7001 α Lyr	.126 ±.006	3.985 ±.006	1.777 ±.045	0.441 ±.023
11	7557 α Aql	.197 ±.005	3.904 ±.011	0.992 ±.031	0.211 ±.023
12	8425 γ Gru	.057 ±.014	4.148 ±.017	2.11 ±.21	0.28 ±.11
13	8728 α PsA	.149 ±.010	3.944 ±.015	1.09 ±.06	0.18 ±.04

* Interferometric determination (Herbison-Evans *et al.* 1971)

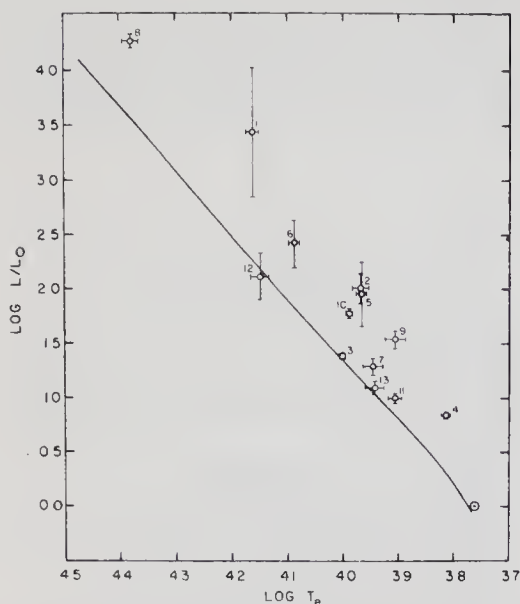


FIG. 5.—H-R diagram based upon the empirical effective temperatures and luminosities for program stars with reliable trigonometric parallaxes. The numbers identify the stars as listed in Table 8. The error bars correspond to the standard deviations given in Table 8. The zero-age main sequence given by Kelsall and Strömgren (1966) for a chemical composition of $X = 0.70$, $Z = 0.02$ is shown, for reference, by the solid curve.

$X = 0.70$, $Z = 0.02$ is shown by the solid line and is based upon Kelsall and Strömgren's (1966) calculations.

VII. DISCUSSION

The effective temperatures derived here, together with the Morton-Adams (1968) temperature scale, are given as a function of $(B - V)$ in Figure 3. The agreement between the two scales is satisfactory for $(B - V) > 0.0$ mag. However, in the region $0.0 < (B - V) < -0.20$ mag the new scale appears to be somewhat cooler than that of Morton and Adams, whereas for $(B - V)$ bluer than -0.20 mag the new scale is considerably hotter. Since the $T_e - (B - V)$ relation is so steep for stars of type earlier than A0, a small error in the color can result in a large change in temperature. However, it appears plausible that these differences in the two scales should exist when one considers how they were derived. The model atmospheres used by Morton and Adams to establish their scale included absorption lines shortward of $\lambda 1600$ only, whereas early-type stars have considerable blanketing in the $\lambda \lambda 2000-3000$ region (Underhill 1972). Flux from this region is redistributed to the visual, and if only the visual spectrum is compared with model atmospheres one would infer a spuriously high temperature, as did Morton and Adams. For the earliest type stars, however, visual parameters become insensitive to tem-

perature whereas large, easily detected changes take place in the bolometric luminosity which are reflected in more rapidly increasing temperatures to earlier spectral types. Thus it appears possible to understand the differences between the two scales, at least qualitatively.

The bolometric corrections and effective temperatures reported here are, with two qualifications, empirical. First, model atmospheres provided the data used in correcting the observed angular diameters for the effect of limb darkening. Second, model atmospheres were used to extend the flux shortward of $\lambda 1100$. For most stars the magnitude of the effect accounted for by models was small, as were the associated uncertainties, and in no case exceed 10 percent in T_e . Thus these nonempirical factors do not seriously compromise the essentially empirical nature of the effective temperatures and bolometric corrections given here.

Finally, it should be pointed out that these values are not likely to be greatly modified in the near future. Further absolute calibration work is going on at Wisconsin and elsewhere; however, on the basis of comparisons with current calibrations it seems improbable that a drastic revision in the derived effective temperatures or bolometric corrections will be required. The only recent calibration in the 1100–1300 Å band is the *Apollo 17* observations of Henry *et al.* (1974). The adoption of this calibration does not change the integrated flux at all. In the 1300–1800 Å band the *Apollo 17* results correspond to approximately a 10 percent decrease in flux, while the recent TD1 calibration given by Humphries *et al.* (1974) would result in an 18 percent decrease. The maximum contribution to the flux in this band is approximately 30 percent, and therefore adoption of these calibrations would result in a decrease in the effective temperature of about 1 percent and a change in the bolometric correction of less than $+0.05$ mag. The TD1 calibration yields an integrated flux in the 1800–3300 Å band of about 8 percent less, while the Colorado calibration by Bohlin *et al.* (1974) corresponds to an 8 percent increase in flux; thus it is unlikely that any large change is to be expected in this spectral interval. These comparisons of recent calibrations are particularly encouraging, since they are based on completely different techniques employing thermal sources, non-thermal sources, or blackbody sensors calibrated in the visual.

Work is underway at Wisconsin to extend the absolute calibration to $\lambda 912$. Again, from various considerations of internal consistency, it seems unlikely that the empirical fluxes will differ a great deal from the model predictions used to extrapolate the flux shortward of $\lambda 1100$. The Narrabri interferometer program has been completed, and more precise angular diameters of early-type stars will not be forthcoming for some time. Thus it would appear that, though the temperature and bolometric correction scales given in this paper will undoubtedly be modified slightly in the future, the values given here are the best likely to be available for some time.

The authors wish to record their thanks to Marilyn Meade who carried out much of the programming and flux integrations required. The work of the stellar interferometer has been supported by the Australian Research Grants Committee, the Research Grants Committee of the University of Sydney, the United States Air Force, and the Science Foundation for

Physics within the University of Sydney. We thank Professor Messel for his support. The University of Wisconsin Space Astronomy Laboratory program has been supported by the National Aeronautics and Space Administration through NAS 5-1348 and NGL 50-002-013.

REFERENCES

- Adams, T. F., and Morton, D. C. 1968, *Ap. J.*, **152**, 195.
 Allen, C. W. 1973, *Astrophysical Quantities* (3d ed.; London: Athlone Press), p. 169.
 Aller, L. H., and Faulkner, D. J. 1961, *Ap. J.*, **140**, 167.
 Arvesen, J. C., Griffin, R. N., and Pearson, B. D. 1969, *Appl. Optics*, **8**, 2215.
 Blaauw, A. 1963, in *Basic Astronomical Data*, ed. K. Aa. Strand (Chicago: University of Chicago Press), chap. 20.
 Bless, R. C., Code, A. D., and Fairchild, E. T. 1976, *Ap. J.*, **203**, in press.
 Bless, R. C., and Savage, B. D. 1972, *Ap. J.*, **171**, 293.
 Boggess, A., and Borgman, J. 1964, *Ap. J.*, **140**, 1636.
 Bohlin, R. C., Frimout, D., and Lillie, C. F. 1974, *Astr. and Ap.*, **30**, 127.
 Bradley, P. T., and Morton, D. C. 1969, *Ap. J.*, **156**, 687.
 Carruthers, G. R. 1969, *Ap. J. (Letters)*, **156**, L97.
 Cashdollar, K., and Code, A. D. 1975, in preparation.
 Code, A. D. 1960, in *Stellar Atmospheres*, ed. J. L. Greenstein (Chicago: University of Chicago Press), p. 50.
 ———. 1973, in *IAU Symposium No. 54, Problems of Calibration of Absolute Magnitudes and Temperatures of Stars*, ed. B. Hauck and B. E. Westerlund (Dordrecht: Reidel), p. 131.
 Code, A. D., Houck, T. E., McNall, J. F., Bless, R. C., and Lillie, C. F. 1970, *Ap. J.*, **161**, 377.
 Conti, P. S., and Smith, L. F. 1972, *Ap. J.*, **172**, 623.
 Davis, J. 1974, private communication.
 Davis, J., and Webb, R. J. 1970, *Ap. J.*, **159**, 551.
 ———. 1974, *M.N.R.A.S.*, **168**, 163.
 Duncan, C. H. 1969, *Radiation Scales and the Solar Constant*, Goddard Space Flight Center Report No. X-713-69-382.
 Hanbury Brown, R., Davis, J., and Allen, L. R. 1974, *M.N.R.A.S.*, **167**, 121.
 Hanbury Brown, R., Davis, J., Lake, R. J. W., and Thompson, R. J. 1974, *M.N.R.A.S.*, **167**, 475.
 Harris, D. L. 1963, in *Basic Astronomical Data*, ed. K. Aa. Strand (Chicago: University of Chicago Press), chap. 14.
 Hayes, D. S. 1970, *Ap. J.*, **159**, 165.
 Hayes, D. S., and Latham, D. W. 1975, *Ap. J.*, **197**, 593.
 Henry, R. C., Weinstein, A., Feldman, P. D., Fastie, W. G., and Moos, H. W. 1975, *Ap. J.*, **201**, 613.
 Herbison-Evans, D., Hanbury Brown, R., Davis, J., and Allen, L. R. 1971, *M.N.R.A.S.*, **151**, 161.
 Hickok, F. R., and Morton, D. C. 1968, *Ap. J.*, **152**, 203.
 Hiltner, W. A., Garrison, R. F., and Schild, R. E. 1969, *Ap. J.*, **157**, 313.
 Humphries, C. M., Jamar, C., Malaise, D., and Wroe, H. 1974, *Astr. and Ap.*, submitted.
 Johnson, H. L. 1963, in *Basic Astronomical Data*, ed. K. Aa. Strand (Chicago: University of Chicago Press), chap. 11.
 ———. 1965a, *Ap. J.*, **141**, 923.
 ———. 1965b, *Comm. Lunar and Planet. Lab.*, **3**, 73.
 Johnson, H. L., and Borgman, J. 1963, *Bull. Astr. Inst. Netherlands*, **17**, 115.
 Johnson, H. L., Mitchell, R. I., Iriarte, B., and Wiśniewski, W. Z. 1966, *Comm. Lunar and Planet. Lab.*, **4**, 99.
 Johnson, H. L., and Morgan, W. W. 1953, *Ap. J.*, **117**, 313.
 Kelsall, T., and Strömberg, B. 1966, *Vistas In Astronomy*, Vol. **8**, ed. A. Beer and K. Aa. Strand (London: Pergamon Press), p. 159.
 Klinglesmith, D. A. 1971, *Hydrogen Line Blanketed Model Stellar Atmospheres*, NASA SP-3065.
 Kuiper, G. P. 1938, *Ap. J.*, **88**, 429.
 Kurucz, R. L., Peytremann, E., and Avrett, E. H. 1972, *Blanketed Model Atmospheres for Early Type Stars*, (Washington: Smithsonian Institution Press).
 Labs, D., and Neckel, H. 1968, *Zs. f. Ap.*, **69**, 1.
 Lesh, J. R. 1968, *Ap. J. Suppl.*, **17**, 371.
 Matthews, T. A., and Sandage, A. R. 1963, *Ap. J.*, **138**, 30.
 Mihalas, D. 1972, *Non-LTE Model Atmospheres for B and O Stars* (Boulder: National Center for Atmospheric Research), NCAR-TN/STR-76.
 Mihalas, D., and Morton, D. C. 1965, *Ap. J.*, **142**, 253.
 Mitchell, R. I., and Johnson, H. L. 1969, *Comm. Lunar and Planet. Lab.*, **8**, 1.
 Morgan, W. W., and Keenan, P. C. 1973, *Ann. Rev. Astr. and Ap.*, **11**, 29.
 Morton, D. C. 1969, *Ap. J.*, **158**, 629.
 Morton, D. C., and Adams, T. F. 1968, *Ap. J.*, **151**, 611.
 Oke, J. B. 1964, *Ap. J.*, **140**, 689.
 Oke, J. B., and Schild, R. E. 1970, *Ap. J.*, **161**, 1015.
 Peytremann, E. 1972, *Astr. and Ap.*, **17**, 76.
 Popper, D. M. 1959, *Ap. J.*, **129**, 647.
 Stuart, F. E. 1969, *Ap. J.*, **157**, 1255.
 Underhill, A. B. 1972, in *The Scientific Results from the Orbiting Astronomical Observatory (OAO-2)*, ed. A. D. Code (Washington: NASA SP-310), p. 367.
 Van Altena, W. F. 1974a, private communication.
 ———. 1974b, *A.J.*, **79**, 826.
 Van Citters, G. W., and Morton, D. C. 1970, *Ap. J.*, **161**, 695.
 Van de Hulst, H. C. 1949, *Rech. Astr. Obs. Utrecht*, Vol. **11**, part 2.
 Worley, C. E. 1969, *A Catalog of Visual Binary Orbits* (Washington: United States Naval Observatory).

R. C. BLESS and A. D. CODE: Washburn Observatory, University of Wisconsin, Madison, WI 53706

J. DAVIS and R. HANBURY BROWN: Chatterton Astronomy Department, School of Physics, University of Sydney, Sydney, N.S.W. 2006, Australia

A STUDY OF γ^2 VELORUM WITH A STELLAR INTENSITY INTERFEROMETER

R. Hanbury Brown, J. Davis, D. Herbison-Evans and L. R. Allen

(Received 1969 November 11)

SUMMARY

The stellar intensity interferometer at Narrabri Observatory has been used, for the first time, to make observations of a multiple star (γ Vel). Measurements have been made in the continuum at $\lambda 4430$ and in the C 111-IV emission feature at $\lambda 4650$. The observations at $\lambda 4430$ give the angular size of the semi-major axis of the binary system γ^2 Vel and the angular diameter of the Wolf-Rayet component, while the observations at $\lambda 4650$ give the angular size of the extended region responsible for the emission feature. The results have been combined with spectroscopic and photometric data to find the distance of γ Vel, the radius, absolute magnitude and emergent flux ($\lambda 5460$) of the Wolf-Rayet star, and the radius and emergent flux ($\lambda 4650$) of the emission region. The surface gravity and effective temperature of the Wolf-Rayet star have been estimated and the size of the emission region has been found to correspond to the critical Roche equipotential lobe around the Wolf-Rayet star. It is concluded that a stellar intensity interferometer can be applied profitably to the study of close binaries and emission-line stars.

1. INTRODUCTION

The major programme of the stellar intensity interferometer at Narrabri Observatory is the measurement of the angular diameters of single hot stars. A description of the instrument (1, 2), the technique (1, 3) and some of the first results on single stars (3) have already been published. Recently we have started to explore the application of the interferometer to the study of more complex stars and as part of this programme we have observed γ Vel. This system consists of a single star γ^1 Vel which is separated by $41''$ from a binary star γ^2 Vel which is about 2.5 magnitudes brighter. The binary star γ^2 Vel is of considerable interest because the brighter component is a Wolf-Rayet star of type WC8 with strong emission lines of ionized carbon. By observing such a star with the interferometer it is possible, at least in principle, to find the angular diameters, angular separation and brightness ratio of the two components of the binary and some of the parameters of their orbit; from measurements in an emission line it is possible to find the angular size and shape of the region responsible for the emission. These measurements, combined with photometric and spectroscopic data, should yield the effective temperatures, absolute magnitudes, distance and radii of the stars, together with the physical size of the emission region. In the present paper we report the results of a first attempt to apply this technique to γ^2 Vel. We believe that the results are of interest not only because they provide new data about a rare type (WC8) of star, but also because they demonstrate an important application of the intensity interferometer.

2. OBSERVATIONS

Observations of γ Vel at $\lambda 4430$ and $\lambda 4650$ were made in the period January–March 1968 using the procedure described in detail by Hanbury Brown, Davis & Allen (1). The observational data have been reduced to give the mean correlation at each baseline following Hanbury Brown *et al.* (3).

2.1 Observations at $\lambda 4430$

The observations at an effective wavelength of 4430 \AA were made with the interference filters used in the single star programme (3). These are centred on $\lambda 4430$ and have a bandwidth of 100 \AA selected to avoid prominent features in the spectra of hot stars. It follows that the correlation measured at $\lambda 4430$ is the resultant, in the continua, due to the three component stars which comprise the γ Vel system. Observations were made at six baselines in an effort to define the shape of the correlation curve for this complex object and the baselines together with the mean correlation at each baseline, normalized to an arbitrary scale (3), are listed in Table I.

TABLE I

Observational Data

Epoch of observations	Baseline (m)	$\overline{c_N(d)} \pm \sigma$ Arbitrary units		Observing time (h)	Wavelength of observations (\AA)
January–February 1968	9.97	441	43	14.1	4430
	29.5	365	53	11.3	
	55.1	306	53	12.7	
	85.5	297	52	14.1	
	121.1	116	51	10.6	
	188.4	70	42	19.0	
February–March 1968	9.97	2560	210	11.8	4650
	29.5	1100	140	21.3	
	43.2	410	210	8.6	
	56.5	560	200	9.6	

2.2 Observations at $\lambda 4650$

A second series of observations was made to measure the angular extent of the region giving rise to the C III–IV emission feature at $\lambda 4650$ in the spectrum of γ^2 Vel. For this purpose the $\lambda 4430$ filters were replaced by filters with a bandwidth of 25 \AA centred on 4650 \AA . These observations measured the resultant correlation from the component stars, seen in the continua of their spectra, and from the emission region, seen in the C III–IV spectral feature. The four baselines used, together with the mean correlation at each baseline normalized to an arbitrary scale, which differs from the $\lambda 4430$ scale, are listed in Table I.

3. RESULTS

The analysis of the observations is complicated by the fact that in one case, for $\lambda 4430$, we are dealing with a triple system and in the other case, for $\lambda 4650$, we are dealing with a triple system plus an emission region. Fortunately, the analysis can be simplified because the contribution from γ^1 Vel to the observed correlation is small. Firstly, γ^1 Vel is much fainter than γ^2 Vel and is responsible for only

9.5 per cent of the light at $\lambda 4430$ and 3.5 per cent at $\lambda 4650$. Secondly, γ^1 Vel is $41''$ from γ^2 Vel and, since this separation is resolved by a baseline of the order of 1 mm, it will be completely resolved by the individual reflectors. Therefore, at $\lambda 4430$, γ^1 Vel contributes less than 1 per cent of the correlation which would be expected at zero baseline if γ Vel were a single star. At $\lambda 4650$ the corresponding contribution to the zero baseline correlation is approximately 0.1 per cent. These contributions are small compared with the observational uncertainties at all the baselines used and they have been ignored in the analysis.

3.1 Results for $\lambda 4430$

Since the contributions of γ^1 Vel can be neglected, the observations at $\lambda 4430$ can be considered as due to γ^2 Vel alone; that is, due to a binary star with components classified on the MK system as WC8 and O7 (4).

The correlation, $c(d)$, observed as a function of baseline d , for a binary star, will have the form

$$c(d) = A \left[\beta^2 \Gamma_1^2(d) + \Gamma_2^2(d) + 2\beta |\Gamma_1(d)| |\Gamma_2(d)| \cos \frac{2\pi d \eta}{\lambda_0} \right] / (1 + \beta)^2 \quad (1)$$

where A is an instrumental constant, $\Gamma_1^2(d)$ and $\Gamma_2^2(d)$ are the correlation factors (3) for the two component stars, β is the brightness ratio of the two stars ($\beta > 1$), λ_0 is the effective wavelength of observation and η is the angular separation of the two stars projected onto the baseline of the interferometer. For the purpose of the analysis the component stars were assumed to appear as circular discs of uniform intensity (3) so that,

$$\Gamma^2(d) = \left| \frac{2J_1(\pi \theta_{UD} d / \lambda_0)}{\pi \theta_{UD} d / \lambda_0} \right|^2 \quad (2)$$

where θ_{UD} is the angular diameter of the star.

For a given baseline $c(d)$ will vary during the period of observation as η changes due to the rotation of the binary system in the sky with hour angle and also due to the motion of the stars in their orbit. In principle the period (P), time of periastron passage (T), eccentricity (e), longitude of periastron passage (ω), inclination (i), position angle (PA) of the binary orbit, brightness ratio (β) and angular sizes of the components (θ_{UD1} and θ_{UD2}), and the angular size of the semi-major axis of the orbit (θ_a) can be found by fitting theoretical curves of the form given by equation (1) to the observations as a function of time. Some of these parameters can also be obtained from spectroscopic observations. In the case of γ^2 Vel the accuracies of the spectroscopic parameters are better than those obtainable from the interferometer observations with the present signal to noise ratio. Since we are most interested in obtaining values for θ_{UD1} and θ_a from the interferometer observations, spectroscopic values were adopted where available for the other parameters. Furthermore, the terms involving $\Gamma_1(d)$ dominate the correlation curve making the accuracy of the interferometric determinations of β (see section 4.3) and θ_{UD2} rather poor. Hence values were also adopted for these parameters. We note that uncertainties in the adopted parameters have only a small effect on the solutions for θ_{UD1} and θ_a .

The orbital elements P , e and ω given by Ganesh & Bappu (5) and listed in Table IV have been adopted for the final solution; i has been taken to be 70° for the reasons given in Section 4.3, and β to be 2.5 following Smith (6). It is noted that $\beta = 2.5$ is consistent with the present observations (see Section 4.3). If it is

assumed for the present purpose that the effective temperatures (T_e) of the two components are equal, then $\theta_{UD2} = 0.63 \theta_{UD1}$. A preliminary analysis gave $\theta_{UD1} = 0''.44 \times 10^{-3}$ (a value unchanged by the subsequent analysis) and so $\theta_{UD2} = 0''.3 \times 10^{-3}$ was adopted.

In outline the method employed to fit a curve to the observations was the following. The correlation expected for each of the actual periods of observation was computed for every baseline using the above orbital parameters to calculate the projected angular separation of the components and taking into account the changing orientation relative to the baseline with hour angle. The sum of the squares of the residuals (observed minus computed correlation) for the six baselines was then minimized by allowing the computer program to vary the unspecified parameters θ_{UD1} , θ_a , PA , T and A (see equation (1)).

The observational points are plotted in Fig. 1(a) with the computed values of correlation for the parameters of the final solution. Also shown in Fig. 1(a) are the loci of the upper and lower limits to the instantaneous values of the computed correlation. The values of θ_{UD1} and θ_a for the final fit are given in Table II.

TABLE II

Results

Parameter	Angle $\pm \sigma$	
	(10 ⁻³ seconds of arc)	
Angular diameter of equivalent uniform disc for WC8 star (θ_{UD1})	0.44	0.05
Angular semi-major axis of orbit (θ_a)	4.3	0.5
Angular diameter of equivalent uniform disc of $\lambda 4650$ emission region	2.05	0.19

3.2 *Results for $\lambda 4650$*

The object of the observations at $\lambda 4650$ was to measure the angular size of the equivalent uniform disc of the region emitting the C III–IV spectral feature (θ_{ER}). As already noted, the measured correlation includes contributions due to all three stars of γ Vel. The contribution due to γ^1 Vel can be neglected (section 3), but it is necessary to correct the observations for the contributions of the WC8 and O7 components of γ^2 Vel before θ_{ER} can be found. This correction was carried out as follows. In order to keep the analysis tractable, it was assumed that the emission region is spherical and concentric with the WC8 component. The association of the emission region with the WC8 star is justified by the fact that the radial velocity curve for the $\lambda 4650$ emission feature is in antiphase with the curves for the absorption lines in the spectrum of the O7 star (5), and the assumption that the emission region is spherical is supported by the fact, as discussed later, that the present observations show no significant departures from a sphere. The assumption was also made that the spectrum of γ^2 Vel at the time of the interferometer observations was the same as that recorded in a photoelectric scan taken at Mt Stromlo in November 1965. From this spectral scan and the spectral transmission curves of the interference filters, the relative contributions to the light flux transmitted by the filters from the WC8 and O7 stars and from the C III–IV emission complex were found. It was assumed, following Smith (6, 7), that the WC8 star was brighter than the O7 star with a brightness ratio of 2.5 as adopted in Section 3.1. In addition to the light fluxes, the individual contributions to the correlation were calculated

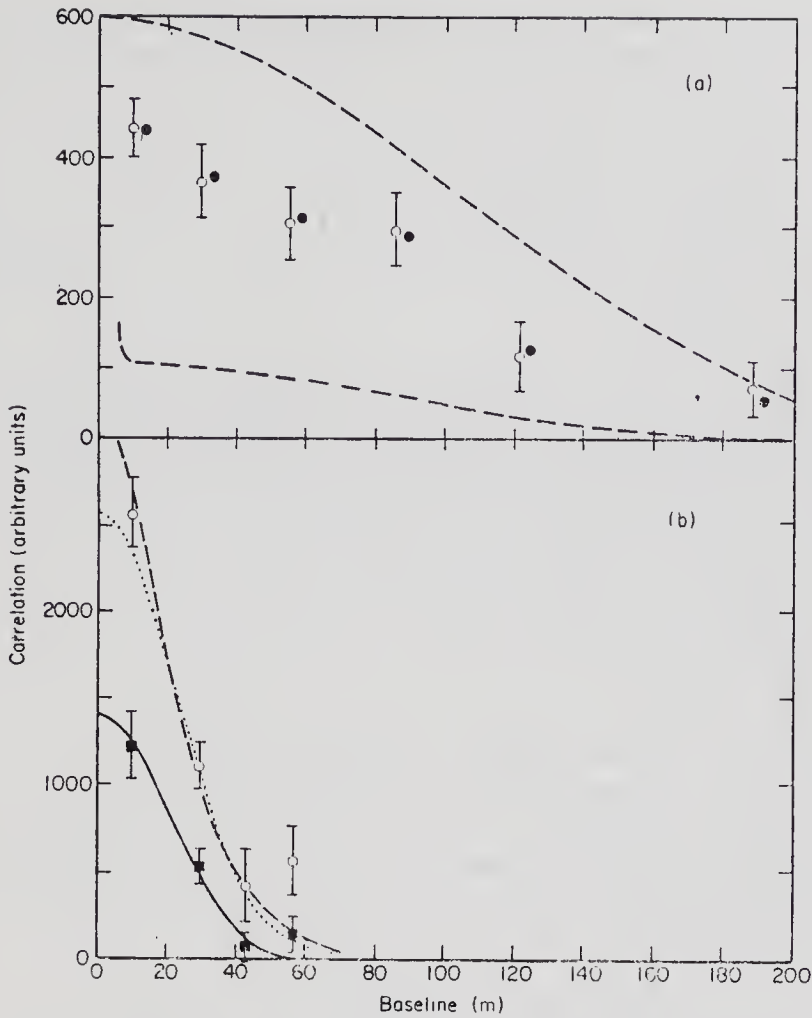


FIG. 1. The observed correlation as a function of baseline (a) At $\lambda 4430$. \circ Observed correlation, \bullet Computed correlation for the periods of observation using the parameters of the final solution, --- Upper and lower limits to the instantaneous theoretical values of correlation for the parameters of the final solution. (b) At $\lambda 4650$. \circ Observed correlation, --- Computed correlation curve for γ^2 Vel (O7 + WC8 + emission region), Computed curve for (WC8 + emission region), \blacksquare Observed correlation with contributions from O7 and WC8 stars removed, ——— Correlation curve fitted to revised observational points to give the angular size of the emission region.

as a fraction of the correlation to be expected from a single star. The effect of the shape of the emission feature on the spectral distribution of the light passing through the filters was taken into account in making the calculations because the parameters σ and B_o (see equation (2) in (I)) are affected in such a way that the correlation due to the emission feature is enhanced relative to that from the continuous spectra.

The correlation curve to be expected from γ Vel was computed by taking a mean angular separation for the WC8 and O7 stars ($\bar{\theta}$) and assuming that the observed correlation is a true average over all hour angles (approximately true). Under these conditions the correlation curve is given by

$$\overline{c(d)} = A \left[\Gamma_1^2(d) + \rho^2 \Gamma_2^2(d) + 2\rho |\Gamma_1(d)| |\Gamma_2(d)| J_o \left(\frac{2\pi \bar{\theta} d}{\lambda_o} \right) \right] / (1 + \rho)^2 \quad (3)$$

where $\Gamma_1^2(d)$ now refers to the WC8 star plus the emission region and $\Gamma_2^2(d)$ to the O7 star as before, and ρ^2 is the ratio of the correlation expected at zero baseline from the O7 star to that expected from the WC8 star plus the emission region. In evaluating this equation an approximate value for θ_{ER} was used, found by applying a rough correction to the observational data for the contributions of the WC8 and O7 stars. The angular diameters of the WC8 and O7 stars were taken to be $0''.44 \times 10^{-3}$ and $0''.3 \times 10^{-3}$ respectively (see Section 3.1) and the mean angular separation of the WC8 and O7 stars was taken to be $\bar{\theta} = 2''.0 \times 10^{-3}$ (corresponding to $\theta_a = 4''.3 \times 10^{-3}$).

The curve computed from equation (3) is shown as a broken line in Fig. 1(b) together with the observed points. The computed curve has been normalized by an arbitrary value of A to give a good fit to the experimental points. Observations of β Ori, made with the $\lambda 4650$ filters at a baseline of 10 m, enable an independent value of A to be determined empirically using the angular diameter of β Ori published previously (3). Satisfactory agreement between the two values of A was obtained but it is noted that for the present purpose, where the aim is to find differences between correlation curves, the value adopted for A is not critical. The correlation curve to be expected for the WC8 star and the emission feature alone was also computed and is represented by the dotted curve in Fig. 1(b). The differences between the two computed curves at each baseline were applied to the observations to remove the contribution due to the O7 star.

Since it has been assumed that the emission region is circular and concentric with the WC8 star the Fourier transform of the equivalent strip brightness distribution of the combination is given by the sum of the Fourier transforms of the emission region and WC8 star taken separately. In other words, if the Fourier transform is represented by F , then

$$F(\text{WC8} + \text{ER}) = \frac{1}{1 + \rho} F(\text{WC8}) + \frac{\rho}{1 + \rho} F(\text{ER}) \quad (4)$$

where ρ^2 is now the ratio of correlation expected from the emission region to that expected from the WC8 star at zero baseline.

The observed values of correlation, with the contributions due to the O7 star removed, are proportional to $|F(\text{WC8} + \text{ER})|^2$. Since symmetry has been assumed it follows that the square root of the corrected values of correlation should be proportional to $F(\text{WC8} + \text{ER})$. No ambiguity in sign exists because at the longest baselines employed for the $\lambda 4650$ observations the combined transform is dominated by $F(\text{WC8})$ which, even at the longest baseline, has a value greater than 0.9 of its zero baseline value. $F(\text{WC8})$ was evaluated using the value for θ_{UD1} found in Section 3.1 and ρ was evaluated from the spectrum and filter characteristics. With these data and equation (4), each observational point was adjusted to give the value of correlation corresponding to the emission region alone. The final values are plotted in Fig. 1(b) and the correlation curve for the equivalent uniform disc, which was fitted to them by the method of least squares, is shown by the full curve. The corresponding value of θ_{ER} is listed in Table II. The uncertainty in θ_{ER} is dominated by the uncertainty in the observational points and any uncertainty arising from the assumptions made in the analysis is small by comparison.

An analysis of the observations made with a baseline of 29.5 m has been carried out in order to place a limit on the asphericity of the emission region. If the emission region is not spherical then as it rotates in the sky with hour angle the observed

correlation should be modulated with a 12-hour period. No significant modulation was found and the available signal to noise ratio puts a limit on any asphericity of $\theta_{\max}/\theta_{\min} < 1.5$.

4. INTERPRETATION OF RESULTS

4.1 Emergent flux and effective temperature of the Wolf-Rayet component

The combination of the angular diameter of a star with the absolute monochromatic flux received from it allows the absolute monochromatic flux at the surface of the star to be calculated (3) and an estimate of the effective temperature of the stellar atmosphere to be made.

The first step is to find the true angular diameter (θ_{LD}) of the star which is related to the angular diameter of the equivalent uniform disc by a limb-darkening law. The limb-darkening law for a WC8 star is not known but following previous work (3) a cosine law has been adopted with a coefficient $U_{4430} = 0.36$. This has been derived from the model atmosphere data given by Grygar (8) assuming $(B-V)_0 = -0.30$. It is noted that θ_{LD} is not sensitive to the value of U_{4430} adopted and a change of ± 0.06 in U_{4430} would not affect the value of θ_{LD} which is given in Table III.

The monochromatic flux at $\lambda 4430$ is not available for γ^2 Vel and therefore the analysis has been carried out at the constant energy reciprocal wavelength ($1.83 \mu^{-1}$) of the V magnitude system (9). The V magnitude for the Wolf-Rayet component was found by subtracting the contribution of the O7 star from V for γ^2 Vel (10) assuming the WC8 star to be 2.5 times brighter than the O7 star (Section 3.1). The resulting value for V is listed in Table III. If, as suggested by many workers, ζ Pup and γ Vel are physically associated in space then the correction for interstellar extinction may be assumed to be the same for both objects. A comparison of the observed colours of ζ Pup (10) with intrinsic colours for an O5 star (11) suggests that $E_{B-V} = 0.05$ mag. The total absorption at $1.83 \mu^{-1}$ due to interstellar extinction has therefore been taken to be 0.15 mag preliminarily, and the corrected V magnitude of the WC8 star is found to be +2.05 as given in Table III.

Following Davis & Webb (12) a value of 3.78×10^{-20} erg cm $^{-2}$ s $^{-1}$ Hz $^{-1}$ for the flux from a star with $V = 0.00$ at $1.83 \mu^{-1}$ has been adopted and, combining this with $V = +2.05$, the flux from the WC8 star at $1.83 \mu^{-1}$ [$f_{\nu}(1/\lambda = 1.83)$] in the absence of interstellar extinction has been calculated. The absolute monochromatic flux at the surface of the star (\mathcal{F}_{ν}) is related to f_{ν} by

$$\mathcal{F}_{\nu} = \frac{4f_{\nu}}{\theta_{LD}^2}. \quad (5)$$

The calculated values of $f_{\nu}(1/\lambda = 1.83)$ and $\mathcal{F}_{\nu}(1/\lambda = 1.83)$ are listed in Table III. For convenience, the brightness temperature (T_{5460}) corresponding to $\mathcal{F}_{\nu}(1/\lambda = 1.83)$ is also listed.

Since a large fraction of the flux from a WC8 star is in the far ultra-violet it has been necessary to resort to the predictions of model atmosphere computations in order to estimate the effective temperature (T_e). A comparison of the empirical value of $\mathcal{F}_{\nu}(1/\lambda = 1.83)$ with the emergent fluxes for the ultra-violet line-blanketed models for O-type stars by Bradley & Morton (13) with $\log g = 3.5$ (Section 4.5) gives a value of $T_e = 30\,100 \pm 4000$ °K. The value of T_e obtained in this way,

TABLE III
The angular diameter, absolute flux and effective temperature of the WC8 component of γ^2 Vel

Parameter	Value	Notes
θ_{UD}	$[0''.44 \pm 0.05] \times 10^{-3}$	Angular diameter of equivalent uniform disc (θ_{UD1} from Table II)
U_{4430}	0.36	Adopted limb-darkening coefficient
θ_{LD}	$[0''.45 \pm 0.05] \times 10^{-3}$	Angular diameter (limb-darkened)
V	+2.20	$V = +1.83$ for γ^2 Vel (10); WC8 assumed 2.5 times brighter than O7 (Section 3.1)
AV	0.00	Interstellar extinction in magnitudes ($AV = 3E_{B-V}$)
V_0	+2.20	V corrected for interstellar extinction
$f_p(1/\lambda = 1.83)$	4.98×10^{-21}	Flux from star outside the atmosphere at $1/\lambda = 1.83 \mu^{-1}$ (λ_{5460}) in the absence of interstellar extinction in $\text{erg cm}^{-2} \text{s}^{-1} \text{Hz}^{-1}$
	0.15 +2.05 5.72×10^{-21}	
$\mathcal{F}_p(1/\lambda = 1.83)$	$[4.2 \pm 0.9] \times 10^{-3}$	Flux at the surface of star at $1/\lambda = 1.83 \mu^{-1}$ in $\text{erg cm}^{-2} \text{s}^{-1} \text{Hz}^{-1}$
	$[4.5 \pm 1.0] \times 10^{-3}$	
T_{5460}	$25\,400 \pm 3400$	Brightness temperature at λ_{5460} in $^\circ\text{K}$
T_e	$28\,000 \pm 3300$	Effective temperature in $^\circ\text{K}$
	$26\,700 \pm 3600$	
	$29\,100 \pm 3600$	

apart from the uncertainty in $\mathcal{F}_\nu(1/\lambda = 1.83)$, is only as good as the models. If the relative energy distributions predicted by the models are incorrect, then T_e will be in error.

The energy distribution for a model with $T_e = 30\,100$ °K has been interpolated from the Bradley & Morton models with $\log g = 3.5$ and is plotted in Fig. 2(a) with the published empirical flux data for comparison. This can only be regarded as a crude check because it is necessary to correct the empirical fluxes for the contribution of the O7 star and this involves assumptions concerning the spectral energy distribution curve for the O7 star. For the present purpose we have assumed, as in Section 3.1, that the WC8 and O7 stars have the same T_e and a brightness ratio of 2.5; in other words, we assume that their relative energy distributions are the same and that the O7 star contributes ~ 29 per cent of the flux at all wavelengths. The empirical data in Fig. 2(a) have been reduced in the following manner. The monochromatic magnitudes of Aller & Faulkner (14) have been reduced to the calibration of Hayes (15) and normalized to $f_\nu = 4.98 \times 10^{-21}$ erg cm $^{-2}$ s $^{-1}$ Hz $^{-1}$ at $1.83 \mu^{-1}$ (i.e. to $V = +2.20$). The data points due to Stecher have been obtained by drawing the continuum on the published spectral scans (16) and reading values from the curve every 100 Å from λ_{3100} to λ_{1900} inclusive. Values for shorter wavelengths were not taken because of the difficulty in defining the continuum and also because of the broad absorption feature between λ_{1700} and λ_{1300} due to the Earth's atmosphere which, as Stecher points out, had not been corrected for in the published curve. All the empirical data have been (i) reduced to fluxes per unit frequency interval, (ii) corrected for reddening with $E_{B-V} = 0.05$ mag using the interstellar extinction curve adopted by Bless, Code & Houck (17) except for $3.5 < 1/\lambda < 6$ where the new data by Stecher (18) have been used, (iii) corrected to remove the contribution from the O7 star, and (iv) converted to fluxes at the stellar surface using equation (5) and θ_{LD} from Table III. All the data referred to so far are narrow band measurements (~ 10 Å) and can be compared directly with the model continuum shown by the curve in Fig. 2(a). Also included in Fig. 2(a) are flux measurements, corrected as described above, by Smith (19) at an effective wavelength of 1376 Å ($7.27 \mu^{-1}$) and by Carruthers (20) at effective wavelengths of 1270 Å ($7.87 \mu^{-1}$) and 1115 Å ($8.97 \mu^{-1}$). These are broad band measurements (~ 1000 Å) and cannot be compared directly with model predictions. Thus the model fluxes plotted in Fig. 2(a) at the effective wavelengths of these three measurements are the predicted fluxes interpolated as above, taking into account the photometer sensitivity curves and the line-blanketed model spectra.

The analysis which is represented by Fig. 2(a) has assumed that interstellar extinction corresponding to $E_{B-V} = 0.05$ mag applies to γ^2 Vel. For comparison the analysis has been repeated assuming no interstellar extinction ($E_{B-V} = 0$). The new empirical value of $\mathcal{F}(1/\lambda = 1.83)$, given in Table III, yields an effective temperature of $28\,000 \pm 3300$ °K when compared with the fluxes predicted by the models. In Fig. 2(b) the empirical fluxes, with no correction for reddening, are plotted with the predicted fluxes for a model with $\log g = 3.5$ and $T_e = 28\,000$ °K extrapolated from the Bradley and Morton models (13).

Inspection of Figs 2(a) and 2(b) suggests that better agreement between the empirical and theoretical fluxes would be given by an intermediate value of the interstellar extinction. Accordingly, a value of $E_{B-V} = 0.03$ mag has been adopted and the analysis repeated once more. The new empirical flux values are listed in Table III with the effective temperature of $29\,100 \pm 3600$ °K derived from a

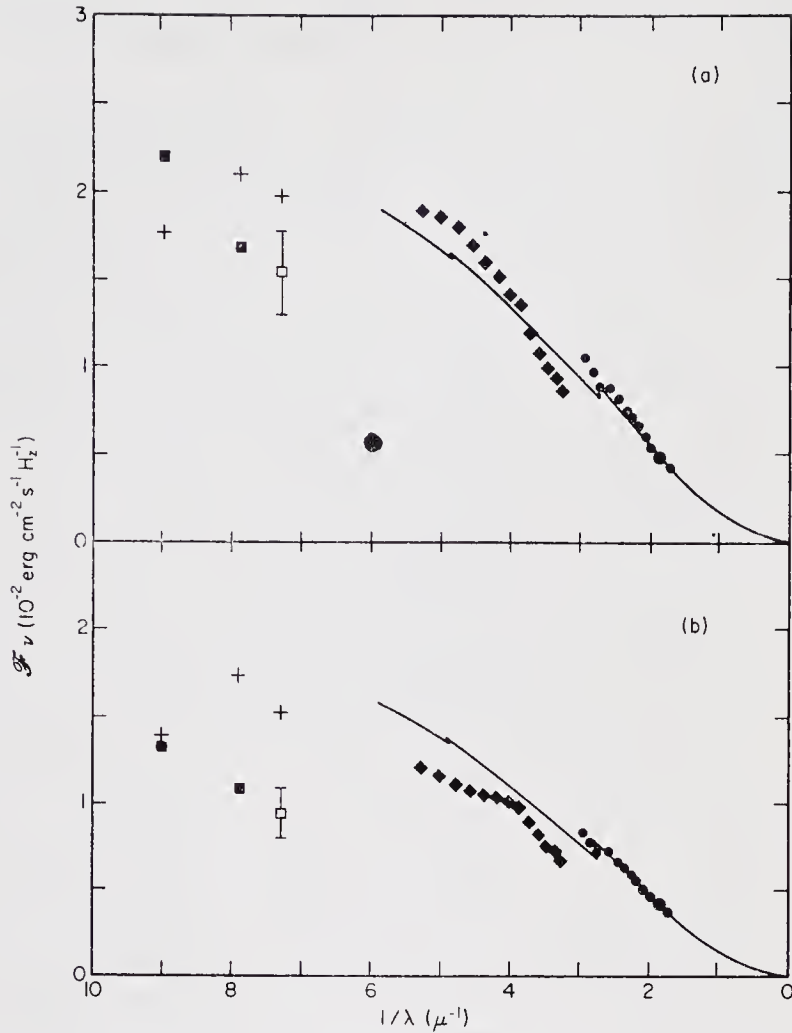


FIG. 2. The empirical fluxes at the surface of the WC8 component of γ^2 Vel compared with the predictions of ultraviolet line-blanketed model atmospheres. ● Flux at $1.83 \mu^{-1}$ (see text), ● Aller & Faulkner (14), ◆ Stecher (16), □ Smith (19), ■ Carruthers (20), — Model continuum, + Model fluxes corresponding to wide band photometric data. (a) Empirical fluxes, assuming $E_{B-V} = 0.05$ mag, compared with a model for $T_e = 30100$ °K and $\log g = 3.5$ interpolated from the models by Bradley & Morton (13). (b) Empirical fluxes, assuming $E_{B-V} = 0.00$ mag, compared with a model for $T_e = 28000$ °K and $\log g = 3.5$ extrapolated from the models by Bradley & Morton (13).

comparison with the fluxes predicted by the models. In Fig. 3 the empirical fluxes, corrected for reddening with $E_{B-V} = 0.03$ mag using the interstellar extinction curve adopted previously, are plotted with the predicted fluxes for a model with $\log g = 3.5$ and $T_e = 29100$ °K interpolated from the Bradley & Morton models (13).

Any comparison of Figs 2(a), 2(b) and 3 should be made with caution because of the underlying assumptions on which they are based. Taken at face value, the general agreement between observation and theory is best for $E_{B-V} = 0.03$ mag as shown in Fig. 3. The agreement is not so good for the broad-band measurements as it is for the narrow-band data and this is particularly true for the broad-band measurements at $7.87 \mu^{-1}$ and $8.97 \mu^{-1}$. There also appears to be a discrepancy between the Aller & Faulkner data and Stecher data in the neighbourhood of

$3 \mu^{-1}$. We note that the kink appearing in the data derived from Stecher's spectral scan at $3.8 \mu^{-1}$ in Fig. 2(b) is largely removed by the application of reddening corrections.

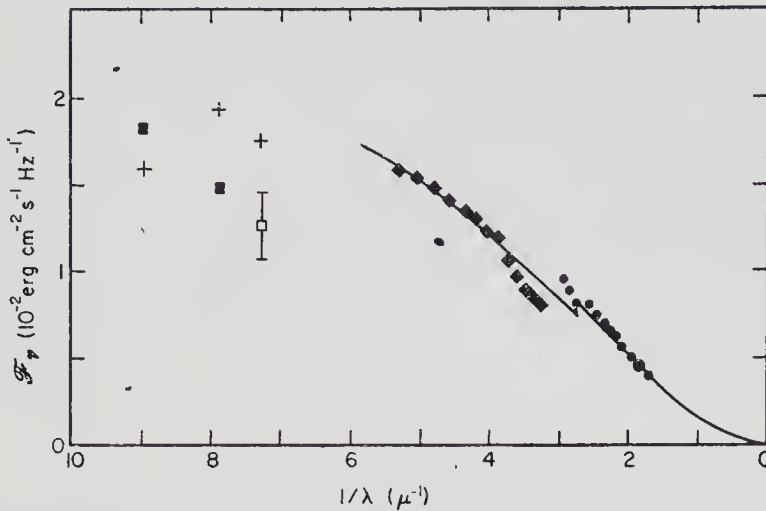


FIG. 3. Empirical fluxes for the WC8 component of γ^2 Vel, assuming $E_{B-V} = 0.03$ mag, compared with a model for $T_e = 29\,100$ °K and $\log g = 3.5$ interpolated from the models by Bradley & Morton (13). The symbols have the same meaning as in Fig. 2.

Two basic assumptions were made in order to construct Figs 2 and 3. Firstly, it was assumed that the ratio in brightness of the two component stars of γ^2 Vel (β) is 2.5. The uncertainty in this adopted value of β (see Section 4.3) introduces an additional uncertainty of ± 2500 °K into the effective temperatures which are listed in Table III. This is appreciably less than the quoted uncertainties in Table III which are due solely to the uncertainty in the angular diameter. The effect of the second assumption, that the WC8 and O7 stars have the same effective temperature (assumed in all cases), is not so easy to assess. It is likely that the O7 star is hotter than the WC8 star and if this was taken into account in correcting the observed fluxes, to give the fluxes for the WC8 component alone, the resultant slope of the continuum would be altered. This would not change the effective temperature deduced from the model atmospheres but it would affect the comparison of the empirical and theoretical flux distributions. However, the effect would be negligible for $\beta = 2.5$ and would only be significant for values of β near the lower limit given in Section 4.3.

We therefore conclude that the agreement between the empirical and theoretical continua in Fig. 3 should not be regarded as convincing evidence for $E_{B-V} = 0.03$ mag. Furthermore, as the effective temperature of an O7 star is not known with any certainty we are of the opinion that the data at present available do not warrant a more detailed analysis. We believe that the value of $T_e = 29\,100 \pm 3600$ °K, based on $E_{B-V} = 0.03$ mag, is the best that can be assigned on the basis of the available evidence.

4.2 Emergent flux at $\lambda 4650$ from the emission region

An estimate of the flux received from the emission region per unit bandwidth at $2.15 \mu^{-1}$ ($\lambda 4650$) was obtained as follows. The monochromatic magnitude for the emission region was deduced by assuming (i) the monochromatic magnitude

at $1.83 \mu^{-1}$ for γ^2 Vel to be the same as the V magnitude and equal to $+1.83$, (ii) the difference in monochromatic magnitude for γ^2 Vel between $1.83 \mu^{-1}$ and $2.15 \mu^{-1}$ to be 0.33 from the data of Aller & Faulkner (14) reduced to Hayes' calibration (15), (iii) the interstellar extinction to be 0.11 mag at $2.15 \mu^{-1}$ and (iv) the difference in monochromatic magnitude between the emission region and γ^2 Vel to be 1.10 from the spectral scan referred to in section 3.2. Thus the monochromatic magnitude of the emission region at $2.15 \mu^{-1}$ is found to be $+0.29$ and for $3.78 \times 10^{-20} \text{ erg cm}^{-2} \text{ s}^{-1} \text{ Hz}^{-1}$ at $1.83 \mu^{-1}$ for $V = 0.00$ this gives a received flux from the emission region at $2.15 \mu^{-1}$ of $2.89 \times 10^{-20} \text{ erg cm}^{-2} \text{ s}^{-1} \text{ Hz}^{-1}$.

Rather than speculate on the intensity distribution across the emission region we have substituted the angular diameter of the equivalent uniform disc given in Table II with the received flux, deduced above, in equation (5) to find the emergent flux from the emission region. Thus, the emergent flux from the 'surface' of the emission region is $(1.17 \pm 0.22) \times 10^{-3} \text{ erg cm}^{-2} \text{ s}^{-1} \text{ Hz}^{-1}$ and this corresponds to a brightness temperature of $T_{4650} = 12\,600 \pm 900 \text{ }^\circ\text{K}$.

4.3 The distance and absolute magnitude

The distance of γ^2 Vel was found by combining the data given in Table II with the spectroscopic measurements by Ganesh & Bappu (5). They observed the C III-IV emission line complex at 4652 \AA and the hydrogen absorption line at 4340 \AA and, on the assumption that these lines give the motions of the WC8 and the O7 star respectively, they derived the orbital parameters shown in Table IV.

TABLE IV

Parameters of γ^2 Vel found by Ganesh & Bappu

Parameter	Value
K(WC8) λ_{4652}	$153.5 \pm 4.4 \text{ km s}^{-1}$
K(O7) λ_{4340}	$43.1 \pm 2.6 \text{ km s}^{-1}$
e	0.17 ± 0.03
ω	$87^\circ \pm 9^\circ$
P	78.5 days
$m(\text{O7}) \sin^3 i$	$46.3 m_\odot$
$m(\text{WC8}) \sin^3 i$	$13.0 m_\odot$

From the data the projected semi-major axis of the orbit ($a \sin i$) is $(2.09 \pm 0.05) \times 10^{13} \text{ cm}$. Although, in principle, the inclination i of the orbit can be found from observations with the interferometer, in the present case we did not make sufficient measurements to establish it with satisfactory accuracy. We shall therefore assume that $\sin i = 0.94 \pm 0.05$, the upper limit being determined by the absence of eclipses and the lower limit by the consideration, following Schwarzschild & Harm (21), that the mass of the O7 star is unlikely to exceed $65 M_\odot$. On this assumption the semi-major axis is $(2.22 \pm 0.13) \times 10^{13} \text{ cm}$ and, taking the measured angular semi-major axis $(4''.3 \pm 0.5) \times 10^{-3}$ from Table II, the distance of γ^2 Vel is $350 \pm 50 \text{ pc}$.

This value of distance can be used to find the absolute magnitude. Thus, taking $V = +1.83$ and $E_{B-V} = 0.03$, the absolute magnitude of γ^2 Vel is

$$M_V[\text{WC8} + \text{O7}] = -6.0 \pm 0.25.$$

Previous estimates of the distance of γ^2 Vel are based on the assumption that it is at the same distance as γ^1 Vel. But the distance of γ^1 Vel is based on an estimate

of its absolute magnitude and this is uncertain. For example, from consideration of the spectral type, Gum (22) adopted $M_V = -2.2$, Aller & Faulkner (14) -3.1 , and Ganesh & Bappu (5) -3.3 ; while from the $H\beta$ photometry of Graham (23) Smith (6) and Morton, Jenkins & Brooks (24) took $M_V = -4.0$. Furthermore, Hiltner, Garrison & Schild (25) give the spectral classification as BI IV which corresponds to $M_V = -3.8$ assigned by Weaver & Ebert (26), -4.0 by Schmidt-Kaler (27) and -4.1 by Blaauw (28). From these values, Gum estimated the distance to γ^1 Vel as 250 pc, Smith as 460 pc and Morton as 450 pc. If we take $V = +4.27$ (10) and $E_{B-V} = 0.03$ then our 'geometrical' distance to γ^2 Vel ($350 \text{ pc} \pm 50$) yields $M_V = -3.5 \pm 0.25$ for γ^1 Vel. This result is reasonably consistent with all these estimates except that of Gum, and suggests that his value (250 pc) for the distance is too low.

As expected from the preceding discussion, our value for the absolute magnitude of γ^2 Vel ($M_V[\text{WC8} + \text{O7}] = -6.0 \pm 0.25$) is not significantly different from -6.4 given by Graham (23), -5.6 by Ganesh & Bappu (5) and -5.6 by Aller & Faulkner (14).

We can also derive from these results the magnitudes of the individual components of γ^2 Vel, but in estimating their uncertainties it is important to take account of the uncertainty in our initial assumption, following Smith (6, 7), that the WC8 star is 1 magnitude brighter than the O7 star. This assumption is supported by our analysis of the interferometer results which show that one component is 1.2 ± 0.6 magnitudes brighter than the other but does not, of course, indicate which of the two stars is the brighter. In the following discussion we shall therefore combine the evidence from the interferometer with our initial assumption and take the WC8 star to be 1 ± 0.6 magnitudes brighter than the O7 star.

As a first step we have examined the effect of this uncertainty on the measured value of θ_a , the angular size of the semi-major axis, and hence on our values for the distance and absolute magnitude of γ^2 Vel. We have found that, if we allow the assumed difference in brightness to vary over the range 0.4 to 1.6 magnitudes, the value of θ_a derived from the interferometer results varies by only 2 per cent. It follows that the uncertainties in the distance and absolute magnitude of γ^2 Vel, given above, are not affected by the uncertainties in the brightness ratio. On the other hand, in estimating the absolute magnitudes of the component stars we must take these uncertainties into account. Thus taking our measured value $M_V[\text{WC8} + \text{O7}] = -6.0 \pm 0.25$ and the difference in brightness to be 1 ± 0.6 magnitudes, the corresponding absolute magnitudes of the component stars are $M_V[\text{WC8}] = -5.6 \pm 0.4$ and $M_V[\text{O7}] = -4.6 \pm 0.7$.

The absolute magnitude which we have found for the WC8 star

$$(M_V \doteq -5.6 \pm 0.4)$$

is consistent with the properties of Wolf-Rayet stars as reviewed by Underhill (29) and by Smith (7). The absolute magnitude of the O7 star ($M_V = -4.6 \pm 0.7$) does not differ significantly from the values assigned to this spectral type of -5.3 by Blaauw (28), -5.2 by Schmidt-Kaler (27) and -4.7 by Weaver & Ebert (26).

4.4 *The radii of the stars and the emission region*

The radius of the WC8 component of γ^2 Vel can be found from the angular diameter measured in the continuum (Table II) and the distance derived in Section

4.3. The measurements were not adequate to give the angular diameter of the O7 star. Thus, if the angular diameter of the WC8 star is $(0''.45 \pm 0.05) \times 10^{-3}$ (θ_{LD} from Table III) and the distance 350 ± 50 pc, the radius of the WC8 star is $17 \pm 3 R_{\odot}$.

The angular diameter of the emission region, measured in the light of the C III–IV emission line complex and assuming it to appear as a uniformly bright disc, is $(2''.05 \pm 0.19) \times 10^{-3}$. At 350 ± 50 pc the corresponding radius of the region is therefore $76 \pm 10 R_{\odot}$. Since the apparent angular size of the semi-major axis a of the binary was found to be $(4''.3 \pm 0.5) \times 10^{-3}$, it follows that the radius of the emission region is $(0.24 \pm 0.04)a$.

It is interesting to compare the observed size of the emission region with the critical Roche equipotential lobe around the Wolf–Rayet star. The dimensions of the Roche lobe have been tabulated by Kopal (30) as a fraction of the semi-major axis and as a function of the mass ratio of the two stars. From the data in Table IV the mass ratio $m(\text{WC8})/m(\text{O7}) = 0.28 \pm 0.02$, where the uncertainty corresponds to the observational uncertainties in $K(\text{WC8})$ and $K(\text{O7})$. The corresponding mean radius of the critical Roche lobe (30) is $(0.26 \pm 0.01)a$. Thus a comparison shows that the observed radius of the emission region $(0.24 \pm 0.04)a$ does not differ significantly from the expected size of the critical lobe and we may provisionally conclude that the envelope responsible for the emission lines of ionized carbon fills the critical Roche equipotential around the Wolf–Rayet star. The observation that the emission envelope is roughly circular in outline, as reported in Section 3.2, is consistent with this conclusion.

4.5 *The surface gravity of the Wolf–Rayet star*

From the value of $m(\text{WC8}) \sin^3 i$ given in Table IV, and the assumed value of inclination ($\sin i = 0.94 \pm 0.05$), the mass of the WC8 star is $15.6 \pm 2.5 m_{\odot}$. If the radius is $17 \pm 3 R_{\odot}$ (Section 4.4), then it follows that the surface gravity of the Wolf–Rayet star is given by $\log g = 3.2 \pm 0.2$ for g in cm s^{-2} .

CONCLUSION

In this paper we have reported some of the first measurements of a binary star made with the stellar intensity interferometer. By combining our measurements with spectroscopic and photometric data we have found values for the distance, radius, absolute magnitude, surface gravity and effective temperature of the Wolf–Rayet component of γ^2 Vel; we have also established the size of the region responsible for the emission lines and shown that it is the correct size to fill the critical Roche equipotential lobe around the Wolf–Rayet star. In reviewing these data, and in assessing the potential value of the method, it should be remembered that our measurement of distance depends only upon measures of angle and velocity. It is therefore likely to be more reliable than a value based on a spectroscopic estimate of absolute magnitude which is usually subject to considerable uncertainties due to the dispersion in the characteristics of individual stars. Our estimate of effective temperature is likely to be more reliable than the results of conventional methods because it is based on a measurement of the absolute emergent flux from the stellar surface. Finally, the radii of the Wolf–Rayet star and of the emitting region are derived from direct measurements and do not depend upon the presence or interpretation of eclipses.

We believe that the results reported here demonstrate that stellar intensity

interferometry can be applied profitably to the study of close binaries and emission-line stars.

ACKNOWLEDGMENTS

The programme of the interferometer has been supported by the Air Force Office of Scientific Research (Office of Aerospace Research) of the United States Air Force under grant (AF-AFOSR-68-1560), the Australian Research Grants Committee, the Research Grant Committee of the University of Sydney and the Science Foundation for Physics within the University of Sydney. We are grateful to Dr D. C. Morton for valuable discussions, to Dr Lindsey Smith for sending us a photoelectric scan of the spectrum of γ^2 Vel made by Mrs Hain, and to Professor H. Messel for his support.

Cornell-Sydney University Astronomy Centre, School of Physics, University of Sydney.

REFERENCES

- (1) Hanbury Brown, R., Davis, J. & Allen, L. R., 1967. *Mon. Not. R. astr. Soc.*, **137**, 375.
- (2) Hanbury Brown, R. & Brovne, A., 1966. *Philips tech. Rev.*, **27**, 141.
- (3) Hanbury Brown, R., Davis, J., Allen, L. R. and Rome, J. M., 1967. *Mon. Not. R. astr. Soc.*, **137**, 393.
- (4) Smith, L. F., 1968. *Mon. Not. R. astr. Soc.*, **138**, 109.
- (5) Ganesh, K. S. & Bappu, M. K. V., 1967. *Kodaikanal Obs. Bull. Ser. A*, No. 183.
- (6) Smith, L. F., 1968. *Mon. Not. R. astr. Soc.*, **140**, 409.
- (7) Smith, L. F., 1968. *Wolf-Rayet Stars*, ed. K. B. Gebbie and R. N. Thomas, *National Bureau of Standards Special Publication 307*, Washington, D.C., 21-64.
- (8) Grygar, J., 1965. *Bull. astr. Inst. Csl.*, **16**, 195.
- (9) Code, A. D., 1960. *Stellar Atmospheres*, ed. J. L. Greenstein, University of Chicago Press.
- (10) Johnson, H. L., Mitchell, R. I., Iriarte, B., Wiśniewski, W. Z., 1966. *Commun. Lunar planet. Lab.*, **4**, 99.
- (11) Johnson, H. L., 1966. *A. Rev. astr. astrophys.*, **4**, 193.
- (12) Davis, J. & Webb, R. J., 1970. *Astrophys. J.*, **159**, in press.
- (13) Bradley, P. T. & Morton, D. C., 1969. *Astrophys. J.*, **156**, 687.
- (14) Aller, L. H. & Faulkner, D. J., 1964. *Astrophys. J.*, **140**, 167.
- (15) Hayes, D. S., 1967. Unpublished dissertation, University of California, Los Angeles.
- (16) Stecher, T. P., 1968. *Wolf-Rayet Stars*, ed. K. B. Gebbie and R. N. Thomas, *National Bureau of Standards Special Publication 307*, Washington, D.C., 21-64.
- (17) Bless, R. C., Code, A. D. & Houck, T. E., 1968. *Astrophys. J.*, **153**, 561.
- (18) Stecher, T. P., 1969. *Astrophys. J. Lett.*, **157**, L125.
- (19) Smith, A. M., 1967. *Astrophys. J.*, **147**, 158.
- (20) Carruthers, G. R., 1969. *Astrophys. Space Sci.*, **5**, 387.
- (21) Schwarzschild, M., & Harm, M., 1959. *Astrophys. J.*, **129**, 637.
- (22) Gum, C. S., 1955. *Mem. R. astr. Soc.*, **67**, 155.
- (23) Graham, J. A., 1965. *Observatory*, **85**, 196.
- (24) Morton, D. C., Jenkins, E. B. & Brooks, N. H., 1969. *Astrophys. J.*, **155**, 875.
- (25) Hiltner, W. A., Garrison, R. F. & Schild, R. E., 1969. *Astrophys. J.*, **157**, 313.
- (26) Weaver, H. F., & Ebert, A., 1964. *Pub. Astr. Soc. Pacific*, **76**, 6.
- (27) Schmidt-Kaler, Th., 1965. *Landolt-Bornstein Numerical Data and Functional Relationships in Science and Technology, New Series group VI*, **1**, 301. Springer-Verlag, Berlin.
- (28) Blaauw, A., 1963. *Basic Astronomical Data*, ed. K. Aa. Strand, University of Chicago Press, Chicago.
- (29) Underhill, A. B., 1966. *The Early Type Stars*, Reidel, Dordrecht.
- (30) Kopal, Z., 1954. *Jodrell Bank Ann.*, **1**, 37.

A STUDY OF α VIRGINIS WITH AN INTENSITY INTERFEROMETER

D. Herbison-Evans, R. Hanbury Brown, J. Davis and L. R. Allen

(Received 28 August 1970)

SUMMARY

Observations of the spectroscopic binary α Vir have been made with the Narrabri stellar intensity interferometer in 1966 and 1970. It has been shown that from interferometric observations alone it is possible to find the angular diameter of the primary, the brightness ratio of the components of the binary, the angular size of the semi-major axis of the relative orbit, the eccentricity, the time of periastron passage, the longitude of the line of apsides, the inclination of the orbit, the position angle of the line of nodes, the period of the orbit and the sense of the orbital motion. For α Vir, spectroscopic observations give values for four of these parameters of higher accuracy than can be obtained from the present interferometric data. Therefore, in the final analysis, these parameters were fixed at their spectroscopic values. The results for the two series of observations are in good agreement and where a spectroscopic parameter could be determined independently from the interferometric observations the agreement with the spectroscopic value is good. Interferometric and spectroscopic results have been combined to obtain the distance of α Vir (84 ± 4 pc) independent of interstellar extinction and luminosity criteria, the masses of the primary and secondary components, and the radius and surface gravity of the primary. The addition of photometric data has enabled the absolute emergent surface flux from the primary at $1.83 \mu^{-1}$ to be determined and, by comparing this surface flux with the predictions of theoretical model stellar atmospheres, the effective temperature of the primary has been estimated. Finally the luminosity of the primary and the absolute magnitudes of both components have been found.

I. INTRODUCTION

The stellar intensity interferometer at Narrabri Observatory has been used primarily to measure the angular diameters of single hot stars. Descriptions of the instrument (1), the technique (2) and some of the first results on single stars (3) have already been published. Recently we have started to explore the application of the instrument to more complex problems and, as part of this programme, we have observed the binary stars γ^2 Vel and α Vir. The results on γ^2 Vel have already been published (4) and the present paper reports the results on α Vir.

The first proposal that an interferometer should be used to observe binary stars was made by Michelson (5) in 1890. Subsequently, some interesting observations were carried out by Anderson (6) and by Merrill (7) who successfully measured many of the principal parameters of the double star α Aur. In principle, observations with an interferometer, made at suitable baselines and times, give the angular diameters and brightness ratio of the components of a binary and their angular separation as a function of time. From this information alone it is possible to find the angular size of the semi-major axis of the relative orbit, the eccentricity, the time of

periastron passage, the longitude of the line of apsides, the inclination of the orbit, the position angle of the line of nodes, the period of the orbit and the sense of the orbital motion.

If these data from an interferometer are combined with conventional photometric and spectroscopic observations, then it is possible, again in principle, to find the distance, absolute magnitude, mass, radius, surface gravity and temperature of both the stars.

Our observations of γ^2 Vel (4) were designed primarily to find the absolute magnitude and temperature of the Wolf-Rayet component and the size of the emission region around it; neither the interferometric nor the spectroscopic data were adequate to find all the parameters of the orbit and, in particular, no attempt was made to find the inclination. In the observations reported here we have chosen to observe a well-known, double-lined, non-eclipsing spectroscopic binary (α Vir) for which adequate photometric and spectroscopic data exist, and we have sought to demonstrate how the principal parameters can be found.

2. SPECTROSCOPIC OBSERVATIONS

Spectroscopic observations of α Vir have been made since 1876 and a brief review of the principal results is to be found in the papers by Struve and his collaborators. For our present analysis we have used the observations by Struve & Ebbighausen (8) in 1933 and 1934, and by Struve *et al.* (9) in 1956, 1957 and 1958. The observed velocities for the primary and secondary, excluding all observations which are marked as affected by blending of lines, were compared in a computer with values derived from a theoretical model and the sum of the squares of the residuals (observed minus computed) was minimized to find the optimum parameters of the orbit. The theoretical model allowed different mean velocities (γ_1 , γ_2) for the two stars and also allowed for a uniform rotation of the line of apsides. The minimization of the residuals and the estimate of the uncertainties in the parameters of the orbit were carried out by the same procedure as described in Section 3.2. The results are shown in Table I. It is important to note that the uncertainties shown in the Table are statistical and make no allowance for any systematic errors in the spectroscopic results.

A comparison of these results with the weighted means of the orbital elements published by Struve *et al.* (9) for 1933 and 1956 shows satisfactory agreement.

TABLE I

An analysis of the spectroscopic data for α Virginis

Parameter	Value
γ_1	$-5.8 \pm 1.3 \text{ km s}^{-1}$
γ_2	$+8.8 \pm 2.1 \text{ km s}^{-1}$
K_1	$123.9 \pm 1.4 \text{ km s}^{-1}$
K_2	$198.8 \pm 1.5 \text{ km s}^{-1}$
ω	$98 \pm 6^\circ$ at JD 2435564
T	JD 2435563.55 \pm 0.07
P	4.014550 ± 0.000032 days
e	0.146 ± 0.009
U	124 ± 11 yr

Furthermore, the orbital elements in Table I predict correctly the epochs of minimum velocity observed by Vogel (10) in 1890, by Baker (11) in 1908 and by Struve and Ebbighausen (8) in 1930.

We note that a recent investigation which has included new spectral data as well as the observations of Struve and his colleagues has led to the conclusion that there is no significant difference between γ_1 and γ_2 for α Vir. This investigation yielded mean values for the remaining parameters in Table I in satisfactory agreement with the values adopted here (N. Lomb and R. R. Shobbrook, private communication).

3. INTERFEROMETRIC OBSERVATIONS

Two series of observations of α Vir have been made with the stellar intensity interferometer at Narrabri. The first series was made in 1966. A method of analysing the results was developed and the final analysis completed in 1970. A second series of observations was made in 1970.

3.1 Method of observation

The observations were all carried out using our standard observing procedure which has been described in a previous paper (1). Briefly the two reflectors of the interferometer are guided to follow the star and their separation, the baseline, is maintained constant and perpendicular to the direction of the star. The correlation is measured over intervals of 100 s and recorded together with the light fluxes received by the two reflectors. The observed correlation is then normalized by the light fluxes and by the gain of the electronic equipment to find the *normalized observed correlation* $\overline{c_N(d)}$ for each interval. Typically these observations are continued for several hours at one baseline and then repeated at other baselines.

3.2 Method of analysis

A computer program was written to calculate the correlation expected from a binary star as a function of time for a given set of orbital parameters. The component stars were assumed to present uniformly bright circular discs. Under these conditions the normalized correlation $\overline{c_N(d)}$ is given by

$$\overline{c_N(d)} = \frac{A}{(1+\beta)^2} \left[\beta^2 \Gamma_1^2(d) + \Gamma_2^2(d) + 2\beta |\Gamma_1(d)| |\Gamma_2(d)| \cos \left(\frac{2\pi\theta_s d \cos \psi}{\lambda_0} \right) \right] \quad (1)$$

where

$$\Gamma_1(d) = \frac{2J_1(\pi\theta_{UD1} d/\lambda_0)}{\pi\theta_{UD1} d/\lambda_0}$$

$$\Gamma_2(d) = \frac{2J_1(\pi\theta_{UD2} d/\lambda_0)}{\pi\theta_{UD2} d/\lambda_0}$$

and λ_0 is the wavelength of observation; θ_{UD1} and θ_{UD2} are the angular diameters (equivalent uniform discs) of the primary and secondary; β is the brightness ratio of the components ($\beta \geq 1$); θ_s is the angular separation of the components projected on to the plane of the sky; ψ is the angle in the plane of the sky between the projection of the line joining the stars and the baseline of the interferometer; A is an instrumental constant, which, in effect, is the normalized correlation to be expected from

an unresolved single star. The parameters of the orbit which enter the calculation are, θ_a the angular semi-major axis, i the inclination of the orbital plane, Ω the position angle of the line of nodes, e the eccentricity, T the epoch of periastron passage, ω the longitude of the line of apsides, P the period of the orbit measured from periastron to periastron, and U the period of rotation of the line of apsides. The sense of rotation of the stars in their orbit and of the line of apsides also enter the calculation.

As a first step in the analysis the values of T , e , P , ω , U and θ_{UD2} were fixed in the computer at the values shown in Table I, leaving six free parameters, i , θ_a , β , Ω , θ_{UD1} and A to be found by comparing the observed and computed correlations. As we shall see later the spectroscopic values of T , e , P and ω are superior in accuracy to those which can be found from the interferometer and, as we expected, the signal/noise ratio of the observations was inadequate to find the value of θ_{UD2} with acceptable accuracy. The 'fixed' values of T , e , P and ω were therefore taken from the spectroscopic data in Table I and the value of θ_{UD2} was estimated with the aid of a preliminary analysis. It was also assumed that the period of rotation of the line of apsides was infinite over the period of observation and hence $U = \infty$ and ω has fixed values appropriate to the mean epochs of observation in 1966 and 1970. Initial values for the 'free' parameters, as a starting point for the programme, were taken from a preliminary analysis (12) and the normalized correlation was computed for each of the intervals of observation.

The calculation was performed as follows: for each interval of Julian date J , the mean anomaly m was computed from

$$m = 2\pi(J - T)/P \quad (2)$$

then the eccentric anomaly E from the first order approximation

$$E = m + \frac{e \sin m}{1 - e \cos m} \quad (3)$$

then the true anomaly v from

$$\tan\left(\frac{v}{2}\right) = [(1+e)/(1-e)]^{1/2} \tan \frac{E}{2} \quad (4)$$

and the angular separation of the stars θ_r from

$$\theta_r = \theta_a(1 - e^2)/(1 + e \cos v) \quad (5)$$

and hence the projected angular separation of the stars in the plane of the sky θ_s was found from

$$\theta_s = \theta_r [1 - (\sin i \cdot \sin \overline{\omega + v})^2]^{1/2}. \quad (6)$$

The position angle ψ of the line joining the stars, relative to the baseline of the interferometer, was computed from

$$\psi = \Omega + \frac{\pi}{2} + \eta + \delta_1 \delta_2 \cos^{-1} \left[\frac{\cos \overline{\omega + v}}{(1 - \sin^2 i \cdot \sin^2 \overline{\omega + v})^{1/2}} \right] \quad (7)$$

where δ_1 is -1 for a clockwise and $+1$ for an anti-clockwise orbit, and δ_2 is $+1$ for $0 < \omega + v < 180^\circ$ and -1 for $180^\circ < \omega + v < 360^\circ$, and the solution to the \cos^{-1} term is chosen to lie between 0 and π . The parallactic angle η is the angle at the star, in the

sky plane, between the vertical circle and the great circle through the star and the poles. η is given by

$$\sin \eta = \cos \phi \sin H / \sin Z \quad (8)$$

where ϕ is the latitude, H is the hour angle and Z is the zenith distance. Finally the values of θ_s and ψ from equations (6) and (7) were substituted in equation (1) to calculate the correlation (c_c) for each interval.

The difference between the observed and the calculated correlation ($\overline{c_N(d)} - c_c$) was then found for each interval, squared, and weighted by the square of the corresponding 'signal/noise ratio'. It can be shown (1) that this signal/noise ratio is proportional to $(I_1 I_2)^{1/2}$ where I_1, I_2 are the light fluxes received by the two reflectors in the interval. The square root of the mean value of the weighted, squared differences is the r.m.s. residual σ_r so that

$$\sigma_r = \left[\sum_M (\overline{c_N(d)} - c_c)_i^2 (I_1 I_2)_i / M \right]^{1/2} \quad (9)$$

where M is the number of intervals observed. The value of σ_r was then minimized by optimizing the 'free' input parameters of the theoretical model using an iterative programme based on the Simplex Method (13).

The uncertainty in the optimized free parameters was found by computing the partial derivatives of the theoretical correlation with respect to each parameter at the time of each observation. These derivatives were then weighted in proportion to the signal/noise ratio by $(I_1 I_2)^{1/2}$, and the resulting matrix of weighted derivatives was multiplied by its transpose, and inverted. The square root of the p th diagonal element of this inverse (x_{pp}) was then multiplied by the r.m.s. residual σ_r to find the r.m.s. uncertainty σ_p in the p th free parameter, where

$$\sigma_p = \sigma_r \sqrt{x_{pp}}. \quad (10)$$

The whole analysis was carried out twice, for clockwise and anti-clockwise orbital motion. Although these two cases cannot be distinguished spectroscopically they can be distinguished by the interferometer, given sufficient observations of high signal/noise ratio, because the orbital motion adds to or subtracts from the parallactic angle.

3.3 Observations in 1966

α Vir was observed for 12 nights in May 1966 with baselines of 10.0, 32.7, 59.7 and 88.3 m for a total time of about 84 hr. The effective wavelength was 4430 Å with a total filter bandwidth of 100 Å. To reduce the amount of computing the normalized correlations at each baseline were averaged over 25 intervals of 100 s to find the normalized observed correlation for periods of 2500 s. The results were then compared with calculated values in the computer to find the optimum values of the six 'free' parameters and their associated uncertainties. A unique minimum in the residual σ_r was found for both choices of the sense of orbital motion and the results are shown in columns 4 and 5 of Table II. The expected value of the residual σ_r is σ_{std} , the normalized r.m.s. uncertainty due to noise in the correlator output (3). We have, therefore, shown σ_r / σ_{std} in Table II, taking values of σ_{std} measured independently for the configuration of the apparatus in 1966.

Table II shows that although the values of Ω and i are significantly different for the two solutions, the residuals σ_r are not. The values of σ_r are both consistent with

TABLE II
Analysis of interferometric observations

(1) Parameter	(2) Symbol	(3) Units	(4) 1966	(5) 1966	(6) 1970	(7) 1970	(8) 1970	(9) 1970	(10) 1970 (Final analysis)
Number of free parameters			6	6	6	6	11	11	6
Inclination of orbit	i	degrees	63 ± 4	76 ± 3	65 ± 2	90 ± 4	65 ± 2	90 ± 4	65.9 ± 1.8
Angular size of primary	θ_{UD1}	10^{-3} arc sec	0.76 ± 0.06	0.74 ± 0.06	0.87 ± 0.04	0.97 ± 0.08	0.88 ± 0.04	0.93 ± 0.05	0.87 ± 0.04
Angular size of secondary	θ_{UD2}	10^{-3} arc sec	(0.4)	(0.4)	(0.4)	(0.4)	~ 0	1.3 ± 0.4	(0.4)
Angular size of semi-major axis	θ_a	10^{-3} arc sec	1.42 ± 0.10	1.42 ± 0.11	1.52 ± 0.05	1.37 ± 0.09	1.52 ± 0.04	1.32 ± 0.11	1.54 ± 0.05
Brightness ratio of components	β		6.2 ± 1.9	6.2 ± 2.0	6.2 ± 0.9	8.1 ± 2.6	6.4 ± 0.9	5.5 ± 1.5	6.4 ± 1.0
Position angle of line of nodes	Ω	degrees	122 ± 5	158 ± 4	132.1 ± 2.1	142.2 ± 3.2	130.8 ± 2.0	142.2 ± 3.4	131.6 ± 2.1
Epoch of periastron passage	T	JD	(2439256.94)	(2439256.94)	(2440678.09)	(2440678.09)	2440678.02 ± 0.08	2440678.16 ± 0.35	(2440678.09)
Eccentricity of orbit	e		(0.146)	(0.146)	(0.146)	(0.146)	0.160 ± 0.021	0.139 ± 0.052	(0.146)
Longitude of line of apsides	ω	degrees	(127)	(127)	(138)	(138)	132 ± 8	150 ± 33	(138)
Inverse period	$1/P$	1/days	(0.249091)	(0.249091)	(0.249091)	(0.249091)	0.2481 ± 0.0006	0.2459 ± 0.0012	(0.249091)
Sense of orbital motion			Clockwise	Anti-clockwise	Clockwise	Anti-clockwise	Clockwise	Anti-clockwise	Clockwise
Instrumental constant	A	arbitrary	1.77 ± 0.06	1.71 ± 0.06	5.01 ± 0.18	4.65 ± 0.19	4.97 ± 0.17	4.91 ± 0.29	5.00 ± 0.19
r.m.s. residual/normalized noise	σ_r/σ_{std}		$0.22/0.20$	$0.23/0.20$	$0.25/0.27$	$0.31/0.27$	$0.25/0.27$	$0.30/0.27$	$0.26/0.27$
Interval over which observations were averaged		seconds	2500	2500	2500	2500	2500	2500	500
Number of intervals used			112	112	158	158	158	158	800

Notes: The values taken from spectroscopic data (Table I) are in brackets. The value of θ_{UD2} in brackets is assumed (see text).

the expected value of $\sigma_{std} = 0.20$. Thus it appears that the signal/noise ratio of these observations is inadequate to distinguish the correct sense of orbital motion from a simple comparison of the 'goodness of fit' of the two solutions. In addition, a more detailed examination suggests that, to solve this particular problem, our choice of baselines could have been better. Fortunately, the difference between the inclinations (i) of the two solutions shows that the clockwise solution must be correct; the high inclination (76°) of the anti-clockwise orbit implies eclipses which are not observed (see Section 4.2).

3.4 Observations in 1970

Following a complete analysis of our 1966 observations we decided to observe α Vir again to check the whole procedure and to increase the precision of the results. Specifically we hoped to improve the accuracy by a different choice of baselines and by taking advantage of improvements to the interferometer which had raised its signal/noise ratio by a factor of about 1.6. The most significant of these improvements was the introduction in 1969 of R.C.A. type 8850 phototubes with high-gain first dynodes.

The second series of observations was made on 16 nights in March and April 1970 with baselines of 19.7, 39.1 and 83.9 m for a total time of about 115 hr. Again the effective wavelength was 4430 \AA with a total filter bandwidth of 100 \AA .

Initially, the observations were analysed in precisely the same way as the 1966 series to find the six free parameters. As for the 1966 data two unique minima were found for the residual σ_r , corresponding to the two senses of orbital motion, and the results are shown in columns 6 and 7 of Table II. The values of σ_r are not inconsistent with the expected value of $\sigma_{std} = 0.27$, measured for the configuration of the equipment used in 1970, but they do differ significantly from one another. The r.m.s. uncertainty in each value of σ_r is about ± 0.02 and so the residual for clockwise rotation (0.25) is three standard deviations less than the residual for anti-clockwise rotation (0.31), thus confirming our earlier conclusion that the clockwise solution must be correct. Furthermore, the inclination of the anti-clockwise solution ($90^\circ \pm 4^\circ$) is again definitely excluded by the absence of eclipses.

A comparison of columns 4 and 6 of Table II shows that the parameters derived from the 1966 and 1970 observations are in satisfactory agreement and that the 1970 results are, as expected, about twice as accurate. The largest differences are in Ω and θ_{UD1} which differ by about 1.9σ and 1.5σ respectively, where σ is their combined uncertainty. It must be noted that the instrumental constants A are widely different because they refer to different configurations of the equipment.

As a further check on the reliability of our results, we have tested their consistency with the spectroscopic data. This we have done by removing the spectroscopic data entirely and allowing the computer to optimize all 11 parameters of the star (θ_a , θ_{UD1} , θ_{UD2} , i , β , Ω , T , e , ω , A and P). Again two minima close to the expected period of the star were found corresponding to clockwise and anti-clockwise rotation and the results are shown in columns 8 and 9 of Table II. The two residuals σ_r differ significantly and show that the clockwise solution is correct. A comparison of the four parameters T , e , ω , and P in Table II with the spectroscopic data in Table I shows that there are no significant differences, but that the spectroscopic data are more precise. The other six parameters agree well with the values shown in columns 6 and 7 for the six 'free' parameter analysis. The value of θ_{UD2} , the angular size of the secondary star, is undetermined because the signal/noise ratio

was inadequate. However, an examination was made of the effects of changes in the assumed value of θ_{UD2} . They were found to be negligible. This can also be seen from a comparison of the solutions in which θ_{UD2} was fixed (columns 6 and 7 in Table II) with those in which it was a free parameter (columns 8 and 9). We conclude from this analysis that our interferometric results are consistent with the spectroscopic data.

Finally, we have tested the dependence of our results on the period over which the observed correlations are averaged. To this end we have averaged the observed correlations over intervals of 500 s, instead of 2500 s, and repeated the calculations shown in column 6 of Table II. Since this is an extensive calculation it has only been carried out for the correct sense of orbital motion (clockwise). For this refined calculation an attempt was made to reject any observations which might be defective. The computer program was therefore modified to reject all observations which differ by more than $2.5\sigma_r$ from the calculated values and, as a result, 19 of the 819

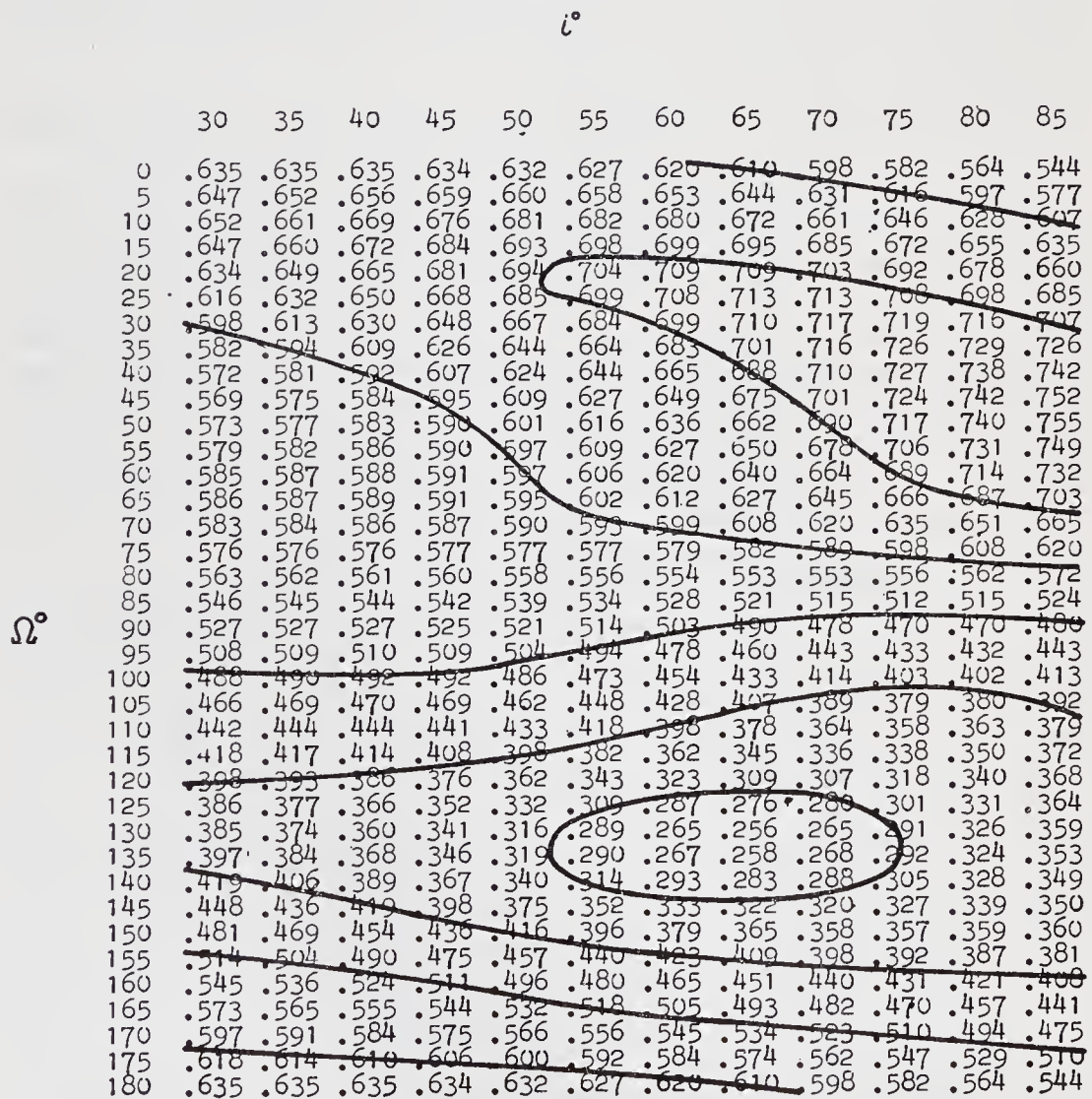


FIG. 1. Map of the r.m.s. residual (σ_r) as a function of the position angle of the line of nodes (Ω) and the inclination (i) with the remaining nine parameters fixed at the values given in column 10 of Table II.

intervals were rejected. A check was made that these rejected observations were not distributed in any systematic way. The results are shown in column 10 of Table II. We note that they are consistent with the results in column 6 of Table II and, since they represent the most exact analysis which it is worth making, we shall take them as our final results for α Vir.

Figs 1 and 2 illustrate the calculations presented above. Fig. 1 is a map of the r.m.s. residual σ_r as a function of the two parameters Ω and i , all the other parameters being fixed at their optimum values. The contours show clearly the unique minimum in σ_r corresponding to the clockwise solution presented in column 6 of Table II. It is fortuitous that in the case of α Vir the orbital period (4.014 days) is so close to 4 days that, over the observation period of 20 days, the binary system presents essentially the same phase every fourth night. In Fig. 2 we have plotted the correlation as a function of hour angle for 12 nights divided into 4 sets; each set is the average of the

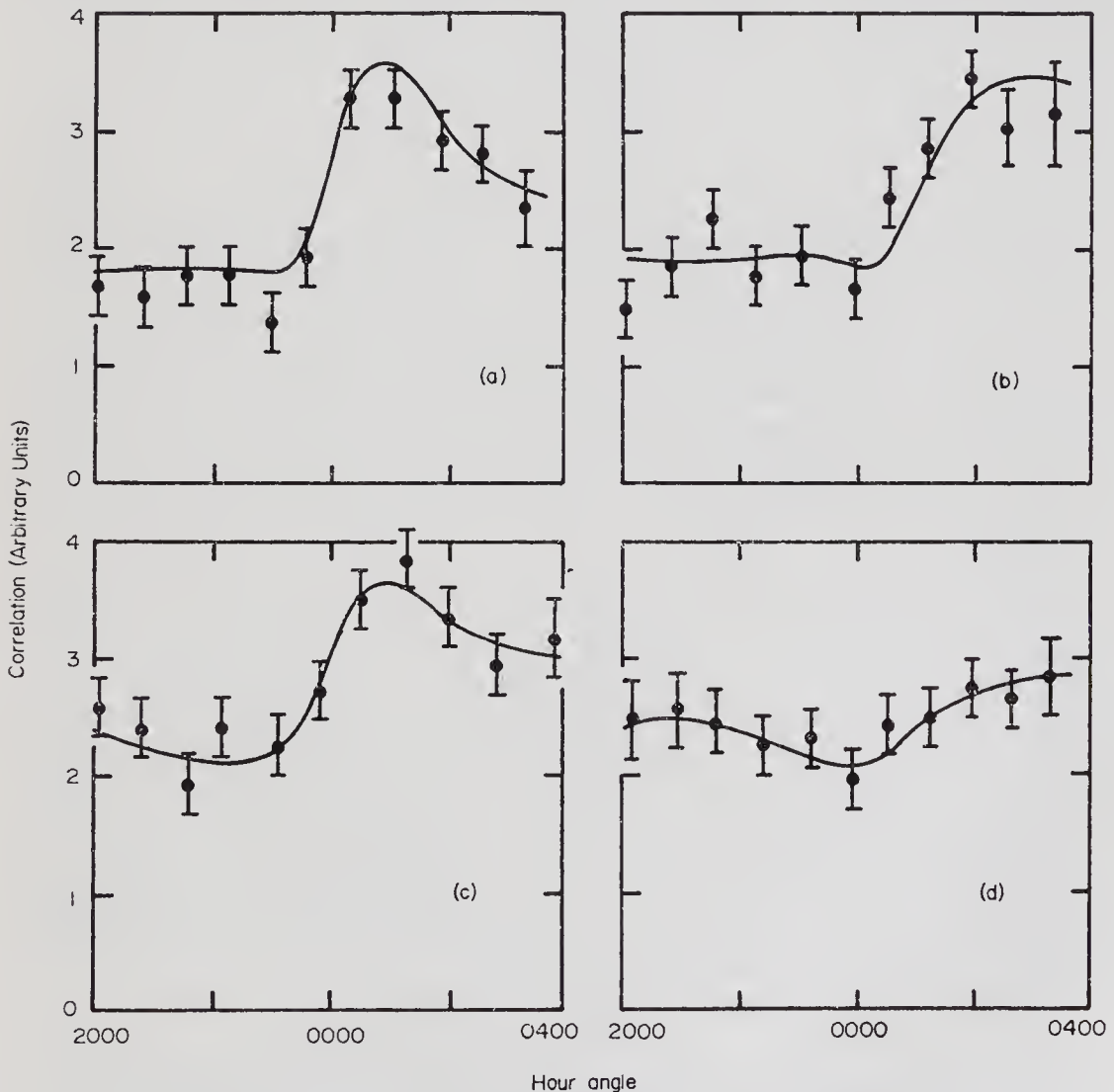


FIG. 2. Variation of correlation from α Vir observed in 1970 with a baseline of 39.1 m for four different 'phases' (see text). Observations for the four 'phases' were combined for the Julian Days of observation as follows: (a) JD2440672, 680 and 692. (b) JD2440673, 677 and 689. (c) JD2440678, 682 and 690. (d) JD2440675, 683 and 691.

The curves represent the average computed correlation for the periods of observation using the parameters of the solution given in column 10 of Table II.

correlation on 3 nights which are themselves separated by either 4 or 8 days. The points show the average of the correlation observed on the 3 nights in 2500 s intervals, and the full line is the average of the correlation calculated for those 3 nights. The curves show clearly the variation of correlation with time for the four different phases of the system.

Detailed lists of all the observations are available and the authors will be glad to supply them to anyone who is interested. We have not included them in the present paper because they are lengthy and we judge that they are not of sufficient interest to justify the space.

3.5 Corrections and errors

In the analysis presented above, the uncertainties in the final parameters have been estimated on the assumption that the weighted differences between the observed and computed correlations represent random errors which are normally distributed. No allowance has been made for systematic errors. An examination of the weighted differences for the results shown in Table II confirms that they are normally distributed. Furthermore, the r.m.s. residual σ_r is, as already noted, consistent with the assumption that the principal source of uncertainty is the statistical noise in the correlator output. Nevertheless, these two tests do not exclude the possibility that there are systematic errors in our measurements. We have, therefore, reviewed all the principal sources of systematic error (timing errors, delay errors, gain calibration, sky and moon background light, non-linearity, effects of elevation, computing approximations, etc.), and have reached the conclusion that, in the present experiments, where the signal/noise ratio is rather low, the systematic errors are small compared with the statistical noise. This conclusion is reinforced by the agreement between the interferometric and spectroscopic parameters discussed in Section 3.4. We shall, therefore, proceed to discuss the results on the assumption that the 'statistical' errors shown in Table II are reasonable estimates of the uncertainties.

There are a number of minor corrections which remain to be discussed. Firstly, the theoretical model assumes that the two stars have circular discs of uniform intensity which do not vary with time. In reality the two stars will be limb-darkened, distorted by rotation and mutual interaction, and the light and radius of the primary will vary because it is a β Cepheid variable (14). Neglect of limb-darkening will not affect the solution for the orbital elements, but it is taken into account in Section 4.1 in finding the true angular size of the primary θ_{LD1} from the angular size of the equivalent uniform disc θ_{UD1} . We have also made estimates of the effects of rotation and tidal distortion on our results and find them to be negligible. The effects of the variations in light of the primary are, to a first order, removed by normalization and theory suggests that the associated periodic changes in radius are too small to be significant in the present context.

In principle, minor corrections should also be made for the effects of partial resolution by the reflectors. The two reflectors themselves are so large (6.5 m diameter) in relation to the baseline that they partially resolve the separation of the two stars when they appear furthest apart, thereby reducing the amplitude of the interaction term in equation (1). In widely-separated binaries this effect limits the use of an intensity interferometer (15), but in the present case calculations show that the only significant effect is to increase the computed value of β , the brightness ratio, by a few per cent. Since this is small compared with the uncertainty in β , no

correction has been made to the data in Table II. Lastly, there is the reflection effect which brightens the inner surfaces of the components of a close binary and thereby reduces their apparent separation as seen by the interferometer. Following Chen & Rhein (16) we have computed the apparent increase in the brightness of the inner surfaces and find that, in the present case, the apparent shift is less than 10^{-3} of the semi-major axis. No correction for the reflection effect has therefore been applied.

4. DISCUSSION

4.1 Combined interferometric, spectroscopic and photometric results

The results of combining the data from interferometric, spectroscopic and photometric observations are shown in Table III.

TABLE III

The parameters of α Virginis

Parameter	Value \pm r.m.s. uncertainty	Source*
Inclination of orbit (i)	$65^{\circ}.9 \pm 1^{\circ}.8$	I
Angular size of primary (limb-darkened) (θ_{LD1})	$(0''.90 \pm 0''.04) \times 10^{-3}$	I
Angular size of semi-major axis (θ_a)	$(1''.54 \pm 0''.05) \times 10^{-3}$	I
Brightness ratio of components (β)	6.4 ± 1.0	I
Position angle of line of nodes (Ω)	$131^{\circ}.6 \pm 2^{\circ}.1$	I
Sense of orbital motion	Clockwise	I
Epoch of periastron passage (T)	JD 2440678.09	S
Eccentricity of orbit (e)	0.146	S
Longitude of line of apsides (ω)	138° at JD 2440678	S
Inverse period ($1/P$)	$0.249091 \text{ days}^{-1}$	S
Period of rotation of line of apsides (U)	124 yr	S
Semi-major axis (a)	$(1.93 \pm 0.06) \times 10^7 \text{ km}$	I + S
Distance	$84 \pm 4 \text{ pc}$	I + S
Mass of primary (m_1)	$10.9 \pm 0.9 m_{\odot}$	I + S
Mass of secondary (m_2)	$6.8 \pm 0.7 m_{\odot}$	I + S
Radius of primary (R_1)	$8.1 \pm 0.5 R_{\odot}$	I + S
Surface gravity of primary ($\log g_1$)	3.7 ± 0.1 [g_1 in c.g.s. units]	I + S
Absolute surface flux of primary (\mathcal{F}_{ν_1} at $1.83 \mu^{-1}$)	$(2.75 \pm 0.24) \times 10^{-3} \text{ erg cm}^{-2} \text{ s}^{-1} \text{ Hz}^{-1}$	I + P
Effective temperature of primary (T_e)	$22400 \pm 1000^{\circ} \text{K}$	I + P
Luminosity of primary ($\log L_1/L_{\odot}$)	4.17 ± 0.10	I + S + P
Absolute magnitude of primary (M_{V_1})	-3.5 ± 0.1	I + S + P
Absolute magnitude of secondary (M_{V_2})	-1.5 ± 0.2	I + S + P

* I = interferometric, S = spectroscopic, P = photometric.

To find the distance of α Vir we first calculated the projected semi-major axis from K_1 , K_2 , P and e in Table I. From the standard relation we found

$$a \sin i = (1.76 \pm 0.05) \times 10^7 \text{ km.} \quad (11)$$

The uncertainty in this result is difficult to estimate. It was noted in Section 2 that the uncertainties in K_1 , K_2 in Table I are only statistical and make no allowance

for systematic errors. An examination of the difference between the results obtained by Struve and his colleagues (9) in 1933 and 1956, together with his comments about the blending and variability of the lines, suggests that there may be significant systematic errors in K_1 and K_2 ; furthermore, we now know (14) that the primary star is a β Cepheid which complicates the interpretation of the spectrum. We have therefore increased the uncertainties given in Table I to cover the range of Struve's results, and we have taken the uncertainty in K_1 to be $\pm 7 \text{ km s}^{-1}$ and in K_2 to be $\pm 5 \text{ km s}^{-1}$. The corresponding uncertainty in $a \sin i$ is that shown in equation (11); the errors in e and P have little effect. The distance of α Vir was then calculated from the projected size of the semi-major axis ($a \sin i$ from equation (11)), the inclination of the orbit and the angular size of the semi-major axis (i and θ_a from column 10 of Table II). The resulting distance is $84 \pm 4 \text{ pc}$ where the major uncertainty is due to the spectroscopic data.

To find the masses of the components of α Vir we first calculated the values of $m_1 \sin^3 i$ and $m_2 \sin^3 i$ from the spectroscopic data. Using the standard relation and the same uncertainties in K_1 and K_2 we have

$$\begin{aligned} m_1 \sin^3 i &= 8.3 \pm 0.6 m_\odot \\ m_2 \sin^3 i &= 5.2 \pm 0.5 m_\odot \end{aligned} \quad (12)$$

The masses given in Table III were found by combining these values with i from column 10 of Table II.

The angular diameter of the primary (θ_{LD1}) was found by correcting θ_{UD1} to allow for limb-darkening. Following a previous discussion (3) we have taken $\theta_{LD1}/\theta_{UD1} = 1.03$ for an assumed limb-darkening coefficient $U_{4430} = 0.39$. The radius of the primary R_1 given in Table III was then found from θ_{LD1} and the distance, and the surface gravity from m_1 and R_1 .

The effective temperature T_{e1} of the primary was found as follows. The absolute monochromatic flux at the Earth (f_ν) from the primary, at the constant energy reciprocal wavelength ($1/\lambda_0 = 1.83 \mu^{-1}$) of the V band (17), was calculated from

$$f_\nu = 3.71 \times 10^{-20} \times 10^{-0.4V} \text{ erg cm}^{-2} \text{ s}^{-1} \text{ Hz}^{-1} \quad (13)$$

where $3.71 \times 10^{-20} \text{ erg cm}^{-2} \text{ s}^{-1} \text{ Hz}^{-1}$ has been adopted as the flux received above the Earth's atmosphere from a star with $V = 0.00$, this being the mean of a new determination by Oke & Schild (18) and the value proposed by Davis & Webb (19) from a review of earlier work. The visual magnitude V of the primary was taken to be $+1.13$ from $V = +0.97$ for α Vir (20) and $\Delta V = 2.0$ (from $\beta = 6.4$ in Table III). Thus, for the primary, $f_\nu = 1.31 \times 10^{-20} \text{ erg cm}^{-2} \text{ s}^{-1} \text{ Hz}^{-1}$ at $1.83 \mu^{-1}$.

At this point we note that ΔV has been determined using a spectroscopic method by Struve (21) who obtained $\Delta V \simeq 2.4$, Petrie (22) $\Delta V = 1.49$ and Struve *et al.* (9) $\Delta V = 1.69$. In view of the spread in values obtained by the spectroscopic method we have chosen to use the interferometric value of $\Delta V = 2.0 \pm 0.2$ throughout our discussion of the results.

The absolute monochromatic flux at the stellar surface (\mathcal{F}_ν) was found next from

$$\mathcal{F}_\nu = \frac{4f_\nu}{\theta_{LD}^2} \cdot 10^{0.4A_\nu} \quad (14)$$

where A_ν is the total interstellar absorption at frequency ν . A comparison of the observed colours of α Vir (20) with the intrinsic colours (23) for a B1.5 IV-V star

mass–luminosity and mass–radius relationships for early type stars. In Figs 3 and 4 we have plotted our results for the primary together with the existing data for binary stars of spectral type A1 and earlier. The data for the mass–luminosity plot in Fig. 3 are taken from the list of Harris, Strand & Worley (28) for ‘reliable’ spectroscopic binaries with the addition of the data for the components of CO Lac by Smak (29). It can be seen that the data for the primary of α Vir are consistent with other binary stars.

The mass–radius data in Fig. 4 are from the compilation by Popper (30) of ‘reliable’ systems with the addition of the data for CO Lac (29). Also included is the point for the primary of α CMa (Sirius), the mass being taken from Harris *et al.* (28)

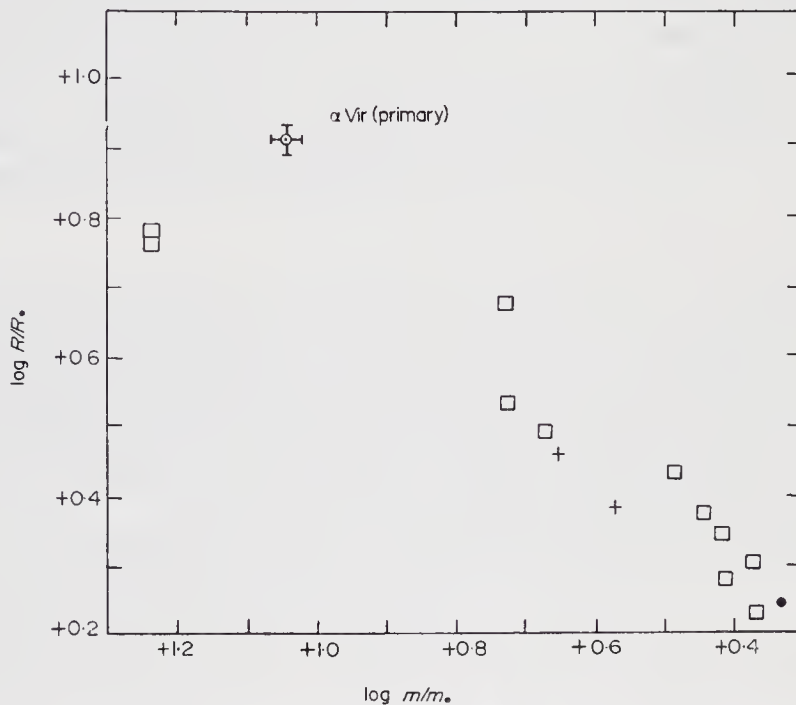


FIG. 4. The empirical mass–radius relation for early-type stars. \square —eclipsing binary data listed by Popper (30); +—CO Lac (Smak (29)); \bullet — α CMa (see text).

and the radius from Hanbury Brown *et al.* (3). The data include only main-sequence components and it can be seen that the primary of α Vir lies above the mean relationship suggesting that it has evolved away from the main-sequence. The position of the primary of α Vir in Fig. 3 is consistent with this conclusion.

The spectral type of the primary of α Vir has been classified as probably B2V by Struve *et al.* (9), B1V by Morgan, Code & Whitford (31) and, more recently, as B1IV by Lesh (32). According to Johnson & Iriarte (33) the absolute magnitudes of types B1V and B1IV are $M_V = -3.6$ and -4.1 , and of types B2V and B2IV are $M_V = -2.5$ and -3.3 . Thus our value of -3.5 ± 0.1 is consistent with a spectral classification between B1 and B2. Our value for the mass of the primary is consistent with this classification. We have already noted that the point for the primary of α Vir lies above the mean relationship for main-sequence components in the mass–radius diagram (Fig. 4) and we conclude that our results are consistent with a spectral classification B1.5 IV–V.

Support for this conclusion is given by the recent observation by Shobbrook *et al.* (14) that the primary of α Vir is a β Cepheid with a period of about 4 hr. It is also

interesting to note that our value for the absolute magnitude (-3.5 ± 0.1) agrees well with the period–luminosity law for β Cepheids found by Leung (34).

The only published spectral classification of the secondary component of α Vir appears to be that by Struve *et al.* (9) who noted that it is probably B₃V, but may be as late as B₇V. Our values for the mass ($6.8 \pm 0.7 m_{\odot}$) and absolute magnitude ($M_{V_2} = -1.5 \pm 0.2$) are consistent with a classification B₃V.

Finally, we must note that, with the parameters in Table III, α Vir may show shallow grazing eclipses. In a rough analysis of this question we have assumed that the primary is flattened at the poles by 4 per cent, due to rotation and mutual distortion, and that both components are limb-darkened with $U_{4430} = 0.4$. Then, with the parameters shown in Table III, we find a grazing eclipse with a depth of approximately 1 ± 1 per cent, where the uncertainty in our estimate is largely due to the uncertainty in the inclination. Unfortunately, the observational evidence for eclipses is complicated by the β Cepheid light variations of the primary and by the mutual distortion of the two stars. According to Shobbrook *et al.* (14), after allowing for these complex effects, there is no residual positive evidence for eclipses and it is unlikely that they exceed 0.5 per cent. Since the depth of a grazing eclipse is critically dependent on so many factors, including our assumptions about limb-darkening, polar flattening and the angular size of the secondary, it is not worth while attempting to refine our parameters of α Vir until more positive evidence from the light curve is available.

5. CONCLUSION

The results presented above demonstrate that all the principal parameters of a double-lined, non-eclipsing, spectroscopic binary star, *including the distance*, can be found by combining observations made with an intensity interferometer with conventional spectroscopic and photometric data. It is of great interest to note, firstly, that the method gives a distance which is independent of interstellar extinction and of spectroscopic criteria of luminosity, and secondly, that it yields the inclination and hence the masses of the two stars.

In conclusion, this preliminary experiment, together with our observations of γ^2 Vel (4) demonstrate the potential value of a high resolution interferometer applied to the study of close binary stars. Given an instrument of greater sensitivity than the existing interferometer it would be possible to establish reasonably precise distances to many binary stars well beyond the useful limits of trigonometrical parallaxes and to extend our meagre knowledge of the masses, radii and absolute luminosities of hot stars.

ACKNOWLEDGMENTS

We are grateful to Professor D. M. Popper for his continued interest in the Narrabri programme and for his valuable advice.

The programme of the interferometer has been supported by the Air Force Office of Scientific Research (Office of Aerospace Research) of the United States Air Force under Grant (AF-AFOSR-68-1560), the Australian Research Grants Committee, the Research Grant Committee of the University of Sydney and the Science Foundation for Physics within the University of Sydney. We thank Professor H. Messel for his support.

Cornell–Sydney Astronomy Centre, School of Physics, University of Sydney

REFERENCES

- (1) Brown, R. Hanbury, Davis J. & Allen, L. R., 1967. *Mon. Not. R. astr. Soc.*, **137**, 375.
- (2) Brown, R. Hanbury & Browne, A., 1966. *Phillips Tech. Rev.*, **27**, 141.
- (3) Brown, R. Hanbury, Davis, J., Allen, L. R. & Rome, J. M., 1967. *Mon. Not. R. astr. Soc.*, **137**, 393.
- (4) Brown, R. Hanbury, Davis J., Herbison-Evans, D. & Allen, L. R., 1970. *Mon. Not. R. astr. Soc.*, **148**, 103.
- (5) Michelson, A. A., 1920. *Astrophys. J.*, **51**, 257.
- (6) Anderson, J. A., 1920. *Astrophys. J.*, **51**, 263.
- (7) Merrill, P. W., 1922. *Astrophys. J.*, **56**, 40.
- (8) Struve, O. & Ebbighausen, E., 1934. *Astrophys. J.*, **80**, 365.
- (9) Struve, O., Sahade, J., Huang, S-S. & Zebergs, V., 1958. *Astrophys. J.*, **128**, 310.
- (10) Vogel, H. C., 1892. *Publ. Potsdam Obs.*, **7**, 127.
- (11) Baker, R. H., 1910. *Publ. Allegheny Obs.*, **1**, 65.
- (12) Herbison-Evans, D. & Cramer, N., 1969. *Proc. astr. Soc. Austr.*, **1**, 295.
- (13) Nelder, J. A. & Mead, R., 1965. *Computer Journal*, **7**, 308.
- (14) Shobbrook, R. R., Herbison-Evans, D., Johnston, I. D. & Lomb, N. R., 1969. *Mon. Not. R. astr. Soc.*, **145**, 131.
- (15) Twiss, R. Q., 1969. *Optica Acta.*, **16**, 423.
- (16) Chen, K-Y, & Rhein, W. J., 1969. *Publ. astr. Soc. Pacific*, **81**, 387.
- (17) Code, A. D., 1960. *Stellar Atmospheres*, p. 50, ed. J. L. Greenstein, University of Chicago Press.
- (18) Oke, J. B. & Schild, R. E., 1970. *Astrophys. J.*, **161**, 1015.
- (19) Davis, J. & Webb, R. J., 1970. *Astrophys. J.*, **159**, 551.
- (20) Johnson, H. L., Mitchell, R. I., Iriarte, B. & Wisniewski, W. Z., 1966. *Commun. lunar planet. Lab.*, **4**, 99.
- (21) Struve, O., 1930. *Astrophys. J.*, **72**, 1.
- (22) Petrie, R. M., 1948. *Publ. Dom. astrophys. Obs.*, **8**, 319.
- (23) Johnson, H. L., 1966. *A. Rev. Astr. Astrophys.*, **4**, 193.
- (24) Bradley, P. T. & Morton, D. C., 1969. *Astrophys. J.*, **156**, 687.
- (25) Van Citters, G. W. & Morton, D. C., 1970. *Astrophys. J.*, **161**, 695.
- (26) Labs, D. & Neckel, H., 1968. *Z. Astrophys.*, **69**, 1.
- (27) Jenkins, L. F., 1963. *Supplement to the General Catalogue of Trigonometric Stellar Parallaxes*, p. 10, Yale University Observatory.
- (28) Harris, D. L., Strand, K. AA. & Worley, C. E., 1963. *Basic Astronomical Data*, p. 287, ed. K. AA. Strand, University of Chicago Press.
- (29) Smak, J., 1967. *Acta Astron.*, **17**, 245.
- (30) Popper, D. M., 1967. *A. Rev. Astr. Astrophys.*, **5**, 85.
- (31) Morgan, W. W., Code, A. D. & Whitford, A. E., 1955. *Astrophys. J. Suppl.*, **2**, 41.
- (32) Lesh, J. R., 1969. *Astrophys. J. Suppl.*, **16**, 371.
- (33) Johnson, H. L. & Iriarte, B., 1958. *Lowell Obs. Bull.*, **4**, 47.
- (34) Leung, Kam-Ching, 1967. *Astrophys. J.*, **150**, 223.

AN ATTEMPT TO DETECT A CORONA AROUND
 β ORIONIS WITH AN INTENSITY INTERFEROMETER
USING LINEARLY POLARIZED LIGHT

R. Hanbury Brown, J. Davis and L. R. Allen

(Received 1974 February 28)

SUMMARY

Observations of the hot supergiant β Orionis have been made with the stellar intensity interferometer at Narrabri using linearly polarized light. The normalized correlation was measured at two baselines with light polarized parallel and perpendicular to the baseline and the results are used to derive two independent measures of the angular size of the star. No significant change of correlation or angular diameter with polarization was observed.

A theoretical analysis is given of the effects of electron scattering on measurements in linearly polarized light. Two cases are considered, scattering by electrons in the photosphere and scattering by electrons in an extended corona. The results are compared with the observations of β Orionis and are used to set an upper limit to the mass loss. It is suggested that with a more sensitive interferometer, using linear polarization, it might be possible to detect coronae and other circumstellar matter around some types of star.

I. INTRODUCTION

Observations of the ultraviolet spectra of some OB giants and supergiants (1) show that they are losing mass. It is to be expected that the scattering of light in the associated corona of free electrons would cause the apparent angular distribution of light across the star to depend upon the plane of polarization. In principle such an effect could be observed with a stellar interferometer using linearly polarized light. In view of the potential value of any technique which yields observational data on the coronae of stars we have used the stellar intensity interferometer at Narrabri Observatory to observe the hot supergiant β Ori (B8 Ia) in linearly polarized light. The present paper is an account of these measurements together with a brief theoretical discussion.

2. OBSERVATIONS OF β ORIONIS

2.1 *The observations*

The stellar interferometer at Narrabri Observatory has been described in detail in several previous publications (e.g. (2), (3)). For the purpose of the present experiment the optical system of the interferometer (2) was modified to incorporate two linear polarizers mounted in front of the phototubes. These polarizers were remotely controlled from the central control desk so that they could be rotated into either of two orthogonal planes, parallel or perpendicular to the baseline. Care was taken that in both positions the planes of polarization of the two polarizers were parallel. Measurements with a spectrophotometer showed that at the wavelength at which the observations were made (4430 Å) the polarizers transmitted 40 per cent of an incident unpolarized beam.

β Ori was observed during 1971 November and December with baselines of 9.95 m and 19.68 m. The first baseline (9.95 m) corresponds to $x \simeq 0.9$, $\Gamma_\lambda^2(d) \simeq 0.8$ (see equation (3)); the second baseline (19.68 m) corresponds to $x \simeq 1.7$, $\Gamma_\lambda^2(d) \simeq 0.5$, a point roughly half-way down the curve of correlation versus baseline where one would expect (Fig. 1) any change of correlation with polarization to be most easily observed. The correlation at these two baselines was measured following the standard procedure described in (2) except that the polarizers were rotated through 90° at intervals of 1000s. At each baseline the observations in the two planes of polarization were therefore closely interleaved in time and, following the standard procedure, observations at the two baselines were also interleaved.

The measurements were corrected for zero-drift of the correlator and normalized by the appropriate values of light flux and correlator gain as described in (3). The final values of normalized correlation for polarization parallel $\overline{c_N(d)}_{\parallel}$ and perpendicular $\overline{c_N(d)}_{\perp}$ to the baseline are shown in Table I together with their rms uncertainties. They are expressed on an arbitrary scale which is not necessarily the same for both polarizations because the scale of normalized correlation is a function of both the shape and width of the overall optical bandpass and these parameters are likely to differ by a small but significant amount for the two polarizations.

TABLE I
Observations of β Orionis in two planes of polarization

Baseline m	Exposure h	Normalized correlation	
		Parallel* $\overline{c_N(d)}_{\parallel} \pm \sigma \dagger$ arbitrary units	Perpendicular* $\overline{c_N(d)}_{\perp} \pm \sigma \dagger$ arbitrary units
9.95	19	10.36 ± 0.23	11.02 ± 0.22
19.68	59	6.21 ± 0.14	6.42 ± 0.14

* Orientation of plane of polarization relative to baseline.

† σ represents the rms uncertainty.

2.2 Analysis of the observations

The values of $\overline{c_N(d)}$ for the two polarizations in Table I cannot be compared directly because of the scale difference; we have therefore treated them as two independent measurements of the star. For each polarization a theoretical curve was fitted to the measured values of normalized correlation following the procedure described in (3). The resulting values of C the normalized correlation at zero-baseline with the effects of partial resolution removed ($\Delta_\lambda = 1$), Δ_λ the partial resolution factor, and θ_{UD} the angular diameter of the equivalent uniform disc are shown in Table II. The normalized correlations at the two baselines $\overline{c_N(d)}/\Delta_\lambda C$ are also shown, and, so that the results for the two polarizations can be compared directly, they have been expressed in a dimensionless form as fractions of their respective zero-baseline correlations $\Delta_\lambda C_{\parallel}$ and $\Delta_\lambda C_{\perp}$; the associated rms uncertainties represent the combined uncertainties in $\Delta_\lambda C$ and $\overline{c_N(d)}$.

3. THEORY

3.1 Introduction

We will now give a brief theoretical discussion of the response of an intensity interferometer to the light from a star in which there is a significant component of

TABLE II
Analysis of results on β Orionis

	Polarization relative to baseline	
	parallel (\parallel)	perpendicular (\perp)
C (arbitrary units)	12.45 ± 0.38	13.37 ± 0.37
θ_{UD} (10^{-3} sec of arc)	2.38 ± 0.07	2.44 ± 0.06
Δ_λ	0.982	0.981
$\frac{c_N(9.95m)}{\Delta_\lambda C}$	0.847 ± 0.032	0.840 ± 0.029
$\frac{c_N(19.68m)}{\Delta_\lambda C}$	0.508 ± 0.019	0.489 ± 0.017

C is the zero-baseline correlation with no partial resolution ($\Delta_\lambda = 1$); θ_{UD} is the angular diameter of the equivalent uniform disc; Δ_λ is the partial resolution factor; $c_N(9.95m)/\Delta_\lambda C$ and $c_N(19.68m)/\Delta_\lambda C$ are the normalized correlations at the two baselines expressed as fractions of the zero-baseline correlation ($\Delta_\lambda C$). All the results are for $\lambda = 4430 \text{ \AA}$.

linear polarization due to electron scattering. Since electron scattering is to be expected in the photosphere of a star as well as in an extended corona, we will estimate the effects of both sources separately.

3.2 The response of an intensity interferometer to unpolarized light from the photosphere

An intensity interferometer measures the correlation between the fluctuations of light intensity at two points separated by a baseline. It has been shown (4) that the time-average of the normalized correlation $c_N(d)$ varies with baseline d as,

$$\overline{c_N(d)} \propto \Delta_\lambda \Gamma_\lambda^2(d) \tag{1}$$

where Δ_λ is the partial coherence factor and $\Gamma_\lambda^2(d)$ is the correlation factor.

The partial coherence factor Δ_λ takes account of the finite size of the light-collectors which may be so large that they partially resolve the star and reduce the correlation. The correlation factor $\Gamma_\lambda^2(d)$ takes account of the variation of correlation with baseline and, in the case where the aperture of the light-collectors is small ($\Delta_\lambda = 1$) and the brightness distribution across the source is circularly symmetrical, it can be shown that it is proportional to the square of the modulus of the Hankel transform of the radial angular distribution of brightness across the source.

Consider a star with a circularly symmetrical disc limb darkened according to the conventional linear law,

$$I(\mu)/I(1) = 1 - u_\lambda(1 - \mu) \tag{2}$$

where μ is the cosine of the angle between the normal at a point on the stellar surface and the line of sight, $I(\mu)$ is the intensity of the light received from the point and u_λ is the limb darkening coefficient. The response of an intensity interferometer to this star, assuming no partial resolution ($\Delta_\lambda = 1$) is given (5) by,

$$\Gamma_\lambda^2(d) = (2/(1 - u_\lambda/3))^2 [(1 - u_\lambda) J_1(x)/x + u_\lambda(\pi/2)^{1/2} J_{3/2}(x)/x^{3/2}]^2 \tag{3}$$

where $x = \pi \theta_{LD} d/\lambda_0$ and θ_{LD} is the true angular diameter of the star.

If curves of $\Gamma_\lambda^2(d)$ are computed from equation (3) for different values of u_λ and for a fixed value of θ_{LD} , it is found (5) that out to the first minimum they are practically indistinguishable in shape but vary in width along the x axis. It follows that in practice u_λ cannot be found from measurements of correlation versus

baseline and for this reason the results of measurements with an intensity interferometer are expressed in terms of θ_{UD} the angular diameter of the *equivalent uniform disc* which is found by fitting the measures of correlation to equation (3) with $u_\lambda = 0$. The true angular diameter θ_{LD} can then be found from θ_{UD} for any assumed value of u_λ using the relation given in (5),

$$\theta_{LD}/\theta_{UD} = [(1 - u_\lambda/3)/(1 - 7u_\lambda/15)]^{1/2}. \quad (4)$$

3.3 *The response of an intensity interferometer to linearly polarized light from the photosphere*

Let us assume that the apparent radial distribution of brightness across a star depends upon the plane of polarization and that the flux emerging from the photosphere in two orthogonal planes is given by

$$\begin{aligned} I_\lambda(\mu, r)/I_\lambda(1, r) &= 1 - u_\lambda(r)(1 - \mu) \\ I_\lambda(\mu, t)/I_\lambda(1, t) &= 1 - u_\lambda(t)(1 - \mu) \end{aligned} \quad (5)$$

where the suffixes r and t refer to light polarized radially and tangentially relative to the centre of the circular disc. The radial distribution of the total flux is then given by an equation of the form of equation (2) where

$$u_\lambda = (u_\lambda(r) + u_\lambda(t))/2 \quad (6)$$

and u_λ represents the limb-darkening coefficient for the total flux.

If we now view this star with an interferometer which accepts only components of the light polarized either parallel or perpendicular to the baseline, as seen from the star, then it follows from an analysis by Sams (6) that equation (3) is modified to

$$\begin{aligned} \Gamma_\lambda^2(d, \parallel) &= (2/(1 - u_\lambda/3))^2 \\ &\times \{[(1 - u_\lambda) J_1(x)/x + u_\lambda(\pi/2)^{1/2} J_{3/2}(x)/x^{3/2} - \{(u_\lambda(r) - u_\lambda(t))/2\} \\ &\times \{J_1(x)/x + (\pi/2)^{1/2} J_{3/2}(x)/x^{3/2} + (2/x^2)(J_0(x) - \sin x/x)\}]^2 \} \end{aligned} \quad (7)$$

where $\Gamma_\lambda^2(d, \parallel)$ is the correlation factor for light polarized parallel to the baseline and it is assumed that there is no partial resolution ($\Delta_\lambda = 1$). The corresponding expression for $\Gamma_\lambda^2(d, \perp)$ with light polarized perpendicular to the baseline is given by interchanging r and t . From equation (7) it can be shown (6) that the angular sizes of the equivalent uniform discs measured in the two polarizations are given by

$$\begin{aligned} \theta_{LD}/\theta_{UD}\parallel &= [(1 - u_\lambda/3)/\{1 - \frac{7}{15}(\frac{3}{4}u_\lambda(r) + \frac{1}{4}u_\lambda(t))\}]^{1/2} \\ \theta_{LD}/\theta_{UD}\perp &= [(1 - u_\lambda/3)/\{1 - \frac{7}{15}(\frac{3}{4}u_\lambda(t) + \frac{1}{4}u_\lambda(r))\}]^{1/2} \end{aligned} \quad (8)$$

where $\theta_{UD}\parallel$, $\theta_{UD}\perp$ are the angular diameters of the equivalent uniform discs measured with light polarized parallel and perpendicular to the baseline respectively and θ_{LD} is the true angular diameter of the star.

3.4 *The effects of scattering by free electrons in the photosphere*

Chandrasekhar & Breen (7) have calculated the polarization of the total flux emerging from a star for the case of pure Thomson scattering by free electrons in a plane parallel atmosphere. They have shown that the flux is polarized and that the percentage polarization increases towards the limb where it reaches about 12 per cent. They give the radial distribution of flux in two polarizations and, for our

purposes, we may approximate their results by the limb-darkening coefficients $u_\lambda(r) = 0.69$ and $u_\lambda(t) = 0.62$. Substituting these values in equations (8),

$$\theta_{UD\parallel} / \theta_{UD\perp} = 0.998. \quad (9)$$

Thus the apparent angular size of the star, measured by an intensity interferometer, should be 1.2 per cent smaller in light polarized parallel to the baseline than perpendicular to the baseline. If we measure the correlation at a baseline where $\Gamma_\lambda^2(d) \simeq 0.5$, that is to say at a point about half-way down the curve of correlation versus baseline, the corresponding change of correlation with polarization is approximately 1 per cent of zero-baseline correlation.

Since this result has been derived for the case of pure electron scattering and no absorption, it is to be expected that it overestimates the polarization of the light from an actual star. For example, Harrington (8) has calculated the polarization for monochromatic radiation emerging from a plane-parallel atmosphere in which the ratio of absorption to total extinction is 0.5. Taking $T_e = 11\,000$ K for β Ori and $\lambda = 4430$ Å the polarization at the limb of the star reaches only about one-quarter of the value given by Chandrasekhar's model. The corresponding change in apparent angular size of the star is reduced from 1.2 per cent to about 0.1 per cent and the change in correlation observed when $\Gamma_\lambda^2(d) \simeq 0.5$ is reduced to about 0.1 per cent of the zero-baseline correlation.

3.5 The effects of scattering by free electrons in a corona

We have considered the effects of scattering in an extended corona of free electrons surrounding a star. For simplicity we took this corona to be spherically symmetrical with an electron density proportional to r^{-2} , where r is the distance to the centre of the star. We also assumed that the optical depth of the corona $\tau < 1$, so that for an approximate theory it was not necessary to consider multiple scattering.

The response of an intensity interferometer was found as follows. The response to the direct light from the stellar disc was calculated from equation (3) assuming the disc to be uniformly bright and the light to be unpolarized. The response to the corona was found by calculating the angular distribution over the corona of the total intensity of the scattered light received in each of two orthogonal planes, parallel and perpendicular to the baseline. For each of these distributions the Fourier transform of the equivalent strip distribution parallel to the baseline was then computed. The final response of the interferometer to the star plus corona was found by combining the responses to the disc and the corona in the appropriate way. The results, calculated by Sams, are shown in Fig. 1.

Curves 2 and 3 in Fig. 1 show the correlation factors $\Gamma_\lambda^2(d, \parallel)$ and $\Gamma_\lambda^2(d, \perp)$ for observations in linearly polarized light with the electric vector parallel and perpendicular to the baseline respectively. Curve 1 shows $\Gamma_\lambda^2(d)$ for the disc of the star alone. The curves were calculated for a corona with an optical depth $\tau = 0.35$ where

$$\tau = \sigma_0 \int_{r_0}^{\infty} N_e(r) dr = \sigma_0 r_0 N_e(r_0) \quad (10)$$

and σ_0 is the scattering cross-section of an electron, r is the distance from the centre of the star, r_0 is the radius of the star and $N_e(r)$ is the electron density at a radial distance r .

Fig. 1 shows that, for $\tau = 0.35$, the change in correlation with polarization reaches a maximum of about 6 per cent of zero-baseline correlation at a point

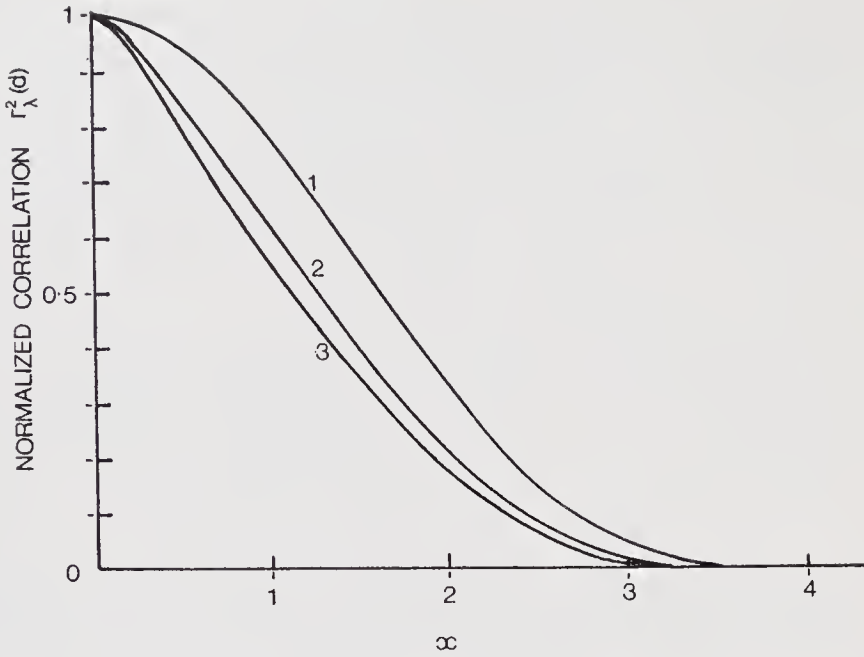


FIG. 1. The variation of correlation with baseline. (1) $\Gamma_{\lambda}^2(d)$ for a uniform disc in unpolarized light. (2) $\Gamma_{\lambda}^2(d, \parallel)$ for a disc plus corona ($\tau = 0.35$) with light polarized parallel to the baseline. (3) $\Gamma_{\lambda}^2(d, \perp)$ for a disc plus corona ($\tau = 0.35$) with light polarized perpendicular to the baseline. The abscissa $x = \pi\theta d/\lambda$, where θ is the angular diameter of the star, d is the baseline and λ the wavelength.

roughly half-way down the curve where $\Gamma_{\lambda}^2(d) \simeq 0.5$; this corresponds to a change in apparent angular diameter with polarization of about 8 per cent. For values of $\tau < 1$ it can be shown that these changes are directly proportional to $\tau/(1 + \tau)$.

4. DISCUSSION

4.1 Interpretation of the results on β Orionis

The results in Table II show that the observed changes in correlation with polarization at baselines of 9.95 m and 19.68 m were:

$$\left[\frac{c_N(9.95 \text{ m})_{\parallel}}{\Delta_{\lambda} C_{\parallel}} - \frac{c_N(9.95 \text{ m})_{\perp}}{\Delta_{\lambda} C_{\perp}} \right] \times 100 = 0.8 \pm 4 \text{ per cent} \quad (11)$$

$$\left[\frac{c_N(19.68 \text{ m})_{\parallel}}{\Delta_{\lambda} C_{\parallel}} - \frac{c_N(19.68 \text{ m})_{\perp}}{\Delta_{\lambda} C_{\perp}} \right] \times 100 = 1.85 \pm 2.5 \text{ per cent} \quad (12)$$

and the observed changes of apparent angular diameter with polarization were,

$$\left[\frac{(\theta_{UD\perp} - \theta_{UD\parallel})}{(\theta_{UD\perp}/2 + \theta_{UD\parallel}/2)} \right] \times 100 = 2.5 \pm 4 \text{ per cent} \quad (13)$$

Thus no significant change of correlation with plane of polarization was observed at either baseline. At a baseline of 19.68 m we will take the upper limit set by the observations to be 4.4 per cent (1σ) of zero-baseline correlation. No significant change in the apparent angular size was observed, the upper limit being 6.5 per cent (1σ).

In Section 3.4 we estimated that any changes in correlation with plane of polarization due to electron scattering in the photosphere of β Ori would be about 0.1 per cent of zero-baseline correlation. The results given above are consistent with this estimate.

In Section 3.5 we estimated that a simple corona of free electrons with a density proportional to r^{-2} and an optical depth of $\tau = 0.35$ would produce, at the optimum baseline, a change of correlation with plane of polarization of about 6 per cent of the zero-baseline correlation. Since it can be shown that for $\tau < 1$ this effect is directly proportional to $\tau/(1 + \tau)$ it follows that the observed limit of 4.4 per cent implies that for β Ori $\tau < 0.25$. Substituting in equation (10), this limit on τ corresponds approximately to $r_0 N_e(r_0) < 4 \times 10^{23} \text{ cm}^{-2}$ and taking $r_0 = 30 R_\odot$, the electron density at the base of the corona $N_e(r_0) < 2 \times 10^{11} \text{ cm}^{-3}$. This limit is consistent with the estimate of $N_e(r_0) \simeq 5 \times 10^9 \text{ cm}^{-3}$ made by Morton (1) for three hot supergiants.

If we assume that β Ori has a corona of fully ionized material, with normal solar abundance, streaming radially outwards with a constant velocity, then

$$\tau \simeq 2 \times 10^8 (dM/dt) / Vr_0 \quad (14)$$

where dM/dt is the mass loss in $M_\odot \text{ yr}^{-1}$, V is the velocity in km s^{-1} , r_0 is the radius of the star in solar units. If we put $V \simeq 500 \text{ km s}^{-1}$ as the escape velocity from the star and take $\tau < 0.25$, then from equation (14) the mass loss from β Ori is $dM/dt < 2 \times 10^{-5} M_\odot \text{ yr}^{-1}$. Again this result is consistent with the estimate of $10^{-6} M_\odot \text{ yr}^{-1}$ inferred from observations of the spectra of some OB giants and supergiants (1).

4.2 Some possibilities of the technique

Our observations of β Ori failed to detect the effects of electron scattering and the analysis presented in Sections 3.4 and 3.5 suggests that to obtain positive results it would have been necessary to improve the sensitivity of the measurements by a factor in the range of 10 to 100. Some improvement might have been gained by longer exposures or by a more refined technique, alternatively the effects of electron scattering might have been detected more easily on some other star; however, for a variety of practical reasons, this is not an attractive programme with the existing interferometer at Narrabri and further work must await the construction of a more sensitive instrument.

It is interesting to enquire what might be expected from a more sensitive instrument. Taking first the main sequence stars, the density at the base of the solar corona is $N_e(r_0) \simeq 10^8 \text{ cm}^{-3}$ which for our simple model of a corona corresponds to the extremely small optical depth $\tau \simeq 5 \times 10^{-6}$. However, the coronal density of other main sequence stars may be higher; for example, De Loore (9) estimates the coronal density of main sequence F stars to be 100 times greater than that of the Sun, corresponding to $\tau \simeq 5 \times 10^{-4}$. Even so, this value of τ is well below the limit reached in the present observations and of any interferometer which can be envisaged; furthermore, it follows from Section 3.4 that, for hot stars, changes of correlation produced by a corona with $\tau < 5 \times 10^{-4}$ would be less than those produced by electron scattering in the photosphere. We may therefore conclude that it is probably not practicable to detect the coronae of main sequence stars by this technique.

There remains however the interesting possibility, which prompted the present work, that it might prove possible to detect more dense coronae. From equation (14) the upper limit of $\tau < 0.25$, established for β Ori, corresponds approximately to $(dM/dt) / Vr_0 < 10^{-9}$ and in Section 4.1 we interpreted this as setting an upper limit to the mass loss of $dM/dt < 2 \times 10^{-5} M_\odot \text{ yr}^{-1}$. This limit is a factor of 20

greater than the mass loss suggested (1) for hot supergiants; however, with a more sensitive instrument it should be possible to lower this limit, possibly by the necessary factor of 20. As we have already noted, this would not necessarily yield the coronal density of a hot supergiant because it might prove impossible to distinguish the effects of electron scattering in the corona from those in the photosphere. However, a more sensitive instrument would certainly allow observations of a variety of stars and might make it possible to verify the high rates of mass loss which have been attributed to some types of star. For example, mass losses which give values of $(dM/dt)/Vr_0 \sim 10^{-10}$, have been derived for some late giants (10) and supergiants (11) and, if the level of ionization is sufficient, the coronae of these stars might be detected. Finally, we have considered here only a crude model of a circularly symmetrical corona but it seems likely that some stars with extended atmospheres, circumstellar shells, rings of material, etc., would produce larger effects than we have estimated and that their structure might be investigated profitably with an interferometer using polarized light.

ACKNOWLEDGMENTS

The programme of the interferometer was supported by the Australian Research Grants Committee, the Research Grants Committee of the University of Sydney and the Science Foundation for Physics within the University of Sydney. We thank Professor Messel for his support and Dr I. D. Johnston and Mr R. T. Kery for their assistance with the observations. We also thank Mr D. Sams for allowing us to use some of his results before publication.

Chatterton Astronomy Department, School of Physics, University of Sydney, NSW 2006, Australia

REFERENCES

- (1) Morton, D. C., 1967. *Astrophys. J.*, **150**, 535.
- (2) Hanbury Brown, R., Davis, J. & Allen, L. R., 1967. *Mon. Not. R. astr. Soc.*, **137**, 375.
- (3) Hanbury Brown, R., Davis, J., Allen, L. R. & Rome, J. M., 1967. *Mon. Not. R. astr. Soc.*, **137**, 393.
- (4) Hanbury Brown, R. & Twiss, R. Q., 1957. *Proc. R. Soc. London, Ser. A*, **243**, 291.
- (5) Hanbury Brown, R., Davis, J., Lake, R. J. W. & Thompson, R. J., 1974. *Mon. Not. R. astr. Soc.*, **167**, 475.
- (6) Sams, D., 1974. *Mon. Not. R. astr. Soc.*, (accepted for publication)
- (7) Chandrasekhar, S. & Breen, F. H., 1947. *Astrophys. J.*, **105**, 435.
- (8) Harrington, J. P., 1970. *Astrophys. Space Sci.*, **8**, 227.
- (9) De Loore, C., 1970. *Astrophys. Space Sci.*, **6**, 60.
- (10) Deutsch, A. J., 1960. *Stars and stellar systems*, Vol. VI, p. 543, ed. J. L. Greenstein, University of Chicago Press.
- (11) Weymann, R., 1962. *Astrophys. J.*, **136**, 844.

EVIDENCE FOR THE DETECTION OF GAMMA RAYS FROM
CENTAURUS A AT $E_\gamma \geq 3 \times 10^{11}$ eV

J. E. GRINDLAY AND H. F. HELMKEN

Center for Astrophysics, Harvard College Observatory and Smithsonian Astrophysical Observatory

AND

R. HANBURY BROWN, J. DAVIS, AND L. R. ALLEN

School of Physics, University of Sydney, Australia

Received 1974 November 27

ABSTRACT

Results of extended observations of the active galaxy NGC 5128 (Cen A) at energies $> 10^{11}$ eV are presented. Data were recorded from three observing periods (1972-1974) in Australia. The atmospheric Cerenkov technique was used, together with partial cosmic-ray rejection, to search for γ -ray-initiated extensive air showers from the direction of Cen A. A 4.5σ (time-averaged) excess over background was detected. Some implications of this probable γ -ray flux are discussed.

Subject headings: cosmic rays—galactic nuclei—gamma rays

I. INTRODUCTION

Centaurus A (NGC 5128), the closest active galaxy, is particularly well suited for observational study. The linear and symmetrical alignment of the extended ($\sim 5^\circ$) and inner ($\sim 4'$) radio lobes have long been recognized as indicative of violent activity in the central galaxy. The recent detection of X-rays from Cen A (Bowyer *et al.* 1970; Kellogg *et al.* 1971; Lampton *et al.* 1972) provides direct evidence that high-energy processes are occurring there. To extend our knowledge of these processes to the highest possible energies, we carried out a search for very high-energy ($\geq 3 \times 10^{11}$ eV) γ -rays from Cen A. The energy range above 10^{11} eV can be studied by ground-based observations of Cerenkov light produced by extensive air showers (EAS) (e.g., Jelley 1967).

II. OBSERVATIONS

We have described (Grindlay *et al.* 1973) our first observations of southern sky objects as possible high-energy γ -ray sources. Employing the atmospheric Cerenkov technique, we conducted these observations in 1972 April-July with an optical intensity interferometer (operated in Narrabri, NSW, by the University of Sydney) converted to detect Cerenkov light from cosmic-ray EAS. Since Cen A yielded the most promising positive effect ($> 3 \sigma$) of 11 objects in the 1972 survey, we continued observing it with highest priority in our 1973 April-June and 1974 March-April observing programs.¹ A double-beam technique (Grindlay 1971) was employed, whereby the two optical reflectors were positioned on a 120-m baseline and pointed so that EAS were initially detected at their electron maxima and simultaneously examined for Cerenkov emission from their penetrating muon cores. Detection of the muon core in ~ 50 percent of the observed EAS rate ($\sim 1 \text{ s}^{-1}$) permits rejection of this fraction of the cosmic-ray back-

ground. A complete description of the technique and apparatus used is given by Grindlay *et al.* (1975).

The detection-system parameters at the zenith are estimated to be as follows: effective solid angle $\Omega \approx 5 \times 10^{-5}$ sr (or "beam" FWHM $\sim 0.45^\circ$), effective collection area $A_c \approx 1.6 \times 10^8 \text{ cm}^2$, and γ -ray energy threshold $E_0 \approx 2 \times 10^{11}$ eV. At the zenith angles $\sim 35^\circ \pm 10^\circ$ for our data, A_c and E_0 were increased by a factor ~ 1.5 .

Several improvements were made to the apparatus after the 1972 observations. The cosmic-ray-rejection efficiency was increased by installing off-axis rejection photomultipliers on both reflectors instead of on only one. Also, both rejection tubes were provided with ultraviolet-transmitting, visible-blocking glass filters (Schott BG-24) to reduce night sky background and improve the detection of the ultraviolet-rich muon Cerenkov pulses. A 26-channel pulse-height analyzer (PHA) measured the sum of the two coincident Cerenkov pulses from the EAS maximum; this covered a range of 20-1 in pulse height and thus in the primary energy. Finally, an expanded data-recording system, including real-time digital recording of all data, was used.

Observations of Cen A were restricted to nights of uniformly high atmospheric transparency in order to obtain reliable statistical comparisons between the EAS rates from Cen A and those from comparison directions. Uniform sky conditions were ensured by accepting an observation only if the EAS rates from the two comparison areas were within 3σ of each other and if a χ^2 test of the distribution of fluctuations each minute of all the EAS rates were random about constant mean values with probability $P(> \chi^2) > 1$ percent. Fewer than 5 percent of all the data recorded were rejected by these criteria. As in our 1972 experiments, the neighboring sky "comparison areas" had the same declination as Cen A but were displaced 10 m in right ascension on either side of Cen A, so that they could be tracked over the identical azimuth and elevation ranges. The com-

¹A complete description of our (other) observations is given in Grindlay *et al.* (1975).

parison areas were also chosen to have sky brightness identical to that of Cen A, and chart recordings of the phototube pulse rates were constant on and off source. When observing Cen A, the beam ($\sim 0.45^\circ$) was centered on the nucleus (Wade *et al.* 1971) of the optical galaxy ($\alpha_{1950} = 13^{\text{h}}22^{\text{m}}31.6^{\text{s}}$, $\delta_{1950} = -42^{\circ}45'30''.0$) and did not include the extended radio lobes. The two comparison regions (off source) were tracked for a total of 15 min, bracketing a period of 15 min on Cen A (on source) to complete a cycle. Unfortunately, the weather conditions in 1973 and 1974 were worse than in 1972. Consequently, although a total of 84 cycles was recorded in 1972, only 55 were measured in 1973 and 65 in 1974.

III. RESULTS

Table 1 lists our 1972 Cen A results (Grindlay *et al.* 1973) as well as those from 1973 and 1974. Total counts both on-source and off-source (sum of two comparison areas) are given, together with the exposure times, the corresponding ON minus OFF rates, and the number of standard deviation σ for the total number of EAS detected and also for the total number of EAS not rejected ("gamma events").

The data show a $\sim 4.5\sigma$ excess of time-averaged, nonrejected gamma events from the direction of Cen A. The sigma values in table 1 were computed assuming that Poisson statistics describe the EAS detection rate both on and off the source. This assumption was checked experimentally by computing the standard deviations of the three EAS detection rates (nonrejected gamma events, rejected EAS, and total detected) each minute for both of the two off-source comparison areas (separately and combined) and for the on-source data. These observed standard deviations were then divided by their corresponding Poisson values, and the distributions of resulting ratios examined. The means of the distributions were all within 3 percent of unity, with standard deviations of about 4 percent. Thus, our data seem to be well described by Poisson statistics.

As an additional check on the statistics of the Cen A results, we have plotted in figure 1 the histograms of all the numbers of standard deviations observed for the ON minus OFF rates for both total EAS and gamma events. A true source should displace the normal Gaussian distribution of detected deviations (d) from a zero mean to a positive value. Each σ deviation is the result obtained in one cycle of 15 min on source and 15

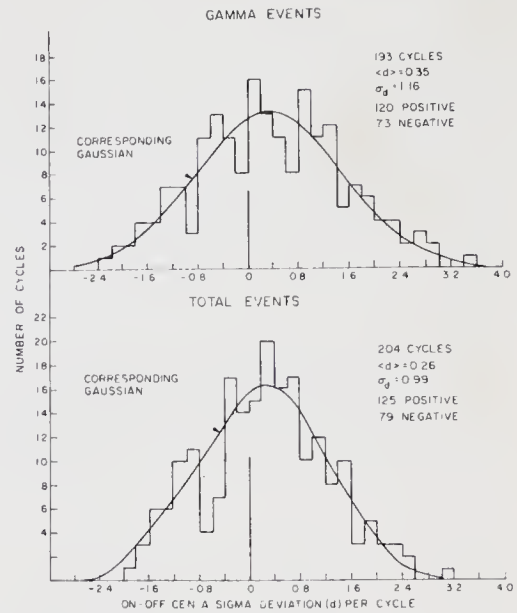


FIG. 1.—Distributions of observed σ for each observation cycle both on and off Cen A. All data (1972–1974) are included. The mean number of standard deviations (per cycle) and the standard deviations of the histograms are shown. The corresponding Gaussian curves fit the histograms with $\chi^2 \sim 0.9$ per degree of freedom.

min off source. A few of the cycles were only 14 min both on and off source. Both distributions are well described by the Gaussians fitted to them. The σ distribution of the gamma events has a mean of $\pm 0.35\sigma$ cycle $^{-1}$ and a standard deviation of 1.16σ cycle $^{-1}$. A fit to the corresponding Gaussian over the 17 bins with ≥ 5 cycles per bin yields $\chi^2 = 12.1$, or 0.86 per degree of freedom [$P(>\chi^2) \approx 60\%$]. The distribution is also consistent with the 4.6σ total (gamma events) effect in table 1, since $0.35\sigma(193)^{0.5} \approx 4.8\sigma$. Similarly, the distribution of total events in figure 1 has a mean of $\pm 0.26\sigma$ cycle $^{-1}$, a standard deviation of 0.99σ cycle $^{-1}$, and $\chi^2 = 0.93$ per degree of freedom [$P(>\chi^2) \approx 55\%$], for a fit to the on-off corresponding Gaussian. Again, the pre-

TABLE 1
SUMMARY OF CENTAURUS A RESULTS

YEAR	TOTAL EAS					NONREJECTED EAS				
	On	Off	Time (min)	On minus Off Rate (min $^{-1}$)	No. of σ	On	Off	Time (min)	On minus Off Rate (min $^{-1}$)	No. of σ
1972...	76660	75601	1289	0.82 ± 0.30	2.7	56471	55167	1240	1.05 ± 0.27	3.9
1973...	35773	35726	782	0.06 ± 0.34	0.2	15463	15297	662	0.25 ± 0.26	1.0
1974...	64759	63757	975	1.03 ± 0.37	2.8	39853	39139	975	0.73 ± 0.29	2.5
Sum	177192	175084	3046	0.69 ± 0.19	3.6	111787	109603	2877	0.76 ± 0.16	4.6
Mean of rates weighted by σ^{-2}				0.63 ± 0.19	3.3				0.66 ± 0.16	4.2

dicted total effect is $\sim 3.7 \sigma$, as compared with 3.6σ in table 1.

The results in table 1 suggest that the 1973 ON minus OFF source rates are a $\sim 2 \sigma$ negative fluctuation from the mean of the 1972 and 1974 data. Although this does not necessarily require source variability, we shall cite below independent evidence for corresponding changes in the Cen A microwave source.

Our results in table 1 are thus consistent with having detected at the $> 4 \sigma$ confidence level a flux of $F_\gamma \sim 0.66 \pm 0.16$ gamma events min^{-1} , or given the detector parameters,

$$F_\gamma(\geq 300 \text{ GeV}) \simeq (4.4 \pm 1) \times 10^{-11} \text{ photons cm}^{-2} \text{ s}^{-1} \quad (1)$$

averaged over the 3 years of observations.

The Cen A data in 1973 and 1974 were recorded with a 26-channel PHA system. We have thus attempted to

investigate the spectral distribution in the range ~ 300 – 3000 GeV of the apparent flux given in equation (1) by combining the pulse-height channels in three groups. Each group has a gain increase by an additional factor ~ 2 above the detector threshold. In figure 2, we have plotted the pulse-height spectrum detected off source for 1285 min of 1973 + 1974 Cen A PHA data. Some representative points of the individual PHA channel counts above threshold are plotted, and they follow closely a straight-line power law ($\alpha = -2.67$). This close agreement in slope with the expected cosmic-ray spectrum confirms the linear relationship over this range between detected Cerenkov pulse heights and cosmic-ray primary energy E_0 . We have therefore fixed the energy scale on the x-axis in figure 2 by using the known cosmic-ray flux and the previously mentioned Narrabri detector parameters. The flatter spectrum with $\alpha = -1.7$ shown in figure 2 (dashed line) is a theoretical γ -ray spectrum (Grindlay 1975) for a Compton-syn-

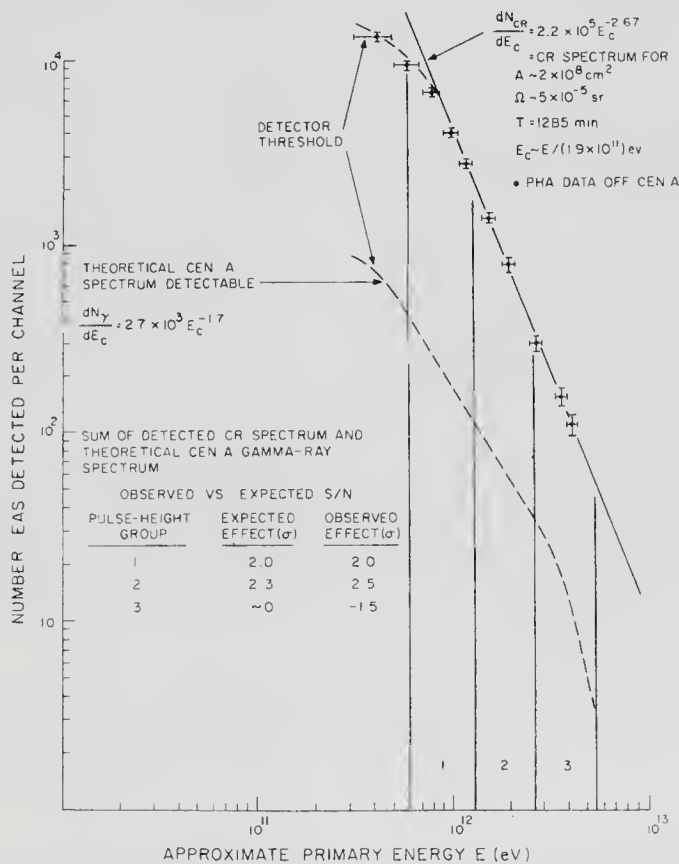


FIG. 2.—Observed off-source pulse-height spectrum of gamma events plotted on the corresponding cosmic-ray primary energy scale. All the PHA data (about 70 percent of the 1973 and 1974 data only) are included. The steep solid-line spectrum is the known cosmic-ray flux for the Narrabri detector parameters given. A Compton-synchrotron model spectrum for the γ -ray flux that could be detected from Cen A is also shown (dashed line) for comparison with the cosmic-ray spectrum. The predicted on-source spectrum is then the sum of the dashed- and solid-line spectra. The resulting predicted signal-to-noise ratios for the pulse-height groups (1–3) are given and compared with the observed values.

chrotron model of the Cen A nucleus. In plotting this curve, we have taken into account the difference (approximately a factor of 2) between the primary energies of γ -ray- and cosmic-ray-initiated EAS yielding the same detected Cerenkov pulse height. The expected total on-source spectrum is the sum of the predicted γ -ray and the observed cosmic-ray spectra. The statistical significance of the difference in the number of counts (expressed in σ) between this combined spectrum and the detected off-source spectrum is listed in figure 2 for pulse-height groups 1-3. The number of sigma actually observed in the three groups is also given. The approximate agreement suggests that the observed Cen A flux is consistent with a flat source spectrum ($\alpha = -1.7$) with a high-energy break at $\sim 10^{12}$ eV, as assumed in the model.

IV. DISCUSSION

The detection of the high-energy γ -ray flux from Cen A given by equation (1) is established at about the 4.5σ level. A relative-likelihood analysis (O'Mongain 1973) also gives a probability of $< 2 \times 10^{-5}$ (or $> 4.5\sigma$) that the total gamma-event excess in table 1 is not due to a γ -ray source.

Since the extended ($\sim 5^\circ$) radio lobes were well outside our beam, they can be excluded as the source. Indications of variability as well as theoretical considerations (Grindlay 1975) can also exclude the inner radio lobes from being the γ -ray source.

A model that assumes that the γ -ray flux originates in the compact nucleus of Cen A by inverse Compton scattering is in reasonable agreement with the observations, as shown in figure 2 and by Grindlay (1975). This model predicts that variations in the γ -ray flux would be associated with those in the microwave flux from the source. There is some evidence that the compact microwave source at the nucleus of Cen A is variable.

The source was discovered by Wade *et al.* (1971) from observations at 2695 and 8085 MHz by the National Radio Astronomy Observatory (NRAO) in 1970 July and 1971 May, between which times a limit of ~ 10 percent was put on its variability. The Stanford group observed the source at 10.7 GHz in 1973 June-August (Price and Stull 1973) and again in 1974 May (Stull 1974). The flux in 1974 was ~ 75 percent higher than that for the previous year. The authors caution that much of this increase may be due to calibration uncertainties at the low elevations required, although they find the difference between their two results and those of NRAO rather striking and they plan future monitoring. Further evidence for a compact source of millimeter radiation in the nucleus of Cen A, possibly variable on a ~ 1 -day time scale, has recently been presented by Kellermann (1974).

We have presented our results of ground-based γ -ray observations of Cen A, which suggest that this active galaxy is the first extragalactic source of very high-energy γ -rays to be detected. When combined with observations of Cen A at lower energies, the results can be used to determine the angular size, the energy content, and the magnetic fields in the source (see, e.g., Grindlay 1975), and should lead to significant progress in our understanding of the origin of radiation from compact sources in galaxies.

This work was supported by the NSF (grant GP 38783), the Smithsonian Institution, the Australian Research Grants Committee, the Research Grants Committee of the University of Sydney, and the Science Foundation for Physics within the University of Sydney. We thank Professor Messel for his support and Dr. T. C. Weekes, G. Gifford, S. Owens, and E. Horine for their assistance with the program.

REFERENCES

- Bowyer, C. S., Lampton, M., Mack, J., and De Mondonca, F. 1970, *A. J. (Letters)*, **161**, L1.
 Grindlay, J. E. 1971, *Smithsonian Ap. Obs. Spec. Rept.*, No. 334.
 ———. 1975, *A. J.*, **199** (in press).
 Grindlay, J. E., Hanbury Brown, R., Davis, J., and Allen, L. R. 1973, *Proc. 13th Int. Cosmic Ray Conf.* (Denver), **1**, 439.
 ———. 1975, submitted to *A. J.*
 Jelley, J. V. 1967, *Progress in Elementary Particle and Cosmic Ray Physics*, **9** (Amsterdam: North-Holland), p. 39.
 Kellermann, K. I. 1974, *A. J. (Letters)*, **194**, L135.
 Kellogg, E., Gursky, H., Leong, C., Schreier, E., Tananbaum, H., and Giacconi, R. 1971, *A. J. (Letters)*, **165**, L49.
 Lampton, M., Margon, B., Bowyer, S., Mahoney, W., and Anderson, K. 1972, *A. J. (Letters)*, **171**, L45.
 O'Mongain, E. 1973, *Nature*, **241**, 376.
 Price, K. M., and Stull, M. A. 1973, *Nature Phys. Sci.*, **245**, 85.
 Stull, M. A. 1974, private communication.
 Wade, C. M., Hjellming, R. M., Kellermann, K. I., and Wardle, J. F. C. 1971, *A. J. (Letters)*, **170**, L11.

L. R. ALLEN, R. HANBURY BROWN, AND J. DAVIS: School of Physics, University of Sydney, Sydney, Australia 2006
 J. E. GRINDLAY and H. F. HELMKEN: Center for Astrophysics, 60 Garden Street, Cambridge, MA 02138

RESULTS OF A SOUTHERN-HEMISPHERE SEARCH FOR
GAMMA-RAY SOURCES AT $E_\gamma \geq 3 \times 10^{11}$ eV

J. E. GRINDLAY AND H. F. HELMKEN

Center for Astrophysics, Harvard College Observatory and Smithsonian Astrophysical Observatory

AND

R. HANBURY BROWN, J. DAVIS, AND L. R. ALLEN

School of Physics, University of Sydney, Australia

Received 1975 March 11

ABSTRACT

The optical intensity interferometer operated by Sydney University at Narrabri, NSW, Australia, was converted in 1972 April to a sensitive detector of atmospheric Cerenkov light from extensive air showers (EAS) with $E_0 > 2 \times 10^{11}$ eV. Its two 7-m aperture optical reflectors were separated by 120 m and pointed by computer at the mean altitude for the maximum development of EAS from the direction of an object to be studied. Off-axis photomultipliers on the reflectors viewed the atmospheric Cerenkov light from the EAS muon cores, thus enabling rejection of ≥ 50 percent of EAS detected as being cosmic-ray-initiated. Possible ($\geq 3 \sigma$) sources were found in 1972 in the directions of Cen A (NGC 5128), the Vela Pulsar, and MP 1451, out of 11 candidate objects studied. The objects included pulsars, unusual X-ray sources, active galaxies, a supernova, and lower energy (~ 100 MeV) γ -ray sources such as the galactic center. Confirmation of the 1972 results was attempted in an improved series of observations in 1973 April–June and 1974 March–April. The Cen A result was confirmed and is reported elsewhere. Upper limits are given here for the other objects, together with evidence for a variable pulsed flux from the Vela Pulsar. Implications of the results are discussed.

Subject headings: cosmic rays — gamma rays — pulsars — X-ray sources

I. INTRODUCTION

At γ -ray energies, the sky is either unexplored or partially surveyed to fluxes of only $\sim 10^{-2}$ of the brightest known source. The most extensive coverage of the sky so far is given by the ~ 30 – 100 MeV observations of Fichtel *et al.* (1975) with the SAS-B satellite, in which several galactic sources were found. Above 10^{11} eV, γ -ray astronomy can be carried out by ground-based detection of the atmospheric Cerenkov light associated with the extensive air showers (EAS) initiated by primary γ -rays. A number of northern-sky objects have been observed by this technique (Weekes *et al.* 1972; Fazio *et al.* 1968; Grindlay 1972; Jennings *et al.* 1974; Chudakov *et al.* 1965), and a partial sky survey is now in progress. However, no observations had been made by use of the Cerenkov technique in the southern hemisphere. There are numerous candidate sources at energies $> 10^{11}$ eV in the southern sky—for example, the galactic center (detected at ~ 100 MeV), as well as unusual X-ray sources in which high-energy cosmic rays and γ -rays may be produced. Thus we began a program in 1972 to observe a number of these objects from Australia using an extension of the Cerenkov technique that had enabled detection of the Crab Pulsar (Grindlay 1972).

The Narrabri optical intensity interferometer (Hanbury Brown *et al.* 1967) has proved suitable for

ground-based γ -ray astronomy. Its two ~ 7 -m aperture optical reflectors can be used as a coincidence pair to detect atmospheric Cerenkov light produced in EAS, as has been shown by Hanbury Brown *et al.* (1969). These observations led, in part, to studies (Grindlay 1971) that showed the possibility of discriminating (partially) between EAS initiated by primary cosmic rays and those initiated by very-high-energy γ -rays. By this “double-beam” technique, the cosmic-ray background can be partially rejected and the sensitivity therefore increased in searches for EAS anisotropies due to high-energy γ -ray sources. In a search for γ -ray point sources, the use of two reflectors in two-fold coincidence and separated by a baseline gives additional discrimination against EAS initiated by primary cosmic rays by reducing the solid angle in which they can be detected, as compared with the use of two reflectors separately. The Narrabri reflectors are especially well suited for this in that they can track a suspected source while preserving the required pointing geometry.

A search for high-energy γ -rays from 11 objects in the southern hemisphere that showed evidence of high-energy processes was carried out with the reflectors of the Narrabri interferometer in the years 1972, 1973, and 1974. A preliminary account of the observations has been given by Grindlay *et al.* (1973, 1974a). We have already presented (Grindlay *et al.*

SEARCH FOR GAMMA-RAY SOURCES

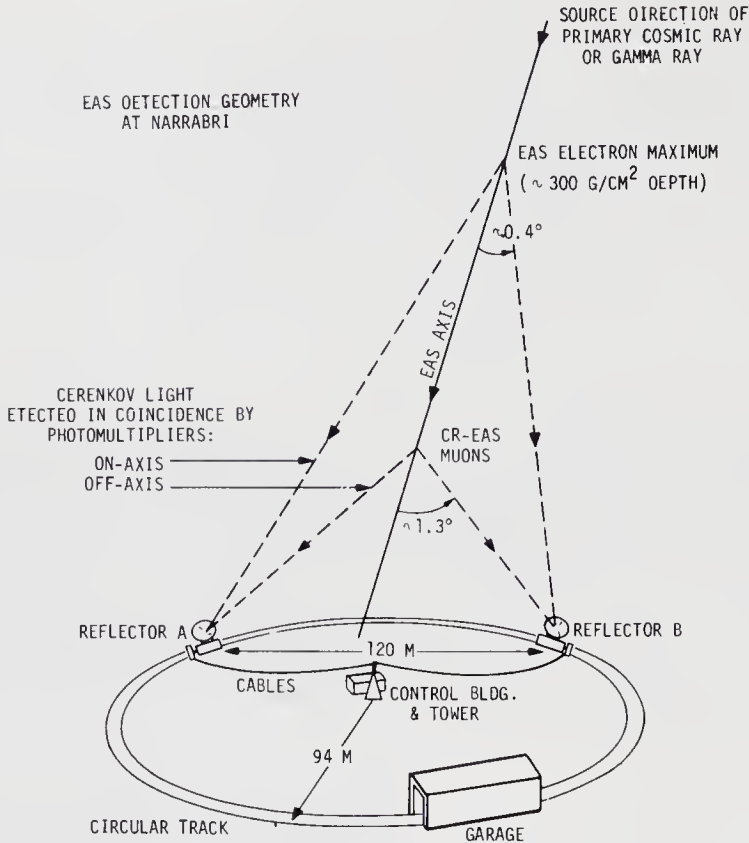


FIG. 1.—Schematic illustration of the double-beam detection of extensive air showers at Narrabri Observatory. A primary cosmic ray or γ -ray with $E_0 \geq 2 \times 10^{11}$ eV initiates an EAS, which reaches its maximum development at $\sim 300 \text{ g cm}^{-2}$ atmospheric depth ($\sim 9 \text{ km}$ altitude). The $\sim 6 \text{ ns}$ pulse of optical Cerenkov radiation from the shower electrons at the maximum is detected in coincidence by reflectors A and B. The reflectors are separated by 120 m on the circular track and are pointed with $\sim 0.4^\circ$ offsets from the “source” direction so that their beams intersect at the EAS maximum. Photomultipliers $\sim 0.9^\circ$ off-axis on A and B then view the EAS at $\sim 1.3^\circ$ from the axis, or at the Cerenkov emission angle for local particles along the EAS axis. Since such particles are primarily muons and would be present only in cosmic-ray (CR) EAS, $\geq 50\%$ of the background can be rejected. The required pointing geometry is preserved while the reflectors follow a source direction under computer control.

1975) our data on Cen A, from which a γ -ray flux was detected at the 4.5σ level. The results of all our remaining observing programs are reported here.

II. OBSERVATIONAL METHOD

To convert the Narrabri reflectors to EAS Cerenkov detectors, the original on-axis photomultipliers were replaced with 5-inch (13 cm) RCA 4522 photomultipliers, chosen for their high speed and good ultraviolet response. In 1972, one of the reflectors was also equipped with two adjacent 4522's, at $\sim 0.7^\circ$ and $\sim 1.4^\circ$ off-axis. In 1973 and 1974, in addition to the on-axis photomultipliers, a single photomultiplier 0.7° off-axis was used on each of the reflectors. These off-axis phototubes were fixed in the same plane as the two on-axis detectors and were connected in

parallel. The EAS detection geometry is illustrated in Figure 1. With a 120-m baseline, EAS from a given source direction were then detected by turning the reflectors from the source direction toward each other by small offsets, which were calculated such that the EAS would be detected at constant atmospheric depth ($\sim 300 \text{ g cm}^{-2}$). This corresponds to an altitude of $\sim 8\text{--}10 \text{ km}$, where the electron components and principal Cerenkov photon production are maximum. The off-axis detectors then “examined” the same EAS, through appropriate three-fold coincidence channels, for the emission (at $\geq 1.3^\circ$ from the EAS axis) that would arise from penetrating muons (Grindlay 1971, 1975a). For the initial observation program, this enabled ~ 40 percent of the detected EAS to be rejected as cosmic-ray-initiated (i.e., containing muons), which increased to ≥ 50 percent when the off-axis

photomultiplier was added to the second reflector in 1973. In 1973 and 1974, both rejection tubes were provided with ultraviolet-transmitting, visible-blocking glass filters (Schott BG-24) to reduce night sky background for the detection of the ultraviolet-rich Cerenkov pulses from local muons.

The solid angle for EAS detection was $\Omega \approx 5 \times 10^{-4}$ sr. The collecting area and γ -ray threshold energy were $A_c \approx 1.6 \times 10^8$ cm² and $E_0 \approx 2 \times 10^{11}$ eV, respectively, for EAS in the zenith; these values increased by a factor ~ 1.5 (Rieke 1970) for the zenith-angle range $\theta \approx 35^\circ \pm 10^\circ$ used in our observations. Our observations of the two objects MP 1451 and Cen X-3 were conducted at larger zenith angles ($\theta \approx 40^\circ \pm 10^\circ$), and so the increase in A_c and E_0 was a factor of ~ 3 . These values of Ω , A_c , and E_0 are consistent with the known cosmic-ray flux and our observed EAS detection rate of ~ 1 s⁻¹ at the zenith; they are also consistent with the calculations of Weekes and Rieke (1974).

Most of the observations were conducted by comparing EAS rates from the source direction with those from neighboring sky comparison areas. The comparison areas were chosen ≥ 2.5 (in right ascension only) on either side of the source for equal sky brightness, and were tracked over exactly the same range of hour angle and hence elevation as was the source. Thus the actual on-source time was ~ 40

percent of the operating time. An exception to this procedure was made for the 1973 observations of Vela, when the pulsar position alone was tracked in an attempt to detect a pulsed flux. Observations in the on-off tracking mode were restricted to moonless nights of uniformly high atmospheric transparency for reliable statistical comparison of the EAS rates on- and off-source. Uniform sky conditions were ensured by (1) the constancy of phototube pulse rates (on chart recordings) on- and off-source, (2) the acceptance of an observation only if the EAS rates from the two comparison areas were within 3σ of each other, and (3) the acceptance of observations for which a χ^2 test yielded a probability $P(>\chi^2) > 1$ percent that the EAS rates were random about constant mean values. In practice, only a few observation cycles on each source were rejected by criteria (2) and (3).

For sources in the 1972 survey where a pulsed flux might be expected, the two EAS types (rejected versus "γ events") were identified and recorded on tape together with a 5-kHz timing signal, as well as with minute markers for absolute time. Before the 1973 program began, a number of improvements were made to the equipment. A new portable clock and a VLF phase-comparison system were installed to give absolute time (UT) to within 50μ s, and the data were recorded with a 10-kHz timing signal derived from this clock so that the arrival time of

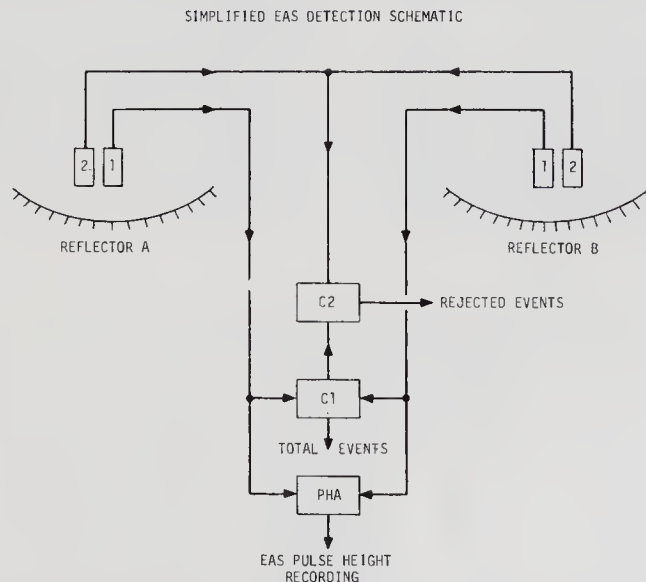


FIG. 2.—Coincidence system diagram for double-beam detection of EAS. The photomultipliers labeled 1 are on-axis of reflectors A and B pointed at EAS maximum (see Fig. 1). Pulses from them are brought through identical networks of amplifiers and discriminators to the inputs of coincidence unit C1. The coincidence output of C1 (total events) triggers the pulse-height analyzer recording of the sum of input pulse heights and appears at the input of coincidence unit C2. The sum of the pulses from the off-axis photomultipliers labeled 2 (with ultraviolet filters), appropriately amplified and delayed, is at the other input of C2. This then records the EAS that are simultaneously detected off-axis closer to the reflectors. Most of these events are due to penetrating local muons and can thus be rejected as cosmic-ray-initiated EAS. Both the C1 and C2 coincidence systems were duplicated with an identical second system (not shown), but with an artificial delay in one side of the input. These systems recorded the random coincidences of each type, which were $< 5\%$ of the real events.

each EAS was known to within 100 μ s. A pulse-height analyzer with 26 channels covering a factor ~ 20 in pulse height was used to measure the sum of the two coincident Cerenkov pulses from the EAS maximum and thus the relative primary energy. Finally, a new data-handling system incorporating real-time digital recording of all the data was introduced. A simplified block diagram is shown in Figure 2.

We observed 11 candidate γ -ray sources during the four moonless and very clear observing sessions, 1972 April–July. The objects were chosen for features (e.g., flat X-ray spectra) suggesting that high-energy processes and γ -ray production might be present. They included pulsars, active galaxies, possible ~ 100 MeV γ -ray sources, and unusual X-ray sources. We shall discuss each briefly in the following presentation of results. The 1973 observing program (April–June) was primarily directed toward confirming positive effects obtained in 1972 on Cen A, the Vela Pulsar, and the pulsar MP 1451. Data were also obtained on the galactic center and a comparison (background) region well off the galactic plane. The weather was generally poor, and only about half the anticipated data were obtained. Therefore, in the 1974 observations (March–April), maximum effort was devoted to Cen A. Because the number of clear observing nights was again less than anticipated, only a few hours of additional Vela data were obtained.

III. RESULTS OF THE OBSERVATIONS

The results are summarized in Table 1. These are the “d.c. analysis” results; they are the EAS rates possibly attributable to γ -rays from the object versus comparison sky. Table 1 does not include our results of analysis for pulsations from several of the objects; these results are given below. The table lists the on-minus-off source rates of detection for all EAS (total

events per minute) and for those not rejected (γ events per minute). The upper limit to the flux corresponding to an excess rate of 3σ above background is also given and was calculated from the γ event rate (off-source) and the detector parameters given above. The ordering of objects in the table is by object class: active galaxies, radio pulsars, a supernova, a quasar, and X-ray sources.

a) Centaurus A

The largest group of data (~ 50 hours on-source) refers to Cen A (NGC 5128), an active radio galaxy and X-ray source, and is discussed in detail elsewhere (Grindlay *et al.* 1975). We tested these data to evaluate the comparison-area tracking method by directly computing the standard deviations of the three EAS detection rates (nonrejected γ events, rejected EAS, and total detected) for each of the two comparison areas, their sum, and the on-source data. The observed standard deviations were then divided by their corresponding Poisson values, and the distributions of resulting ratios examined. The distribution means were all within 3 percent of unity, with standard deviations of about 4 percent. Thus our data seem to be well described by Poisson statistics. We have also applied these tests to data on the other candidate sources with the same results.

The results of all our 1972–1974 data on Cen A, given in Table 1, represent a detection of the source at the 4.5σ level. Since our detector beam did not include the large extended radio lobes of Cen A, the source is within the galaxy NGC 5128. The flux given in Table 1 is an average of the three observing periods. As discussed in Grindlay *et al.* (1975) and Grindlay (1975b), there is evidence that this flux actually varied with changes in the microwave source at the nucleus of NGC 5128.

TABLE 1
SUMMARY OF RESULTS: SOURCE MINUS BACKGROUND EVENT RATES

Object	On-Source Time* (min)	Total Events (min ⁻¹)	γ Events (min ⁻¹)	3σ Flux Upper Limit (10 ⁻¹⁰ photon cm ⁻² s ⁻¹)†
Cen A.....	3046	+0.63 \pm 0.19	+0.66 \pm 0.16	0.44 \pm 0.10 (measured flux)
PKS 1514–24.....	48	–0.13 \pm 1.55	–0.67 \pm 1.46	3.01
PSR 0833–45.....	380	+1.09 \pm 0.54	+0.88 \pm 0.41	0.85
MP 1451–68.....	1008	+0.79 \pm 0.29	+0.75 \pm 0.25	0.26‡
PSR 1749–28.....	325	+1.04 \pm 0.54	+1.17 \pm 0.50	0.99
Supernova 1972e in NGC 5253.....	238	+1.45 \pm 0.73	+0.76 \pm 0.67	1.40
3C 273.....	63	–1.03 \pm 1.20	...	2.50
Galactic center.....	453	–0.71 \pm 0.46	–0.15 \pm 0.38	0.79
Cen X-3.....	200	+0.59 \pm 0.59	+0.31 \pm 0.41	0.43‡
GX 1+4.....	88	–1.22 \pm 1.06	–0.28 \pm 1.01	2.10
GX 340+0.....	324	–0.61 \pm 0.56	+0.07 \pm 0.47	0.98

* Total exposure time on source for 1972–1974 observations. Equal time was spent on background (see text) for each object. An additional 37 hours of exposure on PSR 0833–45 (only) was also recorded for pulsation analysis.

† From γ events min⁻¹ and for integral flux above threshold 3×10^{11} eV.

‡ Integral flux above energy threshold 6×10^{11} eV.

b) PKS 1514-24

Frye *et al.* (1971a) reported detecting a source (Lib γ -1) at ≥ 100 MeV on one of two balloon flights. This source has a location error box that includes the highly variable optical and radio galaxy PKS 1514-24. We tracked the optical position of PKS 1514-24 and the comparison-sky regions for a total of only 48 minutes on 1972 July 5 and 11, and obtained the upper limits shown in Table 1.

c) PSR 0833-45

The Vela Pulsar (PSR 0833-45) was one of our highest priority objects during the 1972 and 1973 observing programs. It had been detected as an X-ray point source (Kellogg *et al.* 1973), and its other similarities to the Crab Pulsar suggested it might also be a pulsed source at $> 10^{11}$ eV. The $+2\sigma$ d.c. result given in Table 1 refers to the observations in 1972 April and May. These data, plus an additional 300 minutes on-source in 1972, were analyzed at the local period of the radio pulsar and added together in phase by using predictions supplied by P. Reichley for the Narrabri Observatory site. The resulting phase distribution of γ -event arrival times is shown in Figure 3. The optical phases predicted for a nondispersed γ -ray pulse are marked by the arrows, where M identifies the phase measured at 408 MHz for us by M. Large at the Molonglo Mills Cross, and R marks the Reichley prediction from his Goldstone 2388 MHz data. The peak we find $\sim 4\sigma$ above the mean of all the data is ~ 3 ms early with respect to the Reichley phase. Changes in the Vela radio pulse shape with frequency (Downs *et al.* 1973), together with the fact that the Mills Cross detects a fixed linear polarization (the plane of polarization rotates during the pulse), possibly accounts for most of the phase discrepancy between M and R in Figure 1. Therefore, it appears

that our 1972 pulsed effect is ~ 3 ms early with respect to the "optical" phase.

The corresponding γ -ray flux would be

$$F_{1972}(\geq 3 \times 10^{11} \text{ eV}) \leq (1.0 \pm 0.33) \times 10^{-11} \text{ photons cm}^{-2} \text{ s}^{-1}, \quad (1)$$

which we regard as an upper limit. The significance of the effect has been estimated by multiplying the probability corresponding to the 4σ effect by 30, the number of phase bins possible for a pulse at arbitrary phase. This reduces the significance of our 1972 Vela results to that of a 3.0σ effect.

This result prompted an extended program of 32 hours of Vela observations in 1973. We tracked the pulsar position only, and not the background, to maximize exposure in an attempt to confirm the 1972 pulsed effect. The data were obtained in April and May with the improved timing system and the pulse-height digital recording system described above. Periodic analysis of all these data with periods and phases again supplied by Reichley yielded no peaks $> 3\sigma$ in the phase-bin plot. Combining the pulse-height analysis channels into four groups of $\sim \times 2$ gain each, however, revealed a 3σ effect at the predicted optical phase for the highest pulse-height (\propto primary energy) events. This would represent a flux

$$F_{1973}(\geq 5 \times 10^{12} \text{ eV}) \leq (7 \pm 3) \times 10^{-13} \text{ photons cm}^{-2} \text{ s}^{-1}, \quad (2)$$

although, again, we consider this result an upper limit.

Finally, in 1974 March, we recorded an additional 3 hours on the pulsar under less than ideal sky conditions. No significant pulsed effect was detected, the

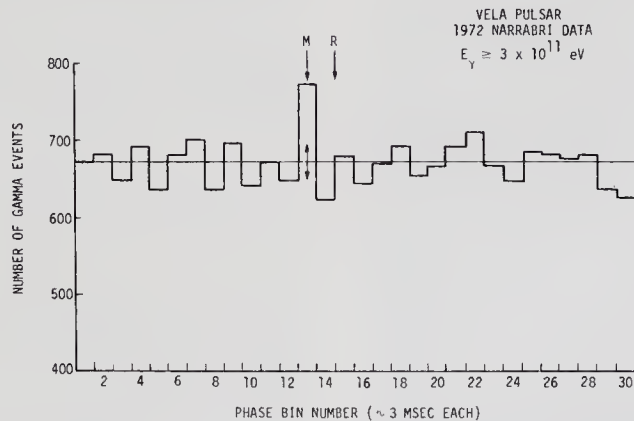


FIG. 3.—Phase histogram of nonrejected (γ event) EAS arrival times recorded on Vela in 1972 April–May and analyzed at the period of PSR 0833-45. M marks the "optical" phase predicted for Narrabri from observations at 408 MHz at Molonglo Observatory, and R is the optical phase predicted by Reichley from Goldstone observations at 2388 MHz. Much of the discrepancy can be accounted for (see text), and the Reichley phase is preferred. The peak in the histogram is 4.0σ above the mean of all the data (horizontal line).

upper limit (3σ) being a factor of ~ 2 above the limit of equation (1).

While these results should be regarded as upper limits, the two 3σ effects are nonetheless interesting. Comparison of our 1972 result, equation (1), with the Crab Pulsar flux at similar energies (Grindlay *et al.* 1974b) requires $n \geq 4$ in any γ -ray pulsar period-luminosity relation $L \propto p^{-n}$ if Vela is at 0.4 kpc and the Crab is at 2 kpc, as usually assumed.

Our 1972 result was obtained within a month of the data of Harnden and Gorenstein (1973), which showed pulsed X-ray emission at ~ 1 keV at a phase ~ 29 ms before the "optical" phase and thus ~ 26 ms before our effect. Albats *et al.* (1974) have reported balloon-flight data from 1972 November showing a pulsed effect at ≥ 20 MeV several milliseconds after the optical phase. While this flux is consistent with an $E^{-0.9}$ integral photon spectrum extrapolated from X-ray energies, our upper limit of equation (1) requires a steepening of the spectral index to at least 1.5 for energies above 20 MeV. Similarly, our reduced flux limit in 1973, equation (2), was obtained within a month of the correspondingly reduced X-ray pulse limit set by Moore *et al.* (1974). Finally, Rappaport *et al.* (1974) reported a similar X-ray upper limit from 1973 November data. Since the statistics of all these "positive" results are not compelling, we conclude that there is no unequivocal evidence for pulsed emission at X-ray energies and above. However, it is possible that, at these energies, there may be a time-variable pulsed flux from PSR 0833, and there could be phase changes as well. Given recent results on the Crab Pulsar at X-ray energies (Forman *et al.* 1974) and at $>10^{11}$ eV (Grindlay *et al.* 1974b), such variability may be characteristic of pulsars. Obviously, observations at higher sensitivity are needed.

d) MP 1451-68

MP 1451-68, a ~ 0.25 s period radio pulsar, was selected for observation in the 1972 survey primarily because its very low dispersion measure of 35726.1 s MHz² (Rankin 1972) suggests that it is one of the closest pulsars. After 631 minutes of exposure on MP 1451 and an equal time on neighboring sky background in 1972 May-July, we obtained an excess rate on-source of $0.99 \pm 0.35 \gamma$ events min^{-1} (Grindlay *et al.* 1973). An additional 377 min were obtained in 1973 June and July, giving an excess rate on-source of $0.49 \pm 0.36 \gamma$ events min^{-1} . The combined totals, listed in Table 1, represent a 3.0σ effect. We have analyzed these data at the pulsar period and added them in phase, using periods and phases predicted by J. Rankin for our site. The predictions were based on measurements made at Molonglo by Large and at Parkes by Rankin. No pulsed effect was found, and the upper limit for pulsed emission (20% duty cycle) is a factor of ~ 2 below that in Table 1. The 3σ d.c. effect, however, suggests that further observations of this object at X-ray and γ -ray energies are warranted, particularly if pulsars are found to have variable phases at high energies.

e) PSR 1749-28

The final radio pulsar chosen for our survey, PSR 1749-28, has a relatively high slow-down rate for its period (~ 0.56 s) and hence a possibly high rate of energy loss. The d.c. upper limit in Table 1 refers to a comparison-sky region displaced $\sim 13^\circ$ in right ascension from the pulsar. The on-source data (1972 June and July) were analyzed at the period and phase of the pulsar predicted for us by Reichley from concurrent radio observations at Goldstone. No significant ($>3\sigma$) pulsed effect was found, and the upper limit for pulsed emission at arbitrary phase is again a factor of 2 below the limit in Table 1. This upper limit is a factor ~ 10 lower in total energy flux (ergs $\text{cm}^{-2} \text{s}^{-1}$) than the 17-42 keV upper limit (1972 April) of Ricker *et al.* (1973). Since PSR 1749 is within 1° of the galactic center, our upper limit to the flux also applies to γ -ray emission from this region near the galactic center.

f) Supernova 1972e (NGC 5253)

After learning of the bright Type I supernova in NGC 5253 (Kowal 1972), we included this object in our observing program. It was not possible to begin these observations until 1972 June 7, which was about a month after the maximum light. Nevertheless, we observed a $\sim 1.5\sigma$ excess over background from this object during June 7-19 and a 1σ excess on July 2 and 5. The flux upper limit for the combined observations is given in Table 1 and is equivalent to a total γ -ray ($E_\gamma > 3 \times 10^{11}$ eV) energy flux limit of $\leq 2.6 \times 10^{-11}$ ergs $\text{cm}^{-2} \text{s}^{-1}$. This can be compared with the energy flux measured at the same time in the visual ($m_v \sim 10$) (Kirshner *et al.* 1973), which was $\sim 2 \times 10^{-9}$ ergs $\text{cm}^{-2} \text{s}^{-1}$, and with the corresponding X-ray upper limit of $\leq 2 \times 10^{-10}$ ergs $\text{cm}^{-2} \text{s}^{-1}$ (Canizares *et al.* 1974). Our γ -ray upper limit also corresponds to a total energy limit of $<10^{46}$ ergs in high-energy ($>3 \times 10^{11}$ eV) photons during our month of observations if NGC 5253 is at 4 Mpc (Sersic *et al.* 1972). This value can be compared with the limit $<10^{50}$ ergs established by Fazio *et al.* (1968) for the supernova Zwicky 1968h at similar energies, although that limit was for a period within a few days of maximum light.

g) 3C 273

On 1972 July 2 and 5, we conducted on-off observations of 3C 273, the only quasar examined in our survey. Since this was the only object we observed that transited north of our local zenith, we did not reverse the off-axis photomultiplier mountings (see Fig. 1 and associated discussion), as would have been required to employ the cosmic-ray-rejection system. Thus, our upper limit in Table 1 refers to total EAS only. The limit is a factor of ~ 3 above that set by Weekes *et al.* (1972) at the same energy.

h) Galactic Center

The galactic center was another principal object of our survey since it is observed as a source up through

100 MeV gamma-ray energies (Kniffen *et al.* 1973). The 1972 observations, conducted during June 8–13, used a comparison area displaced 15 minutes in right ascension from the galactic center. No significant effect was observed (Grindlay *et al.* 1973), and so in 1973 we used comparison areas displaced 45 minutes in right ascension in case there was a broad extended source. A total of 250 minutes exposure was obtained from 1973 May 29–June 5, resulting in a -0.2σ effect.

The combined total of all our galactic-center data is given in Table 1. Our 3σ flux upper limit, when combined with that of Weekes *et al.* (1972) [$F(>2.2 \times 10^{12} \text{ eV}) < 5.8 \times 10^{-12} \text{ photons cm}^{-2} \text{ s}^{-1}$], is consistent with a power-law integral spectral index $\alpha < -1.3$ at these energies, which itself is consistent with the limiting value $\alpha < -1.4$ obtained from extrapolating the 100 MeV flux of Kniffen *et al.* (1973) to our energies. We note that if the 100 MeV flux is primarily due to π^0 decays from cosmic-ray interactions, a steep spectrum with $\alpha \simeq -1.67$ is expected. Such a spectrum would be detectable at our energies with a factor ~ 3 increase in sensitivity. We also note that our upper limit in Table 1 requires that no flat inverse Compton component of the 100 MeV spectrum (Kniffen *et al.* 1973) extend to $\sim 10^{11}$ eV without a break.

i) Centaurus X-3

We now turn to our observations of X-ray sources. The most promising of these, it seemed, was the pulsing X-ray binary Cen X-3. Cosmic-ray production is envisaged in some models of X-ray binaries (e.g., Brecher and Morrison 1973), and a γ -ray flux might be expected. We observed the *Uhuru* position (Giacconi *et al.* 1972) of Cen X-3 in the on-off tracking mode during 1972 April 11–18. The observations on April 16 and 18 were recorded as the X-ray source was entering an eclipse, according to an ephemeris kindly supplied by E. Schreier. The remaining observations were near the phase of maximum X-ray emission in the 2.08714 day period. Our results in Table 1 are for the total of these data, which gave a $+1\sigma$ effect. No significant difference occurred between the effects observed at different orbital phases of the X-ray source. We have analyzed these data for the 4.84 s pulse period present in the X-ray data, and again no significant effect was found. The upper limit in Table 1 also applies to pulsed γ -ray emission with a duty cycle of ~ 50 percent, as is found for the X-rays.

j) GX 1+4

This highly variable X-ray source was reported by Lewin *et al.* (1971). Observed from 18–50 keV, it was found to have a flat spectrum (power-law spectral index $\alpha = 1.4 \pm 0.7$ or $kT = 28 \pm 12$ keV) with intensity variations on a time scale of minutes. Since Frye *et al.* (1971b) have tentatively associated this source with G γ 2 + 3, which they observed at 100 MeV, an extrapolation to $\geq 10^{11}$ eV of the combined spectrum would predict an easily observable ($> 10^{-10}$

photons $\text{cm}^{-2} \text{ s}^{-1}$) flux. We conducted on-off observations on 1972 June 9, 14, and 16, and employed the source position given by Giacconi *et al.* (1972) for the associated source 2U 1728–24 and comparison regions displaced 5° in right ascension. Our upper limit to the high-energy flux is given in Table 1. This upper limit restricts the spectral index to $\alpha < -1.5$ in an extrapolation from the 100 MeV flux reported by Frye *et al.* (1971b).

k) GX 340+0 (3U 1642–45)

The X-ray source GX 340+0 (3U 1642–45) was observed by Lewin *et al.* (1969) to have a hard spectrum. Together with the positional agreement with the 100 MeV source G γ 341+1 reported by Frye *et al.* (1971b), the hard spectrum encouraged us to observe this object. We conducted on-off observations from 1972 May 11–19, using the original *Uhuru* source position (Giacconi *et al.* 1972) and comparison areas displaced on either side by 10 minutes in right ascension. The *Uhuru* source position is also within 10 arcminutes (and thus within our beam) of the radio pulsar PSR 1642–45. The *Uhuru* source is variable by a factor of ~ 3 (Giacconi *et al.* 1972), as apparently is also the case at hard X-ray energies, since Ricker *et al.* (1973) reported an upper limit a factor of ~ 3 below the flux given by Lewin *et al.* (1969). As we did not record our observations of this object with high time resolution, it was not possible to search for either the pulsar period or other fast time variation. Further observations were not planned, in view of the lack of any positive effect in our d.c. result. The upper limit in Table 1 again restricts $\alpha < -1.5$ in an extrapolation from the 100 MeV result given by Frye *et al.* (1971b).

IV. CONCLUSIONS

The survey has shown that a number of sources of hard X-rays and possibly of 100 MeV γ -rays are not strong sources of high-energy γ -rays with $E_0 \geq 3 \times 10^{11}$ eV (i.e., the fluxes are $\leq 10^{-10}$ photons $\text{cm}^{-2} \text{ s}^{-1}$). It has also set limits to the high-energy flux from the galactic center that are consistent with a π^0 source spectrum and not with an inverse Compton component extending to high energies. Limits for the X-ray sources we observed (e.g., Cen X-3) are consistent with accretion models in which essentially no very-high-energy photon flux is expected. They can be used to constrain X-ray source models (e.g., Brecher and Morrison 1973) involving pulsar-like (i.e., rotating magnetized white dwarfs or neutron stars) mechanisms in which cosmic rays are accelerated to very high energies.

An interesting result is the evidence presented above for a variable-intensity pulsed flux from the Vela Pulsar. While our 3σ effects on Vela are certainly not compelling in themselves, their temporal association with the X-ray results may be the first evidence of correlated variability in pulsars at high energies.

The most promising result, however, is the detection of Cen A (Grindlay *et al.* 1975). This result has the consequence of establishing that detectable sources apart from the Crab Pulsar do indeed exist at photon energies $> 10^{11}$ eV. The constraints such a flux imposes make it then possible to construct rather detailed models for the sources (e.g., Grindlay 1975*b*).

If further improvements in the Cerenkov technique of detecting γ -rays can be made, giving, for example, an additional factor of ~ 3 in sensitivity, a more extensive survey of candidate point sources would be justified. Such a system would detect Cen A in 5 hours (rather than in the 50 hours on-source required here), and would enable many promising objects to be examined. It is possible that the reflectors of the very-large-intensity interferometer, proposed as a successor to the Narrabri instrument, will enable such a gain in sensitivity to be achieved.

We are indebted to G. G. Fazio for early discussions leading to this collaborative program, and to T. C. Weekes for assistance from Mount Hopkins Observatory. We thank P. Reichley, M. Large, and J. Rankin for supplying us with pulsar timing data. One of us (J. E. G.) was a Harvard Junior Fellow during the course of this work and thanks the Society of Fellows of Harvard University for support. This work was supported by the National Science Foundation (grant GP-38783), the Smithsonian Institution, the Australian Research Grants Committee, the Research Grants Committee of the University of Sydney, and the Science Foundation for Physics within the University of Sydney. We thank Professor Messel for his support, and G. Gifford, S. Owens, R. Thompson, and E. Horine for their assistance with the program.

REFERENCES

- Albats, P., Frye, G. M., Thomson, G. B., Hopper, V. D., Mace, O. B., and Thomas, J. A. 1974, *Nature*, **251**, 400.
- Brecher, K., and Morrison, P. 1973, *Ap. J. (Letters)*, **180**, L107.
- Canizares, C. R., Neighbours, J. E., and Matilsky, T. 1974, *Ap. J. (Letters)*, **192**, L61.
- Chudakov, A. E., Dadykin, V. L., Zatspin, V. I., and Nesterova, N. M. 1965, *Cosmic Rays* (Proc. P. N. Lebedev Inst.), *Trans. Consultants Bureau*, **26**, 99.
- Downs, G. S., Reichley, P. E., and Morris, G. A. 1973, *Ap. J. (Letters)*, **181**, L143.
- Fazio, G. G., Helmken, H. F., Rieke, G. H., and Weekes, T. C. 1968, *Ap. J. (Letters)*, **154**, L83.
- Fichtel, C. E., Hartman, R. C., Kniffen, D. A., Thompson, D. J., Bignami, G. F., Ögelman, H., Özel, M. E., and Tümer, T. 1975, *Ap. J.*, **198**, 163.
- Forman, W., Giacconi, R., Jones, C., Schreier, E., and Tananbaum, H. 1974, *Ap. J. (Letters)*, **193**, L67.
- Frye, G. M., Albats, P. A., Zych, A. D., Staib, J. A., Hopper, V. D., Rawlinson, W. R., and Thomas, J. A. 1971a, *Nature*, **233**, 466.
- . 1971b, *ibid.*, **231**, 372.
- Giacconi, R., Murray, S., Gursky, H., Kellogg, E., Schreier, E., and Tananbaum, H. 1972, *Ap. J.*, **178**, 281.
- Grindlay, J. E. 1971, *Smithsonian Ap. Obs. Spec. Rept.* No. 334.
- . 1972, *Ap. J. (Letters)*, **174**, L9.
- . 1975a, *Phys. Rev. D.*, **11**, 517.
- . 1975b, *Ap. J.*, **199**, 49.
- Grindlay, J. E., Hanbury Brown, R., Davis, J., and Allen, L. R. 1973, *Proc. 13th Internat. Cosmic Ray Conf. (Denver)*, **1**, 439.
- Grindlay, J. E., Helmken, H. F., Hanbury Brown, R., Davis, J., and Allen, L. R. 1974a, *Proc. 9th ESLAB Symposium on Gamma-Ray Astronomy*, ed. B. G. Taylor, p. 279.
- . 1975, *Ap. J. (Letters)*, **197**, L9.
- Grindlay, J. E., Helmken, H. F., and Weeks, T. C. 1974b, *Proc. 9th ESLAB Symposium on Gamma-Ray Astronomy*, ed. B. G. Taylor, p. 301.
- Hanbury Brown, R., Davis, J., and Allen, L. R. 1967, *M.N.R.A.S.*, **137**, 375.
- . 1969, *ibid.*, **146**, 399.
- Harnden, F. R., and Gorenstein, P. 1973, *Nature Phys. Sci.*, **241**, 107.
- Jennings, D. M., White, G., Porter, N. A., O'Mongain, E., Fegan, D. J., and White, J. 1974, *Il Nuovo Cimento*, **20B**, 71.
- Kellogg, E., Tananbaum, H., Harnden, F. R., Gursky, H., Giacconi, R., and Grindlay, J. 1973, *Ap. J.*, **183**, 935.
- Kirshner, R. P., Willner, S. P., Becklin, E. E., Neugebauer, G., and Oke, J. B. 1973, *Ap. J. (Letters)*, **180**, L97.
- Kniffen, D. A., Hartman, R. C., Thompson, D. J., and Fichtel, C. E. 1973, *Ap. J. (Letters)*, **186**, L105.
- Kowal, C. 1972, *IAU Circ.* No. 2405.
- Lewin, W. H. G., Clark, G., Gerassimenko, M., and Smith, W. 1969, *Nature*, **223**, 1142.
- Lewin, W. H. G., Ricker, G. R., and McClintock, J. E. 1971, *Ap. J. (Letters)*, **169**, L17.
- Moore, W. W., Agrawal, P. C., and Garmire, G. 1974, *Ap. J. (Letters)*, **189**, L117.
- Rankin, J. 1972, private communication.
- Rappaport, S., Bradt, H., Doxsey, H., Levine, A., and Spada, G. 1974, *Nature*, **251**, 471.
- Ricker, G. R., Gerassimenko, M., McClintock, J. E., Ryckman, S. G., and Lewin, W. H. G. 1973, *Ap. J. (Letters)*, **186**, L111.
- Rieke, G. H. 1970, *Smithsonian Ap. Obs. Spec. Rept.* No. 301.
- Sersic, J. L., Pastoriza, M., and Carranza, G. 1972, Preprint No. 1, Observatorio Astronomico, Universidad Nacional de Cordoba, Argentina.
- Weekes, T. C., Fazio, G. G., Helmken, H. F., O'Mongain, E., and Rieke, G. 1972, *Ap. J.*, **174**, 165.
- Weekes, T. C., and Rieke, G. H. 1974, *Proc. 9th ESLAB Symposium on Gamma-Ray Astronomy*, ed. B. G. Taylor, p. 287.

L. R. ALLEN, R. HANBURY BROWN, and J. DAVIS: School of Physics, University of Sydney, Sydney, Australia 2006

J. E. GRINDLAY and H. F. HELMKEN: Center for Astrophysics, 60 Garden Street, Cambridge, MA 02138

The detection of very high energy gamma rays by Čerenkov light

R HANBURY BROWN

Raman Visiting Professor, Indian Academy of Sciences, Bangalore 560 006

This lecture is concerned with the detection of gamma rays in the energy range 10^{11} – 10^{12} eV. Balloons and satellites carrying scintillation counters, nuclear emulsions, spark chambers, gas Čerenkov counters can be used in the range 10^6 – 10^9 eV, but at higher energies the flux is too low; *e.g.* at 10^{11} eV we are concerned with ~ 1 event $\text{day}^{-1} \text{m}^{-2}$. By the use of the Čerenkov light technique which I shall describe it is possible to detect these very low fluxes because one can use the earth's atmosphere as a Čerenkov detector and obtain a 'collecting area' of the order of 10^4m^2 .

A second interesting point about this range is that it represents the highest electromagnetic frequency at which we are likely to be able to receive radiation from distant parts of the Universe. This is because gamma rays are absorbed in interstellar space by photon-photon interaction with starlight and, more importantly, with the universal 3°K radiation. At about 10^{14} eV the optical depth of space is $\tau \simeq 1$ at a distance of $\sim 10^{23}$ cm (1 parsec = 3×10^{18} cm). Thus photons of energy greater than about 10^{14} eV will never reach us from distant galaxies.

The technique which I shall describe relies on the fact that when a gamma ray of very high energy impinges on the earth's atmosphere it produces an extensive air shower. The initial gamma ray Compton-scatters or converts to an electron pair and these electrons produce more electrons and so on. An air shower develops which we shall call a γ -EAS. When a cosmic-ray proton enters the atmosphere it also produces an extensive air shower which we shall call a P -EAS, where P represents the fact that most cosmic-ray showers are initiated by protons. The incoming cosmic-ray proton also produces a shower, but the most abundant product of the initial processes are pions. These pions decay into muons ($\pi^{\pm} \rightarrow \mu^{\pm} + \nu$) and these muons do not interact with the atmosphere if their energy is $< 10^{12}$ eV and they do not decay if $E > 5 \times 10^9$ eV. The number of muons produced is given roughly by,

$$N_{\mu} (E_{\mu} > 10^{10}) = 0.01 E_{(\text{primary GeV})}^{0.875}$$

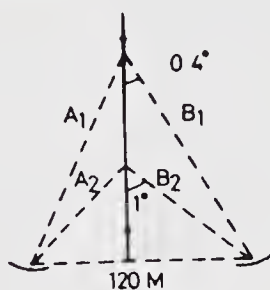
These muons reach the ground and there are roughly ~ 5 muons on the average for showers in the energy range we detect.

The principal difference between the cosmic-ray showers and the gamma-ray showers is that the γ -EAS contain less muons. The cross-section for photo-production of pions is about 1% of that for collision with protons. It is therefore

possible to discriminate, at least for some showers, between γ -EAS and P -EAS by observing the muon core.

The technique of Čerenkov light detection depends upon the fact that the charged particles produced in the showers (mainly electrons) produce Čerenkov radiation. This radiation arrive at the ground as a pool of light with a diameter of roughly 200 m and with a 'thickness' of a few nanoseconds. The maximum light of the EAS is produced at about 8 km above the earth and, if you could see it, would look like a burst of light with an overall angular size of the order of 0.4° . The muon core is roughly collimated because it does not interact much with the atmosphere and will produce a Čerenkov flash at an angle of approximately 1° to its path. The whole problem of detecting γ -ray events is to sort them out from the far more numerous cosmic-ray events. For example the cosmic-ray rate $\simeq 60 \text{ min}^{-1}$ at Narrabri, whereas the γ -ray events were only $0.5 \text{ events min}^{-1}$. The purpose of the 'muon-core' rejection system is, of course, to reduce the background of cosmic-ray events as far as possible.

The reflectors of the Narrabri stellar interferometer were modified for this work after they had completed their stellar programme in 1971. The work itself was a joint programme with the Centre for Astrophysics in Cambridge, Massachusetts. The normal phototubes were replaced by 5 inch RCA 4522 photomultiplier. Two phototubes were mounted at the focus of each reflector to produce two beams per



reflector, the intersection of the beams $A_1 B_1$ is at about 8 km above the earth's surface and is used to detect the light from the P -EAS and γ -EAS. The field of view is $\simeq 0.5^\circ$. The off-set beams $A_2 B_2$ are in the same plane as $A_1 B_1$ and are used to detect the Čerenkov flash from the muon core. The outputs of the photomultipliers are taken to discriminators which respond to pulses of a certain minimum height and then to coincidence counters, etc. The counting rate in A_1, B_1, A_2 and B_2 is measured. One coincidence counter gives $(A_1 \times B_1)$, the total shower rate. A linear adder gives $(A_2 + B_2)$ and then a coincidence counter gives $(A_1 B_1) \times (A_2 + B_2)$. From this information it is possible to get three different counts, total counts, rejected (cosmic-ray) counts, and non-rejected counts (cosmic-rays + γ -rays).

The main phototubes $A_1 B_1$ operate in total light, the offset phototubes $A_2 B_2$ have filters which pass ultraviolet preferentially. The object of the ultraviolet filters is to suppress the effect of starlight relative to Čerenkov light in the offset tubes. Even so the system only rejects about 50% of the cosmic rays giving us effectively $a\sqrt{2}$ gain in signal/noise ratio.

The detection of very high energy gamma rays by Cerenko light

The parameters of the equipment were, collecting area in sky for showers $\simeq 1.6 \times 10^4 \text{ m}^2$ in the zenith; solid angle $5 \times 10^{-5} \text{ ster}^{-1}$, sensitivity $E_{\text{primary}} > 2 \times 10^{11} \text{ eV}$. All these parameters are increased by about 1.5 at a zenith angle of 35° .

Observational programme

All the observations must be made with a very clear sky on moonless nights. The two reflectors are spaced 120 m and set to track a point 8 km above the ground in the direction of the source. The counts of A_1, B_1, A_2, B_2 etc are registered for 15 min from the source and 15 min from a comparison area. The comparison area is divided into 2 parts on either side of the source. The first comparison area is observed for 7 min over a certain range of elevation (ΔE_1), the source is then observed for 15 min over a range of elevations ($\Delta E_1 + \Delta E_2$), the second comparison area is then observed over a range of elevation ΔE_2 . It is important that the range of elevation for the source and comparison area should be *precisely* the same because the cosmic-ray background ($\simeq 60 \text{ counts min}^{-1}$) varies with zenith angle as about $\cos Z^{-2.8}$.

The whole observational technique is complicated by the fact that the interferometer was designed for following stars using a computer assisted by automatic photo-electric star-guiding. When tracking a γ -ray source there is no star-guiding and the pointing errors have to be first calibrated using stars and then fed into the control system manually every 5 min.

The programme started in 1972 with a survey of a number of objects which one might conjecture to be γ -ray sources, (a) supernova N.G.C. 5253, (b) radio-galaxies (Cen-A, 3 C-273), (c) pulsars (0833, MP 1451, PSR 1749), (d) X-ray sources (Cen-X3, Lib γ^{-1} , GX-340, GX 1 + 4).

The galactic centre

Positive results of low significance were obtained on only Cen-A, and the 3 pulsars (total power, not pulsed measurements). All the other sources showed no sign of γ -rays. In 1973 an effort was made to detect Cen-A, the pulsars. In the case of the pulsars observations were made with precise timing so that the pulses could be superimposed at the pulsar period. About 30 hours of tracking PSR 0833 showed a pulse of γ -rays with a significance of only $+3\sigma$ at the phase of the radio pulse as given by Molonglo radio telescope and displaced by about 3 msec from the phase given by Reichley (?). The strength of this pulsed effect was not sufficient to explain the total-power result obtained on PSR 0833 in 1972. Cen-A gave a positive result of low significance. The weather was very bad and cut down the programme very severely.

In 1974 we concentrated on Cen-A and because the weather was again very bad we only got 2 hours observations of PSR 0833. (These latter observations have not yet been analyzed). Cen-A showed again a positive result.

The only positive result which we are at the moment prepared to put forward is *the detection of high-energy gamma rays from Cen-A*. Table I summarizes the results. It shows that the overall significance of the positive effect is $+4.6\sigma$. The

Table 1. Summary of Cen-A results

<i>Total EAS</i>					
Year	ON	OFF	Time (min)	ON-OFF Rate (min ⁻¹)	No. Sigma
1972	76660	75601	1289	0.82 ± 0.30	2.7
1973	35773	35726	782	0.06 ± 0.34	0.2
1974	64759	63757	975	1.03 ± 0.37	2.8
SUM	177192	175084	3046	0.69 ± 0.19	3.6
				Mean of rates weighted by $\sigma^{-2} = 0.63 \pm 0.19$	3.3
<i>Non-Rejected EAS</i>					
1972	56471	55167	1240	1.05 ± 0.27	3.9
1973	15463	15297	662	0.25 ± 0.26	1.0
1974	39853	39139	975	0.73 ± 0.29	2.5
SUM	111787	109603	2877	0.76 ± 0.16	4.6
				Mean of rates weighted by $\sigma^{-2} = 0.66 \pm 0.16$	4.2

results have been analyzed rigorously. For example for every run the counts in the two comparison areas have been compared and if they differ by $> 3\sigma$ the run has been thrown out—this gives us some sort of protection against rapid changes in atmospheric transparency. We have also examined in detail the statistical distribution of all the counts to check that everything is normal and that our positive result does not depend, for example, on a few exceptional runs. On the basis of these results I think we can claim with reasonable confidence that Cen-A is a source of high energy γ -rays. Substituting the parameters of our equipment the gamma-ray rate from Cen-A is

$$Rate (E > 3 \times 10^{11} eV) = 4.4 + 1 \times 10^{11} \text{ photons cm}^{-2} \text{ sec}^{-1}$$

Interpretation

If we assume that the source of γ -rays from Cen-A is the central compact radio, x-ray and infrared source then it appears that the γ -rays are probably produced by inverse Compton scattering of high-energy photons (e.g. x-ray photons) by relativistic electrons. We shall assume that the radio γ -x-rays are produced by synchrotron emission. For a compact isotropic source we can show that,

$$\frac{\text{inverse compton flux}}{\text{synchrotron flux}} = \frac{\text{radiation energy density}}{\text{magnetic energy density}}$$

and derive the following relations,

$$F_{\gamma} \propto \text{constant} \frac{\nu_c^{-\alpha}}{\Omega B (1 + \alpha)}, \tag{1}$$

$$\theta = \Omega^{1/2} = 9.3 \times 10^8 F_{\nu_0}^{1/2} \nu_0^{-5/4} B^{1/4}, \tag{2}$$

The detection of very high energy gamma rays by Cerenkov light

where F_γ is the I.C. flux of γ rays, B is the magnetic field (gauss), θ is the angular size of the source in arc secs, ν_0 is the synchrotron self-absorption 'turnover' frequency in the radio spectrum, F_{ν_0} is the radio flux at ν_0 .

It follows that,

$$\theta^2 = \Omega = \text{constant} \frac{1}{F_\gamma B^{(1+\alpha)}},$$

$$\theta^2 = \Omega = \text{constant} B^{1/2},$$

and so $B = \text{constant} F_\gamma^{-[1/(1.5+\alpha)]}$.

Thus the measurement of F_γ would allow us to find B and θ uniquely if, for example, we knew the radio spectrum, without measuring θ . There are other possible combinations of the data. The interesting thing is that the γ -ray flux gives us a new kind of information about the parameters of the source.

Unfortunately when we turn to Cen-A we find that neither the radio spectrum, nor the angular size are known satisfactorily. For example take the flux measurements in the literature,

$$2695 \text{ MHz } 2.4 \pm 0.2 \text{ f.u.},$$

$$8085 \text{ MHz } 2.9 \pm 0.2 \text{ f.u.},$$

$$10,700 \text{ MHz } 4.4 \pm 0.3 \text{ f.u.},$$

or the diameter information,

$$\theta > 10^{-3} \text{ arc secs from V.L.B.I.}$$

$$\theta \sim 1'' \text{ at infrared}$$

$$\theta < 0.5'' \text{ at 2695 and 8085 MHz.}$$

$$\theta < 15' \text{ at x-rays.}$$

A model of CEN-A

Our measurements of the γ -ray flux from CEN-A do not refer to a single energy. The pulse heights were measured in a 26-channel pulse height analyzer and we have divided them into three groups. We have then calculated the γ spectrum of a model to fit the S/N ratio observed in these 3 pulse height groups. We have assumed in the absence of better information, that the 'turn-over' frequency in the radio spectrum is $\nu_0 = 3 \text{ GHz}$ and that $F_{\nu_0} = 3 \text{ flux units}$, and that the radio spectrum is given by,

$$df/d\nu = 4.4 \times 10^{-16} \nu^{-0.7} \text{ erg cm}^{-2} \text{ sec}^{-1} \text{ Hz}^{-1}$$

We then calculate the spectrum of the inverse compton radiation for a model to match our 3 pulse height (*i.e.* energy) groups. We find that a reasonable match is obtained if,

$$\theta (\text{Cen-A}) = 1.3 \times 10^{-3} \text{ arc sec.}$$

$$B (\text{Cen-A}) = 10^{-1} \text{ gauss.}$$

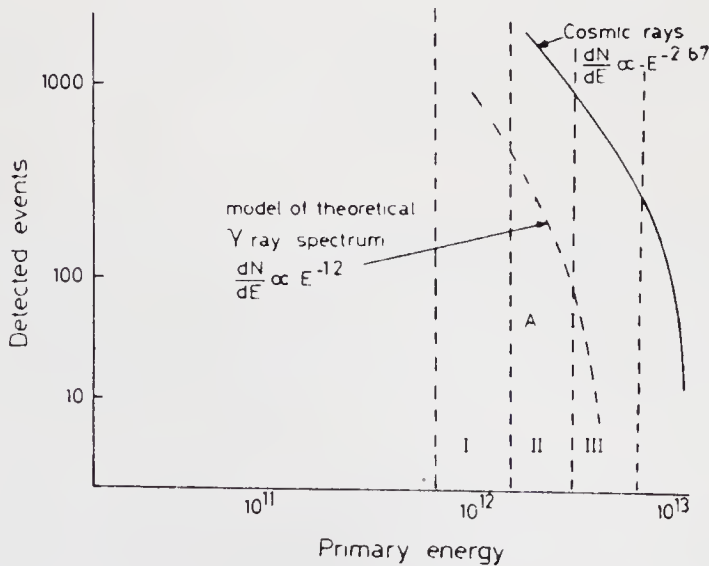
The total I.C. luminosity is $2 \times 10^{40} \text{ ergs sec}^{-1}$ which is 10% of the synchrotron luminosity. The size of the source at the distance of CEN-A is $\approx 0.025 \text{ psc} \approx 1 \text{ light month}$.

This model is of course speculative because the necessary radio data do not exist. It is interesting to compare these data with the compact source in M 87 which is believed to be about 0.1 pc in size, with 3 C 273 which is $\sim 1 \text{ pc}$, with 3 C 84 which is $\sim 2 \text{ light years}$, and with NGC 1275 which is about 1 light year.

Calculation of the total energy stored in the compact source of CEN-A shows that it is insufficient to supply the extended sources for the time required. The energy in the compact source must therefore be replenished continuously and the mechanism by which this occurs is, like all the other compact sources, one of the principal and intriguing mysteries of astrophysics today.

Note on spectrum

The spectrum of the model looks like this.



I, II, and III correspond to pulse height ranges. The maximum S/N is obtained in channel II and then falls off sharply in III. The inflection in the theoretical spectrum at A (for γ rays) is connected with the variation of cross-section for inverse-compton production (*i.e.* transition from Thomson to Klein-Nishina).



Australian Academy of Science

The Matthew Flinders Lecture

Measuring the Size of the Stars

by R. Hanbury Brown

Delivered at the Academy of Science on
29 April 1982

Occasional Paper Series Number 3

I am going to discuss a topic which would, have interested the lively-minded scientist and navigator whose memory we honour by the Matthew Flinders Lecture. I am going to talk about attempts to answer some ancient questions about the night sky — what is the size and shape of the stars, and how hot are they? I am not going to mention the planets or the Moon; in the context of my talk they are too suburban.

For most of history our knowledge of the stars has been limited to measuring their positions on a map of the sky and to the making of crude estimates of their brightness. Before the invention of the telescope and the photographic plate, these measurements were made by the naked eye using simple mechanical aids. At first, people used arrangements of standing stones such as Stonehenge, and later they evolved sophisticated mechanical instruments such as those used by Tycho Brahe at Uraniborg in the 16th century. The last great observatories to be built without telescopes were erected in India by Jai Singh in the early 18th century; interestingly they were built roughly a 100 years after the introduction of the telescope into astronomy and 50 years after the foundation of the Royal Observatory at Greenwich.

The introduction of the telescope in the early 17th century made it possible to see fainter stars and to make more precise measurements of their position, but it told us very little about the stars themselves. The accuracy of pre-telescopic observatories was, at best, not much better than 1 minute of arc;* by the mid-18th century the positions of the bright stars had been measured with telescopes to about 5 seconds of arc.*

The introduction of the spectroscope to astronomy in the mid-19th century revolutionized stellar astronomy. By telling astronomers about the colour of the stars — more precisely about the spectral distribution of their light — it expanded their narrow preoccupation with celestial mechanics (a tedious subject in the days before the electronic computer) into the vigorous study of astrophysics. It was after the introduction of the spectroscope that we really started to know something about the stars; until then we knew that they made pretty patterns in the sky, but we had no idea what they were made of, nor why they differ so much in size and temperature.

The introduction of photography to astronomy, also in the 19th century, greatly extended the use of both the telescope and the spectroscope and

made it possible to measure the brightness of stars more accurately. More recent inventions, such as the photo-electric detector and the image-tube, have extended even further our ability to measure the positions and movements of the stars and the spectral distribution and intensity of their light.

But what progress has been made in studying their size, shape and surface? Going back to the 16th century for a moment, Tycho Brahe reached the conclusion by looking at the stars that a first magnitude star presents a disc of 120 seconds of arc in diameter, and a fifth magnitude star, roughly the faintest star you can see, has a disc of 30 seconds of arc. When Galileo turned his telescope to the stars he found that Tycho was quite wrong; the stars, even when “magnified” by the telescope, still looked like points of light. This was not, may I remind you, a matter of idle curiosity. It had an important bearing on one of the trickiest questions of the day: whether or not the orthodox Ptolemaic cosmology, as taught by the Church, was true. If, as Copernicus had suggested, the Earth travels around the Sun, then it was to be expected that the apparent positions of the nearest stars would, during the course of a year, show parallax; that is, they would appear to move very slightly in position relative to more distant stars. Careful observations by Tycho Brahe, for example, had shown that the stars did not appear to move annually or, to be more exact, that any such movement must be less than 1 minute of arc. This limit set a minimum possible distance to the stars and, combined with Tycho’s estimates of their angular size, implied that if the Earth really does go around the Sun then the stars must be bodies of incredible size, as large as the whole orbit of the Earth around the Sun. Very few people were prepared to believe that the stars are so large, and Tycho himself refused to accept the Copernican system.

But to Galileo the discovery that the stars looked like points of light, even through a telescope, was of great importance, because it made the Copernican theory more plausible. Indeed he tried to measure the angular size of the bright star Vega by a different method. He hung a fine silk cord vertically and then measured the distance from the cord at which he had to stand so that it just occulted the star. By careful experiment he reached the conclusion that the angular size of Vega was 5 seconds of arc. About 350 years later Vega was measured again at Narrabri Observatory in New South Wales; Galileo’s result was found to be roughly 1500 times too large. Nevertheless the measurement served his purpose. It showed that Tycho’s estimate of the angular size of stars was much too big, and gave a plausible explanation for

* Small angles are measured in minutes and seconds of arc. 1 degree of angle = 60 minutes of arc = 3600 seconds of arc.

the failure of the stars to show parallax; quite simply they were too far away and, indeed, their parallax was so small that it was not detected until 1832. In passing I can't help noting that Isaac Newton, as usual, got the right answer! He assumed that the stars are similar bodies to the Sun and calculated how far away the Sun would have to be so that it gave us as much light as a first magnitude star. He found that at that distance the angular size of the Sun would be about 2×10^{-3} seconds of arc which, as we now know, is a reasonable estimate of the angular size of a first magnitude star.

The first successful measurement of the angular size of a star was made by Michelson and Pease in

1920. Using a new type of instrument, a stellar interferometer, they measured the angular diameter of the red super-giant Betelgeuse (α Orionis) to be 0.047 seconds of arc.

Michelson's Stellar Interferometer

A simplified outline of Michelson's stellar interferometer is shown in Fig. 1. Light from a star was received on two small movable mirrors M_1 , M_2 and was reflected to the fixed mirrors M_3 , M_4 which in turn reflected it to the Cassegrain focus of the telescope at O. The mirrors M_1 , M_2 were mounted on a beam, and their separation could be altered at will by the observer. The mirrors were so oriented that the two images of the star were

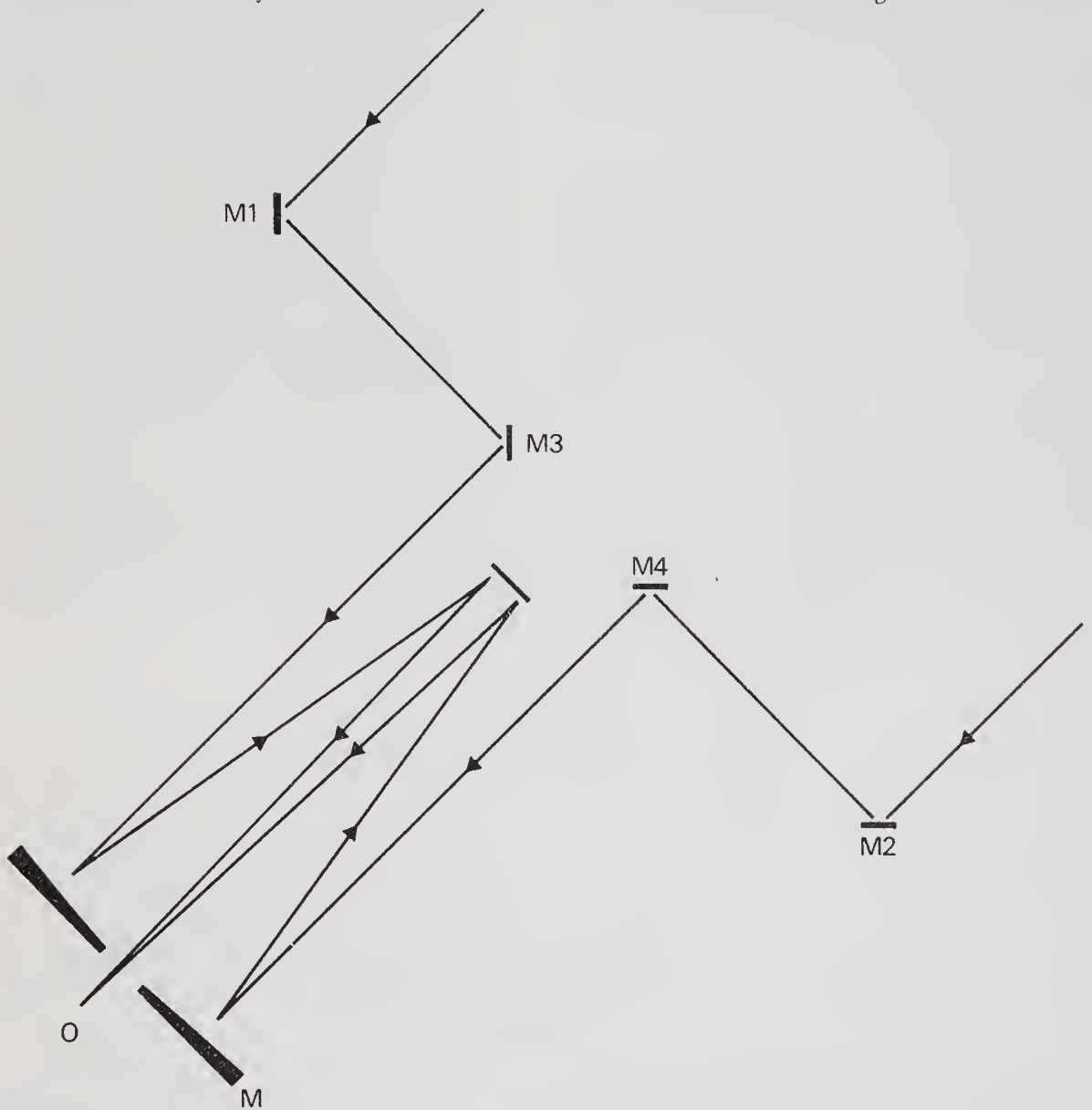


FIGURE 1. A simplified outline of Michelson's stellar interferometer.

superimposed in the focal plane and, when the instrument was in proper adjustment, this image was crossed by alternate bright and dark bands called fringes. The contrast or "visibility" of these fringes is a measure of the "mutual coherence", in other words of the similarity, of the light beams received at the two spaced mirrors. If the spacing between the two mirrors is made very small, so that effectively they are in the same place, then the mutual coherence has a value of unity — that is to say, the two light beams are identical, and the visibility of the fringes is said to be high. As the two mirrors are separated they begin, so to speak, to see different "views" of the star and the mutual coherence, and hence the visibility of the fringes, decreases until they disappear. The exact relationship between fringe visibility and mirror separation depends upon the wavelength of the light used, the angular size of the star, and the way in which the light is distributed across the disc of the star.

Fig. 2 shows how the fringe visibility (V) varies with mirror separation (d) for a star with a uniformly bright disc of angular diameter (θ) when measured with light of wavelength (λ). The curve shows us that as the two mirrors are separated the fringe visibility decreases and falls to zero when they are separated by a distance

$$d = 1.22\lambda/\theta$$

and so, if we measure the separation at which the

fringes disappear, we can find the angular size of the star.

Results with Michelson's Interferometer

The first model of Michelson's interferometer was mounted on the 100-inch Hooker telescope at Mt. Wilson. The observer watched the fringes in an eyepiece and increased the separation of the mirrors until the fringes disappeared; the fringes produced by Betelgeuse disappeared when Pease increased the mirror separation to 121 inches or 3.05 m, giving the angular size of the star as 0.047 seconds of arc.

Pease went on to measure five more stars (see Table I) and that was all the instrument could do. It was limited by the maximum separation between the two small mirrors which was about 20 ft or 6 m. As a consequence the smallest angle which could be measured was 0.02 seconds of arc which, although a very small angle by ordinary standards, is not small enough to measure an average star or "main sequence" star. All the 6 stars measured by Pease are giants or super-giants and are about as representative of the normal stellar population as people over 20 stone are typical of our own.

In an effort to measure more stars, Hale and Pease built a much larger interferometer but, despite determined efforts, it failed to work satisfactorily and the work was discontinued. Let us

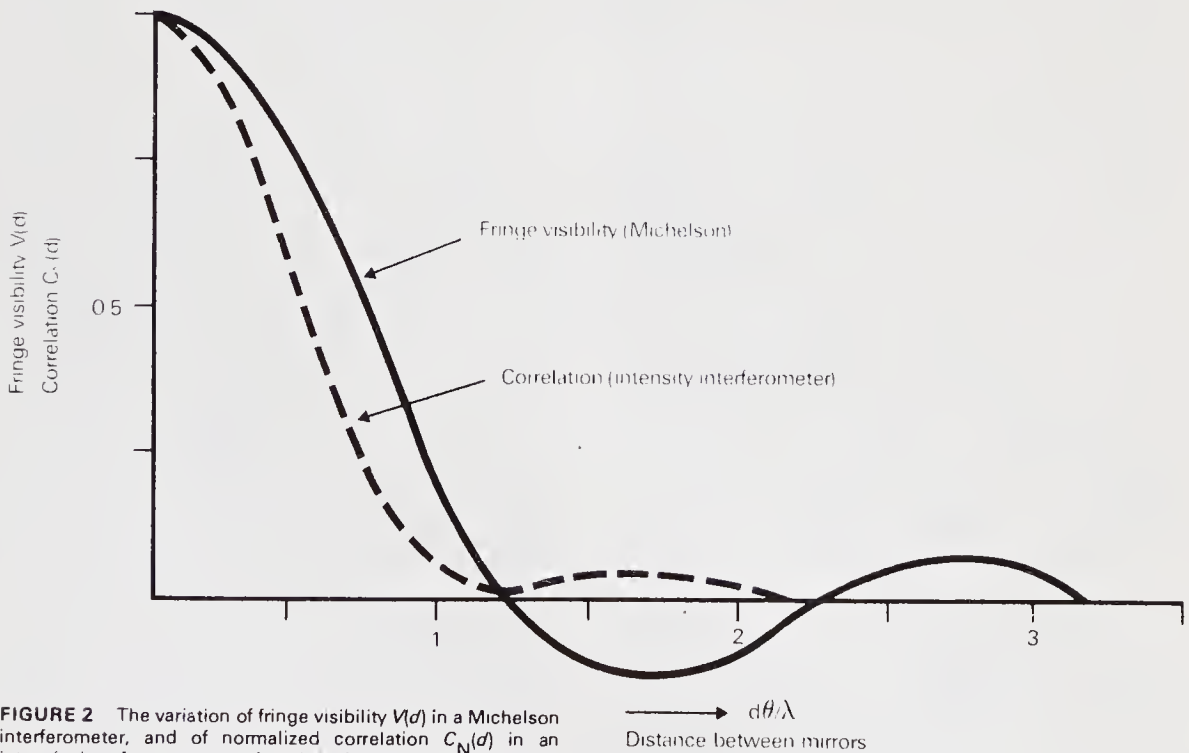


FIGURE 2 The variation of fringe visibility $V(d)$ in a Michelson interferometer, and of normalized correlation $C_N(d)$ in an intensity interferometer, as a function of the distance d between the two mirrors. θ = angular diameter of star, λ = wavelength of light.

now look briefly at two of the major difficulties which prevented this development.

The Limits Set by the Atmosphere and by the Need for Mechanical Precision

Why, we may ask, go to all this trouble? Why not look at the star directly with the 100-inch telescope? After all, as Sir George Airy showed in 1835, the minimum angle θ which a telescope can resolve is given by,

$$\theta = 1.22\lambda/D$$

where D is the diameter of the first lens or mirror. This formula is identical with that for the resolving power of Michelson's interferometer, so why bother with an interferometer? Unfortunately, the light from the stars is randomly bent and delayed on its way to Earth by turbulence in the Earth's atmosphere. The characteristic size of the turbulent elements is about 10 cm and they move with the wind. Because these elements differ in refractive index they introduce random patches of phase and amplitude into the starlight falling on the telescope and, roughly speaking, limit its resolving power to that of a telescope with the diameter of a single patch, roughly 10 cm. As a consequence the actual image of a star seen through a telescope, no matter how large or optically perfect, depends upon the site and the weather but is seldom less than 1 second of arc. In other words, larger telescopes have been built mainly because they collect more light and not because they show us the size of the

stars; for most of the time their angular resolving power is not much better than that of a 10 cm telescope. This is, of course, one of the many reasons why astronomers should migrate to the Moon.

The success of Michelson's interferometer showed that it was not so badly upset by the atmosphere as the 100-inch telescope on which it was mounted; nevertheless, it was by no means immune. As far as we can see it worked because the two little separate mirrors (M_1 , M_2 in Fig. 1) were comparable in size with the 10 cm turbulent elements of the atmosphere and so the phase and amplitude of the light across them was reasonably uniform, at least for short periods of time. They were therefore able to form fringes, although as the patches of "seeing" drifted across the field these fringes moved. In fact the fringes danced about in the focal plane and only when they were not moving too fast could the observer see and measure them. As one might expect, the observed visibility of the fringes depended upon the state of the atmosphere and, as we shall see, these atmospheric effects are one of the major obstacles to measuring the angular size of the stars.

The other great limitation to making an interferometer significantly larger than Michelson's original instrument is the need for mechanical precision. In Michelson's interferometer the two beams of light from the separated mirrors must be brought together at the focus through paths which are very closely equal in length. The maximum difference which can be tolerated depends on the

TABLE I
Stars measured by Michelson and Pease

Star		Type		Angular diameter $\times 10^{-3}$ seconds of arc
Arcturus	∞ Bootis	Giant	K2	20
Aldebaran	∞ Tauri	Giant	K5	20
Antares	∞ Scorpii	Super-giant	M1-M2	40
Scheat	β Pegasi	Giant	M2	21
Mira	σ Ceti	Giant	M6	47
Betelgeuse	∞ Orionis	Super-giant (variable)	M1-M2	34 \rightarrow 47

bandwidth* of light which is to be used; the larger this bandwidth is made the tighter the tolerance. For example, if we choose to look at the fringes by eye with an optical bandwidth of, say, 100 nm then the fringes will vanish completely if the two paths differ by five wavelengths of light. If then we want reasonably accurate results, we must build the instrument with sufficient rigidity, and we must point it at the star with sufficient precision, to ensure that the two paths are equal to about 1 wavelength of light or about half a micron, or, very roughly, one millionth of a metre. That is, I need hardly point out, a very tight mechanical tolerance for a large moving instrument.

These two limitations, the effect of the atmosphere and the need for excessive mechanical precision, prevented the further development of Michelson's interferometer. A second model with a separation of 50ft. (15m) was built around 1930 by Hale and Pease. It proved extremely difficult to see the fringes, let alone to form an estimate of

their visibility and, despite several years work, no reliable measurements of stars were made. It seems that the original 20 ft. (6 m) interferometer was near the limit of technique at that time. Clearly a considerable advance was needed before an instrument which could measure a representative sample of stars could be built. But before we go on to the next stage, let me remind you of what such an instrument must be able to do.

The Different Types of Star

We know from their spectra that stars differ greatly in temperature and in the amount of light which they emit (luminosity). They are classified by their spectral type which, for historical reasons, follows the curious sequence OBAFGKM which corresponds to their surface temperatures. Thus type O stars are hot, blue and large, and type M stars are cool, red and small. If we plot luminosity against spectral type or temperature we get the remarkable pattern in Fig. 3 which is known as a Hertzsprung-Russell Diagram or H-R diagram for short. The vast majority of stars lie on the band marked *main sequence* and are what I mean by *average* stars. They shine by converting hydrogen into helium and their position on the main sequence is determined very largely by their mass; heavy stars are at the hot end and light stars at the cool

* The bandwidth of a beam of light corresponds to the range of wavelengths in the beam. For example visible light is composed of wavelengths between about 400 nm (blue) and 700 nm (red) and therefore has a bandwidth of 300 nm. The bandwidth of the light in an interferometer can be controlled by coloured filters.

1 nm = 1 nanometre = 10^{-9} metre.

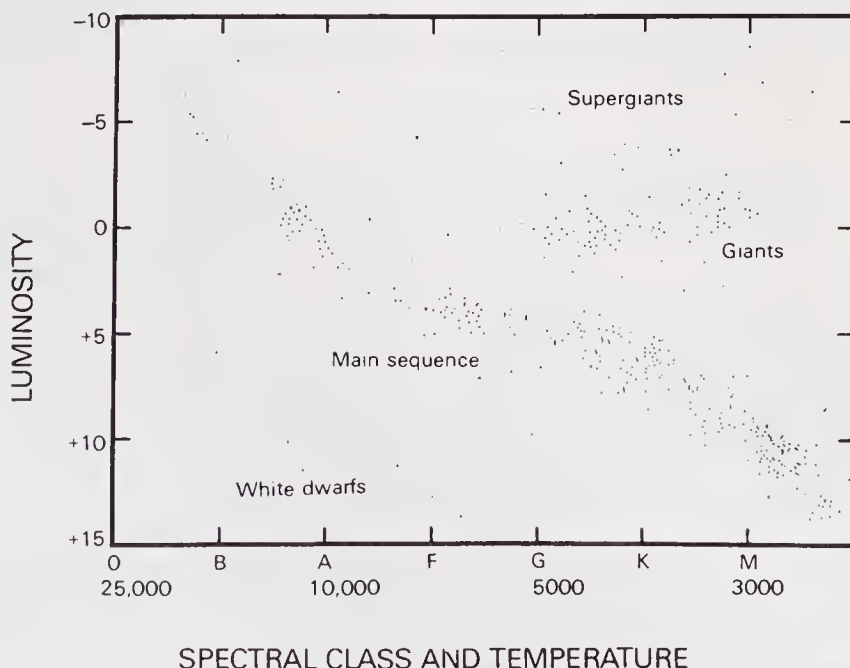


FIGURE 3 The Hertzsprung-Russell diagram for stars of known distance.

end. When they have exhausted a substantial fraction of their hydrogen all sorts of strange things happen. They leave the main sequence and become giants or supergiants, enormously large stars with distended and tenuous envelopes. What happens to them in the end depends largely upon their mass; a given star may blow up as a supernova, evolve into a white dwarf or a neutron star or, perhaps, form one of those darlings of modern astrophysics, a black hole. But we haven't time for all that. The point I want to make is that the vast majority of stars, whose structure and evolution we claim to understand, lie on the *main sequence*; they are the *average* stars. If now we want to measure the angular size of an average star we must be ready to measure extremely small angles, much smaller than the 0.02 seconds of arc which was achieved by Michelson's interferometer.

The actual range of angles which we must measure depends, of course, on how large a sample of the main sequence we wish to make. Contrary to what one might expect, it is the very hot stars which present the greatest difficulty. Although they are physically the largest stars on the main sequence, they are so rare that the nearest specimens are very far from the Earth and hence have a very small angular size. In fact if you want to collect a sample of only 10 of the hottest stars (type O) — and that is very few — you must be prepared to measure an angle of about 10^{-4} seconds of arc; roughly the apparent size of the head of a pin over Perth as seen from Canberra. To do this the separation of the two mirrors of a Michelson interferometer would have to be about half a kilometre!

A new Type of Stellar Interferometer for Measuring the "Radio-Stars"

No further progress was made in measuring the angular size of the stars until a new type of interferometer was developed at the Jodrell Bank Experimental Station of the University of Manchester (U.K.) in 1950. At that time the major problem in radio-astronomy was to discover the nature of the discrete sources of radio waves which had recently been discovered, the two strongest being in Cassiopeia and Cygnus. In those days we called them *radio stars*, but we didn't know whether they were really like stars, nebulae or galaxies. One obvious way to find out something more about them was to measure their angular size. The simplest way of doing this was to make a radio analogue of Michelson's interferometer using two separated antennae and a central radio receiver to record interference fringes as the radio source passed through the antenna beam. However, if these mysterious sources should really prove to be stars, then, to measure them, we would need an

enormously long interferometer; for example, to measure an angle of 0.01 seconds of arc at a working wavelength of 1 m we would need a baseline between the two antennae of 20,000 km. Nowadays it is technically possible to make such an instrument but in those days it would have been extremely difficult. The major technical obstacle was that such an interferometer would require two independent local oscillators with a frequency stability which, at that time, could not be achieved. That was not the only obstacle, but it looked to us to be the worst.

It was to get around this particular difficulty that in 1949 I proposed a new form of interferometer, an *intensity interferometer*, shown in Fig. 4. Two spaced antennae A_1, A_2 were connected to *completely independent* superheterodyne receivers R_1, R_2 which had similar bandwidths and were tuned to same carrier frequency. A narrow band of low-frequencies (1 to 2.5 KHz), in the outputs of their square-law detectors, was selected by band-pass filters and these two low-frequency signals were brought together by radio-link or by telephone line: their *correlation*, or in other words their similarity, was then measured by multiplying them together in a linear multiplier. It can be shown that this correlation $C_n(d)$, when suitably normalized by the signal levels, is equal to the square of the fringe visibility $V^2(d)$ which the source would give in a Michelson interferometer with the same baseline d . Thus,

$$C_n(d) = V^2(d)$$

and by measuring $C_n(d)$ as a function of the separation between the antennae we can find the angular size of a radio star.

This new type of interferometer apparently solved the problem of working with an enormously long baseline: it did not require coherent local oscillators at the two receivers, and the problem of combining their low-frequency outputs seemed to be relatively simple. It could be done by radio link, telephone line or even, perhaps, by tape-recorder. Furthermore, the difficult problem of equalizing the time-delay in the two arms of the interferometer was simplified. The maximum permissible time delay between the two arms of an intensity interferometer is governed by the low-frequency bandwidth of the intensity fluctuations which are taken to the multiplier, and not by the pre-detector bandwidth of the receiver; in practice this makes it much simpler to control the time-delay in an instrument with a long baseline.

The way was now clear to measure the angular size of the radio stars. We built the first instrument on 125 MHz and tested it on the Sun. It worked according to plan and we started to measure the two principal radio stars in Cygnus and Cassiopeia.

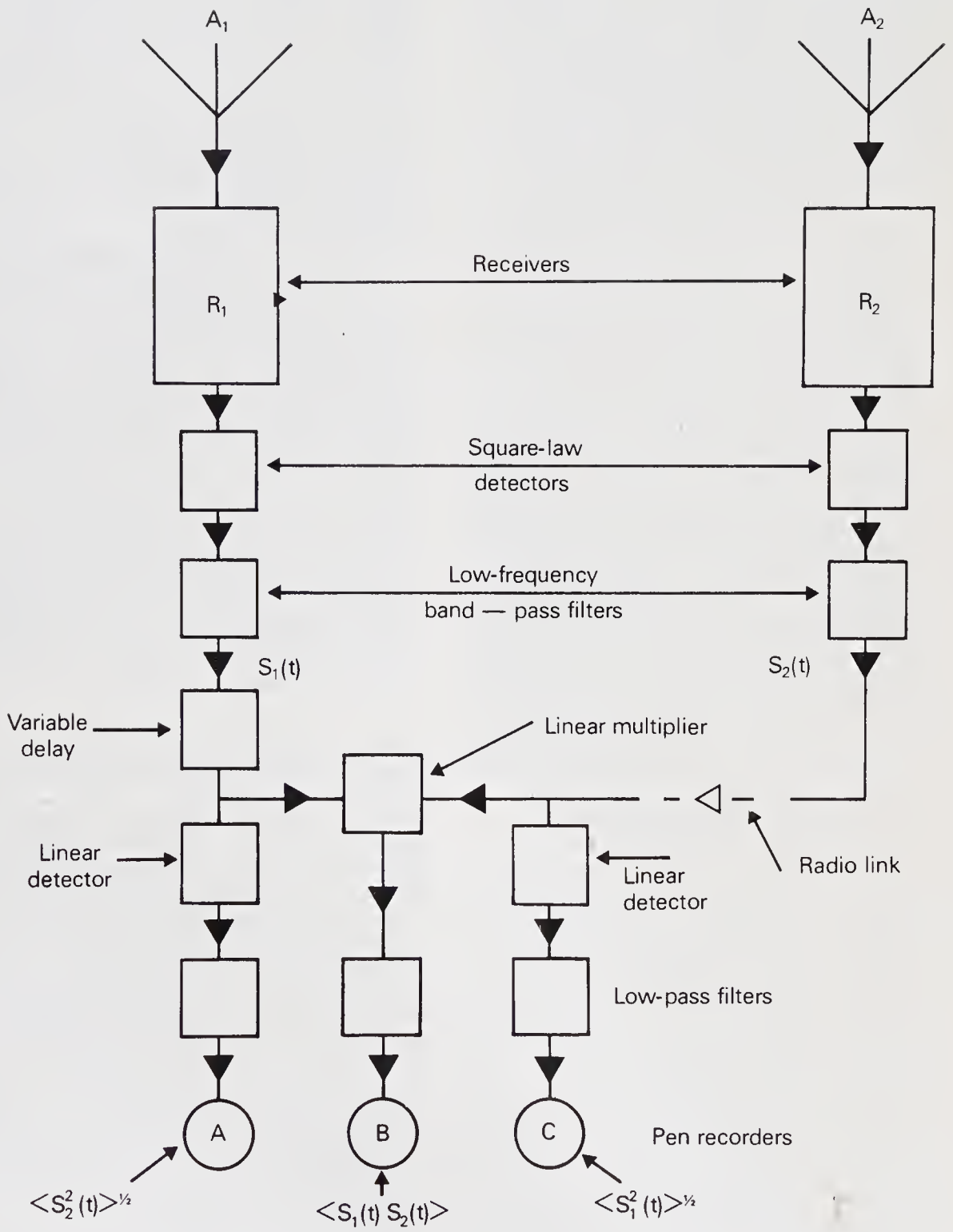


FIGURE 4 A simplified outline of a radio intensity interferometer.

Much to our surprise we didn't need a baseline of 20,000 km; we resolved both the sources with baselines less than 4 km. The radio stars were not stars at all, they were much bigger. We had used a steam-roller to crack a nut. The work could have been done — as it was done elsewhere — with a “Michelson” radio interferometer. All the same, it was all worth while because it showed us how to solve the problem of making an optical interferometer with the necessary resolving power to measure a reasonable sample of main-sequence stars.

The Theory of an Intensity Interferometer for Light Waves

It was while watching our first radio intensity interferometer in operation that my colleague, Richard Twiss, and I realized that we had overlooked one of the principal features of an intensity interferometer — it works well through a turbulent medium. Much to our surprise the measurements of the radio stars were not significantly affected by violent scintillations due to turbulence in the ionosphere. We couldn't help wondering whether the same principle might not be applied to make an optical stellar interferometer which would overcome the effects of turbulence in the atmosphere. We decided to look into the theory of an intensity interferometer for light waves.

Although in principle the theory is the same for radio as for light, it is much easier for a radio engineer to understand and accept an intensity interferometer than a physicist. At first sight, a radio engineer fails to see how the thing can possibly work because, by using independent radio receivers, the relative phase of the “signals” at the two separated antennae is irretrievably lost; under those circumstances it is difficult to see how there can be any “interference”. The answer is that although the relative phase of the two “high-frequency signals” from the source is indeed lost, the relative phase of the “low-frequency” fluctuations in their intensities is not. If in a classical Michelson interferometer we measure both the amplitude (V) and phase (θ) of the fringe patterns as seen with different lengths of baseline, then we can extract from this information both the absolute position of the source in the sky and the angular distribution of brightness across the source. If in an intensity interferometer we measure only the correlation between the low-frequency fluctuations in intensity then all we can find is the square of the fringe visibility $|V^2|$ and not its phase. This gives us no information whatever about the position of the source in the sky but it does give us some, but not all, of the information which we want about the angular size of the source. In

principle the angular distribution of brightness across the source is given by the Fourier transform* of $V\theta$; if therefore we measure only $|V^2|$ and throw away θ , our knowledge of the true angular distribution is limited. The extent to which we can reconstruct the true distribution from $|V^2|$ alone is too lengthy and complicated a subject to discuss here. Broadly speaking, if one is prepared to assume a model for the source, for example that it is centro-symmetric, then one can find the angular distribution from a knowledge of $|V^2|$ alone. For most of our work described here such an assumption was perfectly adequate.

The operation of an intensity interferometer can be explained quite simply using Fourier analysis, and can also be visualized by thinking, for example, about the relative phase at two separated radio receivers of an audio-frequency note modulated onto a carrier. In fact we had little trouble convincing radio engineers and radio-astronomers that our interferometer was sound in principle. Not so the physicists — radio engineers don't worry about photons, but physicists do, and it is the behaviour of photons in an intensity interferometer which worries them.

Consider for a moment the simple intensity interferometer for light waves shown in Fig. 5. Light from a star falls on two separated photoelectric detectors and gives rise to the photoelectric currents (i_1, i_2). The low-frequency fluctuations in these currents are correlated in a linear multiplier and, as in the radio interferometer, the normalized output of this multiplier is proportional to the square of the fringe visibility in a classical Michelson interferometer. The angular size of a star can therefore be measured by observing this correlation for different spacings between the phototubes.

This optical system can be analysed much in the same way as the radio interferometer if we recognize the fact that the probability of emission of a photoelectron is proportional to the intensity, that is to say to the square of the amplitude, of the incident light. It follows that the photoelectric surface may be treated in the same way as a square-law detector in a radio receiver. In fact Richard Twiss and I showed that in the photoelectric current there are two fluctuating components, *wave noise* due to fluctuations in the

* The angular distribution of brightness over a distant source of light can be represented as the superposition of a set of harmonic variations of brightness with different angular frequencies, in the same way as a short burst of sound may be analyzed into component frequencies. The amplitude and relative phase of these frequencies is given by the Fourier transform.

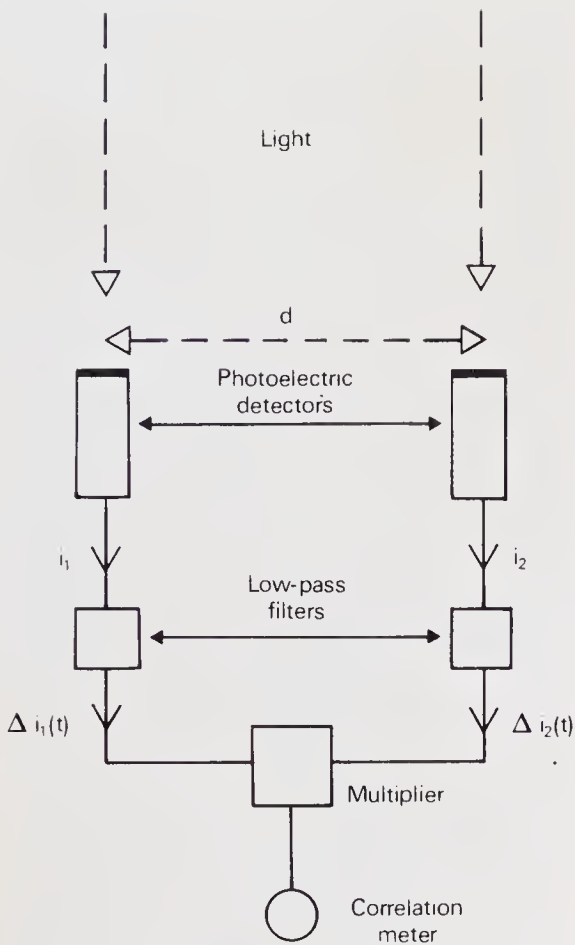


FIGURE 5 A simplified outline of an intensity interferometer for light waves.

intensity of the incident light and *photon noise* due to the discrete charge of the photoelectrons. The same thing is true of the output of a radio receiver; at radio wavelengths wave noise is much greater than photon noise, because the radio photon has little energy; at optical wavelengths the photon noise is much greater than the wave noise because the energy of the optical photon is large. It is, of course, the two wave noise components, corresponding to the fluctuations in intensity, which are correlated in both optical and radio interferometers.

Thus the theory of an optical intensity interferometer is straightforward if one thinks of light as a wave. Admittedly one must calculate the random fluctuations due to photon noise because they limit the sensitivity, but that is a familiar source of noise in all phototubes and vacuum tubes.

The trouble really started when we proposed the interferometer shown in Fig. 6. The light from the star falls on two separated phototubes, which are capable of resolving the pulses of current due

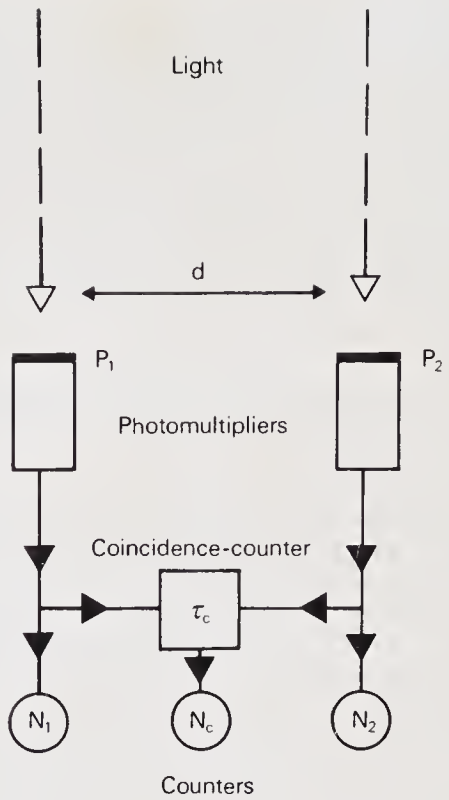


FIGURE 6 A simplified outline of a coincidence-counting intensity interferometer for light waves.

to single photons. The outputs of these phototubes are taken to a coincidence counter which registers a coincidence if two photons arrive within a time τ_c of one another. We showed that the coincidence rate of photons arriving at the two phototubes is a function of the mutual coherence of the light at the two photocathodes; when the coherence or fringe visibility is high, the coincidence rate is high and vice-versa. In fact the angular diameter of the star can be measured by observing the coincidence rate, when suitably normalized for signal levels and corrected for random coincidences, as a function of the separation between the phototubes. We also showed that the performance of the *coincidence-counting* interferometer in Fig. 6 is equivalent to that of the "linear-multiplier" interferometer in Fig. 5, provided that both systems receive the same number of photoelectrons per unit optical bandwidth and that the resolving time of the coincidence counter is equal to the reciprocal of the electrical bandwidth of the linear multiplier. In short, we analysed the performance of a photon-

counting system by quantum theory and showed that it is completely equivalent to one in which light is treated as a wave.

To a surprising number of physicists, brought up to think of photons as being rather like ping-pong balls, the idea that photons should arrive in pairs when the light at the two detectors is mutually coherent was patently absurd. They told us so in person, brandishing a copy of one of the sacred texts of quantum theory (Dirac, Schrödinger, Heitler and so on), by letter, in publications and by actually doing experiments which showed that we were wrong. At the most basic level they would ask how, if photons are emitted at random by a red-hot poker, can they appear in pairs at two detectors — how do they team up, do they wait for each other? At a more sophisticated level, they would point out that the number of photons in a beam of radiation and the phase of the beam are non-commuting operators and that our system was invalidated by an uncertainty principle. There were many other objections and laboratory experiments were performed, for example in Canada and Hungary, which showed that we were wrong.

We tried our best to answer all these objections and to quieten people down. Not only were we interested in seeking truth but also money. We wanted to raise enough money to build a full-scale interferometer, and raising funds for an unconventional project is not made easier by a considerable body of opinion which regards the whole proposal as 'unsound'. In fact most of these objections were answered directly out of the sacred texts of quantum theory. There are really no problems once one has accepted the fact that quantum theory is not a mental picture of what light is "really" like, but is a method of calculating what will probably happen in a particular situation. We found people reluctant to accept the idea that a photon cannot be visualized as a discrete object in flight from emission to absorption. We had to convince them that the concept of photons is limited in use to processes of emission and absorption and can be very misleading as a picture of light "on the wing".

To answer the experimental evidence that photons are not correlated in coherent beams of light we had to take a good hard look at the experiments. In all cases it turned out that the people concerned had not worked out an adequate theory of the effect and were working with experimental arrangements which were far too insensitive to detect the correlation. For example, we analysed the Hungarian experiment in detail; at first sight it looked quite a reasonable experiment, but our analysis showed that it would have taken

100 billion (10^{11}) years to show a significant correlation!

To cut a long story short, we published a complete theory of the intensity interferometer and carried out three laboratory experiments to verify it. In two of these experiments we used a linear multiplier to show the correlation between the fluctuations in two coherent beams of light from a high-pressure mercury arc. In one experiment, performed in Sydney by Richard Twiss and Alec Little, we used a coincidence-counter to show the coincidence between the arrival times of photons in two coherent beams from a mercury isotope lamp.

A Pilot Model of an Optical Stellar Interferometer

By the end of 1954 we were ready to build a pilot model of a stellar intensity interferometer to demonstrate that the method actually worked and to verify our prediction that the measurements would not be significantly affected by atmospheric scintillation. We chose to measure the brightest star in the sky, Sirius (α Canis Majoris), a main-sequence type A star whose angular size had never previously been measured. To save time and money I borrowed two large anti-aircraft search lights from the Army (see Fig. 7). They had reflectors 156 cm in diameter; we removed their arc lamps and substituted photomultipliers. The electronic "correlator" had to be built from scratch and proved to be quite a difficult technical problem; the overall electrical bandwidth of the correlator and phototubes was about 38 MHz.

Observations of Sirius were made for a total time of 18 hours. As seen from Jodrell Bank, Sirius reaches a maximum elevation above the horizon of 20 degrees and can only be observed for a total of 4 hours on any one night. That part of England is not noted for its clear skies — it is even worse than Canberra — and it took us about five months to get 18 hours of clear sky without moonlight. The measurements were made at four different baselines between 2.5 and 9 m and the results gave an angular diameter of Sirius of $7.1(\pm 0.55) \times 10^{-3}$ seconds of arc. Our best modern value, as measured some years later at Narrabri Observatory, is $5.89(\pm 0.16) \times 10^{-3}$ seconds of arc.

The experiment demonstrated that the method worked and gave a result which was in reasonable agreement with the theoretical size of Sirius as deduced from its spectrum and its brightness. Sirius, being at such a low angle of elevation, was always scintillating violently and so it was not possible to compare the measurements with and without scintillation. Apart from the fact that the system worked, we learned some simple, but

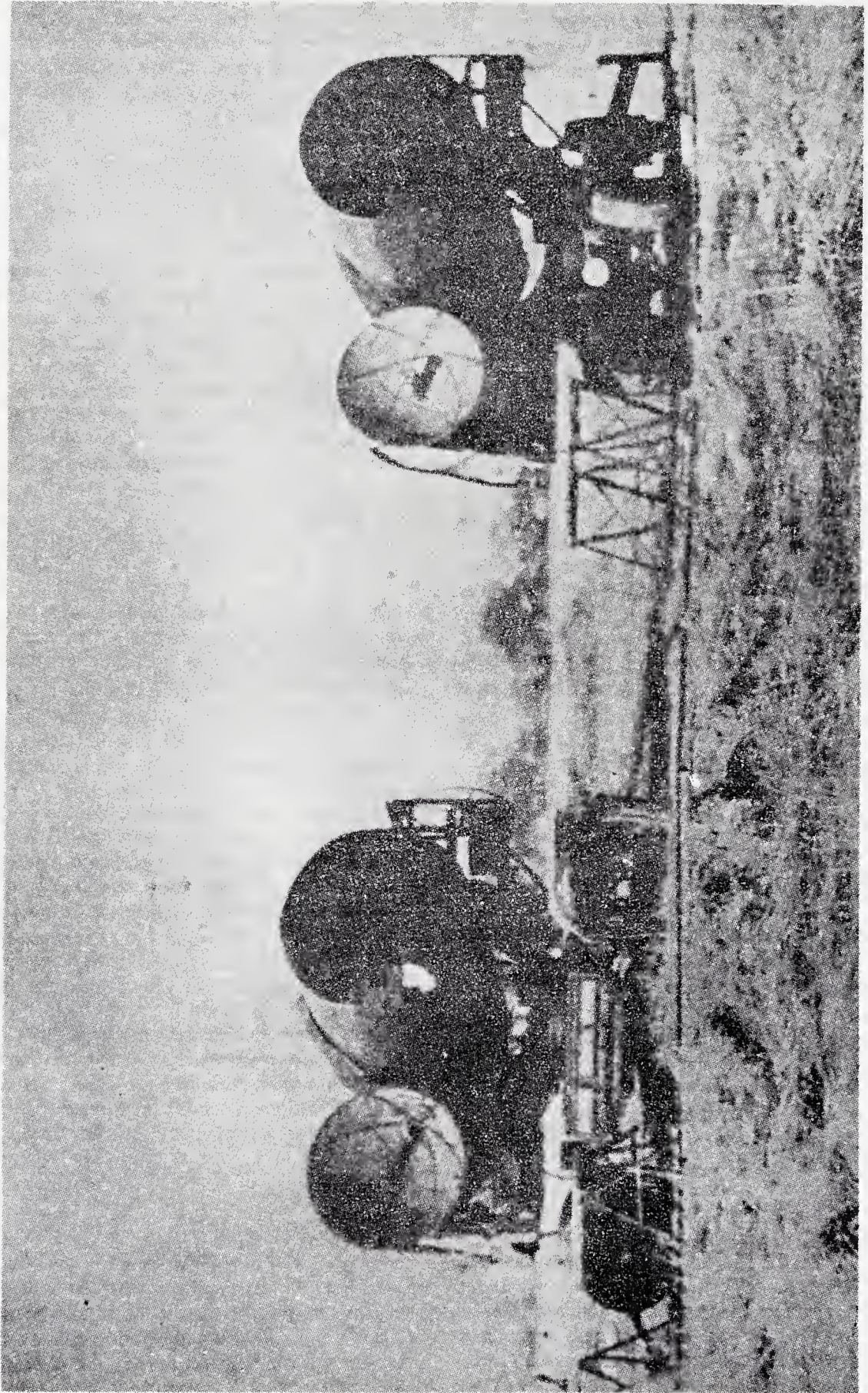


FIGURE 7 Pilot model of intensity interferometer used in 1955 to measure the angular diameter of Sirius.

useful, lessons from this pilot experiment. We learned, for example, that it is essential to screen the leads from the phototubes to the correlator with extreme care in order to exclude radio and television signals. We also learned that dew forms on large exposed mirrors at night and that it is essential to heat them.

The Stellar Intensity Interferometer at Narrabri Observatory

By 1956 we were ready to build a full-scale instrument to measure a reasonable sample of main-sequence stars. The size of this sample would be limited by the size of the light-collectors which we could afford. Our original aim was to build an instrument capable of measuring about 200 stars and costing less than £100,000 sterling, and we proposed to instal it in Haute Provence. In the event we designed an instrument which would measure about 50 stars, cost £225,000 and we installed it at Narrabri in New South Wales. I won't bother you with the details of raising the money, which, in those days was difficult enough but easier than it is now. Suffice it to say that most of the funds came from the Department of Scientific and Industrial Research in the U.K. with the help of Professor P. M. S. Blackett (later Lord Blackett) and from the Nuclear Research Foundation with the help of Professor Harry Messel. In the later stages a very helpful contribution to the capital cost and the running expenses was made by the United States Air Force — those were the golden days before the Mansfield Amendment which, as you may remember, insisted that funding of research by military agencies in the U.S.A. must be "mission-oriented".

Most of the instrument was built in U.K.; the glass mirrors and the electro-hydraulic motors were made in Florence. Delivery of the instrument to the Narrabri Observatory of the School of Physics (University of Sydney) started in January 1962.

The Equipment

The general layout of the interferometer is shown in Fig. 8. The light from the star was received on two very large reflectors carried on trucks running on a railway track laid in a circle 188 m in diameter. These mobile trucks were connected to a central control room by cables suspended from catenary wires attached at one end to a tower in the centre of the circle and at the other to a tender towed by each truck.

The reflectors themselves are shown in Fig. 9; they were 6.5 m in diameter and were each composed of 252 hexagonal mirrors in a paraboloidal mosaic with a focal length of 11 m.

Following our experience in U.K., each mirror was heated by a pad to prevent the formation of dew. At the focus of each reflector there were two phototubes; a main "signal" phototube which received most of the light and an auxiliary phototube for automatic star-guiding. An optical system in front of the main phototube defined the wavelength and bandwidth of the light received; for most of the time we used optical filters with a centre wavelength of 443 nm and a total bandwidth of 10 nm.

The movements of the two reflectors were controlled by an analogue computer. To follow the star in azimuth the reflectors moved around the track, and to follow it in elevation they tilted about a horizontal axis. To compensate for irregularities in the track, the pointing of the reflectors was automatically corrected by the star-guiding phototubes. The length of the baseline could be controlled from a minimum of 10 m to a maximum of 188 m and, while observing a star, the reflectors moved as though they were joined together by a beam which was always at right angles to the direction of the star. This arrangement has two great advantages: firstly, the length of the effective baseline remains constant throughout an observation; secondly, the problem of equalizing the pathlengths in the two arms of the interferometer is greatly simplified.

The output currents of the main phototubes were carried to the central control room by coaxial cables suspended from the catenary. In the control room they were connected to an electronic correlator which amplified the fluctuations in the two phototube currents in a bandpass of 10–100 MHz, and then multiplied them together and printed out their product or *correlation* every 100 seconds together with several other quantities such as the amount of light received by each mirror from the star. The electronic correlator was the hardest part of the whole installation to develop because, by conventional stands, the correlations which we had to measure were extremely small. We were, for example, concerned to measure reliably integrated correlations with an r.m.s. signal/noise ratio of the order of 3/1 in a period of several hours; this places very severe limits on the maximum permissible zero-drift in the correlator output. We solved this problem by a rather elaborate system of "phase-switches", but it took us a long time to do; nowadays it would be much easier using high-speed digital electronics.

It was not easy to put such a complicated instrument together in the bush, but by August 1963 we had it working sufficiently well to measure the bright star Vega (α Lyrae), the same star as Galileo had tried to measure 350 years before. We

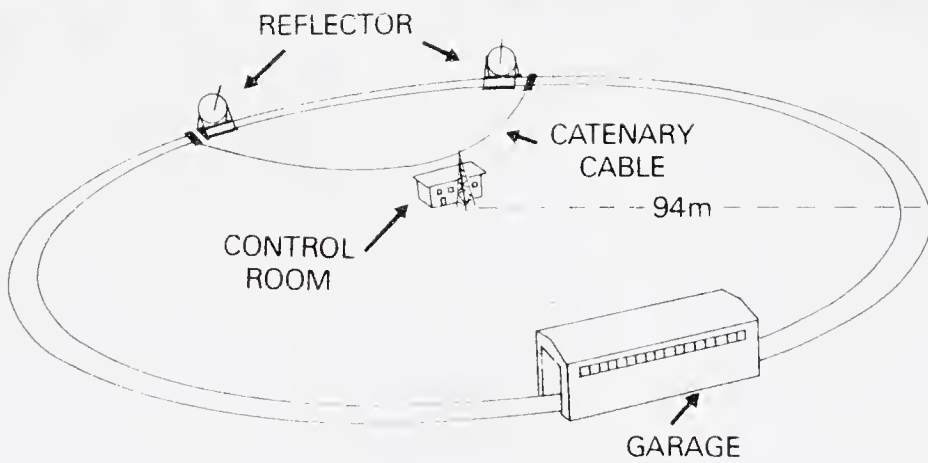
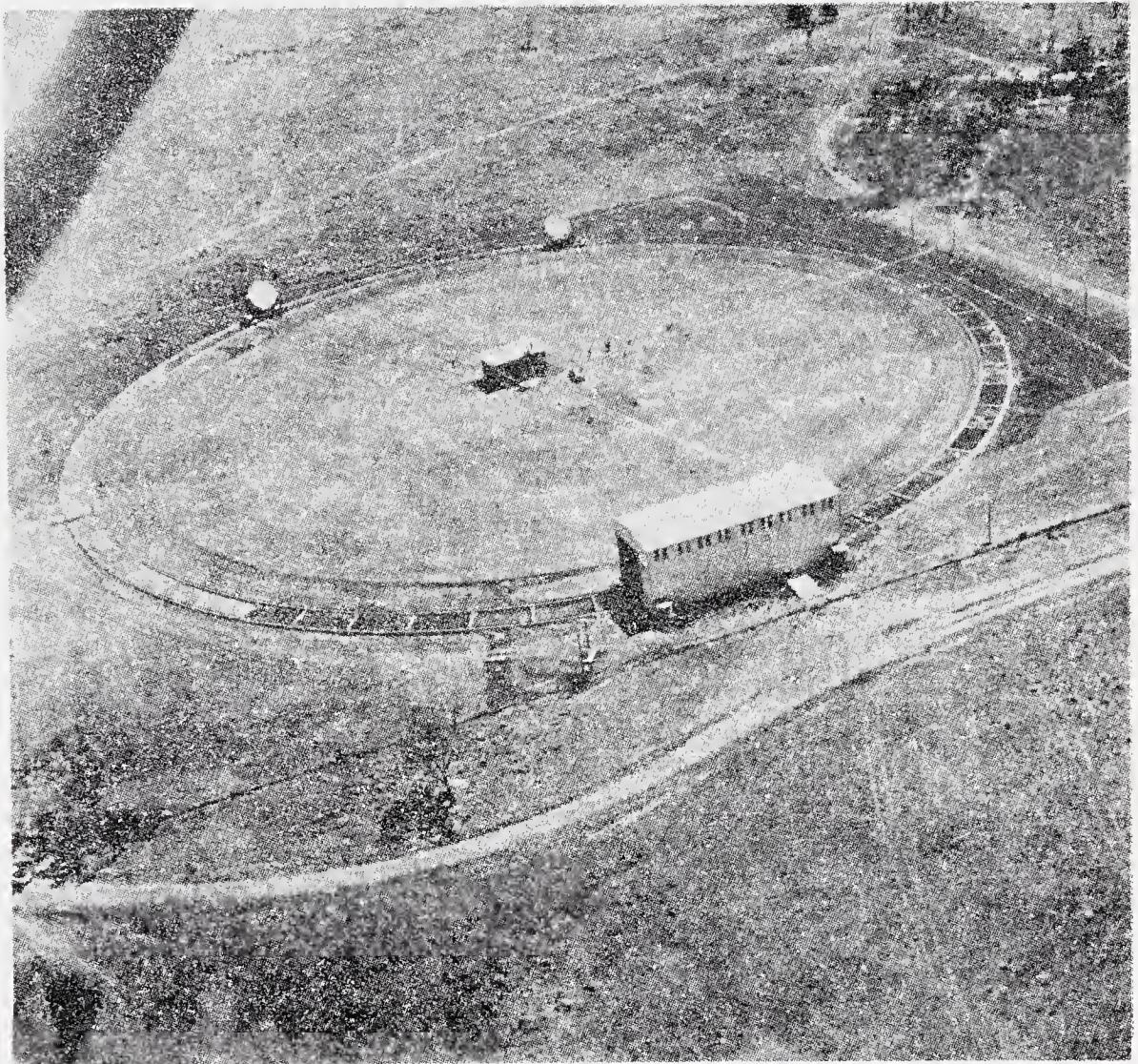


FIGURE 8 Aerial view of the intensity interferometer at Narrabri Observatory in New South Wales

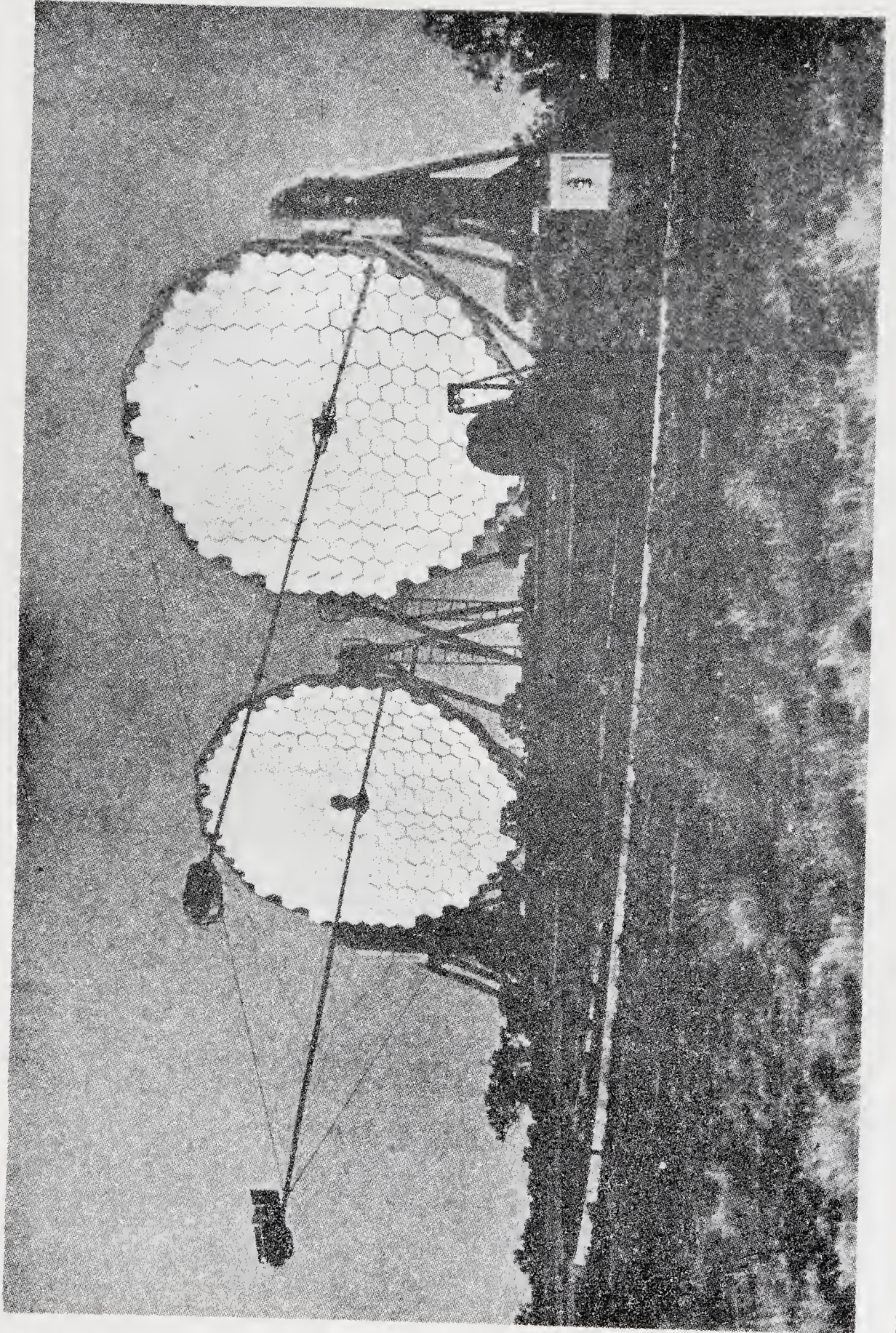


FIGURE 9 The two reflectors of the intensity interferometer at Narrabri Observatory.

started the main observing programme in May 1965. It required 2500 hours of actual exposure to stars under conditions of low wind, no moon and clear sky, and it took seven years to complete.

Our work at Narrabri had three principal objectives. Firstly, we aimed to make a worth-while contribution to stellar astronomy by measuring a significant sample of single stars. Secondly, we explored some of the many other applications of high-angular resolving-power to observational astronomy. Thirdly, we developed the technique itself.

The Angular Diameters of Single Stars

In the course of a seven-year observing programme we measured 32 single stars in the spectral range type O to type F; some of them were measured more than once to establish the repeatability of our results. Our sample of stars was limited by the sensitivity of the equipment to stars brighter than magnitude + 2.5 and hotter than the Sun (type G). Thus, to measure the angular size of a star of magnitude + 2.5 with an uncertainty of about ± 5 per cent required an exposure of at least 100 h. The sample was not limited by the resolving power of the instrument; with a baseline of 188 m it was capable of resolving an angle of 2×10^{-4} seconds of arc which was more than adequate for any star bright enough to measure.

Our measurements were combined with observations of light-flux and parallax to give three important pieces of information about these 32 stars. Firstly we found their *emergent flux* or, in other words, the amount of radiation which is emitted by unit area of their surface. At first sight it seems rather odd that one can find out how bright the actual surface of a star is without going there, but in fact one can. Thus if we combine our measurement of the angular diameter θ with a photometric measurement of the light flux F_λ received from the star at a wavelength λ , then the light flux F_λ emitted by unit area of the star's surface is,

$$F_\lambda = 4f_\lambda/\theta^2$$

These values of F_λ are fundamental to a comparison of actual stars with theoretical models of stellar atmospheres.

If now with a photometer we measure f_λ over the whole spectrum of the star, we can find another fundamental piece of information, its *effective temperature* T_e , where

$$\sigma T_e^4 = \int_{\lambda} f_\lambda d\lambda$$

and σ is Stefan's constant.

For our 32 stars we combined our measurements of angular size with photometric measurements of

their flux distribution to find their effective temperatures. Most of the photometry was done on the ground using conventional methods, but for the hotter stars, where much of the radiation is ultra-violet and does not reach the Earth, the measurements were made from the Orbiting Astronomical Observatory (OAO-2) in collaboration with the University of Wisconsin. Using these results we have established a scale of effective temperature for stars in the spectral range type O to type F. These effective temperatures provide an essential link between the observed properties of stars and the theories of stellar structure and atmospheres. Previous determinations of the temperature scale have been made by comparing the theoretical spectra of stars at different assumed temperatures with the observed spectra of stars of different spectral types. Thus, the significance of our results is that they give the first temperature scale for hot stars to be based entirely on *measurements* and not on theory. At one end of the scale is the type O star ζ Puppis with an angular diameter of about 0.4×10^{-3} seconds of arc and a temperature of 32,500 deg. K; at the other end is the type F star, α Canis Minoris (Procyon) with an angular diameter of about 5.5×10^{-3} seconds of arc and a temperature of 6,500 deg. K.

An Exploration of the Uses of an Interferometer

Although measuring the angular sizes and temperatures of single stars was the main programme, the bread and butter, of Narrabri Observatory and took an unconscionable time, we did manage to fit in some other interesting experiments. We were mainly concerned, not with the future of the existing interferometer, but with the possible uses of a new and more sensitive instrument which we hoped some day to build.

One of the most interesting experiments which we did was to observe the bright spectroscopic binary star Spica (α Virginis). We observed this star for a total of 115 hours and recorded the correlation in 10-second intervals at a number of different baselines. We then put these observations, roughly 40,000 of them, into a computer and compared them with a theoretical model of a binary star in which all the parameters could be varied. Our model of a binary star had 13 parameters of which 6 [e.g. period, epoch and eccentricity of the orbit] were already well-known from spectroscopic observations. We found the remaining 7 parameters which cannot be found spectroscopically [e.g. the inclination of the orbit] by optimizing the match between the model and the observations in the computer. In this way we reached a complete description of Spica. An

interesting feature of this description is that it included the *distance* of Spica which we found from the spectroscopic measurements of velocity, the apparent angular size of the orbit and its angle of inclination. We found the distance of Spica from the Earth to be 84 ± 4 parsecs or 275 ± 13 light years. It is interesting to note that the uncertainty in the distance of Spica derived by measures of parallax is roughly ± 50 per cent. Thus our result is roughly 10 times more accurate than the conventional measurement and is by far the greatest stellar distance to be known accurately.

There were several other interesting experiments which we managed to do. I will only mention some of them briefly to show that there are many new things, besides measuring angular sizes, which one can do with a high-resolution interferometer. For example, we tried to measure the "limb-darkening" of Sirius or, in other words, the distribution of light over its disc; we didn't succeed completely, but we got a long way towards it. We looked for evidence of a corona surrounding the hot star Rigel (β Orionis) by comparing its angular size in two orthogonal polarizations and hoping to see the effect of light scattering by electrons in the corona. We measured the apparent angular size of the bright Wolf-Rayet star γ Velorum in a narrow spectral line and found the size of the emission region surrounding it. We explored the effects of rotation on the apparent shape of the rapidly rotating star Altair (α Aquilae).

There was, however, one attractive experiment we could not do. In principle it should be possible to establish the distance of a Cepheid variable by measuring the changes in its angular size as it pulsates and combining these changes with spectroscopic measurements of the motion of its atmosphere. Such an experiment might give an independent calibration of the Cepheid distances and would be well worth trying. Unfortunately there were no Cepheids bright enough for the Narrabri interferometer to measure. Nevertheless the experiments which we did succeed in doing showed, beyond doubt, that there are many new and valuable measurements on stars which could be made with a more powerful instrument.

Development of the Technique

In this programme we sought to understand as completely as possible the operation and limitations of the stellar intensity interferometer. As one of the major advantages claimed for the technique is that the measurements are not significantly affected by atmospheric scintillation, we set out to test this claim on Sirius. Firstly, on the assumption that the effects of scintillation are likely to vary from night to night, we compared the dispersion

in the correlation observed on 126 nights with the dispersion expected due to the random noise alone: there was no significant difference. We also measured the correlation from Sirius as a function of its elevation above the horizon and, at the same time, recorded the scintillation index. We showed that there was no significant variation of correlation with scintillation even when the star was observed at only 15° above the horizon. It is in fact quite remarkable how free the observations are from the effects of the atmosphere.

Another important thing we did was to search for possible sources of false correlation. In particular we looked at two interesting possibilities, the effect of Cerenkov light pulses from the night sky due to cosmic rays and the possibility that starlight is modulated by radio waves in passing through the ionosphere. The first of the effects, the correlation due to Cerenkov pulses, had been advanced, some years before, as a serious objection to our whole programme. To investigate this effect we replaced the electronic correlator by pulse-counting equipment and measured the rate of coincident Cerenkov pulses with different separations between our two reflectors and also as a function of relative alignment. Our experiments put the effects of Cerenkov radiation on a firm quantitative basis. They showed that any false correlation due to Cerenkov pulses was negligible in the Narrabri interferometer and would remain negligible in a more sensitive instrument.

The modulation of starlight by radio waves in the ionosphere was reported in 1971 and, although it appeared to us to be highly improbable, we considered it worth while to look for it. We examined the spectral distribution of the output noise from our phototubes in the spectral range 0–100 MHz when looking at bright stars; we failed to see any modulation.

There were many other technical experiments to check the reliability of the measurements and I will not describe them here. Suffice it to say that we established to our own satisfaction that the measurements made by the interferometer were reliable and repeatable and that, as far as we could detect, they were free from any significant systematic errors.

The Next Step

Long before the programme at Narrabri was finished (in 1972) we had started to think about the next step. A careful look at the existing interferometer showed that a worth-while improvement in performance could not be achieved by any reasonable programme of modifications. As so many research workers have done before us, we came to the conclusion that what we really

needed was a larger and more expensive instrument! We made a detailed study of all the astronomical programmes which we wanted to carry out and reached the conclusion that the ideal next step would be to develop a new instrument, 400 times more sensitive and with a resolving power 20 times higher; in other words, it would reach stars of magnitude +9 and resolve an angle of about 10^{-5} seconds of arc.

The next question was how to achieve this step forward and, not surprisingly, we haven't answered it yet, although we think we know how to do it. Our first obvious move was to design a more powerful intensity interferometer. In a very detailed study which took us, off and on, about 4 years we reached the conclusion that we could not achieve our ideal sensitivity (magnitude +9); it was relatively easy to achieve a resolving power of 10^{-5} seconds of arc. We therefore designed the largest instrument which we considered practicable to build and finance. The layout was radically different from the Narrabri instrument and is illustrated by the model shown in Fig. 10. Four flat coelostat mirrors ran on a straight railway track, several kilometres in length, and reflected the light from the star into four fixed paraboloids each 15 m in diameter. The instrument operated simultaneously in 10 different spectral channels and had an electrical bandwidth of 1000 MHz. We estimated that it would reach stars of magnitude +7.3 in an exposure of 100 hours; in other words, it would be 100 times more sensitive than the Narrabri instrument. The estimated cost was about \$A3m in 1972 dollars.

There is little doubt that this very large intensity interferometer would, if it were to be built, make a substantial contribution to stellar astronomy. Nevertheless it would be both large and expensive and, taking a long-term view, we considered it important to find out, before we committed our small group to a lifetime of building a larger intensity interferometer, whether or not there was a better way of doing the job. There were three contemporary developments which made us think, a small double-star "Michelson" interferometer using "active optics" developed at Monteporzio (Italy) by Richard Twiss, a "speckle interferometer" in France, and the increasing use of the Moon to occult radio sources and visible stars. We looked carefully at all these things and came to the conclusion that although "speckle interferometry" offered high sensitivity it did not look to be the most promising way of getting the high accuracy which our stellar programme demands. We had learned in our contacts with astrophysicists that most of the interesting questions in stellar astronomy demand high precision; it is of little use to measure

angular sizes with a precision of 10 per cent when what is really needed is 1 or 2 per cent. Much the same thing could be said about the occultation of stars by the Moon. The technique did not appear to offer us the high resolution, high precision and flexibility which we were seeking. It is limited to the occasional measurements of stars which the Moon happens to occult and is therefore totally unsuitable to most of the programmes in which we were interested.

To cut a long story short, we reached the conclusion that a modernized form of Michelson's stellar interferometer might, as far as we could see, offer us the superior economy and sensitivity which we sought. In theory a Michelson interferometer, in which the two beams of light are brought together before they are detected, offers a higher sensitivity than an intensity interferometer in which the two beams are detected separately. A Michelson interferometer therefore uses smaller light collectors and should be not only more sensitive but cheaper to build provided, of course, that the two major problems of atmospheric scintillation and the need for very high mechanical precision can be overcome.

As far as we could see there was a good chance that both these problems could be solved by modern techniques (narrow-band filters, photoelectric detectors, active optics, laser-controlled servos, etc.) which were not available to Michelson. We estimated that, using all these "modern conveniences", a Michelson interferometer might be built to reach stars of magnitude +8 or perhaps +9 with exposures of a few hours and that, if everything went as we expected, it should be possible to build an instrument with a baseline of several hundred metres to achieve most, but not all, of the resolving power we sought.

Modernizing Michelson's Stellar Interferometer

Reluctantly we put the plans for a larger intensity interferometer on one side and started work on a pilot model of a modernized version of Michelson's interferometer. As a first step we are building an interferometer with a fixed baseline of 11 m to measure a few of the bright stars which were measured at Narrabri so that we can check its results. At each end of the 11 m baseline there are two small coelostat mirrors mounted on concrete plinths; they reflect the light from the star into pipes which can, if necessary, be evacuated and which carry the light to the optical system in the centre. This optical system is quite complicated (Fig. 11) and I am not going to describe it in detail; but I shall point briefly to some of the main features which differ from Michelson's original

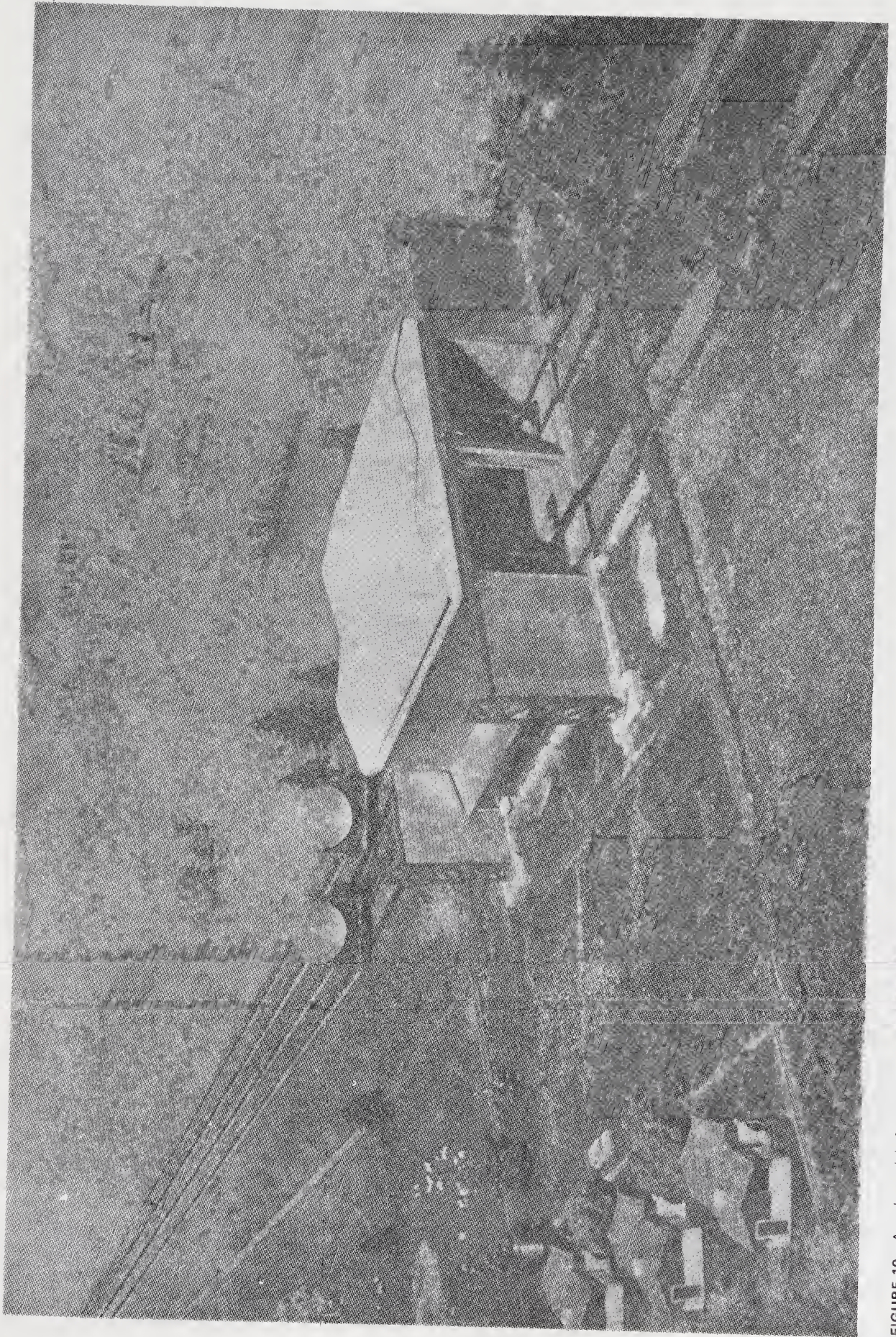


FIGURE 10 A scale model of a very large intensity interferometer using four coelostats running on straight tracks. The central building houses four stationary paraboloids.

instrument. First of all the whole instrument does not move. The equalization of the path differences in the two arms is therefore not achieved, as it was in the original instrument, by pointing the whole thing at the star; it is carried out by "optical path length compensators" (OPLC) which consist of retro-reflectors moving on linear tracks under the control of a computer and a laser fringe-counting interferometer. The effects of atmospheric scintillation are minimized in three ways, firstly by the use of small mirrors, which restrict the phase and amplitude variations of the starlight over the input beam, and secondly by the use of "active optics" which remove the effects of angular scintillation. The small mirrors (T) are tilted by a high-speed servo-system and piezo-electric actuators so that they maintain the beam of light in each arm of the instrument parallel to the optical axis with an accuracy of the order of 0.1 seconds of arc. Thirdly, atmospheric effects are minimized by the use of a large number of very short exposures of a few milliseconds which are made possible by the use of photon-counting detectors and a computer. There is, of course, no observer who has to assess the visibility of fringes. The two beams of light are brought together in a beam-splitter and interfered; the resulting interference is then measured by two photon-counting photoelectric detectors whose output is taken to a computer. The computer

calculates the fringe visibility for each exposure, lasting perhaps 5 milliseconds, and integrates these values to give the final result for an exposure which may last for minutes or hours.

The need for high mechanical precision and rigidity is overcome, we hope, in two ways. Firstly, the whole instrument is stationary, massive and mounted on rock. Secondly the optical bandwidth is made narrow (by the prisms and slits in Fig. 11) so that the path lengths in the two arms of the instrument can be kept sufficiently equal without unreasonable mechanical difficulty. For example, if we make the optical bandwidth 0.2 nm then the difference in the pathlengths of the two arms must not exceed 100 μm if the loss of fringe visibility is to be less than 1 per cent, and that is a mechanical tolerance which we can contemplate with equanimity.

At the present time this new instrument, after six years in the laboratory, is almost complete. We are installing it, by courtesy of the Director, in the grounds of the National Measurement Laboratory in Sydney. We hope, next year, to find out how well it actually works.

Conclusion

The long-term aim of the work which I have been talking about is to develop ways in which we can see the size and shape of the stars or, more

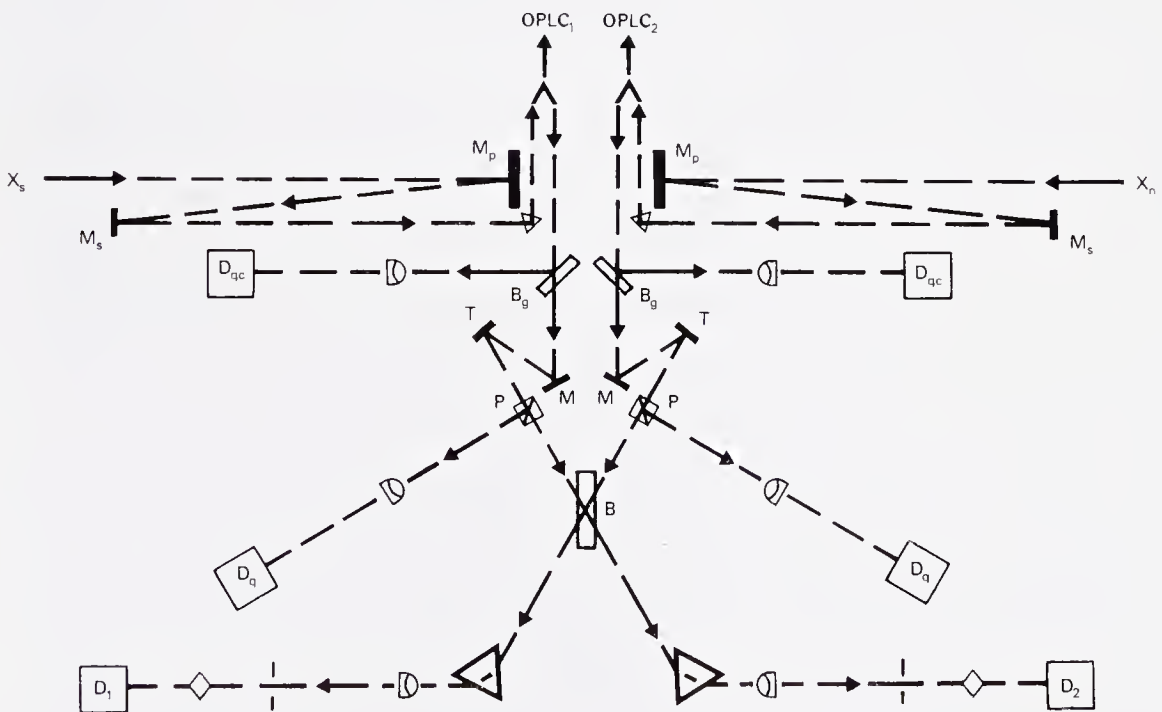


FIGURE 11 The optical system of a modernized version of Michelson's stellar interferometer.

pompously, to apply very high angular resolving power to optical astronomy. Some years ago I initiated an, analogous programme for radio-astronomy at Jodrell Bank; it took years to develop, but paid off, and is still paying off, handsomely. I see no reason why the same thing should not be true of optical astronomy. It is too often forgotten that the progress of science depends intimately on developing new methods of observations.

We have so far demonstrated one successful technique, the intensity interferometer; indeed we used it to measure, for the first time, main sequence stars. We want now to take the next step and, because the intensity interferometer is both large and expensive — like radio-telescopes — we have gone back to take a closer look at square one, Michelson's stellar interferometer. There are, as yet, no answers to the simple questions: can it be made to perform reliably through the Earth's atmosphere or must it wait until someone can afford to put it in space? What are the limits to its sensitivity and resolving power and would it be cheaper to build than an intensity interferometer? Before we can go forward confidently we must have answers to these questions and we hope to have some of them soon. If, as we have reason to expect, the answers prove to be encouraging then our next step will be to expand our pilot model into a full-scale instrument to tackle some of the exciting programmes which we can foresee. I am convinced that there is a rewarding future for this type of work.

★★★★★★★★

I need hardly point out that most of the work which I have been describing is the work of a group, of which Dr J. Davis, Dr L. R. Allen and Dr W. Tango are the members. Since my retirement, the group has been led by Dr Davis.

Select Bibliography

General Books

- Light Waves and their Uses*, by A. A. Michelson. Chicago University Press, 1902.
The Intensity Interferometer, by R. Hanbury Brown, Taylor and Francis, London, 1974.

Scientific Papers

General Theory

- A New Type of Interferometer for use in Radio Astronomy*, by R. Hanbury Brown and R. Q. Twiss, *Phil. Mag.*, **45**, 663, 1954.
Interferometry of the Intensity Fluctuations in Light, by R. Hanbury Brown and R. Q. Twiss.
- I. *Basic theory: the correlation between photons in coherent beams of radiation*, *Proc. Roy. Soc. (Lond.)*, Series A, **242**, 300, 1957.
 - II. *An experimental test of the theory for partially coherent light*, *Proc. Roy. Soc. (Lond.)*, Series A, **243**, 291, 1957.
 - III. *Applications to astronomy*. *Proc. Roy. Soc. (Lond.)*, Series A, **248**, 199, 1958.
 - IV. *A test of an intensity interferometer on Sirius A*. *Proc. Roy. Soc. (Lond.)*, Series A, **248**, 222, 1958.

The Work at Narrabri Observatory

- The Stellar Interferometer at Narrabri Observatory*, by R. Hanbury Brown, J. Davis and L. R. Allen.
- I. *A Description of the Instrument and the Observational Procedure*, *Mon. Not. R. astr. Soc.*, **137**, 375, 1969.
 - II. *The Angular Diameters of 15 Stars* (with J. M. Rome), *Mon. Not. R. astr. Soc.*, **137**, 393, 1967.
- Empirical Effective Temperatures and Bolometric Corrections for Early-type Stars*, by A. D. Code, J. Davis, R. C. Bless and R. Hanbury Brown, *Ap. J.* **203**, 417, 1976.

Future plans

- An 11 metre Michelson stellar interferometer*, by J. Davis, *New Zealand J. Sci.*, **22**, 451, 1979.

Reprinted from *Statistical Physics* (eds: N. Mukunda, A.K. Rajagopal and K.P. Sinha), Suppl. to *J. Indian Inst. Sci.*, 1975, pp. 139-154.

Bosons and stars

R HANBURY BROWN, F.R.S.,

Raman Visiting Professor, Indian Academy of Sciences, Raman Research Institute,
Bangalore 560 006

PART I

Introduction

The development of the intensity interferometer started in about 1950 at the Jodrell Bank Experimental Station of the University of Manchester. At that time one of the major problems in radio-astronomy was to measure the apparent angular diameters of the so-called 'radio-stars' which at that time were unknown. If their angular sizes proved to be comparable with those of the visible stars then it would be necessary to measure angles $\sim 1/100$ th arc sec or less and this would require baselines $\sim 20,000$ km at a wavelength of 1 m.

An obvious way to make these measurements would have been to make a radio analogue of Michelson's stellar interferometer; however the construction of such an instrument capable of operating with very long baselines presented problems which, with the techniques available in 1950, looked extremely difficult, perhaps insoluble. The principal difficulty envisaged was to preserve the relative phase of the signals received at two widely separated aerials. In practice it would be necessary to heterodyne these signals to a lower frequency before recording them on magnetic tape or transmitting them by telephone line or radio link. This would involve the use of two independent local oscillators of very high stability and it is not until quite recently that suitable oscillators have been developed. Other difficulties would be the effects of ionospheric scintillation on the fringe pattern and the equalization of the overall path delays in the two arms of the system. For these reasons I tried to find another technique suitable for very long baselines.

The principle of the intensity interferometer was discovered by trying to evolve a system which would work with independent local oscillators. In the course of thinking about this problem I visualized the low-frequency output noises from two separated and independent receivers as displayed on separate cathode-ray oscilloscopes. I realized that these noises would represent the envelope or 'modulation' of the radio-frequency carriers and that in the case of a plane wave from a distant source, they would look the same even if the two receivers had independent local oscillators. This idea led directly to the intensity interferometer.

The first intensity interferometer

The first intensity interferometer was built in collaboration with R. C. Jennison and M. K. Das Gupta at 125 MHz. It used two fairly large aerials, one of which was mobile, connected to superheterodyne receivers with independent local oscillators. The low-frequency outputs of these receivers in a band 0–1000 Hz were brought together by means of a radio link and then multiplied together. The time delays in the two paths were equalized by a suitable delay. This instrument was tested on the Sun and then used to measure the angular diameters of the intense radio sources in Cygnus and Cassiopeia. In the event these two sources were resolved with a maximum baseline of about 15 km and the very long baselines which we had visualized were not required.

It was while watching the transit of these radio sources through the beam of this instrument that we noted that the mean, normalized, correlation was not affected by quite severe ionospheric scintillation. We immediately made a theoretical analysis of this rather remarkable property of the instrument and realized that the same technique might be applied to optical astronomy. For many years progress in measuring the angular diameters of visible stars had been arrested by the technical difficulties of achieving adequate resolving power and by the effects of atmospheric scintillation and for this reason, in collaboration with Dr. R. Q. Twiss, I set about analyzing the application of the intensity interferometer to light waves. Once we had mastered the difficulties of photons, which had not worried us when working with radio waves, we estimated the signal to noise ratio of an optical intensity interferometer and discovered to our great disappointment that, to measure even a small number of stars, we should need two telescopes comparable in size with the 200 inch telescope; furthermore one of these telescopes must be mobile. In view of the unreasonable cost of such a proposal we abandoned it.

However, some months later we realized that in an optical intensity interferometer it is not necessary to form an image of the star. All that is needed is to collect the light from the star on the two photocathodes. In practice this meant that the two separated telescopes could be of relatively crude construction and that an optical intensity interferometer could be built at reasonable cost.

The principles of an optical intensity interferometer

If a plane wave of white light is incident on a photo-detector we can consider the output current to have three principal components; a D.C. component (i_{DC}), a noise-like component ($\overline{j_N^2}$) called *particle noise*, and a component ($\overline{j_C^2}$) called *wave noise*.

The *particle noise* is due to the stochastic relation between the wave and the ejection of photoelectrons and is given by the well-known formula for shot noise,

$$\text{particle noise} = \overline{j_N^2} = 2ei_{DC} \Delta f, \quad (1)$$

where Δf is the electrical bandwidth of the phototube plus any filters which follow it. Equation (1) assumes that this bandwidth is rectangular.

The *wave-noise* can easily be found from standard formulas used in electrical engineering if we assume that the photo-detector behaves as a square-law detector and that,

$$P(t) \Delta t = a I(t) \Delta t, \tag{2}$$

where $P(t)$ is the probability of ejection of a photoelectron in a time Δt , a is the quantum efficiency and $I(t)$ is the intensity of the light. A proof of this formula has been given by several authors, notably by Mandel, Sudarshan and Wolf, *Proc. Phys. Soc.* **84**, 435 (1964). The result is,

$$\text{wave noise} = 2i_{\text{DC}}^2 \Delta f / \Delta \nu = \bar{j}_C^2, \tag{3}$$

where $\Delta \nu$ is the optical bandwidth. Thus the total noise in the output of the detector is given by;

$$\bar{j}_N^2 + \bar{j}_C^2 = 2ei_{\text{DC}} \Delta f [1 + i_{\text{DC}}/e\Delta \nu], \tag{4}$$

which we can write,

$$\text{total noise} = \text{particle noise} [1 + \text{number of photoelectrons } S^{-1}\text{Hz}^{-1}]. \tag{5}$$

You will recognize that this is what one would expect from a stream of particles obeying Bose Statistics.

If we now multiply the two outputs together the particle noises in the two detectors will obviously be uncorrelated but the wave noises will be correlated if the light is mutually coherent at the two photo-cathodes. Thus it can be shown that, if the intensities at the two cathodes are $I_1(t)$ and $I_2(t)$ where,

$$\begin{aligned} I_1(t) &= \langle V_1^*(t) V_1(t) \rangle, \\ I_2(t) &= \langle V_2^*(t) V_2(t) \rangle, \end{aligned} \tag{6}$$

and $V_1(t)$, $V_2(t)$ are analytic signals and $V_1^r(t)$, $V_1^i(t)$, $V_2^r(t)$, $V_2^i(t)$ are Gaussian random variates, then

$$\langle \Delta I_1(t) \Delta I_2(t) \rangle = \bar{I}_1 \bar{I}_2 |\gamma_{12}|^2, \tag{7}$$

where γ_{12} is the complex degree of coherence of the two light fields.

Using the relation in equation (2) we can now show that the correlation C_d between the wave noises in the two detectors is given by,

$$C_d = \langle \Delta i_1(t) \Delta i_2(t) \rangle = a^2 \cdot e^2 \bar{I}_1 \bar{I}_2 (\Delta f / \Delta \nu) |\gamma_{12}|^2. \tag{8}$$

Thus by measuring the correlation between the two wave noises as a function of the separation d between the detectors we can find $|\gamma_{12}|^2$ which is the square of the fringe visibility in a Michelson interferometer. From the van Cittert-Zernike theorem we

can now find the angular size of the star since $|\gamma_{12}|^2$ is the square of the modulus of the Fourier transform of the intensity distribution across the star reduced to an equivalent strip parallel to the baseline.

It should be noted that in measuring $|\gamma_{12}|^2$ we lose the phase of the Fourier transform and so we cannot distinguish between symmetrical and asymmetrical distributions. This fact was pointed out to Michelson by Lord Rayleigh in 1892 (*Phil. Mag.* **34**, 407, 1892).

The most interesting feature of an intensity interferometer is the temporal coherence. It follows from the Wiener-Kinchin theorem that, if we introduce a delay τ into one arm without altering the spatial coherence, then

$$C(\tau)/C(0) = \frac{\int_0^{\infty} G_{12}(f) \exp(-2\pi if\tau) df}{\int_0^{\infty} G_{12}(f) df}, \quad (9)$$

where $G_{12}(f)$ is the mutual spectral density of the *electrical fluctuations*. If we substitute in equation (9) a practical value of the electrical bandwidth ($\Delta f = 100$ MHz), then it follows that the correlation would be reduced to zero by inserting a time delay $\sim 5 \times 10^{-9}$ s in one arm of the interferometer and that it would be reduced by only 10 per cent by a time delay of about 10^{-9} s or by a path difference of about 30 cm. It is this property of an intensity interferometer which makes it possible to construct a stellar interferometer of sufficient size to resolve hot stars and main sequence stars and to make precise observations through a scintillating atmosphere, as we shall see in my second lecture.

The correlation between photons

A consequence of the correlation between intensity fluctuations at two separated points is that the arrival times of photoelectrons in two spaced detectors must be correlated. One may therefore say that photons tend to arrive at the two detectors in pairs. Nobody worried about this point when we published the theory of the radio intensity interferometer, however it was a very different matter when it came to optics. Our proposals to build an optical interferometer operating on the same principle met with vigorous criticism from many physicists. Apart from theoretical objections that a correlation between photons violated the laws of quantum mechanics, two laboratory experiments, one in Hungary and one in Canada, were carried out and published. Both these experiments claimed to show *experimentally* that no such correlation existed and that this was to be expected from quantum theory.

At the time of these criticisms Dr. Twiss and I were trying to raise money to build an optical interferometer and it was essential that we should refute them. We therefore analysed both experiments theoretically and published the results. We showed that in one case it would have taken 10^{11} years to measure a significant correlation and in the other at least 1000 years. Neither experiment had been carried out under conditions in which one could expect to observe correlation.

Two laboratory experiments

We also carried out two laboratory experiments. In the first experiment carried out at Jodrell Bank (University of Manchester) we illuminated a pinhole with a high-pressure mercury arc using the 4358 Å line of mercury and observed this pin-hole with two spaced photoelectric detectors. The optical layout was arranged, by means of a half-silvered mirror, so that the separation of the detectors as seen from the pin-hole could be varied at will. The outputs of the two detectors were correlated in a wide-band linear correlator which multiplied the output fluctuations together linearly and integrated their average cross-product. We showed that the output fluctuations were correlated and that the magnitude of this correlation and its variation with the separation of the detectors was in agreement with theory.

In this first experiment the number of photons entering each photodetector was so great that the individual pulses were superimposed and appeared as a continuous waveform of noise. In order to demonstrate more clearly the correlation between the arrival time of individual photons we therefore set up another experiment. In this second experiment the two high gain photomultipliers were illuminated by a source of light with a very high specific intensity or apparent temperature. For this purpose we used a mercury isotope lamp excited by radio-frequency. The optical layout was similar to the first experiment but the electronic equipment was different. The output of each photomultiplier was connected to a coincidence counter with a coincidence time (τ_c) of about 3.5×10^{-9} s. The rate of arrival of photoelectrons (N_1, N_2) was measured in each channel and also the number of coincident pulses (N_c). The mutual coherence of the light at the two detectors was then varied, as in the first experiment, and the ratio of the 'excess' coincidence rate to the random rate was measured as a function of this coherence.

In the practical case when $\tau_c \gg 1/\Delta\nu$ it can be shown that

$$\bar{N}_c = \bar{N}_1 \bar{N}_2 2 \tau_c [1 + \frac{1}{2} |\gamma_{12}|^2 \tau_0/2 \tau_c]; \quad (10)$$

if, however, $\tau_c \ll 1/\Delta\nu$ then it can be shown.

$$\bar{N}_c = \bar{N}_1 \bar{N}_2 2 \tau_c [1 + \frac{1}{2} |\gamma_{12}|^2]. \quad (11)$$

Both these equations correspond to unpolarized light. The random rate is given by

$$\text{random rate} = \bar{N}_1 \bar{N}_2 2 \tau_c \quad (12)$$

and it can be seen from equations (10) and (11) that the coincidence rate is given by equation (12) when $|\gamma_{12}|^2 = 0$, that is to say when the light on the two photo-detectors is mutually incoherent. It is interesting to note from equation (11) that the coincidence rate is increased by a factor of 3/2 when the light is unpolarized and fully coherent at the two detectors and by a factor of 2 when the light is polarized. This latter conclusion is analogous to the behaviour of the density of bosons in a boson gas and corresponds to the tendency of bosons to bunch.

In this second laboratory experiment the ratio of 'excess' coincident photoelectrons to random was found to be 0.0193 ± 0.0016 p.e. which is in satisfactory agreement with the theoretical value of 0.0207 deduced from equation (10).

Conclusion

These two laboratory experiments supported our theoretical study of photon correlation and thus confirmed that an intensity interferometer could be made to work at optical wavelengths. In my second lecture I shall describe how we applied this result to measuring the angular diameters of visible stars.

PART II**Introduction**

In this lecture I am going to outline how the work on the intensity interferometer has been applied to the solution of a classical problem in optical astronomy, measuring the apparent angular diameters of the bright visible stars. Up till the time of Galileo it was thought that the angular diameters of bright stars were of the order of a few minutes of arc. However, Galileo was deeply concerned with this question because it was relevant to his arguments with the Church about the heliocentric model of the solar system. If in truth the earth travelled round the Sun then the nearest 'fixed' stars should appear to move in the sky and the amount of this movement depends upon their distance. To estimate their distance he needed to know their angular diameter and Galileo, characteristically, set out to measure the angular diameter of the bright star Vega. He hung a silk cord and measured the distance from the cord at which he had to stand so that it appeared to occult Vega. This careful experiment, described in his 'Dialogue concerning the two Chief World Systems', gave a value of 5 arc sec for Vega. The angular diameter of Vega measured with the stellar intensity interferometer at Narrabri Observatory is $3.08 (\pm 0.07) \times 10^{-3}$ arc sec. So Galileo's result was too large, nevertheless it was an improvement on previous ideas and adequately supported his arguments. The next notable attempt to solve this problem was made by Newton who calculated that the apparent angular size of a first magnitude star should be about 2×10^{-3} arc sec. He arrived at this reasonable result by assuming that the stars are similar in size and brightness to the Sun. Finally the first actual measurement of a star was carried out by Michelson and Pease using a 20 ft interferometer at Mt. Wilson. In December 1920 they measured the angular diameter of α Orionis to be 0.047 arc sec.

Michelson's interferometer

In Michelson's interferometer the light from two small separated mirrors is combined to form fringes which cross the diffraction image of the star. The fringe visibility V is measured as a function of the mirror separation and it can be shown that,

$$V = \frac{I_{\max} - I_{\min}}{I_{\max} + I_{\min}} = |\gamma_{12}|, \quad (1)$$

where I_{\max} , I_{\min} represent the maximum and minimum intensities in the fringe pattern and $|\gamma_{12}|$ is the degree of coherence of the light at the two mirrors.

Now if we wish to measure a bright hot star like ζ Puppis at a wavelength of 4000 \AA we shall need to separate the two mirrors by roughly 200 m and this is clearly going to present severe mechanical problems. Furthermore to preserve the fringe visibility any differential delay (τ) or path difference between the two arms of the interferometer must be such that

$$\tau \ll 1/\Delta\nu \quad \text{or} \quad \ll \Delta\lambda/C, \quad (2)$$

where $\Delta\nu$ and $\Delta\lambda$ are the optical bandwidth. Thus if $\Delta\lambda = 1000 \text{ \AA}$ then any differential delay must be $\ll 10^{-14} \text{ s}$, corresponding to a path difference of about $3 \times 10^{-6} \text{ m}$. This is clearly very difficult to achieve in a large instrument. Quite apart from the difficulties of achieving the necessary mechanical stability there are serious troubles due to atmospheric scintillation which can introduce random time delays as large as 10^{-12} s into the light reaching the two mirrors. As a consequence the fringes move rapidly about in the focal plane and also may vanish completely because the limits of temporal coherence are exceeded.

At first sight it would appear comparatively simple to avoid these difficulties by simply reducing the optical bandwidth $\Delta\lambda$ until all these stringent limits on path difference and time delay are relaxed to values which can be achieved in practice. However, such a reduction in bandwidth would, if carried sufficiently far, greatly reduce the sensitivity of the instrument. This loss of sensitivity cannot be regained by simply increasing the size of the mirrors because their maximum size is very severely restricted by the requirement that the light should be in phase over the whole mirror surface. In practice the correlation length of atmospheric scintillations at the earth's surface probably restricts the diameter of the mirrors to roughly 10 cm for much of the time.

As a consequence of these difficulties efforts to increase the resolving power of Michelson's interferometer have, up till the present date, failed. Only 6 stars, all cool giants or supergiants, were measured with the original 20 ft instrument and efforts to make a 50 ft model at Mt. Wilson in the years following 1930 failed and the work was discontinued. No main sequence star or star hotter than about 3000 K was ever measured. As we shall now see these difficulties can be overcome by using an intensity interferometer.

The choice of intensity interferometer

As we saw in Lecture I there are two forms of intensity interferometer, one using a linear multiplier and one using a coincidence counter. At first sight the coincidence counter is the more attractive from the point of view of the electronic engineer because it avoids the technical problem of multiplying two wide-band noise voltages together and recording the time-average of their cross-product. In practice this is difficult to achieve without introducing troublesome random drifts into the zero of the cross-product and this trouble can be largely circumvented by the use of counters and digital techniques. Nevertheless the coincidence-counter interferometer is not practical for astronomy because, to limit the number of photoelectrons per second to

a rate which can be counted, requires the use of extremely narrow optical bandwidths. These bandwidths cannot be achieved in the poorly collimated beams from very large and coarse optical reflectors; furthermore, even if they could be achieved, it is not clear how the pass-bands of the filters in front of the two detectors could be matched with the necessary precision. For this reason the 'coincidence-counter' interferometer cannot, as yet, be applied to astronomy and we chose to develop a stellar interferometer using a linear multiplier.

The intensity interferometer applied to astronomy

As we saw in Lecture I the intensity interferometer has the interesting property that the temporal coherence ($C(\tau)/C(0)$ in equation 9, Lecture I) is given by the Fourier transform of *electrical* bandwidth and *not* of the optical bandwidth. Therefore, if we put $\Delta f = 100$ MHz then, for a 10 per cent loss in correlation we can tolerate differential time delays between the two arms of 10^{-9} s or path difference of 30 cm. It follows that by the use of an intensity interferometer we can surmount the two major difficulties in extending Michelson's interferometer. Firstly we need only make an instrument in which any mechanical path differences are small compared with 30 cm, and this allows us to build an instrument with the very long baselines which are required to resolve a significant sample of stars. Secondly we can work through a scintillating atmosphere because the random time delays due to the atmosphere ($\sim 10^{-12}$ s) are small compared with 10^{-9} s. Furthermore we can, if we wish, use mirrors which are very much larger than the coherence length (~ 10 cm) of the atmospheric scintillation pattern. Remember that we are not concerned to preserve the relative phase of the light waves at the two detectors, nor does it matter if the phase is preserved over the mirror surface provided only that any differential time delays in the light reaching the photo-cathode from any part of the mirror are $\ll 10^{-9}$ s.

There are, of course, attendant disadvantages to using an intensity interferometer. A minor one, as noted in Lecture I, is that we lose the phase of the Fourier transform. A more serious disadvantage is that the signal/noise ratio is poor and in practice this means that we must use very large light collectors and very long exposures on faint stars.

The stellar interferometer at Narrabri Observatory, New South Wales, Australia

The work described in Lecture I led to the design and construction of a stellar intensity interferometer which was intended to extend the original work of Michelson to main sequence stars, and especially to hot stars.

First let me discuss the signal/noise ratio of the instrument. If we simplify the rather complicated formulae for the signal/noise ratio of an intensity interferometer we can write,

$$(S/N)_{\text{RMS}} = An a (\Delta f T)^{1/2} |\gamma_{12}|^2 \sqrt{\text{LOSSES}} \quad (3)$$

where A is the area of the light collectors, n is the number of photons $\text{S}^{-1} \text{Hz}^{-1}$

received from the star, α is the quantum efficiency, Δf is the electrical bandwidth, T is time of observation, and the term 'LOSSES' includes loss of light in the optical system, excess noise in the phototubes and correlator and excess noise due to light from the night sky, etc. For the interferometer at Narrabri we may put $A = 30 \text{ m}^2$, $\alpha = 0.20$, $\Delta f = 100 \text{ MHz}$, $\text{LOSSES} = 0.20$, $n = 5 \times 10^{-5} \text{ photons m}^{-2} \text{ s}^{-1}$. For an unresolved zero-magnitude star in the zenith ($|\gamma_{12}|^2 = 1$) we find

$$(S/N)_{\text{RMS}} \approx 36 \sqrt{T}, \quad (4)$$

where T is in hours. If we take 3/1 as the lowest workable signal/noise ratio in one hour then it follows that the limiting magnitude for stars in the zenith is about +2.5.

It can also be shown that the limiting temperature, that is to say the coolest star on which one can work, has a surface temperature of roughly 6000 K. This limits the instrument to measuring stars with spectral types earlier than about F8.

The maximum baseline of the interferometer is about 188 m and was designed to be sufficient to measure the hottest star (ζ Puppis) brighter than magnitude +2.5. In making this decision we took the temperature of ζ Puppis to be 50,000 K. In the event it turned out to be considerably lower, 31,000 K, and so the baseline proved to be somewhat longer than necessary.

The interferometer at Narrabri consists of two large mosaic reflectors about 6.7 m in diameter running on a circular railway track 188 m in diameter. The reflectors themselves are parabolic in shape and are formed by a mosaic of hexagonal mirrors, each mirror having spherical curvature. At the focus of each reflector the light is passed through an interferometer filter with a bandwidth of 100 Å centred on 4430 Å. It is then focussed on to the cathode of a photomultiplier and the output of this photomultiplier is carried by a coaxial cable, suspended from a catenary wire, to the centre of the track. In the centre there is a control building which houses the electronic correlator and the computer which controls the movements of two reflectors.

The reflectors are controlled so that they maintain a constant preset separation (the baseline) and move around the track so that this baseline is always normal to the direction of the star from the centre of the track. This configuration has the advantage that, for any preset separation, the resolving power remains constant throughout an observation; furthermore the light arrives at the same time at both reflectors and the cables carrying the signals from the two reflectors to the central correlator are always the same length and under precisely the same conditions of tension and temperature. The disadvantages of this circular configuration is that it cannot easily be expanded if it is desired to increase the resolving power of the instrument.

In operation the reflectors move around the track to follow the star in azimuth and they tilt about a horizontal axis to follow it in elevation. They are mounted on turntables, carried by moving trucks, and can be rotated on these turntables so that, as the baseline is varied, their lines of sight can be maintained parallel to each other. These movements are all controlled by a computer in the control building. However, because the track is not perfect, the direction in which the reflectors point is uncertain by about ± 15 arc min and to take care of this there is also an automatic photoelectric guiding system for each reflector. This system keeps the reflector pointing at the

star with an r.m.s. error of about ± 1 arc min which is small compared with the field of view (~ 15 arc min).

The outputs from the two photomultipliers are multiplied linearly together in an electronic correlator with an overall bandwidth of roughly 100 MHz. This correlator proved to be the most difficult part of the whole instrument to develop and is a fairly complicated instrument. The main technical difficulty is to measure the cross-product of two wide-band noise-like voltages without introducing random zero-drifts which are comparable with the statistical uncertainty in observations which may last for several hours. This problem was successfully solved only after several years of development work.

The output of the correlator is recorded by an electric typewriter which prints a measurement of the average light flux received by each reflector every 100 s and the time-average of the correlation in that period.

To make an observation the interferometer is directed at the star and the correlation is recorded for several hours at different baselines. The total exposure time necessary to measure the angular diameter of a star of magnitude + 2.5 with an uncertainty of $\pm 5\%$ is about 100 h.

Results

Careful tests have been made to establish that there is no significant source of correlation other than the star which is being observed. For example it was suggested that the Čerenkov light pulses due to cosmic rays might produce a significant correlation. This question has been studied in detail at Narrabri and we have shown conclusively that our measurements are not affected by any sources of correlation other than the star under observation.

The main programme of the Observatory has been to measure the angular diameters of single stars. Thus, if we measure the angular diameter (θ) we can find the flux emerging from unit area of the star's surface from the relation

$$F_{\lambda} = 4f_{\lambda}/\theta^2, \quad (5)$$

where F_{λ} is the *emergent flux* and f_{λ} is the flux received at the earth as measured by a photometer. The quantity F_{λ} is of basic importance in the theory of stellar atmospheres.

If we know F_{λ} we can then find the effective temperature T_e of the star from the relation,

$$\int_0^{\infty} F_{\lambda} d\lambda = \sigma T_e^4, \quad (6)$$

where σ is Stefan's constant. If f_{λ} is not known over the whole spectral range then it is necessary to use a grid of model atmospheres calculated for a range of values of T_e and to choose the model which corresponds most closely to the measured value of F_{λ} . However, if f_{λ} can be measured over all significant parts of the star's spectrum

then it is possible to find the star's effective temperature entirely from observations. Perhaps I should note that this is not rigorously true because one has to make a small theoretical correction for the effects of limb-darkening; however, this correction is very small.

Altogether the angular diameters of 32 *single* stars have been measured at Narrabri and I underline 'single' to emphasize the difficulty of finding single stars. Several of the well-known stars in our original observing list (*e.g.* β Cen, σ Sgr, δ Vel) proved to be close-spaced doubles when viewed with the interferometer and we had to reject them from our programme. For all these 32 stars we have measured the flux f_λ over the whole significant spectral range including the ultra-violet. To achieve this we have measured f_λ ourselves in the visible range and collaborated with the University of Wisconsin to find f_λ from satellite observations in the ultra-violet. We have thus succeeded in finding the effective temperatures of these 32 stars, ranging in spectral type from O5 to F8, based *entirely* on observations and independent of model atmospheres. Not only do these measurements represent the first entirely observational measurements of the effective temperatures of hot stars but they include the first measurements of the angular diameters of main sequence stars which have ever been made.

In addition to this work on single stars we have used the stellar interferometer at Narrabri in a number of other programmes. For example we have measured the angular separation of the well-known binary star Spica (α Vir) as a function of time and from these data found the *inclination* and *angular diameter* of the orbit. By combining these measurements with spectroscopic observations of the velocities of the two stars we have found the *distance* of Spica to be 84 ± 4 parsecs. It is interesting to note that this represents an increase in precision of at least 10 times over the classical method of measuring the parallax of a star at that distance.

In other experiments which I shall not attempt to describe we have used a narrow-band filter tuned to an emission line to measure the angular size of the region of excited gas surrounding the Wolf-Rayet star (γ Vel). We have also measured the angular size of the central star by observations in the continuum. We have also observed the distortion in shape of the fast rotating star Altair and we have measured the limb-darkening across the disc of Sirius.

In conclusion the work of the Narrabri stellar interferometer is now complete because it was originally designed only to work on a limited number of bright stars. There are, however, a number of extremely interesting observations which could be made with a more sensitive instrument and in particular I would like to mention the observation of Cepheid variables which pulsate in radius. I hope that, at some future date, we shall be able to attract the necessary financial support to take the next step.

The work I have described has been carried out by the Chatterton Astronomy Department of the School of Physics of the University of Sydney. In particular I would like to acknowledge the work of Dr. J. Davis and Dr. L. R. Allen.

CONCERN ABOUT THE CONTROL OF SCIENCE

R. Hanbury Brown

If we go back 100 years to the days when this University was founded, modern science—the sort of science we are talking about here—was a little more than a child, albeit a fast-grown, good-looking child. During that century this child has grown out of all recognition; some would say it has lost its good looks and some that it has grown too big for its boots. Even before this University was founded Lord Kelvin (1) had already pointed out that the infant science was growing exponentially. Lord Kelvin was right. For the 100 years which followed his speech the number of people engaged in scientific research and in the application of science grew at about 5 per cent per annum. The scientific community doubled in size roughly every 14 years, and, for every scientist living at the time this University was founded, there are more than 100 alive today. This is also true of scientific knowledge if we equate knowledge with data; the number of scientific journals has increased by about one hundred times in the last century. If however we try to measure quality rather than quantity, understanding rather than information, then it rather looks as though the rate of growth decreases as we raise our standards. Some authors who have looked at this question (*e.g.* Rescher (2)) have concluded that the rate at which really significant advances have been made has not increased but has remained roughly constant for many years. As science advances, the problems get harder. However one thing is certain; the cost has increased exponentially. A century ago the cost of science to a nation in manpower and resources was negligible; today the cost to many countries is a significant fraction of their Gross National Product. No wonder there are difficulties due to the impact of science on society! Too much has happened too quickly.

What other changes have there been? One of the most noticeable, I suggest, is the change in the patrons of science. A hundred years ago scientific research was done mainly in the Universities. Today it plays a major role in both military and industrial affairs. Roughly half of all the world's research and development is devoted to armaments; about 90 per cent of the other half is devoted to applied research and development and only about 10 per cent is devoted to basic research.

What Francis Bacon (3) said 350 years ago has come true. 'Knowledge and power', he told us 'meet in one'. Taking a long term view, one of the major historical events of the last 100 years has been this meeting. Science has in fact increased our power over nature and we have learned that this power can be used for good or for evil; now we must learn to use it wisely.

Most of us now fear science in the hands of the military—as nuclear warfare—many of us fear it in the hands of industry—as nuclear power—and some of us fear

it in the hands of the scientists themselves—as genetic engineering and so on—. Most of the ills of the world seem to be blamed on science. The trouble is, of course, that science has come to be identified in the public mind almost wholly with its applications and we are losing sight of its moral and cultural value. This was not always so, and it is an attitude which I believe to be as mistaken as, say, the identification of the Christian faith with religious wars on the excesses of the Inquisition. At one end of the scale, the friendly end, there are those who demand that science should be more relevant, at the other, there are those who demand that it should be stopped. But, as we all know, there is no way back. When Adam and Eve ate from the tree of knowledge they were not offered the option of forgetting; they were expelled from the Garden of Eden, but they kept their knowledge. As Adam said to Eve on leaving the Garden, according to a cartoon in the *New Yorker*, ‘My dear, we live in an age of transition’. So it is with us; we live in the transition from an age when science and power were separate to one in which, in Bacon’s words, they have met as one. We have no option but to learn to live with science.

How then shall we make better use of science? Should we try harder to make it give us what we want? And if so, who is to decide what we want? To what extent can we institutionalize wisdom?

The Distinction between Basic and Applied Science

Let me begin with a brief word about what I mean by basic and applied science. Conventionally this distinction is based on primary intention or purpose of scientific work to achieve some recognized practical goal it is said to be applied or, in jargon borrowed from the military mission-oriented. On the other hand its primary purpose is to increase our knowledge and understanding of ourselves or of the world around us, the work is said to be basic or curiosity-oriented. One difficulty in making this distinction is, of course, that the intentions of most scientific workers are often mixed, especially when they are engaged in long term projects. They may be neither wholly practical nor wholly fundamental; furthermore the intention of the sponsors of the work may well differ from the intention of those who are engaged in it! I shall use the word ‘technology’ to mean the whole body of know-how, including the scientific knowledge, which is involved in producing some practical result. There is much more to technology than applying the results of scientific research.

Clearly there is a symbiotic relation between all these activities and I am reluctant to draw distinctions between them. Nevertheless if we are to discuss the control of science, then it is essential that we should not lose sight of the distinction between basic and applied science, even if it is often blurred.

The Control of Applied Science and Technology

First let us talk about how to get what we want from applied science as it comes to us embodied in new technology. This question is not new; it has been with us since the beginning of human history, but in the last 200 years it has become more compli-

Concern about the control of science

cated and urgent. Ever since the start of the Industrial Revolution there has been an increasing need to control technology. In the 19th century the efforts to do so were concerned mainly with the regulation of trade and, in particular, of monopoly; in the present century they have been concerned with a much wider range of social issues. Thus in many countries there are already long-established agencies to protect health, safety, the environment and so on and they act to control some of the immediate effects of new technology. However, in recent years it has become increasingly clear that, if we are to get what we really want from new technology, we must extend and strengthen our methods of control. Many of our current problems, such as nuclear power and waste disposal, supersonic aircraft, the effects of computers and microprocessors on employment, the use of toxic chemicals, and so on are too novel, too complex, and too socially pervasive to be controlled exclusively by legislation or by regulatory agencies which are mainly concerned with short-term calculations of those specific costs and gains which can be quantified. In dealing with these problems we must look beyond the immediate effects of new technology to more remote, secondary effects; to do this we need to employ a wide range of expertise and we must be prepared to assess risks and to weigh costs and benefits which cannot be quantified—an economist's nightmare—! A classic example has been the debate on the use of the insecticide D.D.T. Its obvious benefits to agriculture and to the control of malaria have had to be weighed against a large number of secondary effects, such as its accumulation in human and animal tissue, its effects on the production of microsomal enzymes in vertebrates, its effects on wild-life and its persistence in the soil. Literally thousands of scientific papers have been written on these topics and the debate has involved a wide ranges of experts from biochemists to lawyers.

For some time it has been abundantly clear that these questions about technology are not just technical problems to be decided by technical experts; they are also political problems to be decided on behalf of society as a whole. If we are to avoid a technocracy, then we must learn to improve the methods by which society learns about and debates the proposals, options and potentialities offered by applied science and technology, and especially we must strengthen the methods by which it imposes its own values and objectives on what is done. This should not be seen as a purely negative, regulatory function but as a positive opportunity to get more of what we want.

The extent to which this can be done, and how to do it, obviously depends on the political structure of a particular country and on how its social objectives and ideals are translated into action, and on its stage of development. For that reason I shall discuss the subject only in the broadest outline. The first step towards a better system is, I suggest, to improve the methods by which complex technical problems, involving social questions, are presented and debated in the public arena. This is, of course, something to which a University, such as this, can aim to contribute. Scientific and technical problems should be presented so that well-informed decisions can be made by people who are not themselves scientific or technical experts. This is not just a matter of putting the scientific evidence into simple language, although that must be done; it is also a matter of presenting it so that the assumptions and values on which it is based are exposed. The scientific view of reality is objective

in the sense that it is based on observations which can be verified, but it is subjective in the sense that the scientific observer must choose what observations to make. This choice is influenced by the values and aims of the observer and, for that reason, scientific evidence, especially about complex problems, may not be value-free. Therefore, in assessing scientific evidence and in resolving differences between conflicting scientific views, for example those on the use of nuclear energy, it is important to be aware of the extent to which the evidence itself is influenced by unspoken values and assumptions. As a society we must learn to treat the scientific expert more as a counsellor and colleague and less as an oracle.

A start in this business of assessing technology has already been made. In the USA, for example, the legislative arm of the Government established the Office of Technology Assessment in 1972 as an independent advisory body with the primary task of keeping the Congress informed on technological issues. It has, I believe, done useful work in a variety of fields including energy policy. At about the same time the Office of Science and Technology, in the Executive Arm of the Government, commissioned some interesting studies through the MITRE corporation of the techniques of assessing the social impact of new technology. Nearer to home there is the work of the OECD and the Council of Europe. In fact there is a rapidly growing literature on the ways in which technical and social considerations can be combined; it abounds with impressive words like relevance-tree and cross-impact-matrix analysis. A recent and extraordinarily lengthy report (4) on 'Technological Change in Australia' quotes the following remark on technology assessment, 'there can hardly ever have been a tool of which we have accumulated so little experience and which has been so extensively analysed in terms of scope, methodology and institutional arrangements'. As an astronomer I am reminded of the science of Cosmology which has been described as 'too many theories chasing too few facts'. What we really need now is more practical experience.

Turning now to the actual methods of control, an ideal system should not, I suggest, be over-centralized; nor can it be truly pluralistic. Perhaps the best description is to say that it should be decentralized, but concerted in the interest of the community as a whole. An ideal system should cope not only with current proposals for new technology, but it should also look ahead and be empowered to influence future developments. However, because the difficulties of planning applied research and development increase so rapidly with the time which separates them from application, it seems likely that, in practice, most of the effective control of new technology must necessarily be exercised at, or close to, the point where it is embodied in concrete proposals. A recent example which comes to mind is the proposal to build a communication satellite for Australia. The problems are not all technical; many of them are social. They include, for example, the assessment of the effect of satellite television on the diversity and independence of the whole television network.

Our ability to look ahead is limited by so many factors. Firstly there is the major difficulty of foreseeing, and agreeing on, any but the most basic needs of society. Then there is the tricky problem of assessing the relevance of any particular piece of research to those needs. The tidy-minded should remember that most of the major discoveries on which our modern science and technology rest, like X-rays, radio

Concern about the control of science

activity and antibiotics, were made largely by accident. Discoveries are not made by directives.

There is another, less obvious, constraint to our ability to plan ahead. It stems from the fact that science advances on what Vannevar Bush (5) called an endless frontier. The topics of science, all the way from topology to palaeontology, are interdependent. They move forward together and only a limited advance ahead of this frontier can be made on a narrow sector. For example the recent advances in genetics were made possible by advances in molecular physics, which in turn were made possible by the development of X-ray diffractometers and electronic computers. Thus if we choose to concentrate our resources on some particular goal whose solution is not yet in sight, for example the cure of cancer, we may pour enormous funds into existing research programmes only to find that we have not made much progress. Indeed if our efforts divert funds from other branches of science, they may even prove to be counter-productive; our problem may be one whose solution must await a general advance of science and technology over a wide front. In science, as in many other things, there is a time to every purpose under the heaven.

For all these reasons it seems likely that the most effective way in which society can influence the application of science is by supporting work towards goals which are not too far ahead and on which it can agree. The necessary basic knowledge to reach these goals must be judged to exist or to be well within reach. There are plenty of worthwhile goals in that category, especially, I need hardly add, in the poorer parts of the world.

If we do succeed in strengthening the control by society of applied science and technology, shall we kill the goose that lays the golden eggs? On the face of it one would say that the scientists engaged in applied research would then know what they ought to be working on and so stop wasting their time. But I doubt if things really work that way. It is much easier, particularly in a democracy, to stop things than to get them moving in the direction you want; furthermore scientists like to go their own way!

It is, I think, more likely that improved social control of applied science and technology will reduce the pace of innovation. That might not be such a bad thing after all; we need more time to get used to what we already have. Judging from the effects of regulation on the pharmaceutical industry, control will also increase the costs. We shall get fewer golden eggs and they will be more expensive; but that, I suggest, we must accept as the cost of getting more of what we really want and, in particular, as the cost of getting less of what we do not want.

On the credit side of the account I would hope that in debates on the applications of science more people will come to appreciate the values on which science is based—for example, the high value placed on critical assessment of evidence rather than on the statements of authority. Hopefully they would come to see science less as an instrument of control and domination and more as a guide to enlightened action.

The Value of Basic Research

Now let us discuss basic research. I have, by-the-way, avoided calling it 'pure' research because I feel that expression to be misleading and faintly ridiculous. I

suppose that we should ask, first, why we bother to do any basic research at all? After all you do not have to look very far to find people who think it is a waste of time, and the most likely failure of any system by which society tries to guide science is that the views of such people might prevail. Although basic research accounts for only a small fraction of the total world effort on scientific research and development, its importance to science is disproportionately great. I hope, therefore, that you will bear with me if I discuss it at disproportionate length.

If we look at the many official reports and surveys of science policy, the first reason which they usually give for the support of basic research is that it is an investment in the future. They invite us to see it, so to speak, as the seed-corn of the future material benefits which we can expect to flow from applying new knowledge. Indeed many economists (6) have argued that governments must support basic research because the free market will always fail to support it adequately. Hence in a welfare economy the government, they say, has an obligation to fill the gap between the level of research and development which the market will support and the level that is socially desirable. It is implicitly assumed in this argument that research and development, including basic research, is an economic activity which can be justified in economic terms. At first sight this looks plausible, if not self-evident, but in fact it has not proved easy to demonstrate for any one country and that, of course, is what interests Governments and tax-payers. Thus if we look at the statistics (7) for the period 1951–1960 there is no clear correlation between the rate of economic growth of a country and the amount which it spends on research. However we should not, I suggest, attach too much weight to, such a simple economic analysis which excludes so many important historical factors. For example—Japan, at that time, was importing and licensing much of its new technology. The rapid growth of its GNP did not, therefore, correlate well with its comparatively low expenditure on research.

However in recent years this situation has changed. The Japanese have recognized that without indigenous research, their technology would eventually become out of date. For one thing, countries with advanced technology are not always willing to export their latest ideas to their competitors.

Thus the relation between expenditure on research and material progress remains difficult to demonstrate in hard economic terms. As a consequence, there is no simple economic index by which any one country can measure how much it should spend. Nevertheless, if we look at science as whole and on a sufficiently long time-scale, then we can see clearly the part played by basic research. What we see is, I suggest, not a simple linear process in which basic research is followed simply by development and production, but a complex interaction in which the driving forces flow in both directions. Broadly speaking the social needs, and the technology of any given time, make possible the application of some basic scientific advance. But it is, of course, necessary to have already made that scientific advance. One can for example look at the development of the transistor at the Bell Telephone Laboratories in 1947 and see that it owed a great deal to the classic papers on the theory of semiconductors written by an academic physicist, A. H. Wilson (8), in 1931 and to technical advances in the purification of germanium. In turn Wilson's work was one of the first applications of the quantum theory, which itself can be traced back to attempts, early in the present century, to understand the spectrum of a black-body.

Concern about the control of science

The quantum theory itself made use of mathematics which was developed in the 19th century, and so on back into the mists of time. A more systematic demonstration is the study published in 1976 by Julius Comroe and Robert Dripps (9). In an impressive analysis of the origins of the ten major clinical advances in the diagnosis, treatment and prevention of cardiovascular and pulmonary diseases, they found that over 60% of the 529 key scientific articles on which these advances were based, were related to basic research. If this argument, that basic research is essential to the advance of material welfare, is to carry its proper share of the weight, it must be strengthened by many more studies like that of Comroe and Dripps.

A second reason for the support of basic research, found in most official reports, is that it contributes to national prestige. To quote a study published by the Science Council of Canada (10), 'The prestige of a nation is to some degree predicated on her contributions of basic knowledge, although such prestige is, to a large extent, restricted to the scientific community'. This is an argument which I distrust. In times of plenty it can be used to justify a spectacular project, like sending a man to the moon, in which the scientific value is not commensurate with the expense; in times of economy it disappears entirely from sight.

A third reason for the support of basic research, also to be found in most official reports, is that it builds up a body of expert knowledge and a group of highly trained people who, especially in a small country, act as an interface between imported technology and industry, and also contribute to higher education. This is, an important, but limited argument; it is limited because many people will claim that there are other, more economical ways, of achieving the same ends.

Finally there is a fourth reason, that basic research is a cultural activity. This argument often suffers, I suggest, from the use of the word 'culture' which in many people's mind conjures up a vision of chamber music and folk dancing. As usually expressed it presents science as an activity like music or painting—*ars pro gratia artis*—science is reduced to an ornament of society. Let me illustrate my point by quoting from the Report of the Royal Commission on Australian Government Administration (11), 'Like the arts', it says, 'science is one of the graces of life, and its presence as an aspect of a particular society is seen as a mark of civilization commanding respect from other societies. Since this activity can no longer be effectively performed by the wealthy amateur, a civilized community will, it is argued, properly support it'. This argument is uncomfortably reminiscent of the old arguments for supporting an aristocracy. I cannot see it standing up to the Treasury in a time of economy!

Thus the conventional apologia for basic science presents it as a source of material progress and of trained people, and as a prestigious ornament of society.

If now we ask the people who actually do basic research why they do it, many of them would add another reason to the list. They would say that they do basic research because they enjoy it; they want to find out something new and get the credit for it.

I have always found this sort of argument unconvincing. It would be better if scientists, when talking about basic research, said more about the nature of science and less about its value to themselves. As Gerald Holton (12) has written, 'The progress of science to-day is threatened not only by the loss of financial support and of good people, not only by diversion of its energy to applied or engineering work

that may not yet be bolstered by enough basic knowledge, and not only by confusion and disenchantment of the wider public. No, what seems to me the most sensitive, the most fragile part of the total intellectual ecology of science is the understanding, on the part of scientists themselves, of the nature of the scientific enterprise'.

May I add a few arguments for basic research which, I believe, will illuminate the nature of the scientific enterprise but will not, I suspect, carry much weight with the funding agencies. As I see it the major cultural function of science is that it brings our world-outlook, our *Weltanschauung*, into a closer correspondence with reality and in so doing it dispels superstition, criticizes our fantasies and yet enriches our imagination.

Consider for example the effect of some of the advances in science which have taken place during the last 150 years. The study of fossils, the theory of biological evolution and the discoveries of modern astronomy have greatly enlarged our ideas about the origin of life as seen on a cosmic time scale, and about the place of the Earth, as seen in cosmic space. The quantum theory and the theory of relativity have shown us that our experience of objects in the everyday world is no guide to the behaviour of objects which are either very small or moving very fast. In this century we have learned by experience to treat the so-called fundamental particles, of which we are all made, as symbols describing interactions rather than as independent objects with intrinsic properties. Modern science, at least modern physics, has moved quite a long way from the so-called mechanistic outlook of the 19th century, a fact which seems so often to be overlooked by its' critics. Meanwhile down to earth and more urgently, it is the environmental sciences which have reminded us in recent years that we live on a finite planet with limited resources and that, if we want to survive, we must learn to look further ahead and take more care than we do now. Clearly if our world-outlook is to be realistic, as it must be if we are to survive, then we must keep an eye on the changing picture of the world presented by science. What that picture has to tell us is an essential component of wisdom.

Another good reason why we must always update the scientific picture of the world is that we need it not only as a tool, but also as a guide to right action; by which I mean action which is right from a moral, and not merely from a political or economic, point of view. As William Blake says in his *Jerusalem*; 'He who would do good to another must do it in Minute Particulars. General Good is the plea of the scoundrel, hypocrite and flatterer, for Art and Science cannot exist but in minutely organized Particulars'. Consider for example how the Minute Particulars offered by medical science have improved our attitude towards mental illness and the way in which we treat it. Enlightened action may be driven by compassion, but it must often be guided by understanding. Seen in that light, the pursuit of science is a moral imperative of a good society.

Finally let me put forward one of the oldest arguments for basic science—that it inspires wonder, if not reverence for creation, and that, surely, is something we should welcome if we want to live in harmony with this mysterious world. Religion tells us that life has a purpose and meaning beyond our control and beyond our understanding; it points to the idea of the holy. Irreligion tells us to feel, think and act as though man is the measure of all things. Science is a dynamic revelation of the world which points unambiguously to the fact that we are part of nature, surrounded by the

Concern about the control of science

mysteries of time, space, matter and consciousness. On the one hand it reminds us, as does religion, that the world is not of our own making. On the other hand it shows us to what extent our future can be shaped by our own hands. It tells us that, if we are to make the best of that future, we must find out as much as we can about ourselves and the world around us.

The Control of Basic Research

How then are we to get the best out of basic research? There are constraints; the most obvious being that science is a social activity and is embedded in history. Inevitably our choice of topics for research will be strongly influenced by the current pre-occupations of society. The physics and mathematics of the 17th and 18th centuries were influenced by navigational problems of exploring the world, and in our own time the exploration of the solar system has been promoted by the military interest in space research. What research we choose to do will also be influenced by the scientific theories and fashions of the day, by what Thomas Kuhn (13) calls the paradigms of science. The acceptance and recognition which our work evokes from our scientific peers will be influenced by fashions in both science and society.

A second constraint is, I need hardly say, the supply of competent people and money. Nowadays research in most branches of science is so expensive that, if it is to be done at all, it needs a grant; and so, inevitably, basic research is controlled through the supply of money.

This brings us to a major question; how much should we spend on basic research? As we have already seen, there is no clear-cut economic answer to that question; furthermore, unlike the arts, public appreciation of basic science cannot be measured by attendance at concerts and art galleries. At present the decision, as far as I can see, is taken largely by 'keeping up with the Joneses' or, in other words, by looking to see what other countries are doing. For this reason the funding of basic research is peculiarly vulnerable to changes in the cultural climate so we should aim to make it less vulnerable.

We might try, I suggest, to develop, a more convincing case, preferably an economic case, for the support of basic research than keeping up with the Joneses. We might also pay more attention to the public relations of science. It is just as important that the public should understand the value of science, as it is that the scientists should understand the value of his work to society—if I may digress for a moment, I suggest that one thing we might do is to encourage more television productions like Bronowski's 'Ascent of Man' or Attenborough's 'Life on Earth', and the publication of semi-popular journals which take a broad view of science such as the new American Journal 'Science 80'. I think they do more for science than a cartload of official surveys.

When it comes to the handing out of the money for individual research projects in basic science, how shall we choose who to give it to? We cannot avoid this choice; to divide the money equally, among everybody who would like to have it, is not only impractical but is a sure prescription for mediocrity.

We must, of course, strike a balance between what I shall call the external and in-

ternal criteria. By external criteria I mean the sort of thing that any good administrator would consider straight away, the size and cost of the project, its suitability to the resources of the particular country, the competence of the people involved, its social importance, and so on. And I shall say no more about that because I am sure all of us here are good administrators! But what about the internal criteria? They should, I suggest, favour ideas which are not only bright and innovative but which are relevant to the general advance of science rather than to social need. An idea or discovery which is most relevant to science is one which sheds the most light on other topics in science, and thereby advances the frontiers of knowledge at more than one point. In the long term science must advance on a wide frontier, and it is not always possible to forecast the relevance of one part of this frontier to another; for example many of the mathematical tools on which modern physics is based were developed, but not applied, in the 19th century.

Paradoxically the future needs of society are best served by research which is not constrained by those needs. In fact most of the fundamental advances on which modern science rests were made by people who were seeking to know and to understand, and not necessarily to apply what they found. For example, in the study of clinical advances in the field of cardiovascular and pulmonary diseases, to which I have already referred, Comroe and Dripps (9) found that over 40% of the work on which these advances were based were not clinically-oriented at the time it was done. In their own words, it was done by scientists who 'sought knowledge for the sake of knowledge'. As Thomas Huxley wrote to Charles Kingsley in 1860, 'Science seems to me to teach in the highest and strongest manner the great truth which is embodied in the Christian conception of entire surrender to the will of God. Sit down before the fact as a little child, be prepared to give up every pre-conceived notion, follow humbly to whatever abysses nature leads, or you shall learn nothing'.

Who shall give out the money for basic research? It follows from the preceding discussion that this is pre-eminently a scientific matter and must be done by the scientists. To be sure the total amount which is spent on basic research is a matter to be decided by the Government of a country, but the detailed disbursement of that money can only be done effectively by a group of scientists acting on behalf of the scientific community. In an ideal world the system would be pluralistic and there would be more than one group. If these people are to be up-to-date they must be working scientists; if they are to ensure that science advances on a wide frontier, they must be drawn from as wide a range of scientific disciplines as possible. I am, of course, describing a system of 'peer review' which is open to the well-known criticisms that it is too conservative, that it is closed to public debate, that it is potentially a mutual-admiration society and so on. My own experience of one such system, The Australian Research Grants Committee, shows that most of these faults can be avoided by simple administrative measures such as limiting the term of service of any one member and by the extensive use of independent assessors of research projects and so on. No system is perfect but a system which puts the detailed control of basic research largely in the hands of scientists is to be preferred to one that puts it in the hands of politicians, the public or Government departments. Almost the reverse is true of the control of applied research. Just as the values of science are not a good guide to its social applications, so the values of society are not a good

Concern about the control of science

guide to the conduct of scientific research. So, in the control of applied science let us remember the responsibility of science to society; in the control of basic research, let us not forget the responsibility of society to science.

In conclusion may I take my own advice and expose the assumptions and values on which this talk has been based. I have assumed, as one of the main articles of scientific faith, that it is both possible and good to seek knowledge of the world; I have not assumed, as is so often done, that the application of this knowledge must inevitably benefit society.

As I said at the beginning of this talk, one of the major events of the last 100 years has been the meeting of knowledge and power; let us make sure that, before your next centenary, they are joined by wisdom.

October 16, 1980

References

- (1) William Thomson (Lord Kelvin) Presidential Address to the British Association for the Advancement of Science, 1871.
- (2) Nicholas Rescher, *Scientific Progress*, Blackwell, Oxford, 1978.
- (3) Francis Bacon, *Novum, Organum*, Book I.
- (4) *Technological Change in Australia*, Australian Government Publishing Service, Canberra, 1980.
- (5) Vannevar Bush, *Science the Endless Frontier*, U.S. Government Printing Office, Washington, D.C., 1945.
- (6) See for Example, K. Arrow, 'Economic Welfare and the Allocation of Reserves for Invention', in *The Rate and Direction of Inventive Activity*, Princeton, 1962.
Also, R. R. Nelson, 'The Simple Economics of Basic Research', *J. Pol. Econ.*, 67, 297-306, 1959.
- (7) See for Example, B. R. Williams, *Research and Economic Growth—What should we expect?* *Minerva*, 3, No. 1. 57-71, 1964.
- (8) A. H. Wilson, *Proc. Roy. Soc. A.* 133, 458-491, and *A.* 134, 277-287, 1931.
- (9) J. H. Comroe and R. D. Dripps, *Science* 192, 105-111, 1976.
- (10) Basic Research, Background Study No. 21 for the Science Council of Canada, Information Canada, Ottawa, 1971.
- (11) Report of the Royal Commission on Australian Government Administration, Australian Government Publishing Service, page 312, Canberra, 1976.
- (12) Gerald Holton, *The Mainsprings of Scientific Discovery*, in the *Nature of Scientific Discovery*, ed. O. Gingerich, Smithsonian Institution Press, Washington D.C., 1975.
- (13) T. S. Kuhn, *The Structure of Scientific Revolutions*, University of Chicago, 1962.

SCIENCE AND FAITH—A PERSONAL VIEW

R. Hanbury Brown

Science is a word that worries me. Like the word Art it shows signs of wear: it has been used for too many things. Many of us, I suspect, especially when we go round galleries of Modern Art, have misgivings about the meaning of the word Art. I often feel the same way about Science. Advertisements reassure us that some tooth-paste or patent medicine has been 'scientifically' tested, or we are told that scientists have discovered this or that, the origin of the universe or how to grow bigger tomatoes, the public image of a scientist being a man in a white coat standing beside a computer. I often wonder what we mean by science.

To those of you who are not working scientists, let me say that Science, like religion, needs to be lived. It is easy to present the body of Science without the spirit, to show the dry bones without the sense of excitement, of community and progress and of the dedication which Science inspires in so many of her followers.

What, then, is this thing called Science?

A conventional description of Science—the sort of thing one reads in many of the older books in the philosophy of science—goes like this, in three parts.

1. Science, viewed as a process, is a social activity in which we seek to discover and understand the natural world, not as we would prefer or imagine it to be, but as it really is. The characteristic method of Science is the rational, objective, and as far as possible impersonal, analysis of problems based mainly on observational data and experiment.
2. Science, viewed as a product, is the public knowledge of what we have so far found out, and about which the scientific community has agreed. Scientific knowledge is therefore limited to statements on which agreement can be reached and is always open to verification or disproof by anyone. A scientific fact can never be 'original' in the same sense as a work of Art; only its discovery can be truly original, which, incidentally, explains why scientists are so interested in priority of publication and discovery.
3. Science, viewed as an ethical paradigm, is, so Merton¹ tells us, a community

¹R. K. Merton, *The Sociology of Science*, Chicago University Press, 1973.

The author was a pioneer of airborne radar and radio astronomy with Sir Bernard Lovell. While at Jodrell Bank he discovered an entirely new way of measuring the apparent size of radio sources—the invention of the intensity interferometer. He is a Fellow of the Royal Society and of the Australian Academy of Science and Professor of Physics (Astronomy) at the University of Sydney. His latest writing for the layman includes 'Man and the Stars' (OUP, 1978), and 'Cosmology—the last 25 years', CAB Vol 56, No 3

governed by four imperatives—Universalism, Communalism, Disinterestedness and Organised Scepticism. Universalism implies that Science is independent of race, colour or creed: it is essentially international; Communalism implies that scientific knowledge is public knowledge; Disinterestedness is, so to speak, the opposite of propaganda; Organised scepticism requires each individual to accept nothing simply on the word of authority; it is encapsulated in the motto of the Royal Society ‘Nullius in Verba’ which, so I’m told, means ‘don’t take anyone’s word for it’.

Now, many working scientists, not counting amateur philosophers of Science, would probably accept this conventional description of Science as being a fair picture. They might perhaps think of it as being a bit old-fashioned, even romantic, but nevertheless, on the right track. The trouble is, of course, that players often see least of the game and the nature of Science is changing. In fact, it has changed so much in recent years that the conventional description now applies only to that minor, but very important, part of Science which seeks to understand the world, rather than to change it. I shall call this Fundamental Science to distinguish it from Applied Science. I shall, by the way, avoid the usual term ‘Pure Science’ because, in my view, it is absurd to use the word Pure as antonym for Applied; furthermore I doubt whether there is any scientific knowledge which cannot be applied.

To arrive at a more realistic description of modern Science, we must take notice of the fact that in the past few decades Science has been industrialised and has allied itself with power. In changing the world it has changed itself, so that the manifest, dominant activity of Science is no longer the disinterested pursuit of knowledge but the pursuit of knowledge for industry and other social purposes, such as defence, agriculture, health and so on. I won’t weary you with the statistics, but less than five per cent of the World’s expenditure on Science is now devoted to Fundamental Science. The vast majority of scientists are busy applying Science to reach material and social goals and their work is largely controlled by governmental agencies serving national, military and civil interests and by large industrial firms.

The industrialisation of Science has transformed not only the goals of Science but also the practice of Science as a craft. Scientific research has taken on many of the features which we usually associate with industrial processes; much of it is done by large teams using large and expensive machinery. As a consequence, research tends to concentrate in the highly developed countries. It has been estimated that only 4 per cent of the world’s research and development is conducted in areas of the world where 70 per cent of the population live. This change in the craft of Science is also true of most fundamental research. You only have to compare the discovery of moons of Jupiter by Galileo in 1610 with the recent observation of these moons by Voyager I, or to visit a modern high-energy physics laboratory to see how these parts of Science have taken on the character of an industry.

Industrialisation has also transformed the ethos of much of Science, as modern critics, such as Ravetz, Roszak, Habermas, Marcuse, Hilary and Steven Rose, and all the other Jeremiahs of Science, are so fond of telling us. Clearly we must accept the fact that all of the four imperatives which we have listed as governing the scientific community, cannot possibly be obeyed by most of those engaged in Applied Science.

Science and faith—a personal view

I need hardly labour the point that Universalism, Communalism and Disinterestedness are inconsistent with most military or industrial research. Thus, as it has become increasingly industrialised, much of Science has lost some of those precious qualities, such as the disinterested love of truth, which flow from the four imperatives. Inevitably, the public respect for Science has declined and this, in turn, has weakened its authority. This is one of the many reasons why we must always preserve a significant body of Science which is autonomous or, in other words, is not controlled closely by agencies primarily interested in its application.

All science is based on observation and experiment

First let us look at the role of observation and experiment. Histories of Science are usually written in terms of outstanding people like Newton and Einstein and give the impression that the progress of Science depends largely on the development of new theories. It would be nearer the truth to say that all Science, both Fundamental and Applied, depends largely on the development of new instruments. The progress of Astronomy, for example, owes more to two technological inventions, the telescope and the spectroscope, than to any other factor, and yet there are very few astronomers who could tell you who invented them. Likewise, Biology and Medical Science would not have got very far without the microscope; in our own day, the revolutionary knowledge of the structure of complex proteins and the mechanisms of heredity owes much to the X-ray diffractometer and the computer. Science and technology have always gone forward hand in hand. May I remind you that J. B. Conant² once said, 'Science owes more to the steam-engine, than the steam-engine owes to Science'.

In discussing our knowledge of the world it is always salutary to remember that it is often initiated, and always limited, by our present tools of observation. It is true that theories often precede and suggest observations, but, in the long run, all theories must be consistent with observations if they are to survive.

Science and values

Turning again to our conventional description, it says that Science is based on the impersonal analysis of observational data. This leads to the question, how much of our scientific picture is impersonal and how much does it reflect our own values! Any student of history knows part of the answer. Science is a social activity and as such its history cannot be separated from the history of anything else.

Quite clearly the choice of the topics of Science is strongly influenced by our current interests and values. As one would expect, at any given time, our scientific picture shows some aspects of Nature in much greater detail than others because they are of greater current interest; they may perhaps be relevant to industry or war. In the 15th and 16th centuries, for example, when the world was being explored and

²J. B. Conant, *Science and Common Sense*, New Haven, 1961.

opened up to trade there was a strong mercantile interest in developing navigation, which necessarily involved quite abstruse and fundamental studies of the motion of the Moon and the distance of the Sun.

In our own times we don't have to look any farther than Space Research to see the connection between our detailed knowledge of the surface of the Moon and military interests. In the civil field only a small fraction of the world's research and development is directly concerned with the needs of the poorest, but relatively large, fraction of the world's population.

There is, I think, no need to pursue this obvious connection between the topics of Science and the values of Society any further; but before we leave it I would like to draw your attention to an interesting, and less obvious paradox in the pursuit of relevance. The demand that Science should be more relevant to the things which Society values and that scientists should be more socially responsible is, I believe, usually justified and certainly to be expected as the cost of science to the community increases. There is, however, one problem which is so often overlooked. The relevance of scientific work can only be judged on a short-time scale; over long periods it is impossible. It takes roughly one generation for the results of new experimental science to reach application and much longer for new mathematics. Thus most of the recent ideas of modern Physics depend upon mathematics which was invented, but not applied, in the previous century. I doubt whether many of the discoveries on which modern Science rests, such as the discovery of the electron, would have been funded by agencies assessing their relevance. The farther scientific work is from application the more vulnerable it is to the demands of relevance. Paradoxically, our interests are best served, in the long run, by fundamental research which is guided more by the internal logic of Science than by the immediate needs of Society. Experience shows that to advance our understanding of the world we must seek knowledge for its own sake. Necessity is the mother of invention but not of discovery.

It is also clear that our values influences what we accept as 'scientific knowledge'. There are many examples of this, particularly in fields of science which are 'immature' in the sense that their main principles have not been established. It may be that the available facts are not decisive, so that theory plays too large a part in the conclusions, or perhaps the conclusions themselves are very sensitive to the choice of the factors on which they are based. In these circumstances, what we accept as Science may well depend on our current prejudices and preoccupations. Thus the history of the theory of the heliocentric Universe, from Copernicus onwards, reflects on one side a religious preference for a man-centred Universe and on the other a mystical idea about the central importance of the Sun coupled with a preference for conceptual economy. Nearer our time there is the opposition to the probabilistic ideas of quantum mechanics, for example by Einstein, on the grounds of a prejudice against a universe ruled by chance. In the comparatively immature, but extremely complex, science of genetics, we can point to the well-worn example of the theories of environmental genetics advanced in the 1940s by the agronomist T. D. Lysenko, ideas which were accepted as Science in the USSR largely because they were politically and ideologically welcome. Judging from recent controversies in the USA it is still difficult to get value-free Science on analogous questions of heredity and environment.

Science and faith—a personal view

In brief, at any given epoch, the process and the product of Science are both coloured by the current values of Society.

The nature of reality

Let us now look more closely at what, in conventional description, is implied by discovering and understanding the world 'as it really is'.

Most of us know perfectly well what is meant by 'reality'. A stone is real, not imaginary; it is a solid, inert lump which, if thrown through our window will break the glass. And yet modern Science tells us that the inside of this stone is mostly space, very peculiar space filled with vacuum fluctuations and 'virtual' particles; and in this space there are protons, electrons, and so on which sometimes behave as waves and sometimes as billiard balls and which may, themselves, be made up of other mysterious entities called quarks. To be sure, Science agrees that our stone is inert and if we want to throw it back we can predict its path precisely by Newton's Laws of motion or, even more precisely, by Einstein's General Theory of Relativity. But if we enquire more closely we find that this apparently simple quality of inertia is itself a mystery; some scientists think that it depends upon the interaction of the stone with all the other bodies in the Universe, and some do not.

Clearly our concept of a 'real stone' is an abstraction from the wider properties of stones based on our experience of seeing and feeling stones. It is a metaphor which, in terms of our everyday experience, describes something more fundamental, more complicated and essentially mysterious. Broadly speaking, we can think of the whole scientific picture of the world in the same way, as a metaphor which describes and relates the abstractions we make by observation from a more complex, possibly infinitely complex, reality. These abstractions are chosen and limited, partly by our own theories and values and partly by our tools of observation, and so our picture of reality is necessarily incomplete and provisional. It can never claim to be absolute truth; but it is the best picture we have.

Does 'reality' reflect the structure of our minds?

There is another more profound question which we can ask about the impersonal nature of scientific knowledge. But, first, may I remind you of Eddington's³ parable of the ichthyologist who explored the life of the ocean with a net which had a two-inch mesh. He came to the conclusion that all fish are longer than two inches. This little parable prompts us to ask to what extent scientific knowledge is shaped and limited by the structure of our minds?

Our experience of Physics in this century has made us cautious of answering this question. We have found that all the phenomena of Nature cannot be explained or described in terms of our familiar, common-sense, concepts of space, time, causality, identity, and even of locality. Common sense cannot interpret the behaviour

³A. S. Eddington, *The Philosophy of Physical Science*, Macmillan, Cambridge, England, 1939.

of objects which are very small, like atoms, or very large, like the Universe, or moving with speeds approaching the velocity of light. To bring this behaviour within the discipline of Science we have had to learn to think in new ways. A good example is to be found in quantum mechanics where we have had to exchange certainty for probability. We have reached the remarkable conclusion that it is fundamentally impossible to predict what an individual particle or proton will certainly do, no matter how much we know about it. We can only predict what it will probably do by a calculus which involves waves of probability. These waves of probability cannot be detected by any physical observation; they exist, so to speak, only in our mathematical minds.

What, we may ask, must the world be like, in order that man may know it? Shall we always be able to develop uncommon-sensical concepts to relate and predict phenomena as yet undiscovered? It remains to be seen.

Is the observer part of the picture?

There is yet another question which brings out the nature of scientific knowledge rather well. How does this knowledge depend upon the act of enquiry? Is the observer, so to speak, part of the picture? The commonsense answer is obviously 'yes' when we are looking at living things, especially at ourselves, and I shall say no more about that; but it is 'no' when we are looking at the inanimate world. In thinking about inanimate things we distinguish sharply between the observer and the observed. We think of stones as having objective existence which is quite independent of us. As Gertrude Stein might have said, 'A stone is a stone is a stone'.

One of the great surprises of the present century has been to learn from Physics that this common-sense view of our relations with the inanimate world is wrong or, to be kinder, is only an approximation of the truth. As I have already said we now realise that our concept of a 'thing' is based on a limited set of abstractions which we ourselves choose to make from a more complex reality. Thus the concept of a thing, and the intrinsic properties which we ascribe to it, depend upon what particular set of abstractions we select; in other words, it depends on the particular class of observations which we choose to carry out and therefore also on the theory which guides our choice. One of the most common intellectual errors is to confuse a concept or symbol with reality and to use it outside its proper domain of validity; in religious terms this is the sin of idolatry.

In the present century physicists have come to realize that by making different abstractions from reality it is possible to arrive at quite different, even contradictory, concepts of the 'thing' which is being observed. A familiar, but not unique, example of this remarkable fact is to be found in the theory of light. As you will know the modern theory of light accepts that light behaves either as an indubitable wave or as an indubitable particle depending on the type of observation we choose to make. We have given up trying to make common-sense out of its properties, and if asked what light is really like, we can only answer 'light is like light', and offer a mathematical theory which will predict its behaviour in any given situation. The point is, of course, that light is neither a particle nor a wave, but something infinitely more

complicated, something we can't visualize in terms of everyday experience. And yet these two concepts, the particle and the wave, are both valid within their own limited domain; physicists call them complementary.

Perhaps I should emphasize that because it is possible to arrive at two apparently contradictory images of the same thing—for example, light—it does not follow that scientific knowledge is subjective. Admittedly, the observer does enter our picture of the world by selecting the particular set of abstractions on which the picture is based. Furthermore, these abstractions cannot be thought of as being intrinsic to the thing itself, they are interactions between the thing and the observer. Nevertheless, the actual observations of these interactions, the data on which our picture is based, remain truly objective. They are independent of the particular observer and can be verified by anyone, even by a machine. In brief, they are public knowledge.

Before we go any further, may I draw your attention to two important, and unfamiliar ideas in this discussion of scientific knowledge. First, that a particular concept of reality is valid only in a limited domain. Secondly, that it is possible to arrive quite objectively at two contradictory, but nevertheless, complementary concepts of the same thing, both of which are valid within their own field. Truth, indeed, has many faces.

Does science progress?

I must now say something about the progress of Science because to the working scientist one of the principal attractions of Science is its sense of progress. Such a sense is, of course, not unique to Science nor has it always been like that. For example, Vasari⁴ writing in the 16th century conveys the sense of progress in the Art of that time towards the goal of more perfect representation. And yet there was then no sense of progress in Science. It came later, in the next century, with the questioning of ancient authority and the rise of experimental method. Since the 17th century, Science and Technology have become our major paradigms of progress, and Astronomy has given us an almost unlimited future into which we can progress. Nowadays, the idea—or should I say the ideal?—of Progress, is so pervasive that it is hard to realize how recent and vulnerable it is. It is, by the way, equally hard to realize how recent and vulnerable is our belief in the value of scientific truth.

The Progress of Science is not, as Francis Bacon⁵ tried to persuade us, a simple matter of adding detail to detail. In pursuing the larger goals of Science—the cause and cure of cancer or the structure of matter—the great art is to ask the right questions, to choose problems which are relevant and soluble from the vast reservoir of unsolved problems. As any scientist knows this cannot always be done, and research sometimes grinds to a halt until it is rescued by a new insight or a happy accident. Now and again someone discovers something immensely useful like X-rays or penicillin entirely by accident, or illuminates a whole range of problems by

⁴G. Vasari, *Lives of the Most Eminent Painters, Sculptors, Architects*, ed. R. N. Linscott, Random House, 1959.

⁵Francis Bacon, *Novum Organum*, Bk. 1.

discovering the structure of DNA. When this happens, there is a step forward which usually leads to the discovery of new phenomena and to a wider understanding of the relations between phenomena which are already known.

Some historians, such as T. S. Kuhn⁶, have pictured the progress of science as a proliferation of ever deeper and narrower specialities. They agree that it progresses, as measured by the number of problems solved, but they see these problems as being set by the whims of the scientists themselves and they discern no overall movement towards some central truth. This is a view of Science which I believe to be misleading. I see no reason to suppose that the progress of Science must converge on some central truth. To borrow a phrase from J. B. Bury⁷, the idea looks to me suspiciously like an 'illusion of finality'. For one thing it is characteristic of all advances in Science that they pose more new questions than they answer. As long as this continues to happen, Science will progress. To take one example from many, in the present century advances in Nuclear Physics have solved the old important problems in Astrophysics of how the stars get their energy and how the heavy elements were formed. And yet, they have created more unsolved problems in Astrophysics than there were before, among them the complicated problem of how all the elements heavier than hydrogen were formed.

A more realistic view does not see the progress of Science simply as a proliferation of new data and narrower specialities, but as the development of more and more powerful generalisations, laws of Nature, which extend our ability to explain, relate, and predict the diverse phenomena which mark the frontiers of Science. Newton, for example, saw the connection between the fall of an apple and the motion of the Moon. In that sense, Science is getting easier, not harder, to understand.

It is often argued that the progress of Science is slowing down and that, one day, it will stop. Admittedly the rate at which significant new ideas are produced has not kept pace with the enormous expansion of Science, but it is obvious why this should be so. It is not, as so often is suggested, due to exhaustion of the subject; the number of problems has increased. It is not due to an unmanageable mass of data; that problem is being solved by technological advances in data-handling. It is due to the simple fact that each advance in Science gets progressively harder to make, not only harder but more costly as well. Our tools of observation, on which progress depends, must be more powerful and elaborate, and, in real terms, they cost more. If anything, other than a loss of will, stops the progress of Science it is most likely to be the sheer cost of new tools. But we haven't got to that stage yet and, even if the rate of progress does slow down, that is not necessarily a bad thing. Society needs more time to get used to new things and new ideas.

In brief, I believe, with most scientists, that Science does progress in a worth-while way and that in the long run distortions in our picture of the world due to errors or cultural influences fade with time, leaving us with a progressively truer image of the world. An important article of the creed of Science is '*Veritas temporis filia est*' —Truth is the daughter of Time.

⁶T. S. Kuhn, *The Structure of Scientific Revolutions*, University of Chicago Press, 1962.

⁷J. B. Bury, *the Idea of Progress*, Macmillan, 1932.

Why bother about science?

Why should we bother about Science? Most people, if asked that question would, I guess, talk about the practical uses of Science. They would point to the very real contributions which Science and Technology have made to our health and wealth. No doubt they would also point to some of the things they fear like pollution, nuclear power, genetic engineering and so on. Some, perhaps rather few, would point to the contributions that Science has made to our culture in the same way as music and painting. Science, they would say, is worthwhile for its own sake—*ars pro gratia artis*.

In my view, these arguments for Science are too shallow. Science is not just a modern cargo cult; nor is it just an ornament of Society; nor is it just an intellectual pastime. Modern Science is one of the greatest achievements of the mind and spirit of man, it is not to be treated simply as an instrument of social or political purpose. It is one of the main, indispensable pillars on which our civilisation and our hopes for the future rest. May I point to some of the reasons why I believe this to be true.

Science and right action

The simple equation of truth with goodness, and of knowledge with right action, was spelled out in the 17th and 18th centuries. It flourished when men came to look more to perfectibility in the future than at perfection in the past. The progress of Science, urged on by Francis Bacon, played a significant part in this reorientation. We have today inherited this precious belief in the possibility of progress, but we have learned that it demands not only knowledge but also vision and wisdom. To act rightly we must always be making value judgements in which we weigh profit and loss, freedom and justice, beauty and truth, and to do this we need all the Science we can get. Most of the problems of the modern world involve detailed scientific knowledge, and it is the obvious responsibility of scientists to alert us to the social implications of scientific advances and to help us, in terms we can understand, to apply them wisely. As William Blake wrote, 'He who would do good to another must do it in Minute Particulars. General Good is the plea of the scoundrel, hypocrite and flatterer, for Art and Science cannot exist but in minutely organised Particulars'.

Science and Weltanschauung

Let us now turn to the influence of Science on our world-view. One of the four main elements in the ethos of Science, as I said before, is 'Organised Scepticism'. Not the sort of quality to inspire devoted enthusiasm, but, nevertheless, invaluable to society. We must remember that one of the dangers to any society especially since the development of mass communications, is that it might become credulous. The antidote to credulity is scepticism.

Anyone who has studied the trial of Galileo, the controversy over evolution between Wilberforce and Huxley or the 'monkey' trials at Dayton, will know that

human institutions preserve ideas as a rock preserves fossils. One of the principal cultural functions of Science is to prevent this happening, and to keep our ideas flexible and, above all, realistic by pointing continuously to the way the world, to the best of our current knowledge, actually is. In doing so, Science fulfils the classic role of destroying superstition.

Consider, for a moment, the profound changes in our world view brought about by Copernicus when he removed the Earth from the centre of the Universe, and by Newton when he developed the science of celestial mechanics. In the present century we have seen equally great changes. The earth is now a planet of a minor star in a galaxy of billions of other stars, and the galaxy itself is one among millions and millions of other galaxies which stretch away as far as our most powerful telescopes can see. The same sort of readjustment of perspective has taken place in time. Modern cosmology has given us an immense past and an equally immense future. Astrophysics has shown us how the heavy elements of which we are all made were evolved in stars from primeval hydrogen. Thus Astronomy, Geology, and Biology have placed the evolution of the Earth and Man in a vast tract of time. There are, of course, many questions which are unanswered, like the origin of the planets or of living matter, but the general perspective of our place in time and space is now fairly clear. What effects this new perspective will have on our culture it is still too early to say; but one thing we can already see, all Modern Science, the whole study of evolution from the Big Bang to man, points to an old and powerful idea, to the unity of Man and his environment, and to his need to live in harmony with it. And there is more to come; what, for example, will be the effects on our society of understanding the mechanism of heredity, the mechanism of mind? Or even, perhaps, communication with other worlds?

If our ideas about ourselves and the world we live in are to be flexible and realistic, as they must, then we shall have to keep an eye on the picture of the world presented by Science. We must always be prepared to revise our ideas in the light of what we see; and this, of course, applies equally well to the teaching of the Church. A static view of the world belongs to the Middle Ages.

Science and imagination

I now want to say a word about imagination because the prophets of the counter-culture (*e.g.* T. ROSZAK⁸) are always telling us that Science is an enemy of the imagination and I believe this to be profoundly untrue. To be sure wisdom and vision both need imagination, but history shows us clearly that imagination must always retain contact with 'objective truth', the sort of truth which Science offers. Beliefs and institutions guided by unrestrained imagination go stale and, sooner or later, turn into fantasy—and very nasty fantasies too. Consider, for example, the religious practices of the Aztecs. Not only does Science keep imagination's feet on the ground, but it enriches it because, as Bronowski⁹ was so fond of pointing out, 'the strength

⁸T. Roszak, *The Making of a Counter Culture*, Faber, London, 1970.

⁹J. Bronowski, *A Sense of the Future*, M.I.T. Press, Cambridge, Mass, 1977.

Science and faith—a personal view

of the imagination, its enriching power and excitement, lies in its interplay with reality—physical and emotional'. No one could have foreseen or imagined the beauty and the complexity of Nature as revealed by Science.

Science and faith

How, in our own times, can we make it easier for Faith and Science to work together as Faith and Art have done in previous centuries? Newton certainly thought that it could be done in his day and so did the Deists after him. But it didn't take long for Science and Religion to become enemies—what went wrong? The fault, needless to say, lay on both sides. In their enthusiasm for Celestial Mechanics or for the Theory of Evolution many scientists, like Laplace, saw no need for God. The supporters of Religion, on the other hand, confused the powerful symbolic ideas which they had inherited from the past with reality, and so they fought a losing battle with Science. Thus, Thomas Huxley won his battle about evolution with Bishop Wilberforce. No doubt he should have won, but not, I think, so easily.

To this day there are people who carry on these old battles, but fight under different banners and on different ground. Some, for example, tell us that the ideals of Science have been so eroded by its alliance with power that it has little to offer us, apart from material goods. This argument, I suspect, we have heard before in the context of the Church. To save time, I suggest that it is no more a valid reason for turning away from the values of Science than it was for turning away from Christian Faith. Others attack Science because they say it removes the sense of mystery from the world and dehumanises us by its emphasis on objectivity. Like Laplace's *Systeme du Monde*, the scientific 'single vision' of the world has no place for the supernatural, no need for God.

This second view of Science is, I suppose, still one of the main obstacles to a closer alliance with Faith. There is, of course, no simple solution to this difficulty, but there are some ideas and attitudes which, I believe, are helpful.

To start with I think that we must dispel the idea that Science removes mystery from the world. It is true, of course, that Science does remove minor mysteries, such as the mechanism of heredity, but in doing so it shows us where the major mysteries really are.

As I said earlier, our scientific knowledge is based on abstractions which we choose to make from a more complex, essentially mysterious reality. All our ideas about the world, about time, space, fundamental particles, light and so on, are therefore symbolic entities which are themselves mysterious. As for the great mysteries which stand in the shadows of all human thought, such as the origin and purpose of the world, modern Science cannot be accused of sweeping them away. The mystery of Creation is intact, pushed back by 20 billion years, but, nevertheless, where it always was—in the beginning. Nor has Science anything to say about the purpose of the world. It has told us a good deal about the setting of the play but not about the plot. In brief, everything we know is bounded by mysteries. Science relates us to these mysteries impersonally through objective knowledge; Art and Religion relate us to them personally through beauty, meaning and purpose. Thus in the domain of

R Hanbury Brown

Science, as the critics rightly point out, there is no room for the supernatural; what they overlook is that the natural is mysterious enough.

Secondly, I think we must accept that the scientific vision of the world is neither a rival nor an alternative to any other point of view. It is an essential part of learning to be at home in this mysterious Universe and of making the best of it and of ourselves. At the same time, we must recognise that the 'public' vision of the world is not the only one. Modern Physics has demonstrated, for all to see, the importance of complementarity in human understanding. It seems that there are many things, perhaps everything, which cannot be understood from one point of view. It is therefore essential to explore other points of view but, as Science tells us, it is equally important to realise that every point has a limited field over which the vision is true.

Finally, I suggest that we should accept the pursuit of Science as a moral duty. To regard it as an enemy of Faith is to live in the last century. Not only is it essential to making a better world, but it is a dynamic revelation of the marvellous and mysterious world in which we live.

As the poet says,¹⁰

Unless the eye catch fire,
The God will not be seen,
Unless the ear catch fire,
The God will not be heard,
Unless the tongue catch fire,
The God will not be named,
Unless the heart catch fire,
The God will not be loved,
Unless the mind catch fire,
The God will not be known.

Modern Science can, I believe, help Faith to set the mind on fire.

¹⁰T. Roszak, *Where the wasteland ends*, Doubleday, 1973.

This article is a lightly edited version of an address to a Conference on 'Faith, Science and the Future, organised by the World Council of Churches at the Kresge Auditorium at the Massachusetts Institute of Technology on July 12 this year. The audience of approximately 1,000 comprised delegates to the conference, observers, students, and representatives of the press, radio and television. Delegates were mainly clergy, theologians and scientists. They came from all over the world.

